Astrophysics and Space Science Library 418

Eija Laurikainen
Reynier Peletier
Dimitri Gadotti *Editors*

Galactic Bulges

ASSL

Springer

Astrophysics and Space Science Library

Volume 418

Editorial Board

More information about this series at http://www.springer.com/series/5664

Eija Laurikainen • Reynier Peletier • Dimitri Gadotti
Editors

Galactic Bulges

Springer

Editors
Eija Laurikainen
Astronomy and Space Physics
University of Oulu
Oulu, Finland

Reynier Peletier
Kapteyn Institute
University of Groningen
Groningen, The Netherlands

Dimitri Gadotti
European Southern Observatory (ESO)
Santiago, Chile

ISSN 0067-0057 ISSN 2214-7985 (electronic)
Astrophysics and Space Science Library
ISBN 978-3-319-19377-9 ISBN 978-3-319-19378-6 (eBook)
DOI 10.1007/978-3-319-19378-6

Library of Congress Control Number: 2015949217

Springer Cham Heidelberg New York Dordrecht London

Cover Illustration: In the cover the 3.6 μ images of one nearby galaxy, NGC 4565, is shown. The images are from the Spitzer Survey of Stellar Structure in Galaxies (PI Kartik Sheth).

Printed on acid-free paper

Springer International Publishing AG Switzerland is part of Springer Science+Business Media (www.springer.com)

Preface

The main motivation for this book was our impression that when observers talk about bulges in galaxies, they do not necessarily mean the same thing as people making theoretical models. Even among the observers, it is not always clear what they mean by *classical* and *pseudobulges*. According to most researchers, classical bulges are highly relaxed systems typically formed in galaxy mergers or by coalescence of massive gas clumps at high redshifts, whereas pseudobulges have more disc-like properties. Some people divide pseudobulges further into *discy pseudobulges*, defined as small central discs in the plane of the galactic disc, and *boxy/peanut bulges* which are actually dynamically heated, vertically thick inner parts of bars. Galaxies can also have central star clusters, usually called nuclear clusters, which structures are not called bulges in this book (see the review by Cole and Debattista). In recent years significant progress has been made both on the theoretical and observational sides, including galactic and extragalactic research. In this book we try to bring all these communities closer to each other.

Most probably many of us share the Copernican approach trying to understand the universe with some simple beautiful theory. Such an attempt is the current paradigm of structure formation, i.e., the hierarchical growth of dark matter halos (ΛCDM), and the subsequent formation of bulges and discs from baryonic matter. However, there is always lurking a possibility that something important is hidden in the myriad of details in the observations, which might eventually lead to something unexpected. This book is an attempt to review our current understanding of galactic bulges both from the observational and theoretical points of view, written by specialists in the field. An inspiring historical and philosophical review about the concept of the bulge is given by Barry Madore, who encourages us to refresh our minds to see galactic bulges with open eyes. The main achievements in the field and the outstanding yet unresolved problems are discussed by John Kormendy.

One of the problems in the current paradigm is why hierarchical clustering produces so many giant galaxies which have only small bulges or even no bulges at all, and also, why so few of the bulges are classical. Galaxy simulations can convincingly make bulge-less dwarf galaxies, but it is still a puzzle what makes also so many bright disc galaxies almost bulge-less. Echoing the morphology-density

relation discovered in the early 1980s, the fraction of classical bulges is a strong function of galaxy environment, i.e., massive bulges appear mainly in galaxy clusters or in small groups of galaxies. Major merger models convincingly explain bulges in the brightest galaxies in the nearby universe, but problems appear when Milky Way mass galaxies, or galaxies having masses lower than that, are considered.

There is observational evidence showing that even half of the galaxies at high and moderate galaxy inclinations have boxy/peanut- or X-shape inner morphology, generally associated to bars. This is the case also with the Milky Way (see the reviews by Shen and Li and Gonzalez and Gadotti), where no clear evidence of a classical bulge is seen, or at least its presence is debated. We may even ask whether the central mass concentrations in most of the Milky Way mass galaxies actually form part of a bar? Interestingly, the average surface brightness profiles of field galaxies, up to $z = 2$, seem to show the astonishing fact that mass is gradually accumulated to the discs at all radial distances from the galaxy center (van Dokkum et al. 2013, ApJL, 771, 35). In this process the Sérsic index of the total surface brightness profile increases, which makes it challenging to distinguish possible merger-built bulges (or galaxies) from those formed by disc instability (or slow accretion events) during the last few gigayears. Needless to say, it would be important to integrate secular evolution into the paradigm of galaxy evolution.

In the theoretical models, strong feedback from supernovae is generally used to delay star formation, thus inhibiting the formation of massive bulges. Intriguing reviews in this book are given, by Brooks and Christensen for merger models and by Bournaud for models where bulges form at high redshifts from gas-rich giant clumps, which gradually drift to the central regions of galaxies. A promising way of explaining the observed low mass bulges in the clumpy universe is obtained in models where a balance appears between feedback and gas accretion, occurred via cold flows or wet minor mergers. Such a balance seems to explain well also the observed cosmic star formation rate at different redshifts (Almeida et al. 2014, A&ARv, 22, 71). In the merger models, a promising channel for making low mass bulges is to add a new superbubble feedback mechanism to the models. A manifestation of strong feedback in galaxies is the observed large metal enrichment of the interstellar medium, which is significant not only in galaxies, but quite unexpectedly also in their environments at large distances from the galaxies (Peeples 2015, Nature, 517, 444). Does this mean that feedback is indeed extremely efficient in massive galaxies? Or alternatively, does there exist a large number of unseen, gas depleted dwarfs hidden in the darkness, galaxies which have expelled their metals in supernova explosions to the interstellar medium? Or, should we rather think that the potential bulge mass actually resides in thick discs or small stellar halos?

In any case, the puzzle of the observed low mass bulges in the nearby galaxies still remains, in particular because the many processes adding mass to the bulge accumulate during the Hubble time. In the review by Combes, this problem has been approached from the MOND (Modified Newtonian Dynamics with no need for dark matter) point of view, which reduces relaxation and thus also suppresses the formation of classical bulges. As also the dynamical timescale for the giant clumps

to drift into the central regions of galaxies is increased, the bulges that form are less massive.

Although the modelers are handling the issue of structure formation of galaxies in a clever manner, sometimes it remains a problem that the observers are not capable of giving an unambiguous picture of the properties of bulges and discs in the actual universe. In this book we try to take one step forward trying to make order in the wild way of using the different concepts of bulges. Bulges are flux concentrations in the central regions of galaxies, but as they are often divided into classical and pseudobulges, we try to systematize the way of using these concepts. However, a word of warning should be in place here. As discussed by Madore in this book, at the early days of extragalactic research, colorful expressions were used to describe the central flux concentrations in galaxies, without attempting to associate them to any specific physical processes. Perhaps we, too easily, do so.

An excellent review of discy pseudobulges is given by Fisher and Drory. They highly recommend to use multiple criteria to distinguish those structures. It is generally assumed that the bar-related boxy/peanuts appear in galaxies seen only edge on, but there is recent observational and theoretical evidence showing that such structures can actually be traced at all galaxy inclinations (Laurikainen and Salo and Athanassoula, in this book). While using the criteria by Fisher and Drory, this somewhat complicates the separation of discy and boxy bulges from each other. Kinematics and stellar populations of bulges are reviewed by Falcón-Barroso and Sánchez-Blázquez, based on the most recent high-quality observations of bulges. These observations are approaching the precision needed for detailed comparison with the properties of the Milky Way bulge. Perhaps one of the challenges in the interpretation still is how to connect the right structure components to the corresponding properties in stellar populations and kinematics. Here, the recently commissioned and forthcoming high-resolution integral field spectrographs (IFUs) are expected to make a great improvement.

One of the oldest ways of studying the nature of bulges has been to look at their three-dimensional structures. In this a nice journey through the past to the present is given by Méndez-Abreu in this book. Historically, the similarity of the intrinsic shapes of bulges and elliptical galaxies is why their formative processes have often been associated to each other. Support to this interpretation comes from many scaling relations of the photometric and kinematic parameters of the bulges and discs (though exceptions also exist). A word of warning of using simple scaling relations to make such conclusions is given by Zaritsky in his review. He suggests that a better way of distinguishing classical and pseudobulges could be based on the idea that only the classical bulges are dynamically complete subsystems satisfying the virial theorem. Although the discs in general also satisfy the virial theorem, that is not expected to be the case for the dynamically incomplete pseudobulges.

The amazing history of the discovery of the supermassive black holes (SMBHs) and their connection to galactic bulges is extensively reviewed by Graham. SMBHs were first discovered in massive quasars, but in 1998 Magorrian suggested that most nearby galaxies might actually harbor a black hole. Nowadays the black holes are detected even in bulge-less galaxies, and a small black hole is found also in the

center of the Milky Way. A lot of passion has been dedicated to explain why the connection between bulges and SMBHs exists and how that works for the classical and pseudobulges. Sparks of that passion are visible also in this book, where ample space is given to different opinions on this subject, as becomes obvious from the sections written by Graham and Kormendy. The topic is definitely important, and the efforts trying to explain that connection go hand in hand with our improved understanding of the structure formation in galaxies.

For the editors, this has been an interesting journey through the world of galactic bulges, and the thoroughly written reviews have taught us a lot. Also, the excellent external referees of the manuscripts of this book have done their work with the same seriousness, as when reviewing normal articles in the refereed astronomical journals.

Acknowledgments We acknowledge the DAGAL Marie Curie Initial Training Network (PI Johan Knapen) for an inspiring research environment, which brought us editors in touch with Ramon Khanna, Senior Astronomy Editor at Springer. This was a critical starting point to this project, as was also the encouragement of Françoise Combes for us to approach Springer with this project. We also warmly thank Heikki Salo for his substantial help while editing this book.

Oulu, Finland — Eija Laurikainen
Groningen, The Netherlands — Reynier Peletier
Santiago, Chile — Dimitri Gadotti
April 2015

Contents

List of Contributors

Evangelie Athanassoula Aix Marseille Université, CNRS, LAM (Laboratoire d'Astrophysique de Marseille), UMR 7326, 13388 Marseille 13, France

Frédéric Bournaud Laboratoire AIM Paris-Saclay, CEA/IRFU/SAp, CNRS/INSU, Université Paris Diderot, 91191 Gif-sur-Yvette Cedex, France

Alyson Brooks Rutgers University, Piscataway, NJ, USA

Charlotte Christensen Grinnell College, Grinnell, IA, USA

David R. Cole Jeremiah Horrocks Institute, University of Central Lancashire, Preston, Lancashire, UK

Françoise Combes Observatoire de Paris, LERMA, CNRS, 61 Av. de l'Observatoire, 75014 Paris, France

Victor P. Debattista Jeremiah Horrocks Institute, University of Central Lancashire, Preston, Lancashire, UK

Niv Drory McDonald Observatory, The University of Texas at Austin, Austin, TX, USA

Jesús Falcón-Barroso Instituto de Astrofísica de Canarias, Vía Láctea s/n, La Laguna, Tenerife, Spain

David B. Fisher Center for Astrophysics and Supercomputing, Swinburne University of Technology, Hawthorn, VIC, Australia

Dimitri Gadotti European Southern Observatory, Alonso de Cordova 3107, Vitacura, Santiago, Chile

Oscar A. Gonzalez European Southern Observatory, Alonso de Cordova 3107, Vitacura, Santiago, Chile

Alister W. Graham Center for Astrophysics and Supercomputing, Swinburne University of Technology, Hawthorn, VIC, Australia

John Kormendy Department of Astronomy, University of Texas at Austin, Austin, TX, USA

Eija Laurikainen Astronomy and Space Physics, University of Oulu, Oulu, Finland

Zhao-Yu Li Key Laboratory for Research in Galaxies and Cosmology, Shanghai Astronomical Observatory, Chinese Academy of Sciences, Shanghai, China

Barry F. Madore Observatories of the Carnegie Institution of Washington, Pasadena, CA, USA

Jairo Méndez-Abreu School of Physics and Astronomy, University of St Andrews, North Haugh, St Andrews, UK

Heikki Salo Astronomy and Space Physics, University of Oulu, Oulu, Finland

Patricia Sánchez-Blázquez Departamento de Física Teórica, Universidad Autónoma de Madrid, Madrid, Spain

Juntai Shen Key Laboratory for Research in Galaxies and Cosmology, Shanghai Astronomical Observatory, Chinese Academy of Sciences, Shanghai, China

Dennis Zaritsky Steward Observatory, University of Arizona, Tucson, AZ, USA

Referees

Ronald Buta: University of Alabama, Tuscaloosa, AL, USA
Mark den Brok: University of Groningen, Groningen, The Netherlands
Enrico-Maria Corsini: Universitá di Padova, Padova, Italy
Bruce Elmegreen: Watson Research Center, Yorktown Heights, NY, USA
Eric Emsellem: European Southern Observatory, Garching, Germany
Chris Hayward: California Institute of Technology, Pasadena, CA, USA
Stacy McGaugh: Case Western Reserve University, Cleveland, OH, USA
Ortwin Gerhard: Max Planck Institute for Extraterrestrial Physics, Garching bei München, Germany
Panos Patsis: Research Center for Astronomy, Academy of Athens, Athens, Greece
Philippe Prugniel: Université de Lyon/Observatoire de Lyon, Saint Genis Laval, France
Sven de Rijcke: Department of Physics & Astronomy, Ghent University, Ghent, Belgium
Roberto Saglia: Max-Planck-Insitut für extraterrestrische Physik/Universitäts-Sternwarte München, München, Germany
Francesco Shankar: School of Physics and Astronomy, University of Southampton, Southampton, UK

Chapter 1
Bulges: Seen from a Philosophically-Informed Historical Perspective

Barry F. Madore

Abstract Most every graduate student in astronomy today knows what the "bulge" of a spiral galaxy is by name and what it looks like. A century ago few professional astronomers knew, or even cared. We trace the early and quite casual usage of the term (and its competitors) and then follow the later and gradually more strict adoption of the term "bulge", needed to call out a major component of galaxy morphology. In the specific context of the Milky Way "The Galactic Bulge" was a proper name. Only later, as they were seen and measured in other galaxies, were these same structural features to become known generically as "bulges". That term finally won out over its more unwieldy competitors such as the "amorphous central region", the "unresolved nuclear region" or the highly ambiguous term "central nucleus".

1.1 Introduction

A bulge. The very word brings to mind a three-dimensional object, implicitly in juxtaposition with some other spatially co-existing object or component that is itself comparatively flat(ter). Taking a two-dimensional projection (i.e., an image) of a galaxy and declaring it to contain a 3D bulge assumes a great deal of prior (passed down, taught and learned) knowledge about galaxies in general, including their components and the intuited relative disposition of those parts in space and time. With further study the stellar make-up of bulges becomes known, the age distributions and chemical composition distributions of those same stars are teased out, and the gross kinematics of selected examples get studied. Slowly the flattened image, still frozen in time, starts to thaw, to become a dynamic, evolving entity, deprojected, inverted and modeled in our collective minds' eye and in our computers over the simulated course of the age of the Universe. A bulge.

B.F. Madore (✉)
Observatories of the Carnegie Institution of Washington, 813 Santa Barbara Street, Pasadena, CA 91101, USA
e-mail: barry@ipac.caltech.edu

E. Laurikainen et al. (eds.), *Galactic Bulges*, Astrophysics and Space Science Library 418, DOI 10.1007/978-3-319-19378-6_1

The same process of understanding might be argued for any and all of the morphological components currently cataloged and studied in galaxies whether they are seen locally, or at the limiting resolution of our best space-based telescopes, looking out to the highest recorded redshifts and earliest times in the assembly of "galaxies", at those distant and formative epochs. But bulges hold a special place in the history of our recent realization and gradual acceptance of galaxies as truly major constituents of the universe. It might be argued by some that the bulge of our own Milky Way has, since the dawn of humans on this planet, been visible to all who cared to look at the sky on a moonless night (Fig. 1.1). But it is only with highly informed hindsight that the bulge of our galaxy is in any way obviously akin to the prototypical bulges seen in "extragalactic" nebulae.

Fig. 1.1 The bulge of our Milky Way galaxy passing high above the dome of the 2.5 m duPont telescope at Las Campanas, Chile, as photographed by the author in August 2014. Compare this with the image of the edge-on galaxy NGC 0891 in Fig. 1.2 (below)

1.2 A Bulge by Any Other Name ...

So where did the concept of a bulge come from, and when did the word *bulge* enter our astronomical vocabulary? The answer is not easy to come by. The transition was neither abrupt nor particularly well orchestrated. It just grew.

From surveying in the literature one thing is for clear: none of the luminaries of the time who were studying galaxies in the 1950s or 1960s were using the term "bulge" consistently. Sometimes it was used figuratively and descriptively; sometimes it was used dramatically and for effect. And then too it was often simply inserted almost incidentally.

The term "bulge" appears to have come into commonly accepted astronomical usage by way of two, parallel and somewhat disjoint applications of the word: one in the specific context of the Milky Way and the other in the more general context of the "anagalactic" nebulae. But independently of making the identification of our galaxy and its "bulge" with external galaxies and their "bulges", something else was in play. As we shall see below, in many cases there were colorful attempts to describe features in galaxies without coming out and explicitly naming them. And so the physical objects we now call "bulges" were often (even in the same sentence) referred to as an "amorphous feature", "a central condensation", "a lens-like feature" or "bulge-like". This colorfully flowing prose kept the readers attention but it never categorically graced the feature with a name. The honor of a name seems to have been first and most naturally bestowed upon the central region of the Milky Way. In the galactic context, numerous authors, almost simultaneously, began talking about "the Galactic bulge" as a named feature. And that name stuck sooner and more robustly than using the word "bulge" did for the same structures seen in the nearest galaxies already imaged at that same time. So, we have two parallel stories: one about the description of the Milky Way and the early adoption of the proper name, "the Galactic Bulge", and the other about the nature of galaxies in general and the earliest attempts to describe, without actually naming or self-consistently referring to various features, most notably the central features that we today call "bulges". Walter Baade undoubtedly played a critical role in both of these stories.

In his overview of "The Nebulae", Heber Curtis (1933) makes the distinction between the "Nuclear Portion" of "true spirals" and an outer region which is home to "whorls". In a section entitled "Conspectus of Forms Assumed" Curtis goes on to say that the whorls can come in various flavors, including "Delicate", "Rather compact", "Moderately open", "Two-branched", "Single"; while the "Nuclear Portion" is described as being "Rather large", "Small and bright", "Tri-nuclear", "Quite faint" or "Not apparent". While the term "bulge" has not yet appeared on the scene, it is amusing to note that few of Curtis's other terms and descriptors survived the transition either: *whorls!*

The explicit use of the word "bulge" began turning up by mid-century. Hubble (1943), in a not-often-cited paper, concerning the direction of rotation in spiral nebulae, talks about "dark material scattered through the central *bulge* of a tilted nebula" and repeatedly uses the phrase "central bulge" through the paper, only to

disappoint us, once again, by stating that "half of the central *lens* is blotted out ..." One can only conclude that in his mind "bulge" and "lens" were synonymous. Five years later, this time back in the galactic context, Stebbins and Whitford (1948) reported making a 2μ "sweep across the galactic equator" showing "a *bulge*, agreeing closely in position and form with that previously found a year earlier (Stebbins and Whitford 1947). In this latter paper, they off-handedly attribute Baade with having shown that "the great cloud in Sagittarius ... is undoubtedly the outer region of the *bulge* about the galactic center." Curiously, at about this same time, it was still possible for the AAS (American Astronomical Society) in 1959 to accept a contributed talk entitled "The Visual Milky Way" wherein Sergei Gaposchkin (1959) described "the visual panorama of the whole Milky Way done with *pen and India ink,* drawn during my stay in Australia". He goes on to say that "around Ophiuchus, Sagittarius, and Scorpius there is a definite halo or *bulge*." (emphasis mine throughout). By way of contrast, Fig. 1.1 is a 20 s exposure of the Galactic Bulge using a standard 35 mm camera; no pen and ink required.

We now transition to Baade's charming introduction to the classification of galaxies as found in his 1958 Harvard Lectures as captured and edited by Cecilia Payne-Gaposchkin and published in the book entitled "Evolution of Stars and Galaxies" (Baade 1975). In the opening chapter, "Classification of Galaxies" Baade is quoted as saying:

"In classifying the spirals, Hubble distinguished the groups Sa, Sb and Sc, the distinguishing criteria being essentially the spiral arms. For instance in his description of Sa the spiral arms emerge at the edge of *the central system*; in the earlier spirals both they and the *central lens* are still unresolved, and the arms are densely coiled. As we proceed along the series, the *central nuclear area* shrinks at the expense of the growth of the arms, which by and by uncoil, until finally the *central area* has shrunk to a *semi-stellar point*, and all the mass seems to be in the spiral arms. This is Hubble's original description, but he agreed completely that it would be simpler today to classify the spirals simply by the size of the *central lens*. This with *very large central lenses* can be called Sa; and those with *intermediate central lenses*, Sb; and those where the *lens* has shrunk to a *semi-stellar point* (actually a huge cluster of stars), Sc. In what follows I shall adopt this very simplified system, based on the size of the *central lens*." There can be little doubt that when Baade was using the term "lens" he was referring to what we would today call the "bulge".

The key practitioners in the early days of galaxy classification played pretty fast and loose with their terminology, especially when it came to describing the major features that went into these classification systems. Perhaps they felt that the classification scheme was intrinsically qualitative and so that the terms used could be metaphorical and/or illustrative rather than rigorously defined or even consistently applied. However, science is not poetry, and eventually people need a common language if they are going to build a coherent ontology and then quantify, study and discuss the same unambiguously identifiable features in physical systems. The quantification of galaxy properties more that likely force the nomenclature to become a bit more rigorous.

1.3 Quantification and the Bulge-to-Disc Ratio

de Vaucouleurs (1959a,b) was among the first astronomers to bring quantitative methods to galaxy classification. And he speculated that "It is conceivable that a precise classification along the spiral sequence could be made to depend on the ratio between the integrated luminosities of the *spherical* and *flat* components; i.e., on the fraction of the total luminosity contributed by the central bulge producing the excess of light above the exponential component". And earlier he categorically states "Sub-types, noted Sa, Sb, Sc, are defined by the relative size of the *nucleus* and the degree of resolution and opening of the spiral structure."

However, Sandage (1961), in an implicit but focused rebuttal, is quick to point out "For many years it was thought that the third classification criterion of the relative size of *the unresolved nuclear region* usually agreed with the criterion of the arms. Inspection of large numbers of photographs shows that, although there is general correlation of the criteria, there are Sa galaxies that have *small nuclear regions.* This does not mean that Sa galaxies do not exist with large amorphous central regions devoid of dust and spiral structure we only wish to point out that a large amorphous central region is not a prerequisite for Sa galaxies."

Sandage (1961) in his self-effacing publication, illustrating and annotating Hubble's (posthumous) classification of galaxies, hardly every is the word "bulge" explicitly used when discussing the classic spiral galaxy Hubble Sequence: Sa, Sb and Sc. Indeed, Sandage does repeatedly talk of "unresolved nuclear regions", or "the large amorphous center" of NGC 3898, "the amorphous central region" of NGC 4579, "the completely amorphous central *nucleus*!" (emphasis and italics mine) for NGC 2775, and finally "the peculiar square-shaped nuclear region" of NGC 7332 and the "peculiar 'box-shaped' nucleus" of NGC 128. "Nucleus", "Nuclear Region", "Center", "Central Region" and "Central Nucleus" all dance around what we would now simply call the "Bulge".

A few years later, in an attempt to meld the two worlds (galactic and extra-galactic), and put our Milky Way galaxy into Hubble sequence, Halton Arp (1965) became the first author to explicitly put into print the term "bulge-to-disc ratio" when he said "Probably the *bulge-to-disc ratio* is the physically most important criterion…" in classifying our Milky Way galaxy …"because it is a measure of the proportion of low angular momentum to high angular momentum populations."

At long last the loop had been closed: our Galactic Bulge joined the ranks of extragalactic bulges, and the bulge-to-disc ratio became one of the first *quantitative* measures of galaxy type (Fig. 1.2).

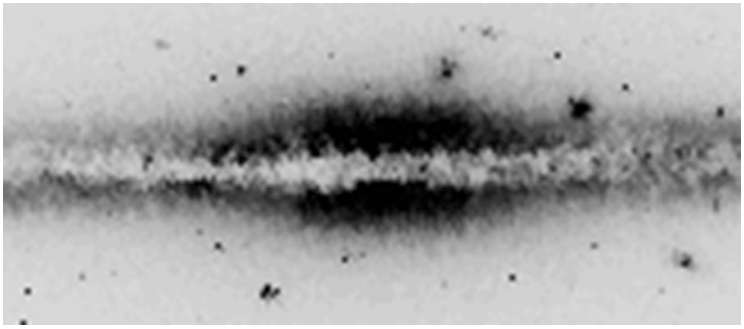

Fig. 1.2 An optical image of the edge-on galaxy NGC 0891. Notice the similarity of this image to that of the bulge of our Milky Way galaxy shown in Fig. 1.1. This and other similar images of other galaxies with dust lanes projected on their "central amorphous regions" must have played an important role in making the case that the Milky Way was just one of many such "Island Universe" galaxies

1.4 CCD Detectors and Large Samples

With the introduction of linear CCD detectors in the mid-1980s the ability to acquire calibrated data on significant samples of galaxies allowed observers to decompose the globally most obvious inner and outer features of galaxies, now regularly referred to (qualitatively at least) as discs and bulges. Using CCDs Steve Kent (1985) measured both components and published "bulge/disc" decompositions for over 100 galaxies of all morphological types. Caught at a time of transition between photographic plates and CCD detectors Dave Burstein (1979) published photographic photometry of 18 S0 galaxies and derived "disc-to-bulge" ratios for 12 of them. This followed close on heels of another photographic "decomposition" study of S0 galaxies undertaken by Kormendy (1977). In this paper Kormendy made a last stand against the use of the word "bulge" and subtitled his Paper III: "Decomposition of Observed Profiles into Spheroid and Disc Components."

Here, perhaps, was a missed opportunity. Most of the quantitative evidence (as gleaned from the fact that the $R^{1/4}$ Law fit the radial light profiles of both bulges and elliptical galaxies) suggested to many that the two systems had much more in common. Perhaps ellipticals were simply discless galaxies, and/or spirals were ellipticals that acquired discs, or even that ellipticals were star piles made from the destruction of many earlier discs. However, as noted in the Introduction, a bulge exists conceptually by virtue of its comparative status with respect to something that it is "bulging out of". Under these circumstances it is cognitively dissonant to even try talking about a bulge without implicitly visualizing a disc (or at least some other additional component). However, if we were to rewind history and declare that the Milky Way and all other spiral galaxies had centrally-located "elliptical components" then the concept of an "elliptical-to-disc ratio" would have unified and simultaneously quantified the entire Hubble classification sequence (not just the

spirals) without any discontinuity, be it linguistic, cognitive or numeric. Kent (1985) came dangerously close when he said "The difficulty of distinguishing between elliptical and S0 galaxies in some cases is emphasized." Thinking of galaxies as being morphologically bimodal (ellipticals versus spirals) produces a very different mindset, as compared to the suggestion that all galaxies are part of a continuum, which to first order is described by an "elliptical-to-disc" ratio. Science is, by design, self-correcting, so the truth will win out, but it is interesting to speculate about the rate of convergence had certain words and suggestive phrases been adopted earlier instead of others.

1.5 Early Unification

In a particularly lucid discussion of the terminological chaos left us by Baade, Hubble and Sandage in their descriptions of the inner reaches of spiral galaxies the Russian astronomer B.A. Vorontsov-Velyaminov (1987) wrote the following (slightly abridged version here):

> As we have seen, Hubble adopted the term "nucleus" without any reservation. Even today authors use the word "nucleus" with no explicit statement of just what is meant; as a result misunderstanding often arises, because different kinds of structures, sometimes quite complicated, may be present near the center of a galaxy. We should therefore recommend the following nomenclature.
> The central formation, generally an amorphous structure standing out in brightness, with a fairly sharp brightness gradient at its edge and containing no spiral arms, will be called the *nuclear region*. We discriminate nuclear regions of several types.
> *Bulge*: A large, nearly globular condensation of light, shaped like an elliptical galaxy. The nuclear regions of type S0 galaxies have this appearance, while type N radio galaxies form a bulge embedded in a rather narrow halo.
> *Lens*: A strongly flattened bulge, in a sense. Bright spiral arms emerge from its periphery. If viewed edgewise, a lens is readily distinguished from a bulge, and looks just like a thick lens in profile. Sa and Sb galaxies usually have a nuclear region of this kind.
> *Nuclear Disc*: A very thin lens structure, with its thickness small compared to its diameter, even at the center. Bright spiral arms emerge at its periphery. When seen face-on, a nuclear disc is nearly uniform in brightness, and in this respect differs from a lens.
> *Nucleus*: A pronounced, nearly globular condensation, resembling a bulge, but smaller in size and luminosity compared to the whole galaxy.
> *Core*: A tiny nucleus, of star-like appearance or almost so. A lens may have a nucleus inside, while a nucleus may in turn contain a core.

Even this admirable attempt to clarify the terminology stumbles a bit when it uses the (optician's term) "lens" to describe the astrophysical "lens" (seen edge-on), and too when the "lens" is described as a "flattened bulge" (in a sense!), leaving one wondering which type of lens is being referred to when a "nuclear disc" is described as "a very thin lens structure" (optical or astrophysical?). And finally we come full circle when we are told that a "nucleus" is simply a "small bulge".

At this point the reader is recommended to consult two chapters in this volume: The vastly superior and thoroughly up-to-date discussion of the properties of bulges

given by Fisher & Drory in "An Observational Guide to Identifying Pseudobulges and Classical Bulges in Disc Galaxies", and the chapter by Laurikainen & Salo entitled "Observed Properties of Boxy/Peanut Bulges" where we are introduced to higher-order structures making up the inner regions of galaxies, including X-shaped morphologies, vertically thick boxy/peanut bulges, and bar/lens bulges.

A final word on extensions to the concept of a bulge. As linear detectors have become more sensitive and surveys using them have become more widespread there will inevitably be new features found that are either at the subtle edge of detectability within known objects or at the other extreme of being so rare that ever larger samples are required to discover just one of them. "Pseudo-bulges" fall in the former category . . . perhaps. The interested reader is referred to the *Annual Reviews* article by Kormendy and Kennicutt (2004) and the chapter by Kormendy in this volume. In the former, the authors discuss the case of M33 , one of the brightest and well studied galaxies in the northern sky. They note that M33 has a "subtle upturn in surface brightness" and go on to pose the question "Does M33 contain a pseudo-bulge?" Without giving away their answer I will instead refer the reader to the image of M33 found in Fig. 1.3. This picture was originally published by Walker (1964) solidly in

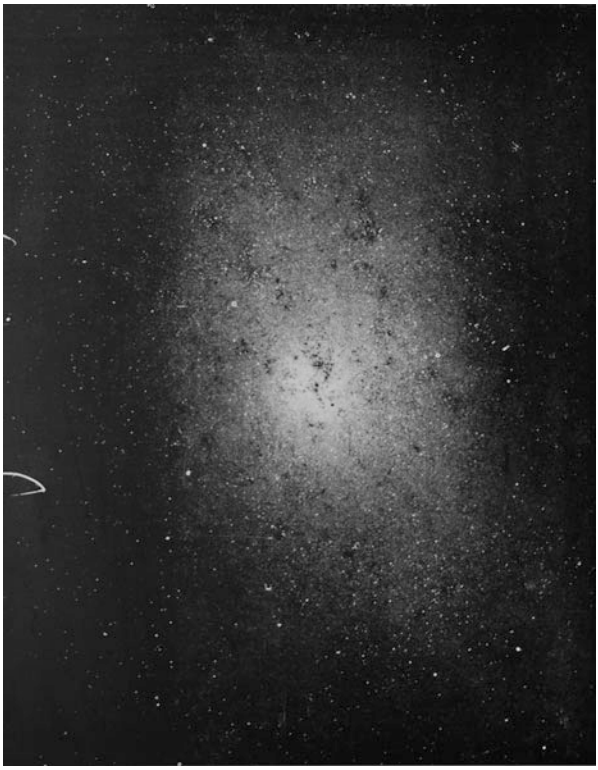

Fig. 1.3 A *color composite* image of M33 (Walker 1964) showing resolved Population I (*blue*) stars in *black* and the unresolved Population II (*red*) stars in *white*

the photographic era, and well before CCDs and linear detectors. What is shown is the result of a photographic combination of images taken in two different (red and blue) bandpasses, differenced and printed to enhance stars and stellar populations of one color extreme or another. They called the technique "composite photography". It gained little traction and has been largely forgotten. Without further comment I will leave it to the reader to decide whether they see a pseudo-bulge in M33 or not, but here is what Walker himself very cautiously claimed. "The fact that the outline of the system of Population II red giants is elliptical indicates that these objects do *not* form a spherical halo around M33 but instead consist of a relatively flattened distribution; whether it is as flat as the system of spiral arms is not clear from the present material."

1.6 Summary

The bulge of M31 was the first extragalactic object seen by the unaided eye in the northern hemisphere. The bulge of the Milky Way was visible for anyone from ancient times onward to see on a clear dark night in the (northern) summer months. The natural correspondence between these two features was not obvious until well into the twentieth Century, so it should come as no surprise that there was no common term being used to describe them both. When discussing the Milky Way, the feature called the "Galactic Bulge" seemed to find its place in astronomical parlance far sooner and with far less equivocation than the multitudes of ways in which the same feature was described in an extragalactic context. In the Galactic setting the Galactic Bulge became a name, albeit a name with descriptive content. Once named, the feature became synonymous with what otherwise would have been one of many ways it could have been described. In the extragalactic context things were still very much in a state of flux, features, names and descriptions included. When Baade described bulges in other galaxies his language was more metaphorical than precise. It was meant to paint an image in the mind's eye of the reader rather than be seen as a well defined and carefully thought out definition of a class. Be it "lens", "bulge", or "amorphous central region" the reader gets the general idea without anything quantitative being measured or implied. Inevitably this all changed as the study of galaxies became more quantitative and especially when digital detectors arrived on the scene. Loose terminology based on visual impressions gave way to quantitative measurements of features and components that could repeatedly identified, deconvolved, extracted, defined and "decisively" named. Initially "bulges" and "discs" were all that you needed to characterize the radial profile of a galaxy. The "bulge-to-disc" ratio became a quantitative measure of all galaxies of all morphological types. Names followed the numbers. Common usage won over descriptive whim; no vote was called for and no declaration was officially made by the IAU. By the mid 1970s "bulges" and "discs" were the only remaining candidates on a ballot that was never cast.

However convoluted and painful it may have been to adopt a commonly accepted name for these features, our consensus does not guarantee uniqueness. The morphological features extracted from one- or two-dimensional images are not obligated to be made up of identical stellar populations, nor do they necessarily have the same histories and/or formation processes; they just happen to look alike, at this time in the evolution of the Universe as originally seen in some particular bandpass. As this volume attests, assessing the detailed stellar content and kinematics of bulges, predicting their future evolution, or modeling their assembly histories, growth and fate are today topics of interest and hot debate.

The early "galaxy morphologists" had no reason to go much beyond classification lightly embedded in a simple interpretive model. But whatever theory of bulge formation might have been offered, philosophers of science could have warned that those theories would fall prey to "underdetermination" by the data. As Pierre Duhem (1954) first noted for the physical sciences (and as Willard Quine (1951, 1975) later broaden and generalized the argument to the pursuit of knowledge in general) for any set of observations there will always be many theories that will be equally able to account for those facts. This is a problem if one is intent on selecting the best of a number of proposed theories (i.e., using the methods of *abduction*, developed by Charles Saunders Pierce, which is "inference to the best explanation"; see for instance Lipton (2004)), but there is an even more insidious problem looming when nature itself has actually taken multiple paths to arrive at apparently (or perhaps even virtually) indistinguishable endpoints. For the case in point, bulges might have formed in a monolithic fashion at one early point in time or they might have formed over an extended period. To Hubble, these two theories would have been decisively "underdetermined" by his classifications derived from photographic images. And now today there are theories of hierarchical assembly over considerable periods of time that are vying with monolithic collapse. And then too the heating of discs, the onset of instabilities, and the dissolution of bars, to name just a few "secular" processes, are also possible (probable?) contenders for modifying "bulges" and/or producing their close relative the "pseudo-bulges". The hope of "reducing" a theory of bulge formation and evolution down to a simple process or to a single input channel may, with hindsight, be found to be a quixotic adventure. Nature is not obliged to conform to the simplest or even the currently best explanations found by its scientists.

References

Arp, H., 1965, ApJ, 141, 43
Baade, W. 1975, Evolution of Stars and Galaxies (Cambridge, Massachusetts: The MIT Press)
Burstein, D., 1979, ApJ, 234, 435
Curtis, H. D. 1933, The Nebulae in Handbuch der Astrophysik: II: Stellar Systems ed. H.D. Curtis, B. Lindblad, K. Lundmark, H. Shapley Evolution of Stars and Galaxies (Berlin: Springer Verlag)

de Vaucouleurs, G. 1959a, Classification and Morphology of External Galaxies in Handbuch der Physik, IV: Stellar Systems ed. S. Flugge (Berlin: Springer Verlag)
de Vaucouleurs, G. 1959b, General Physical Properties of External Galaxies in Handbuch der Physik, IV: Stellar Systems ed. S. Flugge (Berlin: Springer Verlag)
Duhem, P. 1954, The Aim and Structure of Physical Theory (Princeton: Princeton University Press)
Gaposchkin, S., 1959, AJ, 64, 50
Hubble, E. P., 1943, ApJ, 97, 112
Kent, S., 1985, ApJS, 59, 115
Kormendy, J., 1977, ApJ, 217, 406
Kormendy, J., & Kennicutt, R. C. 2004, ARA&A, 42, 603
Lipton, P. 20044, Inference to the Best Explanation (London: Routledge)
Quine, W. V. O. 1951, "Two Dogmas of Empiricism", in "From a Logical Point of View", 2nd Ed., Cambridge, MA: Harvard University Press, p. 20
Quine, W. V. O. 1975, ÒOn Empirically Equivalent Systems of the WorldÓ, *Erkenntnis*, 9, 313
Sandage, A. 1961, The Hubble Atlas of Galaxies (Washington: Carnegie Institution)
Stebbins, J., & Whitford, A. E. 1947, AJ, 52, 131
Stebbins, J., & Whitford, A. E. 1948, AJ, 53, 207
Vorontsov-Velyaminov, B. A. 1987, Extragalactic Astronomy (Chur: Harwood Academic Publishers)
Walker, M. E. 1964, AJ, 69, 744

Part I
Distinguishing the Main Types of Bulges

Chapter 2
The Intrinsic Shape of Galaxy Bulges

Jairo Méndez-Abreu

Abstract The knowledge of the intrinsic three-dimensional (3D) structure of galaxy components provides crucial information about the physical processes driving their formation and evolution. In this paper I discuss the main developments and results in the quest to better understand the 3D shape of galaxy bulges. I start by establishing the basic geometrical description of the problem. Our understanding of the intrinsic shape of elliptical galaxies and galaxy discs is then presented in a historical context, in order to place the role that the 3D structure of bulges play in the broader picture of galaxy evolution. Our current view on the 3D shape of the Milky Way bulge and future prospects in the field are also depicted.

2.1 Introduction and Overview

Galaxies are three-dimensional (3D) structures moving under the dictates of gravity in a 3D Universe. From our position on the Earth, astronomers have only the opportunity to observe their properties projected onto a two-dimensional (2D) plane, usually called the plane of the sky. Since we can neither circumnavigate galaxies nor wait until they spin around, our knowledge of the intrinsic shape of galaxies is still limited, relying on sensible, but sometimes not accurate, physical and geometrical hypotheses.

Despite the obvious difficulties inherent to measure the intrinsic 3D shape of galaxies, it is doubtless that it keeps an invaluable piece of information about their formation and evolution. In fact, astronomers have acknowledged this since galaxies were established to be *island universes* and the topic has produced an outstanding amount of literature during the last century.

In this paper I discuss the main developments and results in the quest to better understand the 3D shape of galaxy bulges. Given the limited space available in this chapter, I have not elaborated on the concept and definition of a bulge, leaving this discussion to another chapter in this volume. In the same way, I have deliberately

J. Méndez-Abreu (✉)
School of Physics and Astronomy, University of St Andrews, North Haugh, St Andrews, KY169SS, UK
e-mail: jma20@st-andrews.ac.uk

E. Laurikainen et al. (eds.), *Galactic Bulges*, Astrophysics and Space Science Library 418, DOI 10.1007/978-3-319-19378-6_2

not included the intrinsic shape of boxy/peanut (B/P) structures located in the center of disc galaxies which some authors associate to galaxy bulges (Lütticke et al. 2000). Currently it is well established that these structures are actually part of the bar and intimately related to their secular evolution (Combes and Sanders 1981; Chung and Bureau 2004). As bars evolve, stars can be moved perpendicular to the disc plane due to a coherent bending of the bar producing its characteristic shape (Debattista et al. 2004; Martinez-Valpuesta et al. 2006). B/P structures share the same photometric and kinematic properties of bars (Méndez-Abreu et al. 2008b; Erwin and Debattista 2013).

On the other hand, I have included a historical review of the evolution of our knowledge of the intrinsic shape of elliptical galaxies. The properties of elliptical galaxies and those of intermediate/massive galaxy bulges have been often considered to be similar (Wyse et al. 1997). This is particularly true when referring to their surface-brightness distributions and shapes. Indeed, it has been common in the literature to rely on both simulations and observations of elliptical galaxies to interpret the observational properties of bulges (e.g., Kormendy and Bender 2012).

This paper is structured as follows. In Sect. 2.2 I describe the basic geometric considerations of the problem and set up the notation used throughout the chapter. In Sect. 2.3 I review our current knowledge on the intrinsic shape of both elliptical and disc galaxies. Section 2.4 introduces the advantages and drawbacks of studying galaxy bulges with respect to ellipticals and a historical perspective of their 3D shape measurements. In Sect. 2.5 I summarize the evolution of the concept of the Milky Way bulge and its intrinsic 3D shape. Section 2.6 addresses the importance of numerical simulations to understand the physical processes that shape galaxy ellipsoids. Finally, in Sect. 2.7 I sketch out the current view on the intrinsic shape of bulges and explore future prospects.

2.2 Setting up the Scene

This section briefly summarizes the basic notation and geometrical considerations to be used during this chapter.

Let (x, y, z) be the Cartesian coordinates on the reference system of the galaxy with the origin in the galaxy center, the $x-$axis and $y-$axis corresponding to the principal equatorial axes of the ellipsoidal component, and the $z-$axis corresponding to the polar axis. Therefore, if A, B, and C are the intrinsic lengths of the ellipsoid semi-axes, the corresponding equation of the bulge on its own reference system is given by

$$\frac{x^2}{A^2} + \frac{y^2}{B^2} + \frac{z^2}{C^2} = 1 \tag{2.1}$$

Let (x', y', z') now be the Cartesian coordinates on the observer reference system. It has its origin in the galaxy center, the polar $z'-$axis is along the line of sight (LOS) and points toward the galaxy. (x', y') represents the plane of the sky.

The equatorial plane (x, y) of the ellipsoid and the plane of the sky (x', y') intersect in the so-called line of nodes (LON). The angle between both planes, i.e., the angle subtended between z and z' is defined as the inclination θ of the ellipsoid. The remaining two Euler angles which allow for the transformation from the reference system of the galaxy to that of the sky are defined as: (i) ϕ is the angle subtended between the $x-$axis and the LON in the ellipsoid equatorial plane, and (ii) ψ is the angle subtended between the $x'-$axis and the LON in the plane of the sky. It is often useful to choose the $x'-$axis to be along the LON, consequently it holds that $\psi = 0$ (see Fig. 2.1).

It is well known that the projection of a triaxial ellipsoid onto the plane of the sky describes an ellipse (Contopoulos 1956; Stark 1977; Binney 1985; Franx et al. 1991), which is usually written as

$$\frac{x_e^2}{a^2} + \frac{y_e^2}{b^2} = 1, \tag{2.2}$$

where x_e and y_e represent the axes of symmetry of the projected ellipse, a and b are the corresponding semi-major and semi-minor axes of the ellipse. The observed ellipticity of the ellipse can be easily derived from the apparent axis ratio as $\epsilon = 1 - b/a$. The x_e axis forms an angle δ with the LON (twist angle), which for convenience is usually made to correspond with the x'-axis. It is worth noting that both the apparent axis ratio ($q = b/a$) and the orientation of the ellipses (δ) depend only, and unambiguously, on the direction of the LOS, i.e., on θ, ϕ, and ψ,

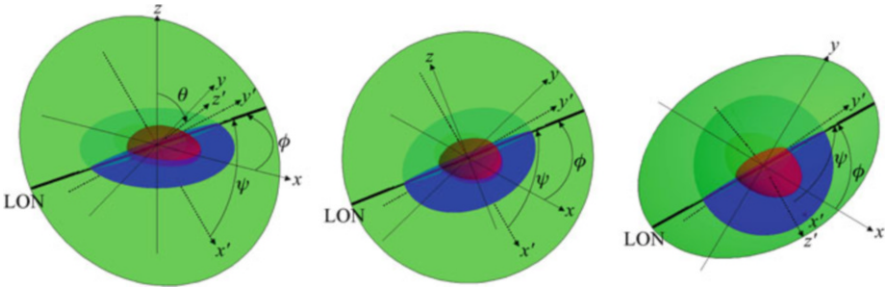

Fig. 2.1 Schematic three-dimensional view of the ellipsoid geometry. The bulge ellipsoid, the disc plane, and the sky plane are shown in *red*, *blue*, and *green*, respectively. The reference systems of both the ellipsoid and the observer as well as the LON are plotted with *thin solid lines*, *thin dashed lines*, and a *thick solid line*, respectively. The bulge ellipsoid is shown as seen from an arbitrary viewing angle (*left panel*), along the LOS (*central panel*), and along the polar axis (i.e., the $z-$axis; *right panel*) (Extracted from Méndez-Abreu et al. (2010). Reproduced with permission from Astronomy & Astrophysics, ©ESO)

and on the intrinsic shape of the ellipsoid, i.e., A, B, and C, see Simonneau et al. (1998) for the full derivation.

Based on this simple geometric representation, if we assume a galaxy is composed of a set of triaxial emitting ellipsoidal shells, which are concentric and coaxial (same axes of symmetry) but non-homologous (intrinsic semi-axes vary with the distance to the center), their projections onto the plane of the sky are concentric ellipses, but non-homologous and non-coaxial. Therefore, the twisting of the galaxy isophotes can be explained just as an effect of the projection of non-homologous triaxial ellipsoids (Williams and Schwarzschild 1979).

2.3 Historical Background on the Intrinsic Shape of Galaxies

Elliptical galaxies are structurally the simplest stellar systems where mathematical techniques can be applied to recover their intrinsic 3D shape. Thus, the huge amount of literature on the subject is not surprising. In fact, the continuously increasing availability of better measurements of the apparent axis ratios of elliptical galaxies have motivated great debate over the years. On the other hand, the similarities between the photometric properties of intermediate/massive bulges and ellipticals (e.g., Gadotti 2009) have usually motivated an extrapolation of the results on the intrinsic 3D shape of ellipticals and their implications on galaxy formation and evolution onto the bulges of disc galaxies. In this section I revisit our current knowledge on the intrinsic shape of elliptical galaxies (Sect. 2.3.1) and, for the sake of completeness, of disc galaxies (Sect. 2.3.2) to put in context the historical background on the intrinsic shape of bulges.

2.3.1 Intrinsic Shape of Elliptical Galaxies

2.3.1.1 Photometric Approach

The first attempt to derive the intrinsic shape of elliptical galaxies was done by Hubble (1926). At that time, it was already realized the importance of relying on statistical methods to recover the 3D shape of galaxies. In fact, Hubble obtained the frequency of intrinsic short-to-long axis ratio under the assumption that elliptical galaxies were oblate ellipsoids with random orientations with respect to the LOS.

Since then, this statistical approach based on the measurement of the apparent axis ratio distribution (AARD) and the assumption that the 3D intrinsic shape is an ellipsoid of revolution, either oblate or prolate, has been extensively used in the literature. For the sake of clarity I briefly outline here the basic statistical concepts.

Let us assume the basic geometry proposed in Sect. 2.2 and define both the intrinsic ellipticity, $Q = B/A$, and intrinsic flattening, $F = C/A$, of the ellipsoid as the corresponding intrinsic axis ratios in the (x, y) and (x, z) planes, respectively.

Therefore, in the case of either a pure oblate ($Q = 1$) or pure prolate ($Q = F$) ellipsoid in Eq. 2.1 can be described by one single parameter. If the polar axis of the ellipsoid forms an angle (θ) with respect to the LOS then the apparent axis ratio of the projected ellipse can be written as

$$F^2 \sin^2\theta + \cos^2\theta = \begin{cases} q^2 & \text{if oblate} \\ q^{-2} & \text{if prolate} \end{cases}. \tag{2.3}$$

Under the realistic assumption of randomly distributed orientations and using Eq. 2.3 where $q = q(\theta)$, the probability $P(q|F)dq$ that a galaxy with intrinsic axis ratio F is observed with an apparent axis ratio in the range $(q, q + dq)$ is

$$P(q|F)dq = \frac{\sin\theta\, dq}{|dq/d\theta|}. \tag{2.4}$$

At this point, the AARD $\zeta(q)$, can be related to the intrinsic probability distribution $\xi(F)$ by

$$\zeta(q) = \int_0^1 P(q|F)\,\xi(F)\,dF. \tag{2.5}$$

The relation between the known (observed) frequency of galaxies of apparent axis ratio $\zeta(q)$ to the unknown frequency $\xi(F)$ of galaxies with intrinsic axis ratio F can be written such as

$$\zeta(q) = \begin{cases} q \displaystyle\int_0^q \frac{\xi(F)dF}{\sqrt{(1-F^2)(q^2-F^2)}} & \text{if oblate} \\ q^{-2} \displaystyle\int_0^q \frac{\xi(F)F^2\,dF}{\sqrt{(1-F^2)(q^2-F^2)}} & \text{if prolate} \end{cases}. \tag{2.6}$$

Based on this approach and using the hypothesis of oblateness, Sandage et al. (1970) derived the intrinsic distribution of flattening $\xi(F)$ for different Hubble types ranging from ellipticals to Sc. They found that the observed axis ratios of 168 elliptical galaxies present in the Reference Catalog of Bright Galaxies (RC1) (de Vaucouleurs and de Vaucouleurs 1964) were well reproduced using a skewed binomial distribution of oblate ellipsoids given by

$$\xi(F) \propto \left(1 + \frac{F - F_0}{\beta}\right)^{\alpha} exp\left[-\alpha\,(F - F_0)\right], \tag{2.7}$$

with main parameters $F_0 = 0.58$ and $\beta = 0.31$ (Fig. 2.2, left panels).

Binney (1978) used the same sample but introducing the prolate approach. Adopting the same functional form for $\xi(F)$ he found values of $F_0 = 0.40$ and $\beta = 0.71$. However, even if using arbitrary analytical representations of $\xi(F)$ can turn out in a good fit of the AARD, in principle they do not have a physical

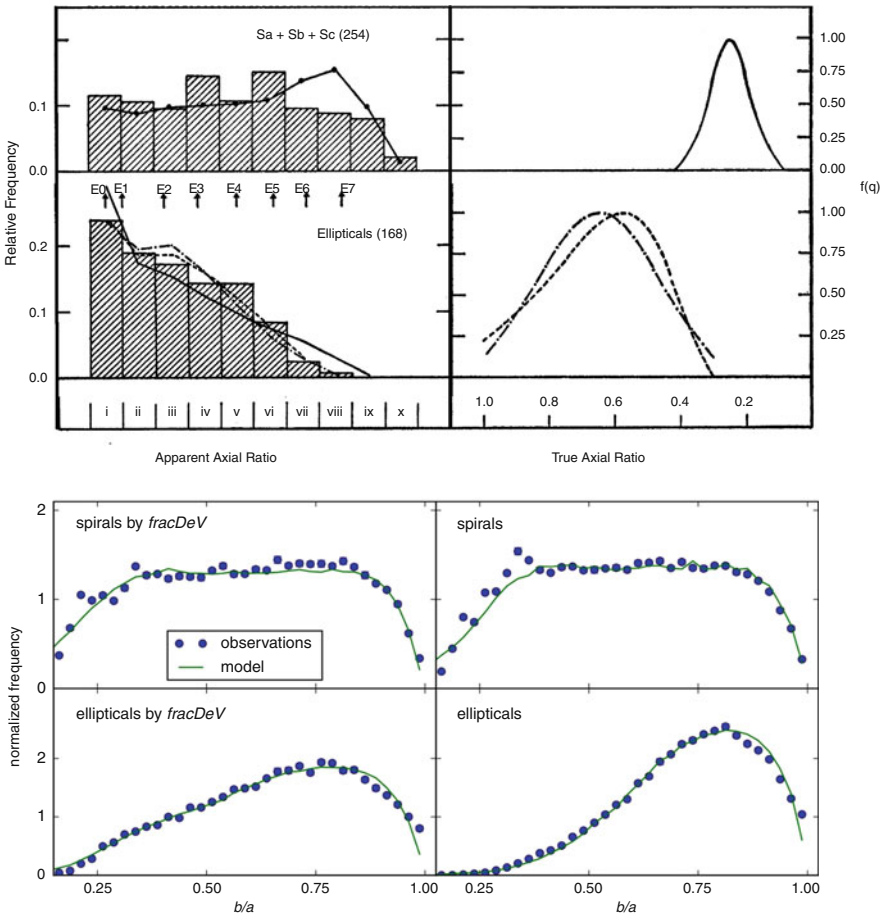

Fig. 2.2 Composite figure showing the evolution of the galaxy samples used in the derivation of the intrinsic shape of ellipticals and discs. *Upper panels*: histograms of the AARD for ellipticals and spiral galaxies. The *over-plotted curves* are predicted ratios for various assumptions of the distribution of intrinsic flattening. On the right, the assumed intrinsic distribution corresponding to the curves on the left (Extracted from Sandage et al. (1970). Reproduced with permission, ©AAS). *Bottom panels*: best fit models to AARD compared to the observations. *Top*: spirals. *Bottom*: ellipticals. *Left*: galaxies selected only by fracDeV, see Abazajian et al. (2005) for definition. *Right*: galaxies selected by Galaxy Zoo morphology and fracDeV (Extracted from Rodríguez and Padilla (2013). Reproduced by permission of Oxford University Press)

motivation. This approximation was improved by Noerdlinger (1979) by solving Eq. 2.6 using the non-parametric inversion technique proposed by Lucy (1974). His results show how under the hypothesis of oblateness the $\xi(F)$ distribution of Sandage et al. (1970) was correct, but he also noticed that a prolate distribution peaking at around $F \sim 0.7$ would produce a good representation of the data as well.

At the same time, some kinematic findings led to the suggestion that the structure of elliptical galaxies can be represented by neither oblate nor prolate ellipsoids of revolution. In fact, the low ratio between rotational velocity and velocity dispersion found in flat systems (Bertola and Capaccioli 1975; Illingworth 1977; Peterson 1978) or the rotation measured along the minor axis of some elliptical galaxies (Schechter and Gunn 1979) were interpreted as resulting from a triaxial structure. From the photometric point of view, the twisting of the inner isophotes of elliptical galaxies was known since the early work of Evans (1951) and it was later confirmed in several works (Liller 1960; Carter 1978; Bertola and Galletta 1979).

As a consequence, Benacchio and Galletta (1980) and Binney and de Vaucouleurs (1981) showed that the AARD could be satisfactorily accounted for also in terms of a distribution of triaxial ellipsoids. Nevertheless, these works still presented significant differences in the predicted number of spherical galaxies mainly due to the differences in the original samples. Other groups reached similar conclusions analyzing higher quality data coming from new CCD detectors (Fasano and Vio 1991).

A new step forward in the methodology to recover the intrinsic 3D shape of galaxies was done by Fall and Frenk (1983). They showed how the inversion of the integral equations for oblate and prolate ellipsoids (Eq. 2.6) can be performed analytically, resulting in

$$\xi(F) = \frac{2}{\pi}\sqrt{1-F^2}\begin{cases} \frac{1}{F}\int_0^F \frac{q\,dq}{\sqrt{F^2-q^2}}\frac{d\zeta}{dq} & \text{if oblate} \\ \frac{1}{F^3}\int_0^F \frac{q\,dq}{\sqrt{F^2-q^2}}\frac{d(q^3\zeta)}{dq} & \text{if prolate} \end{cases}. \tag{2.8}$$

Using this analytical inversion and the largest sample of galaxies to that date (2,135 elliptical galaxies), Lambas et al. (1992) demonstrated how neither oblate nor prolate models could adequately reproduce the data. Contrarily, triaxial ellipsoids with intrinsic axis ratios selected from 1D Gaussians provided an adequate fit to the data. They found a best fit with $Q = 0.95$ and $F = 0.55$. A similar approach was used by Ryden (1992) on a smaller sample of 171 elliptical galaxies. She used a 2D Gaussian combining both intrinsic axis ratios obtaining $Q = 0.98$ and $F = 0.69$. The same sample was later analyzed by Tremblay and Merritt (1995) using a non-parametric technique to test the triaxial hypothesis. They confirmed previous results that discarded a distribution of intrinsic shapes compatible with axisymmetric ellipsoids thus favoring triaxial distributions. Similar conclusions were reached by Ryden (1996) on a larger sample using the same non-parametric approach.

During these years it became increasingly clear that the distribution of intrinsic flattenings of elliptical galaxies was broad and possibly bimodal (Fasano and Vio 1991; Ryden 1992, 1996; Tremblay and Merritt 1995). In fact, combining the galaxy sample described in Ryden (1992) with a new sample of brightest cluster galaxies (BCGs) from Lauer and Postman (1994), Tremblay and Merritt (1996) found that the AARD of galaxies brighter than $M_B \simeq -20$ was different from that of the less luminous ones. This reflected a difference in the shape of low-luminosity and high-

luminosity ellipticals: fainter ellipticals are moderately flattened and oblate, while brighter ellipticals are rounder and triaxial. Recently, Fasano et al. (2010) also found that even if both normal ellipticals and BCGs are triaxial, the latter tend to have a more prolate shape, and the tendency to prolateness is mainly driven by the central dominant (cD) galaxies present in their sample.

The next qualitative leap in studies of the intrinsic shape of elliptical galaxies happened with the advent of the Sloan Digital Sky Survey (SDSS). With respect to previous statistical analyses, SDSS improved not only the number of galaxies under study (an order of magnitude larger) but also the quality and homogeneity of the photometry. All these improvements allowed to study the dependence of the intrinsic shape with other galaxy properties such as the luminosity, colour, physical size, and environment. Using data from the SDSS-DR3 (Abazajian et al. 2005) Vincent and Ryden (2005) found that bright galaxies ($M_r \leq -21.84$) with a de Vaucouleurs profile have an AARD consistent with a triaxiality parameter in the range $0.4 < T < 0.8$, where $T = (1 - Q^2)/(1 - F^2)$, and mean flattening $0.66 < F < 0.69$. The faintest de Vaucouleurs galaxies are best fit with prolate ellipsoids ($T = 1$) with mean flattening $F = 0.51$. Using the SDSS-DR5 (Adelman-McCarthy et al. 2007), Kimm and Yi (2007) were able to reproduce the AARD by using a combination of oblate, prolate, and triaxial galaxy populations. Following the early work of Tremblay and Merritt (1996), they assumed each population having a Gaussian distribution of their intrinsic axis ratios. The best fit to the AARD was found using a fraction of O:P:T=0.29:0.26:0.45 (Oblate:Prolate:Triaxial) with a best triaxial distribution with axis ratios $Q = 0.92$ and $F = 0.78$. In 2008, Padilla and Strauss (2008) used the SDSS-DR6 (Adelman-McCarthy et al. 2008) to derive the intrinsic shape of ellipticals with the main improvement of taking into account the effects of dust extinction. They found that the AARD of elliptical galaxies shows no dependence on colour, suggesting that dust extinction is not important for this sample. The full population of elliptical galaxies was well characterized by a Gaussian distribution in the equatorial ellipticity with mean $Q = 0.89$ and a lognormal distribution of the flattening with mean $F = 0.43$, which corresponds to slightly oblate ellipsoids in agreement with Vincent and Ryden (2005). In a recent paper, Rodríguez and Padilla (2013) have used the SDSS-DR8 (Aihara et al. 2011) and the morphological information from Galaxy Zoo (Lintott et al. 2011) finding that elliptical galaxies have a mean value of $F = 0.58$ (Fig. 2.2, right panels). They concluded that the increase in F is mainly due to the removal of the spiral galaxy contamination thanks to the Galaxy Zoo morphologies. A historical summary in tabular form of all these measurements is shown in Table 2.1.

Owing to the ill-posed problem of deriving the 3D intrinsic shape of elliptical galaxies, its historical perspective is mainly weighted toward statistical methods. As previously showed in this section, the inventiveness of astronomers, the development of statistical methods, and the advent of large surveys have significantly improved our knowledge of the intrinsic shape of elliptical galaxies. Other methods based on the photometric study of individual galaxies have also been developed but to a smaller extent. One of the pioneering works to derive the intrinsic shape of an individual elliptical using its observed ellipticity and isophotal twist was

Table 2.1 Historical summary of the intrinsic shapes of elliptical galaxies

Year (1)	N. Galaxies (2)	Hypothesis (3)	Q (4)	F (5)	Reference (6)
1970	168	Oblate	1	0.58	[1]
1978	168	Prolate	0.4	0.4	[2]
1979	168	Oblate/Prolate	1/0.7	0.55/0.7	[3]
1980	348	Triaxial	0.81	0.62	[4]
1981	196	Oblate/Prolate/Triaxial	1/0.62/0.79	0.62/0.62/0.57	[5]
1992	2,135	Triaxial	0.95	0.55	[6]
1992	171	Triaxial	0.98	0.69	[7]
2005	26,994	Triaxial	0.66–0.85	0.66–0.69	[8]
2007	3,922	Oblate/Prolate/Triaxial	1/0.72/0.92	0.44/0.72/0.78	[9]
2008	303,390	Triaxial	0.89	0.38	[10]
2013	112,100	Triaxial	0.88	0.58	[11]

Notes. (1) Year of publication of the paper. (2) Number of elliptical galaxies in each sample. (3) Hypothesis used to derive the intrinsic shape of the ellipticals. (4) Mean value of the intrinsic ellipticity. (5) Mean value of the intrinsic flattening. (6) Reference of the corresponding paper: [1] Sandage et al. (1970), [2] Binney (1978), [3] Noerdlinger (1979), [4] Benacchio and Galletta (1980), [5] Binney and de Vaucouleurs (1981), [6] Lambas et al. (1992), [7] Ryden (1992), [8] Vincent and Ryden (2005), [9] Kimm and Yi (2007), [10] Padilla and Strauss (2008), [11] Rodríguez and Padilla (2013).

done by Williams (1981). They modeled the elliptical galaxy NGC 0523 assuming a given intrinsic density distribution and finding that the preferred models were prolate in the external regions but increasingly mixed (oblate and prolate) towards the center. This idea was further developed by other authors using more complex models of the density distribution (Fasano 1995; Thakur and Chakraborty 2001). In 2008, Chakraborty et al. estimated the shapes of 10 elliptical galaxies with apparent ellipticities $\epsilon \leq 0.3$, finding that radial differences in the triaxiality parameter can be tightly constrained to values $0.29 < \Delta T < 0.54$. Chakraborty et al. (2011) extended this analysis to three very flat galaxies with ellipticity $\epsilon \sim 0.3$ or more. They found values of the intrinsic flattening of these galaxies around $F \sim 0.5$.

2.3.1.2 Kinematic Approach

Determining the distribution of the 3D intrinsic shape of elliptical galaxies is also possible by combining photometric and kinematic information. In a first attempt, Binney (1985) used simple kinematical models to understand the ratio of rotational motion along both the major and minor isophotal axes of the galaxy. Using a sample of 10 ellipticals he found that elliptical galaxies were not well represented by axisymmetric oblate or prolate models. Franx et al. (1991) revisited this approach by using a larger sample of 38 elliptical galaxies and studying the probability distribution of photometric ellipticities and kinematics misalignments. In particular,

they explored the possibility that the angular momentum could not be aligned with the polar axis of the galaxy but it may have any orientation within the plane containing the short and the long axis (x, z). They found that a variety of models was able to reproduce the observations. Models with all galaxies being triaxial with well-aligned angular momentum were indistinguishable from models with all galaxies being oblate with nonaligned angular momentum.

A different standpoint to statistical studies implies an investigation into the intrinsic shape of elliptical galaxies using detailed individual dynamical modeling of the galaxy kinematics. Tenjes et al. (1993) modelled the photometric and stellar kinematic measurements of three elliptical galaxies adopting a specific form for the intrinsic density and streaming motions. They found tightly constrained geometries with $0.7 < Q < 0.8$ and $0.4 < F < 0.6$. This methodology was further improved in a series of papers by Statler (Statler 1994a,b; Statler and Fry 1994). He showed how using not only their apparent shapes and velocity field misalignments, but also the velocity field asymmetry, it is possible to place tighter constraints on the intrinsic shape of ellipticals. Using this approach Bak and Statler (2000) derived the intrinsic shape of 13 elliptical galaxies finding that although photometric studies give similar results for the flattening, none is able to put real constraints on triaxiality even when large samples are studied, hence demonstrating the need to include kinematic data in the models. Figure 2.3 show the probability distribution of intrinsic axis ratio for nine galaxies with significant rotation in their sample. It is clear that most of the galaxies can be well described by nearly oblate models but some of them present significant triaxiality or even prolateness. van den Bosch and van de Ven (2009) investigated how well the intrinsic shape of elliptical galaxies can be recovered by fitting realistic triaxial dynamical models to simulated photometric and kinematic observations. They found that for axisymmetric galaxies, the models are able to exclude triaxiality but the intrinsic flattening is nearly unconstrained. On the other hand, the shape of triaxial galaxies can be accurately determined when additional photometric and kinematic complexity, such as the presence of isophotal twist or a kinematically decoupled core is observed.

Recently, Weijmans et al. (2014) studied the intrinsic shape of the early-type galaxies described in the ATLAS^{3D} survey (Cappellari et al. 2011). Using a purely photometric approach and assuming axisymmetry, they found that the fast rotator population was much flatter than the slow rotator population, as expected from their dynamical status. Moreover, when the kinematic misalignment is included as a constraint in the analysis, they demonstrated that fast rotators are still better represented to oblate ellipsoids.

2.3.2 Intrinsic Shape of Disc Galaxies

In this section I briefly summarize our current understanding about the intrinsic 3D shape of discs. Bulges are embedded into the disc light and axisymmetry is usually a requirement to derive the bulge intrinsic shape. However, although the discs of

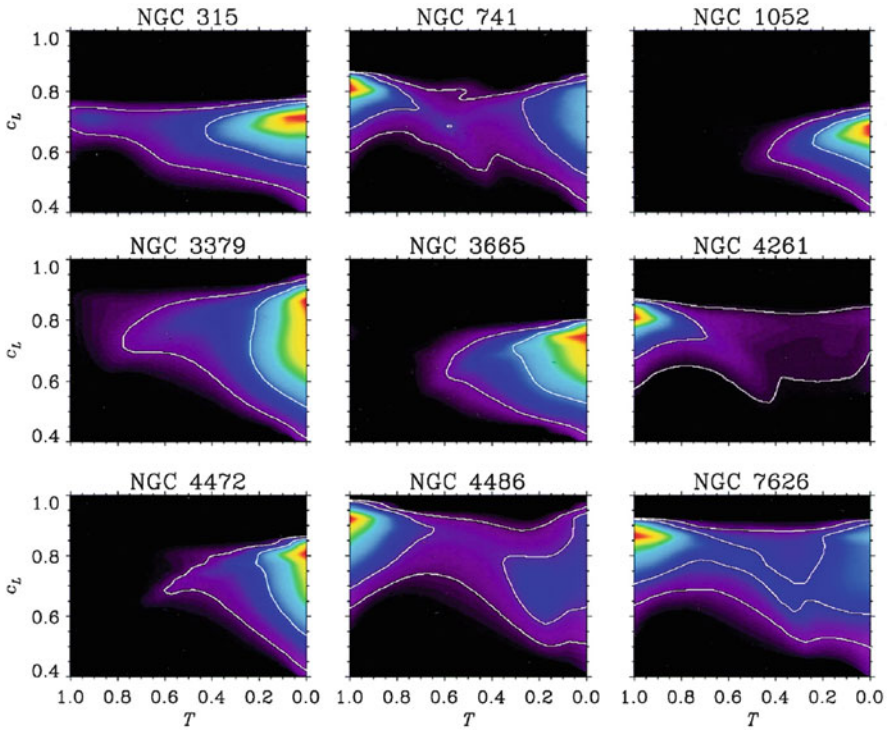

Fig. 2.3 Posterior probability densities in the plane of intrinsic triaxiality, T, and flattening, c_L (F in this chapter), for each of the nine galaxies that show significant rotation in Bak and Statler (2000). Contours indicate the 68 % and 95 % highest posterior density regions. In each panel, round prolate galaxies are at the *top left*, flattened oblate galaxies at *bottom right*, and objects in between are triaxial. Most galaxies are well represented by oblate models but prolate and triaxial are also allowed in many galaxies, e.g., NGC 741, NGC 4486, or NGC 7626 (Extracted from Bak and Statler (2000). Reproduced with permission, ©AAS)

lenticular and spiral galaxies are often considered to be infinitesimally thin and perfectly circular, their intrinsic shape is better approximated by flattened triaxial ellipsoids.

The disc flattening, defined analogously as for ellipticals (Sect. 2.3.1), can be directly determined from edge-on galaxies. It depends both on the wavelength at which discs are observed and on galaxy morphological type. Indeed, galactic discs become thicker at longer wavelengths (Dalcanton and Bernstein 2002; Mitronova et al. 2004) and late-type spirals have thinner discs than early-type spirals (Bottinelli et al. 1983; Guthrie 1992).

Determining the distribution of both the intrinsic flattening and ellipticity of discs is possible by a statistical analysis of the AARD of randomly oriented spiral galaxies. Similarly for elliptical galaxies, Sandage et al. (1970) analyzed the spiral galaxies listed in the RC1. They concluded that discs are circular with a mean

flattening of $\langle F \rangle = 0.25$. However, the lack of nearly circular spiral galaxies ($q \simeq 1$) rules out that discs have a perfectly axisymmetric shape. Indeed, Binggeli (1980), Benacchio and Galletta (1980), and Binney and de Vaucouleurs (1981) have shown that discs are slightly elliptical with a mean intrinsic ellipticity $\langle 1 - Q \rangle = 0.1$. These early findings were based on the analysis of photographic plates of a few hundreds of galaxies. They were later confirmed by measuring ellipticities of several thousands of objects in CCD images and digital scans of plates obtained in wide-field surveys. Lambas et al. (1992) found that pure oblate models failed to reproduce the AARD of spiral galaxies, whereas nearly oblate models with $F \sim 0.2$ and $Q \sim 0.9$ produce a good fit with values similar to those of Sandage et al. (1970). These values were confirmed later on by different authors (Fasano et al. 1993; Alam and Ryden 2002; Ryden 2004). Like the flattening, the intrinsic ellipticity depends on the morphological type and wavelength. The discs of early-type spirals are more elliptical than those of late-type spirals and their median ellipticity increases with observed wavelength (Ryden 2006). Furthermore, luminous spiral galaxies tend to have thicker and rounder discs than low-luminosity spiral galaxies (Padilla and Strauss 2008). In Sánchez-Janssen et al. (2010) they studied the role of stellar mass in shaping the thickness of galaxy discs. They found that the intrinsic thickness distribution of discs has a characteristic *U-shape* and identify a limiting mass $M_\star \approx 2 \times 10^9 M_\odot$ below which low-mass galaxies start to be systematically thicker. Recently, Rodríguez and Padilla (2013) analyse a sample of 92,923 spiral galaxies extracted from the SDSS-DR8, and taking into account the effects of dust in their analysis, they found a distribution of flattening with mean $F = 0.27$ and ellipticity $Q = 0.22$, i.e., disc are less round than in previous studies (Fig. 2.2, right panels).

Despite the large effort made to understand the intrinsic 3D shape of galaxy discs, it is still unclear whether the inferred slight triaxiality could be due to the presence of substructure in galaxy discs or if it really reflects truly triaxial potential in spirals.

2.4 The Intrinsic Shape of Extragalactic Bulges

The study of the intrinsic shape of bulges presents similarities, advantages, and drawbacks with respect to that of elliptical galaxies. Bulges are ellipsoidal systems located in the center of disc galaxies, thus, the main drawback with respect to elliptical galaxies is that their analysis requires the isolation of their light distributions from other structural galaxy components. However, it is worth noting that a similar problem is faced in elliptical galaxies when defining a characteristic radius to measure the global axis ratio of the galaxy (Fasano and Vio 1991). The most common approach to identify a global axis ratio for the bulge is by performing a photometric decomposition of the galaxy surface-brightness distribution. In this method, the galaxy light is usually modeled as the sum of the contributions from the different structural components, i.e., bulge and disc, and eventually lenses, bars, spiral arms, and rings (Prieto et al. 2001; Laurikainen et al. 2005). A number of two-dimensional parametric decomposition techniques have been developed to this

aim, such as: GIM2D (Simard 1998), GALFIT (Peng et al. 2002), BUDDA (de Souza et al. 2004), GASP2D (Méndez-Abreu et al. 2008a), GALPHAT (Yoon et al. 2011), or IMFIT (Erwin 2015). On the other hand, the main drawback on the study of galaxy bulges, i.e., the presence of other components such as the main disc, represents in turn the main advantage. The presence of the galactic disc allows for accurately constraining the inclination of the galaxy. Hence, under the assumption that the two components share the same polar axis (i.e., the equatorial plane of the disc coincides with that of the bulge) it allows for the determination of the inclination of the bulge. This is crucial to solve one of the main concerns when dealing with elliptical galaxies.

2.4.1 Photometric Approach

Galaxy bulges were initially thought as axisymmetric ellipsoids placed at the center of disc galaxies. The first piece of photometric evidence against this idea was given by Lindblad (1956). He showed a misalignment between the major axes of the disc and bulge in M31, realizing that this would be impossible if both the disc and bulge were oblate. This photometric misalignment is similar to the isophote twist observed in elliptical galaxies and used as an indication of triaxiality in these systems (Williams and Schwarzschild 1979). The extensive study undergone by Kent (1984) showed that the twisting isophotes between the central and outer parts of disc galaxies are quite common, but it was not until 1986 when Zaritsky and Lo (1986) properly studied the deviations from axisymmetry in the bulges of spiral galaxies. They found bulge-to-disc misalignments in their sample of 11 spiral galaxies hence confirming the high incidence of non-axisymmetric bulges in ordinary spirals and placing some parallelisms with elliptical galaxies. Beckman et al. (1991) also found compelling photometric evidence for triaxiality in the bulge of NGC 4736.

The first quantitative estimation of the intrinsic 3D shape of galaxy bulges using a statistical approach was performed by Bertola et al. (1991). They measured the bulge AARD and the misalignments between the major axes of the bulge and disc in a sample 32 S0–Sb galaxies. Under the hypothesis that discs are circular, they found that these bulges are triaxial with mean axial ratios $\langle Q \rangle = 0.86$ and $\langle F \rangle = 0.65$. Interestingly, they also demonstrated that a random projection of the probability distribution function of the bulges axis ratios fit sufficiently well to the AARD of the elliptical galaxies presented in Binney and de Vaucouleurs (1981). The results were interpreted as both populations of objects having the same origin.

Fathi and Peletier (2003) derived the intrinsic ellipticity of bulges by analyzing the deprojected apparent axis ratio of the galaxy isophotes within the bulge radius. This work did not assume any geometrical model for the galaxy but only that the disc be circular. They found $\langle Q \rangle = 0.79$ and $\langle Q \rangle = 0.71$ for the bulges of 35 early-type and 35 late-type disc galaxies, respectively. Despite the different methodologies, these results were in good agreement with previous results by Bertola et al. (1991).

Along the same lines, none of the 21 disc galaxies with morphological types between S0 and Sab studied by Noordermeer and van der Hulst (2007) harbors a truly spherical bulge. They reach this conclusion by assuming bulges to be oblate ellipsoids and comparing the isophotal axis ratio in the bulge-dominated region to that measured in the disc-dominated region. A mean flattening $\langle F \rangle = 0.55$ was obtained which is slightly lower than the value found by Bertola et al. (1991).

The number of galaxy bulges under study increased by an order of magnitude with the work of Méndez-Abreu et al. (2008a). They measured the structural parameters of bulges and discs of a sample of 148 early-to-intermediate spiral galaxies using a 2D photometric decomposition. They computed the probability distribution function of the intrinsic ellipticity from the bulges AARD, disc ellipticities, and misalignments between bulges and discs position angles. They suggested that about 80 % of the sample bulges are triaxial ellipsoids with a mean axial ratio $\langle B/A \rangle = 0.85$, confirming that bulges are slightly triaxial structures.

The vertical extension of galaxy bulges remains usually hidden from observations except for edge-on galaxies. Mosenkov et al. (2010) obtained a median value of the flattening $\langle F \rangle = 0.63$ for a sample of both early- and late-type edge-on galaxies using near infrared photometry. These results match well with the early findings by Bertola et al. (1991).

As well as for elliptical galaxies a number of works have attempted to quantify the intrinsic shape of individual bulges using only photometric data. The pioneering work of Varela et al. (1996) used a combination of geometrical deprojection and photometric inversion to work out the actual shape of the galaxy bulge in NGC 2841. They found that a family of triaxial ellipsoids with variable axis ratios is necessary to explain the photometric properties of its bulge. In 1998, Simonneau et al. derived a set of equations defining the three intrinsic axes of a triaxial ellipsoid as a function of the measured geometry of a galaxy bulge and disc (axis ratios and position angles) and the unknown Euler angle ϕ (see Sect. 2.2 for definition). This seminal paper promoted the work of Méndez-Abreu et al. (2010). They introduced a new method to derive the intrinsic shape of bulges based upon the analytical relations between the observed and intrinsic shapes of bulges and their surrounding discs. Using the equations derived in Simonneau et al. (1998) and introducing physical constraints on the accessible viewing angles, they found the following relation between the intrinsic semi-axes of the bulge and their observed properties

$$\begin{aligned} \frac{2\,\sin(2\phi_C)}{F_\theta}\,F^2 &= \sin(2\phi_C-\phi_B)\sqrt{(1-Q^2)^2-\sin^2\phi_B\,(1+Q^2)^2} \\ &\quad -\sin\phi_B\cos(2\phi_C-\phi_B)\left(1+Q^2\right)^2, \end{aligned} \tag{2.9}$$

where ϕ_B, ϕ_C, and F_θ are functions of the observed quantities a, b, δ, and θ, see equations 12, 13, and 43 of Méndez-Abreu et al. (2010). Therefore, Eq. 2.9 directly relates the intrinsic 3D shape of the bulge with its observed properties. Unfortunately, the relation between the intrinsic and projected variables also depends on the spatial position of the bulge with respect to the disc on its own reference system (i.e.,

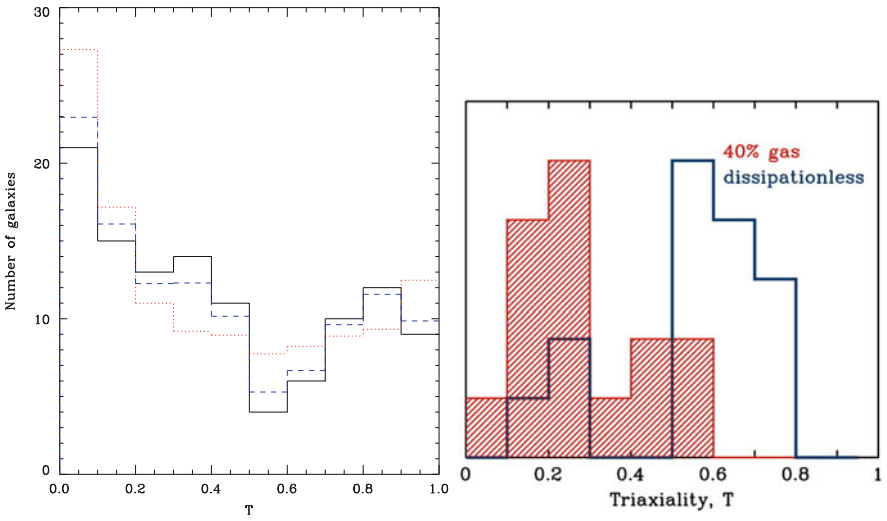

Fig. 2.4 Composite figure showing the similar bimodal distribution of triaxiality parameters from observations (*left panel*) and simulations (*right panel*). *Left panel*: distribution of the triaxiality parameter T obtained from the sample of Méndez-Abreu et al. (2010) (*continuous line*) and for a simulated sample with both 30 % and 100 % of bulges hosting a nuclear bar (*dashed* and *dotted lines*), respectively (Extracted from Méndez-Abreu et al. (2010). Reproduced with permission from Astronomy & Astrophysics, ©ESO). *Right panel*: distribution of both dissipational (*hatched histogram*) and dissipationless (*solid line*) mergers remnant triaxiality parameter from Cox et al. (2006). In both panels oblate galaxies have $T = 0$, prolate galaxies have $T = 1$, and all values in between are triaxial (Extracted from Cox et al. (2006). Reproduced with permission, ©AAS)

on the ϕ angle) and therefore, as well as for ellipticals, a deterministic solution of the problem cannot be given. However, the statistical analysis provided in Méndez-Abreu et al. (2010) allows us to obtain the probability distribution function of both semi-axis ratios, Q and F, for every single bulge, thus imposing tight constraints on its actual shape. Applying this technique to the sample of bulges presented in Méndez-Abreu et al. (2008a) they found a bimodal distribution of the triaxiality parameter (Fig. 2.4, left panel). In particular, bulges with Sérsic index $n \leq 2$ exhibit a larger fraction of oblate axisymmetric (or nearly axisymmetric) bulges, a smaller fraction of triaxial bulges, and fewer prolate axisymmetric (or nearly axisymmetric) bulges with respect to bulges with $n > 2$. Despite no correlations being found between the intrinsic shape of bulges and other properties such as bulge luminosity or velocity dispersion, the differences with the bulge surface-brightness distribution hint towards the presence of different bulge populations as suggested by Kormendy and Kennicutt (2004).

2.4.2 Evidences of Triaxiality from Kinematic Measurements

Early kinematic studies of galaxy bulges were shown to rotate more rapidly than elliptical galaxies (Kormendy and Illingworth 1982). In fact, the kinematic properties of many bulges are well described by dynamical models of oblate ellipsoids which are flattened by rotation with little or no anisotropy (Davies and Illingworth 1983; Jarvis and Freeman 1985; Fillmore 1986; Corsini et al. 1999; Pignatelli et al. 2001). However, there are also kinematic evidences supporting a triaxial shape in a non-negligible fraction of these bulges. In 1989, two independent works of Bertola et al. (1989) and Gerhard et al. (1989) reached the same conclusion about the triaxial bulge of the Sa galaxy NGC 4845. Using a combination of photometric and kinematic measurements they restrict the intrinsic axis ratio of its bulge to $Q = 0.74$ and $F = 0.6$. Their works were mainly supported by the presence of non-circular gas-motions in the galaxy center. In a non-axisymmetric potential, the shape of the rotation curve will depend on the position of the LOS and the major axis of the non-axisymmetric component. A slowly rising rotation curve or one in which a bump of extreme velocities is seen near the center are indications of triaxiality (Gerhard et al. 1989). Based on these considerations, and building on the early work of Lindblad (1956), Berman (2001) demonstrated the presence of a triaxial bulge in the Andromeda galaxy (M31) by using a hydrodynamical simulation to match the observed properties of the galaxy. Further evidences for non-circular gas motion in galaxy centers can be found in Falcón-Barroso et al. (2006) and Pizzella et al. (2008). Other kinematic evidence for the existence of triaxial bulges comes from the presence of velocity gradients along the galaxy minor axis. Corsini et al. (2003) found minor axis rotation in 80 % of their early-type spiral sample. In a series of papers, Coccato et al. (2004, 2005) found that 60 % of the unbarred galaxies show a remarkable gas velocity gradient along their optical minor axis. This was achieved by combining their own data with that present in the literature (Revised Shapley-Ames Catalog of Bright Galaxies) (Sandage and Tammann 1981).

Despite the importance of adding kinematic information to determine the intrinsic shape of the bulges, and contrary to the works on elliptical galaxies (e.g., Statler 1994a), there is not a well-established methodology to quantify the degree of triaxiality of bulges using the combined photometric and kinematic information, yet.

2.4.3 Polar Bulges

Polar bulges, as well as their analogous polar rings (Whitmore et al. 1990), are elongated structures perpendicular to the plane of the galaxy disc. A common signature of both the orthogonally decoupled bulge systems and the polar ring

galaxies is that both contain a structural component whose angular momentum vector is roughly parallel to the major axis of the host galaxy.

Vertical elongation is not a common feature of bulges. Indeed, most bulges can be assumed to be flattened by rotation (see Sect. 2.4.2). Furthermore, orthogonally decoupled bulges are usually not even *allowed* in most statistical works since the condition $A > B > C$ is commonly used, see Bertola et al. (1991). Méndez-Abreu et al. (2010) relaxed this condition and found that only 18 % of the observed bulges have a probability >50 % of being elongated along the polar axis with no bulges reaching a probability >90 %. In fact, to date NGC 4698 (Bertola et al. 1999), NGC 4672 (Sarzi et al. 2000), and UGC 10043 (Matthews and de Grijs 2004) are the only spiral galaxies known to host a prominent bulge sticking out from the plane of the disc.

The case of NGC 4698 is particularly intriguing since it hosts also a polar nuclear stellar disc aligned with its polar bulge and thus perpendicular to the main disc. This galaxy was recently revisited by Corsini et al. (2012) and its intrinsic shape was derived using the methodology proposed by Méndez-Abreu et al. (2010). They found a slightly triaxial polar bulge elongated along the vertical direction with axis ratios $Q = 0.95$ and $F = 1.60$. This result agrees well with the observed kinematics presented in Bertola et al. (1999) and with a model where the nuclear disc is the end result of the acquisition of external gas by the pre-existing triaxial bulge on the principal plane perpendicular to its shortest axis and perpendicular to the main disc of the galaxy.

2.5 The Intrinsic Shape of the Milky Way Bulge

Owing to its vicinity, the Galactic bulge has always been targeted as the ideal benchmark for structure, kinematic, and stellar populations studies of bulges. In fact, it can be studied at a unique level of detail, in comparison to external galaxies, thanks to the possibility of measuring the properties of individual stars. However, our *inside view* of the Galaxy generally restricts our knowledge to pencil beam areas around the Galactic center due to either the high extinction, the crowding, or the superposition of multiple structures along the LOS, making studies of the inner Galactic regions challenging. The structure of the Galaxy has accounted for a significant amount of literature in the past and the topic has come back in the limelight in recent years. In this section I briefly review the Galactic bulge topic focusing on its intrinsic shape heading the readers to other chapters in this volume for more information about its stellar content and kinematics.

In recent decades it has become clear that the Galaxy is a barred system (Blitz and Spergel 1991; López-Corredoira et al. 2005) and that most likely its central regions are dominated by a boxy bulge created by vertical instabilities within the Galactic bar (Dwek et al. 1995; Martinez-Valpuesta and Gerhard 2011; Ness et al. 2013). The historical evolution of our knowledge of the intrinsic structure of the Galactic bulge

has been written by a succession of progressively larger scale, deeper sensitivity photometric and spectroscopic surveys.

The first attempt to understand the shape of the Galactic bulge was made by de Vaucouleurs and Pence (1978). They found that models ranging from spherical to $F = 0.6$ were able to represent well both the distribution of globular clusters around the Galactic center and the infrared isophotes observed at 2.4μm (Maihara et al. 1978). The flattening of the Galactic bulge was then further constrained with the arrival of the Infrared Astronomical Satellite (IRAS). Using IRAS data, Harmon and Gilmore (1988) and Whitelock et al. (1991) found values of the intrinsic flattening spanning $0.6 < F < 0.8$ using *JHK* near-infrared bands. Similarly, Kent et al. (1991) found that, at first order, the Galactic bulge can be represented by an oblate ellipsoid with $F = 0.61$ using data from the Infrared Telescope (IRT).

The picture changed drastically with the advent of the COBE satellite (Hauser et al. 1990). The new striking image of the Milky Way (Fig. 2.5) provided by the DIRBE experiment on board of COBE allowed Blitz and Spergel (1991), and later on Blitz (1993), to find the first direct evidence for a bar at the Galactic center. Interestingly, they also found the presence of a triaxial bulge structurally distinct from the main bar. The modeling of this triaxial bulge was performed by different teams with different sets of data in the subsequent years. Consequently, different axis ratios represented as 1:Q:F were found: 1:0.33:0.22 (Dwek et al. 1995), 1:0.6:0.4 (Binney et al. 1997),1:0.43:0.29 (Stanek et al. 1997), 1:0.38:0.26 (Freudenreich 1998), 1:0.54:0.33 (López-Corredoira et al. 2000), 1:(0.3–0.4):0.3 (Bissantz and Gerhard 2002), 1:0.5:0.4 (López-Corredoira et al. 2005). In general, these values implied the Galactic bulge to be a triaxial structure with a tendency

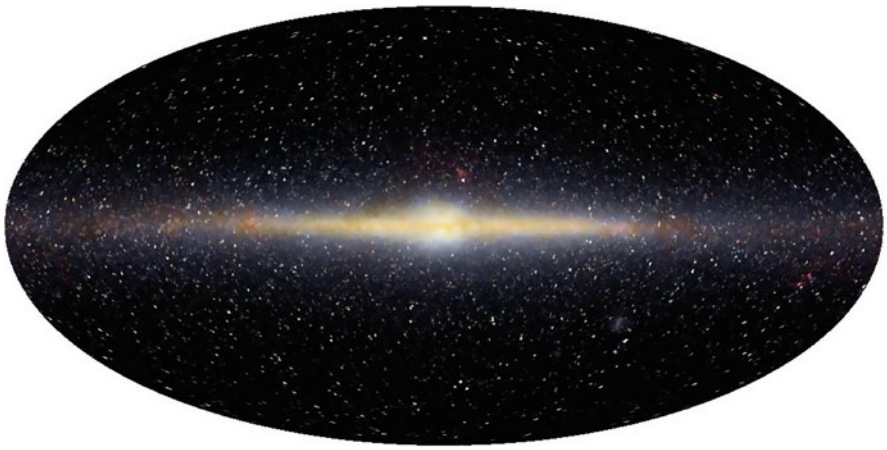

Fig. 2.5 False-colour image of the near-infrared sky as seen by the DIRBE. Data at 1.25, 2.2, and 3.5 μm wavelengths are represented respectively as *blue*, *green* and *red* colours. The image is presented in Galactic coordinates, with the plane of the Milky Way Galaxy horizontal across the middle and the Galactic center at the center (Credits: E. L. Wright (UCLA), The COBE Project, DIRBE, NASA)

to prolateness, thus not in agreement with the triaxial/oblate picture outlined in Sect. 2.4 for extragalactic bulges.

Although the idea of a triaxial bulge worked well at first order, the boxy shape noticed earlier by Kent et al. (1991) and Kent (1992) and confirmed by Dwek et al. (1995) was not recovered by a triaxial ellipsoid. In the meanwhile, different scenarios came up to explain these differences and account for the continuously increasing kinematic and stellar populations information. Alard (2001) suggested the presence of two different bars in the Galaxy by analyzing data from the Two Micron All Sky Survey (2MASS) (Skrutskie et al. 2006). Another possible scenario was worked out by Babusiaux et al. (2010) suggesting a model composed by a classical bulge in the center and a boxy bulge in the outer parts.

Shen et al. (2010) proposed a simple model yet backed up by the high quality stellar kinematics provided by the Bulge Radial Velocity Assay (BRAVA) (Rich et al. 2007). Using N-body simulations they found no evidence for a classical bulge in the Galaxy but the bulge appears to be only part of the bar and therefore not a separated component. Figure 2.6 shows that the inclusion of a classical bulge greatly

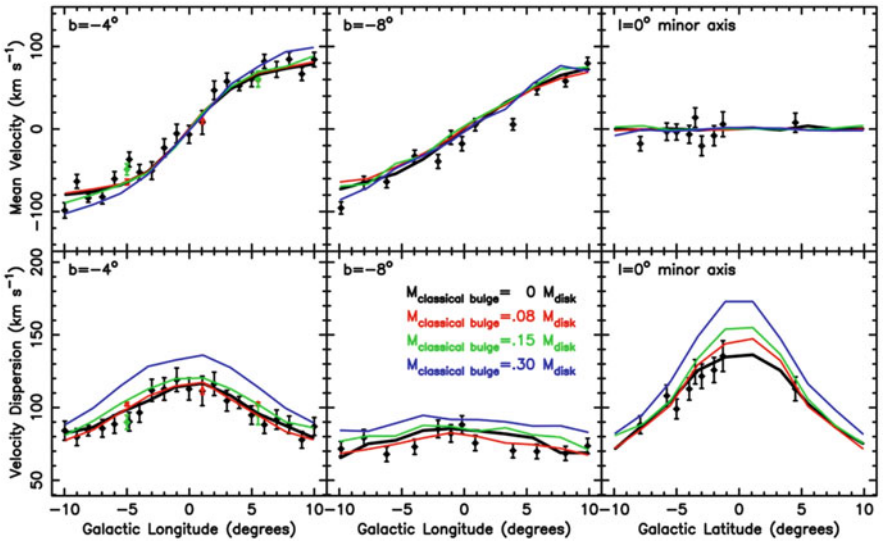

Fig. 2.6 Best models fits to the BRAVA stellar kinematics using different hypothesis on the classical bulge mass. Mean velocity (*top panels*) and velocity dispersion (*lower panels*) profiles of all available kinematic observations presented in Shen et al. (2010). The *left two panels* are for the Galactic latitude b = 4° strip; the *middle two panels* are for the b = 8°; and the *right two panels* are for the l = 0° minor axis. The *heavy black lines* represent the model without a classical bulge. The *red*, *green*, and *blue lines* are for models whose classical bulges have masses of 8 %, 15 %, and 30 %, respectively, of the disc mass. Including a classical bulge significantly worsens the model fits to the data, especially along the minor axis (Extracted from Shen et al. (2010). Reproduced with permission, ©AAS)

worsens the model fit to the data. Models from Shen et al. (2010) rule out that the Milky Way has a significant classical bulge with mass >15 % of the disc mass.

Following this line, Martinez-Valpuesta and Gerhard (2011) demonstrated how the star counts measurements by Cabrera-Lavers et al. (2007) agrees with a scenario composed by a single bar and a boxy bulge. More recent measurements of star counts from the VISTA Variables in The Via Lactea (VVV) (Gonzalez et al. 2011), metallicity gradients from the Abundances and Radial velocity Galactic Origins Survey (ARGOS) (Ness et al. 2013), or stellar kinematics from BRAVA have also been reconciled within this picture (Gerhard and Martinez-Valpuesta 2012; Martinez-Valpuesta and Gerhard 2013).

2.6 The 3D Shape of Bulges in Numerical Simulations

The intrinsic shape of bulges keeps important information about their formation history, with different merger, accretion and assembly scenarios resulting in different shapes. Hence, the comparison of measured intrinsic shapes with the output from numerical simulations represents an intrinsic way to gain insights on their formation. However, numerical resolution problems have often hampered these studies and our interpretation of the shapes of bulges is usually restricted to the analysis of simulated elliptical galaxies.

Cox et al. (2006) studied the structure of ellipsoidal remnants formed by either major (equal-mass) dissipationless or dissipational mergers of disc galaxies. They found a bimodal distribution of the triaxiality parameter in their remnant ellipticals (see right panel in Fig. 2.4). Thus, dissipationless remnants are triaxial with a tendency to be more prolate and with a mean triaxiality parameter $T = 0.55$, whereas dissipational remnants are triaxial and tend to be much closer to oblate with triaxiality $T = 0.28$. This simulated bimodal distribution was compared by Méndez-Abreu et al. (2010) to the triaxiality measured in their sample of 115 galaxy bulges (Fig. 2.4). They concluded that both major dissipational and dissipationless mergers are required to explain the variety of shapes found for bulges. The detailed study presented by Cox et al. (2006) is consistent with previous studies of dissipationless and dissipational mergers (e.g., Barnes 1992; Hernquist 1992; Springel 2000). However, the study of González-García and Balcells (2005) found how the degree of triaxiality of the elliptical remnants in dissipationless mergers also depends on the morphology of the progenitor spirals. The presence of central bulges on the progenitor galaxies produce remnants which tend to be more oblate whereas bulgeless progenitors lead to highly triaxial remnants which seems inconsistent with observations. Therefore, the comparison between simulations and observations are still subject to the range of initial conditions explored by numerical simulations.

On the other hand, even if the similarities between bulges and ellipticals have prompted observers to compare the measured properties of bulges to the properties of simulated elliptical galaxies, the formation path of bulges is likely a more complex process involving the interaction with other galaxy structural components

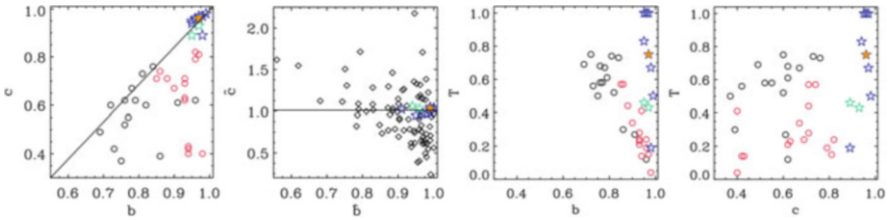

Fig. 2.7 Intrinsic shape of bulges and elliptical galaxies obtained from numerical simulations. A comparison with observed bulges is shown in the second panel. The *blue* and *green stars* in all panels represent the bulge remnants after suffering intermediate/minor mergers. The location of the progenitor bulges is shown with orange stars. The elliptical remnants of major mergers with pure exponential stellar discs (*black circles*) and containing 40 % of gas (*red circles*) are also shown. *First panel*: intrinsic ellipticity b (Q in this chapter) versus the intrinsic flattening c (F in this chapter) *Second panel*: as panel 1 but adding the observed distribution of bulges in Méndez-Abreu et al. (2010) (*black diamonds*). *Third* and *fourth panels*: triaxiality parameter as a function of the intrinsic ellipticity and flattening (Extracted from Tapia et al. (2014). Reproduced with permission from Astronomy & Astrophysics, ©ESO)

(Kormendy and Kennicutt 2004; Athanassoula 2005). The recent work by Tapia et al. (2014) has started to fill the gap on studies about the intrinsic shape of galaxy bulges from numerical simulations. They analysed a set of $N-$body simulations of intermediate and minor dry mergers onto S0s to understand the structural and kinematic evolution induced by the encounters. In their experiments, the progenitor bulges are nearly spherical. The remnant bulges remain spherical as well ($Q \sim F > 0.9$), but exhibiting a wide range of triaxialities ($0.20 < T < 1.00$), remarking how the definition of this shape parameter is too sensitive to nearly spherical systems. Figure 2.7 (second panel) shows how the axis ratios derived from these simulations (open stars) are hardly reconcilable with the observations (black diamonds) by Méndez-Abreu et al. (2010). Still, the strong triaxiality agrees with the structure of elliptical remnants resulting from major-to-intermediate mergers (Cox et al. 2006).

2.7 Concluding Remarks and Future Prospects

I present here a review of our current understanding of the intrinsic 3D shape of galaxy bulges. The approach taken in this review is largely observational and follows the historical development of the field. Thus, a journey through the past and present of our knowledge on the intrinsic shape of other galaxy ellipsoids such as elliptical galaxies or galaxy discs was needed to put the problem in context. The major conclusions of this review are:

- The observational data representing the whole population of elliptical galaxies is consistent with a mixed model, combining partly oblate and partly prolate galaxies, although a more likely alternative points towards at least some fraction

of the ellipticals being triaxial ellipsoids. Triaxiality is also supported by several photometric and kinematics properties, as well as for detailed modeling of individual galaxies.
- The intrinsic shape of ellipticals shows a dependence on galaxy luminosity. Bright ellipticals are in general triaxial with a tendency to be rounder whereas faint ellipticals are more flattened with a tendency to be oblate ellipsoids.
- Even if uncertainties due to the lack of number statistics have been overcome with the advent of recent surveys, the data can still be reproduced by a wide variety of intrinsic shape distributions. Furthermore, a proper interpretation of the data is complicated by the fact that the AARD and kinematic misalignments are often a function of the radius. Therefore it is generally impossible to characterize the full shape of a single elliptical galaxy with only one or two parameters.
- Galaxy discs are, in general, well represented by nearly oblate models with $Q \sim 0.9$. Their intrinsic flattening is also well constrained to values spanning $0.2 < F < 0.3$.
- The population of galaxy bulges can be modeled as slightly triaxial ellipsoids with a tendency to be oblate. This population has typical intrinsic flattenings of $F \sim 0.65$. However, individual galaxies can have a variety of intrinsic flattenings with some extreme cases sticking out the plane of the disc, these are called polar bulges.
- The distribution of the triaxiality parameter of galaxy bulges is strongly bimodal. This bimodality is driven by bulges with Sérsic index $n > 2$. According to numerical simulations they can be explained assuming a combination of major dissipational and dissipationless mergers during their formation.
- Despite previous findings showing a triaxial bulge in the Milky Way, more recent studies have found that is more likely a boxy bulge produced by the vertical instabilities of the Galactic bar. Owing to recent kinematic measurements a classical bulge with mass >15 % of the disc mass can be ruled out.

Despite the study of the intrinsic shape of elliptical galaxies has a long track record, our knowledge of the 3D shape of bulges is still in its infancy. Therefore, further work on the topic is needed to fully exploit its possibilities. A few guidelines to this future prospects are outlined in the following:

- From a photometric point of view, even if new methodologies have been developed they need to be applied to larger samples of galaxy bulges. The number of elliptical galaxies recently analyzed to recover their intrinsic shape is several orders of magnitude larger than the current samples of galaxy bulges. Large number statistics have led to the discovery of important relations for elliptical galaxies, such as the different shapes of bright and faint ellipticals, and similar studies can be crucial for galaxy bulges. This is particularly relevant in the current picture of bulge formation with a different population of classical and pseudobulges dependent of the galaxy mass (Fisher and Drory 2011).
- An even more promising path, already explored in elliptical galaxies, is the use of combined information from photometric and kinematic data. In particular, the common use of integral field spectroscopy is now providing an exquisite detail

of the stellar and gaseous kinematics on large sample of galaxies. This wealth of information together with the development of galaxy dynamical modeling can provide a proper understanding of the intrinsic shape of galaxy bulges.
- It is doubtless that the comparison of the derived intrinsic shape of bulges with the state-of-the-art numerical simulations is a promising way to gain insights on the formation and evolution of bulges. However, there is still a lack of simulations with a large variety of initial and physical conditions interested on a structural analysis of the different galaxy components, and in particular, in the intrinsic shape evolution of galaxy bulges.
- Historically, galaxy bulges were thought as single-component objects at the center of galaxies. This picture is now questioned since different bulge types with different formation paths have been found coexisting within the same galaxy (see Méndez-Abreu et al. 2014, and references therein). A proper separation of different bulges types, as well as the identification of possible unresolved nuclear structures such as bars, rings, etc, must be accounted for to improve our knowledge on bulge formation and evolution.
- The study of the intrinsic shape of elliptical galaxies at high redshift has recently suffered a boost thanks to the arrival of high spatial resolution surveys on large fields of view (see Chang et al. 2013, and references therein). This kind of studies can provide an in-situ view of galaxy evolution and their application to the intrinsic shape of bulges will be key to further progress on this topic.

Acknowledgements I would like to thank the editors E. Laurikainen, R.F. Peletier, and D. Gadotti for their invitation to take part in this volume. I would also like to thank A. de Lorenzo-Cáceres and J. Argyle for a careful reading of this manuscript. JMA acknowledges support from the European Research Council Starting Grant (SEDmorph; P.I. V. Wild).

References

Abazajian K. et al., 2005, AJ, 129, 1755
Adelman-McCarthy J. K. et al., 2008, ApJS, 175, 297
Adelman-McCarthy J. K. et al., 2007, ApJS, 172, 634
Aihara H. et al., 2011, ApJS, 193, 29
Alam S. M. K., Ryden B. S., 2002, ApJ, 570, 610
Alard C., 2001, A&A, 379, L44
Athanassoula E., 2005, MNRAS, 358, 1477
Babusiaux C. et al., 2010, A&A, 519, A77
Bak J., Statler T. S., 2000, AJ, 120, 110
Barnes J. E., 1992, ApJ, 393, 484
Beckman J. E., Varela A. M., Munoz-Tunon C., Vilchez J. M., Cepa J., 1991, A&A, 245, 436
Benacchio L., Galletta G., 1980, MNRAS, 193, 885
Berman S., 2001, A&A, 371, 476
Bertola F., Capaccioli M., 1975, ApJ, 200, 439
Bertola F., Corsini E. M., Vega Beltrán J. C., Pizzella A., Sarzi M., Cappellari M., Funes J. G., 1999, ApJ, 519, L127
Bertola F., Galletta G., 1979, A&A, 77, 363

Bertola F., Vietri M., Zeilinger W. W., 1991, ApJ, 374, L13
Bertola F., Zeilinger W. W., Rubin V. C., 1989, ApJ, 345, L29
Binggeli B., 1980, A&A, 82, 289
Binney J., 1978, MNRAS, 183, 501
Binney J., 1985, MNRAS, 212, 767
Binney J., de Vaucouleurs G., 1981, MNRAS, 194, 679
Binney J., Gerhard O., Spergel D., 1997, MNRAS, 288, 365
Bissantz N., Gerhard O., 2002, MNRAS, 330, 591
Blitz L., 1993, Nature, 364, 757
Blitz L., Spergel D. N., 1991, ApJ, 370, 205
Bottinelli L., Gouguenheim L., Paturel G., de Vaucouleurs G., 1983, A&A, 118, 4
Cabrera-Lavers A., Hammersley P. L., González-Fernández C., López-Corredoira M., Garzón F., Mahoney T. J., 2007, A&A, 465, 825
Cappellari M. et al., 2011, MNRAS, 413, 813
Carter D., 1978, MNRAS, 182, 797
Chakraborty D. K., Diwakar A. K., Pandey S. K., 2011, MNRAS, 412, 585
Chakraborty D. K., Singh A. K., Gaffar F., 2008, MNRAS, 383, 1477
Chang Y.-Y. et al., 2013, ApJ, 773, 149
Chung A., Bureau M., 2004, AJ, 127, 3192
Coccato L., Corsini E. M., Pizzella A., Bertola F., 2005, A&A, 440, 107
Coccato L., Corsini E. M., Pizzella A., Morelli L., Funes J. G., Bertola F., 2004, A&A, 416, 507
Combes F., Sanders R. H., 1981, A&A, 96, 164
Contopoulos G., 1956, ApJ, 124, 643
Corsini E. M., Méndez-Abreu J., Pastorello N., Dalla Bontà E., Morelli L., Beifiori A., Pizzella A., Bertola F., 2012, MNRAS, 423, L79
Corsini E. M., Pizzella A., Coccato L., Bertola F., 2003, A&A, 408, 873
Corsini E. M. et al., 1999, A&A, 342, 671
Cox T. J., Dutta S. N., Di Matteo T., Hernquist L., Hopkins P. F., Robertson B., Springel V., 2006, ApJ, 650, 791
Dalcanton J. J., Bernstein R. A., 2002, AJ, 124, 1328
Davies R. L., Illingworth G., 1983, ApJ, 266, 516
de Souza R. E., Gadotti D. A., dos Anjos S., 2004, ApJS, 153, 411
de Vaucouleurs G., de Vaucouleurs A., 1964, Reference Catalogue of Bright Galaxies. University of Texas Press, Austin
de Vaucouleurs G., Pence W. D., 1978, AJ, 83, 1163
Debattista V. P., Carollo C. M., Mayer L., Moore B., 2004, ApJ, 604, L93
Dwek E. et al., 1995, ApJ, 445, 716
Erwin P., 2015, ApJ, 799, 226
Erwin P., Debattista V. P., 2013, MNRAS, 431, 3060
Evans D. S., 1951, MNRAS, 111, 526
Falcón-Barroso J. et al., 2006, MNRAS, 369, 529
Fall S. M., Frenk C. S., 1983, AJ, 88, 1626
Fasano G., 1995, Astrophysical Letters and Communications, 31, 205
Fasano G., Amico P., Bertola F., Vio R., Zeilinger W. W., 1993, MNRAS, 262, 109
Fasano G. et al., 2010, MNRAS, 294
Fasano G., Vio R., 1991, MNRAS, 249, 629
Fathi K., Peletier R. F., 2003, A&A, 407, 61
Fillmore J. A., 1986, AJ, 91, 1096
Fisher D. B., Drory N., 2011, ApJ, 733, L47
Franx M., Illingworth G., de Zeeuw T., 1991, ApJ, 383, 112
Freudenreich H. T., 1998, ApJ, 492, 495
Gadotti D. A., 2009, MNRAS, 393, 1531
Gerhard O., Martinez-Valpuesta I., 2012, ApJ, 744, L8
Gerhard O. E., Vietri M., Kent S. M., 1989, ApJ, 345, L33

Gonzalez O. A., Rejkuba M., Minniti D., Zoccali M., Valenti E., Saito R. K., 2011, A&A, 534, L14
González-García A. C., Balcells M., 2005, MNRAS, 357, 753
Guthrie B. N. G., 1992, A&AS, 93, 255
Harmon R., Gilmore G., 1988, MNRAS, 235, 1025
Hauser M. G. et al., 1990, in Astrophysics and Space Science Library, Vol. 166, IAU Colloq. 123: Observatories in Earth Orbit and Beyond, Kondo Y., ed., p. 19
Hernquist L., 1992, ApJ, 400, 460
Hubble E. P., 1926, ApJ, 64, 321
Illingworth G., 1977, ApJ, 218, L43
Jarvis B. J., Freeman K. C., 1985, ApJ, 295, 324
Kent S. M., 1984, ApJS, 56, 105
Kent S. M., 1992, ApJ, 387, 181
Kent S. M., Dame T. M., Fazio G., 1991, ApJ, 378, 131
Kimm T., Yi S. K., 2007, ApJ, 670, 1048
Kormendy J., Bender R., 2012, ApJS, 198, 2
Kormendy J., Illingworth G., 1982, ApJ, 256, 460
Kormendy J., Kennicutt, Jr. R. C., 2004, ARA&A, 42, 603
Lambas D. G., Maddox S. J., Loveday J., 1992, MNRAS, 258, 404
Lauer T. R., Postman M., 1994, ApJ, 425, 418
Laurikainen E., Salo H., Buta R., 2005, MNRAS, 362, 1319
Liller M. H., 1960, ApJ, 132, 306
Lindblad B., 1956, Stockholms Observatoriums Annaler, 19, 7
Lintott C. et al., 2011, MNRAS, 410, 166
López-Corredoira M., Cabrera-Lavers A., Gerhard O. E., 2005, A&A, 439, 107
López-Corredoira M., Hammersley P. L., Garzón F., Simonneau E., Mahoney T. J., 2000, MNRAS, 313, 392
Lucy L. B., 1974, AJ, 79, 745
Lütticke R., Dettmar R.-J., Pohlen M., 2000, A&AS, 145, 405
Maihara T., Oda N., Sugiyama T., Okuda H., 1978, PASJ, 30, 1
Martinez-Valpuesta I., Gerhard O., 2011, ApJ, 734, L20
Martinez-Valpuesta I., Gerhard O., 2013, ApJ, 766, L3
Martinez-Valpuesta I., Shlosman I., Heller C., 2006, ApJ, 637, 214
Matthews L. D., de Grijs R., 2004, AJ, 128, 137
Méndez-Abreu J., Aguerri J. A. L., Corsini E. M., Simonneau E., 2008a, A&A, 478, 353
Méndez-Abreu J., Corsini E. M., Debattista V. P., De Rijcke S., Aguerri J. A. L., Pizzella A., 2008b, ApJ, 679, L73
Méndez-Abreu J., Debattista V. P., Corsini E. M., Aguerri J. A. L., 2014, A&A, 572, A25
Méndez-Abreu J., Simonneau E., Aguerri J. A. L., Corsini E. M., 2010, A&A, 521, A71+
Mitronova S. N., Karachentsev I. D., Karachentseva V. E., Jarrett T. H., Kudrya Y. N., 2004, Bull. Special Astrophys. Obs., 57, 5
Mosenkov A. V., Sotnikova N. Y., Reshetnikov V. P., 2010, MNRAS, 401, 559
Ness M. et al., 2013, MNRAS, 432, 2092
Noerdlinger P. D., 1979, ApJ, 234, 802
Noordermeer E., van der Hulst J. M., 2007, MNRAS, 376, 1480
Padilla N. D., Strauss M. A., 2008, MNRAS, 388, 1321
Peng C. Y., Ho L. C., Impey C. D., Rix H., 2002, AJ, 124, 266
Peterson C. J., 1978, ApJ, 222, 84
Pignatelli E. et al., 2001, MNRAS, 323, 188
Pizzella A., Corsini E. M., Sarzi M., Magorrian J., Méndez-Abreu J., Coccato L., Morelli L., Bertola F., 2008, MNRAS, 387, 1099
Prieto M., Aguerri J. A. L., Varela A. M., Muñoz-Tuñón C., 2001, A&A, 367, 405
Rich R. M., Reitzel D. B., Howard C. D., Zhao H., 2007, ApJ, 658, L29
Rodríguez S., Padilla N. D., 2013, MNRAS, 434, 2153

Ryden B., 1992, ApJ, 396, 445
Ryden B. S., 1996, ApJ, 461, 146
Ryden B. S., 2004, ApJ, 601, 214
Ryden B. S., 2006, ApJ, 641, 773
Sánchez-Janssen R., Méndez-Abreu J., Aguerri J. A. L., 2010, MNRAS, 406, L65
Sandage A., Freeman K. C., Stokes N. R., 1970, ApJ, 160, 831
Sandage A., Tammann G. A., 1981, A revised Shapley-Ames Catalog of bright galaxies
Sarzi M., Corsini E. M., Pizzella A., Vega Beltrán J. C., Cappellari M., Funes J. G., Bertola F., 2000, A&A, 360, 439
Schechter P. L., Gunn J. E., 1979, ApJ, 229, 472
Shen J., Rich R. M., Kormendy J., Howard C. D., De Propris R., Kunder A., 2010, ApJ, 720, L72
Simard L., 1998, in ASP Conf. Ser., Vol. 145, Astronomical Data Analysis Software and Systems VII, R. Albrecht, R. N. Hook, & H. A. Bushouse, ed., Astronomical Society of the Pacific, San Francisco, p. 108
Simonneau E., Varela A. M., Munoz-Tunon C., 1998, Nuovo Cimento B Serie, 113, 927
Skrutskie M. F. et al., 2006, AJ, 131, 1163
Springel V., 2000, MNRAS, 312, 859
Stanek K. Z., Udalski A., SzymaŃski M., KałuŻny J., Kubiak Z. M., Mateo M., KrzemiŃski W., 1997, ApJ, 477, 163
Stark A. A., 1977, ApJ, 213, 368
Statler T. S., 1994a, ApJ, 425, 458
Statler T. S., 1994b, ApJ, 425, 500
Statler T. S., Fry A. M., 1994, ApJ, 425, 481
Tapia T. et al., 2014, A&A, 565, A31
Tenjes P., Busarello G., Longo G., Zaggia S., 1993, A&A, 275, 61
Thakur P., Chakraborty D. K., 2001, MNRAS, 328, 330
Tremblay B., Merritt D., 1995, AJ, 110, 1039
Tremblay B., Merritt D., 1996, AJ, 111, 2243
van den Bosch R. C. E., van de Ven G., 2009, MNRAS, 398, 1117
Varela A. M., Munoz-Tunon C., Simmoneau E., 1996, A&A, 306, 381
Vincent R. A., Ryden B. S., 2005, ApJ, 623, 137
Weijmans A.-M. et al., 2014, MNRAS, 444, 3340
Whitelock P., Feast M., Catchpole R., 1991, MNRAS, 248, 276
Whitmore B. C., Lucas R. A., McElroy D. B., Steiman-Cameron T. Y., Sackett P. D., Olling R. P., 1990, AJ, 100, 1489
Williams T. B., 1981, ApJ, 244, 458
Williams T. B., Schwarzschild M., 1979, ApJ, 227, 56
Wyse R. F. G., Gilmore G., Franx M., 1997, ARA&A, 35, 637
Yoon I., Weinberg M. D., Katz N., 2011, MNRAS, 414, 1625
Zaritsky D., Lo K. Y., 1986, ApJ, 303, 66

Chapter 3
An Observational Guide to Identifying Pseudobulges and Classical Bulges in Disc Galaxies

David B. Fisher and Niv Drory

Abstract In this review our aim is to summarize the observed properties of pseudobulges and classical bulges. We utilize an empirical approach to studying the properties of bulges in disc galaxies, and restrict our analysis to statistical properties. A clear bimodality is observed in a number of properties including morphology, structural properties, star formation, gas content & stellar population, and kinematics. We conclude by summarizing those properties that isolate pseudobulges from classical bulges. Our intention is to describe a practical, easy to use, list of criteria for identifying bulge types.

3.1 Introduction

This paper reviews those observed properties of bulges that reveal the bimodal nature of the central structures found in disc galaxies. Our aim is to collect a set of empirical properties of bulges that can be used to diagnose bulges into the two subcategories commonly referred to as *pseudobulges* and *classical bulges*. Despite a long history of studying bulges in disc galaxies (Sandage 1961), and the knowledge that bulges are very common, being found in upwards of $\sim$80 % of bright galaxies ($>10^9$ $M_\odot$; Fisher and Drory 2011), only recently have systematic studies of the bimodal nature of bulges become frequent in the literature.

Kormendy and Illingworth (1982) have shown that bulges in disc galaxies separate by internal kinematics: some rotate rapidly like a disc whereas others are dominated by random motions (Kormendy and Illingworth 1982). Also, the review

D.B. Fisher (✉)
Center for Astrophysics and Supercomputing, Swinburne University of Technology, P. O. Box 218, Hawthorn, VIC 3122, Australia
e-mail: dfisher@swin.edu.au

N. Drory
McDonald Observatory, The University of Texas at Austin, 1 University Station, Austin, TX 78712, USA
e-mail: drory@astro.as.utexas.edu

E. Laurikainen et al. (eds.), *Galactic Bulges*, Astrophysics and Space Science Library 418, DOI 10.1007/978-3-319-19378-6_3

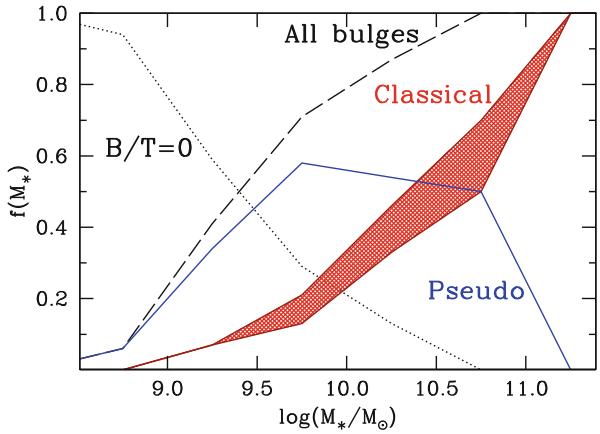

Fig. 3.1 The frequency of bulge types correlates with total galaxy mass. The four curves indicate the frequency of pseudobulges (*blue solid line*), classical bulges (*red filled region*), galaxies with no bulge (*dotted line*) and all bulges (*dashed line*) as a function of total galaxy mass. The classical bulges are shown as a shaded region because an attempt has been made to account for composite pseudobulge-classical systems. The higher value for a given mass includes this estimate, the lower value is for galaxies whose bulges are pure-classical bulge systems. There is a clear sequence of bulgeless galaxies existing at low mass, pseudobulges in intermediate mass galaxies and classical bulges in high mass galaxies

by Wyse et al. (1997, and references therein) demonstrates clearly that bulges are a heterogeneous class of objects. Bulges are shown to vary significantly in their ages and metallicities, and not all bulges show properties that are similar to elliptical galaxies. The observation that there is more than one type of bulge introduces the possibility that bulges as a class could be the end result of more than one mechanism of galaxy evolution.

In Fig. 3.1 we show a result that illustrates simple evidence that bulge type is connected to the evolution of galaxies. The figure shows the frequency of bulge types for the brightest ∼100 galaxies in the local 11 Mpc volume. The type of bulge a galaxy contains changes systematically as galaxy mass increases. Similarly, galaxies with blue, young, stellar populations have been shown to have very different bulges than those of red, old galaxies (Drory and Fisher 2007). These results suggest that bulge type is connected to the phenomena that drive galaxy evolution. Being able to diagnose bulge types in galaxies is therefore both useful to understand the properties of an individual galaxy, and also to understand galaxy evolution in general.

At present, we know of three main mechanisms that allow a galaxy to grow bulge mass (as measured by an increase in the bulge-to-total luminosity ratio from bulge-disc decompositions). These are merging processes (Hammer et al. 2005; Aguerri et al. 2001), slow secular evolution (Kormendy and Kennicutt 2004; Athanassoula 2005a), and rapid internal evolution due to disc instabilities during the "clumpy" phase (Elmegreen et al. 2008; Inoue and Saitoh 2012). It is therefore critical that

we are able to identify the properties of bulges that potentially isolate features associated with each of these formation channels. Given that realistically the end result of bulge formation and evolution is likely a composite object, recognizing "pure" examples of each formation channel (i.e. the most extreme cases along a spectrum of properties) will be necessary to disentangle the physical processes involved.

In this review we will concentrate on work separating bulges into the dimorphic classes mentioned above. These two categories have been given names, the most popular of which seem to be "pseudobulges"[1] and "classical bulges". In short, pseudobulges are bulges that have properties that historically we associate with dissipative phenomena (active star formation, rotating kinematics, young stars). Alternatively, some authors refer to such bulges as "discy bulges" (Athanassoula 2005a). Kormendy and Kennicutt (2004) give a thorough review, though now 10 years old, of pseudobulge properties. Their review focuses largely on exemplary cases, while the review here will focus on statistical results, which can be applied to large sets of galaxies. "Classical bulges", in turn, are those bulges that exhibit properties resembling elliptical galaxies, such as smooth distribution of stars, old stellar age, and kinematics dominated by random motions. The term "classical" refers to this being the widespread preconception about bulges for much of the twentieth century (Wyse et al. 1997). Using a terminology that is based on preconceptions that are no longer widely held seems a bit archaic. Nonetheless, we accept the concept in language signification (known as *Saussurean Arbitrariness*), in which historic meaning or sound of a word is not as important as the meaning we ascribe to it now, and simply adopt the most popular terms of the present day ("pseudobulges" and "classical bulges"). For further reading on bulge properties we refer the reader to the aforementioned reviews by Kormendy and Kennicutt (2004) and Wyse et al. (1997), and also the lecture notes by Gadotti (2012) and Kormendy (2013).

3.1.1 Definition of a Bulge

Before discussing the separate kinds of bulges, it is necessary to define what is meant by the term "bulge" when applied to galaxies. The most commonly used definition of bulges is based on the observed rise in surface brightness above the disc that is observed at the center of many intermediate-type galaxies. Disc components of galaxies are often well described by an exponential decay with increasing radius of their surface brightness (Freeman 1970). Many galaxies contain a centrally located structure that is brighter than the inward extrapolation of the disc's exponential surface brightness, and this component is not associated with

[1]Editorial comment: the criteria used to distinguish discy pseudobulges in this review do not unambiguously separate them from boxy/peanut/barlens structures (see Chap. 4).

a bar. This central structure is often identified as a "bulge". Bulges of this type are often identified using bulge-disc decomposition techniques (Kormendy 1977b), commonly using the Sérsic function (Sérsic 1968) to describe the surface brightness of the bulge. Defining bulges using surface photometry has the advantage that it is straightforward, empirically based, and can be applied to large numbers of galaxies. In principle one can use large data sets like the Sloan Digital Sky Survey to characterize bulges in $>10^4$ galaxies (Lackner and Gunn 2012).

Identifying bulges in bulge-disc decomposition is by nature parametric, but disc galaxies could have non-exponential components in their centers (similar to bars). Therefore, identifying extra light as a separate component may be misleading and physically meaningless. An alternate view of this is that in some intermediate-type galaxies, the bulge-disc decomposition simply reflects an empirical description of the surface brightness profile of star light. Another weakness of this method is that bulge-disc decomposition using the Sérsic function (described below) appears deceptively simple, yet the procedure carries with it a high degree of degeneracy.

Bulges are also identified as a 3-dimensional structure that "bulge" from the disc plane in the z direction. These structures are most easily identified in edge-on galaxies where bulging central structures are observed in the vast majority of massive galaxies (Kautsch et al. 2006). A significant caveat, however, to studying bulges in edge-on systems is that dust extinction from the disc significantly affects the light of the bulge, especially in galaxies with smaller bulges. Secondly, boxy bulges (Bureau and Freeman 1999) which are the result of bars (Athanassoula 2005b) can complicate the interpretation of bulge thickness. Two edge-on galaxies could have equally thick centers, one with a boxy-bulge and the other with a round thick bulge, which would be missed by blanket thickness cuts.

Kinematics can be used to identify a low-angular momentum and higher z-dispersion structure at the center of a high angular momentum thin disc. For example Fabricius et al. (2014) show that kinematics of the intermediate-type galaxy NGC 7217 clearly separates into two components one with high dispersion (the bulge) and the second with low dispersion (the disc). These components are consistent with a photometric bulge-disc decomposition. Ideally such procedure could be carried out on large numbers of galaxies in forthcoming data releases of SAMI (Croom et al. 2012) and MaNGA (Bundy et al. 2014). However, it is not clear that either survey has sufficient spatial or spectral resolution to apply this technique.

3.1.2 Outline

Kormendy and Kennicutt's (2004) review and Athanassoula (2005a) make a strong case that multiple types of bulges exist, and that this is likely reflecting different channels of bulge formation and galaxy evolution. In this review, we discuss the identification of bulges of different types, attempting to provide practical means of classifying bulges.

3.2 Identifying Pseudobulges with Morphology

There are multiple lines of reasoning that motivate the morphological distinction of different bulge types. First, empirically speaking, results from *Hubble Space Telescope* (HST) imaging surveys are quite clear that there is not one single type of morphology that can be associated with regions of galaxies dominated by bulge light. This is in contrast to the description of bulges given in the Carnegie Atlas of Galaxies (Sandage and Bedke 1994), in which bulges are described as having no evidence of a disc or "pure E" morphology. The presence of spiral structure (see, for example, Fig. 3.2) is in stark contrast to this definition. If the structure exhibiting the spiral, ring, or bar pattern is dominating the light then the classifier can be fairly confident that the dynamical state of the system better reflects that of disc kinematics than that of an elliptical galaxy. Morphology is therefore a physically motivated classification. However, we have to remind the reader of the problem in identifying such a discy structure as a distinct component as opposed to just being the physical state of the central disc.

From a certain point of view the simplest means of identifying bulges of different types is morphology. The main requirement is sufficient spatial resolution to identify small-scale features. Data from HST has made this a very straightforward process in which high quality identification of features like spiral structure can be done on nearby galaxies (<50 Mpc). Typically, in this practice the user identifies, by-eye, features that are associated with disc morphology (such as spirals, rings, and bars) inside the region where the bulge dominates the light of the galaxy. Systematic studies comparing morphological bulge classification at different wavelengths would be useful. It stands to reason that broadband photometry at wavelengths in the middle of the optical spectrum (i.e. V to I) are best suited. If the filter is too blue, the light becomes too sensitive to dust effects. Although it has been shown that the morphological features identifying pseudobulges are present in near-IR images (Fisher and Drory 2010), these features become difficult to see at longer wavelengths (e.g. *JHK* bands).

Results from HST reveal that the centers of relatively "early type" galaxies (Sa-Sb) frequently contained spiral structure and show little evidence of a smooth featureless bulge (Carollo et al. 1997). In Fig. 3.2, top left panel, we show an example of nuclear spiral morphology. In this example, NGC 4030, the spiral is face-on and quite easy to identify. When present, the spiral structure frequently extends throughout the entire bulge, and reaches to the very center of the bulge region. In the centers of later type galaxies, such dusty spiral and non-smooth morphology becomes much more common than smooth, round bulges (Böker et al. 2002). In very nearby galaxies, e.g. NGC 5055, the presence of spiral structure that extends all the way to galaxy centers was recognized as early as 1961 in the Hubble Atlas (Sandage 1961). Buta and Crocker (1993) identify a sample of nuclear spirals which they call pseudorings, placing first estimates on sizes (typical diameters of $\sim$1 kpc). The advent of surveys from HST make it clear that nuclear spirals are very common in Sa-Sm galaxies (Fisher and Drory 2011). Fisher and Drory (2008) introduce a

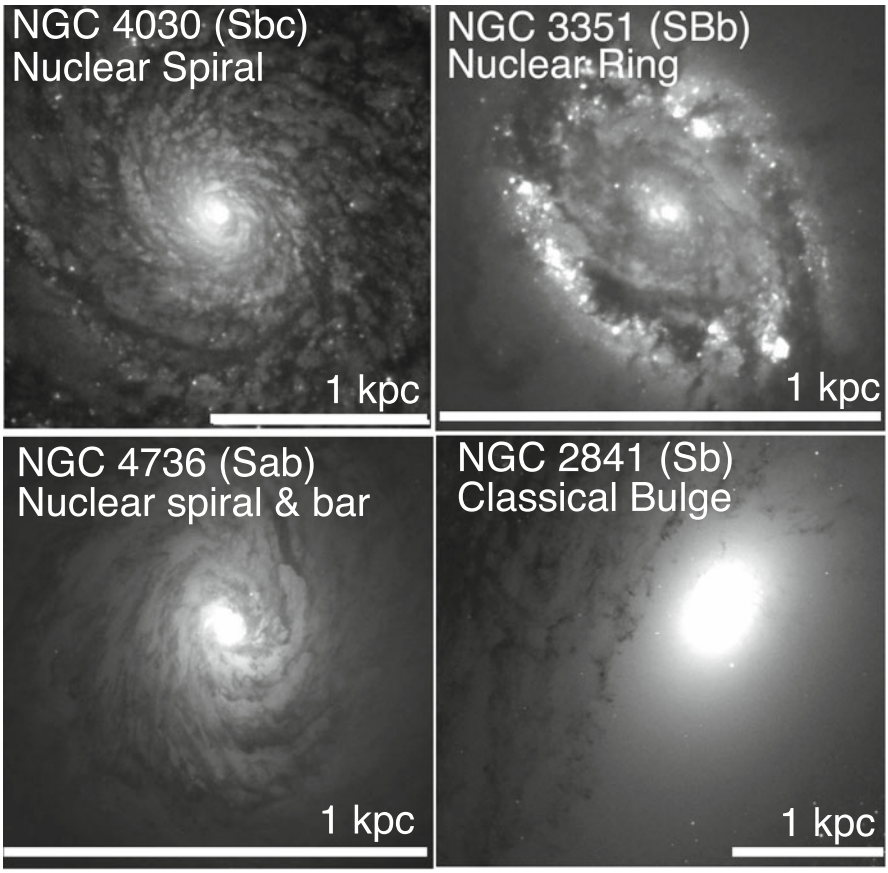

Fig. 3.2 Examples of bulge morphologies are shown using optical images from HST. The detectors and filters are NGC 4030: PC F606W; NGC 3351: PC F606W; NGC4736: PC F555W; and NGC 2841: ACS/WFC F435W. The *white line* in each panel represents 1 kpc. There is an extreme difference in these galaxies between pseudobulge morphologies (nuclear ring, spiral and bar) and classical bulges. In cases such as this, morphological diagnosis of bulge types is relatively straightforward

secondary category of spirals referred to as nuclear patchy spirals. These are almost exclusively found in later type (Sc-Sd) galaxies with very small bulges.

A "nuclear ring" is a ring of stars and/or intense star formation found in the central region (radius <1 kpc) of a disc galaxy (Buta and Crocker 1993; Buta et al. 2007). Nuclear rings are often relatively easy to identify, and they are typically very bright due to their large star formation rates. Nuclear rings are separate from "inner rings" that are commonly found at the end of bars (de Vaucouleurs et al. 1991). Nuclear rings occur in roughly 20 % of spiral galaxies (Knapen 2005). Galaxies with nuclear rings are very likely to be barred (Comerón et al. 2010; Knapen 2005). In Fig. 3.2 we show an example of a prominent nuclear ring in the nearby disc galaxy

NGC 3351. Buta and Crocker (1993) identify galaxies with both nuclear rings and "pseudo-rings". A pseudo-ring is when the ring is not fully formed, and does not extend 360° around the galaxy center. In fact, it may commonly refer to nuclear spirals.

Studies focusing on barred spirals find that secondary (nested) bars are frequent (Erwin and Sparke 2002; Erwin et al. 2004). As many as 40 % of S0-Sa galaxies with bars contain a secondary bar, extending to radii of 0.2–0.8 kpc. Many of the studies on secondary bars focus on early-type galaxies where there is less dust and the bars are easier to identify. Secondary bars in later-type galaxies are easily obscured by dust, and often hard to identify for that reason. Even in unobscured galaxies, it is useful to over-plot isophote contours of the galaxy to identify nuclear bars (as outlined by Erwin and Sparke 2002, also Erwin 2004). In Fig. 3.2 (bottom left panel) we show a galaxy with both a nuclear spiral and a nuclear bar. The bar is aligned north-to-south in the image. A number of simulations focus on the formation of galaxies with nested bars (Heller et al. 2007; Debattista and Shen 2007; Shen and Debattista 2009). These simulations generally find that the nuclear bars are rapidly rotating structures that form easily within barred discs.

Classical bulges are morphologically identified, in the ideal case, as having smooth centrally peaking isophotes that do not show any evidence of disc-like structure such as those described above. In Fig. 3.2 we show NGC 2841 as an example. In the image the smooth classical bulge is seen in the center, and at larger radii the effects from the disc become apparent. The presence of some extinction, indicating dust and gas, does not preclude a system from being a classical bulge; however in classical bulges when defined by morphology, such dust is not a dominant feature, nor is it embedded in a spiral pattern.

There are a number of caveats associated with morphological classification of bulge types. Using morphology as a means of identifying physically distinct phenomena is an inherently biased process by the person doing the identification. Two individuals can come to different conclusions about what is or is not a spiral pattern, or just a wisp of dust. Even with HST data, morphological classification is only possible at very low redshifts $z < 0.05$. Finally, in the absence of Galaxy Zoo type of analysis (e.g. Lintott et al. 2011) morphology is not a quantitative science; this limits both our ability to interpret the meaning and also to apply such analysis to large samples of objects.

Combining all disc-like structures (nuclear rings, nuclear spirals, and nuclear bars) into a single category of "pseudobulges" makes the assumption that these objects are linked. The conditions under which nuclear rings form are likely different than that of a secondary bar, nonetheless, the unifying concept is that all three are structures that are associated with discs. Furthermore, there is no significant differences between the bulge Sérsic index, bulge-to-total ratio or half-light radius of bulges with these structures (Fisher and Drory 2008). The strongest difference appears to be between classical bulges and the rest of bulge morphologies.

In spite of the many caveats, morphological identification of bulge types seems quite useful. Bulges identified as pseudobulges using morphology are more actively forming stars (Fisher 2006), have more disc-like kinematics (Fabricius et al. 2012),

and occupy a different location in structural parameter space (Fisher and Drory 2010) than classical bulges. These correlations establish that by-eye classification can accurately mark important distinctions in bulge types, and will be discussed in more detail in subsequent sections.

3.3 Structural Properties of Bulges: Sérsic Index, Scaling Relations, and Shape of Bulges

Structural parameters returned from bulge-disc decompositions can be a very powerful means to identify pseudobulges. In theory, bulge-disc decomposition software can be run on very large numbers of galaxies. If one can robustly identify bulge-types from the properties in decompositions alone, it is then straightforward to generate strong constraints on the number of bulges of each type in different environments. In practice, this procedure is complicated by inherent degeneracies in the decomposition procedure.

The process of bulge-disc decomposition assumes that the radial surface brightness profile, $I(r)$, of a galaxy can be described by a linear combination of a small number of component structures, such that $I(r) = I_{\rm bulge}(r)+I_{\rm disc}(r)+I_{\rm other}(r)$, where $I_{\rm bulge}$ and $I_{\rm disc}$ describe the bulge and disc, and $I_{\rm other}$ describes any other structure in a galaxy.

There are a few systematic sources of uncertainty that should be taken into account to derive accurate parameters from bulge-disc decompositions. First, a well-known problem is accounting for galaxy structures that are neither bulge nor an exponential disc. Most commonly $I_{\rm other}$ describes light from a bar, but could also refer to rings, nuclei, or bright star forming spiral arms. Not taking a bar into account when modeling the light profile leads to systematic effects, such as overestimating the bulge-to-total ratio (B/T) by as much as a factor of 2, and also systematically overestimating the value of the Sérsic index (Gadotti 2008; Fisher and Drory 2008; Laurikainen et al. 2006). If the galaxy has a central point source, either AGN or nucleus, this must be accounted for as well or else the returned model will have an artificially large Sérsic index and B/T.

Resolution is a crucial parameter for determining accurate Sérsic model parameters of bulge-disc decompositions. If the bulge is of the size of the resolution element, information on the size (half-light radius) and shape (Sérsic index) are completely untrustworthy (Gadotti 2008; Fisher and Drory 2008). Gadotti (2008) suggests that at least 80 % of the half-light radius must be resolved. Fisher and Drory (2010) find that in order to determine accurate Sérsic indices of galaxies with small B/T, a resolution of 100 pc is preferred.

3.3.1 Using Sérsic Index to Identify Bulge Types

Typically, bulge-disc galaxies are decomposed using the Sérsic function (Sérsic 1968) to describe the bulge. In this model the radial light profile in units of mag arcsec^{-2} of a galaxy can be described as

$$\mu_{\rm bulge} = \mu(r_{\rm e}) + b_{\rm n}\left[\left(\frac{r}{r_{\rm e}}\right)^{1/n_{\rm b}} - 1\right], \tag{3.1}$$

where $n_{\rm b}$ is the Sérsic index of the bulge; r represents radius, $r_{\rm e}$ is the radius containing half the light of the bulge, $\mu(r_{\rm e})$ is the surface brightness at $r_{\rm e}$, and $b_{\rm n} = 2.17n_{\rm b} - 0.355$. The above formula, known as the Sérsic function (Sérsic 1968), has been shown by a number of authors to describe the shape of elliptical galaxy profiles quite well (Caon et al. 1994). The case of a Sérsic function with $n_{\rm b} = 1$ is equivalent to an exponential, commonly used to describe discs. The case of $n_{\rm b} = 4$ is equivalent to the de Vaucouleurs profile used historically for E-type galaxies. There are a number of detailed discussions of the Sérsic function and its properties; for further reading see Graham and Driver (2005).

The Sérsic index of bulges is now widely used as a means to identify bulges, based largely on its correlation with other bulge properties (e.g. Fisher and Drory 2008). The first evidence came from early surveys of bulge-disc decomposition in which it was clear that many bulges are better fit by double exponential profiles than by a traditional de Vaucouleurs profile (Andredakis and Sanders 1994; Courteau et al. 1996). This was eventually generalized to show that all bulges are better described using the Sérsic function (Andredakis et al. 1995), and that later-type galaxies tend to have lower values of $n_{\rm b}$. Results using HST images find that bulges with disc morphology are more likely to have shallow, more like exponential, surface brightness profiles (Scarlata et al. 2004).

Using ∼100 galaxies with HST imaging, Fisher and Drory (2008) compare the morphology of bulges to the associated bulge Sérsic index from detailed bulge-disc decompositions. They find that there is a clear bimodal distribution of Sérsic indices in galaxies. To reduce uncertainty in the Sérsic index, the authors created composite surface photometry using HST data to measure the surface brightness profile of the inner 10 arcsec, and a set of deep wide-field images to measure the surface brightness profile of the outer parts of the galaxy (a similar procedure is discussed in Balcells et al. 2003 and Kormendy et al. 2009). The result is a surface brightness profile that covers a very large dynamic range in radius, and is thus able to reduce uncertainty in Sérsic index, and better break the degeneracy between n and $r_{\rm e}$ (Graham et al. 1996). These decompositions reveal that 90 % of bulges with morphology that indicates a pseudobulge (as described in the previous section) have $n_{\rm b} < 2$, and all classical bulges and elliptical galaxies have $n_{\rm b} > 2$. The authors followed up on this result with a larger sample of galaxies with near-IR photometry (still combining HST and in this case Spitzer IRAC 3.6 μm; Fisher and Drory 2010).

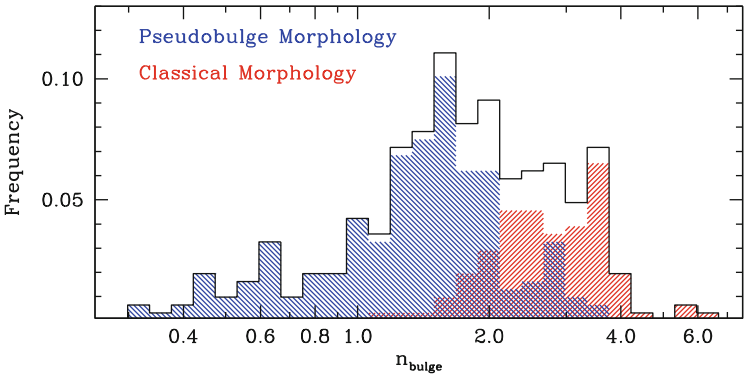

Fig. 3.3 The distribution of bulges Sérsic indices from a sample of 308 nearby bulge-disc galaxies with both published bulge-disc decompositions and available data in the HST archive for bulge morphology diagnosis. The distribution of $n_{\rm bulge}$ in galaxies with classical bulge morphology shown to be clearly different than that of pseudobulges

The result is the same, all classical bulges are found to have $n_{\rm b} > 2$ and over 90 % of pseudobulges have $n_{\rm b} < 2$.

To double check the correlation of bulge Sérsic index with high resolution bulge morphology we compile a sample of 308 galaxies that have both published bulge-disc decomposition and also have data in the HST archive from which we can determine the morphology of the bulge. The sources of $n_{\rm b}$ are Fisher and Drory (2008, 2010, 2011), Fabricius et al. (2012), Fisher et al. (2013), Laurikainen et al. (2010) and Weinzirl et al. (2009). In the case of overlapping galaxies we take the result that is based on the finest spatial resolution, though typically the spread in Sérsic index is not large, $\Delta n_{\rm b} < 0.2$. In a few galaxies ($\sim$10) the spread in $n_{\rm b}$ is large, $\Delta n_{\rm b} > 1$. We drop these galaxies assuming that the Sérsic index is poorly constrained and not trustworthy. The total sample combines decompositions from three independent fitting procedures (described in Fisher and Drory 2008; Weinzirl et al. 2009; Laurikainen et al. 2010), and contains 106 S0-S0/a, 71 Sa-ab, 62 Sb-bc, 61 Sc-cd, 10 Sd-dm galaxies.

In Fig. 3.3 we show the distribution of Sérsic indices in the combined sample. There is a clear correlation between bulge type and Sérsic index. The choice of $n_{\rm b} = 2$ as the dividing line is not arbitrary, but rather is justified by the coincidence of this value with the turnover in the two distributions. This is clearly evident in the figure. The sample contains 102 classical bulges and 87 % of those classical bulges have $n_{\rm b} > 2$, conversely in the sample we identify 205 galaxies as having pseudobulges and 86 % of these have $n_{\rm b} < 2$. If we consider only those galaxies with Hubble type Sa and later, the frequency of classical bulges with $n_{\rm b} < 2$ drops to 7 %, and the frequency of pseudobulges with larger Sérsic index ($n_{\rm b} > 2$) becomes only slightly lower, 11 %. We note that although not completely devoid of gas, S0 galaxies have significantly less dust and gas (Young et al. 2011), therefore identifying features such as nuclear spirals is much more difficult in these galaxies.

In addition, if we restrict the sample to only those galaxies where the resolution is better than 300 pc, the correlation becomes stronger. In the improved-resolution sample, we find that only 6 % of the classical bulges have low Sérsic index and roughly 9 % of pseudobulges have high Sérsic index. If we exclude both S0 galaxies and those galaxies that are poorly resolved, the correlation improves still. In this case only 4 % of classical bulges have $n_b < 2$.

Exactly at what resolution the use of Sérsic index becomes unreliable is difficult to say. Nonetheless, even with the very loose cut applied here we already detect a difference in Sérsic index. As mentioned above, fitting Sérsic functions to galaxy light profiles is a very degenerate procedure. If a bulge diameter approaches the beam width of the data set, clearly using Sérsic index to diagnose bulge types would be unreliable in this scenario. Thus, if bulges are typically ∼2 kpc in diameter, then surveys using SDSS only to measure bulge properties should not extend beyond $z = 0.03$ or a distance of ∼120 Mpc, in which a seeing of 1.5 arcsec would allow for a few resolution elements to sample the bulge.

We remind the reader that this correlation is an empirical result. Broadly speaking, the observation that pseudobulges would have nearly-exponential surface brightness profiles, and thus be more similar to what is observed in discs, is consistent with the general observation that pseudobulges are disc-like. Yet, the physical reason that such a sharp dividing line in Sérsic index at $n_b = 2$ exists separating bulges of different morphological types, is not well understood. Furthermore, the exact distribution of Sérsic indices for pseudobulges and classical bulges is hard to establish for multiple reasons. First, if classical bulges and elliptical galaxies are truly a single class of object, then ellipticals should be included in any analysis of surface brightness profiles. Including early-type galaxies would lead to more galaxies with larger Sérsic index (Caon et al. 1994; Kormendy et al. 2009; Blanton et al. 2005). Secondly, galaxies in which both a pseudobulge and classical bulge are present would complicate this analysis. Such systems have been estimated to make up ∼10 % of bulge-disc galaxies (Fisher and Drory 2010). Thirdly, it is difficult to compile large samples of unbiased pseudobulge identification methods that are independent of the Sérsic index. Nuclear morphology enabled by the HST archive and Sérsic index are the most widely available sources of pseudobulge detection. It is difficult to obtain, for example, kinematics with sufficient spatial and spectral resolution on a large number of galaxies. Also, as we will discuss later using star formation rates and/or stellar populations is subject to biases in the detected systems.

The correlations of structural properties with Sérsic index show a distinct change at $n_b = 2$ (Fisher and Drory 2008, 2010). In Fig. 3.4 we show the correlation of bulge Sérsic index with half-light radius and effective surface brightness. Bulges with $n_b > 2$ show behavior consistent with that of E-type galaxies, that is to say a positive correlation between galaxy size (or luminosity) and Sérsic index (e.g. Graham et al. 1996; Khosroshahi et al. 2000; Kormendy et al. 2009; Falcón-Barroso et al. 2011). Bulges with $n_b < 2$ do not participate in these correlations, and in fact show a lack of scaling relationships between n_b and other structural quantities. This is clearly evident in $r_e - n_b$ parameter space.

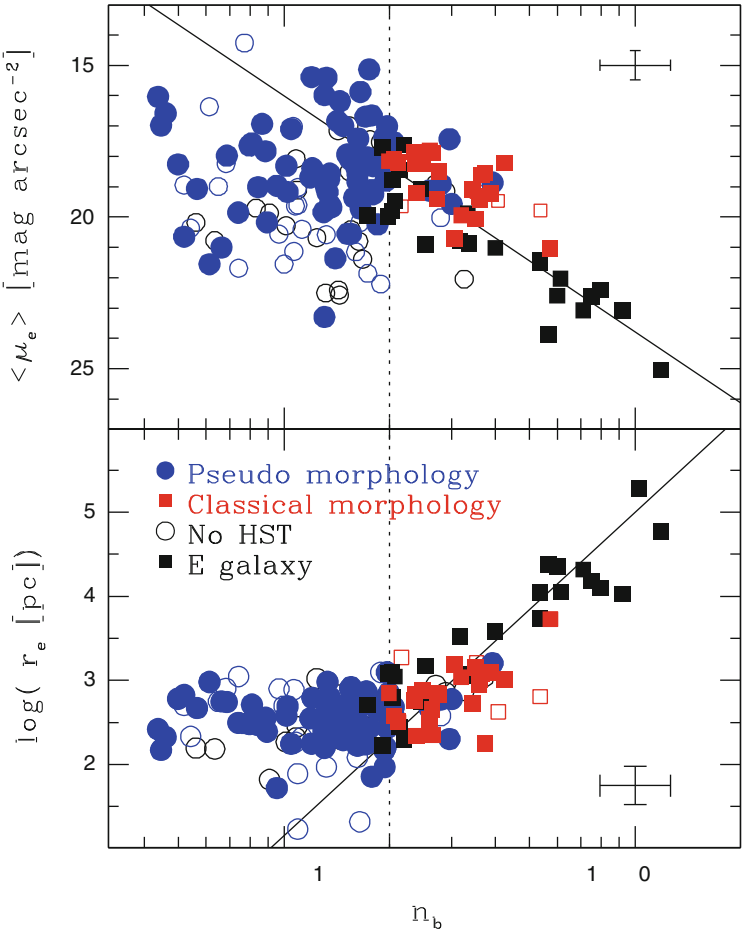

Fig. 3.4 The above figure, adapted from Fisher and Drory (2010), shows the correlation of bulge Sérsic index with structural properties of bulges. There is a clear and distinct break in these correlations at Sérsic index of $n_b = 2$. This break is consistent with a picture in which bulges with larger Sérsic index ($n_b > 2$) are physically similar to elliptical galaxies, and those with smaller Sérsic index ($n_b < 2$) are a different class of object

In following sections we will discuss in more detail the correlations of bulge Sérsic index with kinematic, interstellar medium, and stellar population properties of bulges. Bulges with $n_b < 2$ are observed to have higher fractions (and surface density) of gas (Fisher et al. 2013), which is more actively forming stars (Fisher et al. 2009; Gadotti 2009; Fisher and Drory 2010), and has more disc-like kinematics (Fabricius et al. 2014) when compared to bulges with $n_b > 2$. These results, and those in Fig. 3.4, suggest that the Sérsic index is sensitive to physical differences between bulge types.

3.3.2 *Differences in Bulge Types Fundamental Plane Parameter Space*

Elliptical galaxies follow a very well-known set of correlations between surface brightness, radius, and velocity dispersion, known as the "fundamental plane" (Djorgovski and Davis 1987; Faber et al. 1989; Kormendy 1977a; Bender et al. 1992). These relationships are derived from the assumption that elliptical galaxies are virialized systems, with small – but significant – deviations corresponding to variation in mass-to-light ratios and the non-homology of such galaxies. Because simulations predict that structural scaling relations like the fundamental plane are likely to emerge through the merging processes that form elliptical galaxies through violent relaxation (e.g. Boylan-Kolchin et al. 2006), it would seem reasonable that if pseudobulges, which are more discy, form significantly differently than elliptical galaxies and classical bulges they would not necessarily occupy the same correlation.

There is, however, a danger to using the fundamental plane to identify bulge types. There is no independent theory that predicts the location of pseudobulges in these correlations, and there is nothing to say that in certain projections of fundamental plane correlations pseudobulges and classical bulges would not overlap. We will continuously argue throughout this review, that there does not seem to be a single ideal way to identify pseudobulges and classical bulges. A comprehensive approach that combines multiple indicators of bulge types is therefore called for.

Carollo (1999) shows that the centers of spiral galaxies that contain pseudobulges have lower surface density than classical bulges. The location of bulges in projections of the fundamental plane is studied with larger samples using full bulge-disc decomposition in Gadotti (2009) and also Fisher and Drory (2010). Both of these works find results that are consistent with Carollo (1999), that is a population of bulges with lower surface brightness than corresponding elliptical galaxies of similar size or luminosity.

In Fig. 3.5 we show the relationship between $< \mu_e >$ and r_e (Kormendy 1977a). The data set we use in this figure is taken from Fisher and Drory (2010) (left panels) and Gadotti (2009) (right panels). The data set from Fisher and Drory (2010) is considerably finer spatial resolution and uses near-IR data less affected by variations in mass-to-light ratios and extinction. The Gadotti (2009) sample is a much larger, uniformly selected sample of nearly 10^3 galaxies from SDSS, and therefore offers a statistically sound data set. Both of these studies find essentially the same result, a significant fraction of bulges deviates toward low surface brightness. Furthermore, those bulges that deviate from this relation are much more likely to have low Sérsic index. Based on these results, reproduced in Fig. 3.5, it is clear that if a bulge deviates significantly toward low surface brightness from the Kormendy (1977a) relation, then this is strong evidence that this bulge is a pseudobulge.

Identifying bulges as classical bulges because they are consistent with the $< \mu_e > -r_e$ relationship, however, is less robust. Gadotti (2009) marks bulges contained within the spread of the Kormendy (1977a) relation as classical bulges.

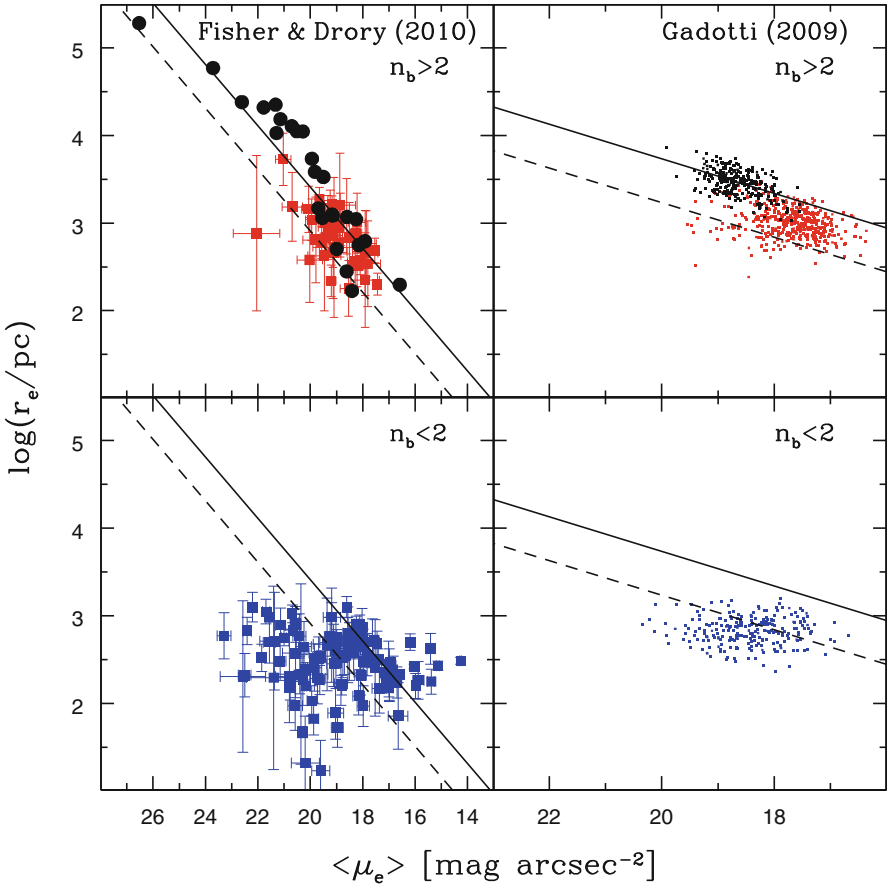

Fig. 3.5 Here we show the relationship of $< \mu_e > -r_e$ for bulges (*red* & *blue squares*) and elliptical galaxies (*black circles*) using data from composite profiles of HST/NICMOS, Spitzer 3.6 μm and 2MASS data (the magnitude scale is set to match 3.6 μm scale) from Fisher and Drory (2010) (*left*), and SDSS *i* Gadotti (2009) (*right*). In both cases we show a correlation fit to the ellipticals (*solid line*) and a line set to contain the spread in elliptical galaxies (*dashed line*). The results of these studies are essentially consistent, there is a significant population of bulges that deviates toward lower surface brightness from this projection of the fundamental plane

They argue that at least in this parameter space, these bulges are structurally similar to elliptical galaxies. This makes the assumption that other physical processes cannot make a bulge with similar values of surface brightness and size. Absent a result from simulations, we cannot know if that assumption is true.

We can look at the properties of those bulges that are consistent with the Kormendy (1977a) relation to determine how homogeneous a class they are. In Fig. 3.6 we show the distribution of 3.6 − 8.0 μm color (Fisher and Drory 2010) and $D_n(4000)$ (Gadotti 2009) for the bulges that are consistent with the Kormendy

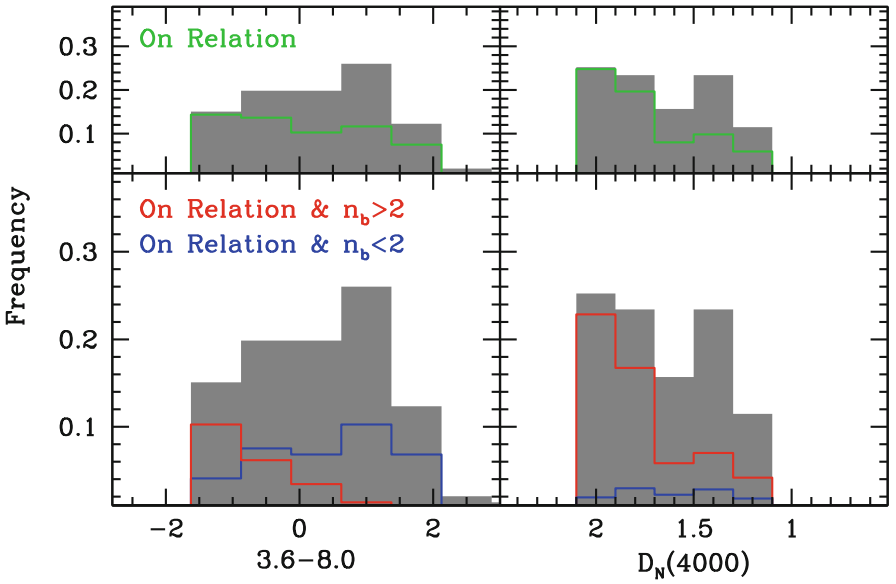

Fig. 3.6 The above figure aims to examine the properties of bulges that are consistent with the $< \mu_e > -r_e$ relationship shown in Fig. 3.5. The *left panels* show distribution of 3.6–8.0 μm colors from Spitzer IRAC data, measured in Fisher and Drory (2010). Higher values of 3.6–8.0 indicate, roughly speaking, larger specific star formation rates. The *left panels* show $D_n(4000)$ values for bulges (excluding E galaxies) from Gadotti (2009). Smaller values of $D_n(4000)$ indicate younger populations. Note that we have inverted the x-axis of $D_n(4000)$ so that in all panels younger, higher star forming bulges are on the *right side of the panel*. The *grey shaded region* shows the distribution for the entire sample. The *green line* represents all those bulges that are consistent with the $< \mu_e > -r_e$ relationship. The *blue line* is those bulges that are consistent with the $< \mu_e > -r_e$ and have $n_b < 2$. The *red line* shows the distribution for bulges consistent with $< \mu_e > -r_e$ and have $n_b < 2$

(1977a) relation. Larger values of $3.6 - 8.0$ μm color imply more active star formation per unit stellar mass. Smaller values of $D_n(4000)$ imply younger stellar populations; for display purposes we plot the $D_n(4000)$ values in reverse order, so in both panels younger, more star forming systems are on the right side of the panel. In both samples it is clear that selecting bulges only by the location in $< \mu_e > -r_e$ parameter space does not uniquely separate bulges. In the bottom panel we show the combination of using both the Kormendy (1977a) relation and n_b as selection criteria for bulge types. In the Fisher and Drory (2010) sample this more cleanly identifies classical bulges as non-star forming systems.

In summary, using the fundamental plane as bulge type diagnostic carries certain caveats. If a bulge significantly deviates toward lower surface brightness from the Kormendy (1977a) relationship between $< \mu_e >$ and r_e, then this is strong evidence that bulge is a pseudobulge, based on studies of its star formation rate, Sérsic index, and nuclear morphology. However, if a bulge has parameters consistent with the fundamental plane, from an empirical point-of-view we cannot say what type of

bulge this is. For example, if the aim of a study is to isolate a sample of bulge-disc galaxies that resemble M31 (a prototypical classical bulge), then using $< \mu_e > -r_e$ alone is clearly insufficient, and as we show in Fig. 3.6 this method selects a number of star forming bulges. Also, Fisher and Drory (2010) show that a number of bulges that are consistent with the Kormendy (1977a) relationship have nuclear morphology that, unlike M31, resembles a disc.

3.4 The Interstellar Medium and Stellar Populations of Pseudobulges and Classical Bulges

Historic work concluded that bulges are uniformly old and devoid of star formation (e.g. Whitford 1978). This led to the widely held view that all bulges are old and inactive. This turns out to be true for some bulges, but it is not universally true by any means. For example, in the prototypical classical bulge of M 31, the dust SED is consistent with being completely heated by the old stars, and shows no evidence for new star formation (Draine et al. 2014), and also the stellar populations indicate a uniformly old population of stars, with mean ages above 12 Gyr (Saglia et al. 2010). However, work in the last 15–20 years shows that many bulges contain cold gas, actively form stars and can have short mass doubling times, and often have intermediate-to-young light-weighted stellar ages.

Peletier and Balcells (1996) show that some bulges are indeed quite blue, and that in general bulges have similar optical colors as the surrounding disc. Similarly, Regan et al. (2001) finds using interferometric observations of CO(1-0), that some bulges are as gas rich (from L_{CO}-to-L_K ratios) as the associated outer disc. In the past 10 years data from Spitzer Space Telescope, GALEX UV telescope, and CO interferometry from BIMA, OVRO, CARMA & PdBI have greatly improved our ability to measure star formation rates in bulges. We can now robustly say that specific star formation rates and gas fractions in the bulge region of nearby galaxies are often very high (Sheth et al. 2005; Jogee et al. 2005; Fisher 2006; Fisher et al. 2009, 2013; Fisher and Drory 2011). Also, bulges can contain young stellar populations (Gadotti and dos Anjos 2001; MacArthur et al. 2004; Peletier et al. 2007; Ganda et al. 2007). See also Kormendy and Kennicutt (2004) for a review.

From a physical perspective it makes sense that pseudobulges would be systematically younger with more active star formation than classical bulges. The present model is that classical bulges formed in the early Universe, either through merging (Aguerri et al. 2001; Robertson et al. 2006) or as the result of clumpy disc instabilities (Noguchi 1999; Elmegreen et al. 2008). The former become less frequent, and the latter are extremely rare below $z \sim 1$. Conversely, galaxies with pseudobulges either did not experience these processes, or they were significantly less pronounced, the resulting galaxy was able to evolve secularly for long periods of time and still does. Some of them still contain significant amount of gas to fuel internal evolution of the bulge. Also, the presence of a classical bulge may in fact

stabilize a galaxy against star formation, and especially the secular inflow of gas (Martig et al. 2009). This process known as "morphological quenching" may act to reinforce a correlation with bulge structural properties and bulge star formation rates.

Before going on, we must point out a simple, yet critical, caveat to using stellar populations, star formation rates, and gas fractions to identifying pseudobulges. Gas stripping by cluster environments (as described by Kenney et al. 2004) can shut down star formation in a galaxy. If such a galaxy had previously formed a pseudobulge, that bulge would quickly appear inactive and old. Also, simulations show that pseudobulges can form in dissipationless systems (Debattista et al. 2004). It is therefore important that one should not use the absence of star formation alone as a reason to suggest a galaxy does not contain a pseudobulge.

To be clear, when we refer to "bulge" star formation rates and gas masses what we really mean is the star formation rate (or gas mass) inside the region of the galaxy where the bulge dominates the light. Cold gas, and thus star formation, happens in a thin disc (García-Burillo et al. 1999) of scale height of $\leq$100 parsecs. Bulge-disc decompositions, however, do not typically consider the thickness of the bulge. Indeed, the thickness of pseudobulges is very poorly constrained. Some are likely very thin (as argued by Kormendy 1993), however, given the common presence of resonant phenomena it is likely that many are thickened. If the goal is to understand how properties of the bulge evolve, however, then comparing the entire mass (or luminosity) of the bulge stars to the entire rate of star formation in a bulge seems appropriate.

3.4.1 A Brief Aside on Measuring Star Formation Rates in Bulges

The measurement of star formation rates in galaxies, *SFR*, is typically done by means of a tracer of the amount of young stars present. This field has greatly advanced in the past decade (Kennicutt 1998; Calzetti et al. 2007; Kennicutt et al. 2009; Leroy et al. 2012; Kennicutt and Evans 2012). Because the emission from O and B stars heavily dominates the UV spectral range, it is straightforward to argue that $SFR \propto L_{\rm UV}$. The calibration of such a relationship can be found in Salim et al. (2007). For bulges, data from the GALEX UV space telescope is well suited to resolve $\sim$1 kpc in galaxies within 40 Mpc. An alternative approach is to use emission from HII regions, typically this is done using the Hα flux, assuming in this case that $SFR \propto L_{H\alpha}$.

A difficulty to estimating the emission from young stars is that dust absorbs UV/optical emission. This is especially important for galaxy centers (i.e. bulge regions), which experience more extinction (Peletier et al. 1999; MacArthur et al. 2004). In fact, we know from studies of our own galaxy that star formation can occur

in heavily obscured regions (for review Evans 1999; Kennicutt and Evans 2012), and therefore much of the light may be missed in optical observing campaigns.

One way to overcome the effects of extinction would be to measure the flux of a Hydrogen emission line in the near-infrared range (e.g. Pa α emission). However, such measurements can be difficult to make, and are often low signal-to-noise. Alternatively, data from *Spitzer Space Telescope* allows us to directly probe the re-radiation in the infrared of the energy absorbed by the dust in the UV/optical, for example using emission at 24 μm (Calzetti et al. 2007). A common approach in the current literature is to combine different star formation tracers (e.g. Kennicutt et al. 2009) to account for both the unobscured star formation (traced by UV or Hα) and the obscured star formation (traced by infrared emission).

The 8 μm emission is dominated by polycyclic aromatic hydrocarbons (often called PAHs). At present, and with respect to measuring the properties of bulges, a significant advantage of 8 μm maps available from Spitzer is that they have significantly finer spatial resolution (beam size of Spitzer IRAC 8 μm data is $\sim$2 arcsec, roughly 3 times better than 24 μm maps with MIPS). However, flux from the 8 μm emission is not reliable as a direct, one-to-one, indicator of the star formation rate. Calzetti et al. (2007) show that the correlation between continuum-corrected 8 μm flux and Pa α flux depends on both environment and metallicity. In light of this, we limit our use of PAH emission to mostly an on/off metric of activity, separating star forming bulges (bright 8 μ emitting bulges) from non-star forming systems.

A second issue in measuring star formation in galaxy bulges is the contamination of the metrics of star formation by old stars. Old stellar populations make a measurable contribution of light at UV wavelengths and lead to an overestimate of the star formation rate (e.g. Cortese et al. 2008). Also, old stars can heat dust and thereby increase the 24 μm flux. These problems are especially pronounced in bulges where the surface density is very high. In this case the flux in tracers used to probe star formation is actually a combination of contributions from old and young stars. Leroy et al. (2012) study this in galaxy discs by modeling the diffuse emission. They find that typically roughly 20 % of the emission at 24 μm can be attributed to evolved stellar populations. Fisher et al. (2013) investigate bulges specifically and find similarly that in typical star forming bulges the star formation rate is decreased by roughly 20 % when accounting for old stellar populations. Both Leroy et al. (2012) and Fisher et al. (2013) show that this effect is stronger in regions of low star formation. Fisher et al. (2013) also shows, as expected, that this effect is more pronounced when the surface density of star light is higher. For example, in the bulge of M31, Draine et al. (2014) find that essentially all of the dust emission is accounted for by heating by stellar populations.

3.4.2 Active Star Formation and More Gas is Strongly Correlated with Bulge Types

Though there is a long history of evidence that many bulges are actively forming stars, and that star formation is likely significantly altering the stellar structure of a bulge (Kormendy and Kennicutt 2004, for review, and outlined above), direct comparisons to bulge classifications began mostly recently. A general summary is that if a bulge is star forming, statistically speaking it likely has other pseudobulge properties (e.g. $n_{\rm b} < 2$, discy nuclear morphology). Conversely, if a bulge is not star forming it can have a large mix of properties, consistent with the discussion above. Also, a small subset of galaxies have star forming centers, but quiescent discs; these systems also have large bulge Sérsic index. A plausible scenario to explain these systems could be the recent accretion of a satellite directly into the galaxy center (e.g. Aguerri et al. 2001).

Fisher (2006) uses data from Spitzer Space Telescope and archival HST data to directly compare the morphological diagnosis of bulge types to the 3.6–8.0 μm color profiles of galaxies with pseudobulges and those with classical bulges. In this case, 3.6–8.0 μm color is a very rough proxy for specific star formation rate (star formation rate divided per unit stellar mass). They find that in galaxies with classical bulges, the color of the disc indicates active star formation, however there is a sharp break near ∼1 kpc where the color profile transitions to a non-starforming bulge. In contrast, there is no such transition in galaxies with pseudobulges. The pseudobulge is forming stars similarly to the outer disc. Fisher and Drory (2010) follow this by calculating the 3.6–8.0 μm color for ∼180 galaxies, and study other indicators of bulge type (morphology, Sérsic index, and $\mu_{\rm e} - r_{\rm e}$). They find that if a bulge has mid-IR colors satisfying 3.6–8.0 > 0, then that bulge has properties that resemble a pseudobulge (e.g. low n_b).

In Fig. 3.7, we compare the specific star formation rate and gas surface density of bulges to the bulge Sérsic index, using data from Fisher et al. (2009, 2013) and Fisher and Drory (2011). The results here re-iterate the results of these papers. In both panels, it is clear that active star formation and high surface densities of gas are exclusively found in bulges with low Sérsic index. It is worth pointing out that there is no a priori reason that the bulge Sérsic index would correlate with the bulge gas density; a similar correlation is recovered if one measures bulge gas density with a fixed radius (e.g. 500 pc) and if one uses the bulge radius as done here. These correlations imply that the separation of bulge types is likely tied to a physical distinction. The results in Fig. 3.7 continue to motivate that the separation of bulges into at least two categories is informative to the physics of galaxy evolution.

Using the star formation rate (or gas surface density) of a bulge alone to identify it as a pseudobulge or classical bulge is, statistically speaking, somewhat ambiguous. 8 % of bulges that have active star formation (defined as $SFR/M > 10^{-11}$ yr^{-1}) also have $n_{\rm b}$ that is significantly larger (considering error bars) than $n_{\rm b} = 2$. A similar result is true when considering $\Sigma_{\rm gas} > 75$ M$_\odot$ pc^{-2}. Therefore, if one discovers that a bulge has a very active gas rich center, this is strong evidence for

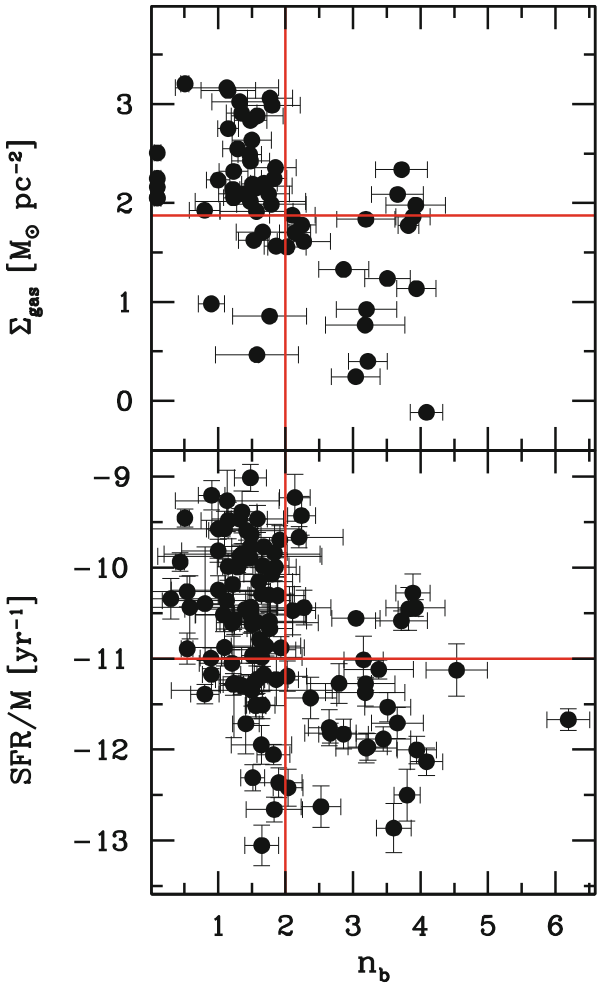

Fig. 3.7 The above figure compares the specific star formation rate (*bottom panel*) and gas surface density (*top panel*) of bulges to the bulge Sérsic index (Data are taken from Fisher et al. (2009), Fisher and Drory (2011) and Fisher et al. (2013). The *vertical lines* indicate the commonly used pseudo-classical bulge dividing line of $n_b = 2$, the *vertical lines* are set to guide the eye for $SFR/M = 10^{-11}$ yr and $\Sigma_{gas} = 75\ M_\odot\ pc^{-2}$)

that bulge being a pseudobulge. However, it is clear that when the star formation or gas density is low, one should not infer the bulge type. We recommend using star formation as a "second tier" method for identifying pseudobulges and classical bulges. For example if other metrics give ambiguous results but the bulge is very actively forming stars one could then conclude that the bulge is a pseudobulge.

3.4.3 Stellar Population Indicators and Bulge Types

Stellar population indicators in bulges show a wide range in properties (for a brief review see Peletier 2008). The topic of stellar populations is quite broad with a large variety of techniques and results that could easily fill its own review. We will concentrate on those results in which correlations, or the notable lack thereof, are relevant as diagnostics of bulge type. There is no set of stellar population parameters that is typical of a bulge. As mentioned before, an overwhelming majority of studies shows that the historic assumption that all bulges are uniformly old is simply not supported by the data (e.g. de Jong 1996; Peletier and Balcells 1996; Carollo et al. 2001; Proctor and Sansom 2002; Moorthy and Holtzman 2005).

There has been mixed evidence that optical color can be used as a means of identifying pseudobulges. Early results were promising. For example, Peletier and Balcells (1996) found a large spread in ages of bulges, and that average stellar age of bulges correlates with that of discs (young bulges are in young discs). This was confirmed in a much larger samples by Gadotti and dos Anjos (2001) and MacArthur et al. (2004). Carollo et al. (2001) find that the average $V - H$ color of exponential bulges with discy nuclear morphology (i.e. pseudobulges) is bluer than that of $r^{1/4}$ bulges.

Studies of the color of larger samples of bulges suggest that a single broadband color using optical or near infrared filters do not correlate strongly enough with other indicators of pseudobulges for reliable use. In Fig. 3.8 we show the distribution of bulge colors from Gadotti and dos Anjos (2001) (grey shaded area). We also cross-reference the sample from Fig. 3.3 against three papers which contain samples of

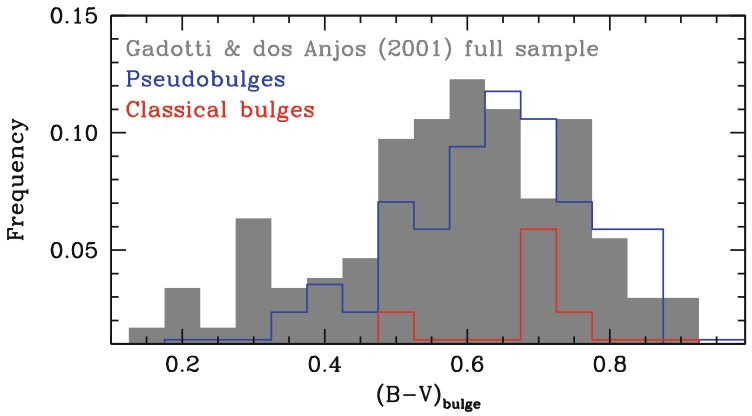

Fig. 3.8 Distribution of $B - V$ for bulges in the Gadotti and dos Anjos (2001) sample of galaxies (*shaded region*). The *blue line* represents those bulges that are identified as pseudobulges and the *red line* represents those that are classified as classical bulges (by combining Sérsic index, nuclear morphology and the Kormendy relationship). Though classical bulges are rarely found to be *blue*, pseudobulges very often have *red* optical colors

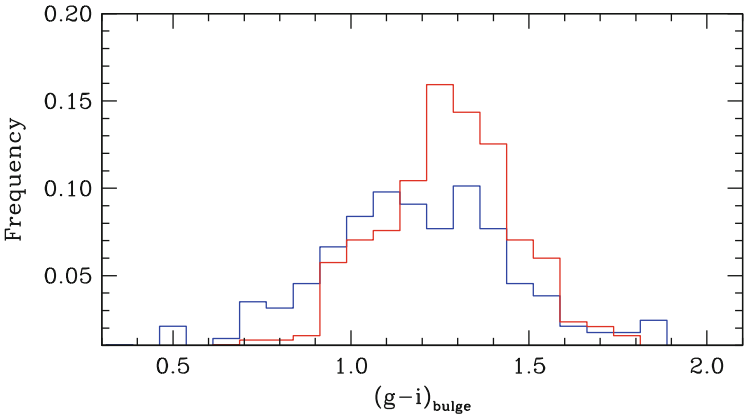

Fig. 3.9 Distribution of $g - i$ for bulges in the Gadotti (2009) sample of galaxies. The *blue line* represents those bulges that are identified as pseudobulges and the *red line* represents those that are classified as classical bulges (by combining Sérsic index, and the Kormendy relationship)

the same bulge color (Gadotti and dos Anjos 2001; Möllenhoff 2004; Fisher et al. 2013).[2] Pseudobulges are identified as bulges which have any of the following: $n_b < 2$, nuclear morphology that resembles a disc, and/or low surface brightness outliers from $\mu_e - r_e$ relation. The Gadotti and dos Anjos (2001) sample is shown to ensure that our bulge classification sample is not significantly biased. The distribution of classical bulges clearly skews to the redder colors, similar to Carollo et al. (2001). Blue bulges are far more likely to be pseudobulges. However unlike the previous methods of identifying pseudobulges there is not a significant range in this parameter over which classical bulges are not found.

The lack of a strong correlation between bulge color and type is likely not due to sample selection. Gadotti (2009) finds a similar result using $g - i$ colors. In Fig. 3.9 we show the distribution of bulge colors for the 670 bulge-disc galaxies from Gadotti (2009). Fernández Lorenzo et al. (2014) find a similar result with 189 galaxies, albeit the sample is biased only to include isolated galaxies.

Gadotti (2009) also compare the stellar populations tracer $D_n(4000)$ (Kauffmann et al. 2003) to bulge types (determined from bulge-disc decompositions). The break in the optical spectrum which occurs at 4000 Å is smaller for younger stellar populations (Bruzual A. 1983; Kauffmann et al. 2003, for description see), and is a good identifier of young or bursty populations. Gadotti (2009) find indeed that pseudobulges have on average smaller values of $D_n(4000)$ and therefore pseudobulges are more likely to be young, but again there is not a significant range that isolates one type of bulge.

[2]Fisher et al. (2013) use SDSS $g - r$, which we convert to $B - V$ via Smith et al. (2002) transformations.

Taken all together, these results suggest that there tends to be a preference for pseudobulges to be blue *on average* compared to classical bulges. This particular subject could benefit from a work with both a well-defined and large sample of galaxies that is well resolved. However, based on the data that presently exists, optical color on its own is not a reliable indicator of bulge-type.

Similar to the results from optical colors, studies of bulge ages using more robust techniques such as absorption line indices or spectroscopic synthesis, return mixed results (see Renzini 2006 and references therein for a discussion of these techniques). Proctor and Sansom (2002) shows that bulges are younger on average and have fewer metals than early type galaxies. Both Moorthy and Holtzman (2005) and Thomas and Davies (2006) find a wide spread in ages, and that many bulges in later type (Sb-Sbc) galaxies are quite old. MacArthur et al. (2009) find, similarly, that the fraction of mass in bulges that was formed in the past gigayear is quite small. Zhao (2012) uses the Sloan Digital Sky Survey to measure the stellar populations of bulges in a sample of 75 isolated galaxies. Bulge types are diagnosed using both Sérsic index and the $\mu_e - r_e$ relation, and they find that on average pseudobulges have more prolonged star formation than classicals. Zhao (2012) find no classical bulges that are younger than $\sim$6 Gyr (mass weighted age), conversely roughly 30 % of pseudobulges are found to be younger than this. However, the average age difference between the two populations of bulges is not very large.

Differences in stellar population indicators do exist between the bulges of different types. A particularly significant difference is found in the absorption line indices of bulges (Peletier et al. 2007; Ganda et al. 2007). It is well known that for elliptical galaxies the Mg_2 line index correlates well with velocity dispersion (e.g. Bender et al. 1992). Peletier et al. (2007) and Ganda et al. (2007) show that many bulges fall below this relation, especially those bulges with low velocity dispersion centers and/or those bulges in late-type galaxies.

In Fig. 3.10 we show that a strong connection exists between bulge type and absorption line indices, specifically Mg b and Fe5150. For this figure we show the central values of pseudobulges, classical bulges and elliptical galaxies taken from a sample combining data from Ganda et al. (2007), Peletier et al. (2007) and Kuntschner et al. (2010). We have classified bulges using bulge Sérsic index and bulge morphology. No classical bulge or elliptical galaxy has Mg b < 2.35 Å, conversely over 2/3 of pseudobulges have lower values. (See Ganda et al. 2007; Peletier et al. 2007; Kuntschner et al. 2010 for a discussion of these Lick indices.) Similarly, the lowest value of Fe5150 in classical bulges and elliptical galaxies is 3.97 Å whereas roughly 50 % of pseudobulges are found below this limit. As we show in Fig. 3.10, the Lick indices become particularly powerful when combined with the velocity dispersion. In each panel the dashed line is a best fit relationship to the E galaxies and classical bulges, the solid line represents a relation with the same slope, yet offset down in Mg b such that it separates pseudobulges and classical bulges.

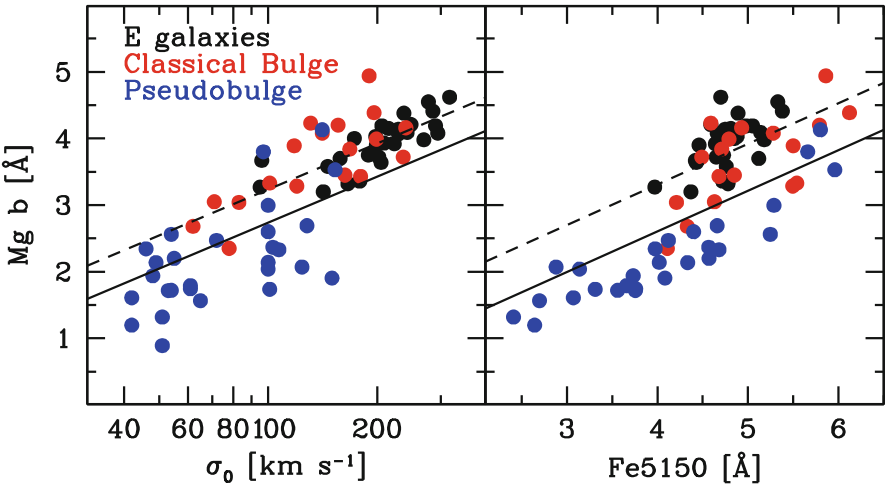

Fig. 3.10 The $Mg\ b - \sigma$ relationship for elliptical galaxies and bulges. We have restricted the control sample (*black dots*) to only the E galaxies from the SAURON sample to ensure that no pseudobulge galaxies are included. We take the bulge values from Peletier et al. (2007) and Ganda et al. (2007). Quantities for pseudobulges (identified with nuclear morphology, Sérsic index and the $\mu_e - r_e$ relation) are plotted as *blue points*, and the *red points* represent classical bulges. The *dashed line* is offset 0.5 Å below the best fit relation *(solid) line*. Only pseudobulges are found below this line

Based on this data set a bulge is a pseudobulge if it meets any of the following criteria:

1. Fe5150 $<$ 3.95 Å,
2. Mg b $<$ 2.35 Å,
3. $\Delta Mg\ b < 0.7$ Å compared to the $Mg - \sigma$ correlation,
4. $\Delta Mg\ b < 0.7$ Å compared to the $Mg - Fe$ relation.

All low Mg b outliers to the $Mg - \sigma$ relation are also outliers to the $Mg - Fe$ relation, but the reverse is not true. Conversely, there is more spread in the classical bulges in $Mg - Fe$. We also stress that because the sample of bulges includes a number of old S0 galaxies from the SAURON survey, using these Lick indices to identify pseudobulges and classical bulges appears to be robust against age. So it seems that using both of these relationships together would be a powerful tool for identifying pseudobulges, especially in the near future in which surveys such as SAMI and MANGA will measure absorption line strengths for large numbers of galaxies.

3.5 Identifying Pseudobulges and Classical Bulges with Kinematic Properties

Kinematic measurements of bulges provided some of the earliest evidence for the dichotomous nature of bulges. Kormendy (1982) points out that some bulges in barred discs are kinematically more similar to discs than those in unbarred discs. This kinematic similarity is indicated by the ratio of peak rotation velocity to bulge velocity dispersion, which is taken as a proxy of the ratio of "ordered-to-random motions." Indeed, use of the $V/\sigma - \epsilon$ parameter space can distinguish pseudobulges from classical bulges, as shown by Kormendy (1993), Kormendy and Kennicutt (2004) and Kormendy and Fisher (2008). However, these studies rely on very small samples, fewer than 20 bulge-disc galaxies, and are thus difficult to control. At present, it is safe to say that bulges with values well above the "oblate line" in the $V/\sigma - \epsilon$ parameter space are considered to be rotating bulges, and thus from a theoretical perspective would be "pseudobulges", but it is difficult to estimate empirically, using currently available data, how often a bulge that has low Sérsic index would also be found in the "disc" region of the $V/\sigma - \epsilon$ diagram.

Central velocity dispersion alone does not completely separate bulge types. The distribution of σ_0 for a sample of ∼100 S0-Sc galaxies is shown in Fig. 3.11. To construct the kinematic sample we use data from published sources that have

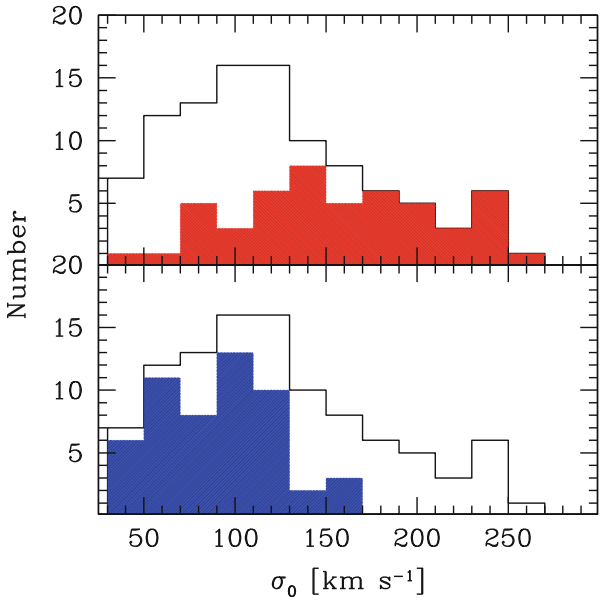

Fig. 3.11 Distribution of central velocity dispersions for galaxies with published σ_0 in the sample from Fig. 3.3. As before, pseudobulges are indicated by *blue shaded region*, and classical bulges by *red*. There is clearly significant overlap between the two samples

sufficient velocity resolution to measure the central dispersion of bulges ($\sigma_{bulge} \geq 50\,\mathrm{km\,s^{-1}}$), and also have sufficient spatial resolution to isolate the absorption line kinematics in the bulge region ($r_{bulge} \sim 1\,\mathrm{kpc}$) that also have available bulge-disc decompositions from the sample used in Fig. 3.3 of this review. We use velocity dispersions from Héraudeau et al. (1999), Barth et al. (2002), Ganda et al. (2007), Kuntschner et al. (2010) and Fabricius et al. (2012). In this comparison we identify pseudobulges as having $n_b < 2$ or prominent disc-like nuclear morphology as described earlier. Zhao (2012) finds that the distribution of central velocity dispersions of pseudobulges is essentially the same when they identify pseudobulges using Sérsic index or with the Kormendy relation. On average, pseudobulges have lower central velocity dispersion than classical bulges ($< \sigma_0 >_{pseudo} \sim 90\,\mathrm{km\,s^{-1}}$, compared to $\sim 160\,\mathrm{km\,s^{-1}}$ for classical bulges). There is a strong decline in the number of pseudobulges with $\sigma > 130\,\mathrm{km\,s^{-1}}$. However, roughly $\sim 1/3$ of the classical bulges in this sample have $\sigma < 130\,\mathrm{km\,s^{-1}}$. It is for this reason that σ_0 alone cannot be used to statistically isolate all pseudobulges from classical bulges. When a bulge has particularly high velocity dispersion ($\sigma > 130\,\mathrm{km\,s^{-1}}$) then it is most likely a classical bulge.

A large sample of uniform measurements of velocity dispersion preferably with integral field spectroscopic measurements in bulge-disc galaxies would have significant value in understanding pseudobulge and classical bulge properties, nonetheless the result in Fig. 3.11 does not appear to depend on the sample. Both Fabricius et al. (2012) and Zhao (2012) find essentially the same result that we report here.

Kormendy and Kennicutt (2004) shows that bulges that are low-σ outliers to the Faber and Jackson (1976) relation between bulge magnitude and velocity dispersion, are likely pseudobulges. However, there is a significant amount of spread in this correlation, and similar to the $\mu_e - r_e$ if a bulge is co-located in parameter space with this relationship it does not mean the bulge is a classical bulge.

Significant correlations between bulge type and the radial structure of kinematics have been seen by a number of authors (e.g. Falcón-Barroso et al. 2006; Comerón et al. 2008; Fabricius et al. 2012). In Fig. 3.12 we show the basic result (in this case taken from Fabricius et al. 2012) that galaxies with classical bulges have centrally peaking velocity dispersion profiles, where galaxies with pseudobulges do not. For this result, Fabricius et al. (2012) identifies pseudobulges using Sérsic index and bulge morphology. This is consistent with the overall picture of classical bulges and pseudobulges. In this case a classical bulge is considered to be a separate component from the disc, and the classical bulge is dynamically hotter than the disc. In the center of the galaxy the classical bulge dominates the light and the measured kinematics. At large radius the disc dominates the light, and measured kinematics have lower dispersion. The intermediate radii show the transition between these two regimes. Pseudobulges, conversely do not have a hotter separate component, they are often thought of simply as high surface density centers of discs, therefore kinematically they do not break from the behavior of the disc. Fabricius et al. (2012) quantifies the kinematic profile shape with the logarithmic derivative $\mathrm{d}\log(\sigma)/\mathrm{d}\log(r)$. The logarithmic derivative correlates well with bulge

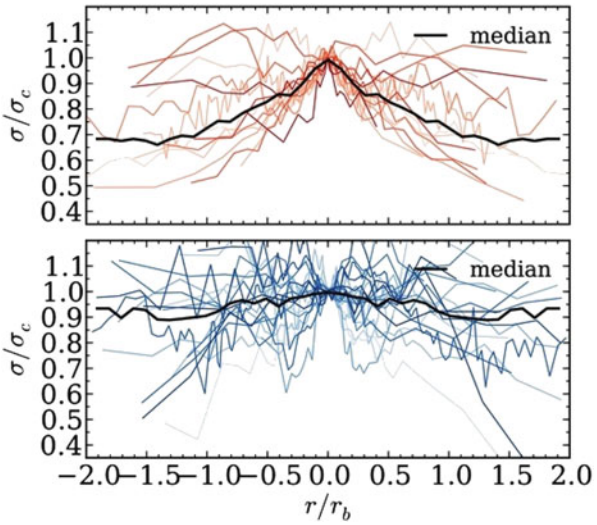

Fig. 3.12 Here we re-plot a result from Fabricius et al. (2012) that shows how the radial profile of the velocity dispersion in pseudobulges is much flatter than that found in galaxies with classical bulges

type. Galaxies with classical bulges ($n_b > 2$ and E-type morphology) have more negative values (i.e. more centrally peaking $\sigma(r)$).

Peletier (2008) notes that all the bulges with central velocity dispersion minima in the samples of Ganda et al. (2007) and Peletier et al. (2007) also are low-Mg b outliers (as described above). Comerón et al. (2008) studies the properties of so-called σ-drop galaxies (galaxies with a central minimum in velocity dispersion). They find that dusty structures that would, in this review, be classified as indicative of pseudobulges are very common in these galaxies. They also find a higher fraction of circumnuclear star formation in σ-drop galaxies.

Fabricius et al. (2012) shows that combining V/σ with metrics of the profile shape can be very powerful for identifying pseudobulges. Galaxies with classical bulges have low values of V/σ and central cuspy surface brightness profiles. Essentially the result is physically sound; if a bulge is dominated by dispersion and has a higher dispersion compared to the surrounding disc then it is almost always a classical bulge. Conversely, pseudobulges are not found in the same region of parameter space. Fabricius et al. (2012) finds that outliers to this rule tend to be galaxies that in line-of-sight velocity distributions that these galaxies have multiple kinematic components that are affecting the measurement of the shape of the velocity profile. The drawback to this method is that it requires sufficient velocity resolution to measure the kinematics of the disc, and therefore may be inaccessible to surveys such as MANGA and SAMI.

3.6 Composite Pseudo-Classical Bulges

Assuming that galaxies either have only a pseudobulge or a classical bulge is most likely an oversimplification. Bulges that consist of both a thin, starforming pseudobulge and a hot-passive classical bulge are very likely present in some galaxies. There has been very little work done on composite bulges. This is definitely an area that could use more work, though results, by the nature of the problem, are likely to be difficult to interpret.

Fisher and Drory (2010) argue that scaling relations can be used to identify some mixed-case bulges. Bulges that are high mass or high surface brightness outliers from fundamental plane scaling relationships are likely to be composite. In these systems, a classical bulge is assumed to be on a scaling relation, for example the $\mu_e - r_e$ correlation of E galaxies. The pseudobulge component increases the mass, without strongly affecting the value for the effective radius. They use models to show that in the limit that the mass of the classical component is larger than that of the pseudo-component this is true. Fisher and Drory (2010) find that bulges that are co-located in fundamental plane parameter space with models of composite pseudo-classical bulges have lower specific SFR than the median pseudobulge, and also have $n_b \sim 1.8 - 2.1$. They show by modeling that adding a high Sérsic index bulge to a low Sérsic index pseudobulge tends to produce an intermediate range n_b. Fisher and Drory (2011) use these results to estimate that roughly 10–20 % of bulges in the local 11 Mpc, fit this description. This is only a rough estimate. Much more work is needed to truly get a robust estimate of the frequency of composite bulge systems.

Erwin et al. (2015) uses stellar kinematics to model the internal structures of several examples of galaxies which contain both a pseudobulge and classical bulge. These models generally find a small compact structure which is referred to as a classical bulge, with a diffuse structure around it that has dynamics that are more consistent with discs, which they call the pseudobulge.

The take away is that the presence of a pseudobulge in a galaxy does not necessarily imply that there is not an old, dynamically hot component of stars within that system. In the future, as integral field spectroscopy becomes more common, dynamical modeling which, places estimates on the maximum fractional mass of a hot stellar component in pseudobulges of ranging properties (B/T, SFR/M_{star}, n_b, etc.) may prove very useful.

3.7 Summary

In this review we have highlighted a number of observed properties that mark empirical differences between classical bulges and pseudobulges. We certainly do not always understand the underlying physical reason for these observed differences. For example, why $n_b \sim 2$ seems to be such a good dividing line between bulge types is not clearly understood. An alternate approach is to base

diagnostic methods on physically motivated arguments (such as an assumption on the star formation history, or the structural properties). However, physically motivated arguments can be specious, especially when we consider that theoretical understanding of bulge formation is incomplete at best. For example, a decade prior to writing this review the most popular theory to explain the population of bulges was major mergers. At present, this is no longer an ubiquitously accepted theory, rather it is thought by many that some mixture of turbulent clump instabilities early on and secular evolution in more recent epochs combine to generate many bulge properties (e.g. Elmegreen et al. 2008; Genzel et al. 2008; Obreja et al. 2013).

Below, we summarize the empirically-determined properties of pseudobulges and subsequentially classical bulges. A very important feature is that pseudobulge properties are not always the complement of classical bulge properties. For example, if a bulge is star forming (and there is no interaction present) this is very good evidence that the bulge is a pseudobulge, but when the bulge is not star forming this does not imply the bulge is classical. It could be either pseudobulge or classical bulge.

The diagnostics are divided into two categories. Those in the top categories (or category I diagnostics) are properties in which the parameter shows a relatively clean separation between almost all pseudobulges and classical bulges. The category II diagnostics are those in which a range in parameter is only occupied by a single bulge type, however does not identify the whole population of bulges. If one wishes to statistically identify all bulges of a certain type in a sample, then a category I diagnostic should be used. Alternatively, if one has a single galaxy, or a sample of bulges and simply wishes to know if these are bulges of a certain type then category II diagnostics may be sufficient. For classical bulges there is a third category which are necessary, but not sufficient properties of classical bulges.

3.7.1 Observational Definition of Pseudobulges

Here we list the empirically-determined properties associated with bulges that resemble discs, i.e. pseudobulges.

I – **Optical morphology** in the region where the bulge light is dominant shows spiral or ring structure, when measured at high spatial resolution (FWHM $\leq$ 100 pc). A description of this can be found in Section 2.

I – **Sérsic index** of bulge stellar light profile in a bulge-disc decomposition is less than 2. Both Fisher and Drory (2008, 2010), also Fig. 3.3 of this review, show that the turnover in the distribution between classical bulges and pseudobulges is at $n_b \sim 2.1$, and below $n_b = 2$ almost no classical bulges are observed.

I – **Correlations with absorption line strengths** are very well connected to bulge types (Peletier et al. 2007; Ganda et al. 2007). As we show in Fig. 3.10, a bulge is a pseudobulge if ΔMg b < 0.7 Å compared to either the correlations of Mg-σ or Mg-Fe. Below we discuss how the absolute value of absorption correlates with bulge type.

I – **Velocity dispersion profile shape** thus far is the best kinematic method to identify pseudobulges and classical bulges (Fabricius et al. 2012). A bulge is identified as a pseudobulge if the logarithmic derivative of the velocity dispersion profile is greater than $dlog(\sigma)/dlog(r) \geq -0.1$ and $< v^2 > / < \sigma^2 > \geq 0.35$. An extreme version of this result are the so-called σ-drop galaxies which have a local minimum in velocity dispersion that is located where the bulge is, these galaxies would have a positive value for $dlog(\sigma)/dlog(r)$, and thus be pseudobulges.

II – **Low surface brightness outliers from scaling relations** are found to be pseudobulges (Carollo et al. 2001; Gadotti 2009; Fisher and Drory 2010). However, many bulges that are co-located with fundamental plane projections also show evidence of being pseudobulges (low n_b, high SFR/M_{star}, Fisher and Drory 2010 and Fig. 3.6). If a bulge is co-located with a projection of the fundamental plane, then this does not discriminate between being a pseudobulge or a classical bulge.

II – **Specific star formation rate** can be indicative of bulge types. If the region in which the bulge dominates the light has $SFR/M_{star} \geq 10^{-11}$ yr^{-1} then the bulge is very likely to be a pseudobulge (Fisher 2006; Fisher et al. 2009). However, if the bulge is less active, where $SFR/M < 10^{-11}$ yr^{-1}, the bulge could be either a pseudobulge or classical bulge. Care should be take also to determine if the galaxy is presently experiencing an interaction, in such cases correlations between SFR/M_{star} and other parameters, such as n_b become less robust.

II – **Absorption line strength** a bulge is found to be a pseudobulge if Fe5150 < 3.95 Å and/or Mg b < 2.35 Å. In the sample of SAURON based observations presented in Fig. 3.10 (Peletier et al. 2007; Ganda et al. 2007), no classical bulge is found with absorption lines below this range. However, this selection does not include all pseudobulges, and therefore in a statistical study should be used in combination with other diagnostics.

II – **Low – σ outliers** to the Faber and Jackson (1976) relation between bulge magnitude and central velocity dispersion of the bulge are found by Kormendy and Kennicutt (2004) to be pseudobulges. However, if a bulge is co-located with the Faber and Jackson (1976), we cannot determine – from this information alone – if it is a pseudobulge or classical bulge.

II – **Extremely blue optical colors** statistically speaking optical color does not appear to be a good indicator of bulge type, however the small subset of bulges with very blue optical colors $B - V < 0.5$ are found to be pseudobulges, and classical bulges are rare for $B - V < 0.65$.

3.7.2 Observational Definition of Classical Bulges

We note again that classical bulges are not always the complement of pseudobulges. In some parameter spaces there is significant overlap between the two populations. This could be evidence of a bridging population, but it is also very likely that

not every metric of galaxy properties is uniquely manifested by a single galaxy evolution mechanism.

The obvious condition is that first a classical bulge must not satisfy any of the criteria listed under the definition of pseudobulges.

I – **Optical Morphology** is found to be simple and free of spiral arms and nuclear rings in the region of the galaxy where the bulge dominates the light. It is important to have good resolution, preferably in the middle of the optical wavelength range ($\sim V$ through I bands). In all but the closest galaxies HST is necessary to diagnose bulge with their morphology.

I – **Sérsic Index** of classical bulges is found to be almost always greater than two, $n_b(classical) > 2$ (Fisher and Drory 2008).

I – **Correlations between absorption line strengths** that are consistent with E galaxies is a property exclusively of classical bulges. Pseudobulges establish correlations that are offset toward lower equivalent widths of absorption.

I – **Strongly centrally peaking velocity dispersion profiles** are a property that appears to be exclusively that of classical bulges. Fabricius et al. (2012) finds that if a bulge has a logarithmic derivative that is more negative than $dlog(\sigma)/dlog(r) < -0.1$ the bulge is a classical bulge.

II – **Central Velocity Dispersion** of pseudobulges is systematically lower than that of classical bulges. If a bulge is found to have $\sigma_0 > 130\,\mathrm{km\,s^{-1}}$ then that bulge is very likely to also show evidence of being a classical bulge, and is not likely a pseudobulge. However, a significant number of classical bulges have lower σ_0 than this.

The following criteria must be satisfied to be defined empirically as a classical bulge, but are not sufficient on their own to identify the bulge as a classical bulge.

III – Classical bulges are **Consistent with the Fundamental plane scaling relationships.**

III – **Low specific star formation rates** and **low central gas surface densities** are found in all classical bulges, that are not presently experiencing a merger. To be identified as a classical bulge we find that $SFR/M_\star < 10^{-11}$ yr^{-1} and $\Sigma_{mol} < 100\,\mathrm{M_\odot\,pc^{-1}}$. Though many pseudobulge also have low star formation activity and likewise are gas poor, therefore an inactive interstellar medium is not sufficient to identify a bulge as being either classical or pseudobulge.

III – **Classical bulges are not extremely blue.** There is no range in optical color that uniquely isolates classical bulges, however if a bulge is extremely blue it is not likely a classical bulge.

Acknowledgements DBF acknowledges support from Australian Research Council (ARC) Discovery Program (DP) grant DP130101460. We are grateful to D. Gadotti, and P. Erwin for making data and results available to us.

References

Aguerri, J. A. L., Balcells, M., & Peletier, R. F. 2001, A&A, 367, 428
Andredakis, Y. C., Peletier, R. F., & Balcells, M. 1995, MNRAS, 275, 874
Andredakis, Y. C., & Sanders, R. H. 1994, MNRAS, 267, 283
Athanassoula, E. 2005a, MNRAS, 358, 1477
—. 2005b, MNRAS, 358, 1477
Balcells, M., Graham, A. W., Domínguez-Palmero, L., & Peletier, R. F. 2003, ApJ, 582, L79
Barth, A. J., Ho, L. C., & Sargent, W. L. W. 2002, AJ, 124, 2607
Bender, R., Burstein, D., & Faber, S. M. 1992, ApJ, 399, 462
Blanton, M. R., Eisenstein, D., Hogg, D. W., Schlegel, D. J., & Brinkmann, J. 2005, ApJ, 629, 143
Böker, T., Laine, S., van der Marel, R. P., Sarzi, M., Rix, H.-W., Ho, L. C., & Shields, J. C. 2002, AJ, 123, 1389
Boylan-Kolchin, M., Ma, C., & Quataert, E. 2006, MNRAS, 369, 1081
Bruzual A., G. 1983, ApJ, 273, 105
Bundy, K., Bershady, M. A., Yan, R., Law, D., Drory, N., R., D., MacDonald, N., Wake, D. A., & Weijmans, A.-M. 2014, ApJ, submitted
Bureau, M., & Freeman, K. C. 1999, AJ, 118, 126
Buta, R., & Crocker, D. A. 1993, AJ, 105, 1344
Buta, R. J., Corwin, H. G., & Odewahn, S. C. 2007, The de Vaucouleurs Altlas of Galaxies (Cambridge University Press)
Calzetti, D., Kennicutt, R. C., Engelbracht, C. W., Leitherer, C., Draine, B. T., Kewley, L., Moustakas, J., Sosey, M., Dale, D. A., Gordon, K. D., Helou, G. X., Hollenbach, D. J., Armus, L., Bendo, G., Bot, C., Buckalew, B., Jarrett, T., Li, A., Meyer, M., Murphy, E. J., Prescott, M., Regan, M. W., Rieke, G. H., Roussel, H., Sheth, K., Smith, J. D. T., Thornley, M. D., & Walter, F. 2007, ApJ, 666, 870
Caon, N., Capaccioli, M., & D'Onofrio, M. 1994, A&AS, 106, 199
Carollo, C. M. 1999, ApJ, 523, 566
Carollo, C. M., Stiavelli, M., de Zeeuw, P. T., & Mack, J. 1997, AJ, 114, 2366
Carollo, C. M., Stiavelli, M., de Zeeuw, P. T., Seigar, M., & Dejonghe, H. 2001, ApJ, 546, 216
Comerón, S., Knapen, J. H., & Beckman, J. E. 2008, A&A, 485, 695
Comerón, S., Knapen, J. H., Beckman, J. E., Laurikainen, E., Salo, H., Martínez-Valpuesta, I., & Buta, R. J. 2010, MNRAS, 402, 2462
Cortese, L., Boselli, A., Franzetti, P., Decarli, R., Gavazzi, G., Boissier, S., & Buat, V. 2008, MNRAS, 386, 1157
Courteau, S., de Jong, R. S., & Broeils, A. H. 1996, ApJ, 457, L73+
Croom, S. M., Lawrence, J. S., Bland-Hawthorn, J., Bryant, J. J., Fogarty, L., Richards, S., Goodwin, M., Farrell, T., Miziarski, S., Heald, R., Jones, D. H., Lee, S., Colless, M., Brough, S., Hopkins, A. M., Bauer, A. E., Birchall, M. N., Ellis, S., Horton, A., Leon-Saval, S., Lewis, G., López-Sánchez, Á. R., Min, S.-S., Trinh, C., & Trowland, H. 2012, MNRAS, 421, 872
de Jong, R. S. 1996, A&A, 313, 45
de Vaucouleurs, G., de Vaucouleurs, A., Corwin, Jr., H. G., Buta, R. J., Paturel, G., & Fouque, P. 1991, Third Reference Catalogue of Bright Galaxies (Volume 1–3, XII, 2069 pp. 7 figs.. Springer-Verlag Berlin Heidelberg New York)
Debattista, V. P., Carollo, C. M., Mayer, L., & Moore, B. 2004, ApJ, 604, L93
Debattista, V. P., & Shen, J. 2007, ApJ, 654, L127
Djorgovski, S., & Davis, M. 1987, ApJ, 313, 59
Draine, B. T., Aniano, G., Krause, O., Groves, B., Sandstrom, K., Braun, R., Leroy, A., Klaas, U., Linz, H., Rix, H.-W., Schinnerer, E., Schmiedeke, A., & Walter, F. 2014, ApJ, 780, 172
Drory, N., & Fisher, D. B. 2007, ApJ, 664, 640
Elmegreen, B. G., Bournaud, F., & Elmegreen, D. M. 2008, ApJ, 688, 67
Erwin, P. 2004, A & A, 415, 941

Erwin, P., Beckman, J. E., & Vega-Beltran, J.-C. 2004, in Astrophysics and Space Science Library, Vol. 319, Astrophysics and Space Science Library, ed. D. L. Block, I. Puerari, K. C. Freeman, R. Groess, & E. K. Block, 775–+
Erwin, P., Saglia, R. P., Fabricius, M., Thomas, J., Nowak, N., Rusli, S., Bender, R., Vega Beltrán, J. C., & Beckman, J. E. 2015, MNRAS, 446, 4039
Erwin, P., & Sparke, L. S. 2002, AJ, 124, 65
Evans, II, N. J. 1999, ARA&A, 37, 311
Faber, S. M., & Jackson, R. E. 1976, ApJ, 204, 668
Faber, S. M., Wegner, G., Burstein, D., Davies, R. L., Dressler, A., Lynden-Bell, D., & Terlevich, R. J. 1989, ApJS, 69, 763
Fabricius, M. H., Coccato, L., Bender, R., Drory, N., Gössl, C., Landriau, M., Saglia, R. P., Thomas, J., & Williams, M. J. 2014, MNRAS, 441, 2212
Fabricius, M. H., Saglia, R. P., Fisher, D. B., Drory, N., Bender, R., & Hopp, U. 2012, ApJ, 754, 67
Falcón-Barroso, J., Bacon, R., Bureau, M., Cappellari, M., Davies, R. L., de Zeeuw, P. T., Emsellem, E., Fathi, K., Krajnović, D., Kuntschner, H., McDermid, R. M., Peletier, R. F., & Sarzi, M. 2006, MNRAS, 369, 529
Falcón-Barroso, J., van de Ven, G., Peletier, R. F., Bureau, M., Jeong, H., Bacon, R., Cappellari, M., Davies, R. L., de Zeeuw, P. T., Emsellem, E., Krajnović, D., Kuntschner, H., McDermid, R. M., Sarzi, M., Shapiro, K. L., van den Bosch, R. C. E., van der Wolk, G., Weijmans, A., & Yi, S. 2011, MNRAS, 417, 1787
Fernández Lorenzo, M., Sulentic, J., Verdes-Montenegro, L., Blasco-Herrera, J., Argudo-Fernández, M., Garrido, J., Ramírez-Moreta, P., Ruiz, J. E., Sánchez-Expósito, S., & Santander-Vela, J. D. 2014, ApJ, 788, L39
Fisher, D. B. 2006, ApJ, 642, L17
Fisher, D. B., Bolatto, A., Drory, N., Combes, F., Blitz, L., & Wong, T. 2013, ApJ, 764, 174
Fisher, D. B., & Drory, N. 2008, AJ, 136, 773
—. 2010, ApJ, 716, 942
—. 2011, ApJ, 733, L47
Fisher, D. B., Drory, N., & Fabricius, M. H. 2009, ApJ, 697, 630
Freeman, K. C. 1970, ApJ, 160, 811
Gadotti, D. A. 2008, MNRAS, 384, 420
—. 2009, MNRAS, 393, 1531
—. 2012, ArXiv e-prints
Gadotti, D. A., & dos Anjos, S. 2001, AJ, 122, 1298
Ganda, K., Peletier, R. F., McDermid, R. M., Falcón-Barroso, J., de Zeeuw, P. T., Bacon, R., Cappellari, M., Davies, R. L., Emsellem, E., Krajnović, D., Kuntschner, H., Sarzi, M., & van de Ven, G. 2007, MNRAS, 380, 506
García-Burillo, S., Combes, F., & Neri, R. 1999, A&A, 343, 740
Genzel, R., Burkert, A., Bouché, N., Cresci, G., Förster Schreiber, N. M., Shapley, A., Shapiro, K., Tacconi, L. J., Buschkamp, P., Cimatti, A., Daddi, E., Davies, R., Eisenhauer, F., Erb, D. K., Genel, S., Gerhard, O., Hicks, E., Lutz, D., Naab, T., Ott, T., Rabien, S., Renzini, A., Steidel, C. C., Sternberg, A., & Lilly, S. J. 2008, ApJ, 687, 59
Graham, A., Lauer, T. R., Colless, M., & Postman, M. 1996, ApJ, 465, 534
Graham, A. W., & Driver, S. P. 2005, Publications of the Astronomical Society of Australia, 22, 118
Hammer, F., Flores, H., Elbaz, D., Zheng, X. Z., Liang, Y. C., & Cesarsky, C. 2005, A&A, 430, 115
Heller, C. H., Shlosman, I., & Athanassoula, E. 2007, ApJ, 657, L65
Héraudeau, P., Simien, F., Maubon, G., & Prugniel, P. 1999, A&AS, 136, 509
Inoue, S., & Saitoh, T. R. 2012, MNRAS, 2819
Jogee, S., Scoville, N., & Kenney, J. D. P. 2005, ApJ, 630, 837
Kauffmann, G., Heckman, T. M., White, S. D. M., Charlot, S., Tremonti, C., Peng, E. W., Seibert, M., Brinkmann, J., Nichol, R. C., SubbaRao, M., & York, D. 2003, MNRAS, 341, 54

Kautsch, S. J., Grebel, E. K., Barazza, F. D., & Gallagher, III, J. S. 2006, A&A, 445, 765
Kenney, J. D. P., van Gorkom, J. H., & Vollmer, B. 2004, AJ, 127, 3361
Kennicutt, R. C., & Evans, N. J. 2012, ARA&A, 50, 531
Kennicutt, R. C., Hao, C., Calzetti, D., Moustakas, J., Dale, D. A., Bendo, G., Engelbracht, C. W., Johnson, B. D., & Lee, J. C. 2009, ApJ, 703, 1672
Kennicutt, Jr., R. C. 1998, ARA&A, 36, 189
Khosroshahi, H. G., Wadadekar, Y., & Kembhavi, A. 2000, ApJ, 533, 162
Knapen, J. H. 2005, A&A, 429, 141
Kormendy, J. 1977a, ApJ, 218, 333
—. 1977b, ApJ, 217, 406
Kormendy, J. 1982, in Saas-Fee Advanced Course 12: Morphology and Dynamics of GalaxiesSaas-Fee Vol. 12: Morphology and Dynamics of Galaxies, 113–288
Kormendy, J. 1993, in IAU Symp. 153: Galactic Bulges, 209–+
—. 2013, Secular Evolution in Disc Galaxies, ed. J. Falcón-Barroso & J. H. Knapen, 1
Kormendy, J., & Fisher, D. B. 2008, in Astronomical Society of the Pacific Conference Series, Vol. 396, Astronomical Society of the Pacific Conference Series, ed. J. G. Funes & E. M. Corsini, 297–+
Kormendy, J., Fisher, D. B., Cornell, M. E., & Bender, R. 2009, ApJS, 182, 216
Kormendy, J., & Illingworth, G. 1982, ApJ, 256, 460
Kormendy, J., & Kennicutt, R. C. 2004, ARA&A, 42, 603
Kuntschner, H., Emsellem, E., Bacon, R., Cappellari, M., Davies, R. L., de Zeeuw, P. T., Falcón-Barroso, J., Krajnović, D., McDermid, R. M., Peletier, R. F., Sarzi, M., Shapiro, K. L., van den Bosch, R. C. E., & van de Ven, G. 2010, MNRAS, 408, 97
Lackner, C. N., & Gunn, J. E. 2012, MNRAS, 421, 2277
Laurikainen, E., Salo, H., Buta, R., Knapen, J., Speltincx, T., & Block, D. 2006, AJ, 132, 2634
Laurikainen, E., Salo, H., Buta, R., Knapen, J. H., & Comerón, S. 2010, MNRAS, 405, 1089
Leroy, A. K., Bigiel, F., de Blok, W. J. G., Boissier, S., Bolatto, A., Brinks, E., Madore, B., Munoz-Mateos, J.-C., Murphy, E., Sandstrom, K., Schruba, A., & Walter, F. 2012, ArXiv e-prints
Lintott, C., Schawinski, K., Bamford, S., Slosar, A., Land, K., Thomas, D., Edmondson, E., Masters, K., Nichol, R. C., Raddick, M. J., Szalay, A., Andreescu, D., Murray, P., & Vandenberg, J. 2011, MNRAS, 410, 166
MacArthur, L. A., Courteau, S., Bell, E., & Holtzman, J. A. 2004, ApJS, 152, 175
MacArthur, L. A., González, J. J., & Courteau, S. 2009, MNRAS, 395, 28
Martig, M., Bournaud, F., Teyssier, R., & Dekel, A. 2009, ApJ, 707, 250
Möllenhoff, C. 2004, A&A, 415, 63
Moorthy, B. K., & Holtzman, J. A. 2005, astro-ph/0512346
Noguchi, M. 1999, ApJ, 514, 77
Obreja, A., Domínguez-Tenreiro, R., Brook, C., Martínez-Serrano, F. J., Doménech-Moral, M., Serna, A., Mollá, M., & Stinson, G. 2013, ApJ, 763, 26
Peletier, R. F. 2008, in Astronomical Society of the Pacific Conference Series, Vol. 390, Pathways Through an Eclectic Universe, ed. J. H. Knapen, T. J. Mahoney, & A. Vazdekis, 232
Peletier, R. F., & Balcells, M. 1996, AJ, 111, 2238
Peletier, R. F., Balcells, M., Davies, R. L., Andredakis, Y., Vazdekis, A., Burkert, A., & Prada, F. 1999, MNRAS, 310, 703
Peletier, R. F., Falcón-Barroso, J., Bacon, R., Cappellari, M., Davies, R. L., de Zeeuw, P. T., Emsellem, E., Ganda, K., Krajnović, D., Kuntschner, H., McDermid, R. M., Sarzi, M., & van de Ven, G. 2007, MNRAS, 379, 445
Proctor, R. N., & Sansom, A. E. 2002, MNRAS, 333, 517
Regan, M. W., Thornley, M. D., Helfer, T. T., Sheth, K., Wong, T., Vogel, S. N., Blitz, L., & Bock, D. C.-J. 2001, ApJ, 561, 218
Renzini, A. 2006, ARA&A, 44, 141
Robertson, B., Bullock, J. S., Cox, T. J., Di Matteo, T., Hernquist, L., Springel, V., & Yoshida, N. 2006, ApJ, 645, 986

Saglia, R. P., Fabricius, M., Bender, R., Montalto, M., Lee, C.-H., Riffeser, A., Seitz, S., Morganti, L., Gerhard, O., & Hopp, U. 2010, A&A, 509, A61
Salim, S., Rich, R. M., Charlot, S., Brinchmann, J., Johnson, B. D., Schiminovich, D., Seibert, M., Mallery, R., Heckman, T. M., Forster, K., Friedman, P. G., Martin, D. C., Morrissey, P., Neff, S. G., Small, T., Wyder, T. K., Bianchi, L., Donas, J., Lee, Y.-W., Madore, B. F., Milliard, B., Szalay, A. S., Welsh, B. Y., & Yi, S. K. 2007, ApJS, 173, 267
Sandage, A. 1961, The Hubble atlas of galaxies (Washington: Carnegie Institution, 1961)
Sandage, A., & Bedke, J. 1994, The Carnegie atlas of galaxies (Washington, DC: Carnegie Institution of Washington with The Flintridge Foundation, ⌊c1994)
Scarlata, C., Stiavelli, M., Hughes, M. A., Axon, D., Alonso-Herrero, A., Atkinson, J., Batcheldor, D., Binney, J., Capetti, A., Carollo, C. M., Dressel, L., Gerssen, J., Macchetto, D., Maciejewski, W., Marconi, A., Merrifield, M., Ruiz, M., Sparks, W., Tsvetanov, Z., & van der Marel, R. P. 2004, AJ, 128, 1124
Sérsic, J. L. 1968, Atlas de galaxias australes (Cordoba, Argentina: Observatorio Astronomico, 1968)
Shen, J., & Debattista, V. P. 2009, ApJ, 690, 758
Sheth, K., Vogel, S. N., Regan, M. W., Thornley, M. D., & Teuben, P. J. 2005, ApJ, 632, 217
Smith, J. A., Tucker, D. L., Kent, S., Richmond, M. W., Fukugita, M., Ichikawa, T., Ichikawa, S.-i., Jorgensen, A. M., Uomoto, A., Gunn, J. E., Hamabe, M., Watanabe, M., Tolea, A., Henden, A., Annis, J., Pier, J. R., McKay, T. A., Brinkmann, J., Chen, B., Holtzman, J., Shimasaku, K., & York, D. G. 2002, AJ, 123, 2121
Thomas, D., & Davies, R. L. 2006, MNRAS, 366, 510
Weinzirl, T., Jogee, S., Khochfar, S., Burkert, A., & Kormendy, J. 2009, ApJ, 696, 411
Whitford, A. E. 1978, ApJ, 226, 777
Wyse, R. F. G., Gilmore, G., & Franx, M. 1997, ARA&A, 35, 637
Young, L. M., Bureau, M., Davis, T. A., Combes, F., McDermid, R. M., Alatalo, K., Blitz, L., Bois, M., Bournaud, F., Cappellari, M., Davies, R. L., de Zeeuw, P. T., Emsellem, E., Khochfar, S., Krajnović, D., Kuntschner, H., Lablanche, P.-Y., Morganti, R., Naab, T., Oosterloo, T., Sarzi, M., Scott, N., Serra, P., & Weijmans, A.-M. 2011, MNRAS, 414, 940
Zhao, Y. 2012, Ap&SS, 337, 719

Chapter 4
Observed Properties of Boxy/Peanut/Barlens Bulges

Eija Laurikainen and Heikki Salo

Abstract We review the observed morphological, photometric, and kinematic properties of boxy/peanut (B/P) shape bulges. Nearly half of the bulges in the nearby edge-on galaxies have these characteristics, which fraction is similar to the observed bar fraction in Hubble types earlier than Scd. B/P bulges are generally detected in the edge-on view, but it has been recently demonstrated that barlenses, which are lens-like structures embedded in bars, are the more face-on counterparts of the B/P bulges. Multi-component structural decompositions have shown that B/P/barlens structures are likely to account for most of the bulge light, including the early-type discs harboring most of the bulge mass in galaxies. These structures appear in bright galaxies, in a mass range near to the Milky Way mass. Also the other properties of these bulges, including morphology (X-shaped), kinematics (cylindrical rotation), or stellar populations (old), are similar to those observed in the Milky Way. Cool central discs are often embedded in the B/P/barlens bulges. Barred galaxies contain also dynamically hot classical bulges, but it is not yet clear to what extent they are really dynamically distinct structure components, and to what extent stars wrapped into the central regions of the galaxies during the formation and evolution of bars. If most of the bulge mass in the Milky Way mass galaxies in the nearby universe indeed resides in the B/P-shape bulges, and not in the classical bulges, that idea needs to be integrated into the paradigm of galaxy formation.

4.1 Introduction

Galaxies in the nearby universe have complex morphological structures and indeed the concept of the bulge depends strongly on how we define it. Bulges can be considered simply as an excess flux above the disc, or they can be defined by detailed morphological, photometric, or kinematic properties. An important question is to what extent these central mass concentrations are associated to the early formative processes of galaxies, and how much are they modified via internal dynamical

E. Laurikainen (✉) • H. Salo
Astronomy and Space Physics, University of Oulu, FI-90014 Oulu, Finland
e-mail: eija.laurikainen@oulu.fi; heikki.salo@oulu.fi

E. Laurikainen et al. (eds.), *Galactic Bulges*, Astrophysics and Space Science Library 418, DOI 10.1007/978-3-319-19378-6_4

processes. Using the notation by Athanassoula (2005) bulges are generally divided to *classical bulges, discy pseudobulges, and boxy/peanut (B/P) bulges*. Classical bulges are the most obvious imprints of galaxy formation at high redshifts, formed in some violent processes, followed by strong relaxation. They are structures supported by velocity dispersion, and also have centrally peaked surface brightness profiles with high Sérsic indexes. Pseudobulges are defined as structures formed by secular evolutionary processes out of the disc material. The concept of a pseudobulge was introduced by Kormendy (1982, 1983) who defined them as flat structures in the central parts of the discs, having excess of light above the disc in the surface brightness profile. Pseudobulges were later extended to include also the vertically thick boxy/peanut bulges, generally associated to bars (Athanassoula 2005; many B/Ps show also X-shape morphology). Since then the flat central mass concentrations have been referred as 'discy pseudobulges'. A division of pseudobulges to these two categories is important, because their observed properties are very different.

The concept of a pseudobulge was created having in mind the relaxed universe where slow secular evolutionary processes are prevalent, not the early gas rich clumpy universe, or the universe where galaxy mergers dominate the evolution. However, it appears that similar internal mechanisms which take place in the local universe, like bar instabilities, can occur also at high redshifts, but in a much more rapid dynamical timescale. As discussed by Brooks and Christensen in Chap. 12 and by Bournaud in Chap. 13, at high redshifts also star formation and the different feedback mechanisms are faster and more efficient. All this can lead to the formation of pseudobulges even at high redshifts, for which reason associating the different bulge types to a unique formative process of bulge is not straightforward. In spite of that the above definition of bulges may still be a good working hypothesis at all redshifts, and give useful insight to the theoretical models.

This article reviews the observational properties of B/P bulges and also gives a historical perspective for the discovery of the phenomenon. The theoretical background of the orbital families is given by Athanassoula in Chap. 14. We have the following questions in mind: (a) what is the observational evidence that B/P bulges are vertically thick inner parts of bars and what are the relative masses of the thin and thick bar components? (b) Are the B/P structures the only bulges in galaxies with this characteristic, or do the same galaxies have also small classical bulges embedded in the B/P bulges? (c) What is our understanding of this phenomenon both in the edge-on and in face-on views? Although the topic is B/P bulges, connections are made also to other type of bulges if that is needed for understanding the phenomenon. Examples of boxy/peanut and X-shape bulges are shown in Fig. 4.1. The unsharp masks further illustrate the X-shape, which may appear weakly also in some bulges with apparent boxy appearance.

An outstanding recent discovery of the Milky Way (discussed in Chaps. 9 and 10 of this book) is that it harbors a boxy (Dwek et al. 1995) or even an X-shape bulge (Li and Shen 2012; Wegg and Gerhard 2013), covering most of the central mass concentration in our Galaxy. In fact, the model by Shen et al. (2010), explaining most of the observed properties of the Milky Way, does not have any classical bulge.

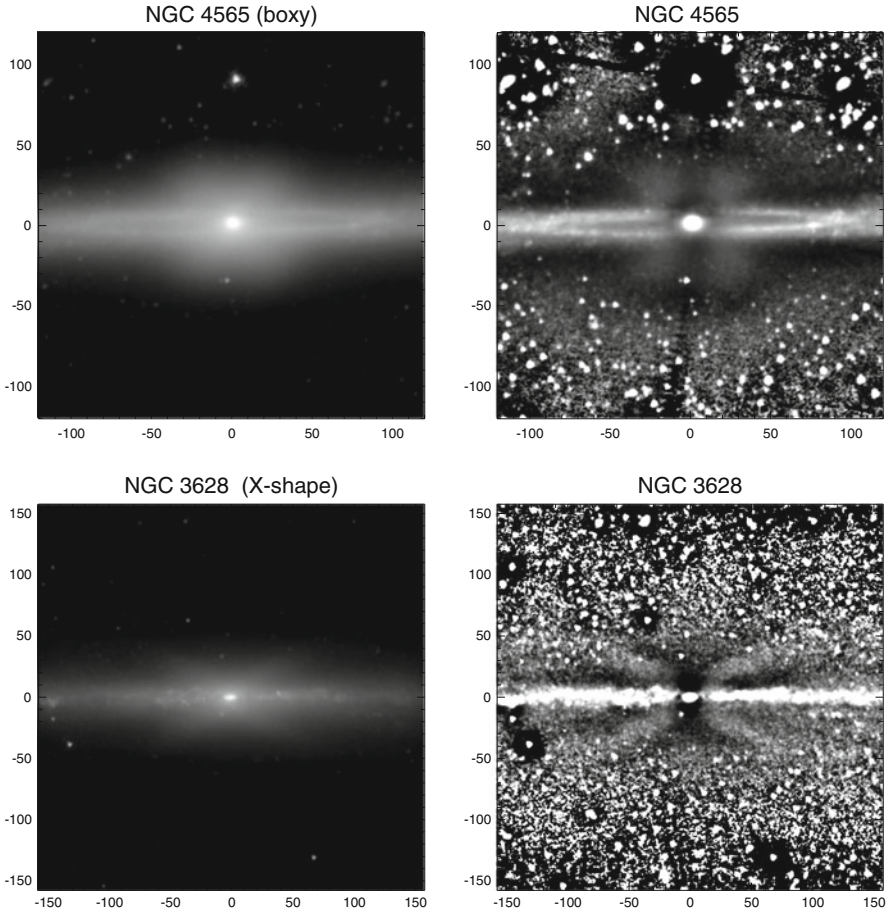

Fig. 4.1 Examples of boxy (NGC 4565) and peanut (NGC 3628) shape bulges, using the 3.6 μm Spitzer space telescope images. Also shown are the unsharp mask images of the same galaxies, which in both galaxies show an X-shape morphology. The units of the x- and y-axis are in arcseconds

We will discuss observations which suggest that actually a large majority of the nearby galaxies in the Milky Way mass range might contain similar boxy or peanut shape bulges, where most of the bulge mass resides.

Good previous reviews of B/P bulges are those by Combes and Sanders (1981), Athanassoula (2005), and Debattista et al. (2006). Critical points in the interpretation of B/P bulges are given in the review by Graham (2011).

4.2 Discovery of B/P Bulges

The earliest notion of boxy bulges goes as far as to 1959, when the (Burbidge and Burbidge 1959) recognized such a structure in NGC 128, which galaxy was later shown in the Hubble Atlas of Galaxies by Sandage (1961). Some years later de Vaucouleurs (1974) paid attention to similar structures in some edge-on galaxies, at a time when bulges were generally thought to be like small ellipticals sitting in the middle of the disc. An interesting new explanation for the B/P bulges was given by Combes and Sanders in 1981: using N-body simulations they showed that when stellar bars form in galactic discs, in the edge-on view they reveal boxy or peanut shapes, similar to those seen in real galaxies. Soon after that a competing astrophysically interesting explanation for the formation of B/Ps was given by Binney and Petrou (1985), who suggested that they might be formed by violent or soft merging of satellite galaxies. Support for the scenario by Combes and Sanders came from the observation that NGC 4565 and NGC 128, with obvious boxy bulges in morphology, appeared to have cylindrical rotation (Kormendy and Illingworth 1982, 1983), which means that the rotational velocity depends only little on the vertical height from the equatorial plane. Kormendy and Illingworth argued that cylindrical rotation might actually be a typical characteristic of boxy bulges, but not of elliptical galaxies. It is also worth mentioning that Bertola and Capaccioli (1977) had already shown that the bulge in NGC 128 is fast rotating and therefore cannot be dynamically hot. However, it is worth noticing that not all bars seen end-on are perfectly round prolate structures.

After the first discoveries of B/P bulges in individual galaxies, systematic studies of B/Ps in galaxies seen in the edge-on view were carried out by Jarvis (1986) and Shaw et al. (1990). They suggested that B/Ps are concentrated to early-type disc galaxies (S0-Sab), and that peanuts are more common than boxy bulges, particularly in the late-type galaxies. They also showed evidence that galaxy environment (cluster/non-cluster, number of nearby companions) is not critical for the formation of the B/P bulges. These observations supported the idea that the B/P-structures indeed form part of the bar as suggested by Combes and Sanders (1981). However, this interpretation was not generally accepted at that time, partly because also 20 % of the elliptical galaxies appeared to be boxy (Lauer 1985). Bender et al. (1989) even speculated that boxy ellipticals might have a similar origin as the cylindrically rotating bulges in disc galaxies. Anyway, as the fraction of galaxies in which B/Ps were identified was only $\sim$20 %, their exact interpretation would not significantly alter the estimated total mass fraction of classical bulges in the nearby universe.

This picture was changed by the studies of Dettmar and Barteldress (1988) and Lütticke et al. (2000a), based on more complete galaxy samples. Inspecting the isophotal contours of the galaxies they found that even 45 % of all S0-Sd galaxies

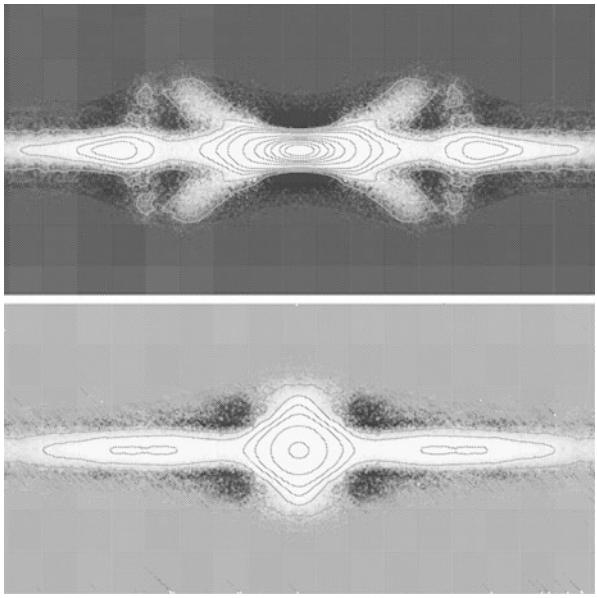

Fig. 4.2 Boxy/peanut bulges seen in the edge-on view in the simulation model by Athanassoula (2005, their figure 6): in the *upper panel* the line of sight is at 90° to the bar major axis, and in the *lower panel* the boxy/peanut is seen end-on (Reproduced with permission of Oxford University Press)

have B/Ps, which is already close to the fraction of barred galaxies: the somewhat larger number of detected bars (∼50–60 %) could be easily understood by the aspect angle of the bar. Namely, bars seen end-on view (along the bar major axis) would look like round structures, similar to the classical bulges (see the simulation model by Athanassoula 2005 in Fig. 4.2).

Lütticke et al. (2004) discovered also a new category of B/P bulges, the so called 'thick boxy bulges'. Such bulges (see Fig. 4.3) are thought to be too extended to form part of the bar, and they also show asymmetries, or signs of recent mergers, which all means that they are not dynamically settled. Although they form only a minority of all B/Ps, they indicate that B/P bulges are not a uniform group of structures. In fact, in the prototype galaxy of 'thick boxy bulges', NGC 1055 (Shaw 1993), the bulge looks very much like a thick disc. This boxy bulge is rotating cylindrically, even in those regions of the observed light distribution where the bulge appears neither boxy nor peanut. Such rotation would be natural even if that structure were interpreted as a thick disc. This interpretation would be interesting, because in that case in traditional terms that galaxy barely has a bulge. In some galaxies even X-shape is visible in the 'thick boxy bulge' (Pohlen et al. 2004).

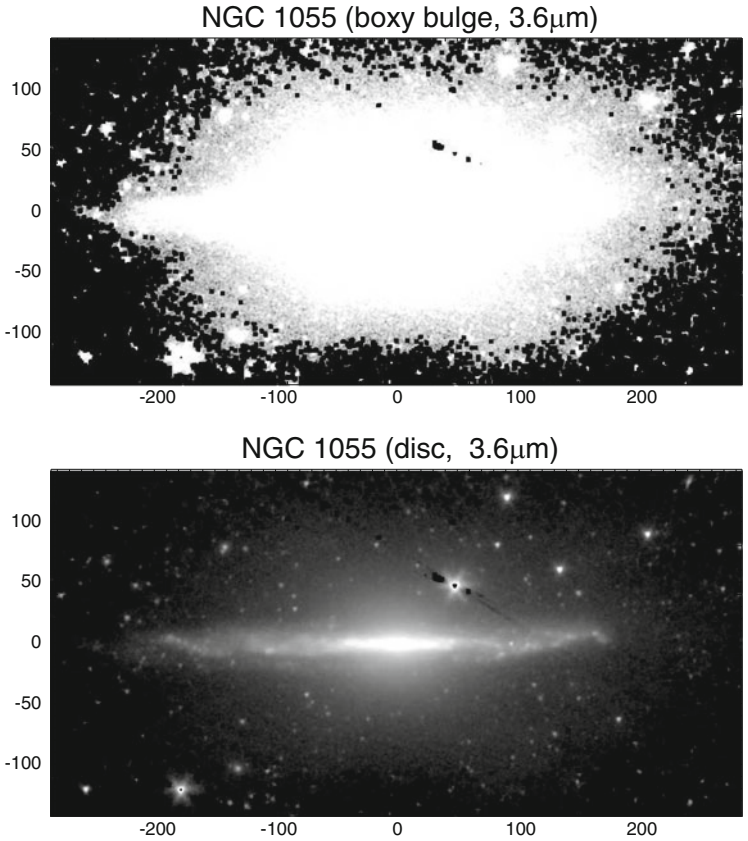

Fig. 4.3 NGC 1055, as an example of a thick boxy bulge. Shown is the 3.6 μm Spitzer space telescope image in two different flux scales

4.3 Properties of the B/P Bulges in the Edge-On View

It was clear that more detailed analysis of the individual galaxies were needed, either to prove or disprove the possible bar origin of the B/P bulges. Such observations, particularly in the near-IR, where the obscuring effects of dust are minimal, were carried out by several groups. The observations were also compared with the predictions of the simulation models.

4.3.1 Direct Images

Morphology of the B/P-structures was systematically studied in the near-IR by Lütticke et al. (2000b). They were able to show that a large majority of these

structures can be associated with bars. In particular, they emphasized that the B/Ps are not just thick bars, but a combination of the vertically thick inner part of the bar, and a central bulge formed differently. They showed that the degree of the boxiness varies with the aspect angle of the bar, e.g. the bulge size normalized with barlength correlates with the level of boxiness of the bulge. These results were consistent with the predictions of the simulation models by Pfenniger and Friedli (1991), and they have been later confirmed by other simulations (Patsis et al. 2002a; Martinez-Valpuesta et al. 2006; Athanassoula and Misioritis 2002; Debattista et al. 2005). Lütticke, Dettmar and Pohlen also measured the vertical thickness of the B/P, both in respect of barlength, and the size of the bulge (e.g. the size of the region with extra light above the exponential disc), in agreement with the predictions of the simulation models. The measured size of the B/P, normalized to barlength was ∼0.4, again in good agreement with the simulation models by Pfenniger and Friedli. Two possible explanations for the small central bulges were speculated by Lütticke et al. (2000b): they could be associated to the primordial bulges (i.e., 'classical bulges'), or to the Inner Lindblad Resonance of the bar where a burst of star formation increases the mass concentration (i.e., 'discy pseudobulges'). This idea has been recently renovated by Cole et al. (2014).

4.3.2 Unsharp Masks

The B/P bulges have been studied by Aronica et al. (2003) using unsharp mask images, which emphasize the sharp features that might appear in galaxies. They pointed out local surface brightness enhancements along the bar major axis on both sides of the bar, which enhancements appeared also in their simulation model after the bar had buckled. To illustrate this in Fig. 4.4 (upper panel) a comparison is made between a simulation model and the bar in ESO 443-042 observed at 3.6 μm. In the same figure we show also a typical barred early-type galaxy, NGC 936, in almost face-on view. Also this galaxy has flux enhancements at the two ends of the bar, and it is tempting to argue that they are the same features as in ESO 443-042. We will come into this issue later.

Unsharp masks were used to study the B/P bulges also by Bureau et al. (2006), but now using a larger sample of 30 galaxies. In fact, in the study by Bureau et al. all the most important morphological characteristics of the B/P/X-shape structures for the edge-on galaxies are summarized, and are collected to our Figs. 4.4 and 4.5:

(a) *Secondary maximum appears along the bar major axis* (upper row in Fig. 4.4), as discussed also by Aronica et al. (2003; see also Patsis et al. (2002a), their Fig. 5e).
(b) *The X-shapes can be centered or non-centered*, e.g. the X-shape either crosses or does not cross the galaxy center (IC 2531 and NGC 4710 in Fig. 4.4).
(c) *Minor-axis extremum* appears (NGC 1381 in Fig. 4.4), e.g., there is a rather narrow and elongated local maximum in the surface brightness profile along the minor axis near the galaxy center.

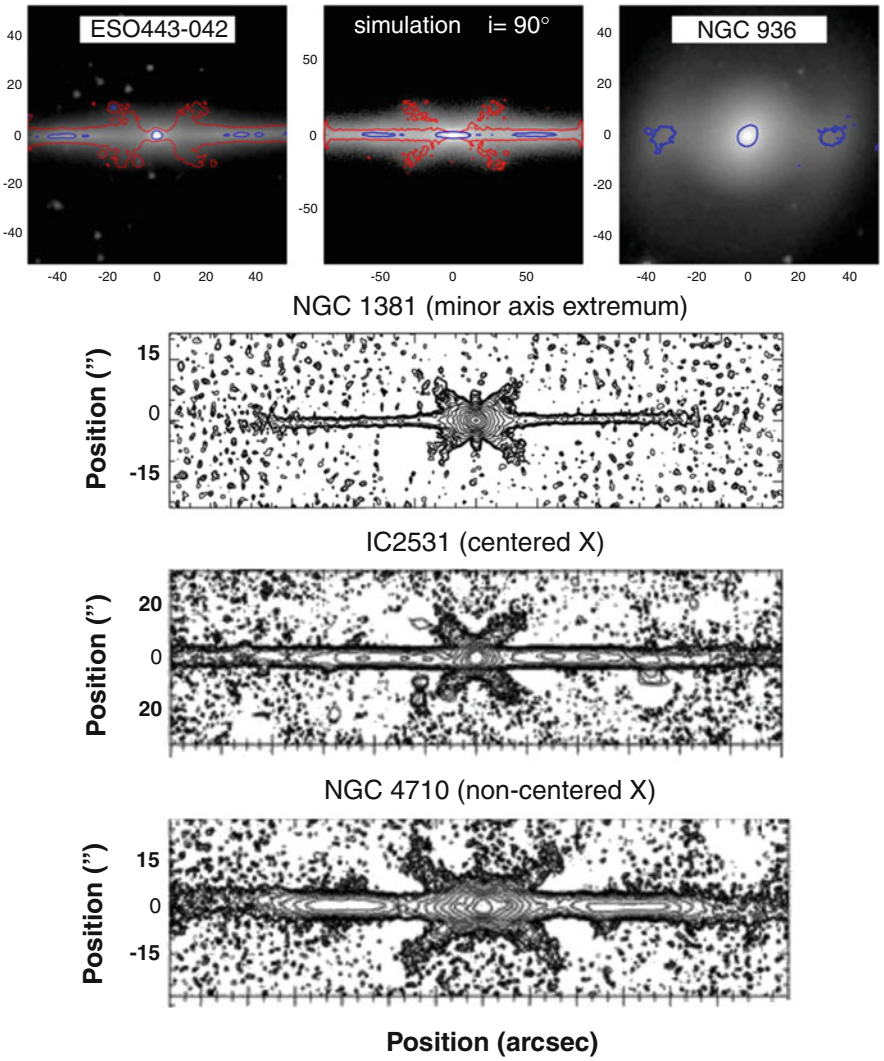

Fig. 4.4 The *upper panel* shows the Spitzer 3.6 μm images for two galaxies with vertically thick inner bar components. For the edge-on galaxy ESO 443-042 it has an X-shape morphology, whereas in NGC 936 it appears as a barlens. Also shown is a simulation model (the same as in Fig. 4.10) in which the bar has buckled in the vertical direction. The contours denote the unsharp masks of the same images: *blue highlights* the brightest regions and *red color* the X-shapes. The *lower panels* show different X-shape morphologies in the edge-on view (Taken from Bureau et al. (2006). Reproduced with permission of Oxford University Press)

(d) *Spiral arms* start from the two ends of the B/P (lower left panel in Fig. 4.5), e.g., symmetric, narrow, and elongated features appear, which on the two sides of the B/P are shifted with each other.

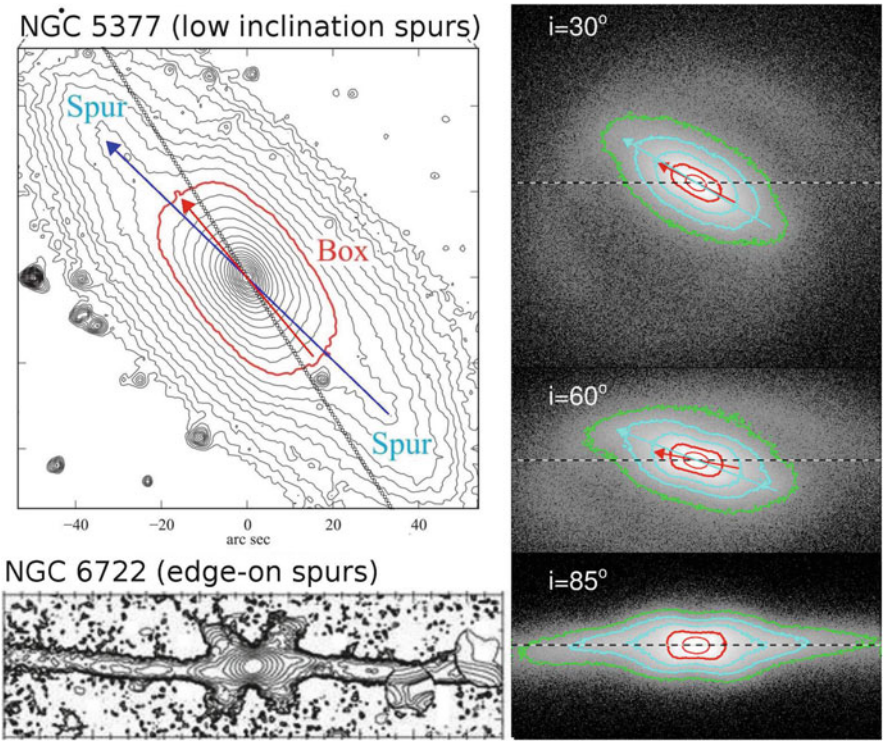

Fig. 4.5 Examples of barred galaxies with B/P-shape bulges at different viewing angles are shown. NGC 5377 shows isophotes from an archival Spitzer IRAC1 (3.6 μm) image, and NGC 6722 is an unsharp mask of the K-band image. NGC 5377 has an inclination of 59°, whereas NGC 6722 is almost edge-on. The broad, nearly rectangular region in NGC 5377 is the boxy bulge, and the "spurs" projecting outside makes the outer part of the bar. As an inclination effect, in both galaxies the "spurs" or "spiral like features", are twisted in respect to each other. *Arrows mark* their position angles, while the *dotted line* is the nodal line of the galaxy disc. Note how the position angle of the vertically thick boxy part falls between the position angles of the bar and the disc. *Right panels* show our simulations for a buckled bar (major axis makes and 35° angle with respect to nodal line), seen at different inclinations. The contours show the isophotes at different surface brightnesses, highlighting the inner and outer parts of the bar

The first two features are typical for the B/P bulges. According to Bureau et al. (2006) even 88 % of the galaxies with B/Ps have a secondary maximum along the bar major axis (in comparison to 33 % in their control sample). Also, 50 % and 38 % of the B/P bulges have off-centered and centered X-shapes, respectively (in 33 % in their control sample with no B/P structures). These features, as well as the minor-axis extremum, have been predicted also by the simulation models by Athanassoula (2005). Whether the X-shape is centered or not, in the models depends on the azimuthal angle of the bar: when viewed side-on the four branches

of the X-feature do not cross the center. However, for the centered X-shapes other explanations, like those related to galaxy interactions, have also been suggested (Binney and Petrou 1985; Hernquist and Quinn 1988; Whitmore and Bell 1988). Altogether, these comparisons showed that the most important characteristics in the morphology of the B/P bulges can be explained by bars.

Concerning the spiral arms, an overabundance in galaxies with B/P bulges was found by Bureau et al. (2006). As a natural explanation for that they suggested that the spiral arms are driven by bars, which is indeed predicted also by the dynamical models. However, it has not been convincingly shown how extended the bar driven spiral arms actually are (see Salo et al. 2010). In fact, looking at the images shown by Bureau et al. the structures that they call as spiral arms are very similar to the features called as 'spurs' by Erwin and Debattista (2013) in their recent study of more face-on barred galaxies (see upper left panel in Fig. 4.5). The 'spurs' can be understood as a combination of galaxy inclination, and the fact that the inner and outer parts of the bar have different vertical thicknesses. When the galaxy is not perfectly edge-on and the major axis of the bar makes an angle with respect of the nodal line, 'spurs' appear to be offset with respect to the major axis of the interior isophotes associated with the boxy bulge (see Fig. 4.5, middle right panel in our simulations). Using the words by Erwin and Debattista, "in an inclined galaxy projection of the B/P creates boxy isophotes which are tilted closer to the line of nodes than are the isophotes due to the projection of the other, flat part of the bar, which form the spurs". Taking into account that not all galaxies in the sample by Bureau et al. are perfectly edge-on, in the two studies we are obviously speaking about the same phenomenon.

Lütticke et al. (2000b) left open the interpretation of the central peaks in the surface brightness profiles of the B/P bulges. However, Bureau et al. (2006) take a stronger view stressing that even the central surface brightnesses can be explained by the processes related to the formation and evolution of bars. They argue that classical bulges are not needed to explain their observations. As a support for this interpretation Bureau et al. showed that the surface brightness is more pronounced along the bar major axis than in the azimuthally averaged brightness, which was suggested to mean that most of the material at high vertical distances belongs to the B/P. In their view the steep inner peak in the surface brightness profile belongs to a flat concentrated inner disc (i.e., a 'discy pseudobulge' in our notation). Alternatively, the central peak belongs to the bar, formed as an inward push of the disc material when the bar was formed. In principle the colors would distinguish between these alternatives, but in the edge-on galaxies the central regions are contaminated by dust and stellar populations of the outer disc.

4.3.3 Structural Decompositions

Two edge-on galaxies with B/P bulges, NGC 4565 and NGC 5746, have been decomposed into multiple structure components by Kormendy and Barentine (2010)

and Barentine and Kormendy (2012). In the classification by Buta et al. (2015) the Hubble types of these galaxies are SB_x(r)ab sp, and (R′)SB_x(r,nd)0/a sp. In direct infrared images the bulges in both galaxies clearly have boxy or even X-shape morphology. The surface brightness profiles were decomposed into an exponential disc, and two bulges (a 'boxy bulge' and a 'discy pseudobulge') fitted with separate Sérsic functions. In both galaxies the boxy bulges were assumed to be bars seen in nearly end-on view. For NGC 5746 there is also kinematic evidence for this interpretation, manifested as a 'figure-of-eight' line-of-sight velocity distribution, typical for boxy bars, which characteristic will be discussed in more detail in the next section.

An interesting outcome of these decompositions is that most of the bulge mass in these massive early-type disc galaxies resides in the boxy bulge. In NGC 4565 the boxy bulge-to-total mass ratio $B_{\rm boxy}/T \sim 0.4$, and $B_{\rm discy}/T \sim 0.06$ (i.e., a 'discy pseudobulge' in our notation). The 3.6 and 8 μm images and the decomposition for this galaxy are shown in Fig. 4.6. Both type of bulges are nearly exponential, along the major axis and perpendicular to that. A more simple decomposition for the same galaxy by Simien and de Vaucouleurs (1986), fitting only one de Vaucouleurs bulge ($n = 4$) and an exponential disc, leads to $B/T = 0.4$, which clearly corresponds to that obtained for the 'boxy bulge' by Kormendy and Barentine. Although the relative mass of bulge is practically the same in these two decompositions, the interpretation from the point of view of galaxy formation is totally different. This is one of those cases where the simple decomposition approach finds a classical bulge, although most of the bulge flux actually belongs to a boxy bar component. A key issue in the structural decompositions is that when there is a central peak in the surface brightness profile, and the various components of the disc are not fitted separately, leads to a massive bulge with large Sérsic index, typical for classical bulges.

Although a systematic study of the decompositions for B/P bulges seen in the edge-on view is still needed, the above discussed decompositions have already shown that there exist massive early-type spiral galaxies which have no classical bulges. Or, at least it is not self-evident how these tiny exponential central bulges should be interpreted.

4.3.4 Diagnostics of Bars in Gas and Stellar Kinematics

Although the B/P morphology can be easily recognized in the edge-on view, in most cases the images alone cannot tell whether those structures indeed form part of the bar or not. Bars in the edge-on view can be easily mixed with rings or lenses. Since the components might have different velocity dispersions which can be hotter than the underlying disc, kinematic tools to identify bars are important.

One such tool suggested by Kuijken and Merrifield (1995, see also Vega Beltran et al. 1997), is the 'figure-of-eight' structure in the line-of-sight velocity distribution (LOSVD) of galaxies, derived from the emission or absorption lines. It is based on

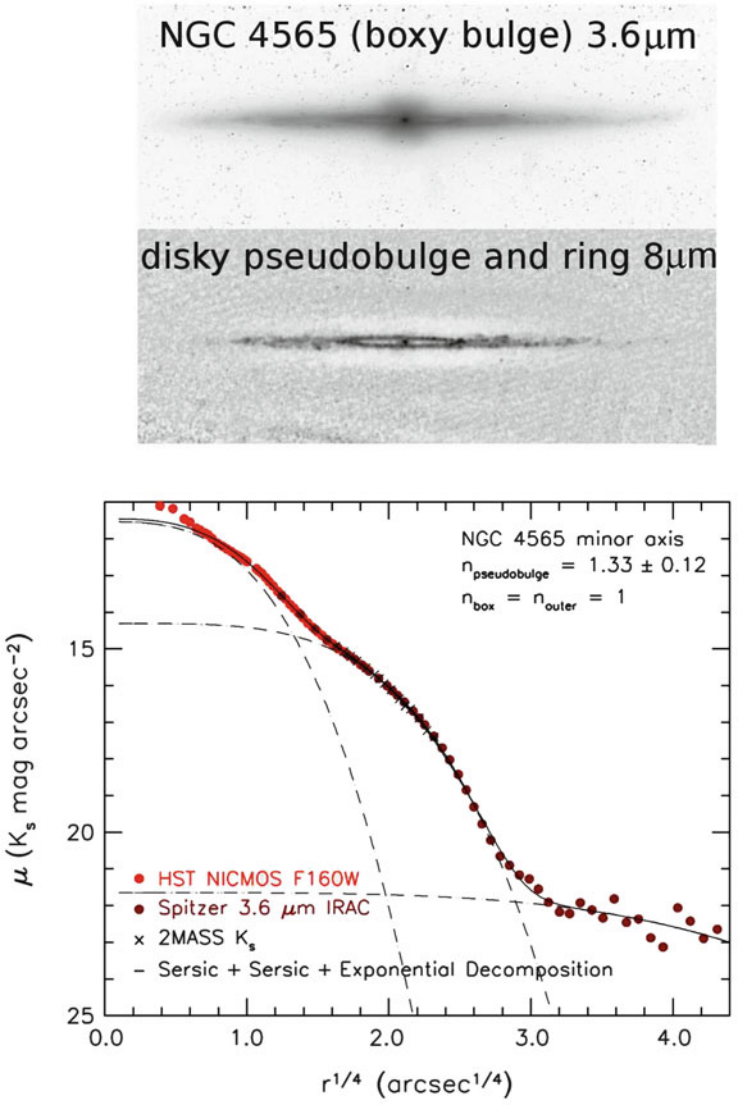

Fig. 4.6 Spitzer/IRAC 3.6 and 8 μm images of NGC 4565 (*upper and middle panels*) are shown to emphasize the boxy bulge, the ring and the tiny central pseudobulge. The *lower panel* shows a composite minor axis surface brightness profile made of the 3.6 μm image (*brown points*), and the Hubble space telescope image at F160W band (*red points*). The central pseudobulge and the boxy bulge are fitted with Sérsic functions and the outer structure with an exponential function. The *solid line* is the sum of the components. The nucleus is not fitted (The figure is taken from Kormendy and Barentine (2010), reproduced with permission of AAS)

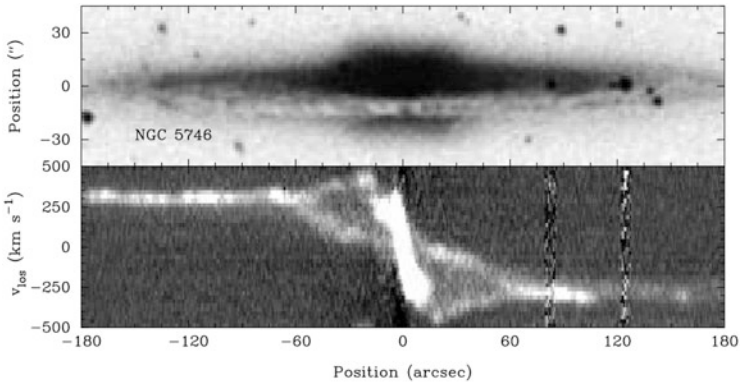

Fig. 4.7 The *upper panel* shows the K-band image of NGC 5746, and the *lower panel* the ionized gas [NII]6584 emission line position velocity diagram taken along the major axis (The figure is taken from Bureau and Freeman (1999), reproduced with permission of AAS)

the idea that the LOSVD has two peaks, one due to particles traveling in bar-related stellar orbits faster than the local circular velocity, and particles that travel more slowly than that. Variations in these velocities then form the 'figure-of-eight' in the diagram where the velocity is shown as a function of galaxy radius (see Fig. 4.7). A good correspondence of these observations with the predictions of the simulation models was obtained by Athanassoula and Bureau (1999), but soon it also became clear that this method works only for strong bars (Bureau and Athanassoula 2005).

The diagnostic tools were further developed by Chung and Bureau (2004, see also the review by Athanassoula 2005), with the main emphasis to distinguish, not only bars in general, but also the B/P bulges within the bars. The identification is based on inspection of the velocity (V_{rot}), the stellar velocity dispersion (σ), and the third and forth terms of the Gauss-Hermite parameters along the major axis (see Bender et al. 1994), which measure the asymmetric (h_3) and symmetric (h_4) deviations of the LOSVD from a pure Gaussian. The h_3 parameter is expected to be a good tracer of the triaxiality of the bulge. The main diagnostics of bars with B/P bulges are shown in Fig. 4.8. They show 'double humped' rotation curves, flat-top or weakly peaked σ-profile, and that h_3-profile correlates with V_{rot} over the projected bar length. Also h_4-profile, although being a weaker indice, shows central and secondary minima. Chung and Bureau (2004) studied 30 edge-on spirals (24 with B/Ps) and showed that even 90 % of them showed kinematic signatures of bars. Not only bars were identified, but also the edges of the B/Ps were recognized in the h_3-profiles. A large fraction (40 %) of those galaxies also showed a drop in the central velocity dispersion, being a manifestation of a dynamically cold central component.

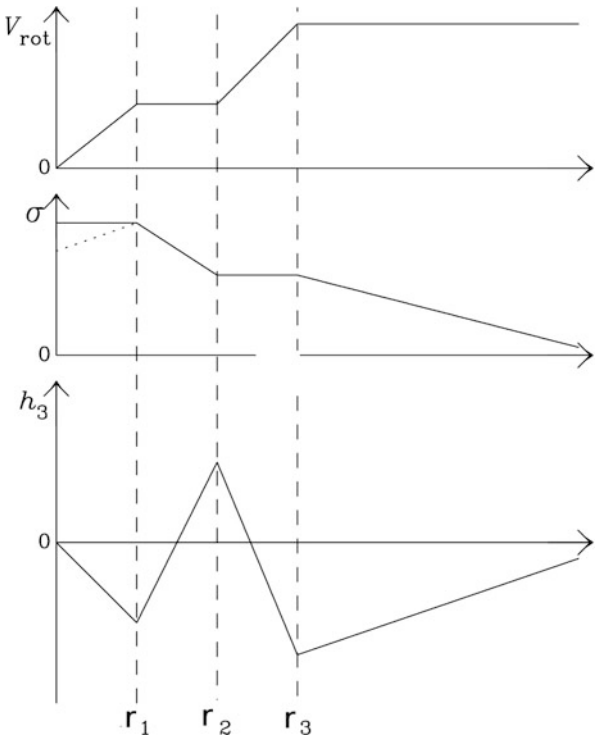

Fig. 4.8 Schematic view of the main diagnostic tools to identify bars and B/P bulges. Shown are the radial profiles of the rotation velocity V_{rot}, the stellar velocity dispersion σ, and third Gauss-Hermite moment parameter h_3. The *vertical dashed lines* indicate the radii of the central disc pseudobulge (r_1), boxy bulge (r_2) and the whole bar (r_3) (The figure is taken from Bureau et al. (2006). Reproduced with permission of Oxford University Press)

4.4 Detection and Properties of B/P-Shape Bulges in Face-On Systems

In face-on view the problem is the opposite: bars are easy to recognize in the images, but the B/P/X-shape structures, which are assumed to be thick in the vertical direction, presumably disappear in the face-on view. In fact, excluding the edge-on galaxies, the B/P-shape structures were expected to be visible only in a narrow range of galaxy inclinations near to the edge-on view. Nevertheless, using the words by Kormendy and Barentine (2010): "as long as face-on and edge-on galaxies appear to show physical differences we cannot be sure that we understand them."

4.4.1 Isophotal Analysis

Isophotal analysis of the image contours has actually appeared to be a powerful tool to identify B/Ps in moderately inclined galaxies. This has been shown in a clear manner by Beaton et al. (2007) for M31 (see also Athanassoula and Beaton 2006 for simulations), which galaxy has an inclination of 77.5°. The main idea is to fit ellipses

to isophotes, and to measure the deviations from the elliptical shapes. The sine (A_4) and cosine (B_4) terms of the Fourier series measure the boxiness and disciness of the isophotes (see Fig. 4.9). In the boxy region B_4 is positive and A_4 is negative. Characteristic for the boxy region is also that the ellipticity increases towards the edge. On the other hand, the position angle is maintained constant throughout the bar region, at least for strong bars. The image of M31 is not shown here, but it would look very much like NGC 5377 in our Fig. 4.5, which galaxy has boxy inner isophotes associated to the boxy bulge, and 'spurs' associated to the more elongated part of the bar.

A similar analysis for a larger number of galaxies has been made by Erwin and Debattista (2013). They studied 78 barred S0-Sb galaxies, covering a large range of galaxy inclinations. The leading idea in their study was to find out an optimal range of galaxy inclinations ($i < 45°$) and the bar's position angles from the nodal line for the detection of B/P. Using a small parameter space they were able to study galaxies in which both the B/P bulge and the large scale bar could be identified in the same galaxies. This allowed also a more reliable estimate for the relative size of the B/P-structure ($R_{\rm boxy}/R_{\rm bar} \sim 0.4$), which appeared to be similar to that predicted by the simulation models of bars (Pfenniger and Friedli 1991; Athanassoula and Misioritis 2002; Debattista et al. 2005), and is also similar to those obtained by Lütticke et al. (2000b) in observations. Also, extrapolating the number statistics of B/P bulges found in the ideal range of all bar/disc orientations and galaxy inclinations, they estimated that even 2/3 of bars might have B/P bulges. Taking into account that a certain fraction of bars at all inclinations must be end-on, this fraction is not far away from the suggestion made by Lütticke et al. (2000b) that all bars might have B/P structures. However, the extrapolation made by Erwin and Debattista for making their prediction is based only on a few galaxies with identified bars and B/P structures in the same galaxies.

A large majority of bars in the sample by Erwin and Debattista (2013) have boxy, rather than peanut-shape isophotes. A given explanation was that in the central regions of the B/P-structures there exist extra inner discs or compact bulges, which smooth out the peanut shape. In fact, the basic assumption in all the morphological and isophotal analysis of the B/P bulges discussed above is that the vertically thick inner parts of bars have either boxy or peanut shapes. However, based on the simulation models by Athanassoula et al. (2014) that is not necessarily the case in the face-on view where they can appear fairly round. In fact, the orbits populating the bars might have more complicated structures than just regular orbits around 3D bar-supporting periodic orbits (see Patsis and Katsanikas 2014a).

4.4.2 Properties of Barlenses

A different approach was taken by Laurikainen et al. (2011) who identified distinct morphological structures called barlenses, in a sample of ∼200 early-type disc galaxies (NIRS0S atlas), observed at fairly low galaxy inclinations ($i \leq 65°$).

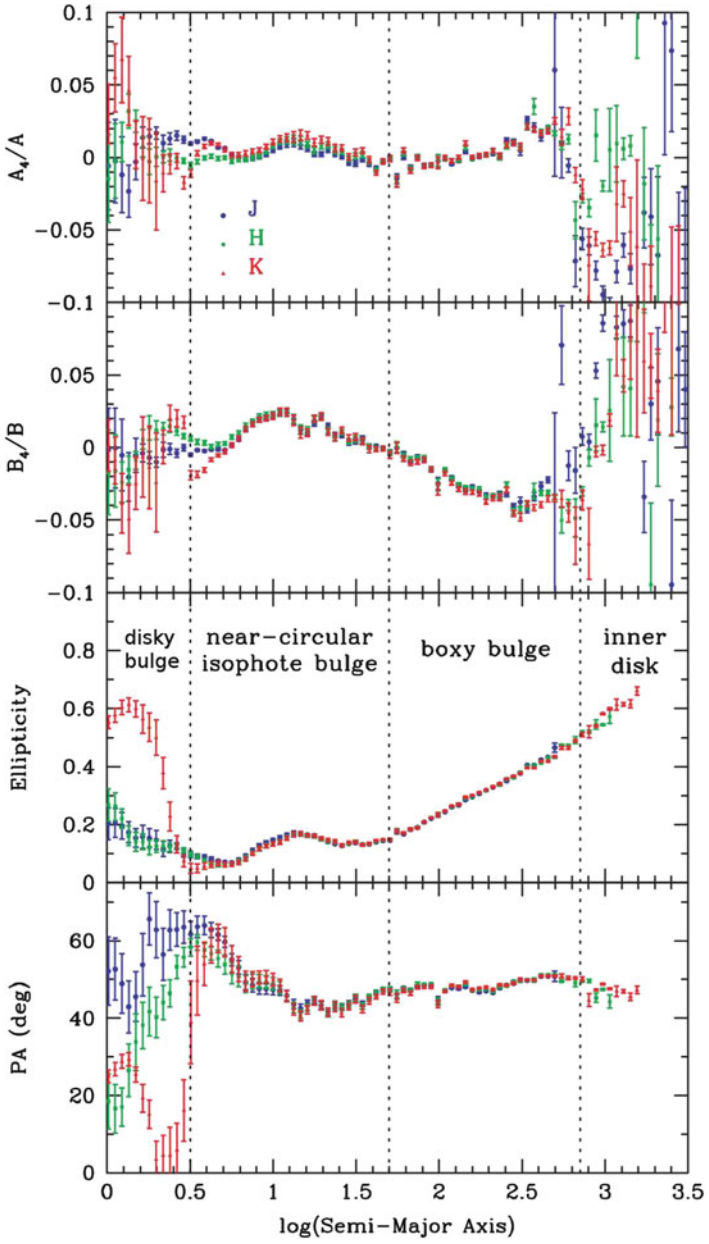

Fig. 4.9 Isophotal analysis of M31 which galaxy has a boxy bulge. Radial profiles (in arcseconds) of the ellipticities and position angles of the isophotes are shown in the *two lower panels*. The *upper panels* show the sine (A_4) and cosine (B_4) terms of the Fourier series of the same isophotes. Shown separately are the measurements in J, H and K-band bands. The regions covering the near-nuclear bulge ('discy pseudobulge' in our notation), boxy bulge, and inner disc (equivalent to 'spurs' in our Fig. 4.5) are shown by *dotted lines* (The figure is taken from Beaton et al. (2007), reproduced with permission of AAS)

Barlenses were recognized as lens-like structures embedded in bars, covering typically half of the barlength. In distinction to nuclear lenses they are much larger, and compared to classical bulges the surface brightness distribution decreases much faster at the edge of the structure. In Laurikainen et al. (2011) and in Buta et al. (2015) barlenses have been coded into the classification. These structures (though not yet called as such) were decomposed with a flat Ferrers function in many S0s already by Laurikainen et al. (2005). This kind of decompositions were summarized in Laurikainen et al. (2010). In Laurikainen et al. (2007) it was speculated that such inner lens-like structures might actually be the face-on views of the vertically thick B/P bulges. If barlenses indeed are physically the same phenomenon as the B/P bulges, that would make possible to have a consistent view of the relative masses of the classical and pseudobulges at all galaxy inclinations.

Two prototypical barlens galaxies, NGC 936 and NGC 4314, are shown in Figs. 4.4 and 4.10. In the images barlenses can be easily mixed with the classical bulges. However, in the surface brightness profiles barlenses appear as nearly exponential, flat sub-sections, both along the major and the minor axis of the bar. Characteristic morphological features for barlens galaxies are the ansae (or handles), which appear at the two ends of the bar (see NGC 936 in Fig. 4.4). It has been shown (Laurikainen et al. 2013) that even half of the barlenses are embedded in that kind of bars. In Sect. 4.3.2 we discussed that such flux enhancements are produced also in galaxy simulations, at the same time when the bar buckles in the vertical direction. This can be considered as further indirect evidence supporting the idea that barlenses indeed form part of a buckled bar. The unsharp mask image of NGC 4314 also shows a structure connecting the barlens to the more elongated part of the bar (see Fig. 4.10). Using the measurements in the NIRS0S atlas Athanassoula et al. (2014) showed that, in respect of the bar, barlenses have very similar sizes as obtained for the B/P bulges by Lütticke et al. (2000b) and Erwin and Debattista (2013).

Morphological structures similar to the observed barlenses are produced by N-body and smoothed particle hydrodynamical simulations by Athanassoula et al. (2013). In Athanassoula et al. (2014) detailed comparisons between the observations and models are shown. In their models barlenses appear in the face-on view without invoking any spheroidal bulge components in the initial models. An example of a barlens in such simulation model, seen both in the edge-on and face-on views, is shown in Fig. 4.10 (two lower left panels). Recent orbital analysis of bars by Patsis and Katsanikas (2014b) have shown that "sticky chaotic" orbits, building parts of bars can appear at high vertical distances in such a manner that when seen in the face-on view they form a boxy inner structure inside the bar (their fig. 8). These bar orbits might be the ones associated to barlenses in some cases. Whether also the X-shape is visible inside the boxy component depends on the specific combination of the orbital families of bars. A more thorough discussion of possible orbits making the barlens is given by Athanassoula in this book.

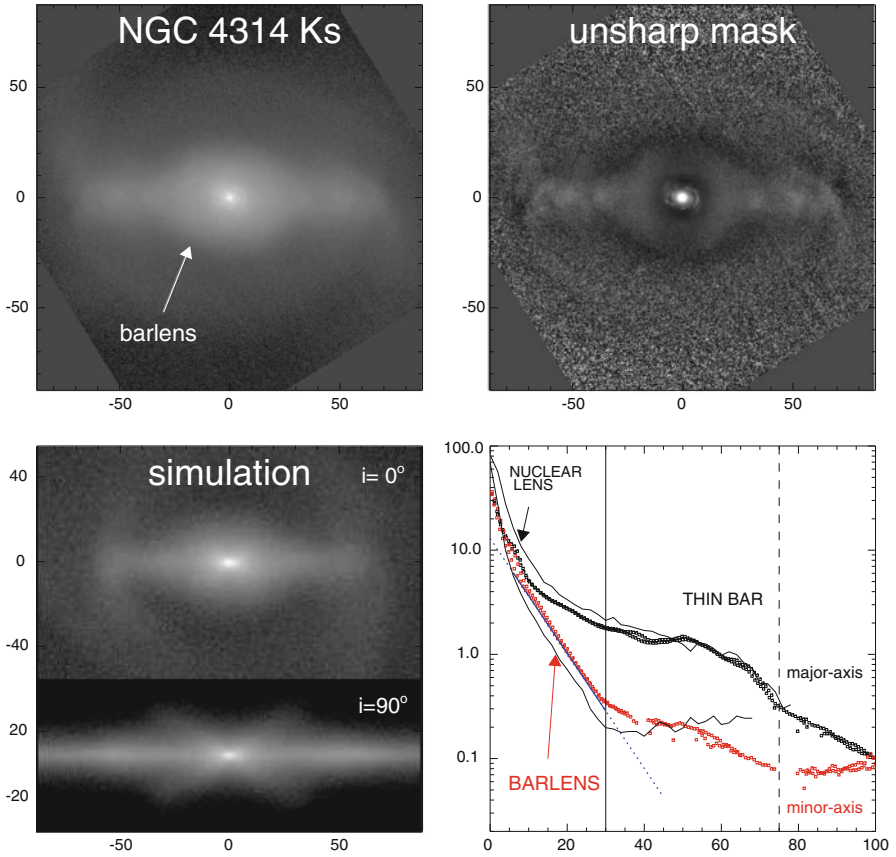

Fig. 4.10 An example of a barlens galaxy NGC 4314, showing the K_s-band image from Laurikainen et al. (2011; *upper left panel*) and the unsharp mask image of that (*upper right panel*). The surface brightness profiles along the bar major (*black symbols*) and minor axis (*red symbols*) are also shown. The *lower left panel* shows the simulation model gtr115 from Athanassoula et al. (2013, 2014), both in the face-on and edge-on view. The simulation model profiles are shown by *solid lines* in the profile plot. Axis labels are in arcseconds in all panels (The figure is taken from Laurikainen et al. (2014), reproduced with permission of Oxford University Press)

4.4.3 Barlenses: The Face-On Counterparts of B/P Bulges

If barlenses and B/P/X-shape bulges indeed were physically the same phenomenon, just seen at different viewing angles, we should see that in the number statistics in a representative sample of nearby galaxies. That has been looked at by Laurikainen et al. (2014) using a sample of 2465 nearby galaxies at 3.6 or 2.2 μm wavelengths, covering all Hubble types and galaxy inclinations (a combination of NIRS0S, and the Spitzer Survey of Stellar Structure of galaxies S^4G). In order to find out all the X-shape structures unsharp masks were done for all these galaxies, in a similar

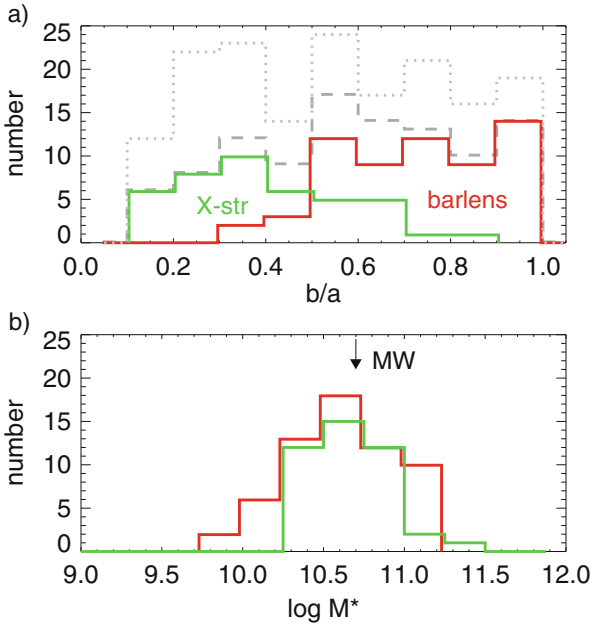

Fig. 4.11 The distributions of (**a**) galaxy minor-to-major (b/a) axis ratios and (**b**) total stellar masses (in units of solar masses) of the galaxies, hosting either barlens (*red*) or X-shape structures (*green*). In these plots a magnitude-limited ($B_T \leq 12.5$ mag) sub-sample of 365 barred galaxies in a combined S^4G and NIRS0S is used. The *grey dashed* and *dotted lines* show the barlens and X-shapes structures, in the magnitude-limited sample and the complete S^4G, respectively (Reproduced with permission of Oxford University Press)

manner as was done previously by Bureau et al. (2006) for a representative sample of edge-on galaxies. Barlenses were recognized in the galaxy classifications of Buta et al. (2015) and Laurikainen et al. (2011). Remarkably, the apparent axial ratios of the galaxies with barlenses and X-shape structures are consistent with a single population viewed from random orientations (Fig. 4.11, upper panel). Although barlenses appear in less inclined galaxies, there is a large overlap in their parent galaxy inclinations, compared to those with X-shape structures. The parent galaxies of barlenses and X-shape structures have similar distributions of total stellar mass (Fig. 4.11, lower panel), and also similar red colors. It is worth noticing that the peak in the mass distribution of these galaxies appears at the Milky Way mass. There are also similarities in the kinematics of barlenses and X-shape structures, which will be discussed in Sect. 4.4.5.

It appears that among the S0s and early-type spirals even half of the barred galaxies have either a barlens or an X-shape structure, and ~30 % if also the non-barred galaxies are included in the statistics (Laurikainen et al. 2014). This is not much less than the 45 % of B/Ps found by Lütticke et al. (2000a) among the edge-on galaxies in the same morphological type bin. The slightly lower B/P fraction by

Laurikainen et al. can be explained by the fact that limiting to X-shape structures, most probably they picked up only the strong bars where the X-shapes are more pronounced (Athanassoula 2005). As Lütticke, Dettmar and Pohlen did not use any unsharp masks we don't know how many of the galaxies in their sample actually have X-shape structures. Most probably not all of them, because boxy isophotes can be identified in the edge-on view even if the bulges have no X-shapes. Fractions of B/Ps has been recently studied also by Yoshino and Yamauchi (2015) in a sample of 1700 edge-on galaxies in the optical region. In order to identify bars a comparison sample of 2600 more face-on galaxies was used. It was then assumed that the bar fraction is the same among the edge-on galaxies. They found that B/Ps appear in 20 % of the galaxies, which fraction is much lower than the 45 % found by Lütticke et al. (2000a). However, according to Yoshino and Yamauchi the fraction of B/Ps they found is very similar to that obtained by Lütticke, Dettmar and Pohlen if the weakest category of B/Ps by Lütticke et al. is omitted.

4.4.4 Structural Decompositions

The assumption that barlenses and B/P bulges are physically the same phenomenon allows us to estimate the relative masses of these components, since this can be done in a fairly reliable manner at moderate galaxy inclinations ($i \leq 65°$) using multi-component decompositions. When the inclination of the disc increases, the reliability of these mass estimates rapidly decreases. The decompositions of Barentine and Kormendy (2012) discussed earlier were made to one-dimensional surface brightness profiles, which is indeed a reasonable approach for the galaxies in the edge-on view. However, applying a similar approach in a more face-on view, in particular when the bar has two components, would dilute the non-axisymmetric structure components, which would appear as one big bulge in the average surface brightness profile (in terms of the flux above the disc). A better approach is to fit the two-dimensional flux distributions of the galaxies.

Examples of the decompositions using a two-dimensional approach and fitting the two bar components separately, allowing also the parameters of the B/P/barlens to vary, are taken from Laurikainen et al. (2014). They used the 3.6 μm Spitzer images to decompose 29 nearby galaxies having either a barlens or an X-shape structure. The bulges (i.e., the central mass concentrations) and discs were fitted with a Sérsic function, whereas the two bar components were fitted either using a Ferrers or a Sérsic function. Representative examples of these decompositions are shown in Fig. 4.12. It appeared that the relative fluxes of barlenses and X-shape bulges form on average even 10–20 % of the total galaxy flux, in comparison to ∼10 % in the central bulges (i.e., a 'discy pseudobulges'). In IC 5240 (Sa) the only bulge seems to be the X-shaped bar component. On the other hand, NGC 4643 ($S0^+$) might have also a small central bulge embedded in the barlens. Looking at the surface brightness profile alone we don't know for sure whether the central peak is really a distinct bulge component, or is it rather formed of the same material as

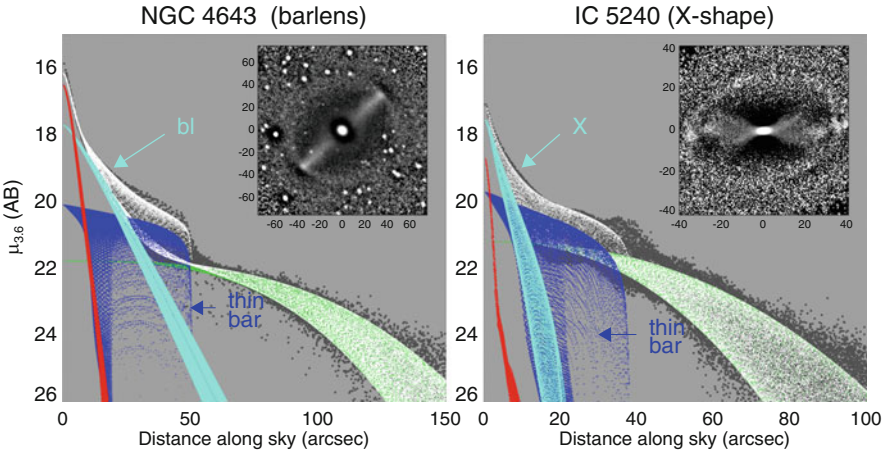

Fig. 4.12 Decomposition models for the barlens and X-shaped galaxies NGC 4643 and IC 5240, which are barred galaxies with Hubble stages $S0^+$ and Sa, respectively. The unsharp mask images are shown in the small *inserts* in the upper corners. *Black dots* are the pixel values of the two-dimensional flux-calibrated 3.6 μm Spitzer images, and *white dots* show the pixel values of the total decomposition models. *Red* and *green dots* show the bulge and the disc components, whereas the *dark* and *light blue* indicate the thin and thick bar (i.e., the barlens and X-shape structure) components (The figure is taken from Laurikainen et al. (2014), reproduced with permission of Oxford University Press)

the rest of the bar, at the epoch of bar formation. The Sérsic index of the central component is $n = 0.7$ indicating that it is not a classical bulge. One possibility is that it is a manifestation of an old pseudobulge formed at high redshift, composed of old stars. That kind of pseudobulges form in the hydrodynamical cosmological simulations by Guedes et al. (2013), via a combination of disc instabilities and minor mergers.

If the B/P bulges (i.e., the barlenses or X-shape structures in the above decompositions) are omitted in the decompositions that would dramatically affect the obtained relative masses of the classical bulges. In the early-type disc galaxies the deduced central bulge will increase from 10 % to 35 % in the sample by Laurikainen et al. (2014), the value 35 % being consistent with the previous more simple bulge/disc/bar decompositions (Gadotti 2009; Weinzirl et al. 2009). In Sect. 4.3.3 we discussed an edge-on galaxy, NGC 4565, for which galaxy the same happens when the simple and more detailed decompositions are compared.

We can compare the decompositions by Laurikainen et al. (2014) with those obtained by Erwin et al. (2003) for NGC 2787 and NGC 3945 . Using a completely different decomposition approach they ended up with similar small relative masses for the central bulges in these two galaxies, just different names were used for the bulges. What is a barlens in Laurikainen et al. (2014), is called as an inner disc by Erwin et al., which discs are a magnitude larger than the central classical bulges, manifested as peaks in the surface brightness profiles. Similar approach

as in Erwin et al. (2003) has been recently taken also by Erwin et al. (2015) for additional seven barred early-type galaxies, but now calling the "inner discs" as "discy pseudobulges". They identified boxy isophotes only in one of those galaxies, but many of them are classified as having a barlens by Laurikainen et al. (2011).

The small central B/P bulges are indeed intriguing, and the obtained nature of those bulges depends on how they are interpreted. As discussed by Chung and Bureau (2004), and more recently by Mendez-Abreu et al. (2014), cool disc components manifesting as nuclear rings or spiral arms, are often embedded in the B/P bulges. An example of a barlens galaxy with similar characteristics is NGC 4314, showing a star forming nuclear ring inside the boxy bulge. However, at least in the near-IR these central cool components are expected to contribute very little in the surface brightness profiles.

4.4.5 Diagnostics of B/P Bulges of Stellar Kinematics

Using simulation models an attempt to identify B/P structures in more face-on galaxies was done by Debattista et al. (2005). The diagnostics largely relies on the analysis of the fourth-order Gauss-Hermite moment, h_4 along the bar major axis. A B/P bulge is recognized as negative double minima in the h_4-profile. These minima appear because the vertical velocity distribution of stars becomes broader, for which reason h_4 is a good proxy for the unobservable vertical density distribution. However, in spite of the smart idea, this method has been applied only for a few galaxies with B/P bulges, like NGC 98 (Méndez-Abreu et al. 2008). The reason is that the observations are very demanding and require a large amount of observing time at large telescopes. The diagnostics for NGC 98 is shown in Fig. 4.13. The size of the B/P is estimated from the radius of the minimum in the h_4-profile, which in this case is 0.35 times the bar semi-major axis length. The same diagnostics has been recently applied for ten more face-on barred galaxies by Mendez-Abreu et al. (2014). They identified B/P bulges in two additional galaxies, and marginally in three more galaxies. In four of these galaxies a dynamically cool central component inside the B/P bulge was the only central bulge, without any sign of a dynamically hot classical bulge.

In the above studies long-slit spectroscopy was used. In principle integral-field unit (IFU) spectroscopy would be ideal to trace the B/P/X/barlens features, but the resolution and the field-of-view have not yet been sufficient for very detailed studies of B/Ps (see the review by Falcon-Barroso in Section 7). So far the largest survey using IFU spectroscopy is the ATLAS^{3D}, in which 260 nearby early-type galaxies, at all galaxy inclinations, have been mapped within one effective galaxy radius (Cappellari et al. 2007; Emsellem et al. 2011). Almost all bulges (86 %) were found to be fast rotating, which is consistent with the idea that most of the bulge mass in the nearby galaxies resides in the B/P/barlens bulges, rotating with the underlying disc (see Laurikainen et al. 2014). Most probably due to the limitations of the observations only a small fraction (15 %) of the fast rotating bulges showed

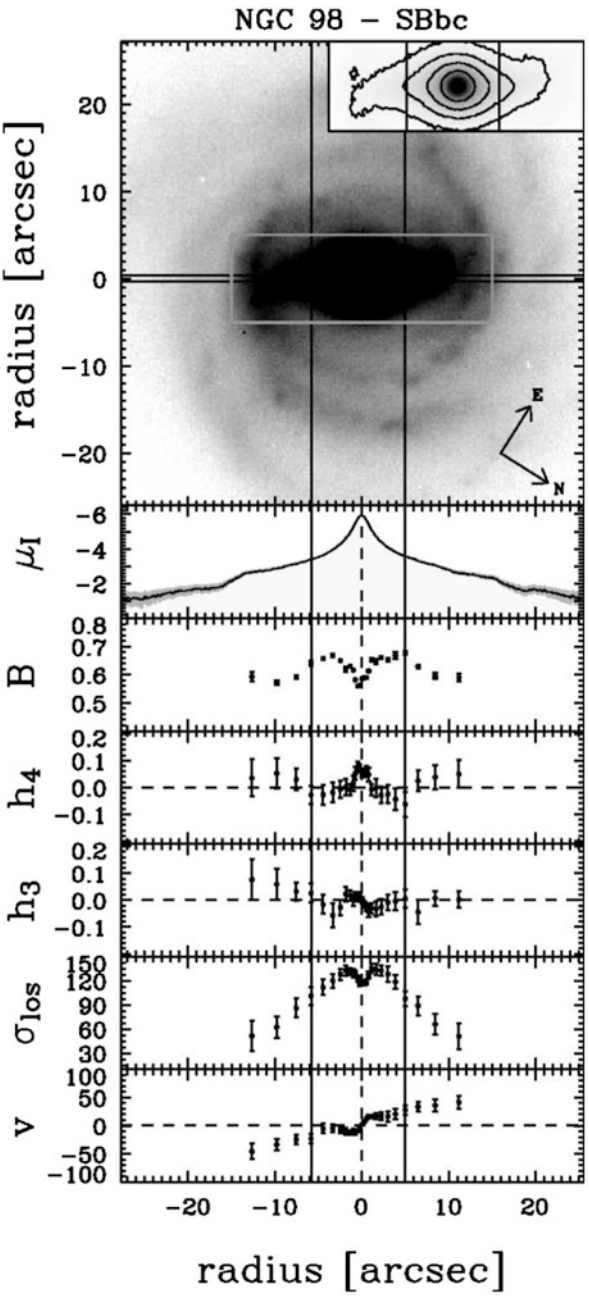

Fig. 4.13 Morphology and stellar kinematics of NGC 98. The *top panel* shows the I-band image, where the slit position and image orientation are also indicated. The *inset* shows the portion of the galaxy image marked with a *white box*. The panels show from top to bottom the radial profiles of surface brightness, broadening parameter B, fourth (h_4) and third (h_3) moments of the Gauss-Hermite series, line-of-sight velocity dispersion (σ_{los}), and the stellar velocity v. The *two vertical lines* indicate the location of the h_4 minima associated with the B/P region in NGC 98 (The figure is from Méndez-Abreu et al. (2008). Reproduced with permission of AAS)

signatures of B/P-structures, in terms of double peaked rotation curves or twisting isophotes (see Krajnovic et al. 2011).

We used the Atlas3D in the following manner. We picked up all those barred galaxies that have either a barlens or an X-shaped structure identified in the images in the sample by Laurikainen et al. (2014), and then looked at what kind of kinematics the Atlas3D finds for those galaxies. We found 27 galaxies in common between the two surveys (11 with X-shapes, 16 with barlenses). It appeared that all these galaxies are classified as regular fast rotators in Emsellem et al. (2011). Half of them have 'double humped' rotation curves, indicative of B/P-structures, but the other half has no particular kinematic features of which the vertically thick bar components could be identified. It is interesting that the fractions of the double humped rotation curves are fairly similar among the galaxies having barlenses and X-shaped structures (56 % and 36 %, respectively), which fractions are much higher than for the bulges in the Atlas3D in general. This is consistent with the idea that barlenses and B/P bulges are manifestations of the same physical phenomenon.

From the point of view of galaxy formation, the interpretation of bulges is complicated because internal dynamical effects in galaxies might modify the kinematic properties of bulges. For example, it has been suggested by Saha et al. (2012) that a small bulge embedded in a bar can absorb angular momentum from the bar, with a consequence that an initially non-rotating classical bulge can transform into a cylindrically rotating triaxial object. Saha and Naab (2013) have also suggested that the appearance of B/P bulges might be connected to the properties of dark matter halos.

4.5 Stellar Populations of B/P Bulges

Stellar populations of bulges in barred and non-barred galaxies have been compared using both absorption line-indices and applying stellar population synthesis methods, but no clear conclusions are derived. Using line-indices for 20 fairly face-on early-type barred galaxies and comparing them with the non-barred galaxies by Moorthy and Holzman (2006), Pérez and Sánchez-Blázquez (2011) found that bulges in barred galaxies are more metal-rich and more α-enhanced than in non-barred galaxies. The α-enhancement is associated to rapid star formation event, which is not expected if bulges formed via vertical buckling during the formation and evolution of bars. Synthetic stellar population methods has been applied for 62 barred and non-barred galaxies by Sánchez-Blázquez et al. (2014), also for fairly face-on galaxies. However, no difference in metallicity or age gradients between barred and non-barred galaxies were found. A sample of 32 edge-on galaxies was studied by Jablonka et al. (2007), and again no difference in the stellar populations of bulges was found between barred and non-barred galaxies.

From our point of view critical questions are do the barred galaxies in the above samples have B/P/barlens bulges or not, and what was measured as a 'bulge'. For the first sample detailed morphological classifications exist for 10 galaxies and it

appears that even half of those have barlenses in Laurikainen et al. (2011). In the second sample 11 barred galaxies have detailed classifications, but none of them have neither B/P nor barlens. In Pérez and Sánchez-Blázquez (2011) the bulges were taken to be the central regions of the galaxies, which means also central regions of barlenses. In most of the bulges studied by them star forming nuclear rings and spiral arms were detected. In these fairly face-on galaxies the star forming structures obviously had a strong impact on the obtained stellar populations and metallicities, and do not tell about the main stellar population of the B/P bulges. It was pointed out already by Peletier et al. (2007) that composite bulges in stellar populations indeed exist. And also, that due to dust in the disc plane, at least in the optical region, the stellar populations and metallicities in the edge-on and face-on views are expected to be different.

Clearly, understanding the different bulge components calls for detailed studies of individual galaxies. Based on the analysis of four early-type galaxies Sánchez-Blázquez et al. (2011) showed that most of the stars in bulges are very old (10 Gyr), as old as in the Milky Way bulge. The same is true for bars, in which the stellar population ages are closer to the bulges than to the discs outside the bars (Pérez et al. 2009). The stellar populations of the B/P bulges in 28 edge-on early-type disc galaxies (S0-Sb) have been studied by Williams et al. (2011, 2012), and compared with the elliptical galaxies. They looked at the properties both in the central regions, covering the seeing-limited part of the boxy bulge, and in the main body of the B/P structures. The central peaks were found to have similar old stellar populations and high stellar velocity dispersion as in elliptical galaxies. However, the main body of the B/P bulge lacks a correlation between the metallicity gradient and σ, which correlation appears in elliptical galaxies. Metallicity gradients are easily produced in a monolithic collapse in the early universe, and at some level also in violent galaxy mergers. But even the non-barred galaxies in their study appeared to have stronger metallicity gradients than the B/P bulges of the same galaxy mass.

In the literature it is often argued that the stellar populations of bulges in S0-Sbc galaxies are similar to those of the elliptical galaxies (Proctor and Sansom 2002; Falcón-Barroso et al. 2006; MacArthur et al. 2009), which similarity breaks only in the later type spirals (see Ganda et al. 2007). However, based on the analysis by Williams et al. (2012), whether the bulges are similar to the ellipticals or not, depends on what do we count as a bulge. If we mean the central peaks in the radial flux distributions, then the answer is that the bulges indeed are much like the elliptical galaxies, but if we are talking about the main body of the B/Ps, then the stellar populations are different from the elliptical galaxies.

An interesting example is NGC 357 (de Lorenzo-Cáceres et al. 2012) for which galaxy all critical diagnostics of B/P-structures have been made, including the isophotal and stellar population analysis, kinematics, and structural decompositions. They found that no single unambiguous interpretation can be given for the bulge. The galaxy has two bars, which further complicates the interpretation. This example demonstrates that based on the same analysis completely different interpretations can be given for the bulge, depending on whether only the central peak, with high rotation and σ drop, is considered as a bulge (i.e., a 'discy pseudobulge' in

our notation), or the larger region with high σ is taken to be the bulge (i.e., the classical bulge in our notation). In their view, a problem in the first interpretation is that the bulge has an old stellar population, generally not accepted for a 'discy pseudobulges'. If a classical bulge is assumed then the problem is the nearly exponential surface brightness profile. If the bulge is interpreted as a classical bulge then there exists also a cool central disc inside that bulge.

But for the interpretation of this particular galaxy there exists also a third possibility, namely that there is a boxy bulge and a central cool disc embedded in that. In this fairly face-on galaxy no B/P is identified in the isophotal analysis, but the galaxy looks very much like NGC 4643, in which galaxy a barlens has been recognized (see Laurikainen et al. 2014). The main bulge with the old stellar population and a small Sérsic index could simply corresponds to the boxy bulge, which can also be dynamically fairly hot. The σ drop could be associated to a central cool disc embedded in the boxy bulge. It is worth noticing that the bulge has similar V-H color as the rest of the galaxy, up to the outer radius of the bar (Martini et al. 2003), which fits into this interpretation. However, the purpose of this paragraph is not to give the 'right interpretation', but rather to demonstrate that not only detailed observations are needed to study the bulges, but also the interpretation depends on the current understanding of bulges.

4.6 Summary and Discussion

Nearly half of the highly inclined galaxies in the nearby universe are found to have B/P/X-shape bulges. Barlenses, which appear in more face-on galaxies, are likely to be physically the same phenomenon. These structures appear in bright galaxies, in a mass range near to the Milky Way mass. Also the other properties of these bulges, including morphology (B/P/X-shape), kinematics (cylindrical rotation or double humped rotation curves), and stellar populations (old), are similar to those observed in the Milky Way. Cool central discs are often embedded inside the B/P/barlens bulges, in which case they are called as composite bulges. Barred galaxies with composite bulges can contain also dynamically hot classical bulges, but it is not yet clear to what extent they, in the Milky Way mass galaxies, are really dynamically distinct structure components, and to what extent stars wrapped into the central regions of the galaxies during the formation and evolution of bars.

A comparison of the observed properties of B/P/barlens bulges with the simulation models have shown that they can indeed be explained as disc structures, possible formed by buckling instabilities soon after the bars were formed. It is unlikely that any significant fraction of B/P bulges were triggered by tidal effects. Independent of the exact isophotal shapes, these structures typically cover nearly half of the bar size, but can be also smaller or larger than that. Also, recent structural multi-component decompositions have shown that most of the bulge mass in these galaxies might appear in the B/P/barlens bulges. The exceptions are the boxy structures appearing in the most massive ($M > 10^{11}\,M_\odot$) slowly rotating galaxies,

which are often elliptical galaxies (sometimes S0s) in classification. Exceptions are also the 'thick boxy bulges', which might actually be manifestations of thick discs in the otherwise almost bulgeless galaxies.

If we believe that most of the bulge mass in the Milky Way mass galaxies indeed appears in the B/P/barlens bulges, it means that the masses of the classical bulges must be very low in all Hubble types, even in the early-type disc galaxies which are usually assumed to contain most of the baryonic spheroidal mass. If we are unwilling to accept this conclusion, then it needs to be explained how the observed morphological and kinematic properties of the B/P/X-shape/barlens bulges are created in galaxies. Why is this view then not accepted as a paradigm in the astronomical community? Actually, the argument that the B/P bulges form part of the bar, has been accepted, but perhaps not the idea that such bar components could contain most of the bulge mass in the Milky Way mass nearby galaxies. One possible reason for that is that the relative masses of bulges are generally estimated from decompositions performed for fairly face-on systems, in which galaxies the massive, round components are often erroneously interpreted as classical bulges.

The explanations discussed for the formation of pseudobulges in this review are related to the evolution of bars. A natural question is then what makes the bulges in the non-barred galaxies? If barred and non-barred galaxies live in similar galaxy environments also the accretion events should be similar, leading to bulge masses not too different from each other. The relative masses of bulges in barred and non-barred galaxies are compared for S^4G sample (Sheth et al. 2010) of 2350 galaxies at 3.6 μm by Salo et al. (2015). For galaxies brighter than $M^* > 10^{10}\,M_\odot$ larger bulge masses were found for barred galaxies ($B/T \sim 0.15$ and $B/T \sim 0.09$, respectively). Since in this study a photometric definition of a 'bulge' was used (excess flux above the disc in the surface brightness profile), this difference most probably reflects the fact that in barred galaxies part of the apparent bulge mass is associated to the B/P/barlens bulge. Also, there is some observational evidence that even in the non-barred galaxies the bulges might have a B/P/barlens origin, once the thin part of the bar has been dissolved (see Laurikainen et al. 2013). The orbital analysis by Patsis et al. (2002b) also predicts that peanuts may form even in galaxies without creating any elongated, vertically thin bar components. Naturally, there exist also other ways of making pseudobulges in the non-barred galaxies, of which minor mergers are one of the most prevalent (see Eliche-Moral et al. 2013).

As a concluding mark we can say that in order to fully understand bulges the same formative processes need to be valid both in the edge-on and in face-on views. Also, it has become evident that bulges are complex systems so that detailed studies of individual galaxies are needed to separate the different bulge components. But even in that case, the interpretation always reflects also the prevalent theoretical understanding of a bulge, regardless of how sophisticated diagnostics are used.

> Zu dem gebrauchten sowohl, wie zum dumpfen und stummen Vorrat der vollen Natur, den unsäglichen Summen, zähle dich jubelnd hinzu und vernichte die Zahl.
>
> Rainer Marie Rilke

Acknowledgements We acknowledge the constructive comments from the referee. We also acknowledge the DAGAL Marie Curie Initial Training Network and the financial support from the Academy of Finland.

References

Athanassoula, E. 2005, MNRAS, 358, 1477
Athanassoula E., and Beaton, R. 2006, MNRAS, 370, 1499
Athanassoula, E., Machado, R., and Rodionov, S. A. 2013, MNRAS, 429, 1949
Athanassoula, E., Laurikainen, E., Salo, H., and Bosma, A. 2014, astro-ph 1405.6726
Athanassoula, E., and Bureau, M. 1999, ApJ, 522, 699
Athanassoula, E., and Misioritis, A. 2002, MNRAS, 330, 35
Aronica G., Athanassoula, E., Bureau, M., Bosma, A., Dettmar, R.-J., Vergani, D., and Pohlen, M. 2003, ApSS, 284, 753
Barentine J., and Kormendy, J. 2012, ApJ, 754, 140
Beaton, R., Majewski, S., Guhathakurta, P. Skrutskie, M. F., Cutri, R. M., Good, J., Patterson, R. J., Athanassoula, E., and Bureau, M. 2007, ApJ, 658, 91
Bertola, F., and Capaccioli, M. 1977, ApJ, 211, 697
Bender, R., Surma, P., Doebereiner, S., Moellenhoff, C., and Madejsky, R. 1989, A&A, 217, 35
Bender, R., Saglia, R., and Gerhard, O. 1994, MNRAS, 269, 785
Binney, J., and Petrou, M. 1985, MNRAS, 214, 449
Burbidge, G., and Burbidge, M. 1959, ApJ, 130, 20
Bureau, M., and Freeman, K. 1999, AJ, 118, 126
Bureau, M., and Athanassoula, E. 2005, ApJ, 626, 159
Bureau, M., Aronica, G., Athanassoula, E., Dettmar, R.-J., Bosma, A., and Freeman, K. C. 2006, MNRAS, 370, 753
Buta, R. Sheth, K., Athanassoula, E., Bosma, A., Knapen, J., Laurikainen, E., Salo, H. et al. 2015, ApJS, 214, 32
Cappellari, M., Emsellem, E., Bacon, R. Bureau, M., Davies, R. L., de Zeeuw, P. T., Falcón-Barroso, J. et al. 2007, MNRAS, 379, 418
Cole, D., Debattista, V. P., Erwin P., Earp, S., and Roskar, R. 2014, MNRAS, 445, 3352
Combes, F., and Sanders, R. H. 1981, A&A, 96, 164
Chung, A., and Bureau, M. 2004, AJ, 127, 3192
de Vaucouleurs, G. 1974, In Formation and Dynamics of Galaxies, IAUS No. 58, edited by J.R. Shakeshalf (Reidel, Dordrecht). p. 335
Debattista V.P., Carollo C., Mayer L., and Moore, B. 2005, ApJ, 628, 678
Debattista V., Mayer L., Carollo M., Moore, B., Wadsley, J., and Quinn, T. 2006, ApJ, 645, 209
Dettmar R., and Barteldress A. 1988, BAAS, 20, 1085
Dwek E., Arendt R. G., Hauser M.G. et al. 1995, ApJ, 445, 716
Eliche-Moral, M. C., González-García, A. C., Aguerri, A. et al. 2013, A&A, 552, 67
Emsellem, E., Cappellari, M., Krajnovic, D., Alatalo, K., Blitz, L., Bois, M., Bournaud, F. et al. 2011, MNRAS, 414, 888
Erwin, P., Beltrán, J., Graham, A., and Beckman, J. E. 2003, ApJ, 597, 929
Erwin, P., and Debattista, V. P. 2013, MNRAS, 431, 3060
Erwin, P., Saglia, R., Fbricius, M. Thomas, J., Nowak, N., Rusli, S., and Bender, R. et al. 2015, MNRAS, 446, 4039
Falcón-Barroso, J., Bacon, R., Bureau, M. et al. 2006, MNRAS, 369, 529
Gadotti, D. 2009, MNRAS, 393, 1531
Ganda, K., Peletier, R., McDermid, R. et al. 2007, MNRAS, 380, 506
Guedes, J., Mayer, L., Carollo, M., and Madau, P. 2013, ApJ, 772, 36

Graham, A. 2011: A review of elliptical and disc galaxy structure, and modern scaling laws, appeared in “Planets, Stars and Stellar Systems”, Vol. 6, Springer Publishing
Hernquist, L., and Quinn, P. J. 1988, ApJ, 331, 682
Jablonka, P., Gorgas, J., and Goudfrooij, P. 2007, A&A 474, 763
Jarvis, B. 1986, AJ, 91, 65
Kormendy, J. 1982, ApJ, 257, 75
Kormendy, J. 1983, ApJ, 275, 529
Kormendy, J., and Illingworth, G. 1982, ApJ, 256, 460
Kormendy, J., and Illingworth, G. 1983, ApJ, 265, 632
Kormendy, J., and Barentine, J. 2010, ApJL, 715, 176
Krajnovic, D., Emsellem, E., Cappellari, M. Alatalo, K., Blitz, L., Bois, M., Bournaud, F. et al. 2011, MNRAS, 414, 2923
Kuijken, K., and Merrifield, M. 1995, ApJ, 443, 13
Lauer, T. 1985, MNRAS, 216, 429
Laurikainen, E., Salo, H., and Buta, R. 2005 MNRAS, 362, 1319
Laurikainen, E., Salo, H., Buta, R., and Knapen, J.H. 2007, MNRAS, 381, 401
Laurikainen, E., Salo, H., Buta, R., Knapen, J.H., and Comerón, S. 2010, MNRAS, 405, 1089
Laurikainen, E., Salo, H., Buta, R., and Knapen, J. H. 2011, MNRAS, 418, 1452
Laurikainen, E., Salo, H., Athanassoula, E., Bosma, A., Buta, R., and Janz, J. 2013, MNRAS, 430, 3489
Laurikainen, E., Salo H., Athanassoula, E., Bosma, A., and Herrera-Endoqui, M. 2014, MNRAS Letter, 444, 80
Li, Z-Y, and Shen, J. 2012, ApJL, 757, 7
de Lorenzo-Cáceres, A., Vazdekis A., Aguerri, J. A. L., Corsini, E. M., and Debattista, V. P. 2012, MNRAS, 420, 1092
Lütticke, R., Dettmar, R., and Pohlen, M. 2000a, A&AS, 145, 405
Lütticke, R. Dettmar, R., and Pohlen, M. 2000b, A&A, 362, 435
Lütticke, R., Pohlen, M., and Dettmar, R. 2004, A&A, 417, 527
MacArthur, L., Lauer, A., González, J., and Courteau, S. 2009, MNRAS, 395, 28
Martinez-Valpuesta, I., Shlosman, I., and Heller, C. H. 2006, ApJ, 637, 214
Martini, P., Regan M., Mulchaey, J., Pogge, R. 2003, ApJS, 146, 353
Méndez-Abreu, J., Corsini, E., Debattista, V. P., De Rijcke, S., Aguerri, J. A. L., and Pizzella, A. 2008, ApJ, 679, 73
Méndez-Abreu, J., Debattista, V. P., Corsini, E. M., and Aguerri, J. A. L. 2014, A&A, 572, 25
Moorthy, B.K., and Holzman, J.A 2006, MNRAS, 371, 583
Patsis, P., Skokos, Ch., and Athanassoula, E. 2002a, MNRAS, 337, 578
Patsis, P., Athanassoula, E., Grosbol, P., Skotos, Ch. 2002b, MNRAS, 337, 1049
Patsis, P., and Katsanikas, M. 2014a, MNRAS, 445, 3526
Patsis, P., and Katsanikas, M. 2014b, MNRAS, 445, 3546
Peletier, R., Falcón-Barroso, J., Bacon, R. Cappellari, M., Davies, R. L., de Zeeuw, P. T., Emsellem, E. at al. 2007, MNRAS, 379, 445
Pérez, I., Sánchez-Blázquez, P., and Zurita, A. 2009 A&A, 495, 775
Pérez, I., and Sánchez-Blázquez, P. 2011 A&A, 529, 64
Pfenniger, D., and Friedli, D. 1991, A&A, 252, 75
Pohlen, M., Balcells, M., Lútticke, R., and Dettmar, R. J. 2004, A&A, 422, 465
Proctor, R., and Sansom, A. 2002, MNRAS, 333, 517
Saha, K., Martinez-Valpuesta, I., and Gerhard, O. 2012, MNRAS, 421, 333
Saha, K., and Naab, T. 2013, MNRAS, 434, 1287
Salo, H., Laurikainen, E., Buta, R., and Knapen, J. H. 2010, ApJL, 715, 56
Salo, H., Laurikainen, E., Laine, J. et al. 2015, ApJL, 219:4
Sánchez-Blázquez, P., Ocvirk, P., Gibson, B. K., Pérez, I., and Peletier, R. F. 2011, MNRAS, 415, 709
Sánchez-Blázquez P., Rosales-Ortega F., Méndez-Abreu, J., Pérez, I., Sánchez, S. F., Zibetti, S., Aguerri, J. et al. 2014 A&A, 570, 6

Sandage A. 1961, The Hubble Atlas of Galaxies", 1961, Washington, D.C.: Carnegie Institution of Washington
Shaw, M., Dettmar, R., and Barteldrees, A. 1990, A&A, 240, 36
Shaw, M. 1993, A&A, 280, 33
Shen, J., Rich, R. M., Kormendy, J., Howard, C. D., De Propris, R., and Kunder, A. 2010, ApJL, 720, 72
Sheth, K., Regan, M., Hinz, J., Gil de Paz, A., Menéndez-Delmestre, K., Munoz-Mateos, J-C, Seibert, M. et al. 2010, PASP, 122, 1397
Simien, F., and de Vaucouleurs, G. 1986, ApJ, 302, 564
Vega Beltran J. C., Corsini E. M., Pizzella A., Bertola, F. 1997 A&A, 324, 485
Weinzirl, T., Jogee, S., Khochfar S., Burkert, A., and Kormendy, J. 2009, ApJ, 696, 411
Wegg, C., and Gerhard, O. 2013, MNRAS, 435, 1874
Whitmore, B. C., and Bell, M. 1988, ApJ, 324, 741
Williams, M., Zamojski, M., Bureau, M., Kuntschner, H., Merrifield, M.R., de Zeeuw, P.T., and Kuijken, K. 2011 MNRAS, 414, 2163
Williams, M., Bureau, M., and Kuntschner, H. 2012, MNRAS, 427, 99
Yoshino, A., and Yamauchi, C. 2015, MNRAS, 446, 3749

Chapter 5
Nuclear Star Clusters and Bulges

David R. Cole and Victor P. Debattista

Abstract Nuclear star clusters are among the densest stellar systems known and are common in both early- and late-type galaxies. They exhibit scaling relations with their host galaxy which may be related to those of supermassive black holes (SMBHs). These may therefore help us to unravel the complex physical processes occurring at the centers of galaxies. The properties of nuclear stellar systems suggest that their formation requires both dissipational and dissipationless processes. They have stellar populations of different ages, from stars as old as their host galaxy to young stars formed in the last 100 Myr. Therefore star formation must be happening either directly in the nuclear star cluster or in its vicinity. The secular processes that fuel the formation of pseudobulges very likely also contribute to nuclear star cluster growth.

5.1 Introduction

Observations with the high resolution instruments on the *Hubble Space Telescope* (*HST*) have revealed that many low to intermediate mass galaxies contain a dense stellar system at their center. They are among the densest stellar systems known. Nuclear stellar systems come in two main morphological types, nuclear star clusters (NSCs), where the stellar distribution is spheroidal, and nuclear discs (NDs).[1] These are not mutually exclusive and NSCs often contain a disc component too, typically comprised of younger stars. These dense stellar systems are common in galaxies across the Hubble sequence.

A connection between NSCs and the formation of their host galaxy is implied by various observed scaling relations between their mass and the properties of their

[1]Editorial comment: NSCs are more compact and less massive than the structures called as bulges. The central discs discussed in the other contributions of this book, generally associated to pseudobulges, are also larger than NSCs.

D.R. Cole (✉) • V.P. Debattista
Jeremiah Horrocks Institute, University of Central Lancashire, Preston PRI 2HE, Lancashire, UK
e-mail: drdrcole@gmail.com; vpdebattista@gmail.com

E. Laurikainen et al. (eds.), *Galactic Bulges*, Astrophysics and Space Science Library 418, DOI 10.1007/978-3-319-19378-6_5

host. These scaling relations provide insight into the physical processes regulating the growth of nuclear stellar systems.

NSCs in late-type disc galaxies are observed to have a mix of populations, including young stars formed within the last 100 Myr. Whether these formed in situ, or arrived as star clusters accreted from the neighborhood of the NSC, gas is needed to make these young stars. Thus NSCs and NDs provide evidence that gas is able to repeatedly reach the centers of late-type galaxies.

5.2 Nuclear Stellar Systems

5.2.1 Properties and Occurrence

NSCs are compact objects with effective radii of order 5 pc and masses ranging from $10^5\,M_\odot$ to $10^8\,M_\odot$, meaning that they have among the highest known average surface densities (Walcher et al. 2005). NSCs have photometric and kinematic properties very similar to those of globular clusters but with higher velocity dispersions. Their absolute visual magnitudes lie between -14 and -10 (Böker et al. 2002; Côté et al. 2006) compared with Milky Way globular clusters which have absolute magnitudes typically in the range -9 to -4 (Harris 1997). Hartmann et al. (2011) found that the NSC in M33 was photometrically and kinematically consistent with being perfectly axisymmetric.

NSCs are present in between 50 % and 75 % of low to intermediate luminosity galaxies. Carollo et al. (1997) found NSCs in 18 of 35 *HST* WFPC2 F606W images of spiral galaxies including early-types, while Böker et al. (2002) found NSCs in 59 of 77 *HST* images of late-type spiral galaxies. Between 66 % and 82 % of early-type galaxies in the *HST* ACS Virgo Cluster Survey have NSCs (Côté et al. 2006), and a similar fraction in the ACS Fornax Cluster Survey (Turner et al. 2012). The presence of a bar does not seem to affect whether NSCs occur or not (Carollo et al. 2002; Böker et al. 2004).

Nuclear discs are also often found in the central regions of galaxies. They span a range of sizes from a few parsecs to of order a kiloparsec in diameter. They can be differentiated from the main galactic disc (if it exists) in that they lie outside of the region where light from the main disc dominates. They are widely observed in galaxies spanning the full range of Hubble types both in late-type (Zasov and Moiseev 1999; Pizzella et al. 2002; Dumas et al. 2007; García-Burillo and Combes 2012) and early-type galaxies (Scorza and van den Bosch 1998; Kormendy and Gebhardt 2001; de Zeeuw et al. 2002; Emsellem et al. 2004; Trujillo et al. 2004; Krajnović et al. 2008; Ledo et al. 2010). Ledo et al. (2010) found that as many as 20 % of early-type galaxies host a nuclear disc. A sample of 48 early-type galaxies observed as part of the SAURON project, revealed that nuclear discs are associated with early-type fast rotators (Krajnović et al. 2008).

5.2.2 Stellar Ages

NSCs in late-type galaxies often consist of multiple stellar populations. Their mean luminosity-weighted ages range from 10 Myr to 10 Gyr (Rossa et al. 2006), very often with evidence of star formation in the last 100 Myr (Walcher et al. 2005, 2006). Spectra reveal that their star formation is bursty, with a duty cycle of a few hundred Myr. For instance, the NSC in M33 had bursts of star formation 40 Myr and 1 Gyr ago (Long et al. 2002). Georgiev and Böker (2014), in a study of NSCs of 228 late-type galaxies, also find that their stellar populations span a wide range of ages and conclude that recent star formation is ubiquitous.

NSCs in late-type disc galaxies are typically elongated approximately in the plane of the main galaxy disc and are often made up of two components, an older spheroidal component, with a younger and bluer disc embedded in it (Seth et al. 2006, 2008b). In the case of NGC 4244, spectra indicate young (<100 Myr) stars in its disc. Integral field spectroscopy reveals that the NSC has rotation in the same sense as the galaxy (see Fig. 5.1) with a relative tilt of 15°. Similarly, the NSC of FCC 277, an elliptical galaxy in the Fornax cluster, is made up of a spheroid and a disc component, both of which are younger than the main galaxy (Lyubenova et al. 2013). Carson et al. (2015) studied *HST* WFC images of 10 of the nearest and brightest NSCs. They found increasing roundness at longer wavelengths inferring the existence of blue discs made up of younger stellar populations as in NGC 4244. Most of these NSCs show evidence in colour-colour diagrams of stellar populations consisting of a mixture of an older population (>1 Gyr) and a younger population (100–300 Myr). Pfuhl et al. (2011) estimated that the NSC in the Milky Way formed ∼80 % of its stars more than 5 Gyr ago, with a deep minimum in star formation 1–2 Gyr ago. The star formation rate then increased again in the last few hundred Myr.

Likewise NDs often exhibit a range of ages with a tendency for young stars to be present. Ongoing star formation is observed in the NDs of NGC 5845 (Kormendy et al. 1994) and NGC 4486A (Kormendy et al. 2005). In the ND manages to have stars more than 2 Gyr younger than the surrounding galaxy (Kormendy et al. 2005). The ND in NGC 4570 shows evidence for recent star formation (van den Bosch et al. 1998). Morelli et al. (2004) found that NGC 4478 has a younger stellar population than the main body of the galaxy, with a prolonged star formation history, whereas NGC 4458 has a uniformly old population. The ND stellar population in NGC 4698 has ages in the range 5–10 Gyr (Corsini et al. 2012). On the other hand, NDs in early-type galaxies have been found to consist mainly of old (>10 Gyr) stars (Krajnović and Jaffe 2004).

5.2.3 Kinematic Decoupling

One phenomenon which suggests that interactions may play a role in the formation of nuclear stellar systems is kinematic decoupling where distinct stellar components

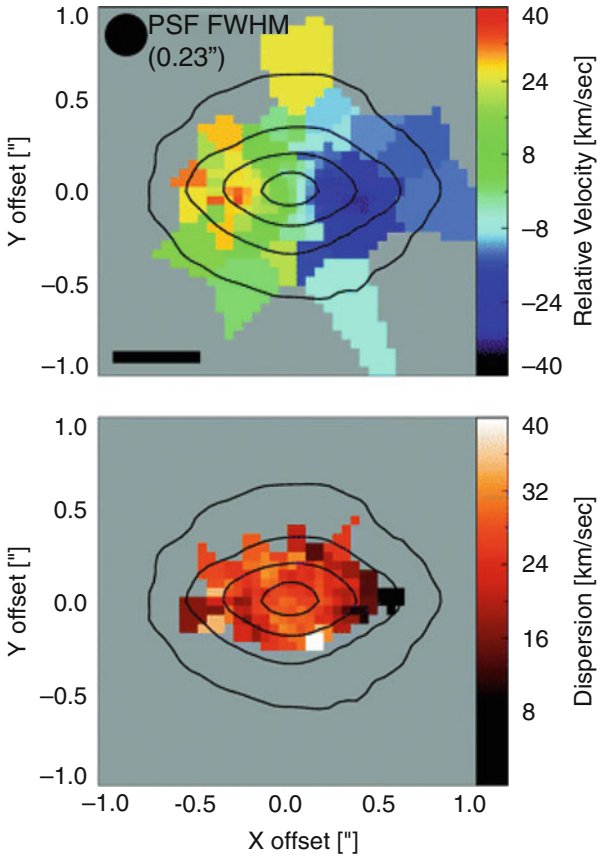

Fig. 5.1 The kinematics of the NSC in NGC 4244. *Top*: The measured radial velocity observed with NIFS. Rotation of 30 km s^{-1} is clearly visible along the major axis. Contours show the K-band isophotes. The *black bar* indicates 10 pc (0.47″). *Bottom*: Velocity dispersion measurements. Figure 2 of Seth et al. (2008b) (Reproduced with permission from Astronomy & Astrophysics)

have large (≥40°) misalignments in their axes of rotation (McDermid et al. 2006). About one third of early-type galaxies in the SAURON sample exhibit this decoupling. Kinematic decoupling has been interpreted as evidence for formation through the capture of external gas. Two types are observed, one on kiloparsec scales, which are generally older than 8 Gyr and found in galaxies with little net rotation, and one which consists of structures on the scale of a few hundred parsec and which have ages ranging from 500 Myr to a Hubble time (McDermid et al. 2006). The ND in NGC 4458 is counter-rotating implying the gas had an external origin (Morelli et al. 2004, 2010). NGC 4698 also displays kinematical decoupling and has a disc rotating perpendicular to the main galactic disc suggesting that the ND formed from externally accreted gas (Bertola and Corsini 1999; Pizzella et al. 2002; Corsini et al. 1999, 2012). While the presence of kinematically decoupled cores

demonstrates that externally captured gas can reach small radii, this by no means implies that the gas also forms a nuclear cluster. For instance, although NGC 4458 has a stellar disc it has been classified as non-nucleated (Lauer et al. 2005).

5.3 Formation

5.3.1 Nuclear Star Clusters

Two principal formation mechanisms have been advanced to explain the formation of NSCs. The first is that NSCs form due to globular clusters falling to the centers of galaxies under the action of dynamical friction and subsequently merge (Tremaine et al. 1975; Capuzzo-Dolcetta 1993; Miocchi et al. 2006; Capuzzo-Dolcetta and Miocchi 2008a,b; Antonini et al. 2012; Antonini 2013; Gnedin et al. 2014). A candidate infalling globular cluster was found in the inner few hundred parsecs of NGC 2139 which could become a NSC in a few hundred Myr (Andersen et al. 2008). An off-center super star cluster with a mass of $1.4^{+0.4}_{-0.5}\times10^7\,M_\odot$ has been observed in NGC 253. This super star cluster is a candidate future NSC (Kornei and McCrady 2009). Georgiev and Böker (2014) present NGC 4654 as an example of galaxies where two star clusters are present at the center. The two star clusters have a mass ratio of order 10:1 and are separated by $\sim$30 pc (in projection). The less massive of the star clusters appear to be young (<100 Myr), supporting the picture of NSC growth due to the accretion of *young* globular clusters onto the center. Nguyen et al. (2014) find a starburst at the center of a SMBH-hosting galaxy Heinze 2–10. This starburst has created several super star clusters within 100 pc of the SMBH and they conclude that the star clusters would merge due to dynamical friction and form an NSC in the next Gyr. Simulations by Capuzzo-Dolcetta (1993) showed that, while the infall of globular clusters is in competition with tidal stripping (which destroys the clusters), nonetheless a fraction of them do manage to reach the nucleus. Fewer massive globular clusters than expected have been found in the inner region of dwarf ellipticals suggesting that the globular clusters missing from the inner regions had been depleted due to their shorter dynamical friction infall times and merging to form NSCs (Lotz et al. 2001, 2004). The infall of globular clusters has been modeled and simulated several times. Agarwal and Milosavljević (2011) modeled the infall (and stripping) of globular clusters analytically and concluded that this process could create NSCs which match the observed NSC masses. Capuzzo-Dolcetta and Miocchi (2008a) show that globular clusters merging at the center of a bulge leads to density-velocity dispersion properties consistent with those of observed NSCs. Analytic modeling of the infall of globular clusters led Gnedin et al. (2014) to the same conclusion; they argue, moreover, that the contrast between the NSC and the background galaxy would be much lower in a massive galaxy like M87, making them harder to detect in such systems. den Brok et al. (2014) studied NSCs in 200 Coma cluster dwarf elliptical galaxies and found a relation between NSC and host

galaxy magnitude of $M_{nuc} = (0.57 \pm 0.05)(M_{gal} + 17.5) - (11.49 \pm 0.14)$, concluding that this is consistent with the predictions of how NSC luminosity scales with host galaxy luminosity, as predicted by the globular cluster merger scenario models of Antonini (2013) and Gnedin et al. (2014). However, they also find that galaxies with higher Sérsic indices tend to have brighter NSCs. They argue that this is due to the brighter galaxies being better able to retain gas and conclude that in situ star formation also plays an important role.

den Brok et al. (2014) showed an example of an unnucleated galaxy with several old globular clusters within it which raises the question of how this galaxy managed to avoid forming a NSC. Hartmann et al. (2011) note that the NSC in M33 appears axisymmetric both photometrically and kinematically. Their simulations of globular cluster mergers produce triaxial NSCs, although this outcome can be avoided if a massive black hole is present. However, in M33 the upper limit on the presence of a black hole is very stringent ($M_{bh} < 3000\,M_{\odot}$, (Merritt and Ferrarese 2001; Gebhardt et al. 2001)) suggesting that its NSC did not form via globular cluster mergers. On the other hand, the NSC in the Milky Way has a rotating sub-structure perpendicular to the Galactic plane (Feldmeier et al. 2014), suggesting that a cluster was accreted. In situ star formation has been proposed as an alternative for forming NSCs (Milosavljević 2004; Bekki 2007). Cen (2001) suggested that at the epoch of re-ionization the external radiation field could create an inward convergent shock leading to the formation of massive dense clusters at the centers of early galaxies with masses and velocity dispersions comparable to those of NSCs. While these could have formed the seeds of some NSCs, the NSCs would have had to grow further since formation to account for the younger populations. Emsellem and van de Ven (2008) showed that the tidal field of a wide range of Sérsic profile spheroids are compressed in the regions where NSCs form; gas falling in is therefore likely to form stars. They found that the mass of the object expected to form would be 0.1–0.5 % that of the host, consistent with the masses of both SMBHs and NSCs. The most direct evidence for the need of in situ star formation comes from modeling the kinematics of the NSC in NGC 4244 (Fig. 5.1). Simulations by Hartmann et al. (2011) find that though the globular cluster merging scenario can reproduce many of the density and kinematic properties of NSCs (see Fig. 5.2), mergers give rise to a central peak in $v_{\rm rms} = \sqrt{\sigma_{\rm los}^2 + v_{\rm los}^2}$, which is not observed in the data. Based on this, they conclude that less than 50 % of the mass of the NSC could have been assembled from the mergers of globular clusters, with the majority due to in situ star formation. On the other hand, they also find a negative vertical anisotropy, $\beta_z = 1 - \sigma_z^2/\sigma_R^2$, confirmed through the independent modeling of De Lorenzi et al. (2013) using the made-to-measure technique (Syer and Tremaine 1996; de Lorenzi et al. 2007). This, they showed, could be produced by the accretion of a globular cluster, accounting for at least 10 % of its mass, on a nearly polar orbit relative to the NSC. They conclude that both in situ star formation and globular cluster mergers played a role in the formation of this NSC. From a sample of over 200 late-type spiral galaxies observed with *HST*, Georgiev and Böker (2014) showed that NSCs are smaller in blue compared to red filters. This can be explained either

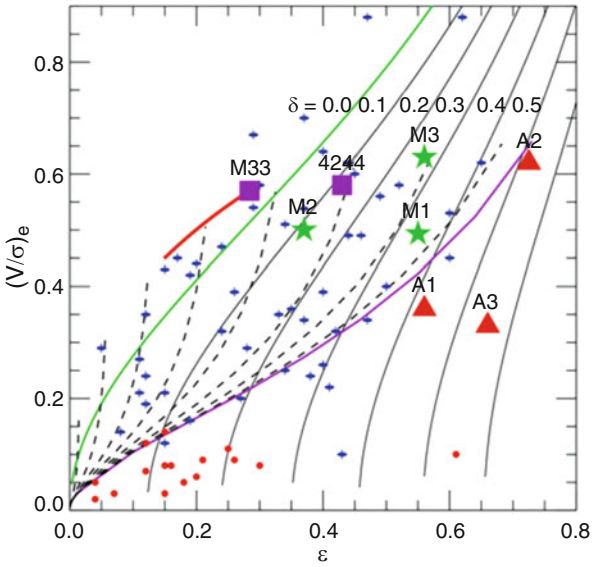

Fig. 5.2 Real and simulated NSCs on the $(V/\sigma, \epsilon)$ diagram of Binney (2005). The *green stars* and *red triangles* indicate the location of the simulated NSCs (M1–M3 & A1–A3) formed by merging infalling globular clusters, while the *magenta squares* are the observed NSCs in NGC 4244 and M33. The observed location for M33 has been projected (*red line*) assuming an inclination of $i = 49°$. For comparison, the *blue symbols* with vertical axes and *red filled circles* are the observed fast and slow rotator early-type galaxies, respectively, from Cappellari et al. (2007). Figure 5 of Hartmann et al. (2011) (Reproduced with permission of Oxford University Press)

by the presence of an AGN or by population gradients within the NSC, possibly indicating ongoing star formation. Turner et al. (2012) studied the nuclei in 43 early-type galaxies in the Fornax cluster. On the basis of globular cluster infall times, they concluded that in low mass early-type galaxies the dominant mechanism for NSC formation is probably globular cluster merging but for more massive galaxies in situ star formation becomes necessary. A picture is being established therefore where both processes, globular cluster mergers and in situ star formation, play a role in NSC formation and which is the dominant mechanism depends on the parameters of the host galaxy (Rossa et al. 2006; Walcher et al. 2006).

5.3.2 Nuclear Disc Formation

The formation of NDs is thought to require in situ star formation. A significant mass of gas needs to be funneled to the nuclear regions to allow this. Such inflows are possible in mergers as shown by hydrodynamical simulations (Mayer et al. 2008, 2010; Hopkins and Quataert 2010; Chapon et al. 2013). Chapon et al. (2013) presented a simulation of the merger of two galaxies with SMBHs (see Fig. 5.3).

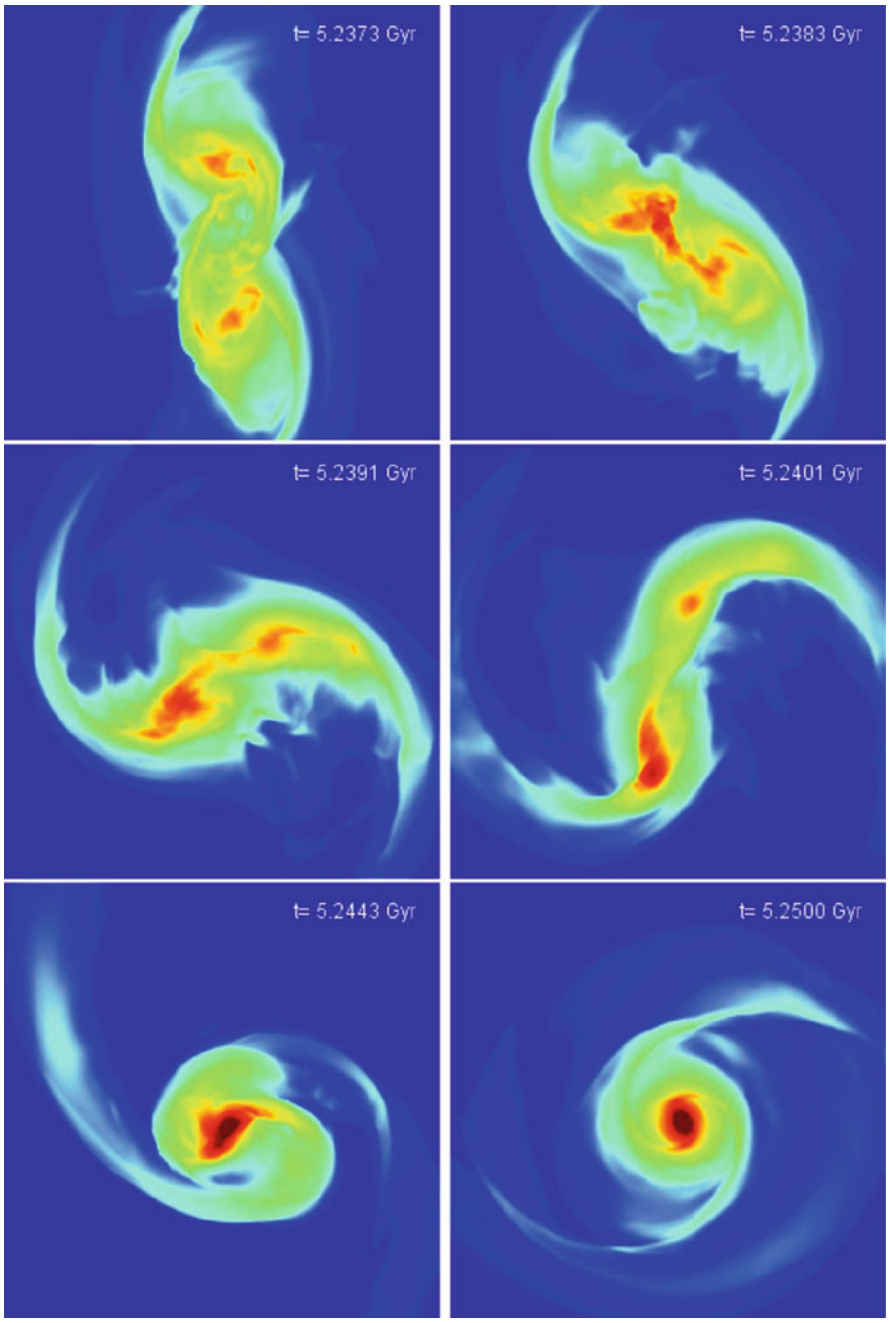

Fig. 5.3 Gas density maps during the final stages of the merger of two galaxies. We are looking down onto the orbital plane of the galaxies and the maps are 1.8 kpc wide. Gas from the two galaxies funnels inwards to form a thick gaseous nuclear disc with two SMBHs orbiting in it in the final image. Figure 1 of Chapon et al. (2013) (Reproduced with permission of Oxford University Press)

After the merger a thick nuclear gas disc forms with a mass $\sim 10^9\,M_\odot$. Nuclear discs have been observed in 17 nearby luminous infra-red galaxies (LIRGs) and ultra-luminous infra-red galaxies (ULIRGs), possibly the results of merger-driven gas funneling to their centers initiating intense star formation (Medling et al. 2014). Meanwhile Hopkins and Quataert (2010) showed that lopsided nuclear discs such as the one in the Andromeda galaxy may form via merger-driven inflows. Instead Ledo et al. (2010) showed that pre-existing NDs are destroyed in mergers.

Secular processes such as the action of a bar can also supply gas to form a ND. The formation of the ND in the edge-on galaxy NGC 7332 was attributed to the presence of a bar (which was inferred from the boxy/peanut-shaped bulge) (Seifert and Scorza 1996; Falcón-Barroso et al. 2004). Barred galaxies have more molecular gas in their central kiloparsec than unbarred galaxies (Sakamoto et al. 1999; Sheth et al. 2005). Enhanced nuclear star formation correlates with the presence of a strong bar in disc galaxies (Wang et al. 2012), and depends primarily on the ellipticity of the bar, not on the size of the bar. However only half of galaxies with centrally concentrated star formation have a strong bar suggesting that processes such as interactions with other galaxies also induce star formation in the nucleus.

Cole et al. (2014) presented a simulation of the formation of an L^* isolated galaxy. After the bar formed, a ND developed (see Fig. 5.4). They demonstrated that gas flows to the center and fuels star formation. The resulting ND is elongated perpendicular to the main bar, suggesting that the stars in the ND are on x2 orbits. The ND can clearly be seen in the kinematics and the stellar metallicity.

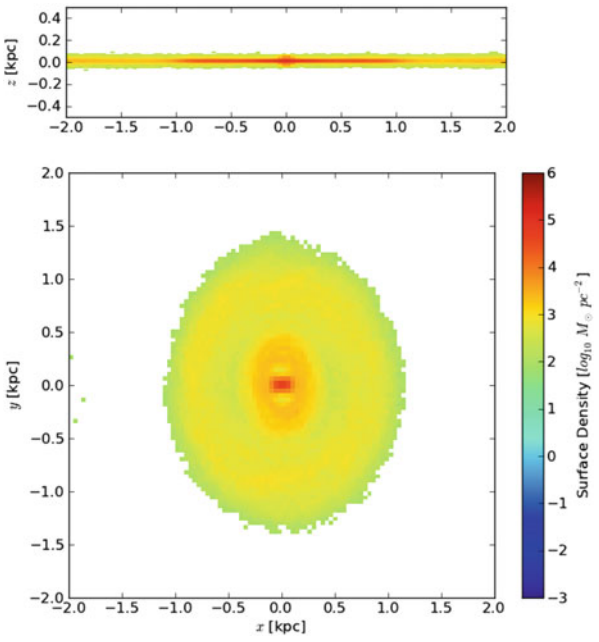

Fig. 5.4 Face-on (*bottom*) and edge-on (*top*) stellar surface density for young stars (<2 Gyr) after 10 Gyr in the simulation of an L^* galaxy. The galaxy has a bar which is oriented along the x-axis. A thin disc of stars can clearly be seen. Figure 4 of Cole et al. (2014) (Reproduced with permission of Oxford University Press)

Given the available data, ND formation through dissipationless processes cannot be excluded. Agarwal and Milosavljević (2011) proposed that NDs form out of the debris of infalling star clusters and Portaluri et al. (2013) showed that such a scenario is consistent with the available kinematic and photometric data. It has also been demonstrated that NDs can be formed from accreted dwarf satellites settling into rotationally supported NDs (Eliche-Moral et al. 2011).

5.4 The Link to Pseudobulges

Just like NSCs and NDs, pseudobulges require the inflow of gas to form. Pseudobulges have proven to be very common, with Fisher and Drory (2011) estimating that they account for ∼80 % of disc galaxies. Kormendy and Kennicutt (2004) reviewed the formation of pseudobulges via the funneling of gas through non-axisymmetric structures, such as bars. They list eight key properties of NSCs which need to be understood if NSCs and pseudobulges are related secular phenomena: (1) NSCs are common, (2) NSCs are rare in irregulars, (3) NSCs are fairly homogeneous in their properties, (4) NSCs are at the centers of their host galaxies, (5) NSCs host young stars, (6) NSCs are not more common in barred galaxies, (7) In the Fundamental Plane NSCs are more similar to globular clusters and, (8) The masses of NSCs correlate with the luminosities of their host galaxies. They argue that points (2), (3), (6) and (7) appear inconsistent with NSCs and pseudobulges being related phenomena. Possible answers to these problems could be that the centers of irregulars are not well-defined (point 2), that globular cluster mergers are responsible for part of the mass assembly of NSCs (points 3 and 7) and the gas flows required for NSCs are not as large as needed for pseudobulges (point 6). Nonetheless, NSCs **are** different. Walcher et al. (2005) tested the idea that NSCs are proto-bulges which form through in situ star formation but whose growth has not been sufficient to form a bulge. On the basis of 9 bulgeless galaxies, they showed that the dynamical properties of the NSCs are very different to those bulges.

How can gas get funneled to NSCs? Kormendy and Kennicutt (2004) invoked bars and ovals to explain the formation of pseudobulges. It has long been recognized that, while bars can drive gas inwards, this gas stalls at the inner Lindblad resonance. Shlosman et al. (1989) proposed that gas can be driven all the way to the center of a galaxy, thereby feeding AGN activity, by means of nested bars, where a small-scale bar resides inside a larger bar. Such double-barred galaxies have been observed in about 25 % of early-type galaxies (Erwin and Sparke 2002). In this scenario the main bar of a galaxy would induce an inward flow creating a nuclear gas disc which could again become unstable leading to further gas infall. Evidence for gas inflow that can be explained by this scenario comes from the molecular gas in NGC 6946 (Schinnerer et al. 2006, 2007), which appears to be streaming along the leading edge of an inner stellar bar about 400 pc long nested inside a large-scale (3.5 kpc) bar.

However, the fact that NSCs do not prefer barred galaxies (Carollo et al. 2002; Böker et al. 2004) suggests that bars are not the sole mechanism responsible for

funneling gas to nuclei. As an alternative, Milosavljević (2004) proposed that the magneto-rotational instability could transport neutral gas inside 100 pc where it could form stars.

NDs can sometimes be directly associated with pseudobulges through the phenomenon of σ-drops, where galaxies have a significant drop in velocity dispersion in their center (e.g. Emsellem et al. 2001). These can be explained by infalling gas forming a dynamically cool ND. Star formation reduces the central velocity dispersion (Wozniak et al. 2003; Comerón et al. 2008). Small NDs have been observed with *HST* in the center of galaxies co-located with σ-drops (Mendez-Abreu et al. 2014).

5.5 Co-Evolution of SMBHs and NSCs

A small fraction of galaxies host both a NSC and a SMBH (Seth et al. 2008a), although the actual fraction could be higher given the difficulties in detecting both in a given galaxy. Neumayer and Walcher (2012) noted that a plot of M_{bh} versus M_{NSC} divides into three regions, one which is NSC dominated, a transition region and one which is SMBH dominated. This led them to speculate that SMBHs form inside NSCs but outgrow and destroy them when the NSC mass is less than 1 % of the SMBH mass. Alternatively, Nayakshin et al. (2009) proposed a competitive feedback to explain the dichotomy between NSCs and SMBHs. Arguing that NSC growth depends on the dynamical time of the nuclear region, they find that there is a transition when the velocity dispersion of the host spheroid is $\sim$150 km s^{-1}. Above this the NSC cannot grow efficiently and below this the SMBH cannot grow efficiently thus explaining why NSCs are mainly found in low and intermediate mass galaxies. Antonini et al. (2012) and Antonini (2013) explained this dichotomy in the globular cluster formation scenario in the presence of a SMBH. For a low mass SMBH, such as the Milky Way's, globular clusters manage to reach the center allowing the NSC to grow. However, if $M_{bh} \sim 10^8\,M_\odot$ then the globular clusters are disrupted before reaching the nucleus.

However Kormendy and Ho (2013) point out that there is no segregation into giants that only contain SMBHs or dwarfs that only contain nuclei. Where SMBHs and NSCs co-exist the ratio of SMBH to NSC mass can vary across a large, and *apparently continuous* range above and below unity. For example in NGC 4026 $\frac{M_{bh}}{M_{NSC}} = 12.4$ (Lauer et al. 2005) whereas in the Milky Way $\frac{M_{bh}}{M_{NSC}} = 0.15 \pm 0.075$ (Launhardt et al. 2002).

Over long timescales, Merritt (2009) showed that NSCs evolve under two competing processes, core collapse by two body interactions, and heating from the surrounding galaxy. Which of these two processes wins out depends on the concentration of the NSC (Quinlan 1996). However, the presence of a SMBH inhibits core collapse implying that in this case a NSC can expand for ever and ultimately be disrupted.

5.6 Scaling Relations

The masses of SMBHs, M_{bh} are well known to correlate with their host galaxy properties including the bulge velocity dispersion, σ_e (Ferrarese and Merritt 2000; Gebhardt et al. 2000; Merritt and Ferrarese 2001; Tremaine et al. 2002; Ferrarese and Ford 2005; Gültekin et al. 2009; Graham et al. 2011; McConnell et al. 2011; Beifiori et al. 2012), the bulge mass, M_{bul} (Magorrian et al. 1998; Marconi and Hunt 2003; Häring and Rix 2004; Sani et al. 2011; Beifiori et al. 2012; Graham 2012) and the bulge luminosity, L_{bul} (Kormendy and Richstone 1995; McLure and Dunlop 2002; Marconi and Hunt 2003; Graham 2007; Gültekin et al. 2009; Sani et al. 2011; McConnell et al. 2011; Beifiori et al. 2012; Graham and Scott 2013). (See Chap. 11 of this volume "Galaxy bulges and their massive black holes" by Alister W. Graham for an up-to-date discussion on SMBH scaling relations and the review by Kormendy and Ho (2013).) Similarly the luminosity and mass of nuclear star clusters and nuclear discs have been found to correlate with their host galaxy properties (Balcells et al. 2003, 2007; Graham and Guzmán 2003; Ferrarese et al. 2006; Wehner and Harris 2006; Graham 2012) which has led to them being lumped along with SMBHs as a generic class of objects, the central massive objects (CMOs), with stellar CMOs being found in less massive galaxies.

The luminosity of stellar CMOs was found to correlate with that of their host bulge in disc galaxies by Balcells et al. (2003, 2007) and a similar correlation was found in a study of dE galaxies in the Coma cluster by Graham and Guzmán (2003). Ferrarese et al. (2006) found that the mass of stellar CMOs in early-type galaxies correlates with both the host galaxy's luminosity and dynamical mass, $M_{dyn}^{gal} \propto \sigma_e^2 R_e^{gal}$ (Fig. 5.5). More importantly they found a common M_{CMO}-M_{gal} relationship for galaxies with either NSCs or SMBHs, with NSCs occupying fainter galaxies with lower σ_e. This common relation suggests that there is a single mechanism responsible for regulating the growth of CMOs. They speculated that stellar nuclei form in all galaxies but in the most massive ones they collapse to a SMBH. A similar common relation between CMO mass and the mass of the host galaxy was also found by Wehner and Harris (2006) in dwarf elliptical galaxies. McLaughlin et al. (2006) proposed that the mechanism responsible for this correlation is momentum-driven feedback, from supernovae in the case of NSCs and from AGN activity in the case of SMBHs.

However the existence of scaling relations between NSCs and SMBHs has recently been questioned. The first indication that stellar CMOs and SMBHs do not, in fact, follow the same scaling relations came in a study of S0-Sbc galaxies by Balcells et al. (2007). They found that the near infra-red luminosities of NSCs scale with host bulge luminosities. However, in contrast to Ferrarese et al. (2006), when they added SMBHs they found a nonlinear dependence between $M_{\rm CMO}$ and $M_{\rm bulge}$. An expanded dataset allowed Graham (2012) to show that NSC mass correlates with host spheroid velocity dispersion as $log[M_{NSC}/M_{\odot}] = 1.57 \pm 0.24 \log[\sigma/70 kms^{-1}] + (6.83 \pm 0.07)$. The slope of this relation, $\sim$2, is much lower than that for SMBHs, $\sim$5. Leigh et al. (2012) found that NSC mass is directly

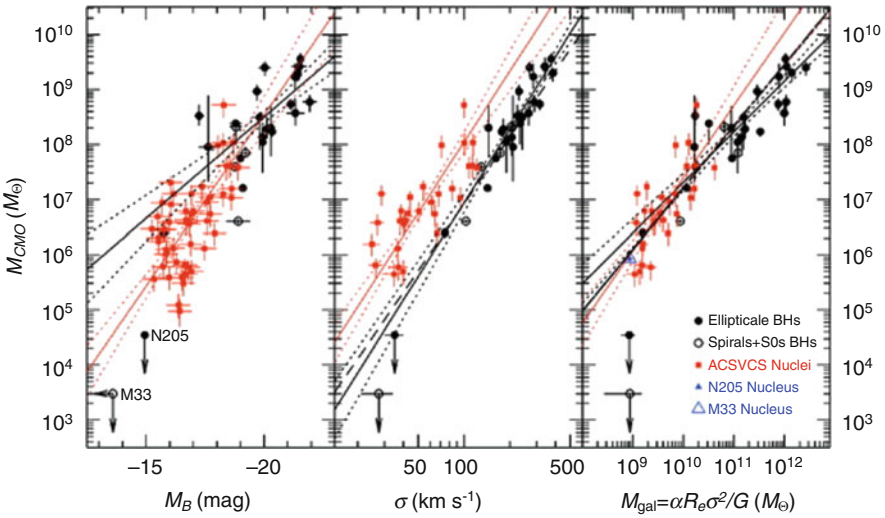

Fig. 5.5 The mass of the CMO versus the blue band magnitude (*left*), velocity dispersion σ (*middle*) and host spheroid dynamical mass (*right*) for SMBHs (*filled and open circles*) and nuclei (*red squares*). The *solid red* and *black lines* show the best fits to the nuclei and early-type SMBH samples, respectively. In the *right panel*, the *dashed line* is the fit obtained for the combined nuclei+SMBH sample. Figure 2 of Ferrarese et al. (2006) (Reproduced with permission of AAS)

proportional to host spheroid mass; the virial theorem then implies an M_{NSC}-σ_e relation with a slope again close to 2. Figure 5.6, taken from Scott and Graham (2013), shows their relations between CMO mass versus galaxy magnitude, σ and galaxy virial mass. These relations can be compared directly with those of Ferrarese et al. (2006), shown in Fig. 5.5, where they find a slope of 2.1 ± 0.3 for the $M_{NSC} - \sigma$ relation, much shallower than the relation found by Ferrarese et al. (2006). A major reason for this difference is their inclusion of NSCs in more massive galaxies and the exclusion of NDs. Erwin and Gadotti (2012) and Scott and Graham (2013) both noted that the mass of NSCs correlates better with the host's total stellar mass, whereas that of SMBHs correlates better with the host spheroid. They conclude that different physical processes regulate NSC and SMBH growth.

Kormendy and Ho (2013) reach a more nuanced conclusion on the relation between SMBHs and NSCs by taking galaxy type into account when studying the ratio of CMO to bulge or galaxy mass. NSCs in spheroidal galaxies are relatively more massive than in late-type galaxies, consistent with the generally held view that spheroidal galaxies are late-type galaxies which have lost baryonic mass. This renders these galaxies less useful for comparing CMO scaling relations. They find that the ratio $(M_{bh} + M_{NSC})/M_{bulge}$ has less scatter than either M_{bh}/M_{bulge} or M_{NSC}/M_{bulge}, suggesting that the evolution of NSCs and SMBHs is tightly coupled. As a fraction of total galaxy mass, instead, both SMBHs and NSCs have a larger relative mass in early-type galaxies compared with late-type galaxies (excluding the

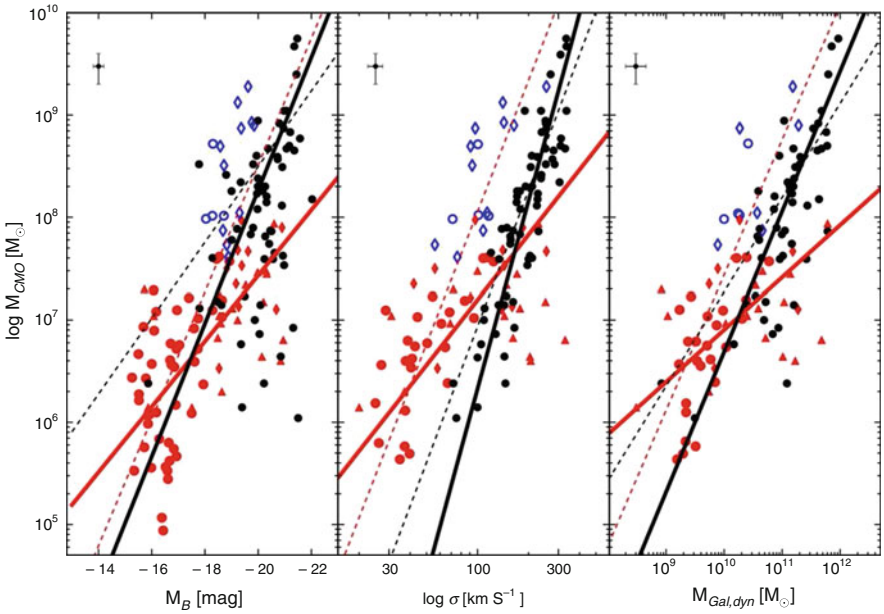

Fig. 5.6 The mass of the CMO versus the B band magnitude, velocity dispersion σ and galaxy dynamical mass for SMBHs (*black dots*), NDs (*open symbols*) and NSCs (*red dots*). The *solid black lines* shows the slope of the relations for SMBHs and the *solid red lines* for NSCs. Figure 2 of Scott and Graham (2013). The scaling relation for SMBHs is updated in Figure 2 of Graham and Scott (2013), and Figure 3 of Scott et al. (2013) (Reproduced with permission of AAS)

spheroidals). Kormendy and Ho (2013) conclude that this hints at SMBHs and NSCs being related.

Although a common scaling relation between NSCs and SMBHs now seems dead, nonetheless the existence of scaling relations between NSCs and their host galaxies still provide important constraints on how their growth is regulated (Silk and Rees 1998; King 2003; Wyithe and Loeb 2003; Di Matteo et al. 2005; Murray et al. 2005; Sazonov et al. 2005; Younger et al. 2008; Booth and Schaye 2009; Johansson et al. 2009; Power et al. 2011). Theoretical models of formation mechanisms make predictions for scaling relations between NSCs and host galaxy properties, based on underlying physics, and these allow us to distinguish how NSCs are formed. The main process proposed is feedback from the CMO, and possibly the effect this has on its galaxy but the exact mechanisms is not yet clear (Silk and Rees 1998; Springel et al. 2005; Booth and Schaye 2009; Fabian 1999; King 2003, 2005, 2010; Murray et al. 2005; McLaughlin et al. 2006; Power et al. 2011; McQuillin and McLaughlin 2012).

5.7 Conclusions

Observations of nuclear star clusters show that these systems can unravel the mass assembly at the centers of galaxies. Their properties give us clues as to how they were formed and the physical processes that contributed to their formation. There is a close connection between the formation of NSCs and their host, as is demonstrated by their scaling relations. Observations support both in situ star formation and globular cluster merging for the formation and growth of NSCs. How much these mechanisms contribute to the growth of NSCs probably depends on whether they are found in early or late-type galaxies or in high-mass or low-mass galaxies. It also seems likely that the morphology of the bulge, whether it is a classical bulge or a discy bulge formed through secular processes, will affect the transport of gas to the nuclear regions of a galaxy where it can form stars. NSCs in early-type galaxies with little gas are unlikely to grow due to dissipational processes. However late-type galaxies show multiple stellar populations with stars of the order of a few hundred Myr old implying recent star formation.

NSCs and SMBHs can co-exist, as can be seen in the Milky Way, but they no longer seem to be two types of a single central massive object. However studying the interrelationship between these two types of nuclear system will contribute to the understanding of all physical processes which are important in their formation. Further investigation of how scaling relations are affected by the presence of a bar, the morphology of the bulge and whether the host galaxy is early- or late-type may allow us to refine our ideas of how they form. There is also a need for higher resolution simulations of the effects of in situ star formation on the kinematics, chemistry and morphology of NSCs. From the information we have gathered so far it is clear that NSC formation is very complicated and their continued study will bring further insights.

Acknowledgements DRC and VPD are supported by STFC Consolidated grant # ST/J001341/1.

References

Agarwal M., Milosavljević M., 2011, ApJ, 729, 35
Andersen D. R., Walcher C. J., Böker T., Ho L. C., van der Marel R. P., Rix H.-W., Shields J. C., 2008, ApJ, 688, 990
Antonini F., 2013, ApJ, 763, 62
Antonini F., Capuzzo-Dolcetta R., Mastrobuono-Battisti A., Merritt D., 2012, ApJ, 750, 111
Balcells M., Graham A. W., Domínguez-Palmero L., Peletier R. F., 2003, ApJ, 582, L79
Balcells M., Graham A. W., Peletier R. F., 2007, ApJ, 665, 1084
Beifiori A., Courteau S., Corsini E. M., Zhu Y., 2012, MNRAS, 419, 2497
Bekki K., 2007, Publications of the Astronomical Society of Australia, 24, 77
Bertola F., Corsini E. M., 1999, in IAU Symposium, Vol. 186, Galaxy Interactions at Low and High Redshift, Barnes J. E., Sanders D. B., eds., p. 149
Binney J., 2005, MNRAS, 363, 937

Böker T., Laine S., van der Marel R. P., Sarzi M., Rix H.-W., Ho L. C., Shields J. C., 2002, AJ, 123, 1389
Böker T., Sarzi M., McLaughlin D. E., van der Marel R. P., Rix H.-W., Ho L. C., Shields J. C., 2004, AJ, 127, 105
Booth C. M., Schaye J., 2009, MNRAS, 398, 53
Cappellari M. et al., 2007, MNRAS, 379, 418
Capuzzo-Dolcetta R., 1993, ApJ, 415, 616
Capuzzo-Dolcetta R., Miocchi P., 2008a, ApJ, 681, 1136
Capuzzo-Dolcetta R., Miocchi P., 2008b, MNRAS, 388, L69
Carollo C. M., Stiavelli M., de Zeeuw P. T., Mack J., 1997, AJ, 114, 2366
Carollo C. M., Stiavelli M., Seigar M., de Zeeuw P. T., Dejonghe H., 2002, AJ, 123, 159
Carson D. J., Barth A. J., Seth A. C., den Brok M., Cappellari M., Greene J. E., Ho L. C., Neumayer N., 2015, ArXiv e-prints
Cen R., 2001, ApJ, 560, 592
Chapon D., Mayer L., Teyssier R., 2013, MNRAS, 429, 3114
Cole D. R., Debattista V. P., Erwin P., Earp S. W. F., Roškar R., 2014, MNRAS, 445, 3352
Comerón S., Knapen J. H., Beckman J. E., 2008, A&A, 485, 695
Corsini E. M., Méndez-Abreu J., Pastorello N., Dalla Bontà E., Morelli L., Beifiori A., Pizzella A., Bertola F., 2012, MNRAS, 423, L79
Corsini E. M. et al., 1999, A&A, 342, 671
Côté P. et al., 2006, ApJS, 165, 57
de Lorenzi F., Debattista V. P., Gerhard O., Sambhus N., 2007, MNRAS, 376, 71
De Lorenzi F., Hartmann M., Debattista V. P., Seth A. C., Gerhard O., 2013, MNRAS, 429, 2974
de Zeeuw P. T. et al., 2002, MNRAS, 329, 513
den Brok M. et al., 2014, MNRAS, 445, 2385
Di Matteo T., Springel V., Hernquist L., 2005, Nature, 433, 604
Dumas G., Mundell C. G., Emsellem E., Nagar N. M., 2007, MNRAS, 379, 1249
Eliche-Moral M. C., González-García A. C., Balcells M., Aguerri J. A. L., Gallego J., Zamorano J., Prieto M., 2011, A&A, 533, A104
Emsellem E. et al., 2004, MNRAS, 352, 721
Emsellem E., Greusard D., Combes F., Friedli D., Leon S., Pécontal E., Wozniak H., 2001, A&A, 368, 52
Emsellem E., van de Ven G., 2008, ApJ, 674, 653
Erwin P., Gadotti D. A., 2012, Advances in Astronomy, 2012
Erwin P., Sparke L. S., 2002, AJ, 124, 65
Fabian A. C., 1999, MNRAS, 308, L39
Falcón-Barroso J. et al., 2004, MNRAS, 350, 35
Feldmeier A. et al., 2014, A&A, 570, A2
Ferrarese L. et al., 2006, ApJ, 644, L21
Ferrarese L., Ford H., 2005, Space Sci. Rev., 116, 523
Ferrarese L., Merritt D., 2000, ApJ, 539, L9
Fisher D. B., Drory N., 2011, ApJ, 733, L47
García-Burillo S., Combes F., 2012, Journal of Physics Conference Series, 372, 012050
Gebhardt K. et al., 2000, ApJ, 539, L13
Gebhardt K. et al., 2001, AJ, 122, 2469
Georgiev I. Y., Böker T., 2014, MNRAS, 441, 3570
Gnedin O. Y., Ostriker J. P., Tremaine S., 2014, ApJ, 785, 71
Graham A. W., 2007, MNRAS, 379, 711
Graham A. W., 2012, MNRAS, 422, 1586
Graham A. W., Guzmán R., 2003, AJ, 125, 2936
Graham A. W., Onken C. A., Athanassoula E., Combes F., 2011, MNRAS, 412, 2211
Graham A. W., Scott N., 2013, ApJ, 764, 151
Gültekin K. et al., 2009, ApJ, 698, 198

Häring N., Rix H.-W., 2004, ApJ, 604, L89
Harris W. E., 1997, VizieR Online Data Catalog, 7202, 0
Hartmann M., Debattista V. P., Seth A., Cappellari M., Quinn T. R., 2011, MNRAS, 418, 2697
Hopkins P. F., Quataert E., 2010, MNRAS, 407, 1529
Johansson P. H., Naab T., Burkert A., 2009, ApJ, 690, 802
King A., 2003, ApJ, 596, L27
King A., 2005, ApJ, 635, L121
King A. R., 2010, MNRAS, 402, 1516
Kormendy J., Dressler A., Byun Y. I., Faber S. M., Grillmair C., Lauer T. R., Richstone D., Tremaine S., 1994, in European Southern Observatory Conference and Workshop Proceedings, Vol. 49, European Southern Observatory Conference and Workshop Proceedings, Meylan G., Prugniel P., eds., p. 147
Kormendy J., Gebhardt K., 2001, in American Institute of Physics Conference Series, Vol. 586, 20th Texas Symposium on relativistic astrophysics, Wheeler J. C., Martel H., eds., pp. 363–381
Kormendy J., Gebhardt K., Fisher D. B., Drory N., Macchetto F. D., Sparks W. B., 2005, AJ, 129, 2636
Kormendy J., Ho L. C., 2013, 51, 511
Kormendy J., Kennicutt, Jr. R. C., 2004, 42, 603
Kormendy J., Richstone D., 1995, 33, 581
Kornei K. A., McCrady N., 2009, ApJ, 697, 1180
Krajnović D. et al., 2008, MNRAS, 390, 93
Krajnović D., Jaffe W., 2004, A&A, 428, 877
Lauer T. R. et al., 2005, AJ, 129, 2138
Launhardt R., Zylka R., Mezger P. G., 2002, A&A, 384, 112
Ledo H. R., Sarzi M., Dotti M., Khochfar S., Morelli L., 2010, MNRAS, 407, 969
Leigh N., Böker T., Knigge C., 2012, MNRAS, 424, 2130
Long K. S., Charles P. A., Dubus G., 2002, ApJ, 569, 204
Lotz J. M., Miller B. W., Ferguson H. C., 2004, ApJ, 613, 262
Lotz J. M., Telford R., Ferguson H. C., Miller B. W., Stiavelli M., Mack J., 2001, ApJ, 552, 572
Lyubenova M. et al., 2013, MNRAS, 431, 3364
Magorrian J. et al., 1998, AJ, 115, 2285
Marconi A., Hunt L. K., 2003, ApJ, 589, L21
Mayer L., Kazantzidis S., Escala A., 2008, Mem. Soc. Astron. Italiana, 79, 1284
Mayer L., Kazantzidis S., Escala A., Callegari S., 2010, Nature, 466, 1082
McConnell N. J., Ma C.-P., Gebhardt K., Wright S. A., Murphy J. D., Lauer T. R., Graham J. R., Richstone D. O., 2011, Nature, 480, 215
McDermid R. M. et al., 2006, MNRAS, 373, 906
McLaughlin D. E., King A. R., Nayakshin S., 2006, ApJ, 650, L37
McLure R. J., Dunlop J. S., 2002, MNRAS, 331, 795
McQuillin R. C., McLaughlin D. E., 2012, MNRAS, 423, 2162
Medling A. M. et al., 2014, ApJ, 784, 70
Mendez-Abreu J., Debattista V. P., Corsini E. M., Aguerri J. A. L., 2014, ArXiv e-prints
Merritt D., 2009, ApJ, 694, 959
Merritt D., Ferrarese L., 2001, ApJ, 547, 140
Milosavljević M., 2004, ApJ, 605, L13
Miocchi P., Capuzzo Dolcetta R., Di Matteo P., Vicari A., 2006, ApJ, 644, 940
Morelli L., Cesetti M., Corsini E. M., Pizzella A., Dalla Bontà E., Sarzi M., Bertola F., 2010, A&A, 518, A32
Morelli L. et al., 2004, MNRAS, 354, 753
Murray N., Quataert E., Thompson T. A., 2005, ApJ, 618, 569
Nayakshin S., Wilkinson M. I., King A., 2009, MNRAS, 398, L54
Neumayer N., Walcher C. J., 2012, Advances in Astronomy, 2012, 15

Nguyen D. D., Seth A. C., Reines A. E., den Brok M., Sand D., McLeod B., 2014, ApJ, 794, 34
Pfuhl O. et al., 2011, ApJ, 741, 108
Pizzella A., Corsini E. M., Morelli L., Sarzi M., Scarlata C., Stiavelli M., Bertola F., 2002, ApJ, 573, 131
Portaluri E., Corsini E. M., Morelli L., Hartmann M., Dalla Bontà E., Debattista V. P., Pizzella A., 2013, MNRAS, 433, 434
Power C., Zubovas K., Nayakshin S., King A. R., 2011, MNRAS, 413, L110
Quinlan G. D., 1996, New Astronomy, 1, 255
Rossa J., van der Marel R. P., Böker T., Gerssen J., Ho L. C., Rix H.-W., Shields J. C., Walcher C.-J., 2006, AJ, 132, 1074
Sakamoto K., Okumura S. K., Ishizuki S., Scoville N. Z., 1999, ApJ, 525, 691
Sani E., Marconi A., Hunt L. K., Risaliti G., 2011, MNRAS, 413, 1479
Sazonov S. Y., Ostriker J. P., Ciotti L., Sunyaev R. A., 2005, MNRAS, 358, 168
Schinnerer E., Böker T., Emsellem E., Downes D., 2007, A&A, 462, L27
Schinnerer E., Böker T., Emsellem E., Lisenfeld U., 2006, ApJ, 649, 181
Scorza C., van den Bosch F. C., 1998, MNRAS, 300, 469
Scott N., Graham A. W., 2013, ApJ, 763, 76
Scott N., Graham A. W., Schombert J., 2013, ApJ, 768, 76
Seifert W., Scorza C., 1996, A&A, 310, 75
Seth A., Agüeros M., Lee D., Basu-Zych A., 2008a, ApJ, 678, 116
Seth A. C., Blum R. D., Bastian N., Caldwell N., Debattista V. P., 2008b, ApJ, 687, 997
Seth A. C., Dalcanton J. J., Hodge P. W., Debattista V. P., 2006, AJ, 132, 2539
Sheth K., Vogel S. N., Regan M. W., Thornley M. D., Teuben P. J., 2005, ApJ, 632, 217
Shlosman I., Frank J., Begelman M. C., 1989, Nature, 338, 45
Silk J., Rees M. J., 1998, A&A, 331, L1
Springel V., Di Matteo T., Hernquist L., 2005, MNRAS, 361, 776
Syer D., Tremaine S., 1996, MNRAS, 282, 223
Tremaine S. et al., 2002, ApJ, 574, 740
Tremaine S. D., Ostriker J. P., Spitzer, Jr. L., 1975, ApJ, 196, 407
Trujillo I., Erwin P., Asensio Ramos A., Graham A. W., 2004, AJ, 127, 1917
Turner M. L., Côté P., Ferrarese L., Jordán A., Blakeslee J. P., Mei S., Peng E. W., West M. J., 2012, ApJS, 203, 5
van den Bosch F. C., Jaffe W., van der Marel R. P., 1998, MNRAS, 293, 343
Walcher C. J., Böker T., Charlot S., Ho L. C., Rix H.-W., Rossa J., Shields J. C., van der Marel R. P., 2006, ApJ, 649, 692
Walcher C. J. et al., 2005, ApJ, 618, 237
Wang J. et al., 2012, MNRAS, 423, 3486
Wehner E. H., Harris W. E., 2006, ApJ, 644, L17
Wozniak H., Combes F., Emsellem E., Friedli D., 2003, A&A, 409, 469
Wyithe J. S. B., Loeb A., 2003, ApJ, 595, 614
Younger J. D., Hopkins P. F., Cox T. J., Hernquist L., 2008, ApJ, 686, 815
Zasov A. V., Moiseev A. V., 1999, in IAU Symposium, Vol. 194, Activity in Galaxies and Related Phenomena, Terzian Y., Khachikian E., Weedman D., eds., p. 279

Part II
Observational Properties of Bulges in Galaxy Surveys

Chapter 6
Stellar Populations of Bulges at Low Redshift

Patricia Sánchez-Blázquez

Abstract This chapter summarizes our current understanding of the stellar population properties of bulges and outlines important future research directions.

6.1 Introduction

The stellar populations of bulges provide a fossil record of their formation and evolutionary history, including insights into the duration and efficiency of the primary epochs of star formation. In the previous chapters we have learned that there are three main type of bulges: the classical, the discy, and the boxy/peanut. All of them show different structural and kinematical properties and different formation scenarios are proposed to explain them. In these scenarios, the star formation history is predicted to be different, e.g., the proposed mechanisms to form classical bulges imply rapid and efficient star formation, while discy bulges are believed to form slowly and at lower redshifts, from the inflow of mainly gaseous material to the center of the galaxy (see Wyse et al. 1997; Kormendy and Kennicutt 2004, for reviews).

Boxy/peanut bulges are believed to be parts of bars seen edge-on and have their origin in vertical instabilities of the disc. Therefore they are expected to have a similar stellar population compared to the inner disc. In principle we should be able to distinguish between different formation scenarios simply by studying the different ages, metallicities and abundance ratios of the bulges. However, the situation is not that straightforward; as discussed in other sections (see e.g. Sect. 6.2.3) internal processes related with disc instabilities can also occur at high redshift and in short timescales. Furthermore, bulges with properties resembling pseudobulges can form, not only by internal processes related with the presence of non-axisymmetric components, but also by accretion of gas and galaxies (Guedes et al. 2013; Querejeta et al. 2015; Eliche-Moral et al. 2011; Obreja et al. 2013). However, getting constraints on the ages, metallicities and abundance ratios in the

P. Sánchez-Blázquez (✉)
Departamento de Física Teórica, Universidad Autónoma de Madrid, Madrid, Spain
e-mail: p.sanchezblazquez@uam.es

E. Laurikainen et al. (eds.), *Galactic Bulges*, Astrophysics and Space Science Library 418, DOI 10.1007/978-3-319-19378-6_6

different types of bulges constitute, undoubtedly, a strong constrain for scenarios of bulge formation and, therefore, several authors have studied the problem. With the exception of the Milky way (MW) and M31, in which we can resolve individual stars, studies of bulges have to deal with integrated properties, through their mean color or absorption lines. Such unresolved stellar population studies have been far less common for bulges than for elliptical galaxies. The reason is that disc galaxies have more dust and ionized gas. The first affects the colors and the second fills the Balmer lines, the most important age diagnostics in the optical. In addition, bulges have, in general, lower surface brightness than ellipticals and the presence of several morphological components, such as discs, bars, rings, etc., complicates the interpretation of the results. Lastly, the light coming from the disc may contaminate the bulge spectrum in a way that is difficult to quantify. This problem is especially acute for studies of stellar population gradients.

Furthermore, over many years, unresolved stellar population studies have been done comparing the integrated colors or absorption lines with the theoretical predictions for single stellar populations (SSP); that is, an essentially coeval population of stars formed with a given initial mass function with the same chemical abundance pattern. While this scenario may not be a bad approximation for massive elliptical galaxies, bulges, especially those formed secularly, are believed to have a more extended star formation history. This means that the young populations, which have low mass-to-light ratios, bias the analyses of composite populations, if present (e.g. Trager et al. 2000).

The relatively low number of studies, the small – and biased – samples, and the difficulties pointed out above have led to a lack of consensus about important results concerning the stellar populations of bulges, as I will show in this review.

However, in the last decade, stellar population models which predict, not only individual spectral features, but the entire synthetic spectra for a population of a given age and metallicity (Vazdekis 1999; Bruzual and Charlot 2003; Vazdekis et al. 2010; Coelho et al. 2007; Walcher et al. 2009; Conroy et al. 2014) have been released. The availability of these models is stimulating the development of numerical algorithms to invert the observed galaxy spectrum onto a basis of independent components (combination of single stellar populations, age-metallicity relation, and dust extinction). Also, new specialized software allows the separation of the light coming from the stars and ionized gas in a reliable manner (e.g. Sarzi et al. 2006). In addition to this, new data from integral field spectrographs (e.g. Bacon et al. 2001; Cappellari et al. 2011; Blanc et al. 2013) are changing the way we see galaxies (Sánchez et al. 2012; Rosales-Ortega et al. 2010). The analysis of these datasets allows one to associate stellar population properties with morphological and kinematical characteristics of the galaxies, making the interpretation of stellar populations more secure. Therefore, the development of the field is very promising and we foresee important advances in the decades to come.

In this section, I will try to review the state of the art in the area, trying to highlight the necessary steps to get a better understanding of the star formation histories of these complex systems. Section 6.2 summarizes the general results obtained with single apertures. Section 6.3 compiles the works on the possible influence of bars in

the stellar populations of bulges and on the stellar populations of bars themselves. Section 6.4 outlines the results obtained with full spectral fitting techniques and Sect. 6.5 reports on the studies of stellar population gradients in bulges. In Sect. 6.6, I show the results about the possible connection between the stellar populations of bulges and discs while in Sect. 6.7 the main results are summarized. In Sect. 6.8, I give some thoughts of what I think the next steps for the study of stellar populations in bulges should be.

6.2 Results Obtained with Single Aperture

6.2.1 General Properties

The first studies of stellar populations in bulges were performed using optical and near-infrared broadband photometry (Balcells and Peletier 1994; Terndrup et al. 1994; Peletier and Balcells 1996; Bell and de Jong 2000; de Jong 1996). These works demonstrated that changes in the bulge colors are linked to galaxy luminosity, potential well, and local surface brightness, with more massive/luminous bulges and higher surface brightness regions being redder than less massive/luminous and lower surface brightness ones. They also showed that early-type bulges are red, as red as elliptical galaxies, and with very little dispersion in their colors (Peletier and Balcells 1996). These results do not apply to the few late-type galaxies analyzed, where significantly bluer colors are measured.

Early interpretation of this data pointed to early-type bulges being as old as ellipticals, the late-type, less massive bulges being younger and/or more metal poor. The small dispersion in the colors was interpreted as being due to small dispersion in the age of early-type bulges (maximum of $\sim$2 Gyr). This, in principle, is in agreement with the classical and discy bulge formation scenarios (see Sect. 6.1) if, as it seems to be the case, secularly formed discy bulges are more common in late-type and in less massive galaxies (Kormendy and Kennicutt 2004; Ganda et al. 2009).[1]

One problem of using colors is the well known age-metallicity degeneracy (Worthey 1994). Bluer bulges can be either younger or more metal poor and, without this information, it is difficult to extract conclusions about their formation mechanisms. Further complications are the presence of emission lines and dust extinction that also affect the colors. In particular, dust extinction depends on the inclination and, therefore, inclination is another parameter that needs to be taken into account when comparing the colors of different types of bulges, and also

[1] Note, however, that a significant number of local massive spiral galaxies appears to have dominant pseudobulges, defined as those bulges with $n < 2$, that includes both discy and boxy/peanut bulges (Kormendy et al. 2010). Furthermore, pseudobulges are also found in S0 galaxies (Laurikainen et al. 2010).

when comparing the results from different studies (see Ganda et al. 2009). All these obstacles make very difficult to extract useful conclusions about the stellar populations of bulges using only colors. For these reasons studies with colors need to be complemented with those using information of the absorption lines with different sensitivities to age and metallicity, and also that they are not affected by dust extinction (MacArthur 2005).

The first spectroscopic studies of bulges analyzed the relation of line-strength indices (the so-called Lick/IDS indices, see Gorgas et al. 1993; Worthey et al. 1994) with the central velocity dispersion (σ hereafter) – used as a proxy for the dynamical mass of the galaxy. Lick/IDS indices measure the strength of the most prominent absorption lines in the optical galaxy spectra and are sensitive to changes of the mean age, chemical abundances and, to a lesser extent, the initial mass function (e.g. Vazdekis et al. 2010; Bruzual and Charlot 2003; Thomas et al. 2003; Schiavon 2007; Conroy and van Dokkum 2012). These studies confirmed the similarity of bulges with elliptical galaxies for early-type galaxies (earlier than Sbc, Bender et al. 1993; Fisher et al. 1996; Idiart et al. 1996).

However, it has been pointed out that this similarity may be due to the fact that the majority of these initial analyses were performed on samples that were biased towards early-type spirals (earlier than Sbc, Kormendy and Kennicutt 2004). In the last few years, however, several studies have included in their samples late-type bulges and analyzed, mostly, the relation between the Mg-sensitive indices (Mg_2 and Mgb) and the central σ. When these bulges were included, differences between elliptical galaxies and bulges were found. However, the nature of these differences is still not clear. Some authors claim that bulges are located below the Mg-σ relation obtained for ellipticals, which is commonly interpreted as bulges having a younger stellar population (Prugniel et al. 2001; Chiappini et al. 2002; Ganda et al. 2007; Morelli et al. 2008). Other authors find that the slope of the Mg-σ is steeper for bulges (Falcón-Barroso et al. 2002), while Trager et al. (1999) and Proctor and Sansom (2002) report that only low-mass bulges depart from the relation between spectral indices and σ drawn by large bulges. On the other hand, other studies do not find any systematic difference in the Mg-σ relation of bulges and elliptical galaxies, but find that the scatter among this relation for bulges is larger than the equivalent one for ellipticals (Moorthy and Holtzman 2006; Peletier et al. 2007). Similar conclusions were obtained using other line-strength indices.

Some of the discrepancies in the conclusions of different studies may be due to differences in the mass distribution (or central σ) of the selected sample. For example, Fig. 6.1 shows the relation between the Mgb and Hβ indices (measured in magnitudes) for a sample of late-type and early-type bulges and elliptical galaxies from Ganda et al. (2007). It can be seen that despite the relations between line-strength indices and σ followed by late-type bulges and early-type galaxies run apparently parallel to each other, the differences may be just related to the different

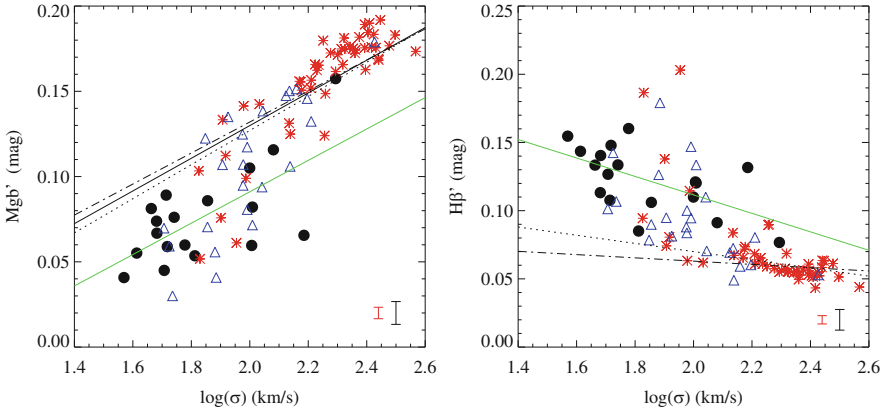

Fig. 6.1 Line-strength indices Mgb′ and Hβ' expressed in magnitudes, against central velocity dispersion. The *black symbols* represent the sample of late-type bulges from Ganda et al. (2007), and the *blue* and the *red symbols*, the sample of Sa galaxies and E and S0 respectively from the SAURON survey. The *dotted* and *dashed-dotted black lines* over-plotted in both panels are the relations obtained by Sánchez-Blázquez et al. (2006a) for low- and high-density environments, respectively, and the *green solid lines* are the relations determined using the late-type galaxy sample. Representative error bars are added at the bottom right of each panel; the *black* one refers to both the early- and late-type spiral samples, while the *red* one refers to the E/S0 galaxies (Figure taken from Ganda et al. (2007). Reproduced with permission of Oxford University Press)

range of central σ. In fact, the differences disappear at low-σ, where even early-type galaxies (E and S0[2]) deviate from the relation defined by massive ellipticals.

Furthermore, bulges, contrary to massive elliptical galaxies, are rotationally supported. Some authors have cautioned (Prugniel and Simien 1994; Falcón-Barroso et al. 2002) that by not taking into account the rotation in the σ measurements, one may be underestimating their binding energy. The contribution to the rotation may by calculated as $0.5\log(1+0.62V^2/\sigma^2)$, as in Prugniel and Simien (1994), where V is the rotational velocity. Falcón-Barroso et al. (2002) claim that a mean $V/\sigma = 0.5$ suffices to bring the bulges back to the Mg_2-σ relation defined by giant ellipticals.[3] Other studies have also claimed a better correlation between the line-strength indices and V_{max} (an indicator of the total potential well) than between line-strength indices and the central σ (Prugniel et al. 2001).

[2]Classically, studies of stellar populations include E and S0 galaxies into the same group.

[3]Note, however, that the majority of low-luminosity elliptical galaxies are also rotationally supported (Emsellem et al. 2011).

6.2.2 Comparison with SSP Models

Nevertheless, the similarity found by some authors between the index-σ relation of bulges and elliptical galaxies may not reflect a real similarity in their stellar content. Line-strength indices are not free from the age-metallicity degeneracy (e.g., Mg_2 and Mgb can be lower in younger or in more metal stellar populations). Therefore, large differences between the ages of bulges and ellipticals could exist, and not be reflected in these relations if there is a complementary age-metallicity relation (e.g. Trager et al. 2000). The advantage of using these characteristics, though, is that the sensitivity to variations of age and metallicity of each different index varies. A way to partially break the age-metallicity degeneracy is to combine indices more sensitive to mean age variations (i.e., the Balmer lines) with those more sensitive to abundance variations in the so-called index-index diagrams. Figure 6.2 shows one of these diagrams combining the composite index

$$[\mathrm{MgFe}]' = \sqrt{\mathrm{Mgb}(0.28\mathrm{Fe5270} + 0.72\mathrm{Fe5335})},$$

which is fairly insensitive to variations of $[\alpha/\mathrm{Fe}]$ abundances[4] (Thomas et al. 2003) and the Balmer index Hβ.

Several authors have used this technique to compare the index values with the predictions of SSP models. These comparisons show that bulges have a large range in SSP-equivalent ages from $\sim$2 to 13.5 Gyr (Peletier et al. 2007; Moorthy and Holtzman 2006) and metallicities. They also report a correlation between both the SSP-equivalent age and metallicity and central σ. In general, they found that more luminous/massive bulges were older and more metal rich. They also inferred that more massive bulges have a larger ratio of α-element[5] with respect to Fe, which is usually interpreted as more massive bulges forming their stars on shorter timescales. The relations were similar to those found for elliptical galaxies (Bica 1988; Jablonka et al. 1996, 2007; Idiart et al. 1996; Casuso et al. 1996; Goudfrooij et al. 1999; Trager et al. 1999; Thomas and Davies 2006; Moorthy and Holtzman 2006; Ganda et al. 2007). On the other hand, Proctor and Sansom (2002) and Prugniel et al. (2001) found that, contrary to what happens in elliptical galaxies, both Fe and Mg were correlated with σ in bulges, resulting in the lack of a tight correlation between

[4]The α elements are those chemical elements predominantly formed via fusion with a helium nucleus. Their most abundant isotopes therefore have nucleon numbers that are multiples of 4 (e.g., O, Ne, Mg, Si, S, Ar, Ca, Ti). These elements are mainly synthesized in Type II supernovae, while Type Ia supernovae produce elements of the iron peak (V, Cr, Mn, Fe, Co and Ni). In chemical evolution models, type II supernovae produce an early enrichment of α-elements followed by a subsequent enrichment of iron-peak, Type Ia supernovae products. In the absence of other modifying factors, this implies that $[\alpha/\mathrm{Fe}]$ can be used as a 'galactic clock' for the duration of the star formation.

[5]What it is usually measured is the Mg abundance through the Mgb index. Other α-elements, like Ca or Ti may follow different patterns (e.g. Conroy et al. 2014; Graves and Schiavon 2008; Cenarro et al. 2004).

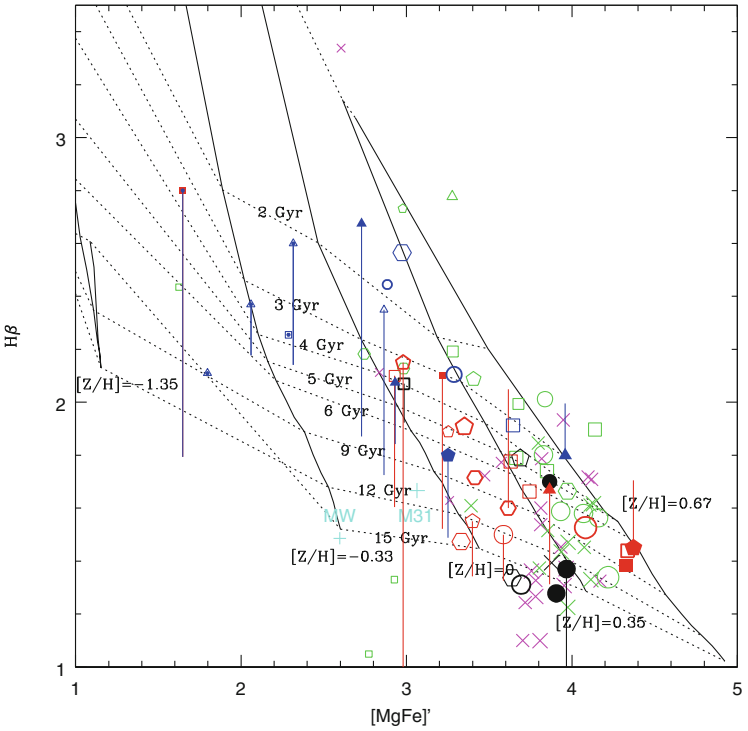

Fig. 6.2 Hβ vs. [MgFe]$'$ in the central regions of bulges and ellipticals. Magenta crosses are galaxies from Trager et al. (1999). *Green symbols* are bulges and ellipticals from Proctor and Sansom (2002). The MW (Puzia et al. 2002) and M31 (Puzia et al. 2005) are shown as '+' symbols. *Blue* and *red symbols* are from Moorthy and Holtzman (2006). The color of the symbol is chosen according to whether they are redder or bluer than B-K = 4. Larger sizes indicate larger central velocity dispersion. Bulges for which there is no color information are in *black*. *Solid lines* represent the predictions of Thomas et al. (2003) for SSPs of constant metallicity (as indicated in the labels) while *dotted lines* represent the predictions for populations of constant age, with age increasing towards the bottom of the panel. For other details regarding the figure see Moorthy and Holtzman (2006) (Reproduced with permission of Oxford University Press)

Mg/Fe (a proxy for [α/Fe]) and σ. This result needs to be corroborated by other studies.

Similar to the results obtained with line-strength indices, a comparison of SSP-equivalent parameters of bulges and ellipticals reveals that both have very similar properties, at least in samples of bulges earlier than Sbc. Figure 6.3 illustrates the relation between the SSP-equivalent ages, metallicities, and [α/Fe], and the central σ for bulges, S0s, and elliptical galaxies (Thomas and Davies 2006). It can be seen that, at a given central σ, the stellar population parameters of bulges and elliptical galaxies are indistinguishable. These results support the idea that bulges (with morphological types earlier than Sbc) were formed with very little influence from the disc, in a process similar to the one that formed elliptical galaxies.

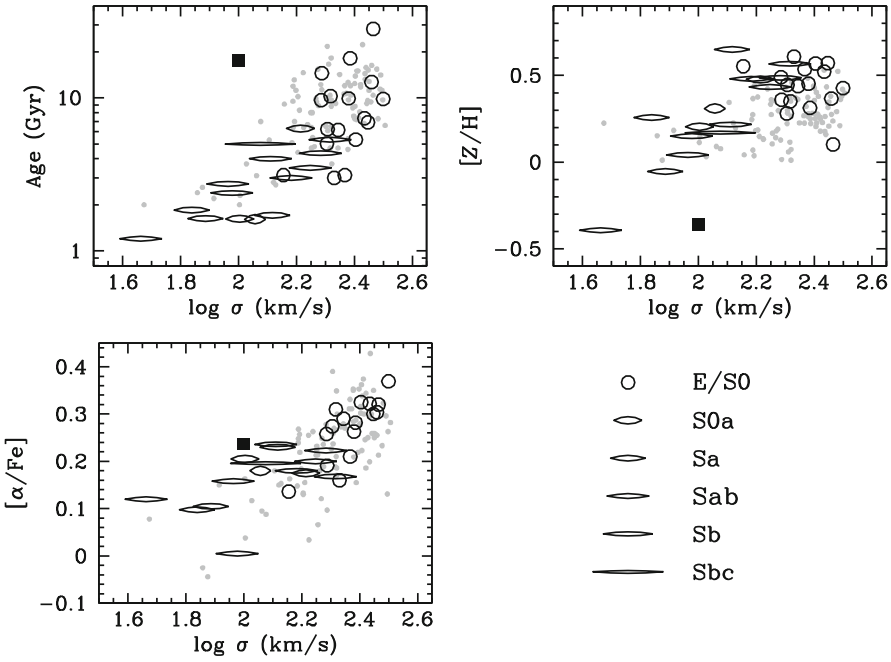

Fig. 6.3 Stellar population parameters *versus* central velocity dispersion. *Open circles* are early-type galaxies from Thomas and Davies (2006), ellipses are spiral bulges with ellipticity increasing for the later-types (see labels in the *right-hand bottom panel*) and the *filled square* is the integrated light of the MW bulge. *Small grey-filled circles* are early-type galaxies from Thomas et al. (2005). Central stellar populations are shown (Figure taken from Thomas and Davies (2006). Reproduced with permission of Oxford University Press)

In samples that contained late-type galaxies (later than Sbc), both Prugniel et al. (2001) and Moorthy and Holtzman (2006, see also Morelli et al. 2008) find three types of bulges in the comparison of line-strength indices and stellar population models: old-metal rich (OMR), young metal rich (YMR) – which are bulges with ages less than 3 Gyr and super-solar metallicities – and metal poor (MP) with sub-solar metallicity. These classes seem to be sensitive to the Hubble type. All the early-type (S0-Sab) bulges are metal-rich. The red early-type bulges are in the OMR region while the blue early-types reside in the YMR region. Metal-poor bulges are all late-types, although late-type bulges are found in all three regions. A comparison of the SSP properties of late-type bulges and elliptical galaxies at a similar σ, however, remains to be done. Therefore, as was the case with the line-strength indices, it is not clear whether late-type bulges are younger for being late-type, or for having low σ.

6.2.3 Relation Between Stellar Population and Structural Properties

A more direct way to test the different proposed scenarios for bulge formation is to compare the stellar population properties of a sample of bulges, which have morphological or dynamical properties that distinguish them as classical, discy, or boxy/peanut bulges. As we have seen in previous sections (see Sect. 6.2.2), there are several observables used to separate bulges and pseudobulges, and also, different authors have employed different properties to perform this task. Carollo et al. (2001) analyzed V, H, and J HST images of a sample of bulges with exponential (typical of discy and boxy/peanut bulges) and $R^{1/4}$ luminosity profiles (typical of classical bulges), finding the former, on average, bluer than the latter (by $\sim$0.4 mag in $< V - H >$), which could be a consequence of a younger and/or lower metallicity stellar population. They also found, in agreement with the results of Peletier and Balcells (1996), that the colors of those bulges showing a $R^{1/4}$ profile were red and very homogeneous, while for the exponential bulges the scatter was significantly larger.[6] They interpreted these results as a delayed formation of the exponential bulges compared with those having an $R^{1/4}$ profile, which formed their stars in the early Universe. Drory and Fisher (2007) used a different approach and separated classical and pseudobulges morphologically. Pseudobulges were those showing nuclear bars, nuclear spirals, and/or nuclear rings, whereas classical bulges were featureless structures being also rounder than the outer disc. Separating the bulges this way and comparing with their visual morphological types, they studied the location of bulges in the color-magnitude diagram. They fond that Sc galaxies and later types do not contain classical bulges and are located almost entirely in the blue cloud in the color-magnitude diagram. Intermediate Sa-Sbc type galaxies, on the contrary, contain both classical and pseudobulges. While 87 % of the galaxies with pseudobulges were in the blue cloud, all galaxies with classical bulges were in the red-sequence. These authors stress that the differences in colors are not due to a different contribution of bulge and disc to the total galaxy color, because blue and red galaxies share a certain range in bulge-to-total (B/T) ratio. This is shown in Fig. 6.4, where the global color of the galaxies is plotted as a function of the B/T ratio. It can be seen that both bulges and pseudobulges coexist in the region of B/T values ranging from 0.05 to 0.45 and that, in this region, classical bulges are redder than pseudobulges. They also found that, in general, pseudobulges classified with the morphological features described above were more diffuse and had lower Sérsic indices than classical bulges.

Another way of separating classical bulges from pseudobulges was adopted by Gadotti (2009) who identified pseudobulges as those lying below the Kormendy relation (Kormendy 1977) defined by elliptical galaxies. He established that pseudobulges defined this way were in general, 0.2 mag bluer in the $(g - i)$ color than

[6] Note, however, that many of the exponential bulges were showing colors as red as the $R^{1/4}$ bulges.

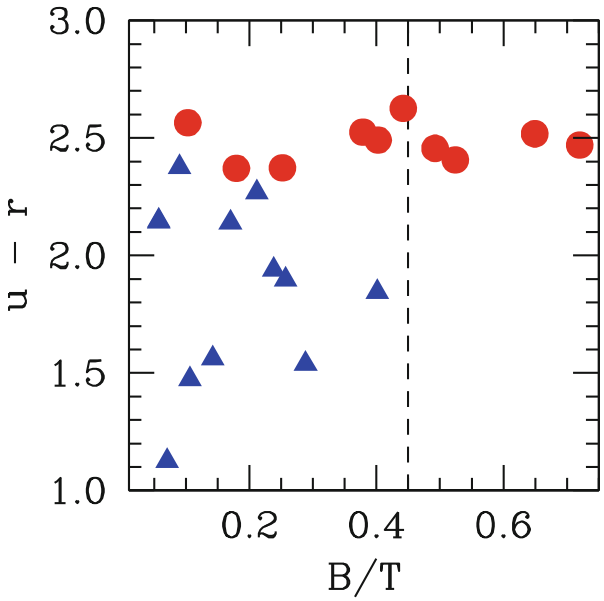

Fig. 6.4 Distribution of bulge-to-total ratios, B/T, of intermediate type (Sa-Sbc) galaxies with pseudobulges (*blue triangles*) and classical bulges (*red circles*) with respect to their global u-r color. The *dashed line* marks B/T = 0.45 above which only classical bulges are found (From Drory and Fisher 2007)

the classical bulges. On the other hand, Fernández Lorenzo et al. (2014), who used the Sérsic index to differentiate between classical and pseudobulges, found that the latter are as red as the former at the same luminosity. Only for the fainter pseudobulges they measured bluer colors.

Again, colors are affected by the age-metallicity degeneracy and dust extinction. In principle more information may be obtained from the study of absorption lines and their comparison with stellar population models. Several works have also compared the line-strength indices of bulges with different structural characteristics (Williams et al. 2012; Gadotti 2009). The first studied a sample of edge-on boxy/peanut bulges finding that they follow the same central index-σ relation as elliptical galaxies (see also Jablonka et al. 2007), although the sample was biased towards early-type galaxies (S0-Sb). On the other hand, Gadotti (2009) found a strong correlation between the D4000 index and the Sérsic index (n), indicating younger populations[7] in galaxies with lower n. On the contrary, for a sample of early-type galaxies, Vazdekis et al. (2004) did not find any correlation between n and age, while they found a strong correlation between n and [Mg/Fe]. The different

[7] Actually the author did not compare the index with stellar population models and, therefore, a variation in metallicity is also possible.

behavior for bulges and ellipticals is very interesting, but more studies of this kind using larger samples are still needed to confirm or refute the trends. Note that the only study targeting specifically boxy/peanut bulges is that of Williams et al. (2012). The rest of studies cited above usually include both discy and boxy/peanut bulges in the same 'pseudobulge' category.

The current lack of consensus between studies may be due to different criteria to separate classical and pseudobulges. Some might include discy and boxy/peanut bulges in the same category, without making any distinction between them. Furthermore, different distributions of the galaxy luminosities can also lead to discordant results. It is clear that low-luminosity, low-mass bulges are bluer than the more massive and brighter ones, but it is not clear if, at the same luminosity, bulges with different structural characteristics share the same color.

6.2.4 Bulges as Composite Systems

Thanks to the 2-dimensional data of the SAURON survey (Bacon et al. 2001), Peletier et al. (2007) (see also Sil'chenko and Afanasiev 2004) noticed that, when present, young stellar populations in their sample of early-type bulges were concentrated near the center, in discs or in annuli suggestive of resonance rings (Byrd et al. 1994). Peletier et al. (2007) realized that the studies comparing the line-strength indices of bulges and elliptical galaxies could be divided into two categories: those targeting inclined galaxies, which do not find any difference between the index-σ relation of bulges and ellipticals, and those sampling almost face-on galaxies, which find younger stellar populations in bulges compared with those of elliptical galaxies, and a large scatter in the line-strength indices at a given σ. The differences are especially visible in galaxies with low σ. They argue that bulges are composite systems, with two or more types of bulges coexisting in the same galaxies. The classical bulge is composed mainly of an old and metal rich population and the discy and boxy/peanut bulge can be younger and contain more metal-poor stars (although it can also be old). The discrepant results obtained in samples of different inclinations can be explained, according to these authors, by the different contribution to the bulge light of different subcomponents (classical, discy, and boxy/peanut). If the young component is a disc, then it is concentrated in the disc plane and would not be seen in edge-on galaxies. These young components, however, do contribute to the integrated light of less inclined samples (if they are limited to the central regions). The result is supported by the observation of central dips in the velocity dispersion maps in 50 % of the galaxies of their sample.

The coexistence of two or more types of bulges (classical, discy, and boxy/peanut) in some galaxies has been pointed out by several authors (Athanassoula 2005; Gadotti 2009; Nowak et al. 2010; Kormendy and Barentine 2010; Erwin 2008) and is supported by theoretical studies (Obreja et al. 2013; Samland and Gerhard 2003). Obreja et al. (2013) propose a picture were the centers of most early-type spirals contain multiple kinematic components: an old and slowly

rotating elliptical-like component, and one or more disc-like, rotationally supported components which are typically young but can also be old.

This 'two component model' also explains the properties of our MW bulge. The MW is considered to have a boxy bulge, yet increased evidence of an old, α-enriched stellar population that formed on a short time-scale, has resulted in a two component model (e.g. Tsujimoto and Bekki 2012). It has been shown that two stellar populations coexist in the Bulge separated in age and metallicity (McWilliam and Rich 1994; Feltzing and Gilmore 2000; van Loon et al. 2003; Groenewegen and Blommaert 2005; Zoccali et al. 2006, 2008; Fulbright et al. 2007), which separation extends somewhat also to kinematics (Zhao et al. 1994; Soto et al. 2007). However, age determinations through color-magnitude diagram shows that most bulge stars in the MW are older than 10 Gyr (Ortolani et al. 1995; Feltzing and Gilmore 2000; Zoccali et al. 2006; Clarkson et al. 2008).

The task of isolating the stellar population properties of the different subcomponents forming a bulge is difficult. Still, it has been tried by some authors. For example, Williams et al. (2011) study the stellar populations of two edge-on boxy/peanut shaped bulges. They place the slit along the major axis and observe with three offset in parallel positions. They found that NGC 1381 has a boxy bulge, with stellar rotation neither cylindrical (as would be expected for bars seen edge-on) nor strongly non-cylindrical, and with a double hump on the rotation curve. The galaxy shows a metallicity gradient but no age gradient and a positive [α/Fe]. They explain the properties of these galaxies in an scenario where NGC 1381 has the three classes of bulges. The classical bulge formed their stars rapidly and explain the general trend in [α/Fe] as a function of height, as disc light (with its lower [α/Fe]) contributes less and less to the integrated spectrum. The boxy appearance is explained by the simultaneous presence of a bar (which appears boxy in projection), and the double hump of the rotation curve hints at the presence of a small discy pseudobulge (see also Sil'chenko et al. 2010).

6.3 The Influence of Bars in Building Up the Bulge

It seems clear that some bulges have central discs (Peletier et al. 2007),[8] often (but not always) with young stars, which is usually linked to disc gas inflow and central star formation caused by internal secular processes, related to the presence of a bar (Friedli and Benz 1995; Norman et al. 1996; Noguchi 2000; Immeli et al. 2004). However, this central rotationally supported younger component does not necessarily form due to internal processes. Major and minor mergers as well as external accretion of gas may result in the formation of a discy bulge (e.g. Guedes et al. 2013; Querejeta et al. 2015). This idea may be supported by some observational studies. For example, Kannappan et al. (2004) found, in a sample of

[8]Editorial comment: we assume that in terms of this book the author means discy pseudobulges.

discy bulges selected based on their blue colors and therefore having young stars, that all of them showed signs of recent interactions.

Hydrodynamical cosmological simulations predict that both secular and external processes contribute to form discy pseudobulges with similar characteristics e.g., they are rotationally supported and have young and metal poor stellar populations (Obreja et al. 2013; Guedes et al. 2013). Eliche-Moral et al. (2011) analyze the effects of minor mergers on the inner part of disc galaxies, finding that also this process is efficient in forming rotationally supported inner stellar components, i.e., discs, rings or spiral patterns (see also Domínguez-Tenreiro et al. 1998; Aguerri et al. 2011; Scannapieco et al. 2010).

A way to quantify the importance of secularly formed discy bulges is to compare the properties of galaxies with and without bars. It has been found that H_α emission is enhanced in the early-type spirals with bars, compared to that in the early-type non-barred galaxies (e.g. Ho et al. 1997; Huang et al. 1996; Alonso-Herrero and Knapen 2001; Jogee et al. 2005; Ellison et al. 2011). However, in spite of that, the evidence supporting the bulge building by bars from the ages of its stars has proven to be elusive. Several authors have made this comparison using samples of face-on galaxies, where it is easy to morphologically identify the bar. The differences, however, have not been firmly established. Moorthy and Holtzman (2006) and Pérez and Sánchez-Blázquez (2011) found hints of lower ages and higher metallicities in barred galaxies, compared to their non-barred counterparts at a given σ.[9] They also found higher $[\alpha/\mathrm{Fe}]$ abundances in barred galaxies with central velocity dispersion $2.2 > \log\sigma\ (\mathrm{km/s}) > 2.35$, but the opposite for $2 > \log\sigma\ (\mathrm{km/s}) > 2.2$. At fixed σ and V_{max}, barred galaxies appear to have larger central values of $[\mathrm{MgFe}]'$[10] (which can be used as an indicator of metallicity independent of $[\alpha/\mathrm{Fe}]$, see above) than non-barred galaxies (or galaxies with elliptical shape bulges) of the same σ or V_{max}. The differences, however, were not very significant in a statistical sense.

On the other hand, Jablonka et al. (2007) found no difference between the stellar population properties of edge-on barred and non-barred galaxies. However, it may be difficult to detect a bar in an edge-on galaxy. de Lorenzo-Cáceres et al. (2012, 2013) analyzed the stellar populations in the center of double-barred early-type S0s and spirals finding some signs of gaseous flows and young stellar populations. This population was not very prominent though. Nevertheless, all the above studies were affected by poor number statistics.

Coelho and Gadotti (2011) observed 575 face-on bulges in disc galaxies, of which 251 contain bars. They found that, for bulges with masses between $10^{10.1}\,\mathrm{M}_\odot$ and $10^{10.85}\,\mathrm{M}_\odot$, the distribution of ages in barred galaxies is bimodal with peaks at 4.7 and 10.4 Gyr. This bimodality is not seen in non-barred galaxies of a similar bulge mass range. The age distribution of barred and non-barred galaxies is, per

[9] Although the differences found by Moorthy and Holtzman (2006) in the $\mathrm{H}\beta$-σ relation between barred and non-barred galaxies disappear when V_{max} is used instead of σ.

[10] This index is defined as $[\mathrm{MgFe}]' \equiv \sqrt{\mathrm{Mgb} \times (0.72\,\mathrm{Fe5270} + 0.28\,\mathrm{Fe5335}}$ in Thomas et al. (2003).

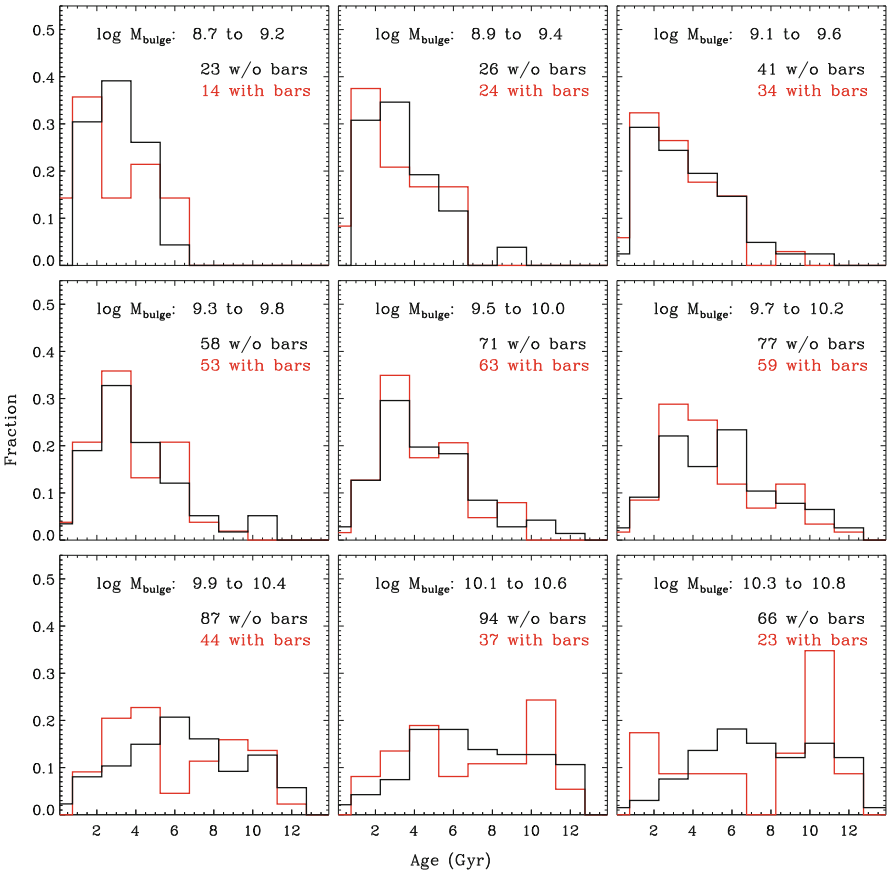

Fig. 6.5 Normalized distributions for bulge ages, for several mass intervals, as indicated. Distributions for barred and non-barred galaxies are shown in *red* and *black lines*, respectively (Figure taken from Coelho and Gadotti (2011). Reproduced with permission of AAS)

contra, similar for bulges of masses lower than $10^{10.1}\,M_{\odot}$ (i.e., the differences are only seen in massive bulges). These authors did not find any difference in the metallicity distribution of barred and non-barred galaxies. These results are summarized in Fig. 6.5 where the distributions of ages for several mass intervals are shown for samples of barred and non-barred galaxies.

Therefore, it is still not clear if there are differences between the stellar populations of galaxies with and without bars. What seems clear though is that, if there are differences, they are only visible in massive, early-type galaxies, a result that is supported by other studies analyzing the molecular gas concentration (Sakamoto et al. 1999). This is often attributed to the fact that early-type galaxies host larger and stronger bars than late-type galaxies (e.g. Buta and Combes 1996), although, as pointed out in Laurikainen et al. (2004, 2007), a longer bar does not

necessarily imply a stronger bar and, in fact, the bar induced tangential forces in early type galaxies are weaker because they are diluted by the more massive bulges.[11]

This does not necessarily mean that bars are not efficient agents in building up bulges. It is still not clear if bars are long-lasting structures or not. If bars are not long-lasting structures but rather recurrent patterns (Bournaud and Combes 2002) then, the fact that we do not find differences between barred and non-barred galaxies would not necessarily imply that bars are not important for secular evolution but, simply, that non-barred galaxies could have been barred in the recent past. However, most numerical simulations show that, once formed, bars are robust structures (Shen and Sellwood 2004; Athanassoula et al. 2005, 2013; Debattista et al. 2006; Berentzen et al. 2007; Villa-Vargas et al. 2010; Kraljic et al. 2012). Furthermore, at least in massive disc galaxies, bars have the same stellar population properties as bulges (old, metal rich, and [α/Fe]-enhanced stellar populations; Sánchez-Blázquez et al. 2011; Pérez et al. 2009) which, in many cases, are very different from that of the disc (see Sect. 6.3). This result also supports (although it does not prove, see Sect. 6.3[12]) the idea that bars formed long ago. The longevity of bars is also suggested in studies of the bar fraction evolution (e.g. Sheth et al. 2008), which find a similar bar fraction at z$\sim$0.8 to that seen at the present-day for galaxies with stellar masses $M_* \geq 10^{11}\,M_\odot$. In addition, non-axisymmetric structures, such as nuclear spirals, can drive gaseous inflows (e.g. Kormendy and Fisher 2005), which could dilute the differences between barred and non-barred galaxies.

6.3.1 Stellar Population of Bars

As the debate of the durability of bars is still open and its influence may be crucial for the formation of bulges, it is important to study the stellar populations hosted by bars. Very few works, however, have dealt with this problem.

Gadotti and de Souza (2006) obtained color gradients in the bar region in a sample of 18 barred galaxies. They interpreted the color differences as differences in stellar ages and concluded that younger bars were hosted by galaxies of later types (see also Gadotti 2008). However, as we mentioned in Sect. 6.2, the effects of age-metallicity degeneracy and dust extinction are strongly degenerate in colors and, therefore, conclusions based on only colors remain uncertain. Pérez et al. (2007, 2009) performed an analysis of the stellar populations of bars in early-type galaxies using line-strength indices. They found that the mean bar values of SSP-equivalent age, metallicity, and [α/Fe], correlate with central σ, in a similar manner as for

[11] Although the majority of authors does not distinguish different types of S0, Laurikainen et al. (2007) also show that early-type S0s have shorter bars than later type S0s, i.e., the trend of longer bars for early-type morphologies reverse in this morphological subclass.

[12] The stars in the bar can form in the disc long time ago, even if the bar have been recently formed.

bulges, pointing to an intimate evolution of both components. Galaxies with high central σ ($>170\,\mathrm{km\,s^{-1}}$) host bars with old stars, while galaxies with lower central velocity dispersion show stars with a large dispersion in their ages.

These authors also analyzed the stellar population gradients along the bars and found three different behaviors: (1) bars with negative metallicity gradients. These bars have young/intermediate stellar populations (SSP-equivalent values <2 Gyr) and have amongst the lowest stellar velocity dispersions of the sample; (2) bars with no metallicity gradients. These galaxies have positive age gradients; and (3) bars with a mean old stellar population and positive metallicity gradients (more metal-rich at the bar ends).

The fact that bars are composed of old stellar populations does not mean that they formed long ago, as the bar might have formed recently out of old stars in the disc. One way to disentangle these two options is to compare the stellar populations of the disc and the bar at the same distances. In Sánchez-Blázquez et al. (2011) this comparison is made for two galaxies, finding that stars in the bar are older and more metal rich than those of the disc. Furthermore, the gradients in both parameters are much flatter in the bar region. In general, they found that the stellar content of the bar is more similar to that of the bulge than to the disc. However, the sample of this study remains small and biased towards early-type bulges. Clearly, a study using larger galaxy samples covering all morphological types is still needed.

6.4 Star Formation Histories

The majority of stellar population studies of bulges are based on the comparison of the observed colors or spectral properties with the predictions of SSP models. While the SSP assumption may not be a bad approximation for massive elliptical galaxies, it is most likely not a good one for spirals, which are believed to have more extended star formation histories (Kennicutt 1993; James et al. 2008).

In cases were the star formation history has been more complicated than just a single burst, the interpretation of the results based on analyses of single-stellar population is difficult. Bulges with an intermediate SSP-equivalent age could have formed all of their stars at intermediate epochs or, alternatively, almost all star formation appeared at very early times, and only a small fraction is generated at more recent epochs.

To avoid these difficulties, some authors have tried to analyze their data assuming more realistic star formation histories. There are several examples in the literature where the stellar population properties have been derived using a parametric approach (Ganda et al. 2007; MacArthur et al. 2004; Kauffmann et al. 2003), where a predefined shape for the star formation history and chemical enrichment is assumed. In this case, some parameters are fixed while others are fitted by comparing the observations with the predictions of the models. Ganda et al. (2007) compared three line-strength indices with the predictions based on two bursts, and on exponentially declining star formation histories. They obtained, respectively, the

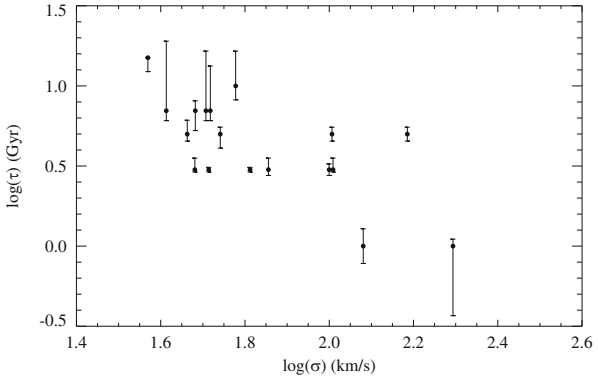

Fig. 6.6 Central aperture values for the *e*-folding time-scale τ against central velocity dispersion σ (both in units of decimal logarithm), in an exponentially declining star formation scenario; the τ values are obtained selecting amongst models with age = 10 Gyr (Figure from Ganda et al. (2007). Reproduced with permission of Oxford University Press)

age, metallicity and mass fraction of the youngest burst, and the e-folding (τ) time in the case of the exponentially declining star formation history. In the first case, they concluded that degeneracies in the parameter space prevented them from extracting useful conclusions. In the second case, they found that bulges with a larger central σ showed shorter e-folding times, more consistent with an instantaneous burst scenario. Low-σ galaxies have larger τ, indicating a more extended star formation history (see Fig. 6.6).

The problem with this approach is that the results depend strongly on the priors – i.e., the wrong answer can be obtained with the wrong assumptions about the star formation history. Furthermore, the use of only a few line-strength indices makes it difficult to break the existing degeneracies in the parameter space, such as the age of the burst versus its strength, or the τ-metallicity degeneracy.

The availability of high-quality stellar libraries and associated stellar population models (e.g. Sánchez-Blázquez et al. 2006b; Vazdekis et al. 2010; Bruzual and Charlot 2003; Conroy and van Dokkum 2012) that predict, not only individual absorption line features, but the whole spectral energy distribution, has allowed the development of new techniques. Fitting the whole spectrum it is possible to obtain, not only SSP-equivalent ages and metallicities, but also more realistic star formation histories. Furthermore, by considering the information provided by the entire spectrum, the age and the metallicity are more easily separated (Sánchez-Blázquez et al. 2011). These techniques are non-parametric – i.e., no predefined shape for the star formation history is assumed. Codes that have been used to study the stellar population properties of galaxies include MOPED (Heavens et al. 2000); VESPA (Tojeiro et al. 2007); STECKMAP (Ocvirk et al. 2006b); STARLIGHT (Cid Fernandes et al. 2005); SEDFIT (Walcher et al. 2006) and ULySS (Koleva et al. 2009). Using these new tools, one can fit an observed spectrum in terms of a model built by a linear combination of a number of SSPs with different ages and

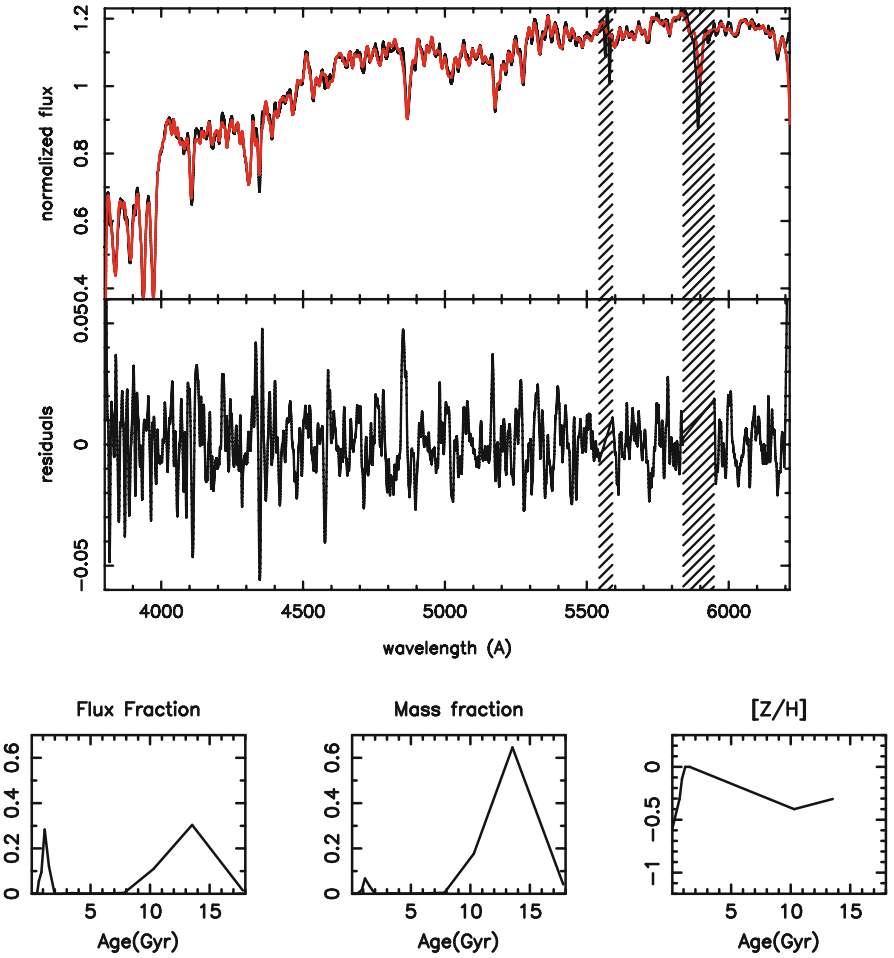

Fig. 6.7 *Top panel*: Example of the fit (*red line*) obtained with STECKMAP for the integrated spectrum of NGC 628 (*black line*). The residuals from the fit (observed-fitted) are also showed. *Hashed regions* indicate those zones that were masked during the fit. *Bottom panels*: Mass, flux fractions and the age-metallicity relation derived with STECKMAP for the integrated spectrum of NGC 628 (From Sánchez-Blázquez et al. (2014). Reproduced with permission from Astronomy & Astrophysics)

metallicities. The kinematics can be calculated at the same time by convolving the model with a Gaussian line-of-sight velocity distribution. In some cases dust can be modeled assuming a reddening law. Figure 6.7 shows an example of a fit to the integrated spectrum of NGC 628 using the STECKMAP code (Ocvirk et al. 2006a,b), together with the derived flux and mass fractions for stars of different ages and the age-metallicity relation (Sánchez-Blázquez et al. 2014).

The problem of inverting a spectrum to derive detailed star formation and chemical enrichment histories is ill-conditioned, i.e., small fluctuations in the data can produce strong variations in the final solution. The different codes try to overcome these issues. The accuracy of the recovered star formation history depends critically on the signal-to-noise of the input spectra and, depending on this value, one can recover more or less different stellar populations described by an age and a metallicity. However, if the spectra have enough signal-to-noise, the different methods can recover reliably both the age distribution and the age-metallicity degeneracy (see, e.g. Cid Fernandes et al. 2005; Ocvirk et al. 2006b; Sánchez-Blázquez et al. 2011).

Robust quantities, even when derived from a spectrum with low signal-to-noise, are the mean values of age and metallicity (Cid Fernandes et al. 2005) weighted with the light (LW) or the mass (MW) of the stars. These are defined as:

$$< A >_{\rm LW} = \frac{\sum_i^N A_i \times {\rm flux}_i}{\sum_i {\rm flux}_i} \tag{6.1}$$

$$< A >_{\rm MW} = \frac{\sum_i^N A_i \times {\rm mass}_i}{\sum_i {\rm mass}_i}, \tag{6.2}$$

where A represents the physical parameter (age or metallicity) and $\rm mass_i$ and $\rm flux_i$ are the reconstructed mass and flux contributions of the stars in the i-th age bin, respectively, as returned by the code. When present, young stars are very luminous in the optical and, therefore, contribute more to the light-weighted values. This means that the light-weighted values of age will be biased towards the youngest stellar components. The mass-weighted values will be less biased, but they are also more uncertain, as the contribution to mass by low-mass faint stars can be very important.

It is interesting to make a comparison between the SSP-equivalent parameters and the averaged ones obtained from the full star formation history. This comparison was made by Trager and Somerville (2009). In their work, the authors derived stellar population parameters from synthetic spectra generated by a hierarchical galaxy formation model. Figure 6.8 shows the comparison of the SSP-equivalent ages and metallicities with the mean values weighted with both light (in the V-band) and mass. As can be seen, the SSP-equivalent ages are always lower than both the luminosity- and mass-weighted averages. In particular, SSP-equivalent ages reflect more closely the age of the last episode of star formation, while luminosity-weighted means, although still biased towards the ages of the youngest components, are closer to the unweighted mean. On the other hand, SSP-equivalent metallicities and abundance ratios are less severely biased.

Some studies have used the non-parametric techniques to analyze the star formation histories of galaxy bulges (MacArthur et al. 2009; Sánchez-Blázquez et al. 2011; González Delgado et al. 2014). The first conclusion from these studies is that the SSP is a very bad approximation for the star formation history of these objects. Furthermore, MacArthur et al. (2009) and Sánchez-Blázquez et al. (2011) found

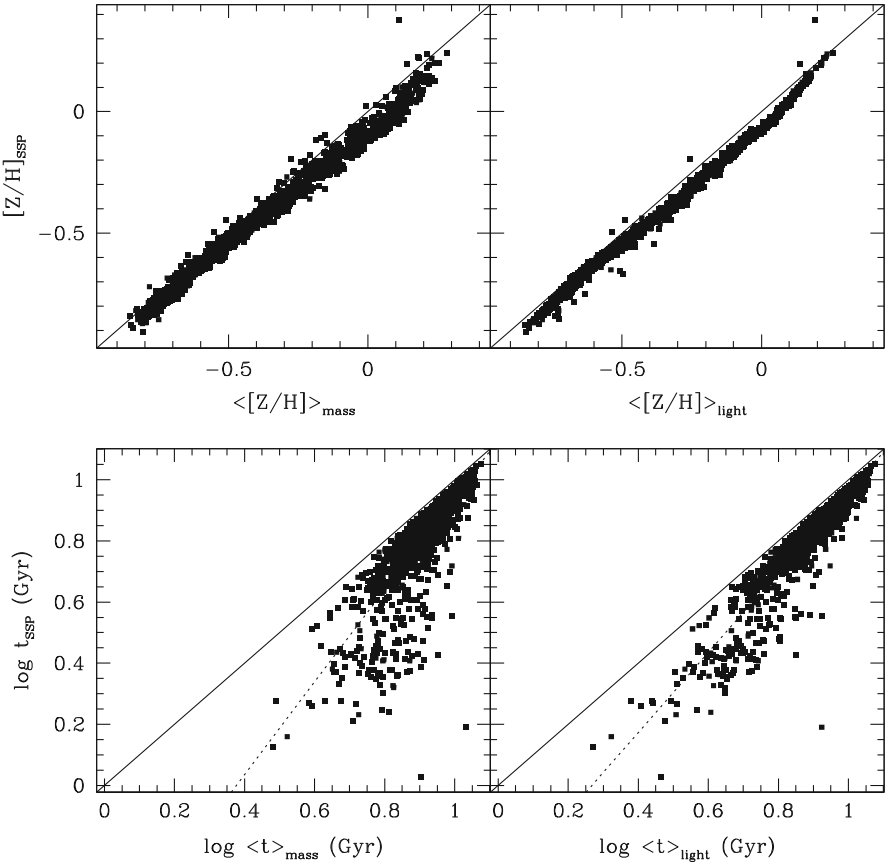

Fig. 6.8 Comparison of the SSP-equivalent age and metallicity as a function of mass-weighted (*left-hand panels*) and V-band light-weighted values (*right-hand panels*) for models of early-type galaxies drawn from 20 realizations of a Coma cluster-size halo (Figure from Trager and Somerville (2009). Reproduced with permission of Oxford University Press)

that in a mass-weighted context, all bulges in their sample were predominantly composed of old stars, independently of their central velocity dispersion. In fact, the previously reported trends of age with central velocity dispersion disappear when mass-weighted values of age are used instead of light weighted ones. This can be seen in Fig. 6.9 from MacArthur et al. (2009).

The result that bulges are dominated, by old stars applies to all types of bulges (early- and late-type, showing different Sérsic index, and with and without bars). However, this type of analysis has been performed on a very low number of galaxies. It would be desirable to extend this work to a complete sample of bulges covering a large range of masses and morphological types. Ideally, one would like to quantify the mass contribution of the young component and correlate this with other properties of the bulges, such as the mass, the environment, the presence of

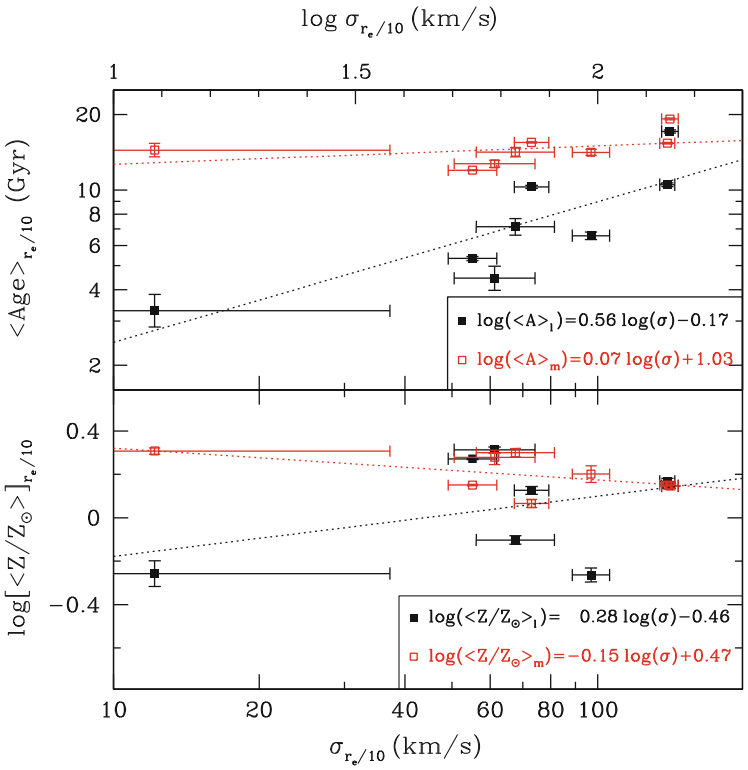

Fig. 6.9 Average age and metallicity as a function of velocity dispersion for a sample of face-on bulges. *Black solid squares* represent light-weighted values while *red symbols* are mass-weighted. The *black* and *red dotted lines* are linear regressions to the light- and mass-weighted data (From MacArthur et al. (2009). Reproduced with permission of Oxford University Press)

bars, and the spiral arm morphology. This would allow one to study the importance of secular versus external mechanisms in building up the central bulges.

Recent works deriving the star formation histories of large samples of spiral galaxies are those performed using the data from the CALIFA survey (Pérez et al. 2013; González Delgado et al. 2014; Sánchez-Blázquez et al. 2014). None of these studies have yet specifically investigated the bulge population. However, Pérez et al. (2013) analyze the mass assembling history of the central parts of galaxies, compared with the rest of the galaxy, for galaxies of all morphological types binned in mass. They found that the galaxies with stellar masses $M_* > 5 \times 10^{10}\,\mathrm{M}_\odot$ have grown their inner part quickly in 5–9 Gyr ago, while lower mass galaxies formed their stars more slowly.

A caveat in all these studies performing full spectral fitting is that they use stellar population models with chemical abundance ratios scaled to solar (e.g. Bruzual and Charlot 2003; Vazdekis et al. 2010). This implies that the models are tuned

to the specific chemistry and star formation history of our MW. This is because the empirical spectral libraries are limited to those stars in the solar neighborhood.

Predictions for the line strengths using the Lick/IDS indices, with variable abundance ratios, have been made for SSPs of different ages and metallicities (Trager et al. 2000; Thomas et al. 2003; Proctor et al. 2004; Tantalo and Chiosi 2004; Lee and Worthey 2005; Annibali et al. 2007; Schiavon 2007), using a semi-empirical approach. However, calculation of the entire spectral energy distribution is more challenging. In fact, in the last few years full spectrum fitting models have been extended to include a variation of elemental abundance patterns, using either theoretical stellar libraries or semi-empirical approaches (Coelho et al. 2007; Walcher et al. 2009; Conroy and van Dokkum 2012). The first studies using full spectral fitting to derive chemical abundance ratios of different elements are starting to appear in the literature, all using samples of early-type galaxies (Conroy et al. 2014; Walcher et al. 2009). This is, however, a challenging task, due to the large number of parameters to fit and possible degeneracies between them.

6.5 Spatially Resolved Stellar Populations in Bulges

Most stellar population studies in bulges have been done using the integrated properties inside a certain aperture. In case of spectroscopic studies, this aperture commonly encloses just the very central parts. However, if we want to have a full understanding of bulge formation, it is necessary to gain knowledge of the variations of the stellar populations with radius. These variations are intimately connected with the dynamical processes that led to the formation of these structures, the degree of dissipation, and the possible re-arrangement of material.

Mergers with gas dissipation or monolithic collapse scenarios predict steep metallicity gradients (Eggen et al. 1962; Larson 1974; Arimoto and Yoshii 1987) and strong gradients in $[\alpha/\mathrm{Fe}]$ (Ferreras and Silk 2002). The predictions for secularly formed bulges are more complicated. As they formed from redistribution of disc stars, the final metallicity gradient will depend on the original gradient in the disc and the scale-length of the final bulge and also on the disc heating (Moorthy and Holtzman 2006). However, lower metallicity gradients are expected to be compared with those of the first scenario. Observationally, the MW bulge manifests many characteristics of a peanut-shaped bulge: it has a clear vertical metallicity gradient, such that the more metal-rich part of the metallicity distribution thins out towards higher latitudes (Minniti et al. 1995; Zoccali et al. 2008; Gonzalez et al. 2011). This result has long been taken as a signature for a classical bulge in the MW. However, recent results have shown that the stars that have been scattered furthest from the disc are the oldest stars and, consequently formed from the least metal-enriched fuel (Freeman 2008; Martinez-Valpuesta and Gerhard 2013). The buckling process may hence establish a negative minor-axis metallicity gradient (which is observed in the MW and NGC 4565, Proctor et al. 2000).

Several articles have studied the variation of the spectral features with radius in bulges (Moorthy and Holtzman 2006; Jablonka et al. 2007; Morelli et al. 2008; Pérez and Sánchez-Blázquez 2011; MacArthur et al. 2009; Sánchez-Blázquez et al. 2011; Ganda et al. 2007), and compared them with stellar population models to obtain either SSP-equivalent parameters or mean values, based on the recovery of the star formation history. These studies find that most bulges have SSP-equivalent or luminosity-weighted negative gradients in metallicity, almost no gradients in age, and slightly positive or null [α/Fe] gradients. Metallicity gradients in the bulge regions are generally steeper than those in the disc region (Moorthy and Holtzman 2006; Sánchez-Blázquez et al. 2011). Figure 6.10 shows the distribution of the SSP-equivalent gradients for a sample of bulges taken from the work of Morelli et al. (2008).

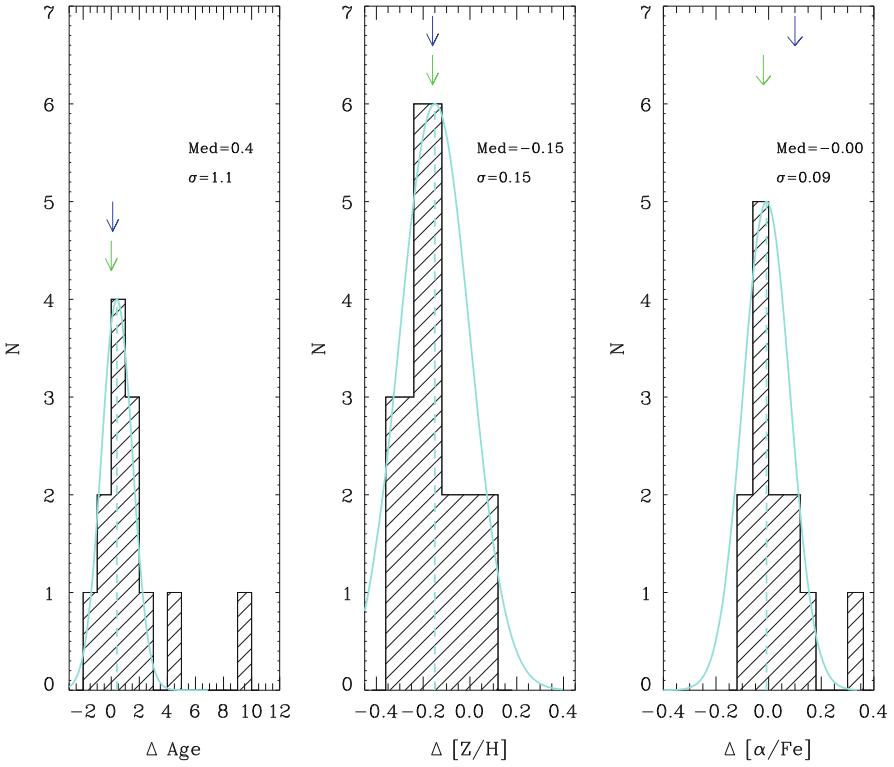

Fig. 6.10 Distribution of the gradients of age (*left*), metallicity (*central*), and [α/Fe] enhancement (*right*) for a sample of galaxies. The *dashed line* represents the median of the distribution and its values is also reported. The *solid line* represents a Gaussian centered on the median value of the distribution. Their σ is approximated by the value containing the 68 % of objects of the distribution and is noted in the inset label. The *green* and *blue arrows* show the average gradient found for early-type galaxies and bulges by Mehlert et al. (2003) and Jablonka et al. (2007), respectively (Figure from Morelli et al. (2008). Reproduced with permission of Oxford University Press)

These gradients are similar to those found in elliptical galaxies, although the quantitative comparison is not that clear. Jablonka et al. (2007) and Morelli et al. (2008) do not find any difference in the magnitude of the bulge gradients and those of elliptical galaxies, while Williams et al. (2012) found that the gradients in boxy bulges are shallower than those in elliptical galaxies at a given σ.

Several studies have also looked for correlations between the gradients and other properties of the galaxies, such as the central σ, the luminosity or mass, in order to check if they are related with the potential well of the galaxy in a similar manner as the central values are. Goudfrooij et al. (1999) and Proctor et al. (2000) found that the gradients were correlated both with the luminosity and central σ, although based on very small samples, while Jablonka et al. (2007) found no such correlation. However, there seems to be a trend that the small bulges have smaller gradients (see also Moorthy and Holtzman 2006; González Delgado et al. 2014). This, in principle, could be attributed to the fact that secularly formed bulges are more common in low mass galaxies.

Possible differences between the gradients of bulges with and without bars have also been explored in a few works, but in none of them any significant differences were found (Moorthy and Holtzman 2006; Jablonka et al. 2007; Pérez and Sánchez-Blázquez 2011). However, Moorthy and Holtzman (2006) reported that, when a positive age gradient was present, it was always in barred galaxies, which could indicate that these objects have more extended star formation in their centers due to bar-driven inflow of gas. This result agrees with that of Gadotti and dos Anjos (2001), who found a greater prevalence of null or positive color gradients in barred galaxies than in non-barred galaxies, which they interpret as an evidence for gradients being erased by bar-driven mixing. Nonetheless, this has not been confirmed in other studies (Jablonka et al. 2007). The reason for the discrepancies could be, once again, galaxy orientations in the samples. The large majority of authors agree that positive age gradients are a consequence of the presence of central discs or nuclear rings, generally associated to recent star formation (e.g. Morelli et al. 2008). As the central discs and rings are likely more common in barred galaxies, this can explain the differences between barred and non-barred galaxies found by Moorthy and Holtzman (2006). They could explain also the lack of differences between barred and non-barred galaxies in the edge-on sample of Jablonka et al. (2007), as these flattened central structures will not contribute to the observed light of the bulge in these orientations.

This interpretation of the age gradients, due to the presence of central younger structures, is supported by the fact that the mass-weighted age gradients are, in the majority of cases, much flatter than the luminosity-weighted or the SSP-equivalent ones. This indicates that the majority of stars in the bulge are old and share a common age, while a small fraction of stars concentrated in central structures are causing the observed radial trends (MacArthur et al. 2009; Sánchez-Blázquez et al. 2011, 2014; González Delgado et al. 2014).

Interestingly, Jablonka et al. (2007) find that the line-strength indices at 1 $r_{\rm eff}$[13] were very similar for all the galaxies in their sample, independent of the mass or morphological type, and that the different gradients come from the differences in their central indices.

A problem in measuring the gradients of age, metallicity, and [α/Fe] in bulges, could be the contamination of their stellar population by the light coming from the underlying disc stellar component. This effect is not important in the galaxy center but it can have an enormous impact in the stellar population estimates of the external parts where the contribution from the disc to the total light is more important. Different authors have tried to quantify, in one way or the other, this contamination from the disc to the bulge light (see Jablonka et al. 1996; Moorthy and Holtzman 2006; Morelli et al. 2008). So far the effect has not been found to be very important, although no extensive tests have been carried out. Studies of edge-on galaxies (Jablonka et al. 2007) do not have this problem. Instead, a drawback in those studies, as mentioned above, is that they are blind to flatter components in the central regions of galaxies.

6.6 The Bulge-Disc Connection

The age distribution of discs is important for constraining scenarios of disc-bulge formation. Correlations between the disc and bulge colors have been found by several authors (Peletier and Balcells 1996; de Jong 1996; Bell and de Jong 2000; Carollo et al. 2001; Gadotti and dos Anjos 2001), which stands both for early and late-type spirals. The similarity in color between inner disc and bulge has been interpreted as implying similar ages and metallicities for these two components, and an implicit evolutionary connection (de Jong 1996; Peletier and Balcells 1996). However, using only colors one cannot directly transform the correlation in colors into correlations of age and/or metallicity.

A correlation of the line-strength index [Mg Fe]$'$, at a radius of one disc scale length from the center, was also found by Moorthy and Holtzman (2006). They interpret this as a correlation between the metallicity of bulge and disc, as this index is more sensitive to variations of metallicity than age, and it is almost insensitive to variations of [α/Fe].

More recently Sánchez-Blázquez et al. (2014) performed a full spectral fitting analysis of a sample of 62 nearly face-on spiral galaxies observed as part of the IFU CALIFA survey (Sánchez et al. 2012). They showed that the slope of the relation between the luminosity-weighted age and metallicity with the central velocity dispersion, is similar in the central parts of the bulges and for the disc at $\sim$2.4 scale-lengths. However, the bulges show higher luminosity-weighted ages and metallicities. Figure 6.11 shows the comparison of the mean values of age and

[13]The radius that contains half of the total luminosity of the bulge.

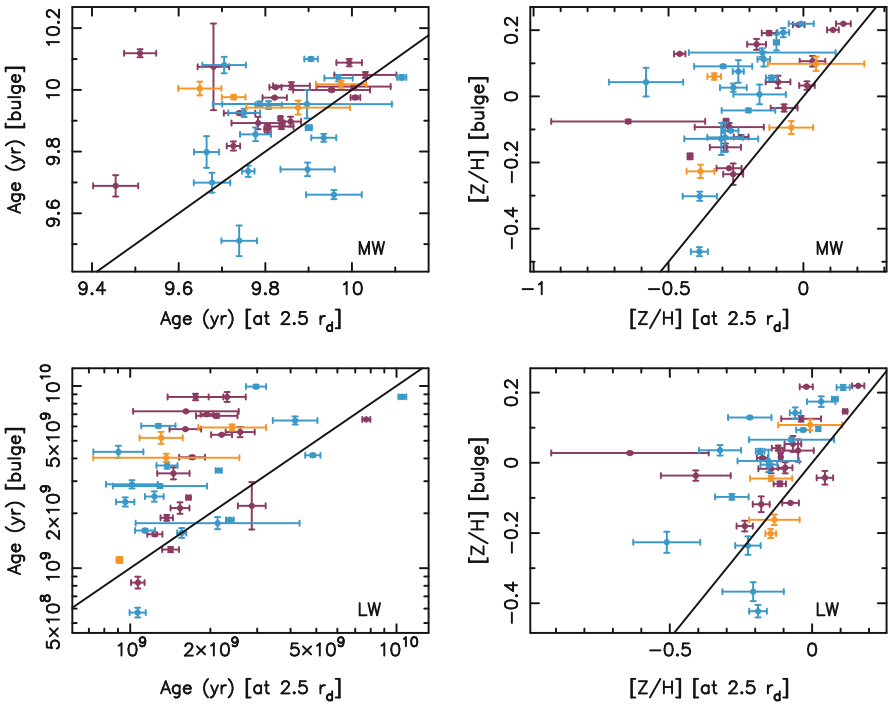

Fig. 6.11 Comparison of the average ages (*left panels*) and metallicity (*right panels*) weighted by both mass (*top panels*) and light (*bottom panels*) measured in the center and at 2.5 scale-lengths of the disc. Different colors indicate if the galaxy is barred (*red*), non-barred (*blue*) or weakly barred (*orange*). The *solid line* represents the 1:1 relation. For more details see Sánchez-Blázquez et al. (2014) (Reproduced with permission of Oxford University Press)

metallicity (both weighted with mass and light) in the center, and at 2.5 scale-lengths of the disc. A Spearman rank order tests shows that, while the metallicities of both components are correlated, the same does not happen with the ages.

Note that the above correlation exists for all early and late-type spirals, classical and pseudobulges. However, such a connection between the radial sizes of bulges and discs exists only for pseudobulges (Fisher and Drory 2008). Therefore, either all bulges formed secularly and some had their bar destroyed, or other physical processes are responsible for this correlation. Several authors have shown that the correlation between the disc and bulge sizes can appear in major or minor merger remnants. While minor mergers tend to preserve the original bulge-disc coupling of the main progenitor, major mergers are capable of rebuilding a bulge-disc coupling from the remnants after having destroyed the original structures of the progenitors (Querejeta et al. 2015, and references therein).

On the other hand, Morelli et al. (2012) rule out significant interplay between the bulge and disc components due to the similarity in the stellar population

properties of bulges hosted in galaxies with very different discs (high- and low-surface brightness).

6.7 Summary

Stellar population studies can provide a critical test needed to understand the basic mechanisms driving bulge formation. However, a clear picture about the stellar populations and their possible correlations with the other parameters of the bulges is still not yet obvious. We have collected the main results obtained from the studies of the observed colors and spectral characteristics of bulges, and of the comparisons with the stellar population models. These characteristics are summarized below:

- Bulges show a wide range of SSP-equivalent ages and metallicities. There is a trend for which more massive bulges have, on average, older stellar populations and higher values of metallicity and [α/Fe].
- Bulges with high Sérsic index n tend to be old and have high [α/Fe], but it is not clear if this trend is due to the existing trend between mass and n.
- There are not strong differences in the stellar populations of bulges and elliptical galaxies at the same mass, but the details of this comparison are still not clear, and the conclusions differ between studies.
- Bulges are often composite systems, with discy, boxy/peanut and classical bulges coexisting in the same galaxy. They usually host different stellar populations. Young stars, when present, are located in the central discs or rings. These young components are not seen in the edge-on samples, which has lead to different conclusions, depending on the galaxy inclination.
- In general terms, there are not very clear differences in the stellar population properties of bulges with and without bars, neither in the central values, nor in the variations with radius. If there are differences, those are only present in massive galaxies, and they show up as an excess of young populations when compared to unbarred galaxies.
- When the mass-weighted mean values of age are considered, all bulges, independent of their mass, seem to be dominated by old stars. The trends between age, metallicity, and mass become much flatter and almost non-existent. This is true for bulges with a variety of structural parameters, such as different Sérsic indices or surface brightness profiles.
- Bulges show mild, negative metallicity gradients, and almost null [α/Fe] and age gradients. The distribution of the slopes is similar to that found in elliptical galaxies. At present, there is no agreement about possible correlation of these gradients with the other parameters of the bulges.
- There is a correlation between the metallicity of the bulge and the disc, but the same is not true for the ages.

6.8 Future Prospects

Although considerable progress has been made in the field, there is still much to be done in order to understand the star formation histories and chemical evolution in the bulges of spirals and S0 galaxies. The first thing we have to deal with is the fact that we cannot make a clean distinction between classical, discy, and boxy/peanut bulges, as many of them coexist in the same galaxy. We need to quantify the preponderance of each component and correlate this with the other properties of the galaxies, like the mass, environment, presence of bars, type of spiral arms, etc. We need also to understand the physical mechanisms that formed each components. For example, numerical simulations have shown that bulges with structural characteristics of pseudobulges can be formed, not only secularly, but also quickly at high redshift, via a combination of non-axisymmetric disc instabilities and tidal interactions or mergers.

Most advances will come from the use of new techniques to derive star formation histories that allow us to distinguish different episodes of star formation. The future is promising: Ocvirk et al. (2008) and Coccato et al. (2011) show the feasibility of separating different components, not only in terms of stellar populations, but also kinematically. This is illustrated in Fig. 6.12, from Ocvirk et al. (2008), where the age-velocity distribution for the bulge is shown in two positions (in the center and outside the bulge dominated region of the galaxy). In this work, the authors model the observed spectrum as a sum of 40 components with different ages but, contrary to the traditional assumption that all components share the same line-of-sight velocity distribution (LOSVD), each component was allowed to have its own non-parametric (not necessarily Gaussian) LOSVD. These authors reconstructed the age-velocity distribution of two bulge regions of the Sbc galaxy NGC 4030.

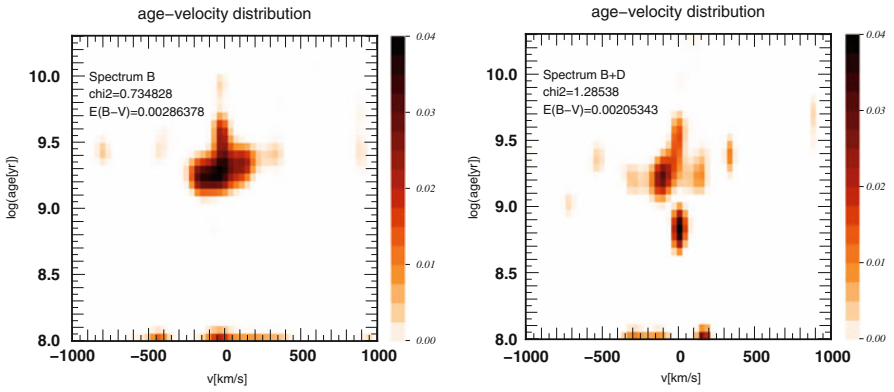

Fig. 6.12 Age-velocity map reconstruction for the center of the bulge spectrum of NGC 4030 (*left*) and for the bulge spectrum 3 arcsec from the center (*right panel*), where a disc component appears on top of the dynamically hot component (From Ocvirk et al. (2008). Reproduced with permission from Astronomische Nachrichten)

They were able to separate two components, one with a relatively young stellar population (∼2 Gyr) and $\sigma \sim 100$ km/s, and an other even younger (∼500 Myr) and kinematically colder ($\sigma \sim 30$ km/s) component. The location (outside the bulge-dominated region of the galaxy), kinematics, and relatively young age of the latter component suggests that it is a young inner disc. The null mean velocity of this structure is expected for the minor axis of the stellar disc. This study demonstrates the feasibility of separating and measuring the age and kinematics of superimposed galactic components from an integrated light spectrum. This type of analysis will be very useful in characterizing the properties of the different components in composite bulges and isolating the properties of their stellar populations.

Furthermore, throughout this review we have mentioned several results that need to be confirmed with larger galaxy samples. Spectroscopic studies of a large samples of bulges with different characteristics are clearly needed to advance in our understanding of the stellar populations of bulges. Ideally, integral field units needs to be used, in order to morphologically separate the different subcomponents. Also, galaxies in different environments needs to be studied. Indeed, the influence of environment has not been investigated thoroughly yet. Morelli et al. (2008) analyzed a sample of bulges in the Coma cluster but they did not compare their results with bulges in other environments. Peletier et al. (1999) did not find any difference in the colors of galaxies in different galaxy environments, and concluded that this parameter does not have a strong influence on shaping the star formation in bulges. Nonetheless, a more comprehensive study remains to be done. A detailed study of the properties of bulges with environment might help us to distinguish between external and internal processes for the formation of bulges.

We expect that instruments that are already operating, such as MUSE (Bacon et al. 2010), with superb spatial resolution, will help us to resolve central components, such as nuclear discs or bars. These data will allow possible coupling of stellar population and kinematic properties, with the morphological characteristics of the galaxies, improving our understanding of bulges in a way it has not been possible before.

Acknowledgements I would like to thank Brad Gibson, Jairo Mendez-Abreu, Pierre Ocvirk, Jesús Falcón-Barroso, Adriana de Lorenzo-Cáceres and also the anonymous referee for suggestions that improved this manuscript. I would also like to thank all the authors who have kindly provided me with figures from their publications.

References

Aguerri J. A. L., Balcells M., Peletier R. F., 2001, A&A, 367, 428
Alonso-Herrero A., Knapen J. H., 2001, AJ, 122, 1350
Annibali F., Bressan A., Rampazzo R., Zeilinger W. W., Danese L., 2007, A&A, 463, 455
Arimoto N., Yoshii Y., 1987, A&A, 173, 23
Athanassoula E., 2005, MNRAS, 358, 1477
Athanassoula E., Lambert J. C., Dehnen W., 2005, MNRAS, 363, 496

Athanassoula E., Machado R. E. G., Rodionov S. A., 2013, MNRAS, 429, 1949
Bacon R., Copin Y., Monnet G., Miller B. W., Allington-Smith J. R., Bureau M., Carollo C. M., Davies R. L., Emsellem E., Kuntschner H., Peletier R. F., Verolme E. K., de Zeeuw P. T., 2001, MNRAS, 326, 23
Bacon R., et al., 2010, in Society of Photo-Optical Instrumentation Engineers (SPIE) Conference Series, Vol. 7735, Society of Photo-Optical Instrumentation Engineers (SPIE) Conference Series, p. 8
Balcells M., Peletier R. F., 1994, AJ, 107, 135
Bell E. F., de Jong R. S., 2000, MNRAS, 312, 497
Bender R., Burstein D., Faber S. M., 1993, ApJ, 411, 153
Berentzen I., Shlosman I., Martinez-Valpuesta I., Heller C. H., 2007, ApJ, 666, 189
Bica E., 1988, A&A, 195, 76
Blanc G. A., Weinzirl T., Song M., Heiderman A., Gebhardt K., Jogee S., Evans II N. J., van den Bosch R. C. E., Luo R., Drory N., Fabricius M., Fisher D., Hao L., Kaplan K., Marinova I., Vutisalchavakul N., Yoachim P., 2013, AJ, 145, 138
Bournaud F., Combes F., 2002, A&A, 392, 83
Bruzual G., Charlot S., 2003, MNRAS, 344, 1000
Buta R., Combes F., 1996, Fundamentals of Cosmic Physics, 17, 95
Byrd G., Rautiainen P., Salo H., Buta R., Crocher D. A., 1994, AJ, 108, 476
Cappellari M., et al., 2011, MNRAS, 416, 1680
Carollo C. M., Stiavelli M., de Zeeuw P. T., Seigar M., Dejonghe H., 2001, ApJ, 546, 216
Casuso E., Vazdekis A., Peletier R. F., Beckman J. E., 1996, ApJ, 458, 533
Cenarro A. J., Sánchez-Blázquez P., Cardiel N., Gorgas J., 2004, ApJL, 614, L101
Chiappini C., Pellegrini P. S., Rité C., Maia M. A. G., Ogando R., Ramos B., Schiavon R. P., Willmer C. N. A., da Costa L., Bernardi M., Alonso M. V., Wegner G., 2002, in Astronomical Society of the Pacific Conference Series, Vol. 253, Chemical Enrichment of Intracluster and Intergalactic Medium, Fusco-Femiano R., Matteucci F., eds., p. 321
Cid Fernandes R., Mateus A., Sodré L., Stasińska G., Gomes J. M., 2005, MNRAS, 358, 363
Clarkson W., Sahu K., Anderson J., Smith T. E., Brown T. M., Rich R. M., Casertano S., Bond H. E., Livio M., Minniti D., Panagia N., Renzini A., Valenti J., Zoccali M., 2008, ApJ, 684, 1110
Coccato L., Morelli L., Corsini E. M., Buson L., Pizzella A., Vergani D., Bertola F., 2011, MNRAS, 412, L113
Coelho P., Bruzual G., Charlot S., Weiss A., Barbuy B., Ferguson J. W., 2007, MNRAS, 382, 498
Coelho P., Gadotti D. A., 2011, ApJL, 743, L13
Conroy C., Graves G. J., van Dokkum P. G., 2014, ApJ, 780, 33
Conroy C., van Dokkum P. G., 2012, ApJ, 760, 71
de Jong R. S., 1996, A&A, 313, 377
de Lorenzo-Cáceres A., Falcón-Barroso J., Vazdekis A., 2013, MNRAS, 431, 2397
de Lorenzo-Cáceres A., Vazdekis A., Aguerri J. A. L., Corsini E. M., Debattista V. P., 2012, MNRAS, 420, 1092
Debattista V. P., Mayer L., Carollo C. M., Moore B., Wadsley J., Quinn T., 2006, ApJ, 645, 209
Domínguez-Tenreiro R., Tissera P. B., Sáiz A., 1998, ApJL, 508, L123
Drory N., Fisher D. B., 2007, ApJ, 664, 640
Eggen O. J., Lynden-Bell D., Sandage A. R., 1962, ApJ, 136, 748
Eliche-Moral M. C., González-García A. C., Balcells M., Aguerri J. A. L., Gallego J., Zamorano J., Prieto M., 2011, A&A, 533, A104
Ellison S. L., Nair P., Patton D. R., Scudder J. M., Mendel J. T., Simard L., 2011, MNRAS, 416, 2182
Emsellem E., et al., 2011, MNRAS, 414, 888
Erwin P., 2008, in IAU Symposium, Vol. 245, IAU Symposium, Bureau M., Athanassoula E., Barbuy B., eds., p. 113
Falcón-Barroso J., Peletier R. F., Balcells M., 2002, MNRAS, 335, 741
Feltzing S., Gilmore G., 2000, A&A, 355, 949

Fernández Lorenzo M., Sulentic J., Verdes-Montenegro L., Blasco-Herrera J., Argudo-Fernández M., Garrido J., Ramírez-Moreta P., Ruiz J. E., Sánchez-Expósito S., Santander-Vela J. D., 2014, ApJL, 788, L39
Ferreras I., Silk J., 2002, MNRAS, 336, 1181
Fisher D., Franx M., Illingworth G., 1996, ApJ, 459, 110
Fisher D. B., Drory N., 2008, AJ, 136, 773
Freeman K. C., 2008, in IAU Symposium, Vol. 245, IAU Symposium, Bureau M., Athanassoula E., Barbuy B., eds., pp. 3–10
Friedli D., Benz W., 1995, A&A, 301, 649
Fulbright J. P., McWilliam A., Rich R. M., 2007, ApJ, 661, 1152
Gadotti D. A., 2008, MNRAS, 384, 420
—, 2009, MNRAS, 393, 1531
Gadotti D. A., de Souza R. E., 2006, ApJS, 163, 270
Gadotti D. A., dos Anjos S., 2001, AJ, 122, 1298
Ganda K., Peletier R. F., Balcells M., Falcón-Barroso J., 2009, MNRAS, 395, 1669
Ganda K., Peletier R. F., McDermid R. M., Falcón-Barroso J., de Zeeuw P. T., Bacon R., Cappellari M., Davies R. L., Emsellem E., Krajnović D., Kuntschner H., Sarzi M., van de Ven G., 2007, MNRAS, 380, 506
Gonzalez O. A., Rejkuba M., Zoccali M., Valenti E., Minniti D., 2011, A&A, 534, A3
González Delgado R. M., et al., 2014, A&A, 562, A47
Gorgas J., Faber S. M., Burstein D., Gonzalez J. J., Courteau S., Prosser C., 1993, ApJS, 86, 153
Goudfrooij P., Gorgas J., Jablonka P., 1999, Astrophysics & Space Science, 269, 109
Graves G. J., Schiavon R. P., 2008, ApJS, 177, 446
Groenewegen M. A. T., Blommaert J. A. D. L., 2005, A&A, 443, 143
Guedes J., Mayer L., Carollo M., Madau P., 2013, ApJ, 772, 36
Heavens A. F., Jimenez R., Lahav O., 2000, MNRAS, 317, 965
Ho L. C., Filippenko A. V., Sargent W. L. W., 1997, ApJ, 487, 591
Huang J. H., Gu Q. S., Su H. J., Hawarden T. G., Liao X. H., Wu G. X., 1996, A&A, 313, 13
Idiart T. P., de Freitas Pacheco J. A., Costa R. D. D., 1996, AJ, 111, 1169
Immeli A., Samland M., Gerhard O., Westera P., 2004, A&A, 413, 547
Jablonka P., Gorgas J., Goudfrooij P., 2007, A&A, 474, 763
Jablonka P., Martin P., Arimoto N., 1996, AJ, 112, 1415
James P. A., Prescott M., Baldry I. K., 2008, A&A, 484, 703
Jogee S., Scoville N., Kenney J. D. P., 2005, ApJ, 630, 837
Kannappan S. J., Jansen R. A., Barton E. J., 2004, AJ, 127, 1371
Kauffmann G., et al., 2003, MNRAS, 341, 33
Kennicutt Jr. R. C., 1993, in Astrophysics and Space Science Library, Vol. 188, The Environment and Evolution of Galaxies, Shull J. M., Thronson H. A., eds., p. 533
Koleva M., Prugniel P., Bouchard A., Wu Y., 2009, A&A, 501, 1269
Kormendy J., 1977, ApJ, 218, 333
Kormendy J., Barentine J. C., 2010, ApJ, 715, L176
Kormendy J., Drory N., Bender R., Cornell M. E., 2010, ApJ, 723, 54
Kormendy J., Fisher D. B., 2005, in Revista Mexicana de Astronomia y Astrofisica Conference Series, Vol. 23, Revista Mexicana de Astronomia y Astrofisica Conference Series, Torres-Peimbert S., MacAlpine G., eds., pp. 101–108
Kormendy J., Kennicutt Jr. R. C., 2004, Annual Review of Astronomy & Astrophysics, 42, 603
Kraljic K., Bournaud F., Martig M., 2012, ApJ, 757, 60
Larson R. B., 1974, MNRAS, 166, 585
Laurikainen E., Salo H., Buta R., 2004, ApJ, 607, 103
Laurikainen E., Salo H., Buta R., Knapen J. H., 2007, MNRAS, 381, 401
Laurikainen E., Salo H., Buta R., Knapen J. H., Comerón, S. 2010, MNRAS, 405, 1098
Lee H.-c., Worthey G., 2005, ApJS, 160, 176
MacArthur L. A., 2005, ApJ, 623, 795
MacArthur L. A., Courteau S., Bell E., Holtzman J. A., 2004, ApJS, 152, 175

MacArthur L. A., González J. J., Courteau S., 2009, MNRAS, 395, 28
Martinez-Valpuesta I., Gerhard O., 2013, ApJ, 766, L3
McWilliam A., Rich R. M., 1994, ApJS, 91, 749
Mehlert D., Thomas D., Saglia R. P., Bender R., Wegner G., 2003, A&A, 407, 423
Minniti D., Olszewski E. W., Liebert J., White S. D. M., Hill J. M., Irwin M. J., 1995, MNRAS, 277, 1293
Moorthy B. K., Holtzman J. A., 2006, MNRAS, 371, 583
Morelli L., Corsini E. M., Pizzella A., Dalla Bontà E., Coccato L., Méndez-Abreu J., Cesetti M., 2012, MNRAS, 423, 962
Morelli L., Pompei E., Pizzella A., Méndez-Abreu J., Corsini E. M., Coccato L., Saglia R. P., Sarzi M., Bertola F., 2008, MNRAS, 389, 341
Noguchi M., 2000, MNRAS, 312, 194
Norman C. A., Sellwood J. A., Hasan H., 1996, ApJ, 462, 114
Nowak N., Thomas J., Erwin P., Saglia R. P., Bender R., Davies R. I., 2010, MNRAS, 403, 646
Obreja A., Domínguez-Tenreiro R., Brook C., Martínez-Serrano F. J., Doménech-Moral M., Serna A., Mollá M., Stinson G., 2013, ApJ, 763, 26
Ocvirk P., Peletier R., Lançon A., 2008, Astronomische Nachrichten, 329, 980
Ocvirk P., Pichon C., Lançon A., Thiébaut E., 2006a, MNRAS, 365, 74
—, 2006b, MNRAS, 365, 46
Ortolani S., Renzini A., Gilmozzi R., Marconi G., Barbuy B., Bica E., Rich R. M., 1995, Nature, 377, 701
Peletier R. F., Balcells M., 1996, AJ, 111, 2238
Peletier R. F., Balcells M., Davies R. L., Andredakis Y., Vazdekis A., Burkert A., Prada F., 1999, MNRAS, 310, 703
Peletier R. F., Falcón-Barroso J., Bacon R., Cappellari M., Davies R. L., de Zeeuw P. T., Emsellem E., Ganda K., Krajnović D., Kuntschner H., McDermid R. M., Sarzi M., van de Ven G., 2007, MNRAS, 379, 445
Pérez E., et al., 2013, ApJL, 764, L1
Pérez I., Sánchez-Blázquez P., 2011, A&A, 529, A64
Pérez I., Sánchez-Blázquez P., Zurita A., 2007, A&A, 465, L9
—, 2009, A&A, 495, 775
Proctor R. N., Forbes D. A., Beasley M. A., 2004, MNRAS, 355, 1327
Proctor R. N., Sansom A. E., 2002, MNRAS, 333, 517
Proctor R. N., Sansom A. E., Reid I. N., 2000, MNRAS, 311, 37
Prugniel P., Maubon G., Simien F., 2001, A&A, 366, 68
Prugniel P., Simien F., 1994, A&A, 282, L1
Puzia T. H., Perrett K. M., Bridges T. J., 2005, A&A, 434, 909
Puzia T. H., Saglia R. P., Kissler-Patig M., Maraston C., Greggio L., Renzini A., Ortolani S., 2002, A&A, 395, 45
Querejeta M., Eliche-Moral M. C., Tapia T., Borlaff A., Rodríguez-Pérez C., Zamorano J., Gallego J., 2015, A&A, 573, A78
Rosales-Ortega F. F., Kennicutt R. C., Sánchez S. F., Díaz A. I., Pasquali A., Johnson B. D., Hao C. N., 2010, MNRAS, 405, 735
Sakamoto K., Okumura S. K., Ishizuki S., Scoville N. Z., 1999, ApJ, 525, 691
Samland M., Gerhard O. E., 2003, A&A, 399, 961
Sánchez S. F., et al., 2012, A&A, 538, A8
Sánchez-Blázquez P., et al., 2014, A&A, 570, A6
Sánchez-Blázquez P., Gorgas J., Cardiel N., González J. J., 2006a, A&A, 457, 787
Sánchez-Blázquez P., Ocvirk P., Gibson B. K., Pérez I., Peletier R. F., 2011, MNRAS, 415, 709
Sánchez-Blázquez P., Peletier R. F., Jiménez-Vicente J., Cardiel N., Cenarro A. J., Falcón-Barroso J., Gorgas J., Selam S., Vazdekis A., 2006b, MNRAS, 371, 703
Sánchez-Blázquez P., Rosales-Ortega F., Diaz A., Sánchez S. F., 2014, MNRAS, 437, 1534

Sarzi M., Falcón-Barroso J., Davies R. L., Bacon R., Bureau M., Cappellari M., de Zeeuw P. T., Emsellem E., Fathi K., Krajnović D., Kuntschner H., McDermid R. M., Peletier R. F., 2006, MNRAS, 366, 1151
Scannapieco C., Gadotti D. A., Jonsson P., White S. D. M., 2010, MNRAS, 407, L41
Schiavon R. P., 2007, ApJS, 171, 146
Shen J., Sellwood J. A., 2004, ApJ, 604, 614
Sheth K., et al., 2008, ApJ, 675, 1141
Sil'chenko O. K., Afanasiev V. L., 2004, AJ, 127, 2641
Sil'chenko O. K., Moiseev A. V., Shulga A. P., 2010, AJ, 140, 1462
Soto M., Rich R. M., Kuijken K., 2007, ApJ, 665, L31
Tantalo R., Chiosi C., 2004, MNRAS, 353, 917
Terndrup D. M., Davies R. L., Frogel J. A., Depoy D. L., Wells L. A., 1994, ApJ, 432, 518
Thomas D., Davies R. L., 2006, MNRAS, 366, 510
Thomas D., Maraston C., Bender R., 2003, MNRAS, 339, 897
Thomas D., Maraston C., Bender R., Mendes de Oliveira C., 2005, ApJ, 621, 673
Tojeiro R., Heavens A. F., Jimenez R., Panter B., 2007, MNRAS, 381, 1252
Trager S. C., Dalcanton J. J., Weiner B. J., 1999, in The Formation of Galactic Bulges, Carollo C. M., Ferguson H. C., Wyse R. F. G., eds., p. 42
Trager S. C., Faber S. M., Worthey G., González J. J., 2000, AJ, 120, 165
Trager S. C., Somerville R. S., 2009, MNRAS, 395, 608
Tsujimoto T., Bekki K., 2012, ApJ, 747, 125
van Loon J. T., Gilmore G. F., Omont A., Blommaert J. A. D. L., Glass I. S., Messineo M., Schuller F., Schultheis M., Yamamura I., Zhao H. S., 2003, MNRAS, 338, 857
Vazdekis A., 1999, ApJ, 513, 224
Vazdekis A., Sánchez-Blázquez P., Falcón-Barroso J., Cenarro A. J., Beasley M. A., Cardiel N., Gorgas J., Peletier R. F., 2010, MNRAS, 404, 1639
Vazdekis A., Trujillo I., Yamada Y., 2004, ApJ, 601, L33
Villa-Vargas J., Shlosman I., Heller C., 2010, ApJ, 719, 1470
Walcher C. J., Böker T., Charlot S., Ho L. C., Rix H.-W., Rossa J., Shields J. C., van der Marel R. P., 2006, ApJ, 649, 692
Walcher C. J., Coelho P., Gallazzi A., Charlot S., 2009, MNRAS, 398, L44
Williams M. J., Bureau M., Kuntschner H., 2012, MNRAS, 427, L99
Williams M. J., Zamojski M. A., Bureau M., Kuntschner H., Merrifield M. R., de Zeeuw P. T., Kuijken K., 2011, MNRAS, 414, 2163
Worthey G., 1994, ApJS, 95, 107
Worthey G., Faber S. M., Gonzalez J. J., Burstein D., 1994, ApJS, 94, 687
Wyse R. F. G., Gilmore G., Franx M., 1997, Annual Review of Astronomy & Astrophysics, 35, 637
Zhao H., Spergel D. N., Rich R. M., 1994, AJ, 108, 2154
Zoccali M., Hill V., Lecureur A., Barbuy B., Renzini A., Minniti D., Gómez A., Ortolani S., 2008, A&A, 486, 177
Zoccali M., Lecureur A., Barbuy B., Hill V., Renzini A., Minniti D., Momany Y., Gómez A., Ortolani S., 2006, A&A, 457, L1

Chapter 7
The Stellar Kinematics of Extragalactic Bulges

Jesús Falcón-Barroso

Abstract Galactic bulges are complex systems. Once thought to be small-scale versions of elliptical galaxies, advances in astronomical instrumentation (spectroscopy in particular) has revealed a wealth of photometric and kinematic substructure in otherwise simple-looking components. This review provides an overview of how our perspective on galactic bulges has changed over the years. While it is mainly focused on aspects related to the dynamical state of their stars, there will be natural connections to other properties (e.g. morphology, stellar populations) discussed in other reviews in this volume.

7.1 Introduction

Galactic bulges have been generally assumed to be simple components that, morphologically closely resemble elliptical galaxies. First photometric decompositions of lenticular and spiral galaxies (e.g. Caon et al. 1993) established that the radial behavior of their surface brightness followed a de Vaucouleurs (1948) or a Sérsic profile (Sersic 1968) with typically high n values. In the mid 1990s, we discovered that bulges in late-type spiral galaxies were smaller and displayed exponential profiles (Andredakis et al. 1995; Courteau et al. 1996; Carollo 1999). This difference observed in the light profiles was also present in their colours, with exponential bulges displaying bluer colours than those with larger Sérsic n (e.g. MacArthur et al. 2004; Ganda et al. 2009). Despite the marked distinction in their light profiles, the variation of colour between bulges and their surrounding discs is rather smooth (e.g. Balcells and Peletier 1994).

Our view of the location of bulges in the major scaling relations (e.g. Faber-Jackson (1976), Kormendy relation (Kormendy 1977), or fundamental plane (Dressler et al. 1987; Djorgovski and Davis 1987)) has also evolved over time. The sample selection biases introduced in the first studies (e.g. predominantly early-type galaxies) showed no significant differences between bulges and elliptical

J. Falcón-Barroso (✉)
Instituto de Astrofísica de Canarias, Vía Láctea s/n, La Laguna, Tenerife, Spain
e-mail: jfalcon@iac.es

E. Laurikainen et al. (eds.), *Galactic Bulges*, Astrophysics and Space Science Library 418, DOI 10.1007/978-3-319-19378-6_7

galaxies (e.g. Kormendy and Djorgovski 1989; Jorgensen et al. 1996; Balcells et al. 2007). With samples nowadays including large numbers of spiral galaxies, our understanding of the situation of bulges in those relations has now drastically changed (e.g. Gadotti 2009; Laurikainen et al. 2010; Erwin et al. 2015).

One aspect in the study of galactic bulges that has radically changed our understanding of their nature (i.e. merger-driven structures around which discs are formed) is their kinematics. While the photometric properties of some bulges already pointed to a high degree of structural similarity with discs (e.g. exponential profiles), this can only be confirmed if their kinematics also follows that displayed by discs (e.g. significant rotation and low velocity dispersions). In a pioneering study Kormendy and Illingworth (1982) investigated the degree of rotational support of a small sample of bulges compared to elliptical galaxies. Figure 7.1 presents an updated version, from Kormendy and Fisher (2008), of the original figure published in 1982. The figure shows that bulges display a much larger degree of rotation than the elliptical galaxies at a given apparent ellipticity. This was the first piece of evidence in the literature indicating that bulges differed dynamically from their otherwise similarly looking, slow rotating, massive early-type counterparts. While we know now that this picture is not accurate, at the time it led to the realization that some bulges are actually discs and therefore may not have formed in merger episodes as most scenarios would assume, but rather formed from internal material through secular processes (Kormendy 1993). These ideas evolved over time and gave rise to the definition of pseudobulges. We refer the reader to Falcón-Barroso and Knapen (2013) for an extensive review, produced by the lecturers of the *XXIII*

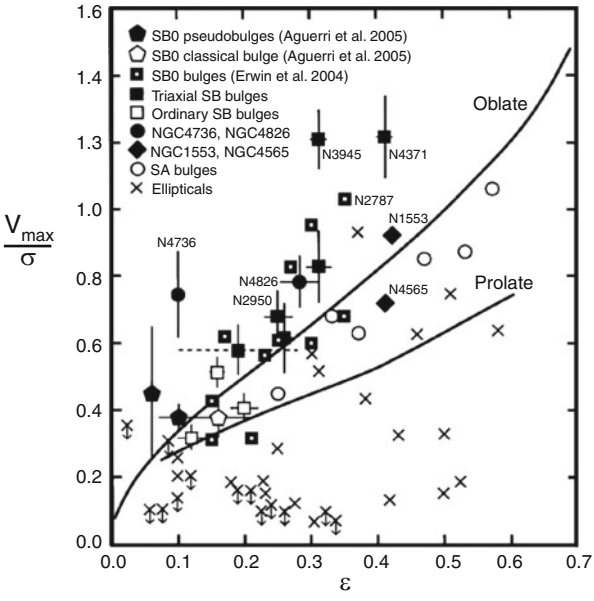

Fig. 7.1 Historical view of the level of rotational support and anisotropy of a sample of elliptical galaxies (*crosses*) and bulges (*remaining symbols*) from Kormendy and Fisher (2008). This is an updated version of the original figure presented in Kormendy and Illingworth (1982). While the physical interpretation of this figure has evolved over time, it was the first piece of evidence suggesting that bulges and massive early-type galaxies were intrinsically different

Canary Islands Winter School of Astrophysics, of bulge formation and evolution in the context of secular evolutionary processes.

In this review I will give an overview of the kinematic properties observed in extragalactic bulges, establishing their connection to the dynamical features produced by bars, and briefly discuss the similarities with the Milky Way bulge. I will also summarize our yet limited knowledge of the kinematics of bulges at high redshift and end with future prospects yet to be explored in this field.

7.2 Kinematic Properties of Extragalactic Bulges

The central regions of galaxies are complex environments often displaying multiple coexisting structural components. It is thus important to define what we mean by a bulge in this context. In this Section I will consider as a bulge the stellar structures in the central regions of galaxies that "bulge" vertically[1] over the disc. The modern view is that there are three type of bulges: classical bulges (with properties akin to elliptical galaxies), discy bulges (with properties akin to discs), and boxy/peanut bulges (which are related to bars, see Sect. 7.3). In addition to bulges, the central regions of galaxies can also host smaller structures such as nuclei, black holes, or nuclear rings (that do not extend vertically beyond the main disc of the galaxy).

The study of bulges is often hampered by the contamination from different sources.[2] In general there are two main components that can affect our measurements: (1) the underlying main disc of the galaxy, as so far there is no indication of truncation of discs in the inner parts of galaxies; (2) dust, that will prevent the full integration along the line-of-sight and thus will only allow to measure properties of stars in front of the dust lanes. These issues are usually solved by observing galaxies in edge-on or face-on configurations. The first one will give a clear view of the bulge above the disc and avoid dust obscuration. It is most useful for prominent bulges in early-type galaxies. The face-on orientation will minimize the effects of the underlying disc. It is best for small bulges in late-type systems, which have higher surface brightness than the disc. The drawback is that if bulges are rotating, their signature will be likely minimal in that orientation.

In the following subsections I will summarize the main kinematic properties of bulges paying particular attention to those works in the literature that have considered these issues more carefully.

[1] Editorial comment: notice that in this review only the vertically thick components are considered as bulges. That definition excludes the "discy pseudobulges" which are defined as structures in the plane of the galactic disc.

[2] It is important to remember that properties observed in galaxies are result of integrating along the line of sight. This averaging depends greatly on the number of components as well as the type of stars contributing most to the light in that direction.

7.2.1 Rotational Support and Level of Anisotropy

Kormendy and Illingworth (1982) were the first to describe the level of rotational support specifically in bulges of galaxies. This was achieved by measuring the maximum rotational velocity observed in the regions above the main disc where the light of the bulge dominates over the central velocity dispersion of the system (V_{max}/σ). The work by Kormendy not only concluded that the level of rotation observed in galactic bulges was larger than that displayed by elliptical galaxies but also, with the aid of model predictions (Binney 1981), concluded that bulges were very likely oblate, have isotropic velocity dispersions, and are flattened by rotation. This study was quickly followed up by Kormendy himself (Kormendy 1982), but also other authors (Davies et al. 1983; Davies and Illingworth 1983) reaching similar conclusions. Our current view on the level of anisotropy of bulges is, however, different (e.g. Cappellari et al. 2007).

The V_{max}/σ–ϵ diagram has been very popular for its power to classify dynamically different kind of galaxies, but most studies have focused on the study of the entire systems and not in their bulge components specifically (e.g. Bender 1988b; Prugniel and Simien 1994; Kormendy and Bender 1996; Rix et al. 1999; van Zee et al. 2004). With the advent of integral field spectroscopy (IFS), this diagram has evolved and led to a parameter (i.e. λ_{Re}, Emsellem et al. 2007) that allows a more robust (and less inclination dependent) kinematic classification of galaxies. λ_{Re} quantifies the level of specific angular momentum in a galaxy within its half-light radius. Applied to large samples of early-type galaxies it allowed the distinction between Slow and Fast rotating galaxies (Emsellem et al. 2007, 2011). Together with model predictions for oblate/prolate, (an)isotropic systems, it can also be used to establish the level of anisotropy of galaxies. This aspect was explored by Cappellari et al. (2007) for the SAURON sample (de Zeeuw et al. 2002) of early-type galaxies. This study shows that the family of Slow Rotators are weakly triaxial, while the Fast Rotators (with V_{max}/σ values similar to those observed in bulges) are typically oblate and display a wide range of anisotropy values. The results of this study indicate that the anisotropy observed in Fast Rotators is mainly due to a flattening of the velocity ellipsoid in the meridional plane ($\sigma_R \geq \sigma_z$), with clear indications that anisotropy is larger for intrinsically flatter galaxies. Given the significant contribution of the bulge to the light in these regions, this result suggests that bulges are actually anisotropic. This is consistent with the level of intrinsic flattening observed in different kind of bulges (see Méndez-Abreu in this volume). In this context, the study of larger samples of bulges in late-type galaxies will be very important to fully characterize their dynamical properties (e.g. CALIFA survey, Falcón-Barroso et al. 2014).

There has been very few attempts in the literature to extract a *clean* measurement of the anisotropy of bulges and are mostly focused on the analysis of the Milky Way bulge. The complications to decompose accurately the contributions of the disc to the velocity ellipsoid in the bulge dominated areas still remains the major hurdle. The best way forward in this topic has come from the use of detailed

dynamical modeling fitting the observed stellar kinematics (e.g. Bottema et al. 1991; Pignatelli and Galletta 1999; Kregel and van der Kruit 2005). Nevertheless, the main limitation of those studies is that often the shape of the velocity ellipsoid is a property imposed in the fitting. The natural step forward is the use of orbit-based dynamics models (e.g. Schwarzschild 1979) to separate the contributions of the bulge, disc, and any other components present in a galaxy and thus obtain their intrinsic properties. These models are quite demanding and require a large number of kinematic constraints. With many IFS surveys providing data for vast amounts of galaxies, it is only a matter of time that we exploit these analysis tools more routinely to study the intrinsic properties of bulges.

7.2.2 Scaling Relations

Many of the scaling relations used to study galaxy evolution are, in essence, different manifestations of the Virial Theorem (Clausius 1870), and relates the kinetic energy of a galaxy with the one provided by its gravitational potential. The relationship between different structural parameters of galaxies (e.g. absolute magnitude, half-light radius, mean surface brightness), are discussed at length in other reviews in this volume. Here we concentrate only on those relations that involve the velocity dispersion of the galaxy (σ).

7.2.2.1 Faber–Jackson Relation

The Faber–Jackson relation establishes the link between the absolute magnitude of a galaxy with its central velocity dispersion (Faber and Jackson 1976). Early-type galaxies form a well defined sequence where more luminous galaxies are also those exhibiting larger velocity dispersions. When it comes to the bulges in particular, the inclusion of bulges of lenticular galaxies hardly introduces any changes in the relation. Bulges of disc dominated spiral galaxies, however, seem to populate different regions in this parameter space, with largest offsets from the relation defined by the ellipticals for those galaxies with latest morphological types (see Fig. 7.2). The observed offset implies that: (1) either the bulges of later-types are brighter at a given velocity dispersion, which would suggest the presence of younger stellar populations (as they are also typically bluer) and/or (2) the dynamics of late-type bulges, at a given absolute bulge luminosity, is closer to that observed in their surrounding discs. Both cases are likely possible given that the velocity dispersion is biased towards the younger population present along the line-of-sight. Note, that despite the potential discy origin of those late-type bulges, the observed relation is not driven by the luminosity of the disc but of the bulge itself (e.g. Balcells et al. 2007).

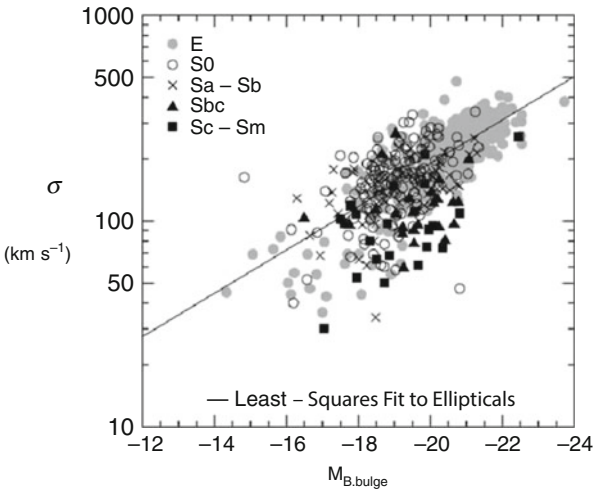

Fig. 7.2 Faber-Jackson relation for galaxies of different morphological types from Kormendy and Kennicutt (2004). Bulges of late-type galaxies deviate systematically from the relation defined by ellipticals

7.2.2.2 $Mg_2 - \sigma$ Relation

A more direct connection with stellar populations is made in the $Mg_2 - \sigma$ relation (e.g. Terlevich et al. 1981). In Fig. 7.3 we show the compilation made by Falcón-Barroso et al. (2002) using their own sample together with that of Bender et al. (1992), Jablonka et al. (1996), and Prugniel et al. (2001) against the reference relation defined for early-type galaxies by Jorgensen et al. (1996). Galaxies displaying larger amounts of ionized gas (i.e. [OIII] equivalent width) are also the ones deviating most from the relation for early-types. This relation is usually considered as a mass–metallicity relation. This is however only true in the absence of young stellar populations. If present, the Mg_2 index is no longer a good metallicity indicator and it becomes quite sensitive to age (e.g. Vazdekis et al. 2010). Galaxies with large amounts of ionized gas are also typically the ones experiencing more intense star formation and thus result into overall younger stellar populations. It is therefore not surprising that the bulges in those galaxies are the ones deviating most from the relation described by the early-type galaxies. Similar conclusions have been reached using much larger samples (e.g. Chiappini et al. 2002), although exploring the dependence with maximum rotational velocity rather than morphological type.

7.2.2.3 Fundamental Plane Relation

The fundamental plane is one of the most studied scaling relations. It relates the half-light radius of galaxies to the mean surface brightness within that radius and the central velocity dispersion of the galaxy. As many other scaling relations, early-type galaxies have been studied extensively (e.g. Dressler et al. 1987; Djorgovski

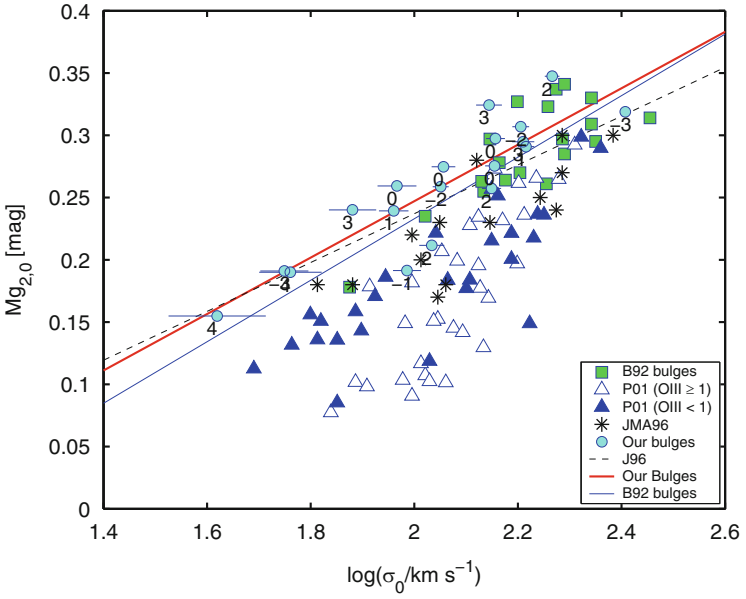

Fig. 7.3 $Mg_2 - \sigma$ relation for galactic bulges presented in Falcón-Barroso et al. (2002). The figure includes samples from this work as well as Bender et al. (1992), Jablonka et al. (1996), and Prugniel et al. (2001). *Dashed line* marks the reference relation for early-type galaxies observed by Jorgensen et al. (1996). Bulges of later-type galaxies, e.g. with larger amounts of ionized-gas and younger stellar populations, deviate most from the reference line (Reproduced with permission of Oxford University Press)

and Davis 1987; Jorgensen et al. 1996; Pahre et al. 1998; Mobasher et al. 1999; Bernardi et al. 2003; D'Onofrio et al. 2008; Hyde and Bernardi 2009; La Barbera et al. 2010; Magoulas et al. 2012; Cappellari et al. 2013). In contrast, the specific location of bulges in the relation has not been explored much and has been limited to galaxies with prominent bulges.

One of the first studies in this respect was carried out by Bender et al. (1992). They showed that bulges of lenticular galaxies followed the relation defined by elliptical galaxies. This result was later confirmed by Falcón-Barroso et al. (2002), who also found that bulges of later-type galaxies (e.g. Sbc) were slightly displaced with respect to the main relation. Bulges presenting the largest offsets were those with younger stellar populations and lower velocity dispersions. These authors showed that the offsets could be removed if one considers the missing rotational support expected in these late-type bulges. As the rotational support of some bulges increases, the measured velocity dispersion is no longer a reliable tracer of their motion. In those cases rotational velocity is a much better probe of those motions. For purely rotationally supported systems the Tully–Fisher relation (Tully and Fisher 1977) is the one often the one invoked. Several studies have confirmed that when the full kinetic energy is accounted for and differences in the stellar

populations are considered, galaxies of all morphological types form a single relation (e.g. Prugniel and Simien 1994, 1996; Cappellari et al. 2006; Graves and Faber 2010; Falcón-Barroso et al. 2011), with remaining scatter typically driven by changes in their mass-to-light ratios (e.g. Cappellari et al. 2013).

7.2.3 Radial Behavior

The study of the kinematic radial properties of galaxies has been one of the most prolific areas in astronomy. Mainly for bulges of early-type galaxies (e.g. Kormendy and Illingworth 1982; Fisher 1997; Héraudeau and Simien 1998; Héraudeau et al. 1999; Falcón-Barroso et al. 2003; Emsellem et al. 2004; Spolaor et al. 2010), over time we quickly started to routinely explore the motions of stars in late-type systems (e.g. Bottema 1989, 1992; Vega Beltrán et al. 2001; Pizzella et al. 2004, 2008; Kregel and van der Kruit 2005; Fabricius et al. 2012). More recently, we have started expanding our understanding of bulges through IFS (e.g. SAURON (Ganda et al. 2006), DiscMass (Martinsson et al. 2013)). While at first only rotational velocity and velocity dispersion was extracted, the arrival of new parametrizations of the line-of-sight velocity distributions (e.g. Gauss-Hermite expansions, van der Marel and Franx 1993) allowed us to identify the presence of kinematic subcomponents in galaxies (see Sect. 7.2.4 for a detailed discussion). Despite displaying clear signatures of rotational support, it is very hard to distinguish between the signal of the bulge and underlying disc in typical rotation curves. A much more fruitful avenue to explore is the study of the radial behavior of the stellar velocity dispersion. With many bulges still having a high degree pressure support (e.g. dynamical support by random motions), it is easiest to identify the contrast between the velocity dispersion of the disc and the bulge-dominated regions.

Fisher (1997) is one of the first studies to correlate the slope of the observed velocity dispersion profile with general properties of their host galaxies (e.g. central velocity dispersion, absolute magnitude, or Mg_2 and Fe line-strength indices). He analyzed a sample of 18 lenticular galaxies and computed the velocity dispersion gradients along the major and minor axes of the galaxies. Compared to bright elliptical galaxies, the velocity dispersion profiles of lenticulars in his sample were much steeper. This is expected given that the profiles reached the low dispersion regimes observed in the disc dominated regions. The contrast between the velocity dispersion in the bulges and discs of his galaxies was therefore large. The intriguing result of this study was to discover that there was no correlation between these gradients and central velocity dispersion (σ_0), absolute magnitude or gradients of metallicity sensitive line-strength indices. The lack of correlation with central velocity dispersion was particularly surprising, as one would expect a larger contrast (i.e. steeper gradient) between the very high central dispersion galaxies and their surrounding disc. At face value, this result suggests that: (1) the sample used in this study did not cover a sufficiently large range of central velocity dispersion values, which could be true as the lowest σ_0 was above $100\,\mathrm{km\,s^{-1}}$ or (2) galaxies with

dynamically hotter bulges (i.e. with larger σ_0) have also hotter discs. At this point, with the current sample it was not possible to discern between the two scenarios.

The next natural step in this direction was to extend the sample to later-type galaxies. Falcón-Barroso et al. (2003) studied the radial kinematic profiles (along the minor axis) of 19 galaxies with morphological types expanding between S0 and Sbc. The sample was carefully chosen to have intermediate inclinations and thus permit access to the bulge with minimal contamination of the disc on one side of the galaxy. Central velocity dispersions ranged from 50 to over 300 km s^{-1}. The analysis of their sample did show remarkably different σ radial profiles. While about half of the sample displayed very steep profiles, the remaining set showed mainly flat profiles. The lack of velocity dispersion gradient in a fair amount of galaxies in the sample was yet another piece of evidence pointing to the discy nature of some galactic bulges. In relation to the properties of the host galaxy, there was a slight tendency for galaxies with flatter profiles to display higher disc central surface brightness. A trend was also found with the ellipticity of the bulge component in the sense that more flattened bulges showed shallower gradients. Despite analyzing galaxies covering a wider range of morphological types, no correlation was found with either morphological type index, bulge Sérsic index n, bulge and disc scale lengths and bulge effective surface brightness. It appears that the discy nature of bulges cannot be established on the basis of spheroid luminosity, as velocity dispersion gradients do not seem to correlate with bulge luminosity or with central velocity dispersion either.

Fabricius et al. (2012) presents the most recent effort in the literature trying to address these issues. In this work 45 S0 to Sbc galaxies were studied with the goal of relating the kinematic information with photometric properties typical of classical and pseudobulges.[3] The sample contained a fair fraction of barred galaxies and displayed a wide range of central velocity dispersions (between ∼50 to 200 km s^{-1}) and absolute magnitudes (from −18 to −21 mag). The galaxies were also moderately inclined with allowed access to the bulge region without being significantly affected by dust in the disc. Figure 7.4 shows the radial behavior of the velocity dispersion along the major and minor axes of the galaxies in the sample. Similarly to Falcón-Barroso et al. (2003), bulges exhibit two types of profiles: steep and flat velocity dispersion profiles. This work provides first tentative evidence for a correlation between the slope of the velocity dispersion profile and the bulge's Sérsic index n.

The study of the stellar kinematics of late-type galaxies has usually been hampered by complex, often dusty, morphologies. Furthermore, bulges in those galaxies are not particularly bright which makes the extraction of any spectroscopic measurement (kinematic in particular) specially harder. With the advent of integral-field spectroscopy, a few studies have allowed a kinematic characterization of

[3]Note that in this work the definition of a bulge differs from the one used in this review. While Fabricius et al. (2012) define bulges as structures with flux above the disc surface brightness profile, here they are also required to extend vertically above the disc.

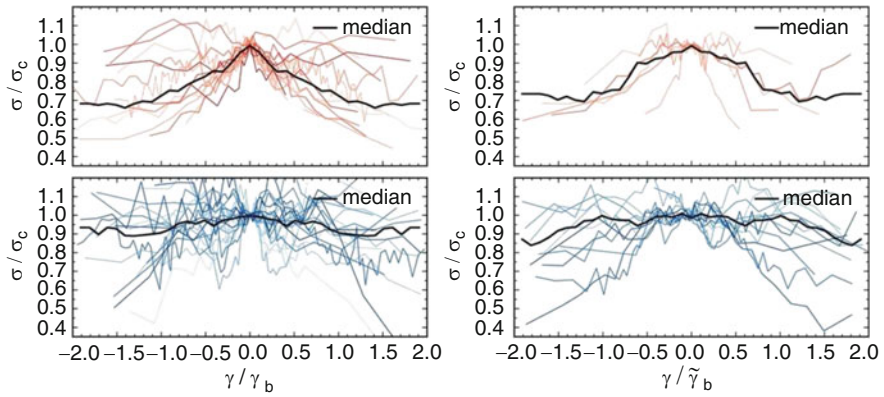

Fig. 7.4 Radial velocity dispersion profiles for a sample of 45 lenticular to spiral galaxies from Fabricius et al. (2012). Profiles have been normalized to their central velocity dispersion and bulge radius. Profiles of classical bulges are plotted in *red* and pseudobulges in *blue*. Major axis profiles are shown on the *left* and minor axis on the *right* columns respectively. The *thick black lines* correspond to the median of the individual profiles (Reproduced with permission of AAS)

bulges in galaxies from Sb to Sd types. Ganda et al. (2006) carried out SAURON observations of 18 spiral galaxies with good *Hubble Space Telescope* photometry available. The velocity dispersion profiles of the galaxies were mostly flat or with positive gradients. Very few galaxies displayed negative gradients. When looking for correlations between these gradients and the morphological type of the galaxies, there was only a slight tendency for earlier types to display negative gradients. Positive gradients were not strongly correlated with latest Hubble types.

The study of velocity dispersion gradients will be soon expanding thanks to the large number of IFU surveys (DiscMass, Bershady et al. 2010; CALIFA, Sánchez et al. 2012; SAMI, Croom et al. 2012; MaNGA, Bundy et al. 2015). However, it is important to remember that not all of them will allow the study of bulges in late-type galaxies due to restrictions in the spatial sampling or their spectral resolution.

7.2.4 Amount of Substructure

So far in this review we have exposed the properties of different kind of bulges, and yet this has gone as far as showing that some bulges exhibit kinematics closer to what it is observed in a disc (e.g. rotation dominated) instead of the classical idea of bulges being pressure supported. Here we will revise the kinematic properties of the different structural components dominating the light in the inner regions of galaxies.

Counter-rotating components are common in galaxies. Large, kpc-scale, kinematically decoupled components (KDCs) are typically found in bright elliptical galaxies (e.g. Bender 1988a; Franx et al. 1989; Carollo et al. 1997; Hau et al.

1999; Davies et al. 2001; Emsellem et al. 2014). They usually contain old stellar populations and are almost indistinguishable from the remaining body of the galaxy. Smaller decoupled components are, however, harder to identify, are made of young stars and reside in lower luminosity early-type galaxies (e.g. McDermid et al. 2006). Large-scale counter-rotation of disc components seems also not so rare: NGC 4550 (e.g. Rubin et al. 1992; Rix et al. 1992), NGC 413 (Jore et al. 1996), NGC 4473 (Cappellari et al. 2004). See Krajnović et al. (2011) for other cases detected through a *kinemetry* analysis (Krajnović et al. 2006). The detection of such extreme cases keeps increasing as new kinematic decomposition techniques are developed (e.g. Coccato et al. 2013; Johnston et al. 2013; Pizzella et al. 2014).

Counter-rotation of bulges is an odd phenomenon. There are very few cases reported in the literature of bulges rotating around a completely different axis than their surrounding discs. One of those striking cases is NGC 4698 (Bertola et al. 1999), where the bulge appears to rotate perpendicular to the stellar disc. Another unusual case is that of NGC 7331 where the bulge was reported to counter-rotate with respect to the disc (Prada et al. 1996, but see Bottema 1999). Numerical simulations suggest mergers of galaxies as the only viable path for the formation of such structures (e.g. Balcells and González 1998; Thakar and Ryden 1998).

A common feature is the presence of co-rotating components (e.g. a nuclear disc) embedded in an otherwise pressure supported spheroidal bulge. The key kinematic signature of these inner discs is a steep rise of the rotation velocity in the inner parts (i.e. faster than the expected rise of the main disc) accompanied by low velocity dispersion values. There is often also an anti-correlation between the velocity and h_3 moment in the locations with lowest velocity dispersion, which is usually an indication of multiple kinematic components. All these features are shown in Fig. 7.5 using the two-dimensional kinematic maps of NGC 4274 from Falcón-Barroso et al. (2006) as an example. The *Hubble Space Telescope* unsharped-masked image reveals the presence of a dusty disc in the inner regions of the galaxy, which is not so obvious in the reconstructed image of the galaxy. The disc has a clear signature in the velocity map, and even more so in the velocity dispersion which is much lower than the values of the surrounding dynamically hot bulge. In this particular case, the very low [OIII]/Hβ emission line ratio suggests that star formation is taking place in the inner disc. The presence of these co-rotating components do not always imply associated young stellar populations. The stellar population analysis carried out by Peletier et al. (2007) of the Falcón-Barroso et al. (2006) sample of 24 Sa galaxies concluded that about half of the galaxies displaying low central velocity dispersion values (so called σ-drops, Emsellem et al. 2001; Wozniak et al. 2003) have mean luminosity weighted ages above 5 Gyr. The incidence of σ-drops in this sample was about 50 %. σ-drops are not only produced by nuclear discs, but can also be caused by nuclear dust spirals and star-forming rings (Comerón et al. 2008). The origin of these components is often related to the inflow of gas, driven by bars, towards the inner regions of galaxies (e.g. Athanassoula 2005). Note, however, that minor mergers could be also responsible for the formation of inner discs and rings in spiral galaxies (e.g. Eliche-Moral et al. 2011).

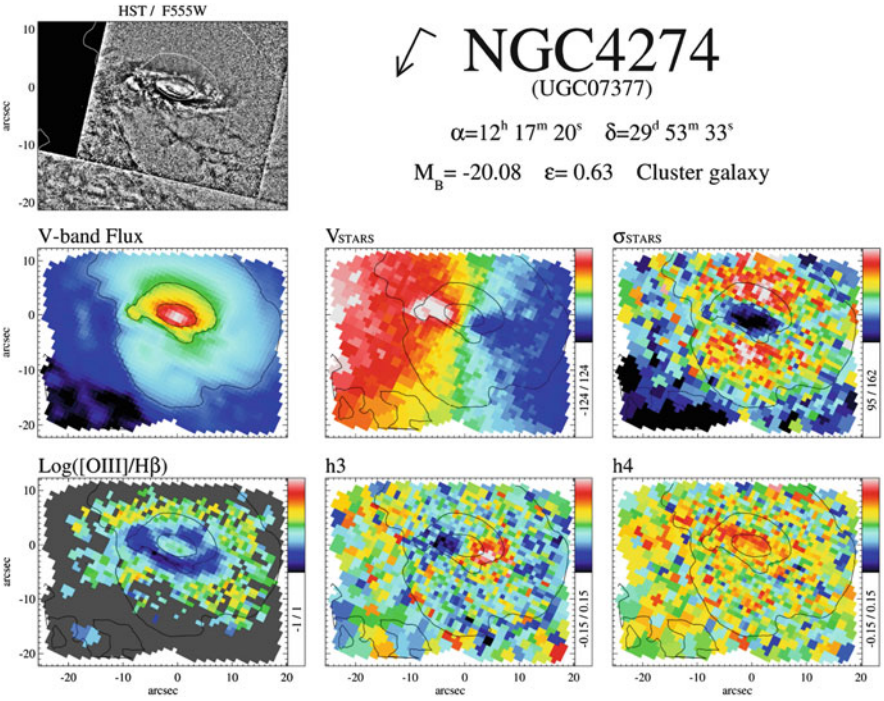

Fig. 7.5 Stellar kinematic maps for NGC 4274 from Falcón-Barroso et al. (2006). The arrow and its associated dash at the top of each figure mark the north and east directions, respectively. (*First row*) HST unsharp-masked image of the galaxy and some basic information. (*Second row*) reconstructed total intensity (in mag/arcsec^2 with an arbitrary zero point), stellar mean velocity V, and stellar velocity dispersion (in km s^{-1}). (*Third row*) [OIII]/Hβ emission line ratio map (in logarithmic scale), and Gauss-Hermite moments h3 and h4 of the stellar line-of-sight velocity distribution (Reproduced with permission of Oxford University Press)

7.3 Relating Bars and Bulges

Bars are prominent components of galaxies, produced by disc instabilities, that can pump disc material above the plane generating central structures that also *bulge* over the thin disc (e.g. Hasan et al. 1993). As we discuss in this section, the kinematic properties of these bars are different from those observed in common bulges. The origin of some type of bulges (e.g. pseudobulges) appears to be tightly connected to secular evolutionary processes induced by bars (see Athanassoula 2005, for a theoretical view of bulge formation in the context of bars). Bars are active agents in the inflow of gas towards the inner regions of galaxies (e.g. Sakamoto et al. 1999). This naturally allows the formation of new structures (e.g. bulges, rings, inner discs, central mass concentration).

The vertical extent of bars is best observed in edge-on galaxies. When the long axis of the bar is perpendicular to our line-of-sight bars are usually called

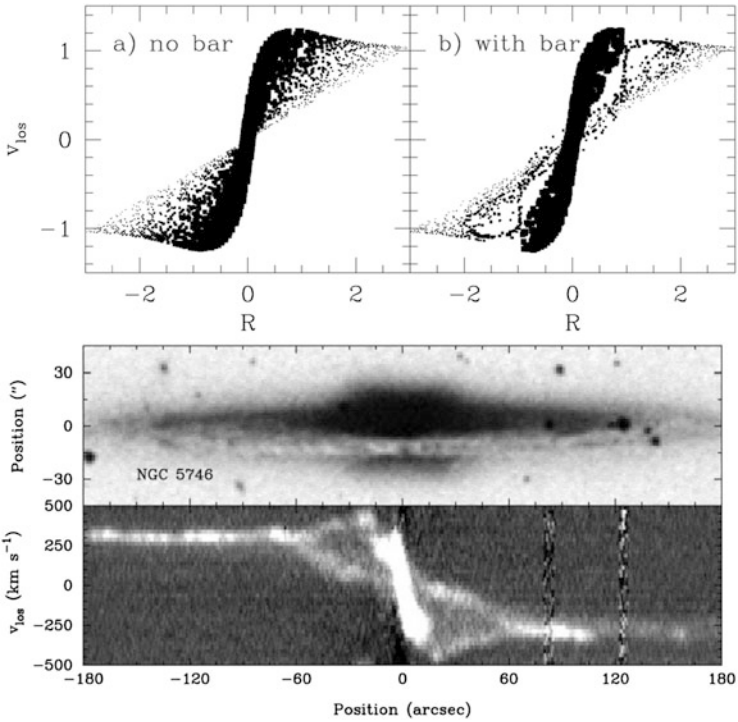

Fig. 7.6 Position–velocity diagrams (PVDs) of barred galaxies. (*Top*) Model prediction for the observed line-of-sight velocity distribution as a function of radius for non-barred and barred galaxies (Kuijken and Merrifield 1995). (*Bottom*) Observed PVD for the boxy/peanut bulge of NGC 5746 (Bureau and Freeman 1999). The kinematic signature of a bar in the observations is very evident (Reproduced with permission of AAS)

boxy/peanut (BP) bulges due to their peculiar shape. Most of the material outside the disc plane has been elevated through bar buckling episodes early in the evolution of the bar (e.g. Martinez-Valpuesta et al. 2006). Kinematically, BP bulges produce a characteristic signature (i.e. a "figure-of-eight") in the Position–Velocity Diagram (PVD). This was first predicted by Kuijken and Merrifield (1995) (see Fig. 7.6, top row). With the aid of analytical models, they determine the location of particles in this diagram for barred and non-barred galaxies. In their view, the gap observed in the PVD of barred galaxies is produced for a lack of available orbits near the corotation radius of the bar. This effect should affect both the stellar and gas components of galaxies. This prediction was nicely confirmed with larger samples of galaxies (e.g. Merrifield and Kuijken 1999; Bureau and Freeman 1999). In the case of Bureau and Freeman (1999), they produced PVDs for a sample of 30 edge-on spiral galaxies with prominent BP bulges. Figure 7.6, bottom row, shows the observed PVD for NGC 5746 that clearly displays the predicted gap.

Another typical kinematic feature of BP bulges predicted by numerical simulations is cylindrical rotation (e.g. Rowley 1988; Combes et al. 1990). The first evidence for cylindrical rotation in galaxies was revealed by Kormendy and Illingworth (1982) for NGC 4565 when studying the stellar kinematics of galactic bulges. References of cylindrical rotation in other galaxies are rather scarce in the literature: IC 3370 (Jarvis 1987), NGC 1055 (Shaw 1993), NGC 3079 (Shaw et al. 1993), NGC 5266 (Varnas et al. 1987), NGC 7332 (Fisher et al. 1994). This lack of cases is likely due to: (1) inclinations effects. Cylindrical rotation is best observed in edge-on galaxies (e.g. Athanassoula and Misiriotis 2002), (2) the fact that most observations with long-slit spectrographs targeted the major and/or minor axes of the galaxies, which makes it difficult to detect. The most recent work addressing this aspect of BP bulges is that of Williams et al. (2011). This study placed long slits parallel to the major axis of five known BP bulges. The surprising result of this study is that not all BP bulges displayed cylindrical rotation. Figure 7.7 shows the analysis for two distinct cases in their sample. While NGC 3390 displays clear signatures of solid-body rotation, IC 4767 presents shallower major axis velocity profiles as a we move away from the disc. This outcome requires further confirmation using larger samples of edge-on galaxies. It will also benefit from studies making use of integral-field spectrographs to map the full two-dimensional kinematics over the BP

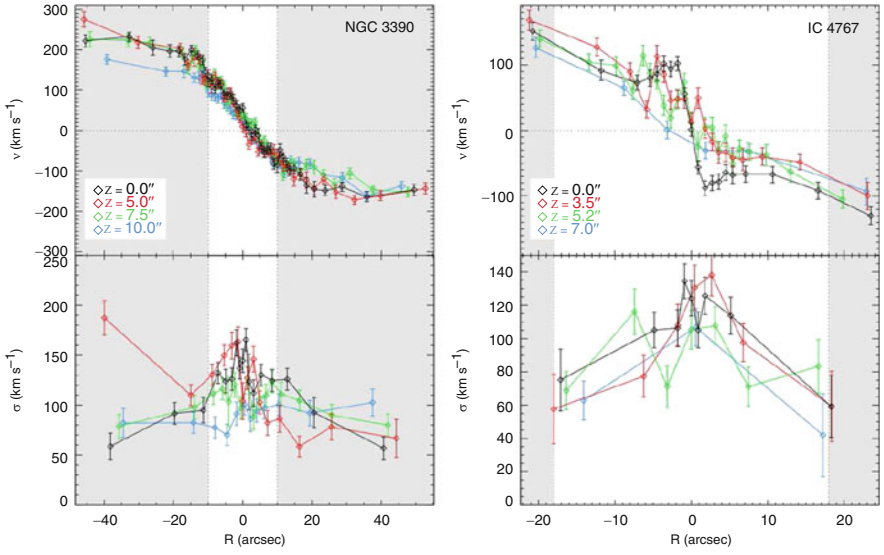

Fig. 7.7 Stellar line-of-sight rotation curves and velocity dispersion profiles for two Boxy/Peanut, edge-on galaxies in the Williams et al. (2011) sample. NGC 3390 shows clear signatures of cylindrical rotation, while IC 4767 does not (i.e. kinematics at increasing distance from the main disc shows different behavior). The *shaded regions* mark the disc dominated regions (Reproduced with permission of Oxford University Press)

dominated region. A glimpse of what this kind of studies can bring is presented in Falcón-Barroso et al. (2004) for the known case of NGC 7332.

Bars are also capable of producing other distinct features in the stellar kinematics of galaxies, which are often related to resonances induced by the bar itself in the host galaxy. Bureau and Athanassoula (2005) established, using N-body simulations, a series of kinematic diagnostics for bars of different strength and orientations in highly-inclined galaxies (see Fig. 7.8): (1) a "double-hump" rotation curves, (2) velocity dispersion profiles with a plateau at moderate radii, and often displaying a σ-drop in the center, (3) a positive correlation between the velocity and the h_3 Gauss-Hermite moment over the length of the bar. Some of these features have been recognized observationally in several studies (e.g. Pence 1981; Kormendy 1983; Bettoni and Galletta 1997; Emsellem et al. 2001; Márquez et al. 2003; Pérez et al. 2009). While having the most potential to unravel the presence of bars, the V–h_3 correlation has been hardly studied observationally (e.g. Chung and Bureau 2004). These diagnostics work best for edge-on galaxies. The kinematic tracer of BP bulges in face-on systems is the h_4 Gauss-Hermite moment. Simulations carried out by Debattista et al. (2005) predict that a negative double minima around the center of the galaxy is an excellent indicator of a BP bulge for a wide range of bar strengths and inclinations. Although the observational requirements to measure this parameter are very demanding, this feature has been nicely confirmed observationally by Méndez-Abreu et al. (2008). Interestingly, Laurikainen et al. (2014) suggest that the barlenses observed in the face-on view of many disc galaxies (e.g. Laurikainen et al. 2011) are effectively the thick part of the BP bulge when seen face-on. See also Athanassoula et al. (2014) for a theoretical interpretation.

There are strong indications that large bulges can have an effect in the strength of a bar. Stronger bars appear in galaxies with low bulge-to-total ratios and central velocity dispersions (Das et al. 2008; Aguerri et al. 2009; Laurikainen et al. 2009). What it is not well established yet, observationally, is the effect a bar would have on the dynamics of a pre-existing bulge. Numerical simulations by Saha and Gerhard (2013) suggest that a pressure supported bulge would gain net rotation as a result of angular momentum exchange with the bar. Rotation of the final composite classical and BP bulge would be close to cylindrical, with small deviations in the early phases of the secular evolution. Therefore, untangling the intrinsic properties of bulges in barred galaxies is a very difficult task that will require detailed dynamical modeling of high quality observations. Numerical tools like the NMAGIC code (de Lorenzi et al. 2007) applied to high-quality, integral-field data (e.g. De Lorenzi et al. 2013) seems the way forward.

The Milky Way bulge is the most vivid example of a complex system. Besides cylindrical rotation, it displays many of the other kinematic signatures of bars summarized above. The origin of the multiple substructures present at the center of our Galaxy (possibly including other types of bulges, e.g. Ness et al. 2014) cannot be solved by inspecting the kinematics alone, as angular momentum transfer is expected between them. Most of the efforts today to solve this puzzle come from relating the observed kinematics to the distinct stellar populations present in those regions. We refer the reader to Oscar González and Dimitri Gadotti's review in this

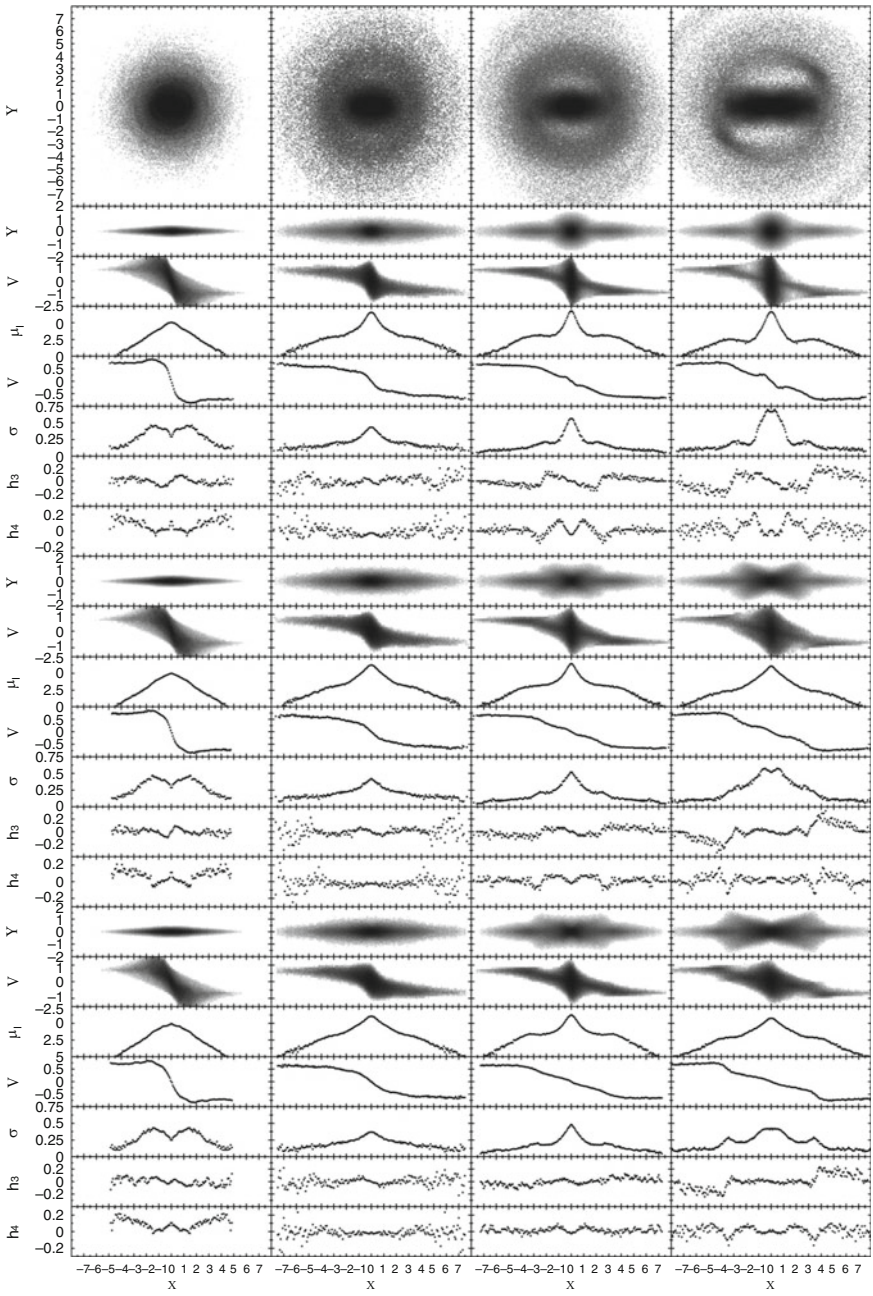

Fig. 7.8 Stellar kinematic diagnostics for barred galaxies in N-body simulations from Bureau and Athanassoula (2005). (*Left to right*) No-bar, weak-bar, intermediate-bar, and strong-bar case. (*Top to bottom*) image, PVD, surface brightness, and kinematic parameters (velocity, velocity dispersion, h_3 and h_4 Gauss-Hermite moments) as a function of bar orientation, from end-on to side-on (Reproduced with permission of AAS)

volume for a comprehensive summary of the properties observed in the Galactic bulge, and also the chapter by Juntai Shen and Zhao-Yu Li for a theoretical view on the possible paths for its formation and evolution.

7.4 Kinematics of Bulges at High Redshift

With typical sizes of a few kiloparsecs, bulges in nearby galaxies would be very difficult to resolve spatially at intermediate to high redshifts even with the best instruments on board of *Hubble Space Telescope*. In addition, the morphologies of galaxies are known to deviate from the standard Hubble sequence from redshift $\sim$1 onwards (e.g. Elmegreen et al. 2008), so we should probably not think of bulges at high-redshift in the same way we think of them in the local Universe. Nevertheless knowing the conditions, in terms of rotational support, of the galaxies that will eventually lead to lenticular and spiral galaxies nearby, can help us to understand the kind of progenitors that will host the variety of bulges we see today.

In the light of the large amount of pseudobulges observed in the nearby Universe, a logical question to ask is: do we see the signatures of secular evolution in bulges at high-z? Numerical simulations reproducing the clumpy galaxies from redshift $z \sim 1$ suggest that bulge kinematics is not very different from the values observed for pressure-supported systems, with (V/σ) values below 0.5 (e.g. Bournaud et al. 2007; Elmegreen et al. 2008). This is likely due to the turbulent nature of clumps merging at the center of galaxies (e.g. Ceverino et al. 2012). Note, however, that the merging and migration of clumps towards the inner regions is an internal process, as it takes place in the disc of galaxies. The physical conditions, in terms of gas supply, for bulge formation at high redshifts are very different from the ones observed in the local Universe. Secular evolution takes place at a much faster pace at high z.

Integral-field observations of galaxies at increasing redshifts confirm the turbulent nature of discs, as revealed by the systematically high velocity dispersion values (e.g. Newman et al. 2013; Wisnioski et al. 2014). Nevertheless, galaxies show a wide range of kinematic properties: from well behaved rotating discs, to dispersion dominated systems, and galaxies with chaotic motions (e.g. Yang et al. 2008; Genzel et al. 2008; Wisnioski et al. 2011; Buitrago et al. 2014). Recent results from the KMOS3D survey (Wisnioski et al. 2014) show that most galaxies, in the main star forming sequence, between redshifts 1 and 2 are rotationally-supported. When combined with other datasets, they measure an evolution of the ionized-gas velocity dispersion which is consistent with the observed changes in the gas fractions and specific star formation rates of galaxies as a function of redshift. This result favors an 'equilibrium' model where the amount of turbulence of a disc is defined by the balance between gas accretion and outflows.

The physical conditions between redshifts 1 and 4 appear to be particularly favorable for the formation of bulges, and yet it appears that it cannot be the only channel to build the (pseudo)bulges observed in the nearby Universe. Mergers seem to be required too (e.g. Ceverino et al. 2014). To complicate the issue further, the

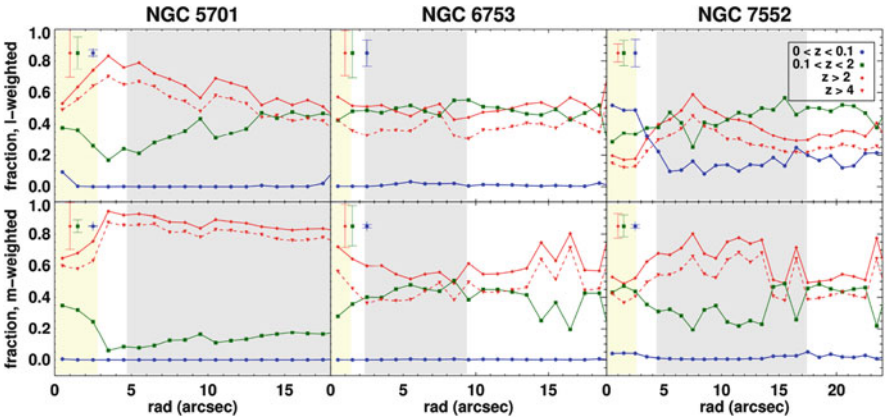

Fig. 7.9 Relative light (*top row*) and mass (*bottom row*) fractions of young, intermediate and old stellar populations as a function of radius present in three galactic bulges studied in Seidel et al. (2015). Uncertainties in the analysis are indicated in the *top left corner*. *Shaded regions* mark the regions where the average light and mass fractions of this study are computed. More than 60 % of the stellar mass in those bulges was already in place beyond $z \sim 4$ (Reproduced with permission of Oxford University Press)

analysis of the star formation histories of different types of bulges (e.g. Seidel et al. 2015) suggest that at least 60 % of the stellar mass of those bulges formed at redshifts beyond 4 (see Fig. 7.9). All these results together indicate that bulge formation most likely happens in a two stage process (e.g. Obreja et al. 2013), with an initial period of rapid build-up (with possible influence of mergers) and a secondary phase (between redshifts 1 and 2) of high star formation activity that would lead to the younger pseudobulge components we see today.

7.5 Concluding Remarks and Future Prospects

Lying at the center and denser regions of galaxies, bulges are a keystone in our understanding of galaxy formation and evolution. It is also their location, shared with other components of galaxies, what makes them so difficult to study. In this review I have tried to provide an overview of the main kinematic features observed in extragalactic bulges.

Identifying the formation scenario for bulges based solely on kinematic grounds is a very difficult task. The orbits of the different structural components in galaxies (e.g. bulges, discs, bars, spiral arms, nuclear discs rings, etc.) are not necessarily well separated in phase-space. The best example of this complexity comes from the observations of the Milky Way bulge. As nicely illustrated in other contributions to this volume (e.g. González and Gadotti, or Sánchez-Blázquez), the combined study of kinematics and stellar populations provides one of the best ways to

discern between different formation scenarios. While this coupling can be achieved relatively easy in the Milky Way (because it is possible to measure the properties of individual stars) this is not an easy task in bulges of other galaxies where all we get is the integrated light along the line-of-sight. Fortunately, with better data, models, and numerical tools we are at the verge of being able to treat other galaxies in the same way we study our own Galaxy. Studies of the coupling between kinematics and stellar populations in external galaxies are now flourishing (e.g. Ocvirk et al. 2008). Initially restricted to galaxies with known distinct counter-rotating components, they are now exploring more regular galaxies (e.g. Johnston et al. 2014).

As remarked many times throughout this review, this new step in the 3D decomposition of galaxies can only be achieved with datasets that allow the uniform exploration of galaxies in the two-dimensions they project in the sky. The first generation of IFU surveys and instruments (e.g. SAURON, ATLAS^{3D}, DiscMass, SINFONI, VIMOS, PPaK) showed us the potential of these datasets to reveal the intrinsic properties of galaxies. The currently ongoing IFU surveys (e.g. CALIFA, SAMI, MaNGA, KMOS^{3D}) will allow the exploitation of these new techniques for very large, morphologically and mass unbiased samples of galaxies. We should not forget though that we can still learn a lot of the physical processes governing galaxies, and bulge formation and evolution in particular, with unique instruments like MUSE. The Milky Way is a unique case, as we will be able to probe the 3D nature of the Galaxy directly thanks to the Gaia space mission.

Acknowledgements J. F-B would like thank D. Gadotti, E. Laurikainen and R.F. Peletier for their invitation to take part in this volume and for their infinite patience waiting for this review. J. F-B acknowledges support from grant AYA2013-48226-C3-1-P from the Spanish Ministry of Economy and Competitiveness (MINECO), as well as from the FP7 Marie Curie Actions of the European Commission, via the Initial Training Network DAGAL under REA grant agreement number 289313.

References

Aguerri J. A. L., Méndez-Abreu J., Corsini E. M., 2009, A&A, 495, 491
Andredakis Y. C., Peletier R. F., Balcells M., 1995, MNRAS, 275, 874
Athanassoula E., 2005, MNRAS, 358, 1477
Athanassoula E., Laurikainen E., Salo H., Bosma A., 2014, ArXiv e-prints:1405.6726
Athanassoula E., Misiriotis A., 2002, MNRAS, 330, 35
Balcells M., González A. C., 1998, ApJ, 505, L109
Balcells M., Graham A. W., Peletier R. F., 2007, ApJ, 665, 1104
Balcells M., Peletier R. F., 1994, AJ, 107, 135
Bender R., 1988a, A&A, 202, L5
Bender R., 1988b, A&A, 193, L7
Bender R., Burstein D., Faber S. M., 1992, ApJ, 399, 462
Bernardi M., Sheth R. K., Annis J., Burles S., Eisenstein D. J., Finkbeiner D. P., Hogg D. W., Lupton R. H., et al 2003, AJ, 125, 1866
Bershady M. A., Verheijen M. A. W., Swaters R. A., Andersen D. R., Westfall K. B., Martinsson T., 2010, ApJ, 716, 198

Bertola F., Corsini E. M., Beltrán J. C. V., Pizzella A., Sarzi M., Cappellari M., Funes J. G. S. J., 1999, ApJ, 519, L127
Bettoni D., Galletta G., 1997, A&AS, 124, 61
Binney J. J., 1981, in Fall S. M., Lynden-Bell D., eds, Structure and Evolution of Normal Galaxies The macroscopic dynamics of elliptical galaxies. pp 55–66
Bottema R., 1989, A&A, 221, 236
Bottema R., 1992, A&A, 257, 69
Bottema R., 1999, A&A, 348, 77
Bottema R., van der Kruit P. C., Valentijn E. A., 1991, A&A, 247, 357
Bournaud F., Elmegreen B. G., Elmegreen D. M., 2007, ApJ, 670, 237
Buitrago F., Conselice C. J., Epinat B., Bedregal A. G., Grützbauch R., Weiner B. J., 2014, MNRAS, 439, 1494
Bundy K., Bershady M. A., Law D. R., Yan R., Drory N., MacDonald N., Wake D. A., Cherinka B., et al. 2015, ApJ, 798, 7
Bureau M., Athanassoula E., 2005, ApJ, 626, 159
Bureau M., Freeman K. C., 1999, AJ, 118, 126
Caon N., Capaccioli M., D'Onofrio M., 1993, MNRAS, 265, 1013
Cappellari M., Bacon R., Bureau M., Damen M. C., Davies R. L., de Zeeuw P. T., Emsellem E., Falcón-Barroso J., Krajnović D., Kuntschner H., McDermid R. M., Peletier R. F., Sarzi M., van den Bosch R. C. E., van de Ven G., 2006, MNRAS, 366, 1126
Cappellari M., Emsellem E., Bacon R., Bureau M., Davies R. L., de Zeeuw P. T., Falcón-Barroso J., Krajnović D., Kuntschner H., McDermid R. M., Peletier R. F., Sarzi M., van den Bosch R. C. E., van de Ven G., 2007, MNRAS, 379, 418
Cappellari M., Scott N., Alatalo K., Blitz L., Bois M., Bournaud F., Bureau M., Crocker A. F., et al. 2013, MNRAS, 432, 1709
Cappellari M., van den Bosch R. C. E., Verolme E. K., Bacon R., Bureau M., Copin Y., Davies R. L., Emsellem E., Krajnovic D., Kuntschner H., McDermid R., Miller B. W., Peletier R. F., de Zeeuw P. T., 2004, Coevolution of Black Holes and Galaxies, p. 5
Carollo C. M., 1999, ApJ, 523, 566
Carollo C. M., Franx M., Illingworth G. D., Forbes D. A., 1997, ApJ, 481, 710
Ceverino D., Dekel A., Mandelker N., Bournaud F., Burkert A., Genzel R., Primack J., 2012, MNRAS, 420, 3490
Ceverino D., Dekel A., Tweed D., Primack J., 2014, ArXiv e-prints
Chiappini C., Pellegrini P. S., Rité C., Maia M. A. G., Ogando R., Ramos B., Schiavon R. P., Willmer C. N. A., et al 2002, in Fusco-Femiano R., Matteucci F., eds, Chemical Enrichment of Intracluster and Intergalactic Medium Vol. 253 of Astronomical Society of the Pacific Conference Series, Mg_2-σ in Early-Type Galaxies and Spiral Bulges.. p. 321
Chung A., Bureau M., 2004, AJ, 127, 3192
Clausius R., 1870, Philosophical Magazine, 40, 112
Coccato L., Morelli L., Pizzella A., Corsini E. M., Buson L. M., Dalla Bontà E., 2013, A&A, 549, A3
Combes F., Debbasch F., Friedli D., Pfenniger D., 1990, A&A, 233, 82
Comerón S., Knapen J. H., Beckman J. E., 2008, A&A, 485, 695
Courteau S., de Jong R. S., Broeils A. H., 1996, ApJ, 457, L73
Croom S. M., Lawrence J. S., Bland-Hawthorn J., Bryant J. J., Fogarty L., Richards S., Goodwin M., Farrell T., et al. 2012, MNRAS, 421, 872
Das M., Laurikainen E., Salo H., Buta R., 2008, Ap&SS, 317, 163
Davies R. L., Efstathiou G., Fall S. M., Illingworth G., Schechter P. L., 1983, ApJ, 266, 41
Davies R. L., Illingworth G., 1983, ApJ, 266, 516
Davies R. L., Kuntschner H., Emsellem E., Bacon R., Bureau M., Carollo C. M., Copin Y., Miller B. W., Monnet G., Peletier R. F., Verolme E. K., de Zeeuw P. T., 2001, ApJ, 548, L33
de Lorenzi F., Debattista V. P., Gerhard O., Sambhus N., 2007, MNRAS, 376, 71
De Lorenzi F., Hartmann M., Debattista V. P., Seth A. C., Gerhard O., 2013, MNRAS, 429, 2974
de Vaucouleurs G., 1948, Annales d'Astrophysique, 11, 247

de Zeeuw P. T., Bureau M., Emsellem E., Bacon R., Carollo C. M., Copin Y., Davies R. L., Kuntschner H., Miller B. W., Monnet G., Peletier R. F., Verolme E. K., 2002, MNRAS, 329, 513
Debattista V. P., Carollo C. M., Mayer L., Moore B., 2005, ApJ, 628, 678
Djorgovski S., Davis M., 1987, ApJ, 313, 59
D'Onofrio M., Fasano G., Varela J., Bettoni D., Moles M., Kjærgaard P., Pignatelli E., Poggianti B., et al. 2008, ApJ, 685, 875
Dressler A., Lynden-Bell D., Burstein D., Davies R. L., Faber S. M., Terlevich R., Wegner G., 1987, ApJ, 313, 42
Eliche-Moral M. C., González-García A. C., Balcells M., Aguerri J. A. L., Gallego J., Zamorano J., Prieto M., 2011, A&A, 533, A104
Elmegreen B. G., Bournaud F., Elmegreen D. M., 2008, ApJ, 688, 67
Emsellem E., Cappellari M., Krajnović D., Alatalo K., Blitz L., Bois M., Bournaud F., Bureau M., et al 2011, MNRAS, 414, 888
Emsellem E., Cappellari M., Krajnović D., van de Ven G., Bacon R., Bureau M., Davies R. L., de Zeeuw P. T., Falcón-Barroso J., Kuntschner H., McDermid R., Peletier R. F., Sarzi M., 2007, MNRAS, 379, 401
Emsellem E., Cappellari M., Peletier R. F., McDermid R. M., Bacon R., Bureau M., Copin Y., Davies R. L., Krajnović D., Kuntschner H., Miller B. W., de Zeeuw P. T., 2004, MNRAS, 352, 721
Emsellem E., Greusard D., Combes F., Friedli D., Leon S., Pécontal E., Wozniak H., 2001, A&A, 368, 52
Emsellem E., Krajnović D., Sarzi M., 2014, MNRAS, 445, L79
Erwin P., Saglia R. P., Fabricius M., Thomas J., Nowak N., Rusli S., Bender R., Vega Beltrán J. C., Beckman J. E., 2015, MNRAS, 446, 4039
Faber S. M., Jackson R. E., 1976, ApJ, 204, 668
Fabricius M. H., Saglia R. P., Fisher D. B., Drory N., Bender R., Hopp U., 2012, ApJ, 754, 67
Falcón-Barroso J., Bacon R., Bureau M., Cappellari M., Davies R. L., de Zeeuw P. T., Emsellem E., Fathi K., et al. 2006, MNRAS, 369, 529
Falcón-Barroso J., Balcells M., Peletier R. F., Vazdekis A., 2003, A&A, 405, 455
Falcón-Barroso J., Knapen J. H., 2013, Secular Evolution of Galaxies
Falcón-Barroso J., Lyubenova M., van de Ven G., the CALIFA collaboration 2014, ArXiv e-prints
Falcón-Barroso J., Peletier R. F., Balcells M., 2002, MNRAS, 335, 741
Falcón-Barroso J., Peletier R. F., Emsellem E., Kuntschner H., Fathi K., Bureau M., Bacon R., Cappellari M., et al. 2004, MNRAS, 350, 35
Falcón-Barroso J., van de Ven G., Peletier R. F., Bureau M., Jeong H., Bacon R., Cappellari M., Davies R. L., et al. 2011, MNRAS, 417, 1787
Fisher D., 1997, AJ, 113, 950
Fisher D., Illingworth G., Franx M., 1994, AJ, 107, 160
Franx M., Illingworth G., Heckman T., 1989, ApJ, 344, 613
Gadotti D. A., 2009, MNRAS, 393, 1531
Ganda K., Falcón-Barroso J., Peletier R. F., Cappellari M., Emsellem E., McDermid R. M., de Zeeuw P. T., Carollo C. M., 2006, MNRAS, 367, 46
Ganda K., Peletier R. F., Balcells M., Falcón-Barroso J., 2009, MNRAS, 395, 1669
Genzel R., Burkert A., Bouché N., Cresci G., Förster Schreiber N. M., Shapley A., Shapiro K., Tacconi L. J., et al. 2008, ApJ, 687, 59
Graves G. J., Faber S. M., 2010, ApJ, 717, 803
Hasan H., Pfenniger D., Norman C., 1993, ApJ, 409, 91
Hau G. K. T., Carter D., Balcells M., 1999, MNRAS, 306, 437
Héraudeau P., Simien F., 1998, A&AS, 133, 317
Héraudeau P., Simien F., Maubon G., Prugniel P., 1999, A&AS, 136, 509
Hyde J. B., Bernardi M., 2009, MNRAS, 396, 1171
Jablonka P., Martin P., Arimoto N., 1996, AJ, 112, 1415
Jarvis B., 1987, AJ, 94, 30

Johnston E. J., Aragón-Salamanca A., Merrifield M. R., 2014, MNRAS, 441, 333
Johnston E. J., Merrifield M. R., Aragón-Salamanca A., Cappellari M., 2013, MNRAS, 428, 1296
Jore K. P., Broeils A. H., Haynes M. P., 1996, AJ, 112, 438
Jorgensen I., Franx M., Kjaergaard P., 1996, MNRAS, 280, 167
Kormendy J., 1977, ApJ, 218, 333
Kormendy J., 1982, ApJ, 257, 75
Kormendy J., 1983, ApJ, 275, 529
Kormendy J., 1993, in Dejonghe H., Habing H. J., eds, Galactic Bulges Vol. 153 of IAU Symposium, Kinematics of extragalactic bulges: evidence that some bulges are really discs. p. 209
Kormendy J., Bender R., 1996, ApJ, 464, L119
Kormendy J., Kennicutt R.C., 2004, ARA&A, 42(1), 603–683
Kormendy J., Djorgovski S., 1989, ARA&A, 27, 235
Kormendy J., Fisher D. B., 2008, in Funes J. G., Corsini E. M., eds, Formation and Evolution of Galaxy Discs Vol. 396 of Astronomical Society of the Pacific Conference Series, Secular Evolution in Disc Galaxies: Pseudobulge Growth and the Formation of Spheroidal Galaxies. p. 297
Kormendy J., Illingworth G., 1982, ApJ, 256, 460
Krajnović D., Cappellari M., de Zeeuw P. T., Copin Y., 2006, MNRAS, 366, 787
Krajnović D., Emsellem E., Cappellari M., Alatalo K., Blitz L., Bois M., Bournaud F., Bureau M., et al. 2011, MNRAS, 414, 2923
Kregel M., van der Kruit P. C., 2005, MNRAS, 358, 481
Kuijken K., Merrifield M. R., 1995, ApJ, 443, L13
La Barbera F., de Carvalho R. R., de La Rosa I. G., Lopes P. A. A., 2010, MNRAS, 408, 1335
Laurikainen E., Salo H., Athanassoula E., Bosma A., Herrera-Endoqui M., 2014, MNRAS, 444, L80
Laurikainen E., Salo H., Buta R., Knapen J. H., 2009, ApJ, 692, L34
Laurikainen E., Salo H., Buta R., Knapen J. H., 2011, MNRAS, 418, 1452
Laurikainen E., Salo H., Buta R., Knapen J. H., Comerón S., 2010, MNRAS, 405, 1089
MacArthur L. A., Courteau S., Bell E., Holtzman J. A., 2004, ApJS, 152, 175
Magoulas C., Springob C. M., Colless M., Jones D. H., Campbell L. A., Lucey J. R., Mould J., Jarrett T., et al. 2012, MNRAS, 427, 245
Márquez I., Masegosa J., Durret F., González Delgado R. M., Moles M., Maza J., Pérez E., Roth M., 2003, A&A, 409, 459
Martinez-Valpuesta I., Shlosman I., Heller C., 2006, ApJ, 637, 214
Martinsson T. P. K., Verheijen M. A. W., Westfall K. B., Bershady M. A., Schechtman-Rook A., Andersen D. R., Swaters R. A., 2013, A&A, 557, A130
McDermid R. M., Emsellem E., Shapiro K. L., Bacon R., Bureau M., Cappellari M., Davies R. L., de Zeeuw T., et al. 2006, MNRAS, 373, 906
Méndez-Abreu J., Corsini E. M., Debattista V. P., De Rijcke S., Aguerri J. A. L., Pizzella A., 2008, ApJ, 679, L73
Merrifield M. R., Kuijken K., 1999, A&A, 345, L47
Mobasher B., Guzman R., Aragon-Salamanca A., Zepf S., 1999, MNRAS, 304, 225
Ness M., Debattista V. P., Bensby T., Feltzing S., Roškar R., Cole D. R., Johnson J. A., Freeman K., 2014, ApJ, 787, L19
Newman S. F., Genzel R., Förster Schreiber N. M., Shapiro Griffin K., Mancini C., Lilly S. J., Renzini A., Bouché N., et al. 2013, ApJ, 767, 104
Obreja A., Domínguez-Tenreiro R., Brook C., Martínez-Serrano F. J., Doménech-Moral M., Serna A., Mollá M., Stinson G., 2013, ApJ, 763, 26
Ocvirk P., Peletier R., Lançon A., 2008, Astronomische Nachrichten, 329, 980
Pahre M. A., Djorgovski S. G., de Carvalho R. R., 1998, AJ, 116, 1591
Peletier R. F., Falcón-Barroso J., Bacon R., Cappellari M., Davies R. L., de Zeeuw P. T., Emsellem E., Ganda K., et al. 2007, MNRAS, 379, 445
Pence W. D., 1981, ApJ, 247, 473

Pérez I., Sánchez-Blázquez P., Zurita A., 2009, A&A, 495, 775
Pignatelli E., Galletta G., 1999, A&A, 349, 369
Pizzella A., Corsini E. M., Sarzi M., Magorrian J., Méndez-Abreu J., Coccato L., Morelli L., Bertola F., 2008, MNRAS, 387, 1099
Pizzella A., Corsini E. M., Vega Beltrán J. C., Bertola F., 2004, A&A, 424, 447
Pizzella A., Morelli L., Corsini E. M., Dalla Bontà E., Coccato L., Sanjana G., 2014, A&A, 570, A79
Prada F., Gutierrez C. M., Peletier R. F., McKeith C. D., 1996, ApJ, 463, L9
Prugniel P., Maubon G., Simien F., 2001, A&A, 366, 68
Prugniel P., Simien F., 1994, A&A, 282, L1
Prugniel P., Simien F., 1996, A&A, 309, 749
Rix H.-W., Carollo C. M., Freeman K., 1999, ApJ, 513, L25
Rix H.-W., Franx M., Fisher D., Illingworth G., 1992, ApJ, 400, L5
Rowley G., 1988, ApJ, 331, 124
Rubin V. C., Graham J. A., Kenney J. D. P., 1992, ApJ, 394, L9
Saha K., Gerhard O., 2013, MNRAS, 430, 2039
Sakamoto K., Okumura S. K., Ishizuki S., Scoville N. Z., 1999, ApJ, 525, 691
Sánchez S. F., Kennicutt R. C., Gil de Paz A., van de Ven G., Vílchez J. M., Wisotzki L., Walcher C. J., Mast D., et al. 2012, A&A, 538, A8
Schwarzschild M., 1979, ApJ, 232, 236
Seidel M. K., Cacho R., Ruiz-Lara T., Falcón-Barroso J., Pérez I., Sánchez-Blázquez P., Vogt F. P. A., Ness M., et al. 2015, MNRAS, 446, 2837
Sersic J. L., 1968, Atlas de galaxias australes
Shaw M., 1993, A&A, 280, 33
Shaw M., Wilkinson A., Carter D., 1993, A&A, 268, 511
Spolaor M., Hau G. K. T., Forbes D. A., Couch W. J., 2010, MNRAS, 408, 254
Terlevich R., Davies R. L., Faber S. M., Burstein D., 1981, MNRAS, 196, 381
Thakar A. R., Ryden B. S., 1998, ApJ, 506, 93
Tully R. B., Fisher J. R., 1977, A&A, 54, 661
van der Marel R. P., Franx M., 1993, ApJ, 407, 525
van Zee L., Skillman E. D., Haynes M. P., 2004, AJ, 128, 121
Varnas S. R., Bertola F., Galletta G., Freeman K. C., Carter D., 1987, ApJ, 313, 69
Vazdekis A., Sánchez-Blázquez P., Falcón-Barroso J., Cenarro A. J., Beasley M. A., Cardiel N., Gorgas J., Peletier R. F., 2010, MNRAS, 404, 1639
Vega Beltrán J. C., Pizzella A., Corsini E. M., Funes J. G., Zeilinger W. W., Beckman J. E., Bertola F., 2001, A&A, 374, 394
Williams M. J., Zamojski M. A., Bureau M., Kuntschner H., Merrifield M. R., de Zeeuw P. T., Kuijken K., 2011, MNRAS, 414, 2163
Wisnioski E., Förster Schreiber N. M., Wuyts S., Wuyts E., Bandara K., Wilman D., Genzel R., Bender R., et al. 2014, ArXiv e-prints:1409.6791
Wisnioski E., Glazebrook K., Blake C., Wyder T., Martin C., Poole G. B., Sharp R., Couch W., et al. 2011, MNRAS, 417, 2601
Wozniak H., Combes F., Emsellem E., Friedli D., 2003, A&A, 409, 469
Yang Y., Flores H., Hammer F., Neichel B., Puech M., Nesvadba N., Rawat A., Cesarsky C., et al. 2008, A&A, 477, 789

Chapter 8
A Universal Kinematic Scaling Relation and Galaxy Bulges

Dennis Zaritsky

Abstract We retrace the development of a kinematic scaling relation, referred to as the Fundamental Manifold (FM), that addresses shortcomings of the commonly used fundamental plane in certain contexts. We then examine whether bulges separately satisfy the FM relation and discuss what the success or failure of such a match implies for the nature of classical- and pseudo-bulges. On the basis of this preliminary analysis we suggest that while classical bulges appear to be independent, dynamically complete subsystems within their host galaxies that satisfy the scaling relation, pseudobulges do not satisfy the scaling relation and so probably consist of an unrepresentative subset of disc stars. This is currently not a unique explanation of the results, but the use of kinematic scaling relations with larger samples, done in a more systematic manner, could lead to a more definitive resolution on the nature of bulges.

8.1 Scaling Relations and Polemics

The nature of galaxy populations is often defined by scaling relations—the tight confinement of a class of systems within an empirical parameter space. For example, Kormendy used photometric scaling relations to draw distinctions between giant ellipticals, dwarf ellipticals, and globular clusters, while describing bulges of disc galaxies as similar to elliptical galaxies (Kormendy 1985). Unfortunately, different populations of galaxies can appear related to one another in certain parameter spaces and distinct in others. For example, in contrast to their appearance in Kormendy's original photometric space, in the space spanned by shape and kinematic measurements, bulges and low luminosity ellipticals are quite distinct (Davies et al. 1983).

As the above example illustrates, scaling relations can span both photometric and kinematic parameters. The two most widely used galaxy scaling relations in all of extragalactic astronomy connect photometric properties to kinematic

D. Zaritsky (✉)
Steward Observatory, University of Arizona, 933 N. Cherry Ave., Tucson, AZ, USA
e-mail: dennis.zaritsky@gmail.com

E. Laurikainen et al. (eds.), *Galactic Bulges*, Astrophysics and Space Science Library 418, DOI 10.1007/978-3-319-19378-6_8

properties, and we refer to such scaling relations as "kinematic scaling relations". One can straightforwardly argue that disc galaxies are a separate galaxy class from spheroidals because while they satisfy a rotation velocity—magnitude scaling relation, otherwise known as the Tully-Fisher relation (Tully and Fisher 1977), spheroids satisfy a size-surface brightness-velocity dispersion scaling, otherwise known as the fundamental plane (Dressler et al. 1987; Djorgovski and Davis 1987).

The literature on scaling relations is extensive and many details are argued about, but the overarching impact of this type of work is that it frames our thinking regarding how stellar systems form and evolve. For example, because of the apparent structural differences between giant and dwarf ellipticals, one might conclude that the formation of giant and dwarf ellipticals involves two distinct processes. Conversely, based on the low scatter of giant ellipticals about scaling relations, one might conclude that there must be only a single formation path for all giant ellipticals. Such arguments have been extended in some cases to identify different subclasses, such as classical vs. pseudobulges, of bulges and to examine the origin of those subclasses (for example, Gadotti 2009; Fabricius et al. 2012). However, as we will discuss, whether classes of stellar systems appear similar or different can often depend on which scaling relations is being applied, even when only considering the most widely used relations.

Because of such ambiguity, scaling relations should primarily be considered as a means to providing constraints for models, rather than intuitive insight into the specifics of the galaxy formation processes. To be clear, if two galaxy populations appear to follow different scaling relations in one parameter space, but the same scaling relation in another, it is difficult to reach a conclusion regarding the degree of similarity between the two populations. However, any model of the formation and evolution of these systems is required to satisfy both observations. So, while it is unquestionable that any scaling relation provides information in the form of a model constraint, it is almost always an overwhelming temptation to ascribe greater meaning to the failures or successes of scaling relations.

Given the degree to which scaling relations are satisfied by galaxies, it is likely that they reflect general dynamical principles of how baryons settle into dark matter potential wells, similar in spirit to those evinced by the existence of universal dark matter profiles (Lithwick and Dalal 2011), more than they represent a requirement for homogeneity in the details of galaxy formation and evolution. The settling process is quite efficient, as evidenced by the small departures of recent mergers, the E+A galaxies, from the fundamental plane (Yang et al. 2008). If recent, significant mergers are relatively ineffective in displacing galaxies from the tightest scaling relationship known, we do not expect secular processes to do much.

Nevertheless, we continue both to attempt to identify scaling relations that apply to all galaxies—bright, faint, spheroidal, disc—and to attempt to find populations of galaxies that violate those scaling relations. The former is an attempt to unearth underlying rules of galaxy formation, or at least structure, and the latter one to find where that equilibrium is disturbed or never attained. Galaxy bulges are the particular class of system that is the focus here. If we find that bulges, or particular subclasses of bulges, fall off a scaling relation that is applicable to all other types of

stellar systems, this deviation would be a gross violation of the framework behind the relationship. Because the deviations might be subtle, the most universal and stringent scaling relations will be the most powerful at uncovering such behavior.

8.2 Key Points About Kinematic Scaling Relations

8.2.1 Once More, From the Beginning

Scaling relations are empirically identified. However, in a search for the most inclusive scaling relation it is best to begin with a simple conjecture and proceed to identify what requirements must be added to derive the observed scaling relations. We begin by assuming that the luminous portions of galaxies satisfy the Virial Theorem.

It is a common misconception that scaling relations are simply rephrased versions of the Virial theorem. Although their origin lies with that theorem, their existence implies additional, non-trivial, physical constraints on the nature of galactic structure. This assertion is clarified by expressing the Virial theorem in a form reminiscent of the FP:

$$\log r_0 = 2\log V_0 - \log I_0 - \log \Upsilon_0 + \log A_0 - \log B_0 - C_0, \tag{8.1}$$

where the subscript 0 indicates quantities measured at a specified radius, r_0: V_0 is a measure of the internal motions within that radius (typically either the circular velocity, velocity dispersion, or some combination), I_0 is the surface brightness within r_0, Υ_0 is the mass-to-light ratio of the matter within r_0, A_0 and B_0 are coefficients arising from the integration of the kinetic and potential energy terms in the virial theorem (setting, for example, $\int_0^\infty mv^2/2\, d\mathbf{r} \equiv AV^2$), and finally C_0 is an integration constant. For this equation to correctly represent the Virial Theorem, r_0 must be selected to encompass the entire system because the Virial theorem is only valid for the system as a whole. However, empirical considerations typically place r_0 somewhere within the luminous portion of galaxies. Once one accepts that accommodation, a reasonable choice for r_0 is the radius that encompasses half the light of the system, r_h, but we no longer have a "physics" guarantee that this equation will hold.

In principle, A_0, B_0, C_0, and Υ_0 can vary from system to system so stellar systems could lie anywhere within the (r_0,I_0,V_0) space. If systems were to scatter throughout the space, there would be no scaling relation. To be specific, solutions of Eq. 8.1 exist for any combination of (r_0,I_0,V_0) if Υ_0, A_0, B_0, and C_0 are unconstrained. However, galaxies do not populate the entire (r_0, I_0, V_0)-space. The more confined the distribution of galaxies within this space, the more restrictive the constraints on

the models. For example, if we were to posit that Υ_0, A_0, B_0, and C_0 are identical for all galaxies, then galaxies would lie on a simple plane given by

$$\log r_0 = 2 \log V_0 - \log I_0 - C_0', \tag{8.2}$$

and in such a scenario all galaxies would be exact, rescaled, replicas of each other (we write C_0' only to distinguish this constant from the original, more general, C_0). Actual galaxies do not satisfy Eq. 8.2, although giant ellipticals satisfy a relationship, the fundamental plane, that is quite similar to this. The value of comparing the actual distribution of galaxies to a scaling relation is that it quantifies the degree to which Nature, through mechanisms beyond the Virial Theorem, is limiting combinations of Υ_0, A_0, B_0, and C_0.

8.2.2 The Fundamental Plane Must Break Down

One of the great successes of observational work on elliptical galaxies is the discovery that giant elliptical galaxies empirically fall on the fundamental plane (FP), which has the form

$$\log r_h = \beta \log \sigma_{v,h} - \gamma \log I_h + \delta, \tag{8.3}$$

where β, γ, and δ are numerical coefficients and the subscript h refers to the values at the half-light radius, r_h. While this equation matches Eq. 8.2 in form if one associates the velocity dispersion σ_v with the kinematic term V, the empirically evaluated coefficients do not match those in Eq. 8.2. If we assume that the structural terms A_0 and B_0 vary little among ellipticals, then within the framework of Eq. 8.1, the existence of the FP implies that $\Upsilon_h \propto \sigma_v^{2-\beta} I_h^{1+\gamma}$. One particular published fit to the FP, $r_h \propto \sigma_v^{1.2\pm0.07} I_h^{-0.82\pm0.02}$ (Cappellari et al. 2006), suggests that $2 - \beta = 0.8 \pm 0.07$ and $1 + \gamma = -0.18 \pm 0.02$, or expressed in another form that $\Upsilon_h \propto \sigma_v^{0.8} I_h^{-0.18}$ for giant elliptical galaxies.

Using a local galaxy sample with direct measurements of Υ_h from Jeans modeling (Fig. 8.1; van der Marel and van Dokkum (2007)) we see both that the power law relationship with exponent 0.8 between Υ_h and σ_v holds for giant ellipticals, and that it must break down for low σ_v ellipticals. This eventual failure arises because the relationship $\Upsilon_h \propto \sigma_v^{0.8} I_h^{-0.18}$ is bounded at the lower end by the stellar value of Υ_h. The value of Υ_h cannot fall below what the stars themselves contribute. It is therefore inarguable that the FP must break down at small values of V, where small is $\sim$100 km s^{-1}. To identify a relationship that fits all spheroids, the relationship tying Υ_h to σ_v and I_h must be more complex than a bivariate power law. This recognition is particularly critical for bulges, which for the most part are likely to have $\sigma_v < 100$ km s^{-1}.

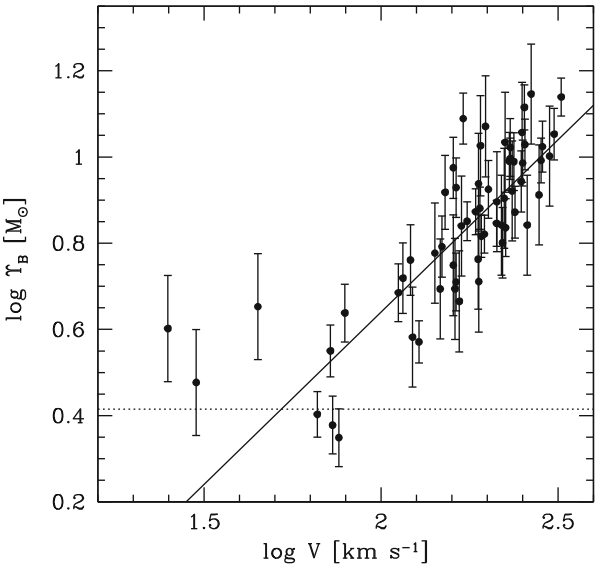

Fig. 8.1 Υ in the B-band (Υ_B) for 62 local galaxies evaluated using Jeans modeling (van der Marel and van Dokkum 2007). Here we take $V = \sigma_v$. The *dotted line* indicates the expected Υ_B for a pure, old, stellar population, while the *solid line* represents the expectation outlined in the text from the Cappellari et al. (2006) FP fit. The agreement between this line and the data for $\log V > 2$ demonstrates that assuming that the structural terms (A_0,B_0) are constant and that it is Υ_h that is varying is valid. The crossing of this line and the lower limit on Υ_h demonstrates that this description is unsustainable for lower V systems. As such, the FP requires modification—but this failure is usually not observed because most existing samples of ellipticals are dominated by $\log \sigma_v > 2$ galaxies (as is the case in this Figure as well) (Figure reproduced from Zaritsky (2012), reproduced with permission from ISRN Astronomy and Astrophysics)

8.2.3 The Bends

Sometimes to avoid having something break, you must allow it to bend. The classic scaling relations, FP (as shown above) and TF, implicitly adopt a power-law scaling between Υ_h and the observables. To avoid values of Υ_h that need to be less than the stellar mass-to-light ratio, one could conjecture that the relationship between $\log \Upsilon_h$ and $\log \sigma_v$ and $\log I_h$ is second order rather than first. There is no a priori reason to expect this functional form, but this ansatz works empirically, which demonstrates usefulness but not uniqueness. Such a relationship was defined and named the Fundamental Manifold (FM), in references to its antecedent the FP (Zaritsky et al. 2006).

We now write

$$\log r_h = 2 \log \sigma_v - \log I_h - \log \Upsilon_h - C'', \tag{8.4}$$

where $\log \Upsilon_h$ is an empirically-determined second-order polynomial in $\log \sigma_v$ and $\log I_h$. We determine the polynomial coefficients relating $\log \Upsilon_h$ to $\log \sigma_v$ and $\log I_h$ by minimizing the final scatter about the final FM relationship (Eq. 8.4). That such an exercise results in a scaling relation with small scatter demonstrates that the breakdown of the FP is related to higher order corrections in σ_v and I_h, but it does not demonstrate that those corrections are the sole provenance of Υ_h. One could alternatively interpret this empirical fit as representing systematic variations in A_0 or B_0 with σ_v and I_h. However, we have shown that the corrections match independently derived measures of Υ_h as measured by gravitational lensing and dynamical modeling (Zaritsky et al. 2011). The application of this polynomial fitting function for Υ_h results in turning the fundamental plane into a curved surface in the (r_h,V_h, I_h) space, and hence the moniker. The additional complexity introduced into the relation between Υ_h and σ_v and I_h enables the relation to fit all spheroidals, from giant ellipticals to ultrafaint dwarfs (Zaritsky et al. 2011), without introducing any additional physical quantities.

8.2.4 A Necessary Simple, Well-Motivated Refinement

Not all galaxies are dynamically supported by random stellar motions. Therefore, σ_v cannot be the appropriate proxy for V in general. In lower luminosity spheroidal galaxies rotation provides an important additional source of dynamical support (Davies et al. 1983; Bender 1990). This support is evident in the classic diagram comparing the ratio of the rotational velocity, v_r, to the velocity dispersion, v_r/σ_v, to ellipticity (Davies et al. 1983), but is also evident in the deviations from the FM when we adopt $V \equiv \sigma_v$, as a function of v_r/σ_v. We show these deviations in Fig. 8.2 using data for ellipticals (van der Marel and van Dokkum 2007) and S0's (Bedregal et al. 2006). Note that this systematic deviation is also a shortcoming of the standard FP and it will have affected comparisons of E's and S0's based on straightforward applications of the FP. Ignoring rotation produces increasing departures from the FM (or FP) independent of galaxy type. Because bulges often have significant rotation, we would again be misled with a straightforward application of the FP or FM.

A natural extension of the FP or FM utilizes a combination of σ_v and v_r to express the complete kinematic support. The commonly suggested combination to account for both rotational and pressure support is expressed as $V = \sqrt{v_r^2/\alpha + \sigma_v^2}$, where α is a parameter that is determined by the internal structure of the system. Unfortunately, the existing data are insufficient to discriminate between choices of α suggested previously (Burstein et al. 1997; Weiner et al. 2006; Kassin et al. 2007; Zaritsky et al. 2011). A standard choice is $\alpha = 2$, although $\alpha = 3$ is also acceptable (Weiner et al. 2006), and Zaritsky et al. (2011) fit the data to argue for $\alpha = 2.68$. The allowed range in values of α is related to the unknown nature of the gravitational potential and the tracer particle distribution function. Within an isothermal potential, if the orbits are isotropic, then $\alpha = 2$, while for other potentials

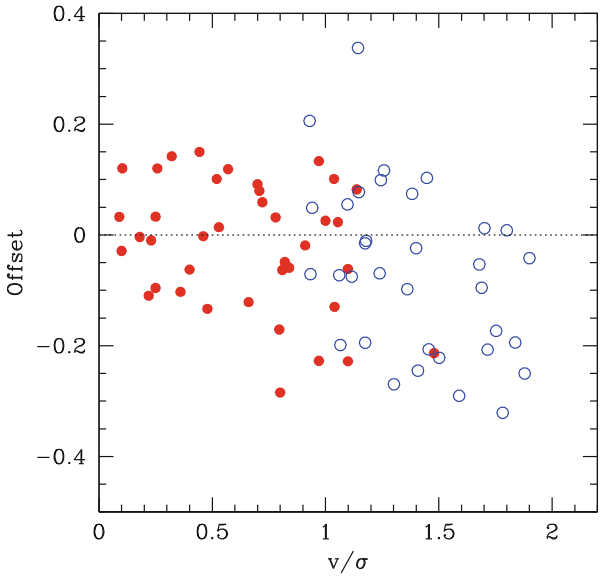

Fig. 8.2 The dependence of FM residual, when assuming $V = \sigma_v$, plotted against v_r/σ_v. The correlation coefficient of the combined sample is −0.58 and the probability is 3.7×10^{-9} that such a trend would arise randomly. We have used the K-band magnitudes for the ellipticals (van der Marel and van Dokkum 2007, *filled circles*) to match the data available for the S0s (Bedregal et al. 2006, *open circles*) (Figure reproduced from Zaritsky (2012), reproduced with permission from ISRN Astronomy and Astrophysics)

and orbital anisotropies the value of $\alpha \neq 2$. Here, we will simply adopt $\alpha = 2$ in defining the V term. Such a correction removes the trend shown in Fig. 8.2.

Finally, we close by showing in Fig. 8.3 the resulting FM relation for a sample that includes galaxies, ultra compact dwarf galaxies, regular dwarf galaxies, and star clusters (Forbes et al. 2008). Despite the heterogeneity of galaxy types the relationship spans 5 orders of magnitude in size.

8.3 Do Bulges Fit In?

The application of a kinematic scaling relation to galaxy bulges, such as FP or FM, must bear in mind at least the points mentioned above:

- The power-law behavior of Υ with V cannot continue to low masses because it implies unphysically small values for low mass systems (the floor value could be lower than that plotted in Fig. 8.1 because of younger stellar populations, but there will be a floor), therefore one should not apply the FP; and
- The scaling relation must include both velocity dispersion and rotation to account fully for dynamical support.

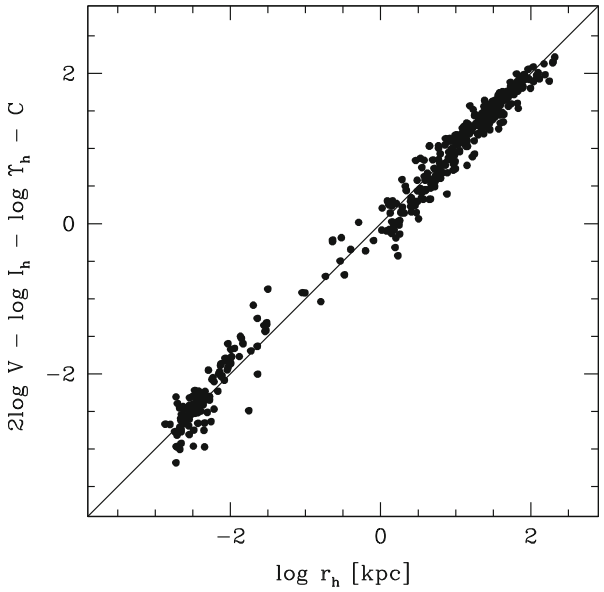

Fig. 8.3 The K-band version of the FM using the Forbes et al. (2008) sample of galaxies, ultra compact dwarfs, dwarf galaxies, and star clusters (Figure reproduced from Zaritsky et al. (2011). Reproduced with permission of AAS)

In addition, for bulges there is the added complexity of dealing with a subsystem within the galaxy. Just as there was no a priori justification for why the Virial Theorem should hold when using measurements that did not reflect the global properties of the system, one may wonder if there is justification for expecting subsystems to trace scaling relations determined from galaxies in their entirety.

If we consider the extreme case where all luminous galaxy components, whether they be stars, gas, stellar clusters, or satellite galaxies, are massless tracers within a fixed gravitational potential (defined by the dark matter), then it if fairly straightforward to conclude that each of these will independently satisfy the Virial Theorem, because they have no influence on each other. This situation is implicitly assumed when measuring galaxies masses, for example, when the stars or gas in the disc, or the clusters or satellites in the halo, are taken to be fair dynamical tracers and the Virial Theorem or some variant is applied. In the case of bulges then, we might expect the Virial Theorem to hold—and the FM to be satisfied—if the bulge stars are truly an independent dynamical system within a galaxy. On the other hand, the Virial Theorem will not hold if by selecting "bulge" stars one is in reality selecting a subpopulation of disc stars that have specific dynamical properties. That is, the Virial Theorem does not hold for a subpopulation of objects, clusters for example, that are selected to be those with the most radial orbits or those that have the largest epicenters—the observed sample must be a representative sampling of the tracer population as a whole.

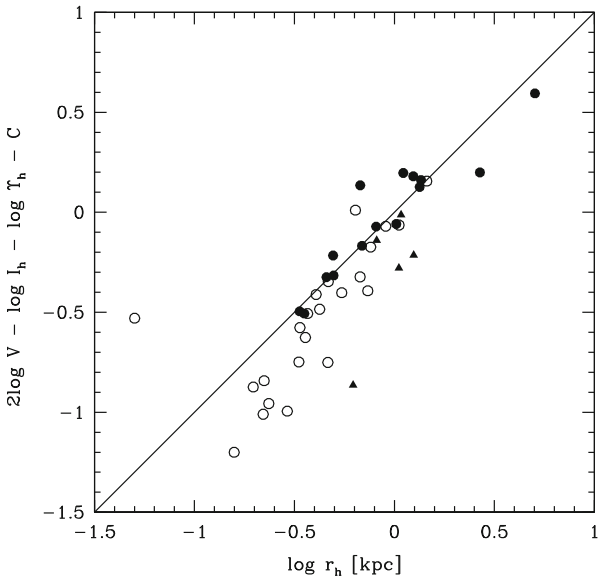

Fig. 8.4 Bulges on the FM. We have taken the data presented by Fabricius et al. (2012) and directly placed those galaxies on the FM as defined for Fig. 8.3. The *filled circles* represent bulges classified as classic by those authors, the *open circles* those classified as pseudo, and the *triangles* those that they were unable to classify. The line is the 1:1 line, as in Fig. 8.3

For our preliminary analysis, used here only as a "proof-of-concept", we use an existing sample of published bulge data (Fabricius et al. 2012) to place bulges on the FM in Fig. 8.4. They adopt the bulge classifications from the literature (Fisher and Drory 2008, 2010), or apply the same technique of examining the images for disc-like structures within the bulge as applied in those literature studies. The results are striking in that the classical bulges, as defined by those authors using only photometric characteristics, are well described by the existing FM relation. We have applied no readjustment or recalibration of the FM shown in Fig. 8.3. We do not even apply a constant shift despite the problem that the bulge data are in H-band and the FM of Fig. 8.3 is in K-band (note that this issue is not as significant as it may appear because the shift will depend on the *relative* color difference across H and K between the Sun and these bulges). The agreement suggests that classical bulges, even though they are embedded within another stellar system, satisfy the FM and that the bulge tracer particles satisfy the Virial Theorem.

In contrast, those bulges classified as pseudobulges fall systematically off the FM, particularly so for those with smaller r_h. Although they could have different mass-to-light ratios (due to younger populations), that difference would need to be systematic, in that the offset from the FM is larger for the smaller bulges, rather than a simple offset along the vertical axis of the plot, as would be the case if pseudobulges systematically consist of younger stellar populations. We provocatively suggest that the failure of the pseudobulges to fall on the FM is due

to pseudobulges not being independent dynamical systems but rather that they are comprised of a subset of special stars drawn from a larger system, presumably the disc. If so, the Virial Theorem should not be expected to hold for such a subset of stars, and therefore pseudobulges should not be expected to fall on the FM.

We caution, however, that there are alternative interpretations of the results shown in Fig. 8.4. For example, it could also be the case that pseudobulges are the one type of dynamical system found so far to have very distinct A_0 or B_0 values. Furthermore, the classification of bulge types is controversial and results often disagree between studies. A proper treatment of this question would attempt to reconcile cases where disagreement exist. For example, some of these galaxies are perhaps better examples of bar and lens systems and viewing angle plays an important role as well (Laurikainen et al. 2011). As always, interpreting the results of comparisons to scaling relationship is fraught with peril, but the basic observational results serve as constraints on models of both classical and pseudobulges.

8.4 Summary

We have highlighted some key modifications of the most standard kinematic scaling relation, the fundamental plane, that are required to incorporate low mass and/or rotationally supported systems. Furthermore, we have summarized the existing findings in the literature that one can empirically derive a fitting function for the mass-to-light ratio within the half-light radius, Υ_h, in terms of the observables V and I_h. Doing so enables one to place all galaxies from the ultrafaints to brightest cluster galaxies on the same scaling relation.

We then explored whether bulges on their own also satisfy this scaling relation. We showed that classical bulges are well described by the scaling relation, suggesting that they are dynamically complete subsystems within galaxies. On the other hand, pseudobulges fall off the FM. One possible explanation is that they are not dynamically complete systems and instead simply represent certain orbit families within the discs of these galaxies. As such, we do not expect the Virial Theorem to hold for those stars separately. As we stressed in the introduction, it is always tempting to read too much into the results of comparisons to scaling relationship. However, the existence of scaling relations and how various populations of objects fall about those scaling relations is a demanding constraint on models of the formation and evolution of those systems.

References

Bedregal, A.G. Aragón-Salamanca, A., & Merrifield, M.R. 2006, MNRAS, 373, 11 25
Bender, R. 1990, A&A, 229, 441

Burstein, D. & Bender, R. & Faber, S. & Nolthenius, R., 1997, AJ, 114, 1365
Cappellari, M. et al. 2006, MNRAS, 366,1126
Davies, R. L., Efstathiou, G., Fall, S.M., Illingworth, G., Schechter, P.L. 1983, ApJ, 266, 41
Djorgovski, S. & Davis, M., 1987, ApJ, 313, 59
Dressler, A. & Lynden-Bell, D. & Burstein, D. & Davies, R. L., Faber, S. M., Terlevich, R. & Wegner, G., 1987, ApJ, 31 3, 42
Fabricius, M.H., Saglia, R.P., Fisher, D.B., Drory, N., Bender, R., and Hopp, U., 2012, ApJ, 754, 67
Fisher, D. B., & Drory, N. 2008, AJ, 136, 773
Fisher, D. B., & Drory, N. 2010, ApJ, 716, 942
Forbes, D.A., Lasky, P., Graham, A.W., and Spilter, L. 2008, MNRAS, 389, 1924
Gadotti, D.A. 2009, MNRAS, 393, 1531
Kassin, S.A. et al. 2007, ApJ, 660, 35
Kormendy, J., 1975, ApJ, 295, 73
Laurikainen, E., Salo, H., Buta, R., & Knapen, J.H. 2011, MNRAS, 418, 1452
Lithwick, Y., & Dalal, N. 2011, ApJ, 734, 100
Tully R. B., Fisher J. R., 1977, A&A, 54, 661
van der Marel, R.P., and van Dokkum, P. 2007, ApJ, 668, 756
Weiner, B.J. et al. 2006, ApJ, 653, 1049
Yang, Y, Zabludoff, A.I., Zaritsky, D., & Mihos, J.C. 2009, ApJ, 702, 1683
Zaritsky, D., 2012, in ISRN Astronomy & Astrophysics, 2012, 12
Zaritsky, D., Gonzalez, A. H. & Zabludoff, A. I., 2006, ApJ, 638, 725
Zaritsky, D., Zabludoff, A.I., and Gonzalez, A.H. 2011, ApJ, 682, 68

Part III
The Milky Way Bulge

Chapter 9
The Milky Way Bulge: Observed Properties and a Comparison to External Galaxies

Oscar A. Gonzalez and Dimitri Gadotti

Abstract The Milky Way bulge offers a unique opportunity to investigate in detail the role that different processes such as dynamical instabilities, hierarchical merging, and dissipational collapse may have played in the history of the Galaxy formation and evolution based on its resolved stellar population properties. Large observation programs and surveys of the bulge are providing for the first time a look into the global view of the Milky Way bulge that can be compared with the bulges of other galaxies, and be used as a template for detailed comparison with models. The Milky Way has been shown to have a boxy/peanut (B/P) bulge and recent evidence seems to suggest the presence of an additional spheroidal component. In this review we summarize the global chemical abundances, kinematics and structural properties that allow us to disentangle these multiple components and provide constraints to understand their origin. The investigation of both detailed and global properties of the bulge now provide us with the opportunity to characterize the bulge as observed in models, and to place the mixed component bulge scenario in the general context of external galaxies. When writing this review, we considered the perspectives of researchers working with the Milky Way and researchers working with external galaxies. It is an attempt to approach both communities for a fruitful exchange of ideas.

9.1 Introduction

What is the origin of the bulge of the Milky Way? The answer to this question is a crucial step towards identifying the history of events that took place during the formation and evolution of the Galaxy as a whole. As a matter of fact, the answer to this question has changed dramatically, since the early times of Galactic bulge archaeology until today, between the two main ideas behind bulge formation: the merger-driven bulge scenario, where a bulge is formed violently and quickly during the early stages of the Galaxy dominated by the gravitational collapse or hierarchical

O.A. Gonzalez (✉) • D. Gadotti
European Southern Observatory, Alonso de Cordova 3107, Vitacura, Santiago, Chile
e-mail: ogonzale@eso.org; dgadotti@eso.org

E. Laurikainen et al. (eds.), *Galactic Bulges*, Astrophysics and Space Science Library 418, DOI 10.1007/978-3-319-19378-6_9

merging of sub-clumps of dark matter carrying baryons and gas (e.g. Abadi et al. 2003; Elmegreen 1999), and the secular evolution scenario where the bulge structure is naturally born from the dynamical evolution of the stellar Galactic disc (Combes and Sanders 1981; Raha et al. 1991; Norman et al. 1996; Athanassoula 2005). Until this day, we cannot say with absolute certainty which one of these scenarios, or if perhaps both, played a major role during the formation of the bulge of our Galaxy.[1]

The reason for this long term debate might lie, ironically, in our greatest strength. The Galactic bulge allows us to investigate its properties by taking advantage of the fully resolved stellar populations – a unique strength that can be understood as the ability to see its properties in a unique level of detail with respect to what we can learn from the observation of external bulges. However, such an advantage also means that nearly 500 sq. deg. of sky must be homogeneously covered in order to obtain the most global picture of the Bulge. To obtain a general characterization of these properties is a crucial step in order to answer the question of the origin of our Galactic bulge.

As a consequence, observational efforts during the last decade have been focused on solving this limitation. As a result, our knowledge regarding the global properties of the Galactic bulge has increased considerably thanks to the advent of dedicated spectroscopic and photometric surveys. We are currently witnessing a revolution in the field of Milky Way bulge research that will also find its place within the bulges of other disc galaxies. It is thus a moment in which the communities of Galactic and Extragalactic research are approaching each other. From this, one cannot expect anything but a fruitful exchange of ideas that will certainly push both fields forward. However, it is not straightforward for members of each community to study the other field, for at least two reasons. The first obstacle is the vast amount of work, rich in details, that one has to become familiarized with. The second obstacle is the jargon employed independently by each group which hampers understanding. This review is a modest first attempt to overcome these obstacles.

[1]To be complete, we must mention the pioneering work of Eggen et al. (1962), who suggested that the first stage in the formation of the Milky Way was a fast ($<10^8$ yr) monolithic collapse of a single massive gas cloud, which could have formed both the Galaxy stellar halo and the bulge. This scenario was later replaced with the merger-driven scenario mostly due to the widely varying ages of different components of the Galaxy and the hierarchical nature of LCDM theory. We refer the reader to Brooks and Christensen (this volume) for a review on merger-driven bulge formation. In the last decade or two, the secular evolution scenario has slowly, but unequivocally, gained terrain over the merger-driven scenario. Another bulge building scenario we do not discuss here has recently been put forward by e.g. Elmegreen et al. (2008, – see review by Gadotti 2012). In this scenario, bulges form by the coalescence of giant clumps in primordial discs. This scenario can explain the formation of spheroids but does not account for boxy/peanuts.

9.2 The Structure of the Milky Way Bulge

The most basic definition of a galactic bulge is that of an over-density that swells up from the plane of the disc. The idea of this natural conception originated from the observations of other disc galaxies, in particular the bulges of edge-on spirals, which allow us to compare them more easily with our own in a purely morphological way.

Within spiral galaxies, we could in principle distinguish between classical bulges and those bulges which are formed via secular evolution, based almost solely on their morphological signatures. Clearly, a proper characterization of the structural properties of the Milky Way bulge would provide us with a valuable set of constraints needed to find its place in the more general scheme of external bulges and, as extensively shown by galaxy formation models, to connect these constraints to the different mechanisms of origin.

After it was first postulated by de Vaucouleurs (1964), followed by Sinha (1979) and Liszt and Burton (1980) among others, Blitz and Spergel (1991) predicted the presence of the bar-like structure for the inner regions of the Galaxy based on infrared observations. Later on, continuing with the exploitation of infrared imaging in order to overcome the strong dust obscuration towards the inner galaxy, the COBE/Diffuse Infrared Background Experiment (Smith et al. 2004) data was used by Weiland et al. (1994) to unambiguously establish the presence of the bar. Soon after, the COBE data further revealed the global B/P morphology of the Milky Way bulge (Dwek et al. 1995).

An important number of Bulge structural studies have been based on the stellar counts of red-clump stars, which are the metal-rich counterpart of the well known globular cluster horizontal-branch stars. The absolute magnitudes of red-clump stars, are found to have little dependence on age and metallicity, making them one of the most powerful tools for deriving distances towards the bulge and therefore tracing its global morphology. This method is based on the construction of the luminosity function of the Bulge towards a given line of sight where the red-clump feature can be easily identified and fitted with a Gaussian distribution to obtain the mean red-clump magnitude (Stanek et al. 1994). Zoccali (2010) and McWilliam et al. (2010) presented the discovery of a split within the red-clump when investigating the luminosity function of the Bulge at latitudes 90: $|b| > 5°$, along the minor axis. Soon enough, McWilliam and Zoccali (2010) and Nataf et al. (2010) provided a wider mapping of this split red-clump in the color magnitude diagram, providing substantial evidence for the bright and faint red-clumps to be the consequence of having two over-densities of stars located at different distances, namely the two southern arms of an X-shaped structure both crossing the lines of sight. Detailed three-dimensional maps were later constructed by Saito et al. (2011), based on the use of red-clump stars observed in the near-IR survey 2MASS, which confirmed the suggestion of McWilliam and Zoccali (2010) that the Bulge is in fact X-shaped due to the prominent vertices of the B/P. Wegg and Gerhard (2013) modelled the distribution of red-clump stars, observed in Vista Variables in the Via Lactea (VVV) ESO public survey, providing the first complete mapping of the

X-shaped Bulge. These X-shaped bulges are commonly observed in external edge-on galaxies and belong to the case of a pronounced B/P structure, that is simply the inner regions of the bar that grow out of the plane of the disc.

Currently, the axial ratios of the bar are constrained to be about 1:0.4:0.3 with a bar size of about 3.1–3.5 kpc diameter and the near end of the bar pointing towards positive Galactic longitudes. Until recently, the position angle of the bar was constrained to a relatively large range of values between ∼20–40° with respect to the Suncenter line of sight. The uncertainty in the bar position angle is likely to be a consequence of measurements done across different latitudes in each study, thus finding a different position angle when looking at different distances from the Galactic plane (Blitz and Spergel 1991; Stanek et al. 1994; Dwek et al. 1995; Binney et al. 1997; Bissantz and Gerhard 2002; Benjamin et al. 2005; Babusiaux and Gilmore 2005; Rattenbury et al. 2007; Cao et al. 2013). As a matter of fact, specific evidence for a longer flatter component of the bar, referred to as the Galactic long bar, has been presented in the literature based on near-IR star counts near the Galactic plane. This long bar is found to have an axis length of 4–4.5 kpc and ratios of 1:0.15:0.03. The position angle of this longer component has been constrained to ∼45° in such studies (e.g. López-Corredoira et al. 2007; Cabrera-Lavers et al. 2007; Hammersley et al. 2000; Churchwell et al. 2009; Amôres et al. 2013). On the other hand, the recent model of the global distribution of red-clump stars from Wegg and Gerhard (2013) provided a precise measurement for the B/P Bulge position angle of $27 \pm 2°$, in agreement with the studies done at larger distances from the Galactic plane. The nature of the long bar has been debated extensively in the literature. Recently, Garzón and López-Corredoira (2014) provided a theory where two co-existing bars, the long bar restricted to the plane latitudes and the B/P thick bar, could be present in the inner Galaxy. However, model observations of barred galaxies led Martinez-Valpuesta and Gerhard (2011), Romero-Gómez et al. (2011), and Athanassoula (2012) to strongly argue that the apparent long bar is an artifact associated with leading spiral features at the end of the shorter primary bar (the B/P Bulge). Furthermore, the co-existence of such independently large scale structures has not been seen in external galaxies. For this reason, the observed properties attributed to different bars in the Galaxy are more likely corresponding to a unique B/P bulge and bar structure formed by the buckling instability process. The long bar would then be explained by the interaction of the outer bar, with the adjacent spiral arm near the plane which produced leading ends that ultimately results in the measurement of a larger position angle (Martinez-Valpuesta and Gerhard 2011).

In the innermost regions ($l < 4°$, $b < 2°$) the bar has been found to change its apparent inclination with respect to the line of sight which has been interpreted as evidence for a possible distinct smaller bar, referred to as a nuclear bar. However, models of a single bar (meaning those that do not include a distinct nuclear bar) have also shown such a change in orientation in the inner regions, most likely due to the presence of a more axisymmetric concentration of stars in the central regions (Gerhard and Martinez-Valpuesta 2012).

Red-clump stars, although an excellent distance indicator for the bulge mean population, still suffer from the usual complications when looking towards the inner

Galaxy such as disc contamination, extinction, and, to a minor extent, the effects of stellar populations. Furthermore, red-clump stars will map the distribution of the variety of stellar ages of the Bulge population, which is not defined beforehand. These uncertainties can be statistically handled when constructing and analyzing the Bulge luminosity function, however their impact on the results will depend on the level of knowledge of the properties of each analyzed field. For this reason, Variable stars, specifically RR-Lyrae, have recently provided a new perspective for the Bulge structural properties. Their well defined period-luminosity relation in the near-IR helps to overcome the effects of dust extinction in the inner Galaxy and they are well spatially distributed across the entire bulge. The period-luminosity relation makes RR-Lyrae an exquisitely accurate distance indicator that unequivocally traces the oldest Galactic population.

Surprisingly, given the vast amount of different tracers that have confirmed a dominant barred structure, RR Lyrae have shown a remarkably different spatial distribution compared to, for example, red-clump stars. While red-clump stars trace the position angle of the bar at all latitudes, a direct comparison with the RR Lyrae distance distribution provided by Dékány et al. (2013) strongly suggests a different morphology for the oldest population in the inner Galaxy. Unlike the red-clump stars, the RR Lyrae stars show a more spheroidal, centrally concentrated distribution. This structural component, populated by stars with ages larger than 10 Gyr, seems to be overlying with the B/P bulge. Figure 9.1 shows a comparison of the projected mean distances obtained from RR Lyrae and those from the mean magnitude distribution of red-clump stars. The figure illustrates the structural difference between the components traced by both distance tracers, with only red-clumps stars following the position angle of the bar. This result presented in Dékány et al. (2013) is perhaps the first purely morphological evidence suggesting a composite Bulge nature, with two different stellar populations overlapping in the inner Galaxy.

The presence of more than one age/metallicity distribution within a B/P bulge has already been seen in dissipative collapse models (e.g. Samland and Gerhard 2003) and also in bulges from cosmological galaxy formation simulations (e.g. Obreja et al. 2013). However, one must be very careful when further linking the different spatial distributions seen in the Galactic bulge with a distinct origin process, namely having a classical bulge and a secularly evolved B/P bulge that originated from the disc. Recently, Ness et al. (2014) gives caution to the fact that different spatial distributions and mean stellar ages can be found in pure B/P bulges without the need of a merger-origin structure to be present, as seen in an N-body + smoothed particle hydrodynamics simulation of a disc galaxy. Certainly, the fine details of the shape traced by RR-Lyrae will be achieved when the complete sample of RR-Lyrae from the VVV survey is available. The mapping of a wider area of the Bulge and the larger sample of sources available in each line of sight will allow for the calculation of precise mean distances with high spatial resolution.

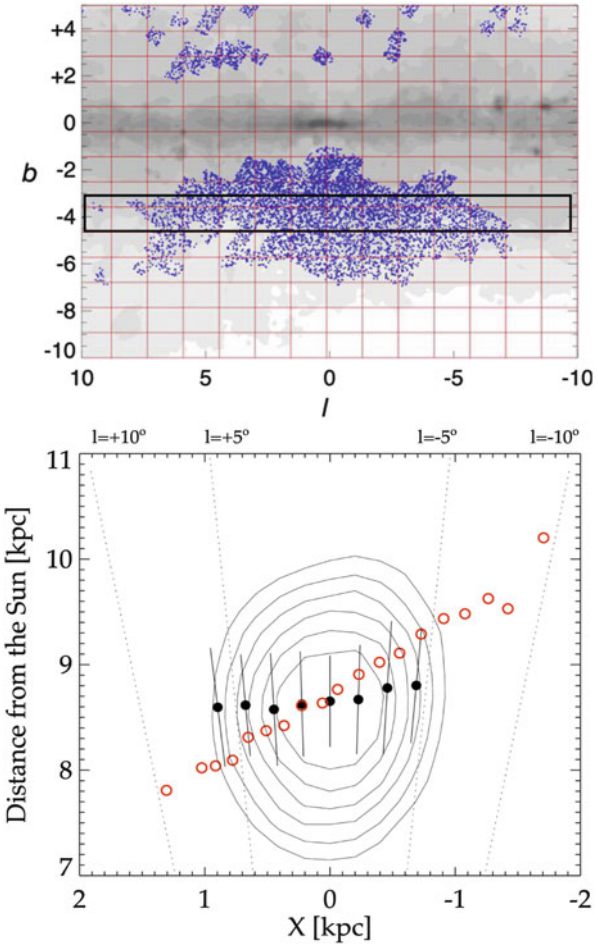

Fig. 9.1 *Upper panel*: Spatial distribution in Galactic coordinates for the 7663 OGLE-III RRab stars in the bulge area of the VVV Survey, from Dékány et al. (2013). The *grey* scale background shows the interstellar extinction map of Schlegel et al. (1998). The *black rectangle* denotes the region at b $= -4$ for which the mean distance of RR Lyrae and RC stars are compared in the *lower panel*. The *lower panel* shows the projected mean distances of RR Lyrae in *black filled circles* and of the *red-clump stars* as *red open circles*. Isodensity contours for the projected distance distribution of the RR Lyrae sample in the analyzed latitude range are also shown. Mean distances of the red clump stars are from the mean magnitudes obtained in Gonzalez et al. (2012) and calculated adopting an absolute magnitude of $M_{Ks,RC} = 1.71$ mag. Distances for the sample of RR Lyrae have been presented in Dékány et al. (2013) and were used here to derive the projected mean distance and 1σ width (*black solid lines*) to each line of sight (*Upper panel* adapted from Dékány et al. (2013))

9.3 The Age of the Milky Way Bulge

Right from the very early discovery of RR Lyrae towards the center of the Galaxy (Baade 1951), perhaps the most common statement found in the literature addressing the Galactic bulge stellar populations is: *The Milky Way bulge stellar population is predominantly old*. The reasons for such a statement are indeed very well funded and are described in this section.

Without a doubt, deep photometric observations towards low extinction regions of the Bulge provided a defining view on the age of its stellar population thanks to the possibility of constructing colour-magnitude diagrams that reached the turn-off position – a useful indicator for the mean age of a given stellar population. However, the effects of differential reddening and, in particular, the uncertainty on the distance modulus of the stars towards a given line of sight does not allow the derivation of an absolute age estimation for the Bulge using the turn-off technique. To overcome these issues, Ortolani et al. (1995) adopted a differential method, based on the position of red-clump stars in the luminosity function. The very small dependence on age and metallicity for the mean magnitude of the red-clump allowed Ortolani et al. (1995) to match its position in the luminosity function to that of an old stellar population, the globular cluster NGC 6528, finding a remarkable agreement between the relative positions of the turn-off. This result provided strong support for the view of the Galactic Bulge being formed in a time scale shorter than 1 Gyr, thus making it as old as the globular cluster population.

Dedicated photometric studies spread across other regions of the Bulge, and based on similar techniques further strengthen the conclusion of a stellar population with a mean age of $\sim$10 Gyr, particularly setting a lower limit on ages higher than 5 Gyr (Zoccali et al. 2003; Valenti et al. 2013; Clarkson et al. 2011). The major issue with these kind of studies is how to deal with the contamination of the foreground disc, in particular with the main sequence of the disc which lies right on top of the Bulge turn-off. Statistical decontamination methods, for example using disc control fields (Zoccali et al. 2003; Valenti et al. 2013), have been used to eliminate foreground stars to some extent. However, the contamination of foreground stars coupled with uncertainties in differential reddening and metallicity distribution effects lead to uncertainties on age determination via the analysis of color-magnitude diagrams that remain of the order of 2 Gyr.

Recently, Clarkson et al. (2008) provided what is perhaps the cleanest, and thus most accurate, age determination of those studies based on the analysis of a colour-magnitude diagram (Fig. 9.2). Clarkson et al. (2008) were able to decontaminate the turn-off position of the Bulge population from that of the nearby disc by using a mean proper motion criteria as the one shown by Kuijken and Rich (2002) with a set of ACS WFC on HST observations taken over 123-orbit HST integrations in the SWEEPS field (l,b)=(1.25°, −2.65°). The study of Clarkson et al. (2011) later concluded that a fraction of only up to a 3.5 % of the Bulge stars can be younger than 5 Gyr. Therefore, this study is in agreement with most of other studies where the Bulge population is found to be dominantly old.

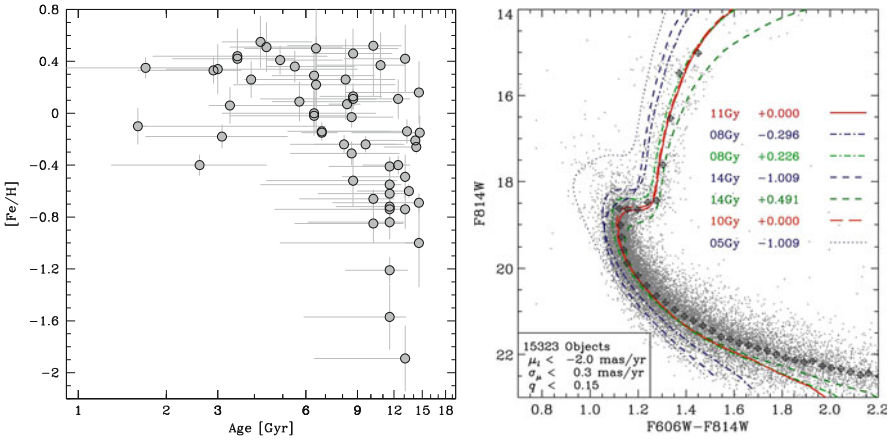

Fig. 9.2 *Left panel*: The metallicity of the microlensed dwarfs of the Bulge as a function of their ages taken from Bensby et al. (2013a). *Right panel*: The color magnitude diagram for proper motion-selected Bulge objects from Clarkson et al. (2008), using similar mean proper motion criteria to Kuijken and Rich (2002) but with a 6σ detection requirement imposed. A set of isochrones with different metallicities and ages is over-plotted to the color magnitude diagram. An alpha-enhanced, solar-metallicity isochrone at 11 Gyr represents the median sequence well above the turn-off. Also shown in the figure are sequences at metallicity [Fe/H]$=$ (-1.009, -0.226, $+0.491$) and ages (8, 10, 14) Gyr (*Left panel* adapted from Fig. 15 in Bensby et al. (2013a), reproduced with permission ©ESO. *Right panel* adapted from Fig. 20 in Clarkson et al. (2008), reproduced by permission of the AAS)

A large percentage of young stars is certainly not expected in a bulge that originates purely from early dissipation or merging processes. These events would take place at early times in the evolution of the galaxy and would occur rapidly. Although some intermediate-age stars could later be added to the bulge by diffusion from the inner disc, the bulk of the bulge stellar population would be old. On the other hand, a significant population of young stars could be found – and might be actually expected – in bulges formed via disc instabilities. So if the Milky Way bulge is indeed dominated by a component formed via disc instability, as seen by its structural properties, then where are those young stars? It is only very recently that a possible answer to this question has been brought to the table, and it was using a completely different approach: the high-resolution spectroscopy of Bulge microlensed stars. The microlensing event, which produces the brightness magnification of a dwarf star in the bulge due to the passing of a foreground lens star, provides a unique opportunity to obtain high resolution spectra of this otherwise unreachable target. Bensby et al. (2013a) have collected enough microlensed dwarfs to investigate the overall metallicity distribution and also their age. While the metallicity distribution of the microlensed dwarfs has been found to be in good agreement with that of the bulge giant stars, their age distribution presented a significant number of young stars: nearly 22 % of the micro-lensed dwarfs were found to be younger than 5 Gyr. As the number of analyzed micro-lensed stars

increases, these findings will be further confirmed or disproved with better statistics in order to refine the actual percentages of young and old stars found in the bulge. Particularly, notice the disagreement between the 22 % of stars younger than 5 Gyr found in the microlensing sample and the corresponding 3.5 % fraction of young stars given in the work of Clarkson et al. (2011).

9.4 The Chemical Abundances of the Milky Way Bulge

9.4.1 The Metallicity Distribution

The characterization of the chemical abundance of Bulge stars is perhaps the field that has evolved most quickly thanks to the advent of multi-object spectrographs in large telescopes. Different surveys have – and still are – pointing towards different regions of the bulge and collecting samples of thousands of stars. The argument for such surveys is clear: it became evident that a few low extinction regions were no longer representative of the global chemical abundance patterns of the Bulge. First attempts to derive the metallicity distribution of the Bulge based on low resolution spectra (e.g. Sadler et al. 1996; Ramírez et al. 2000), together with a small number of available spectra obtained with high resolution (McWilliam and Rich 1994; Fulbright et al. 2006), had shown from the start that the mean population of the bulge was overall metal-rich. The shape of the metallicity distribution was, on the other hand, less clear. Zoccali et al. (2003) used a set of observations using WFI to obtain a photometric metallicity distribution based on the colour of red giant stars. They found a rather broad metallicity distribution, in good agreement with that derived from spectroscopy in the same field but with a larger statistical sample, with [Fe/H] values ranging from −1.0 to 0.4 and which peak at solar metallicity.

With a well-characterized metallicity distribution in Baade's window, it was time to answer the following question: how spatially uniform were these properties? Minniti et al. (1995) had already discussed the possibility for a metallicity gradient in the Bulge, impressively enough based on low resolution spectra of less than a hundred giant stars. It then became the era of multi-object spectroscopy where hundreds of stars could be observed in one single shot. Using FLAMES on the Very Large Telescope, Zoccali et al. (2008) derived the metallicity distribution for different fields along the Bulge minor axis at different latitudes ($b = -4°$, $-6°$, and $-12°$). They found a clear metallicity gradient of $\sim$0.6 dex/kpc, with mean metallicities varying from −0.4 at the largest latitudes and up to solar metallicity at $b = -4°$. This gradient has since then been confirmed thanks to several subsequent observations across different regions and the variation in the metallicity distributions have been further characterised (Johnson et al. 2011; Uttenthaler et al. 2012; Johnson et al. 2013; Ness et al. 2013a; Rojas-Arriagada et al. 2014).

Gonzalez et al. (2013) recently complemented these results by presenting a photometric metallicity map, constructed with the same technique used by Zoccali

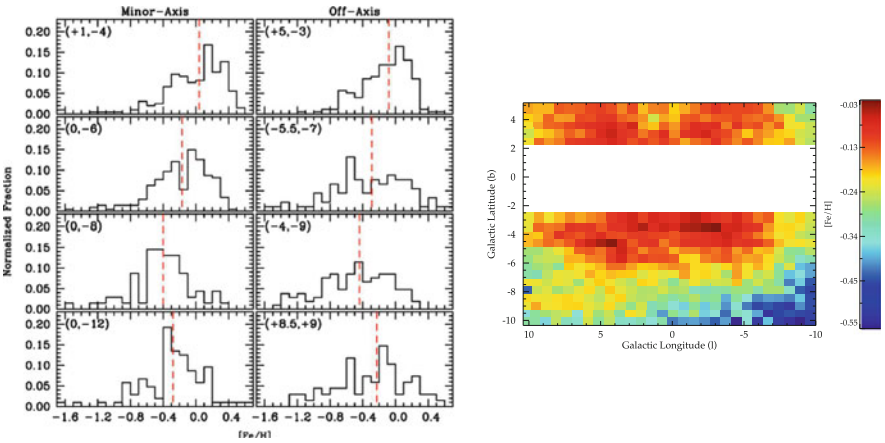

Fig. 9.3 *Left panel*: Metallicity distributions for a compilation of studies taken from Johnson et al. (2013). The $(l, b) = (+1, -4), (0, -6)$ and $(0, -12)$ fields are from Zoccali et al. (2008), the $(0, -8)$ field is from Johnson et al. (2011), the $(+5, -3)$ field is from Gonzalez et al. (2011), and the $(-5.5, -7)$, $(-4, -9)$, and $(+8.5, +9)$ fields are from Johnson et al. (2013). *Right panel*: Map of the mean photometric metallicities of the bulge constructed with the VVV survey data from Gonzalez et al. (2013) (*Left panel* adapted from Fig. 8 in Johnson et al. (2013) reproduced by permission of the AAS. *Right panel* adapted from Fig. 2 in Gonzalez et al. (2013) reproduced with permission ©ESO)

et al. (2008) but based on the Vista Variables in the Via Lactea (VVV) ESO public survey, for almost the entire Bulge region providing the global picture of the Bulge metallicity gradient. The metallicity gradient is therefore strongly established by an increasing number of spectroscopic studies obtained with different techniques and stellar samples (see Fig. 9.3 for a compilation of the latest results). However, the metallicity distributions obtained in the innermost regions of the Bulge ($|b| < 4°$) based solely on high-resolution, near-infrared spectroscopy have provided evidence for the flattening-out of the gradient in the inner 700 pc (Ramírez et al. 2000; Rich et al. 2012).

What is the implication of finding such a metallicity gradient in the Bulge? At first, similarly to the domination of old ages found in Bulge stars, the metallicity gradient was interpreted as direct evidence for a bulge formed as a classical bulge via mergers in the early stages of the galaxy, similarly to elliptical galaxies. It was also interpreted as evidence against the secular evolution scenario, since it was thought that bars would mix the stellar orbits well enough to erase any existing vertical gradient. Models of bar formation in disc galaxies, however, proved otherwise, showing that a bar might produce a gradient similar to the one seen in the Milky Way depending on the original disc radial gradients (Martinez-Valpuesta and Gerhard 2013), vertical gradients (Bekki and Tsujimoto 2011), or both (Di Matteo et al. 2014).

However, the existence of metallicity gradients has also been interpreted as a consequence of having two or more underlying components each one with a

characteristic metallicity distribution. This mixing of components would naturally produce a variation on the mean metallicity according to the bulge region which is being studied. Evidence for such a multiple component scenario has been suggested based on a bimodal metallicity distribution of red clump stars in Baade's window by Hill et al. (2011) and has been also suggested from a similar bi-modality seen in the metallicity distribution of microlensed dwarfs. Both of these distributions show a metal-poor and a metal-rich peaks located approximately at [Fe/H] ~ -0.3 and [Fe/H] $\sim +0.3$, respectively. Recently, the same bi-modality has also been found in the metallicity distributions based on the Gaia-ESO survey observations of the Bulge (Rojas-Arriagada et al. 2014). By producing a Gaussian decomposition of the metallicity distribution functions, Rojas-Arriagada et al. (2014) showed a clear bi-modality in all the analyzed fields with relative sizes of components depending on the specific position on the sky. This change in the relative sizes of each component can be clearly seen in Fig. 9.4.

On the other hand, the ARGOS Galactic bulge survey (Freeman et al. 2013), which consists of the largest sample of homogeneously analyzed RC stars, constructed large-number statistics metallicity distributions at different latitude stripes, using a total of more than 10,500 stars located within a galacto-centric radius of 3.5 kpc. The overall metallicity distribution of the ARGOS survey was interpreted in Ness et al. (2013a), as being composed of five Gaussian components. Each of these components would be sampling a different stellar population and thus any changes in their relative contribution fraction as a function of latitude could be the origin of the observed mean metallicity gradient seen in the Bulge. The metallicity distributions for stars within Galactic longitudes $l = \pm 15°$ and latitudes $b = -5°$, $-7.5°$, and $-10°$ from the ARGOS survey by Ness et al. (2013a) are also shown in Fig. 9.4. This effect has lead the ARGOS survey to suggest the three main components of the metallicity distribution to be associated with the metal rich B/P bulge (mean [Fe/H] $\sim +0.15$), the thick B/P bulge (mean [Fe/H]~ -0.25) and the inner thick disc (mean [Fe/H]~ -0.70).

Although the results from Ness et al. (2013a) are based on the identification of several components, it can be safely understood that most studies converge into a similar conclusion: the bulge metallicity distribution is the result of not a single but of a mixture of populations with at least two main components, one metal-poor and the other metal-rich. Certainly, this is everything that can be concluded from the metallicities alone and one has to be extremely cautious when attempting to link these different components with a given bulge formation scenario. All evidence needs to be considered when interpreting results in terms of such scenarios, i.e. such an assessment must also include the kinematics, spatial distribution and ages of the stars.

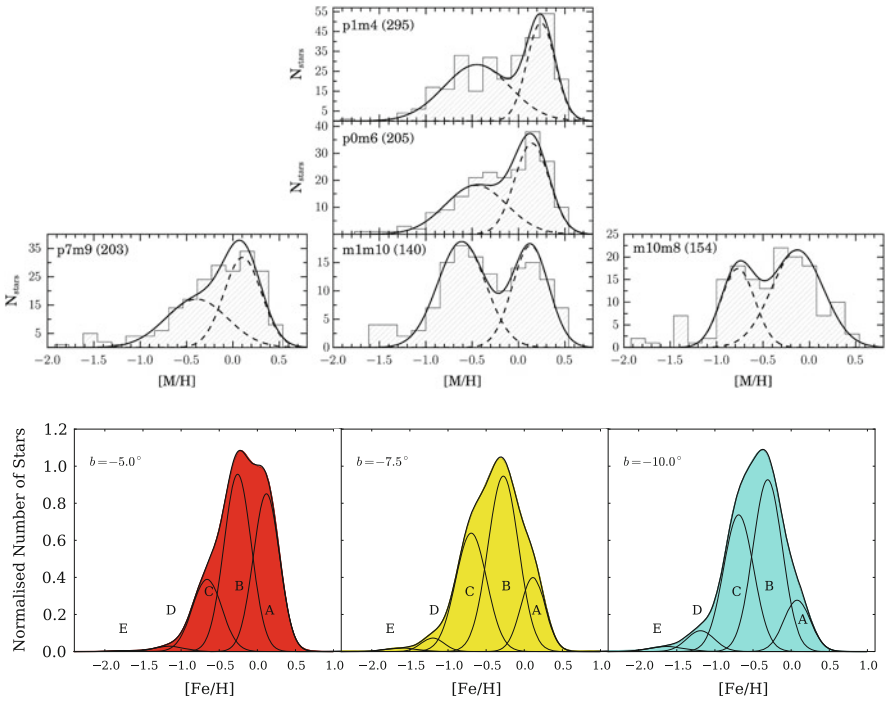

Fig. 9.4 *Upper panels*: Metallicity distributions for the five bulge fields from the ESO Gaia survey, presented in Rojas-Arriagada et al. (2014). *Black dashed* and *solid lines* show the components identified in each field as dashed Gaussian functions, with the sum of them shown as a *solid line*. The three minor-axis fields located at (+1,−4), (0,−6), and (−1,−10) are shown in the *central panels*, and the lateral fields (+7,−9) and (−10,−8) at the left and right. *Lower panels*: Metallicity distributions from the ARGOS survey from Ness et al. (2013b). From left to right at b = −5, −7.5 and −10, for l = ±15. The different contribution of the adopted Gaussian components are marked in each field, with the three main components being A, B and C (*Upper panel* adapted from Figure 6 in Rojas-Arriagada et al. (2014), reproduced with permission ©ESO. *Bottom panel* adapted from Fig. 1 in Ness et al. (2013b))

9.4.2 The Bulge Alpha-Element Abundances

The α-element abundances can provide us with further constraints for the origin of the Bulge stellar populations, specifically with respect to its formation time-scale. Tinsley (1979) suggested that the ratio of [α/Fe] compared to [Fe/H] is a function of the time delay between SNe II, which produce both α- and iron-peak elements (e.g. Woosley and Weaver 1995), and SNe Ia, which yield mostly iron-peak with little α-element production (e.g. Nomoto et al. 1984). Therefore, only after sufficient time has passed for the SNe Ia events to occur, the [α/Fe] ratio will decline from the SNe II value. Clearly, the critical ingredient on this relation is the SNe Ia delay time, for which different production channels might be present.

In the Bulge, the α-element abundances of Bulge stars with [Fe/H]<-0.3 have been found to be enhanced over iron by [α/Fe]$\sim+0.3$ dex (McWilliam and Rich 1994; Rich and Origlia 2005; Cunha and Smith 2006; Fulbright et al. 2007; Lecureur et al. 2007; Rich et al. 2007) calling for a fast formation scenario, while metal-rich stars [Fe/H]>-0.3 showed a decrease in [α/Fe] reaching solar values for metallicities larger than Solar. However, it is important to note that not all elements were found to follow the same yield trends.

A relative approach has been commonly adopted instead of an absolute interpretation of the Bulge α-element ratio. The direct comparison of [α/Fe] values in Bulge stars against those of other galactic components then provides a relative time constraint on the bulge formation. Fulbright et al. (2007), Zoccali et al. (2006), and Lecureur et al. (2007) all came to the conclusion that the [α/Fe] ratio was enhanced by nearly $+0.1$ dex with respect to the trends of both the thin and the thick disc, thus implying a shorter formation time scale for the bulge than from both discs. However, as first pointed out by Meléndez et al. (2008), the bulge α-element over-enhancement with respect to the thick disc was a result of systematic offsets between abundance measurements in dwarf stars of the disc and giant stars from the Bulge. Later on, Alves-Brito et al. (2010) and Gonzalez et al. (2011) confirmed that when giants from the both bulge and the disc are homogeneously analyzed the Bulge followed the same over-abundance in α-elements as the thick disc, both being enhanced with respect to the thin disc at metallicities [Fe/H]<-0.2. At solar metallicities the Bulge stars are found to be α-poor, as poor as those of the thin disc. The way these trends are interpreted is that the metal-poor population of the bulge underwent a similarly fast formation scenario to that of the thick disc, while the metal-rich population of the bulge must have had a longer formation time scale, in similar time-scale to that of the thin disc stars. Similar conclusions have been reached in several other studies carried in different regions of the Bulge (Bensby et al. 2010, 2011; Ryde et al. 2010; Hill et al. 2011; Johnson et al. 2011, 2013, 2014).

However, open questions remain regarding the chemical similarities of Bulge stars with those of the thick disc stars, particularly in light of a few recent findings. Bensby et al. (2013a) suggested that the position in the [α/Fe] – [Fe/H] plot where [α/Fe] starts to decrease (referred to as the *knee* in the literature) is located at higher metallicities in the Bulge than in the thick disc. The position of the *knee* in the bulge may be 0.1–0.2 dex higher in metallicity in the Bulge than in the thick disc thus suggesting that the chemical enrichment of the metal-poor bulge has been somewhat faster than what is observed for the local thick disc. As the sample of Bulge micro-lensed dwarfs increases, it would be of great interest to further confirm the findings of Bensby et al. (2013a). As a matter of fact, a similar result was proposed by Johnson et al. (2014) who also added the analysis of Fe-peak elements finding in particular that Co, Ni, and Cu appear enhanced compared to the disc. It is important

to recall that the results presented in Johnson et al. (2014) have been obtained by comparing Bulge giants to dwarf stars from the local disc. This technique has been shown to suffer from systematic offsets by Meléndez et al. (2008). However, the detailed analysis by Johnson et al. (2014) has been carefully calibrated internally so it would be of great interest to confirm if these results are also found when bulge giant stars are compared to (inner) disc giant stars. These findings certainly highlight the importance of the future multi-object spectroscopic surveys on different galactic components to obtain a definitive answer.

9.5 The Bulge Kinematics

The observational properties of the Bulge regarding the morphology, age and chemical abundances seem to be independently providing evidence for a rather complex bulge stellar population, where at least a metal-poor, α-enhanced population of old stars co-exists with a metal-rich, α-poor population of both old and a fraction of young stars ($\sim$22 % according to Bensby et al. (2013a) but see Clarkson et al. (2011)). It is then natural to evaluate how the kinematics of each of these populations can help to solve the puzzle and answer the question on what is the nature of each of these components.

Following the initial attempts to constrain the kinematics of the bulge stars by measuring their radial velocities (Frogel and Whitford 1987; Rich 1988, 1990; Terndrup et al. 1995; Minniti 1996; Sadler et al. 1996; Tiede and Terndrup 1997) our understanding of the dynamical characteristics of the Bulge has gained an outstanding level of advancement thanks to the recent spectroscopic surveys that are able to sample radial velocities of thousands of M giants and red-clump stars across the Bulge.

In the most general view of Galactic bulge kinematics, the bulge is known to lie between a purely rotating system and a hotter system supported by velocity dispersion, with a $V_{max}/\sigma = 0.65$ (Minniti and Zoccali 2008). The Bulge Radial Velocity Assay survey (BRAVA; Howard et al. 2008; Kunder et al. 2012) was the first to provide a broad view of the bulge kinematics, perhaps finally allowing us to start looking at the Bulge from an extragalactic perspective. The BRAVA survey presented the mean radial velocity and velocity dispersion as a function of longitude, at different Bulge latitudes, showing evidence for cylindrical rotation of the bulge (BRAVA; Howard et al. 2008; Kunder et al. 2012) which is a characteristic feature of boxy/peanuts originating from secularly evolved bars.

The cylindrical rotation seen in M giants of BRAVA, later confirmed using red-clump stars by the ARGOS (Ness et al. 2013b) and GIBS (Zoccali et al. 2014) surveys, was modeled by Shen et al. (2010), who conclude that the bulge could not have more than 8 % of the disc mass in the form of a classical spheroid to reproduce

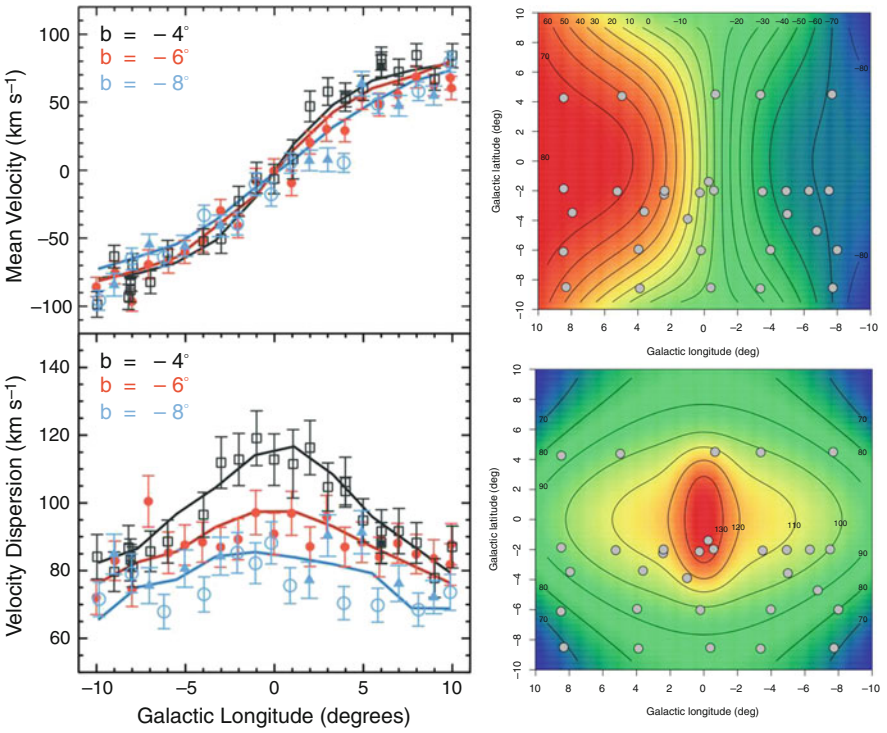

Fig. 9.5 *Left panels*: Velocity dispersion profile (*bottom*) and rotation curve (*top*) for latitudes b = −4°, −6°, and −8° from Kunder et al. (2012). *Solid lines* represent the models from Shen et al. (2010). *Right panels*: Radial velocity (*top*) and radial velocity dispersion (*bottom*) surface in the longitude-latitude plane constructed from the measured rotation profiles at negative latitudes from the GIBS survey by Zoccali et al. (2014). *Grey points* show the positions of the observed fields by the survey, while the *black contour lines* are labeled with the relevant velocity dispersion in km/s (*Left panel* adapted from Figure 11 in Kunder et al. (2012), reproduced by permission of the AAS. *Right panels* adapted from Figures 10 and 11 in Zoccali et al. (2014), reproduced with permission ©ESO)

BRAVA observations. Figure 9.5 shows the agreement between the BRAVA survey measurements at different latitudes compared to the pure disc models from Shen et al. (2010). Also shown in Fig. 9.5 are the radial velocity and velocity dispersion maps for the Bulge constructed by Zoccali et al. (2014) based on the GIBS survey observations.

However, dynamical models such as the one presented by Saha et al. (2012) have shown that if a spheroidal component, i.e. a classical bulge, was already present when the bar was formed then the classical bulge could spin-up and rotate faster than expected for its dispersion supported nature due to the effects of the bar potential

(Saha and Gerhard 2013). In these conditions, the detection of such a component based in kinematics alone would be very difficult (Gardner et al. 2014). Indeed, in order to understand the nature of these components the analysis of a connection between the kinematics and other stellar properties such as metallicity seems to be a key factor. Babusiaux et al. (2010) investigated the connections of metallicity and kinematics, the latter based on radial velocities and proper-motions, for the sample of Zoccali et al. (2008) at different latitudes along the bulge minor axis. They found that the high metallicity stars ([Fe/H]>-0.25) show a larger vertex deviations of the velocity ellipsoid than their metal-poor ([Fe/H]<-0.25) counterpart. Furthermore, metal-rich stars showed an increase in their velocity dispersion with decreasing latitude (moving closer to the galactic plane), while metal-poor stars show no changes in the velocity dispersion profiles. This information led Babusiaux et al. (2010) to associate the more metal-rich stars with a barred population and the metal-poor stars with a spheroidal component or even the inner thick disc. The rotation curves and dispersion profiles of the large sample of stars from the ARGUS survey (Fig. 9.6) led Ness et al. (2013b) to reach a similar conclusion to that of Babusiaux et al. (2010).

An additional piece of the puzzle has been provided thanks to the recent development of our understanding of the structural properties of the Bulge, in particular the discovery of the X-shape. Ness et al. (2013b) and Vásquez et al. (2013) investigated in more detail the connection between the X-shape bulge and its chemo-dynamical properties. Both studies showed that only the metal-rich stars ([Fe/H]> -0.5) trace the split red-clump in the luminosity function and therefore belong to the X-shaped bulge, while the metal-poor stars do not share the same split in magnitude.

Finally, important constraints on the bulge formation history can be obtained by looking at the radial velocities of a large number of stars. However, also having information on the proper motions for some of those stars in order to reconstruct the three-dimensional characteristics of the stellar orbits may become fundamental to disentangle the more complex characteristics of the Bulge. Although proper motions can be derived for large samples of stars based on photometric information obtained with relatively short exposure times, they require a long time baseline ($\sim$10 yr). Therefore, to obtain a very precise astrometric solution in order to reach the required accuracy of a few mas/yr across the bulge is perhaps more a luxury than a requirement. Indeed, studies that have used proper motion information in specific fields, combined with radial velocity measurements, have been able to unravel the perhaps otherwise hidden complexity of the Bulge (e.g. Zhao et al. 1994; Soto et al. 2007; Babusiaux et al. 2010). In this context, Vásquez et al. (2013) provided for the first time an analysis based on both the radial velocities and proper motions for both arms of the X-shape bulge, and were thus able to derive the complete space

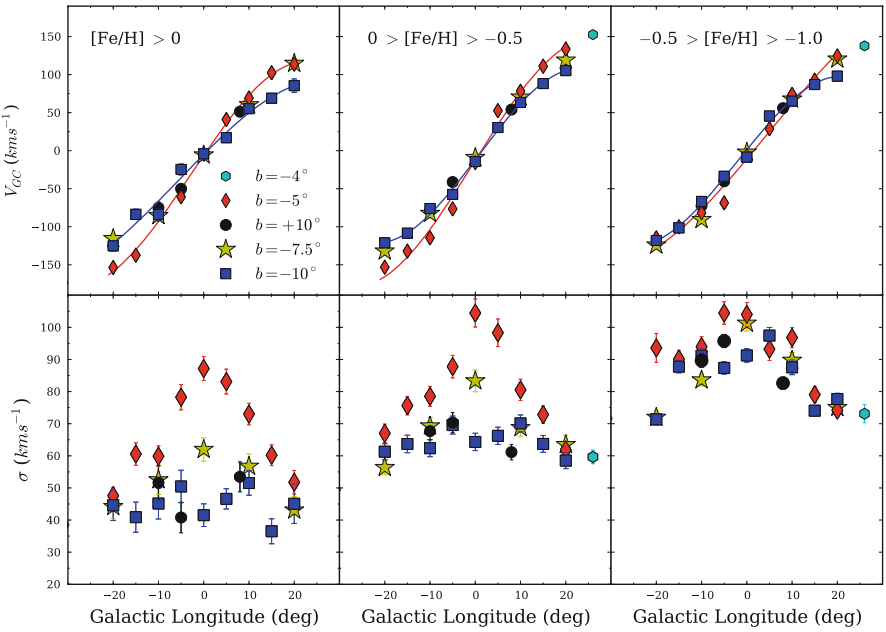

Fig. 9.6 Rotation (*top panel*) and velocity dispersion (*bottom panel*) across the bulge for the 16,600 stars from the ARGO survey with [Fe/H] >-1.0 within <3.5 kpc of the Galactic Center from Ness et al. (2013b). The three plots correspond to different metallicity bins, from *left* to *right* in decreasing [Fe/H]. Note that the discrete bins are used to represent stars of components A, B and C from *left* to *right* shown in Fig. 9.4. Although the rotation curves are similar, the dispersion clearly demonstrates the difference in kinematics of stars with [Fe/H]> -0.5 and with [Fe/H]<-0.5. There are 3,100, 8,600 and 4,900 stars in each plot, from *left* to *right*. The *red diamonds* are b $= -5°$, the *yellow stars* are b $= -7.5°$, the *blue rectangles* are b $= -10°$ and the *black circles* are b $= +10$ (Figure adapted from Figure 6 in Ness et al. (2013b))

velocities in the U, V, W Galactic Cartesian system for a sample of spectroscopic targets in the field l,b $= (0°,-6°)$. As shown in Fig. 9.7, Vásquez et al. (2013) showed how the closer over-density of the X-shaped bulge shows an excess of stars moving towards the Sun, and the far overdensity shows an excess of stars receding from the Sun, as expected from stars on elongated orbits streaming along the arms of the X-shaped bulge. A wider mapping of these are the key signatures of the detailed kinematics of the bulge, thus expanding the study of Vásquez et al. (2013) to other Bulge regions, will become an important ingredient for an accurate modelling of the bulge and will perhaps allow a better identification of its different components (Gardner et al. 2014).

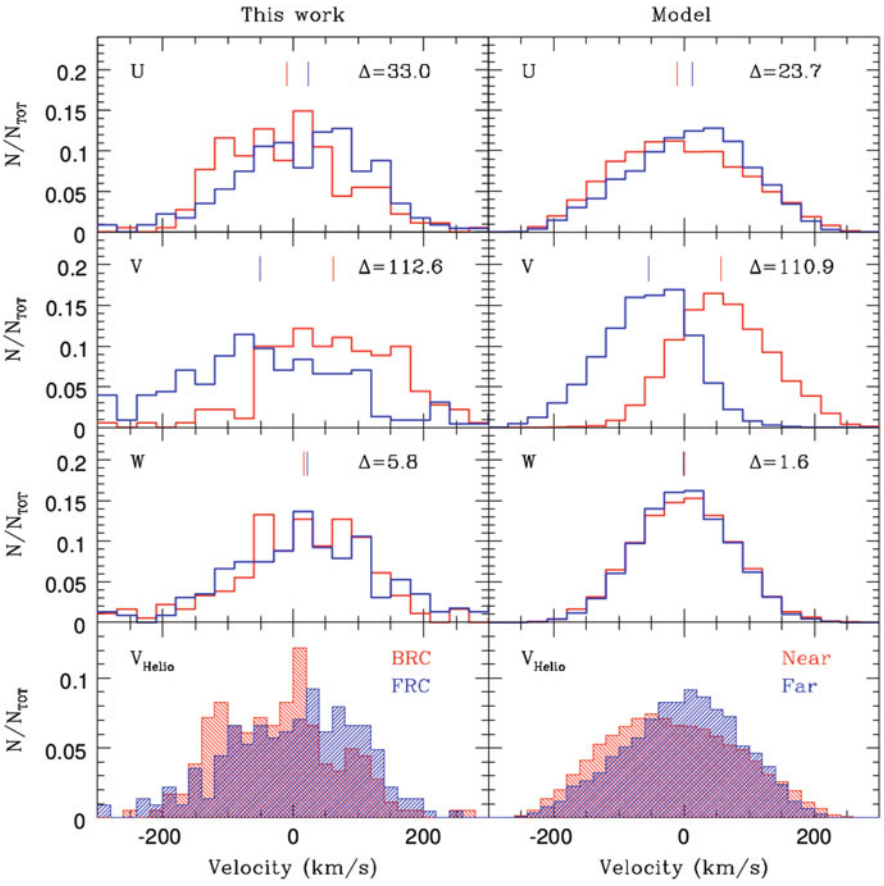

Fig. 9.7 Comparison of the kinematics of the bright and faint red clump of the Bulge with respect to the kinematical model for a strong boxy-peanut bulge (Debattista et al. 2005) obtained from Vásquez et al. (2013). From the model, two samples were selected from the two overdensities formed by the near (*red*) and far (*blue*) arms of the boxy-peanut stellar distribution in the line of sight for (l,b) = (0°, −6°). Colour lines over U, V, and W histograms correspond to the median value for each distribution (Figure adapted from Figure 7 in Vásquez et al. (2013), reproduced with permission ©ESO)

9.6 The Milky Way Bulge in a Nutshell

The properties of the Galactic bulge described above can be summarised as follows:

- The Bulge stellar population properties show independent evidence for a multiple component scenario, with different morphological and dynamical characteristics. The metallicity distribution can be separated in, at least, a main metal-poor and a metal-rich components. Their different contributions across the Bulge produces

a vertical metallicity gradient of ∼0.6 dex/kpc which seems to flatten in the inner 700 pc. From a morphological/structural viewpoint, there is strong evidence of a boxy/peanut, while more recent work points out the existence of a component with different geometrical properties, as seen in the spatial distribution of RR Lyrae stars, which trace the oldest Galactic population (Fig. 9.1). The next two bullet points connect these structural components to differences observed also in chemical content, age and dynamics.

- There is a metal-rich (mean [Fe/H]∼0.3), α-poor population of stars in the bulge, composed mostly by old stars but with a fraction of young stars. This population of stars rotates cylindrically and shows a large vertex deviation consistent with the bar structure traced with a position angle of ∼27 deg. At latitudes $|b| > 5°$ the inner parts of the bar have grown out of the disc plane, originating the boxy/peanut. These metal-rich stars further show the split red-clump in the luminosity function tracing the X-shape of the Bulge.
- The metal-poor bulge population (mean [Fe/H]∼−0.3) is composed predominantly by old stars and it shows an alpha-enhancement similar to that of the local thick disc. The kinematics of these stars follow a more spheroidally distributed population than the one traced by the metal-rich stars, consistent with the structure traced by the bulge RR Lyrae stars. Furthermore, these stars do not trace the X-shape morphology of the Bulge.

9.7 The Milky Way Bulge in the Context of External Galaxies

9.7.1 The X-Shaped Bulge of the Milky Way: How Rare Is This?

It can be argued that while in the context of Galactic research boxy/peanuts are somewhat a recent discussion, in extragalactic studies such structures are known for about twice as much the time. So it came as no surprise to the extragalactic community when evidence suggested that the Milky Way has a boxy/peanut, especially because there is also evidence that it has a bar. Perhaps the first mention in the literature about these deceptively unusually-looking structures is from Burbidge and Burbidge (1959), referring to the prototypical example that is NGC 128 (see also Sandage 1961). More detailed investigation came with de Vaucouleurs (1974), Jarvis (1986) and Shaw (1987). But it was in the pioneering studies of de Souza and Dos Anjos (1987) that the major step of connecting these structures with bars was made for the first time from an observational viewpoint, using a statistical argument. Basically, they argued, the frequency of boxy/peanuts in edge-on lenticulars is similar to that of bars in face-on lenticulars, consistent with the idea that boxy/peanuts are bars seen at a different projection. This conclusion was corroborated years later by Lütticke et al. (2000), who reported a fraction >40 % of boxy/peanuts in disc galaxies covering most of the Hubble sequence (from S0 to Sd classes).

The complicating factor here is of course the fact that bars are difficult to be seen when the inclination angle of the galaxy is too large. Therefore, simulations of barred galaxies played a major role here. In fact, the starting point for this observational connection between bars and boxy/peanuts was the work published in Combes and Sanders (1981). These authors have shown, using collisionless simulations, that bars seen at a given edge-on projection show a very characteristic peanut-like morphology.

A number of studies came thereafter dedicated to extend this connection into a dynamical context. Kuijken and Merrifield (1995) came up with an ingenious diagnostic to test in this context whether boxy/peanuts are just bars seen at a different projection. This consisted in producing diagrams in which the line of sight velocity is plotted against the galactocentric radius for highly inclined or edge-on systems. By producing such diagrams corresponding to orbits in a purely axisymmetric potential, and orbits in a barred potential, they showed that the presence of a bar produces a clear distinctive signature. Because at a region around the bar corotation radius (the radius at which the pattern speed of the bar matches the local circular speed) there are no close, non-self-intersecting orbits available, clear gaps appear in this diagram, producing a figure-of-eight pattern. The matter became then just to produce such diagrams for galaxies presenting boxy/peanuts in order to test for the presence of a bar. Kuijken and Merrifield (1995) did that for NGC 5746 and NGC 5965, providing observational evidence that boxy/peanuts and bars are related phenomena.

More evidence was produced in Merrifield and Kuijken (1999) and Bureau and Freeman (1999). To this point, almost all galaxies with boxy/peanuts studied showed evidence of a bar. In only a few extreme cases the boxy/peanut could have formed through accretion of external material. In addition, none of the galaxies without boxy/peanuts showed signatures of a bar. Further development also happened in the theoretical background. Bureau and Athanassoula (1999) refined and corroborated the orbital study of Kuijken and Merrifield (1995), while Athanassoula and Bureau (1999) provided strong support to the bar detection diagnostic with hydrodynamical simulations.

It must be noted that the detailed morphology of boxy/peanuts, i.e. if they either have a boxy shape, a peanut shape or an X shape, depends on projection effects, as well as the strength of the boxy/peanut. More about X shape bulges can be found in Laurikainen and Salo (this volume), but essentially the X shape is more clear in the strongest peanuts. Techniques such as unsharp masking are able to reveal X shapes more clearly when the peanut is not so pronounced. Therefore, all these morphologies come actually from the same physical process, i.e. the increase in the vertical extent of stellar orbits in the inner parts of the bar. Both simulations and observations point out that boxy/peanuts extend to galactocentric distances which are about a third to a half of the bar semi-major axis (see Erwin and Debattista 2013). What causes this change in the orbits vertical extent is reviewed in detail by Athanassoula (this volume). In the Milky Way, we see the extension of the B/P to galactocentric distances of $\sim$1.5 kpc, which is nearly two-thirds the length of the semi-major axis of the long bar of 2–2.3 kpc (Hammersley et al. 2000; Benjamin et al. 2005; López-Corredoira et al. 2007).

A review on the observed properties of boxy/peanuts in external galaxies is given by Laurikainen and Salo (this volume). They also discuss a structure called barlens, which is interpreted as the projection of boxy/peanuts when seen face-on. This structure was noticed by Laurikainen et al. (2005), who included a model to fit barlenses in their image decompositions. Later, based on Fourier analysis, Laurikainen et al. (2007) suggested that barlenses are part of the bar, while Gadotti (2008) also noticed their existence in a sample of local barred galaxies. However, only in Laurikainen et al. (2011) the term 'barlens' is introduced as a new morphological feature in galaxies. Very recently, more detailed studies have made a robust connection between barlenses and boxy/peanuts (Laurikainen et al. 2014; Athanassoula et al. 2014). This connection implies that also on the plane of the disc, the stellar orbits in the inner part of the bar become wider. Figure 9.8 describes schematically the connection between bars, boxy/peanuts and barlenses.

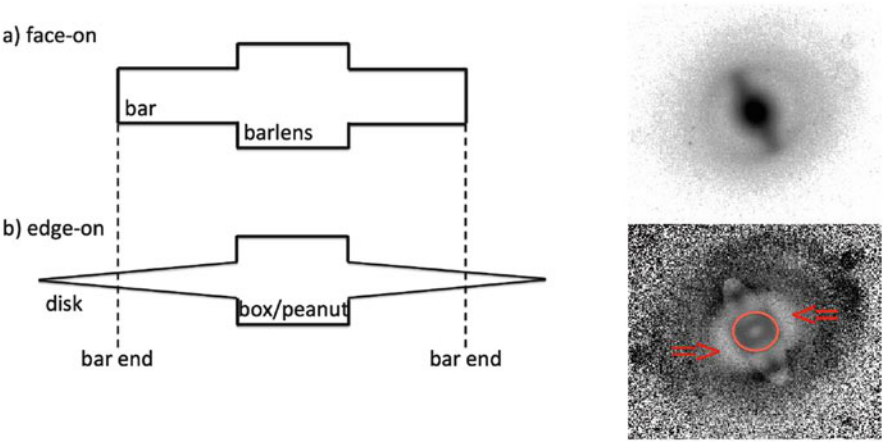

Fig. 9.8 Connection between bars, boxy/peanuts and barlenses. The diagram on the *left* shows a schematic representation of a barred galaxy seen (**a**) face-on, and (**b**) edge-on. boxy/peanuts can be seen at edge-on projections, but the flat, more extended part of bar is difficult to realize, as its vertical extent is similar to that of the disc. The same galaxy seen face-on would reveal the bar and barlens. The barlens and the boxy/peanut appear to be the same structure seen at different projections (see Laurikainen and Salo (this volume) and Athanassoula (this volume)). The panels on the *right* show an *R*-band image of NGC 4608 (*top*), where the bar and barlens can be clearly seen (see also Laurikainen et al. 2005, 2007, 2011). The *bottom panel* shows a residual image, after the subtraction of a 2D model of the bulge, bar and disc of this galaxy. In the residual image the barlens stands out even more clearly. The *red circle* points out the barlens. This circle was not in the original Gadotti (2008) paper, but added now that we understand that the structure is a barlens.[2] The *red arrows* point out empty regions in the disc within the bar radius, where stars from the disc were captured by the bar (*Right panels* adapted from Gadotti (2008))

[2]Editorial comment: barlenses are recognized from direct images – without any assumption of massive classical bulges first subtracted from the images, as done in Fig. 9.8. By definition barlenses are not inner discs embedded in classical bulges.

The presence of barlenses in external galaxies suggests of course that our own Milky Way may have such structural component. Since the stars in barlenses seem to be contained within the disc plane, in the Milky Way, they are seen in projection, in the foreground and background with respect to the Galactic center. They thus complicate even further the interpretation of observations of the Milky Way, such as those discussed above. These stars are stars within the bar and then have chemical properties and ages similar to those of other bar stars – they are boxy/peanut stars. From a kinematical point of view, barlenses are different from discs and this is a promising avenue to separate them from the other stellar populations seen from the Sun at the direction of the Milky Way central regions.

9.7.2 Bulge Formation Scenarios

The formation of bulges in general, and of the Milky Way bulge in particular, have been discussed many times elsewhere (e.g. Aguerri et al. 2001; Kormendy and Kennicutt 2004; Athanassoula 2005; Laurikainen et al. 2007; Hopkins et al. 2010; Fisher and Drory 2010; Gadotti 2012, see also Bournaud, and Brooks and Christensen, this volume). Here we will assess each bulge formation scenario in the light of evidence obtained from data on the Milky Way bulge, as presented above. There is mounting evidence that the Milky Way has a bar and a boxy/peanut, and thus secular evolution processes induced by bars in disc galaxies must have played a non-negligible role in the evolution of the Galaxy. On the other hand, a scenario in which the Galactic bulge was formed in violent processes such as mergers has weak support from data. In fact, an important question that observers must focus now is whether the Galaxy has a merger-built central stellar component at all.

9.7.2.1 Bulges Formed via Disc Instabilities

Dynamical disc instabilities can originate bars, spiral arms and ovals, the latter being just a distortion in the disc stellar orbits that make them acquired less circular orbits, but not as eccentric as those in bars. All these structures, being non-axisymmetric, produce perturbations in the galaxy potential, with the result that material (gas and stars) within the corotation resonance radius loses angular momentum, whereas material outside the corotation radius absorb this angular momentum. The effect is particularly important for the collisional gas component, which thus falls towards the center. At some point, the in-falling gas gets compressed and form stars, contributing to a rejuvenation of the stellar population in the central regions (e.g. Gadotti and dos Anjos 2001; Fisher 2006; Coelho and Gadotti 2011; Ellison et al. 2011).

Because most disc galaxies with bars should have one or two Inner Lindblad Resonances (ILRs) near the center ($\sim$ a hundred to a few hundred parsecs from it), the in-falling gas cannot reach the galaxy center immediately (see Fig. 9.9). Instead,

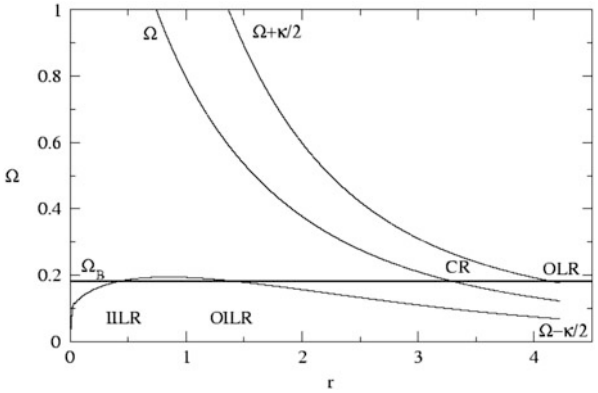

Fig. 9.9 Angular speed of stars in circular orbits in a potential reproducing a disc galaxy with a bar, as a function of the galactocentric distance (in arbitrary units). The bar pattern speed is represented by the *solid horizontal line* (Ω_B). The epicyclic frequency of the stellar orbits is denoted by κ. Barred galaxies present several dynamical resonances. This figure shows schematically how four of the main resonances come to be. Whenever the bar pattern speed is equal to Ω or $\Omega \pm \kappa/2$ this is the position of a dynamical resonance. From the center outwards, the resonances depicted here are: the Inner Lindblad Resonance, the Outer Inner Lindblad Resonance, Corotation, and the Outer Lindblad Resonance. In this case, the main families of stellar orbits change their orientation by 90° at each resonance. This effect is at the origin of a number of dynamical effects in barred galaxies, in particular the transfer of angular momentum from material inside the corotation radius to material outside this radius, and the resulting formation of disc-like bulges.

it usually forms an inner disc, decoupled from the large-scale disc. These inner discs may form nuclear bars and spiral arms, as often observed, and are often called disc-like bulges (see e.g. Athanassoula 2005; Gadotti 2012) or discy pseudobulges, to contrast with the fact that boxy/peanuts are often called as well pseudobulges (see Kormendy and Kennicutt 2004). At the ILRs gas can get accumulated and compressed, often forming a star-bursting nuclear ring.

However, it must be noted that simulations indicate that, initially, the infall of gas within a bar corotation radius occurs rapidly after the formation of the bar, with a time scale of the order of 10^8 years, i.e. a dynamical time (Athanassoula 1992; Emsellem et al. 2014).[3] This means that disc-like bulges not necessarily present ongoing star formation or a very young stellar population, if the bar has formed long ago and have been able to push most of the gas to the center quickly, and if the gas content in the disc is not being replenished. Sheth et al. (2008, 2012) present

[3]Gas outside corotation receives angular momentum from the bar, and other factors govern the gas infall rate at these outer radii, such as dynamical effects induced by spiral arms and the dissipative nature of the ISM. At these distances the infall of gas no longer occurs in a dynamical time scale.

results that suggest that the first long-standing bars[4] formed after redshift 1. These bars are still the ones seen at redshift zero, since bars are difficult to destroy, unless the disc is extremely gas-rich (see Athanassoula et al. 2005; Bournaud and Combes 2002; Bournaud et al. 2005; Kraljic et al. 2012). This means that they first induced star formation at the centers of their host galaxies about 8 Gyr ago. Thus, disc-like bulges with stars as old as 8 Gyr are perfectly possible.

For the disc to be replenished with gas so that the bar can push this gas to the center and produce a new central burst of star formation and rebuilding of the disc-like bulge, it has to fall into the disc plane from a direction not parallel to the galaxy disc, and inside the bar corotation radius. Otherwise, this gas will be pushed outwards by the bar or accumulate at the corotation (see Bournaud and Combes 2002). Evidence for gas infall from directions not parallel to the galaxy disc has recently been presented by Bouché et al. (2013), but how often it occurs is still unknown, as is whether the gas reaches the disc within corotation.

Thus, although Ellison et al. (2011) find that, statistically, barred galaxies present ongoing, central star formation more often than unbarred galaxies, there is still a significant fraction of barred galaxies with star formation rates comparable to those in unbarred galaxies. In addition, Coelho and Gadotti (2011) find that the younger bulges found in barred galaxies have a mean stellar age of a few Gyr. This is in contrast to unbarred galaxies, which show on average older mean stellar ages (see Fig. 9.10). This means that replenishing the disc with gas inside the corotation radius is a phenomenon that does not occur very often. Otherwise, very young stellar populations should be more conspicuous at the centers of barred galaxies.

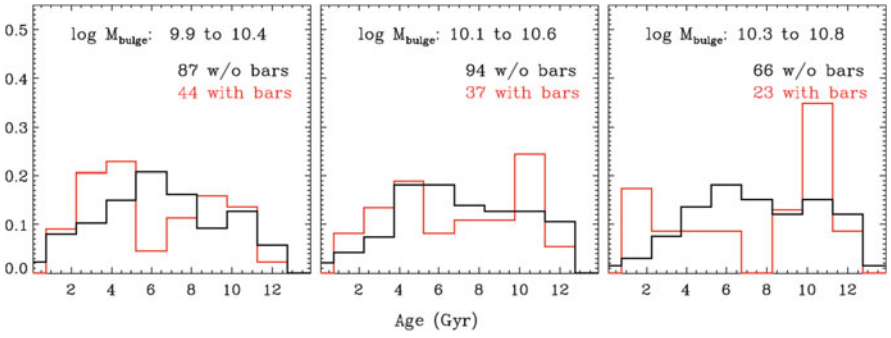

Fig. 9.10 Relative distributions of bulge mean stellar ages for barred and unbarred galaxies in bins of bulge stellar mass, as indicated. For massive bulges, the distribution is bimodal only for barred galaxies, consistent with the picture in which secular evolution processes build disc-like bulges. However, note that the mean stellar ages of such bulges can be as high as a few Gyr (Adapted from Coelho and Gadotti 2011)

[4]Some simulations (Kraljic et al. 2012) have reported the early formation of bars, at redshifts above 1. However, these bars are short-lived. In these simulations, bars formed at ≤ 1 generally persist down to $z = 0$.

As discussed above, Bensby et al. (2013b) find a stellar component in the Milky Way bulge with ages less than 5 Gyr. Although this means that the mean stellar age for the Milky Way bulge as a whole is above this value, this younger component has a mean stellar age thus in very good agreement with the mean stellar ages of the young bulges in other barred galaxies. The bottom line is that stars originating from gas infall to the center through disc instabilities do not necessarily have to be extremely young now. A fraction of these younger stars could be elevated out of the disc plane and populate the boxy/peanut, but most of these stars are expected to be at or near the large scale disc plane.

Some studies using both simulations and observations have suggested that some star formation may occur along the bar as soon as the bar forms and induces shocks in the gas content in the interface between the bar and the disc (see Athanassoula 1992; Phillips 1996; Sheth et al. 2002). However, they also indicate that, due to shearing in the gas clouds when they start falling towards the center, this is interrupted shortly afterwards, and from then on, star formation is limited to components at the bar ends and the disc center. Discs stars trapped by the bar mostly do not leave the bar, keeping their elongated orbits. As it evolves, however, the bar can capture stars from the disc formed more recently (see an example of such capture in the right panels of Fig. 9.8), and thus a fraction of young stars can be present in the bar, as long as there is ongoing star formation in the disc within the radius at which the bar ends, and the bar can grow stronger and keep capturing disc stars. Stars in bars are thus predominantly old, and therefore boxy/peanuts, being just part of bars, should as well be populated mostly by old stars, with some younger component.

For a galaxy as massive as our own, the bar is expected to form at redshifts close to 1 (see Sheth et al. 2012). The ages of the stellar populations seen at the Galactic bulge are thus consistent with the picture of it being built purely from the bar instability in the disc, i.e. the Galactic bulge can well be just a boxy/peanut plus a disc-like bulge, as far as the ages of its stellar populations are concerned.

In trying to assess how the bulge of the Galaxy has formed, the chemical content of its stellar populations are better considered closely with their kinematical properties. Bars and their boxy/peanuts are expected to rotate cylindrically, i.e. the mean stellar velocity is independent of the height above the plane of the disc – as a rigid body. Variations in this pattern are usually attributed to the presence of other structural components with different kinematical properties (see e.g. Williams et al. 2011, and references therein). As discussed above, one stellar population in the Bulge can be described as having high metallicity, low content of α-elements, and kinematics consistent with the eccentric stellar orbits in bars in cylindrical rotation. The α-element content thus indicates that the boxy/peanut formed after the thick disc. In external galaxies, recent evidence suggests that thick discs form early, during the short initial formation stages of the galaxy, which qualitatively agrees with the picture for the Milky Way (Comerón et al. 2011, 2014). Nevertheless, although most of the thick disc stars thus form in situ, a significant fraction of stars in the thick disc may come from the accretion of satellites, and another fraction

(likely smaller), may consist of heated up stars from the thin disc. Evidently, this complicates substantially the interpretation of observations.

Likewise, the observations from the ARGUS survey indicating variations in metallicity within the boxy/peanut (see Sect. 9.4.1), are suggestive of a complex stellar population content in the boxy/peanut itself. This can be a result of similar processes that complicate just as well the stellar population content of the thick disc, as described in the previous paragraph. As discussed in Sect. 9.4, different populations or population gradients in the disc from which the boxy/peanut forms can produce a similar result. However, it can also be the result of more than one buckling event forming the boxy/peanut. In the simulations of Martinez-Valpuesta et al. (2006) a bar goes through a first buckling event about 2 Gyr after the beginning of the simulation, and this event is fast (<1 Gyr). However, a second, powerful buckling event occurs around 5 Gyr later and lasts for about 3 Gyr. How this would affect the chemical content of stars seen today in the boxy/peanut depends on how the stellar population content and kinematical properties of the bar and boxy/peanut vary during these periods. But it is clear that if the bar of the Milky Way has gone through such recurrent buckling, the presence of multiple populations in the boxy/peanut is not surprising. Add this to the complex composition of the thick disc and one sees how complicated the stellar populations can be away from the disc plane.

9.7.2.2 Bulges Formed via Violent Processes

The classical picture of bulges in disc galaxies is that of mini-ellipticals: massive, smooth and extended spheroids with dense centers, with old stellar populations showing α-enhanced chemical composition and relatively low rotational support (as compared to discs). A natural formation scenario for these structural components would be that of a monolithic collapse (Eggen et al. 1962), in which a single gas cloud collapses in short time scales ($<10^8$ yr), producing a violent burst of star formation that originates the stellar halo and the bulge. While this scenario might explain the formation of the first spheroids, it faces many difficulties. It does not reproduce for instance the heterogenous distributions of stellar ages and metallicities observed in bulges (e.g. McWilliam and Rich 1994; Wyse et al. 1997, a monolithic collapse implies a more homogeneous population) and regions of ongoing star formation (e.g. Carollo et al. 1997).

It should be noted, however, that the monolithic collapse scenario was formulated within a perspective that does not include boxy/peanuts, and thus should not be compared against the properties of such observed structures. On the other hand, modern dissipative collapse models similar to the pioneer model of Eggen et al. (1962), that however include as well cosmological ingredients, generate bulges with more realistic properties. Such key ingredients include in particular a long time scale history of accretion of dark matter haloes into the central halo, with the associated evolution of angular momentum and star formation episodes (see e.g. Samland and Gerhard 2003; Obreja et al. 2013).

A natural picture within ΛCDM cosmology is that of merger-built bulges. Brooks and Christensen (this volume) review this picture. Another scenario to explain the formation of classical bulges is the coalescence of clumps in discs at high redshifts. This is also reviewed in this volume by Bournaud.

The evidence from observations of the Galactic bulge as reviewed above, however, give little support to the presence of a massive classical bulge. The observed boxy/peanut and its cylindrical rotation cannot be originated in violent scenarios. On the other hand, the possibility of a small classical bulge embedded within the boxy/peanut is not yet ruled out. Such composite bulges are discussed in the next section.

Nevertheless, we have seen above that there is a component in the Galactic bulge with low metallicity and an α-element content consistent with it being formed concomitantly with the thick disc, i.e. *before* the boxy/peanut. In addition, the morphological properties of this component seem to point out a more spherically distributed structure (see Fig. 9.1). This is revealed by RR Lyrae stars and are properties that are shared by classical bulges. This component has a spatial extent similar to that of the boxy/peanut, but it is not revealed by images such as those from COBE. However, a number of early-type disc galaxies with massive classical bulges show bars, which probably went through a buckling process that originated a boxy/peanut. So it is perfectly plausible to have a classical bulge and a boxy/peanut coexisting in the same galaxy. A possible example is our own massive neighbor, M31. Athanassoula and Beaton (2006) have shown that this galaxy has a bar and a boxy/peanut, and there is evidence that it also hosts a classical bulge (e.g. Courteau et al. 2011, and references therein). 2D decompositions in Gadotti and Erwin (in preparation) show that the classical bulge has a similar extent as the boxy/peanut. The morphology of the M31 bulge (see Fig. 2 in Athanassoula and Beaton 2006) is similar to that seen in the COBE/DIRBE image for the Milky Way, although the vertices of the boxy/peanut are more clearly recognized in the Galaxy (perhaps due to projection effects in M31). Nevertheless the same 2D decompositions of Gadotti and Erwin reveal the X shape outstandingly (see Gadotti 2012). Another critical issue is the understanding of how bright/massive is the component revealed by RR Lyrae stars in the Galaxy, and how does this compare to other classical bulges. It clearly cannot be large enough as to mask the vertices of the boxy/peanut revealed by COBE.

9.7.2.3 Composite Bulges

In the previous subsections, we explored the possibility that the Milky Way has a disc-like bulge, apart from its boxy/peanut. We also remarked about the possibility of a classical bulge. Here we will briefly summarise recent work on the presence of such composite bulges in external galaxies. It is not hard to contemplate the possibility of such composite systems. A pure disc galaxy can form at high redshifts, say $z \sim 3$, and acquire a classical bulge, be it through minor mergers, accretion events or the coalescence of clumps of stars and gas in the disc. At $z \sim 1$ the

same disc – now hosting a classical bulge at its center – might become unstable to the formation of a bar, and develop one. Quickly this bar pushes gas to the central regions of the disc, originating a disc-like bulge. Give it a couple of Gyr and the boxy/peanut is formed. We thus end up with a galaxy containing a classical bulge, a disc-like bulge, and a boxy/peanut.

Gadotti (2009) has shown evidence that 34 % of his disc galaxies hosting classical bulges are galaxies possessing bulges with structural properties typical of classical bulges, but with an intensity of star formation activity characteristic of disc-like bulges. While one cannot rule out the possibility that some classical bulges may present ongoing star formation, it is also plausible that many of these galaxies actually host composite bulges. Those would be composed by an extended classical bulge with an embedded disc-like bulge. Because the classical bulge dominates the disc-like bulge in terms of mass, the composite bulge shows structural properties of classical bulges. However, using the $D_n(4{,}000)$ spectral index, Gadotti (2009) was able to realize the intense star formation in the bulge region. Such star-forming activity, according to this interpretation, occurs at the embedded disc-like bulge. Further evidence for this and other types of composite bulges is presented in Méndez-Abreu et al. (2014).

Kormendy and Barentine (2010) report the existence of a small disc-like bulge embedded in the boxy/peanut of NGC 4565. Nowak et al. (2010) argue that NGC 3368 and NGC 3489 actually have an embedded classical bulge within component(s) built via disc instabilities. Finally, very recently, Erwin et al. (2014) have shown further evidence of such components that appear to be embedded in classical bulges.

It will thus be no surprise if the Galactic bulge is a composite bulge.

9.8 Concluding Remarks

In this review we have presented a summary of current progress towards characterising the properties of the Milky Way bulge. In recent years, the spectroscopic and photometric surveys of the Bulge have provided us with the necessary tools to build a bridge connecting the detailed stellar population properties with a global view of the Galactic bulge. As a consequence, it is now becoming possible to discuss the Bulge properties as seen from an extragalactic perspective. Such a comparison, powered by the increasing number of models to which observations can now be directly compared, is the only way in which we can set the history of events that led to the properties of the Bulge we see today.

The era of surveys looking towards the Galactic bulge was born not only from our intrinsic desire to explore, but also as a response to the increasing complexity in Bulge properties revealed with previous individual observations. The need to further map its morphology, to better constrain the spatial variations of its stellar populations and subsequently connect it with their kinematics required the larger spatial coverage offered by such large-scale observations.

While the dominant B/P nature of the Milky Way bulge has now been well established, it remains to be understood if the observed stellar population properties relate solely to the same structure or if they each have a different origin. Another way to phrase this would be to ask the following question: do the metal-poor, α-element enhanced, old bulge stars belong to a different structure than the B/P, which was formed somehow independently to the buckling instability process of the bar (i.e. as a classical bulge)? Currently, while we have important evidence from the connections between kinematics and metallicities of Bulge stars as well as their spatial distribution, we can only suspect about the presence of different components. However, creating the link between these components and the specific formation scenarios should be done with extreme caution, as a number of processes could have played a specific role at different stages of the assembly of the Galaxy. For example, the coalescence of disc clumps and the accretion of gas could have formed a thin disc, a thick disc, and even a spheroid in the center during the early stages of formation of the Milky Way. The merging history could have also contributed to this assembly, which will depend on gas content, mass ratio and orbital parameters of the mergers, until the formation of a bar and the onset of the buckling instability took place to shape the dominant central component we see today – the B/P Bulge. Only by carrying out an extensive comparison of all the observational properties of Bulge stars with models and external galaxies, can we constrain the importance of all these events during the formation history of the Bulge.

Acknowledgements We are grateful to an anonymous referee for many useful comments. We warmly thank Istvan Dekany for kindly providing us the table of individual distances to the RR-lyrae that we used to produce Fig. 9.1.

References

Abadi MG., Navarro JF., Steinmetz M., Eke VR. 2003, ApJ, 591, 499
Aguerri J.A.L., Balcells M., Peletier R.F. 2001, A&A, 367, 428
Alves-Brito A., Meléndez J., Asplund M., Ramírez I., Yong D. 2010, A&A, 513, A35
Amôres E.B., López-Corredoira M., González-Fernández C., Moitinho A., Minniti D., Gurovich S. 2013, A&A, 559, A11
Athanassoula E. 1992, MNRAS, 259, 345
Athanassoula E. 2005, MNRAS, 358, 1477
Athanassoula E. 2012, MNRAS, 426, L46-
Athanassoula E., Beaton R.L. 2006, MNRAS, 370, 1499
Athanassoula E., Bureau M. 1999, ApJ, 522, 699
Athanassoula E., Lambert J.C., Dehnen W. 2005, MNRAS, 363, 496
Athanassoula E., Laurikainen E., Salo H., Bosma A. 2014, ArXiv e-prints 1405.6726
Baade W. 1951, Galaxies - Present Day Problems. Publications of Michigan Observatory 10, 7
Babusiaux C., Gilmore G. 2005, MNRAS, 358, 1309
Babusiaux C., Gómez A., Hill V., Royer F., Zoccali M., Arenou F., Fux R., Lecureur A., Schultheis M., Barbuy B., Minniti D., Ortolani S. 2010, A&A, 519, A77
Bekki K., Tsujimoto T. 2011, MNRAS, 416, L60

Benjamin RA., Churchwell E., Babler BL., Indebetouw R., Meade MR., Whitney BA., Watson C., Wolfire MG., Wolff MJ., Ignace R., Bania TM., Bracker S., Clemens DP., Chomiuk L., Cohen M., Dickey JM., Jackson JM., Kobulnicky H.A., Mercer E.P., Mathis J.S., Stolovy S.R., Uzpen B. 2005, ApJ, 630, L149

Bensby T., Feltzing S., Johnson JA., Gould A., Adén D., Asplund M., Meléndez J., Gal-Yam A., Lucatello S., Sana H., Sumi T., Miyake N., Suzuki D., Han C., Bond I., Udalski A. 2010, A&A, 512, A41

Bensby T., Adén D., Meléndez J., Gould A., Feltzing S., Asplund M., Johnson J.A., Lucatello S., Yee J.C., Ramírez I., Cohen J.G., Thompson I., Bond I.A., Gal-Yam A., Han C., Sumi T., Suzuki D., Wada K., Miyake N., Furusawa K., Ohmori K., Saito T., Tristram P., Bennett D. 2011, å, 512, A41

Bensby T., Yee JC., Feltzing S., Johnson JA., Gould A., Cohen JG., Asplund M., Meléndez J., Lucatello S., Han C., Thompson I., Gal-Yam A., Udalski A., Bennett D.P., Bond I.A., Kohei W., Sumi T., Suzuki D., Suzuki K., Takino S., Tristram P., Yamai N., Yonehara A. 2013a A&A, 549, A147

Bensby T., Yee JC., Feltzing S., Johnson JA., Gould A., Cohen JG., Asplund M., Meléndez J., Lucatello S., Han C., Thompson I., Gal-Yam A., Udalski A., Bennett D.P., Bond I.A., Kohei W., Sumi T., Suzuki D., Suzuki K., Takino S., Tristram P., Yamai N., Yonehara A. 2013b, A&A, 549, A147

Binney J., Gerhard O., Spergel D. 1997, MNRAS, 288, 365

Bissantz N., Gerhard O. 2002, MNRAS, 330, 591

Blitz L., Spergel D.N. 1991, ApJ, 379, 631

Bouché N., Murphy M.T., Kacprzak G.G., Péroux C., Contini T., Martin C.L., Dessauges-Zavadsky M. 2013, Science, 341, 50

Bournaud F., Combes F. 2002, A&A, 392, 83

Bournaud F., Combes F., Semelin B. 2005, MNRAS, 364, L18

Burbidge E.M., Burbidge GR. 1959, ApJ, 130, 20

Bureau M., Athanassoula E. 1999, ApJ, 522, 686

Bureau M., Freeman K.C. 1999, AJ, 118, 126

Cabrera-Lavers A., Hammersley P.L., González-Fernández C., López-Corredoira M., Garzón F., Mahoney T.J. 2007, A&A, 465, 825

Cao L., Mao S., Nataf D., Rattenbury N.J., Gould A. 2013, MNRAS, 434, 595

Carollo C.M., Stiavelli M., de Zeeuw P.T., Mack J. 1997, AJ, 114, 2366

Churchwell E., Babler B.L., Meade M.R., Whitney B.A., Benjamin R., Indebetouw R., Cyganowski C., Robitaille T.P., Povich M., Watson C., Bracker S. 2009, PASP, 121, 213

Clarkson W., Sahu K., Anderson J., Smith T.E., Brown T.M., Rich R.M., Casertano S., Bond H.E., Livio M., Minniti D., Panagia N., Renzini A., Valenti J., Zoccali M. 2008, ApJ, 684, 1110

Clarkson W.I., Sahu K.C., Anderson J., Rich R.M., Smith T.E., Brown T.M., Bond H.E., Livio M., Minniti D., Renzini A., Zoccali M. 2011, ApJ, 735, 37

Coelho P., Gadotti DA. 2011, ApJ, 743, L13

Combes F., Sanders R.H. 1981, A&A, 96, 164

Comerón S., Elmegreen B.G., Knapen J.H., Salo H., Laurikainen E., Laine J., Athanassoula E., Bosma A., Sheth K., Regan M.W., Hinz JL., Gil de Paz A., Menéndez-Delmestre K., Mizusawa T., Muñoz-Mateos JC., Seibert M., Kim T., Elmegreen D.M., Gadotti D.A., Ho L.C., Holwerda B.W., Lappalainen J., Schinnerer E., Skibba R. 2011, ApJ, 741, 28

Comerón S., Elmegreen B.G., Salo H., Laurikainen E., Holwerda B.W., Knapen J.H. 2014, A&A, 571, A58

Courteau S., Widrow L.M., McDonald M., Guhathakurta P., Gilbert K.M., Zhu Y., Beaton R.L., Majewski S.R. 2011, ApJ, 739, 20

Cunha K., Smith V.V. 2006, ApJ, 651, 491

de Souza RE., Dos Anjos S. 1987, A&AS, 70, 465

de Vaucouleurs G. 1964, Interpretation of velocity distribution of the inner regions of the Galaxy. In: Kerr FJ (ed) The Galaxy and the Magellanic Clouds, IAU Symposium, vol 20, p 195

de Vaucouleurs G. 1974, Structures of Central Bulges and Nuclei of Galaxies. In: Shakeshaft JR (ed) The Formation and Dynamics of Galaxies, IAU Symposium, vol 58, p 335
Debattista V.P., Carollo C.M., Mayer L., Moore B. 2005, ApJ, 628, 678
Dékány I., Minniti D., Catelan M., Zoccali M., Saito R.K., Hempel M., Gonzalez O.A. 2013, ApJ, 776, L19
Di Matteo P., Gomez A., Haywood M., Combes F., Lehnert M.D., Ness M., Snaith O.N., Katz D., Semelin B. 2014, ArXiv e-prints 1411.1416
Dwek E., Arendt R.G., Hauser M.G., Kelsall T., Lisse C.M., Moseley S.H., Silverberg R.F., Sodroski T.J., Weiland J.L. 1995, ApJ, 445, 716
Eggen O.J., Lynden-Bell D., Sandage A.R. 1962, ApJ, 136, 748
Ellison S.L., Nair P., Patton D.R., Scudder J.M., Mendel J.T., Simard L. 2011, MNRAS, 416, 2182
Elmegreen B.G. 1999, ApJ, 517, 103
Elmegreen B.G., Bournaud F., Elmegreen D.M. 2008, ApJ, 688, 67
Emsellem E., Renaud F., Bournaud F., Elmegreen B., Combes F., Gabor J. 2014, ArXiv e-prints 1410.6479
Erwin P., Debattista V.P. 2013, MNRAS, 431, 3060
Erwin P., Saglia R.P., Fabricius M., Thomas J., Nowak N., Rusli S., Bender R., Vega Beltran J.C., Beckman J.E. 2014, ArXiv e-prints 1411.2599
Fisher D.B. 2006, ApJ, 642, L17
Fisher D.B., Drory N. 2010, ApJ, 716, 942
Freeman K., Ness M., Wylie-de-Boer E., Athanassoula E., Bland-Hawthorn J., Asplund M., Lewis G., Yong D., Lane R., Kiss L., Ibata R. 2013, MNRAS, 428, 3660
Frogel J.A., Whitford A.E. 1987, ApJ, 320, 199
Fulbright J.P., McWilliam A., Rich RM. 2006, ApJ, 636, 821
Fulbright J.P., McWilliam A., Rich R.M. 2007, ApJ, 661, 1152
Gadotti D.A. 2008, MNRAS, 384, 420
Gadotti D.A. 2009, MNRAS, 393, 1531
Galaxy Bulges and Elliptical Galaxies. Lecture Notes. Memorie della Societa Italiana, Gadotti D.A. 2012, in press
Gadotti D.A., dos Anjos S. 2001, AJ, 122, 1298
Gardner E., Debattista V.P., Robin A.C., Vásquez S., Zoccali M. 2014, MNRAS, 438, 3275
Garzón F., López-Corredoira M. 2014, Astronomische Nachrichten, 335, 865
Gerhard O., Martinez-Valpuesta I. 2012, ApJ, 744, L8
Gonzalez O.A., Rejkuba M., Zoccali M., Hill V., Battaglia G., Babusiaux C., Minniti D., Barbuy B., Alves-Brito A., Renzini A., Gomez A., Ortolani S. 2011, A&A, 530, A54
Gonzalez O.A., Rejkuba M., Zoccali M., Valenti E., Minniti D., Schultheis M., Tobar R., Chen B. 2012, A&A, 543, A13
Gonzalez O.A., Rejkuba M., Zoccali M., Valent E., Minniti D., Tobar R. 2013, A&A, 552, A110
Hammersley P.L., Garzón F., Mahoney TJ., López-Corredoira M., Torres MAP. 2000, MNRAS, 317, L45
Hill V., Lecureur A., Gómez A., Zoccali M., Schultheis M., Babusiaux C., Royer F., Barbuy B., Arenou F., Minniti D., Ortolani S. 2011, A&A, 534, A80
Hopkins P.F., Bundy K., Croton D., Hernquist L., Keres D., Khochfar S., Stewart K., Wetzel A., Younger JD. 2010, ApJ, 715, 202
Howard C.D., Rich R.M., Reitzel D.B., Koch A., De Propris R., Zhao H. 2008, ApJ, 688, 1060
Jarvis B.J. 1986, AJ, 91, 65
Johnson C.I., Rich R.M., Fulbright J.P., Valenti E., McWilliam A. 2011, ApJ, 732, 108
Johnson C.I., Rich R.M., Kobayashi C., Kunder A., Pilachowski C.A., Koch A., de Propris R. 2013, ApJ, 765, 157
Johnson C.I., Rich R.M., Kobayashi C., Kunder A., Koch A. 2014, AJ, 148, 67
Kormendy J., Barentine J.C. 2010, ApJ, 715, L176
Kormendy J., Kennicutt RC. Jr. 2004, ARA&A, 42, 603
Kraljic K., Bournaud F., Martig M. 2012, ApJ, 757, 60
Kuijken K., Merrifield M.R. 1995, ApJ, 443, L13

Kuijken K., Rich R.M. 2002, AJ, 124, 2054
Kunder A., Koch A., Rich R.M., de Propris R., Howard C.D., Stubbs S.A., Johnson C.I., Shen J., Wang Y., Robin A.C., Kormendy J., Soto M., Frinchaboy P., Reitzel D.B., Zhao H., Origlia L. 2012, AJ, 143, 57
Laurikainen E., Salo H., Buta R. 2005, MNRAS, 362, 1319
Laurikainen E., Salo H., Buta R., Knapen JH. 2007, MNRAS, 381, 401
Laurikainen E., Salo H., Buta R., Knapen J.H. 2011, MNRAS, 418, 1452
Laurikainen E., Salo H., Athanassoula E., Bosma A., Herrera-Endoqui M. 2014, MNRAS, 444, L80
Lecureur A., Hill V., Zoccali M., Barbuy B., Gómez A., Minniti D., Ortolani S., Renzini A. 2007, A&A, 465, 799
Liszt H.S., Burton W.B. 1980, ApJ, 236, 779
López-Corredoira M., Cabrera-Lavers A., Mahoney T.J., Hammersley P.L., Garzón F. 2007, AJ, 133, 154
Lütticke R., Dettmar R.J., Pohlen M. 2000, A&AS, 145, 405
Martinez-Valpuesta I., Gerhard O. 2011, ApJ, 734, L20
Martinez-Valpuesta I., Gerhard O. 2013, ApJ, 766, L3
Martinez-Valpuesta I., Shlosman I., Heller C. 2006, ApJ, 637, 214
McWilliam A., Rich R.M. 1994, ApJS, 91, 749
McWilliam A., Zoccali M. 2010, ApJ, 724, 1491
McWilliam A., Fulbright J., Rich RM. 2010, Chemical Composition of the Galactic Bulge in Baade's Window. In: Cunha K., Spite M., Barbuy B. (eds) IAU Symposium, vol 265, p 279
Meléndez J., Asplund M., Alves-Brito A., Cunha K., Barbuy B., Bessell M.S., Chiappini C., Freeman K.C., Ramírez I., Smith V.V., Yong D. 2008, A&A, 484, L21
Méndez-Abreu J., Debattista V.P., Corsini EM., Aguerri J.A.L. 2014, A&A, 572, A25
Merrifield M.R., Kuijken K. 1999, A&A, 345, L47
Minniti D. 1996, ApJ, 459, 579
Minniti D., Zoccali M. 2008, The Galactic bulge: a review. In: Bureau M., Athanassoula E., Barbuy B. (eds.) IAU Symposium, IAU Symposium, vol 245, p 323
Minniti D., Olszewski E.W., Liebert J., White S.D.M., Hill J.M., Irwin M.J. 1995, MNRAS, 277, 1293
Nataf D.M., Udalski A., Gould A., Fouqué P., Stanek K.Z. 2010, ApJ, 721, L28
Ness M., Freeman K., Athanassoula E., Wylie-de-Boer E., Bland-Hawthorn J., Asplund M., Lewis G.F., Yong D., Lane R.R., Kiss L.L. 2013a, MNRAS, 430, 836
Ness M., Freeman K., Athanassoula E., Wylie-de-Boer E., Bland-Hawthorn J., Asplund M., Lewis G.F., Yong D., Lane RR., Kiss L.L., Ibata R. 2013b, MNRAS, 432, 2092
Ness M., Debattista V.P., Bensby T., Feltzing S., Roškar R., Cole D.R., Johnson J.A., Freeman K. 2014, ApJ, 787, L19
Nomoto K., Thielemann F.K., Wheeler J.C. 1984, ApJ, 279, L23
Norman C.A., Sellwood J.A., Hasan H. 1996, ApJ, 462, 114
Nowak N., Thomas J., Erwin P., Saglia R.P., Bender R., Davies RI. 2010, MNRAS, p 106
Obreja A., Domínguez-Tenreiro R., Brook C., Martínez-Serrano F.J., Doménech-Moral M., Serna A., Mollá M., Stinson G. 2013, ApJ, 763, 26
Ortolani S., Renzini A., Gilmozzi R., Marconi G., Barbuy B., Bica E., Rich R.M. 1995, Nature, 377, 701
Phillips AC. 1996, Star Formation in Barred Galaxies. In: Buta R., Crocker D.A., Elmegreen B.G. (eds) IAU Colloq. 157: Barred Galaxies, Astronomical Society of the Pacific Conference Series, vol 91, p 44
Raha N., Sellwood J.A., James R.A., Kahn F.D. 1991, Nature, 352, 421
Ramírez S.V., Stephens A.W., Frogel J.A., DePoy D.L. 2000, AJ, 120, 833
Rattenbury N.J., Mao S., Sumi T., Smith M.C. 2007, MNRAS, 378, 1064
Rich R.M. 1988, AJ, 95, 828

Rich R.M. 1990, ApJ, 362, 604
Rich R.M., Origlia L. 2005, ApJ, 634, 1293
Rich R.M., Origlia L., Valenti E. 2007, ApJ, 665, L119
Rich R.M., Origlia L., Valenti E. 2012, ApJ, 746, 59
Rojas-Arriagada A., Recio-Blanco A., Hill V., de Laverny P., Schultheis M., Babusiaux C., Zoccali M., Minniti D., Gonzalez O.A., Feltzing S., Gilmore G., Randich S., Vallenari A., Alfaro E.J., Bensby T., Bragaglia A., Flaccomio E., Lanzafame A.C., Pancino E., Smiljanic R., Bergemann M., Costado M.T., Damiani F., Hourihane A., Jofré P., Lardo C., Magrini L., Maiorca E., Morbidelli L., Sbordone L., Worley C.C., Zaggia S., Wyse R. 2014, A&A, 569, A103
Romero-Gómez M., Athanassoula E., Antoja T., Figueras F. 2011, MNRAS, 418, 1176
Ryde N., Gustafsson B., Edvardsson B., Meléndez J., Alves-Brito A., Asplund M., Barbuy B., Hill V., Käufl H.U., Minniti D., Ortolani S., Renzini A., Zoccali M. 2010, A&A, 509, A20
Sadler E.M., Rich R.M., Terndrup D.M. 1996, AJ, 112, 171
Saha K., Gerhard O. 2013, MNRAS, 430, 2039
Saha K., Martinez-Valpuesta I., Gerhard O. 2012, MNRAS, 421, 333
Saito R.K., Zoccali M., McWilliam A., Minniti D., Gonzalez O.A., Hill V. 2011, AJ, 142, 76
Samland M., Gerhard O.E. 2003, A&A, 399, 961
Sandage A. 1961, The Hubble atlas of galaxies
Schlegel D.J., Finkbeiner DP., Davis M. 1998, ApJ, 500, 525
Shaw M.A. 1987, MNRAS, 229, 691
Shen J., Rich RM., Kormendy J., Howard C.D., De Propris R., Kunder A. 2010, ApJ, 720, L72
Sheth K., Vogel S.N., Regan M.W., Teuben P.J., Harris A.I., Thornley M.D. 2002, AJ, 124, 2581
Sheth K., Elmegreen D.M., Elmegreen B.G., et al. 2008, ApJ, 675, 1141
Sheth K., Melbourne J., Elmegreen D.M., Elmegreen B.G., Athanassoula E., Abraham R.G., Weiner B.J. 2012, ApJ, 758, 136
Sinha R.P. 1979, A&AS, 37, 403
Smith B.J., Price S.D., Baker R.I. 2004, ApJS, 154, 673
Soto M., Rich RM., Kuijken K. 2007, ApJ, 665, L31
Stanek K.Z., Mateo M., Udalski A., Szymanski M., Kaluzny J., Kubiak M. 1994, ApJ, 429, L73
Terndrup D.M., Sadler E.M., Rich R.M. 1995, AJ, 110, 1774
Tiede G.P., Terndrup D.M. 1997, AJ, 113, 321
Tinsley B.M. 1979, ApJ, 229, 1046
Uttenthaler S., Schultheis M., Nataf D.M., Robin A.C., Lebzelter T., Chen B. 2012, A&A, 546, A57
Valenti E., Zoccali M., Renzini A., Brown T.M., Gonzalez O.A., Minniti D., Debattista V.P., Mayer L. 2013, A&A, 559, A98
Vásquez S., Zoccali M., Hill V., Renzini A., González O.A., Gardner E., Debattista V.P., Robin A.C., Rejkuba M., Baffico M., Monelli M., Motta V., Minniti D. 2013, A&A, 555, A91
Wegg C., Gerhard O. 2013, MNRAS, 435, 1874
Weiland J.L., Arendt R.G., Berriman G.B., Dwek E., Freudenreich H.T., Hauser M.G., Kelsall T., Lisse C.M., Mitra M., Moseley S.H., Odegard N.P., Silverberg R.F., Sodroski T.J., Spiesman W.J., Stemwedel S.W. 1994, ApJ, 425, L81
Williams M.J., Zamojski M.A., Bureau M., Kuntschner H., Merrifield M.R., de Zeeuw P.T., Kuijken K. 2011, MNRAS, 414, 2163
Woosley S.E., Weaver T.A. 1995, ApJS, 101, 181
Wyse RFG., Gilmore G., Franx M. 1997, ARA&A, 35, 637
Zhao H., Spergel D.N., Rich R.M. 1994, AJ, 108, 2154
Zoccali M. 2010, The Stellar Population of the Galactic Bulge. In: Cunha K., Spite M., Barbuy B. (eds.) IAU Symposium, IAU Symposium, vol 265, p 271
Zoccali M., Renzini A., Ortolani S., Greggio L., Saviane I., Cassisi S., Rejkuba M., Barbuy B., Rich R.M., Bica E. 2003, A&A, 399, 931
Zoccali M., Lecureur A., Barbuy B., Hill V., Renzini A., Minniti D., Momany Y., Gómez A., Ortolani S. 2006, A&A, 457, L1

Zoccali M., Hill V., Lecureur A., Barbuy B., Renzini A., Minniti D., Gómez A., Ortolani S. 2008, A&A, 486, 177

Zoccali M., Gonzalez O.A., Vasquez S., Hill V., Rejkuba M., Valenti E., Renzini A., Rojas-Arriagada A., Martinez-Valpuesta I., Babusiaux C., Brown T., Minniti D., McWilliam A. 2014, A&A, 562, A66

Chapter 10
Theoretical Models of the Galactic Bulge

Juntai Shen and Zhao-Yu Li

Abstract Near infrared images from the *COBE* satellite presented the first clear evidence that our Milky Way galaxy contains a boxy shaped bulge. Recent years have witnessed a gradual paradigm shift in the formation and evolution of the Galactic bulge. Bulges were commonly believed to form in the dynamical violence of galaxy mergers. However, it has become increasingly clear that the main body of the Milky Way bulge is not a classical bulge made by previous major mergers, instead it appears to be a bar seen somewhat end-on. The Milky Way bar can form naturally from a precursor disc and thicken vertically by the internal firehose/buckling instability, giving rise to the boxy appearance. This picture is supported by many lines of evidence, including the asymmetric parallelogram shape, the strong cylindrical rotation (i.e., nearly constant rotation regardless of the height above the disc plane), the existence of an intriguing X-shaped structure in the bulge, and perhaps the metallicity gradients. We review the major theoretical models and techniques to understand the Milky Way bulge. Despite the progresses in recent theoretical attempts, a complete bulge formation model that explains the full kinematics and metallicity distribution is still not fully understood. Upcoming large surveys are expected to shed new light on the formation history of the Galactic bulge.

10.1 A Brief Overview on the Properties of the Galactic Bulge

Most spiral galaxies consist of three main components, an invisible dark matter halo, an embedded flat disc, and a central bulge. The Milky Way is no exception. The Milky Way bulge comprises about 15 % of the total luminosity, and its stellar mass is about $1.2 - 1.6 \times 10^{10} M_{\odot}$ (Portail et al. 2015a). Galactic bulges contain crucial information about the galaxy formation and evolution. Major mergers between

J. Shen (✉) • Z.-Y. Li
Key Laboratory for Research in Galaxies and Cosmology, Shanghai Astronomical Observatory, Chinese Academy of Sciences, 80 Nandan Road, Shanghai 200030, China
e-mail: shen@shao.ac.cn; lizy@shao.ac.cn

E. Laurikainen et al. (eds.), *Galactic Bulges*, Astrophysics and Space Science Library 418, DOI 10.1007/978-3-319-19378-6_10

galaxies generally create a significant classical bulge that is similar to ellipticals in many aspects (see Chap. 12 of this book), whereas the long term internal secular evolution in the disc galaxy tends to build up a pseudobulge (Kormendy and Kennicutt 2004). Understanding the structure of our Milky Way bulge is nontrivial, mostly because of our location in the disc plane and the severe dust extinction in the optical band. One the other hand, a huge advantage being inside the Milky Way is the power to resolve and observe individual stars. Here we briefly summarize the structure, chemical composition, age, and kinematics of the Galactic bulge. More detailed reviews on the observational properties of the Galactic bulge can be found in Zoccali (2010), Rich (2013), Origlia (2014) and Chap. 9 of this book.

Structure. The presence of a triaxial structure in the inner Galaxy was first hinted from gas kinematics (de Vaucouleurs 1964; Binney et al. 1991; Burton and Liszt 1993). The near infrared images from the *COBE* satellite revealed clearly that the Milky Way contains an asymmetric parallelogram-shaped boxy bulge in the center (Weiland et al. 1994). The asymmetry may be explained by a tilted bar; the near end of the bar is closer to us than the far side, consequently it appears to be bigger than the other side (Blitz and Spergel 1991). Measurements of the three-dimensional density distribution of the Galactic bulge using various stellar tracers give a triaxial bar with the semi-major axis $\sim$3–4 kpc and tilted by $\sim$20°–30° between the Sun-Galactic Center (GC) line (i.e., Stanek et al. 1997; Bissantz and Gerhard 2002; Rattenbury et al. 2007b; Robin et al. 2012; Cao et al. 2013; Wegg and Gerhard 2013; Pietrukowicz et al. 2014). This main triaxial bar is sometimes dubbed as "the (boxy) bulge bar" (i.e., boxy pseudobulge in the notation of this book), whose properties still differ among different research groups.

The existence of other bar structures than the main bulge bar is still under active debate. Based on stars counts from the GLIMPSE (Galactic Legacy Mid-Plane Survey Extraordinaire) survey, Benjamin et al. (2005) argued for another planar long bar passing through the GC with half-length 4.4 kpc tilted by $\sim$45° to the Sun-GC line (see also Cabrera-Lavers et al. 2007). If this long bar is confirmed, then its co-existence with the similarly-sized bulge bar is dynamically puzzling, as their mutual torque tends to align the two bars on a short timescale. Also both observations of external galaxies (Erwin and Sparke 2002, 2003) and simulations of long-lived double barred galaxies (Debattista and Shen 2007; Shen and Debattista 2009) have shown that the size ratio of two bars is generally about 0.1–0.2. Using numerical simulations, Martinez-Valpuesta and Gerhard (2011) showed that the observational signatures of the planar long bar may actually be reproduced with a single bar structure. They suggested that the long bar may correspond to the leading ends of the bulge bar in interaction with the adjacent spiral arm heads. Nishiyama et al. (2005) and Gonzalez et al. (2011a) also suggested the existence of a possible secondary inner bar, as the slope of the longitudinal magnitude peak profile of red clumps flattens at $|l| \sim 4°$, deviating from the main bar. With the same single barred *N*-body model, Gerhard and Martinez-Valpuesta (2012) showed that such a slope change may be caused by a transition from highly elongated to nearly axisymmetric isodensity contours in the inner boxy bulge.

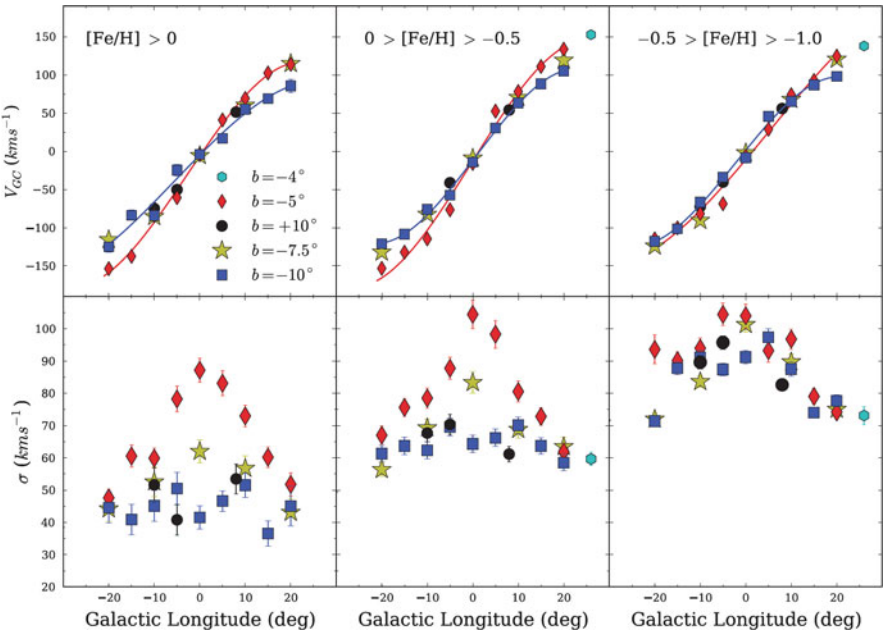

Fig. 10.1 Rotation and velocity dispersion profiles in the ARGOS observations towards the Galactic bulge fields from Ness et al. (2013a). The three columns correspond to three different metallicity bins, decreasing from left to right. Different symbols represent stars in different fields (Reproduced from Ness et al. 2013a)

Chemical composition and stellar age. The chemical composition and the stellar age are crucial parameters to constrain galaxy formation history and to establish the connection to stellar populations in other structural components. The bulk of bulge stars is old with a wide range of metal abundances (McWilliam and Rich 1994; Zoccali et al. 2008), including some of the oldest stars in the Milky Way (e.g. Howes et al. 2014; Schlaufman and Casey 2014). The metallicity distribution in the bulge displays a vertical gradient both on and off the minor axis away from the Galactic plane (Zoccali et al. 2008; Gonzalez et al. 2011b; Johnson et al. 2011, 2012, 2013), while Rich et al. (2012) found no major vertical abundance gradient close to the disc plane ($b \leq 4°$). Ness et al. (2013a) found that stars with [Fe/H] > -0.5 are part of the boxy bar/bulge, and the metal-poor stars are likely associated with thick disc. As shown in Fig. 10.1, although the rotation curves are similar for three different metallicity bins, the metal-poor population ($-0.5 <$ [Fe/H] < -1.0) clearly has higher velocity dispersion and spheroidal kinematics. In Ness et al. (2013a), stars with [Fe/H] $\sim +0.15$ are more prominent close to the plane than the metal-poor stars, appearing as a vertical abundance gradient of the bulge. Most bulge metal-poor stars show enhanced α elements compared to both thin and thick disc stars (Johnson et al. 2011; Gonzalez et al. 2011b; Rich et al. 2012), suggesting a rapid formation timescale with respect of both disc components.

Compared to metallicity, age determination is more difficult and imprecise (see the review by Soderblom 2010 and references therein). The bulk of bulge stars is old (∼10 Gyr) (e.g., Ortolani et al. 1995; Lecureur et al. 2007; Clarkson et al. 2008). However, intermediate-age metal-rich stars are also detected in the bulge region, with the exact relative fraction still under debate (Clarkson et al. 2011; Bensby et al. 2011, 2012; Ness et al. 2014). In addition, there is a nuclear disc of much younger stellar population with ongoing star formation in the central 200 pc (sometimes termed "nuclear bulge"), whose mass is about $1.5 \times 10^9 M_\odot$ (Launhardt et al. 2002).

Kinematics. To study systematically the stellar kinematics, Rich et al. (2007) initiated the Bulge Radial Velocity Assay (BRAVA) project with M giants as tracers covering the whole Galactic bulge (∼9000 stars). The BRAVA survey revealed clear cylindrical rotation of the bulge, i.e., nearly constant rotation regardless of the height above the disc plane (Howard et al. 2008, 2009; Rich et al. 2008; Kunder et al. 2012). BRAVA kinematics also put the Galactic bulge close to the oblate isotropic rotator line in $V_{\max}/\sigma - \epsilon$ diagram (Binney 1978), distinct clearly from a hot slowly-rotating system like the Milky Way halo supported by velocity dispersion. The BRAVA radial velocity distribution was well reproduced by a self-consistent N-body model of a pure-disc Galaxy by Shen et al. (2010), with no need for a significant classical bulge (see Sect. 10.2).

The Abundance and Radial velocity Galactic Origins Survey (ARGOS) obtained radial velocities and stellar parameters for 28,000 stars in the bulge and inner disc of the Milky Way galaxy across latitudes of $b = -5°$ and $-10°$ (Freeman et al. 2013). The cylindrical rotation of the bulge was also confirmed in the ARGOS data (Ness et al. 2013a). They found a kinematically distinct metal-poor population ($[\mathrm{Fe/H}] < -1.0$), which may be related to the thick disc or halo. In the commissioning observation of APO Galactic Evolution Experiment (APOGEE) towards the Galactic bulge region, a high Galactocentric velocity ($V_{\mathrm{GSR}} \sim +200\,\mathrm{km\,s^{-1}}$) and cold ($\sigma \sim 30\,\mathrm{km\,s^{-1}}$) stream was reported and suggested as the bar supporting orbits (Nidever et al. 2012). However, Li et al. (2014) suggested that stars that self-consistently make up a typical bar potential do not generate a distinct cold high velocity stream observed from the solar perspective. A smooth high velocity shoulder instead does exist in many bulge fields; it roughly corresponds to the tangential point between the line-of-sight and the bar-supported orbits as shown in the distance-velocity diagram. The cold high velocity peaks could be due to other substructures in the disc, unless the APOGEE survey preferentially selects stars with particular characteristics. Recent Giraffe Inner Bulge Survey (GIBS) observed 24 Galactic bulge fields and confirmed the cylindrical rotation and the lack of a significant cold high velocity peak in the radial velocity distribution (Zoccali et al. 2014). Besides the radial velocity, the proper motion is also an important parameter (e.g., Rattenbury et al. 2007a). Given the stellar distance, the transverse velocities can be estimated. In the Baade's window, the velocity ellipsoid of metal-rich stars shows a vertex deviation in the radial versus transverse velocity, consistent with the bar supporting orbits (Soto et al. 2007).

Based on the radial velocity and the [Fe/H] measurement of three minor axis fields, Babusiaux et al. (2010) identified two distinct population: the metal-rich

population with bar-like kinematics and the metal-poor population corresponding to an old spheroid or a thick disc (also see Hill et al. 2011; Rojas-Arriagada et al. 2014). The metal-rich population demonstrates smaller velocity dispersion and lower α-element enhancement compared to the metal-poor population (Johnson et al. 2011; Uttenthaler et al. 2012). Across the bulge fields in ARGOS survey, the metal-poor population ([Fe/H] < -1.0) was also found to be kinematically distinct with large velocity dispersion and non-cylindrical rotation (Ness et al. 2013b).

X-shaped structure. A recent development in the bulge structural study is the discovery of an intriguing X-shaped structure (Sect. 10.3). Recently, two groups independently reported the bimodal brightness distribution of the red clump (RC) stars, which can be considered a good standard candle (Stanek and Garnavich 1998), in the Galactic bulge (McWilliam and Zoccali 2010 hereafter MZ10; Nataf et al. 2010). MZ10 suggested that the bimodality is hard to explain with a naive tilted bar since the line of sight crossing the bar can only result in stars with one distance. One possibility speculated by Nataf et al. (2010) is that one RC population belongs to the bar and the other to the spheroidal component of the bulge. Another puzzling fact is that distances of the bright and faint RCs are roughly constant at different latitudes, which was hard to understand with a naive straight bar. MZ10 proposed that these observed evidences can be well explained with a vertical X-shaped structure in the bulge region. The existence of this particular structure was later verified by Saito et al. (2011). They found that the X-shaped structure exists within (at least) $|l| \leq 2°$, and has front-back symmetry. Around $b = \pm 5°$, two RCs start to merge, due to severe dust extinction and foreground contamination (MZ10; Wegg and Gerhard 2013). From numerical simulations, as demonstrated in Li and Shen (2012) and Ness et al. (2012), the buckled bar naturally reproduces the observed X-shape properties in many aspects. The X-shape extends to about half the bar length with similar tilting angle as the bar. The observed north-south symmetry of the X-shape indicates that it must have formed at least a few billion years ago (Li and Shen 2012).

10.2 A Fully Evolutionary Bar Model as the Basis of Understanding the Galactic Bulge

Theoretical modeling of the Milky Way bulge made intense use of N-body simulations. The basis of a successful Galactic bulge model is a fully evolutionary bar model that developed naturally from the bar instability of a cold massive disc. Here we describe a successful high-resolution bar model developed in Shen et al. (2010, hereafter S10), which was initially motivated to match the BRAVA stellar kinematic data. N-body bar models to explain the Galactic bulge were already attempted in early studies such as Fux (1997) and Sevenster et al. (1999), but little stellar kinematic data were available to constrain their models.

S10 simulated the self-consistent formation of a bar that buckles naturally into a thickened state, then scaled that model to fit the BRAVA kinematic data on bulge rotation and random velocities. BRAVA measured the stellar radial velocities of

M-type giant stars whose population membership in the bulge is well established. These giants provide most of the 2 μm radiation whose box-shaped light distribution motivates bar models. S10 used nearly 5000 stellar radial velocities in two strips at latitude $b = -4°$ and $b = -8°$ and at longitude $-10° < l < +10°$, and a strip along the minor axis ($l \equiv 0°$). The strong cylindrical rotation was found in the preliminary BRAVA data (Howard et al. 2009) consistent with an edge-on, bar-like pseudobulge (Kormendy 1993; Kormendy and Kennicutt 2004), although a precise fit of a bar model to the data was not available. The success prompted S10 to construct a fully evolutionary N-body model that can fit the radial velocity data of BRAVA.

S10 used a cylindrical particle-mesh code (Shen and Sellwood 2004) to build fully self-consistent N-body galaxies. The code is highly optimized to study the evolution of disc galaxies, and it allows S10 to model the disc with at least 1 million particles to provide high particle resolution near the center where the density is high. They tried to construct the simplest self-consistent N-body models that fit the BRAVA data, avoiding contrived models with too many free parameters. Initially, they contained only an unbarred disc and a dark halo. The profile of the Galactic halo is poorly constrained observationally; S10 adopted a rigid pseudo-isothermal halo potential which gives a nearly flat initial rotation curve between 5 kpc and 20 kpc. A simple halo form allows S10 to run many simulations quickly, which greatly facilitates a parameter search. A rigid halo also omits dynamical friction on the bar, but the central density of this cored halo is low enough so that friction will be very mild. Since the bulge is embedded well interior to the core radius of the halo, the exact profile of the dark halo at large radii is not critical.

The process of bar formation and thickening in S10 is physically understood. First a bar develops self-consistently via the bar instability from the initially unbarred, thin disc. Bar formation enhances the radial streaming motions of disc particles, so the radial velocity dispersion quickly grows much bigger than the vertical one. Consequently the disc buckles vertically out of the plane like a firehose (Fig. 10.2)[1]; this is the well known firehose or buckling instability (e.g., Toomre 1966; Combes et al. 1990; Raha et al. 1991). It raises the vertical velocity dispersion and increases the bar's thickness. This happens on a short dynamical timescale and saturates in a few hundred million years. The central part of the buckled bar is elevated well above the disc mid-plane and resembles the peanut morphology of many bulges including the one in our Galaxy.

S10 found the one that best matches our BRAVA kinematic data after suitable mass scaling, out of a large set of N-body models. The barred disc evolved from a thin exponential disc that contains $M_{\rm d} = 4.25 \times 10^{10} {\rm M}_{\odot}$, about 55 % of the total mass at the truncation radius (5 scale-lengths). The scale-length and scale-height

[1]It is puzzling why no galaxy has been caught in the process of violent buckling as shown in Fig. 10.2. The saturation timescale of the buckling instability is very rapid (about a few hundred Myr), but it is not short enough to miss out the violent buckling phase if one can observe thousands of edge-on barred galaxies. Perhaps this implies that the buckling instability must have happened in the very early assembly stage of disc galaxies, which is much harder to observe.

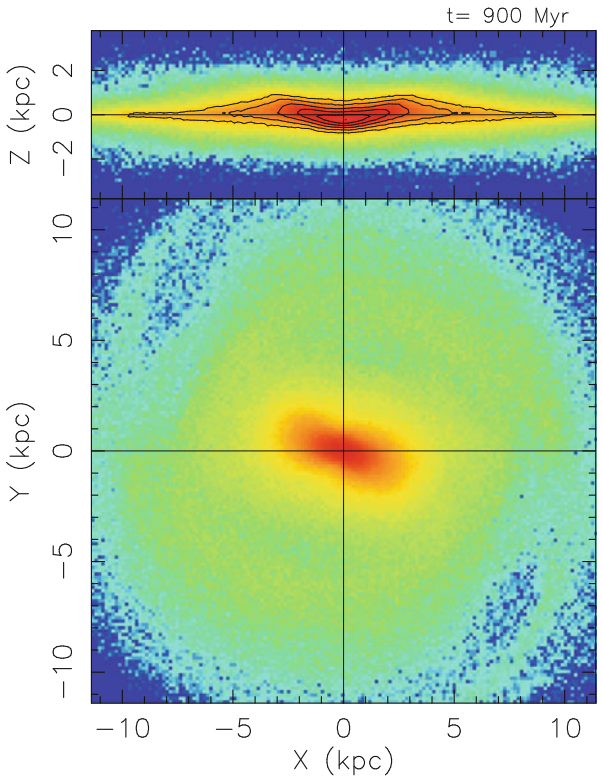

Fig. 10.2 Shortly after its formation, the bar becomes vulnerable to the vertical firehose/buckling instability (Toomre 1966; Raha et al. 1991). The figure illustrates the vigorous buckling instability that makes the initially thin bar bend out of the disc plane, reaching a considerable maximum distortion. After the buckling instability saturates on a short dynamical timescale (in a few hundred million years), the bar is greatly thickened in the vertical direction, giving rise to the boxy shape. (see Fig. 10.4)

of the initial disc are ∼1.9 kpc and 0.2 kpc, respectively. The disc is rotationally supported and has a Toomre-Q of 1.2. The amplitude of the final bar is intermediate between the weakest and strongest bars observed in galaxies. The bar's minor-to-major axial ratio is about 0.5–0.6, and its half-length is ∼4 kpc. Figure 10.3 shows the pattern speed of the bar ($\Omega_p \approx 39$ km/s/kpc) and locations of the Lindblad resonances. The bar properties in the best-fitting model are comparable to those obtained in other independent studies. The left panel of Fig. 10.4 shows face-on and side-on views of the projected density of the best-fitting model in S10. A distinctly peanut shaped bulge is apparent in the edge-on projection. Figure 10.4 (right panel) shows the surface brightness distribution in Galactic coordinates in solar perspective. Nearby disc stars dilute the peanut shape, but the bar still looks boxy. The asymmetry in the longitudinal direction can be understood as a perspective effect; the near end of the bar (at positive Galactic longitude) is closer to the Sun, so

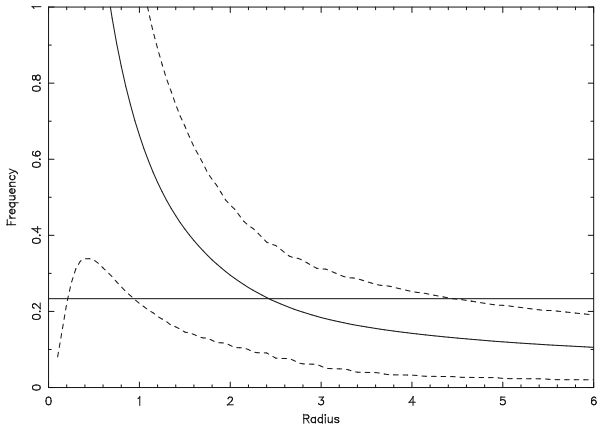

Fig. 10.3 The *horizontal line* marks the pattern speed Ω_p of the quasi-steady bar in internal simulation unit with $R_\mathrm{d} = G = M_\mathrm{d} = 1$. Here $\Omega_p \approx 39\,\mathrm{km/s/kpc}$ in physical units. The *solid line* shows the curve of the circular angular frequency Ω, and the *dashed lines* mark $\Omega \pm \kappa/2$ at around $t = 4.8\,\mathrm{Gyr}$ (Reproduced from Shen (2014) with permission of AAS)

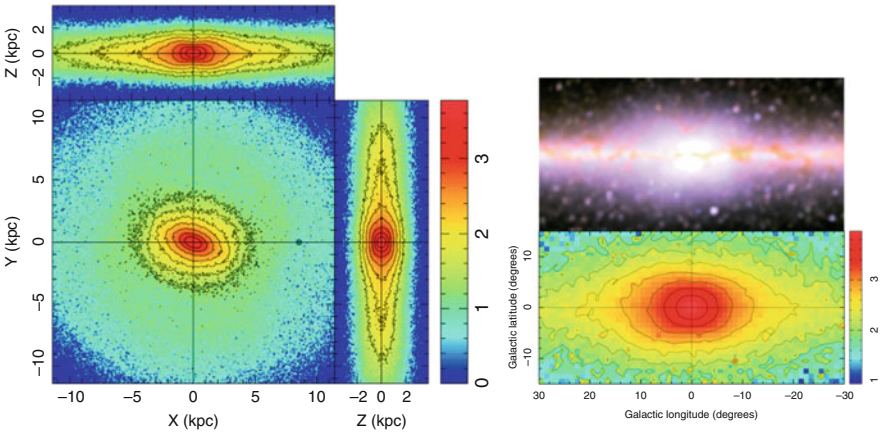

Fig. 10.4 *Left three panels*: face-on and side-on views of the surface density of our best-fitting model as seen from far away. The Sun's position 8.5 kpc from the Galactic center is marked along the $+x$ axis. The Galaxy rotates clockwise as seen in the face-on projection. *Right panels*: The COBE DIRBE composite image of the Milky Way bulge and model's surface brightness map in solar perspective. Both the model and observed image show the box-shaped, edge-on bar that appear bigger on its near side (positive longitude side) (The *left panel* is reproduced from Shen et al. (2010) with permission of AAS)

it appears bigger and taller than the far side. Both the boxy shape and the asymmetry are in good agreement with the morphology revealed by the near-infrared image from the COBE satellite (Weiland et al. 1994).

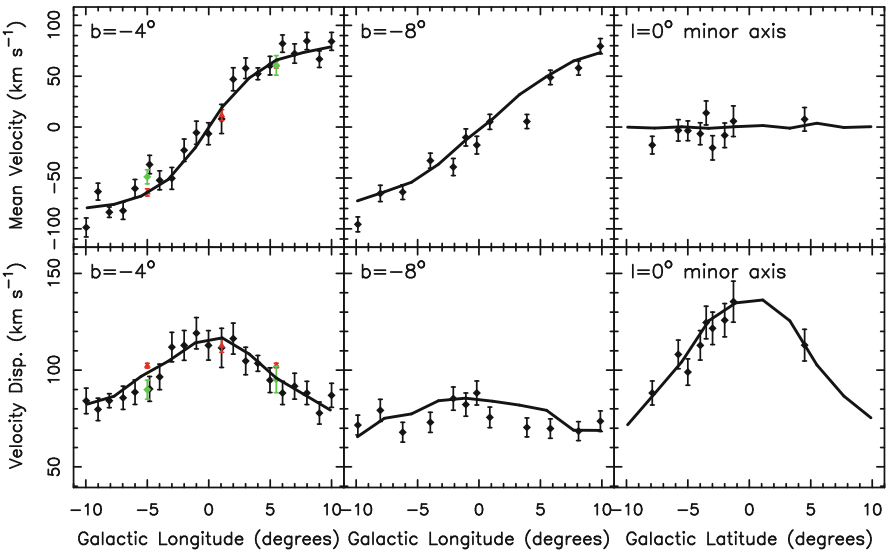

Fig. 10.5 (*top*): Mean velocity and velocity dispersion profiles of the best-fitting model (*black lines*) compared to all available kinematic observations. The *left two panels* are for the Galactic latitude $b = -4°$ strip; the *middle two panels* are for the $b = -8°$ strip; and the *right two panels* are for the $l = 0°$ minor axis. The *black diamonds* and their error bars are the BRAVA data; the *green diamonds* are for M-type giant stars (Rangwala et al. 2009), and the *red triangles* are the data on red clump giant stars (Rangwala et al. 2009). This is the first time that a single dynamical model has been compared with data of such quality. The agreement is striking (Reproduced from Shen et al. (2010) with permission of AAS)

Figure 10.5 compares the best-fitting model kinematics in S10 (solid lines) with the mean velocity and velocity dispersion data from the BRAVA and other surveys. All velocities have been converted to Galactocentric values (the line-of-sight velocity that would be observed by a stationary observer at the Sun's position). For the first time, this model is able to simultaneously match the mean velocities and velocity dispersions along two Galactic latitudes ($-4°$ and $-8°$) and along the minor axis. The model comparison with the complete BRAVA data release was also impressive (Kunder et al. 2012).

S10 also provided some constraints on the bar angle between the bar and the Sun-galaxy center line. Using both the fit to the velocity profiles and the photometric asymmetry, they found that the overall best-fitting model has a bar angle of $\sim 20°$, which agrees reasonably well with other independent studies (e.g., Stanek et al. 1997; Rattenbury et al. 2007b; Cao et al. 2013; Wegg and Gerhard 2013).

The best-fitting model in S10 contains no classical bulge component. S10 also tested whether or not a significant classical bulge is present, since it could have been spun up by the later formation of a bar, flattened thereby and made hard to detect. They found that including a classical bulge with $> \sim 15\,\%$ of the disc mass considerably worsens the fit of the model to the data, even if the disc properties are

accordingly re-adjusted. If the pre-existing classical bulge is overly massive, then it becomes increasingly hard to match both the mean velocity and velocity dispersions simultaneously (see also Saha et al. 2012).

The BRAVA kinematic observations show no sign that the Galaxy contains a significant merger-made, "classical" bulge. S10 demonstrated that the boxy pseudobulge is not a separate component of the Galaxy but rather is an edge-on bar. This result also has important implications for galaxy formation. From a galaxy formation point of view, we live in a pure-disc galaxy. Our Galaxy is not unusual. In fact, giant, pure-disc galaxies are common in environments like our own that are far from rich clusters of galaxies (Kormendy et al. 2010; Laurikainen et al. 2014). Classical bulgeless, pure-disc galaxies still present an acute challenge to the current picture of galaxy formation in a universe dominated by cold dark matter; growing a giant galaxy via hierarchical clustering involves so many mergers that it seems almost impossible to avoid forming a substantial classical bulge (Peebles and Nusser 2010).

10.2.1 The Bulge Structure May Be Younger than Its Stars

A common misconception about the secularly evolved bar model is that it seems inconsistent with the old age of bulge stars that formed on a short timescale ($\sim$1 Gyr), as demonstrated by their α-element enhancement. It is important to make a distinction between the assembly time of the bulge/bar and the age of the bulge stars; the Galactic bulge structure may be younger than its stars. The stars in our Galactic bar are older than most disc stars, but those stars could have formed over a short period of time long before the bar structure formed (Wyse 1999; Freeman 2008). Their old age (e.g., Zoccali et al. 2003; Fulbright et al. 2007; Clarkson et al. 2008) is therefore not an argument against the internal secular evolution model.

10.2.2 Could the Vertical Metallicity Gradient be Produced in a Simple Bar Model?

Although the general bulge morphology and kinematics are well explained by this simple and self-consistent model, a potential difficulty of the simple model is how to explain the observed vertical metallicity gradient (e.g., Zoccali et al. 2008; Gonzalez et al. 2011b). Intuitively one may expect that any pre-existing vertical metallicity gradient should be erased due to mixing in the violent buckling process. Thus the vertical metallicity gradient has been suggested as the strongest evidence for the existence of a classical bulge in the Milky Way.

S10 proposed a plausible solution that an abundance gradient can still be produced within the context of secular bar/bulge formation if some of the vertical

thickening is produced by resonant heating of stars that scatter off the bar (Pfenniger and Norman 1990). If the most metal-poor stars are also the oldest stars, then they have been scattered for the longest time and now reach the greatest heights away from the disc plane.

Recently Martinez-Valpuesta and Gerhard (2013) challenged the widespread belief that secularly evolved bar/bulge models cannot have metallicity gradients similar to those observed in our Galaxy. Using a similar boxy bulge/bar simulation as in S10, they were able to successfully reproduce the observed vertical metallicity gradient and longitude-latitude metallicity map similar to that constructed by Gonzalez et al. (2013), provided that the initial unbarred disc had a relatively steep radial metallicity gradient. One important assumption is that the pre-existing radial metallicity gradient is set up during the buildup of the precursor disc prior to bar formation. They proposed that if the Galactic bar/bulge formed rapidly from the precursor disc at early times, the violent relaxation may be incomplete during the bar and buckling instabilities, thus transforming radial pre-existing metallicity gradients to vertical gradients in the final boxy bulge. They further proposed that the range of bulge star metallicities at various latitudes may be used to constrain the radial gradient in the precursor disc. In their study, they tagged particles with some metallicity and no chemical evolution was considered. If their result is confirmed in more detailed studies, then the vertical metallicity gradient is no longer a strong argument against the secularly-evolved bar/bulge model.

10.2.3 Merits of the Simple Self-consistent Bar/Bulge Model

The main advantage of a simple self-consistent bar/bulge model such as the one in S10 lies in its simplicity; S10 tried to construct the simplest self-consistent *N*-body models that fit the BRAVA data, avoiding contrived models with too many free parameters. In addition, the S10 model is not just a static model but rather one that evolved naturally to this state from simple initial conditions. The bar is self-consistently developed from a massive cold precursor disc embedded in a cored halo. So it has relatively few parameters to tweak, unlike the more complicated chemo-dynamical models.

Secondly, physical processes dictating the formation and evolution of the bar/bulge can be well understood. The formation of evolution of the bar is a natural outcome of two well-studied dynamical instabilities, namely the bar instability creating the bar and the subsequent firehose/buckling instability that thickens the bar vertically (see Sellwood 2014 for a comprehensive review on these instabilities). The buckling instability also helps the Milky Way to develop an intriguing X-shaped structure (Sect. 10.3). The different components of the early inner Galaxy (thick disc, old and younger thin discs) probably become trapped dynamically within the bulge structure (Ness et al. 2013b).

Thirdly and probably most importantly, despite its simplicity, the best-fitting model of S10 also ties together several isolated results (e.g., photometric bar

angle, kinematic bar angle, successful kinematic fits in the context of observed cylindrical rotation, reasonable bar length and bar pattern speed, resulting constraint on a classical bulge, the vertical metallicity gradient, and explaining the X-shaped structure) into a coherent picture, cemented by an *N*-body model in which the bar evolves naturally and without complicated fine-tuning. At current stage, it is still unrealistic to expect a full chemo-dynamical model to match all observed properties of the Galactic bulge. The simple bar model was designed to serve as a physically-motivated starting point, then one can gradually incorporate more complexities of the Milky Way bulge on top of it.

10.3 The X-Shaped Structure in the Galactic Bulge

RCs are good standard candles commonly used in the studies of the Galactic bulge. The apparent magnitude of RCs in high-latitude bulge fields shows a clearly bimodal distance distribution, often termed "split red clump". This bimodal distribution was discovered in the 2MASS data (MZ10, Saito et al. 2011) and the OGLE data (Nataf et al. 2010), then confirmed also in the ARGOS sample (Ness et al. 2012). The RCs seem to be distributed in a vertically-extended X-shaped structure (MZ10). This X-shape was initially puzzling; it seemed difficult to explain them using a tilted naive ellipsoidal bar.

This X-shaped structure does not have a straight-forward explanation in classical bulge formation scenarios, but it is a natural consequence of the bar buckling processes (see Sect. 10.2) if it is properly modeled (Combes et al. 1990; Raha et al. 1991; Bureau and Freeman 1999; Athanassoula 2005; Martinez-Valpuesta et al. 2006). Li and Shen (2012) analyzed the same best-fitting Milky Way bar/bulge model in S10, and demonstrated that it can qualitatively reproduce many observations of the X-shaped structure, such as double peaks in distance histograms (MZ10, Nataf et al. 2010) and number density maps (Saito et al. 2011).

Li and Shen (2012) found that an X-shaped structure is clearly discernible in the inner region of the side-on view of the S10 best-fitting bar/bulge model (top panel of Fig. 10.6b). They fitted and subtracted the underlying smooth component from the side-on bar model, then the X-shaped structure is highlighted in the bottom panel of Fig. 10.6b (Li and Shen 2012). Figure 10.6a shows the distance distributions of particles towards the Galactic bulge, where double peak features similar to observations can be clearly identified. The bottom row shows that at a given latitude b the peak positions are roughly constant. As the longitude decreases, the peak at larger distances becomes stronger. The top row shows that at a given longitude l the separation of the two peaks increases as the line of sight is further away from the Galactic plane. These results nicely agree with the observations of the X-shaped structure (MZ10). Along the bar major axis, the end-to-end separation between the inner two edges of the X-shaped structure is $\sim$2 kpc. For the outer two edges, the end-to-end separation is $\sim$4 kpc. The size of the X-shaped structure along the bar is estimated by averaging the two separations, which yields $\sim$3 kpc.

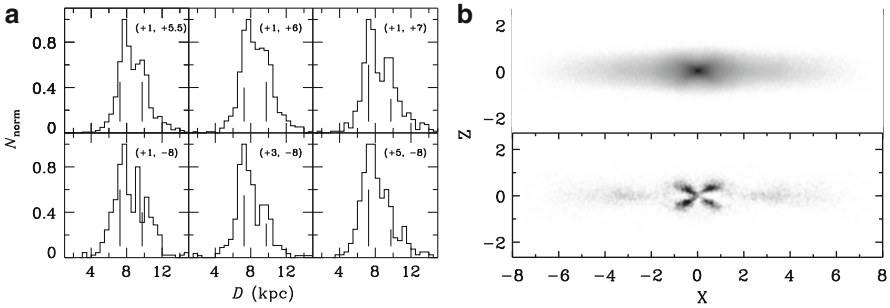

Fig. 10.6 (**a**). *Left panels*: Distance distributions of particles in the S10 model in the Galactic bulge fields at a given longitude (*top row*) and latitude (*bottom row*); (**b**). *Right panels*: Demonstration of the X-shape structure with the *upper panel* showing the side-on view of the bar in the S10 model and the *lower panel* showing the residual after fitting and subtracting the underlying smooth light contribution. The vertical X-shaped structure is highlighted in this residual image. The length unit is $R_{\rm d} = 1.9\,$kpc (Reproduced from Li and Shen (2012) with permission of AAS)

It is worth noting that the value is much less than the bar's full length (∼8 kpc). Similarly, the end-to-end vertical separation between the inner two edges of the X-shaped structure is ∼1.2 kpc. For the outer two edges in the vertical direction, this separation is ∼2.4 kpc. Therefore the vertical size of the X-shaped structure in the S10 model is ∼1.8 kpc. By summing up the pixels with positive values in the X-shaped region, Li and Shen (2012) estimated that the light fraction of this X-shaped structure relative to the whole boxy bulge region is about 7 %. It is still uncertain how much mass is contained in the X-shape. More sophisticated analysis by Portail et al. (2015a), based on the reconstructed volume density of the Galactic bulge from Vista Variables in the Via Lactea survey (VVV) (Wegg and Gerhard 2013), suggests an off-centered X-shape enclosing about 20 % of the bulge mass. Recently Nataf et al. (2015) studied the X-shape properties based on OGLE-III observations, and also found good agreement with the models in S10 and Ness et al. (2012).

Li and Shen (2012) also demonstrated that the X-shaped structure becomes nearly symmetric with respect to the disc plane about 2 Gyr after the buckling instability gradually saturates. The observed symmetry (MZ10) probably implies that the X-shaped structure in the Galactic bulge has been in existence for at least a few billion years.

Based on the ARGOS sample, Ness et al. (2012) found that the X-shaped structure is mainly composed of the metal-rich stars rather than the metal-poor ones (also see Uttenthaler et al. 2012; Gilmore et al. 2012). However, this conclusion is questioned by Nataf et al. (2014) who demonstrated that there may be a bias of metallicity on the RCs distance determination. In the future larger and unbiased samples are required to answer this question unambiguously.

The existence of the X-shaped structure in our Milky Way provides extra evidence that the Galactic bulge is shaped mainly by internal disc dynamical instabilities instead of mergers, because no other known physical processes can

naturally develop such a structure. De Propris et al. (2011) studied the radial velocity and abundances of bright and faint RCs at $(l, b) = (0°, -8°)$, and found no significant dynamical or chemical differences. This may suggest that the two RCs indeed belong to the same coherent dynamical structure, which can be naturally made in the formation of the bar/boxy bulge.

Orbital structure studies are essential for understanding the properties of the X-shaped structure, which is the outcome of the collective buckling instability. The backbone orbits of a three-dimensional buckled bar are the x_1 tree, i.e., the x_1 family plus a tree of three-dimensional families bifurcating from it (Pfenniger and Friedli 1991). It is widely believed that the X-shaped structure may be supported by orbits trapped around the three-dimensional x_1 family (also known as banana orbits due to their banana shape when viewed side-on) (e.g., Patsis et al. 2002; Skokos et al. 2002). Recent work by Portail et al. (2015b) classified orbital families in the peanut/X-shaped bulges and suggested brezel-like orbits, whose origin could be closely related to the $x_1 mul_2$ family (Patsis and Katsanikas 2014a), as the main contributor to the X-shape. Qin et al. (2015) also found that stars in the X-shaped bulge do not necessarily stream along simple banana orbits. Clearly, more studies on the orbital structure and vertical resonant heating (e.g. Quillen et al. 2014) are desired to make more specific predictions for the Milky Way.

The detailed kinematics of the near (bright) and far (faint) sides of the X-shape may be a useful tool to probe the underlying orbital structure. Several observational studies have explored the X-shape kinematics. With about 300 RCs in $(0°, -6°)$, Vásquez et al. (2013) found a weak anti-correlation between the longitudinal proper motion and radial velocity in both bright and faint RCs. However, they found no significant correlation between the latitudinal proper motion and the radial velocity. These results were interpreted as possible streaming motions along the X-shaped arms. In bulge fields at $b \sim 5°$, Poleski et al. (2013) reported the asymmetric mean proper motion difference between the near and far sides in both l and b directions; this difference is linear for $-0.1° < l < 0.5°$, but roughly constant for $-0.8° < l < -0.1°$. The linear part was attributed to the streaming motions in the X-shape.

Numerical simulations can provide comprehensive understanding of the X-shape kinematics. The kinematic imprints of the X-shape onto the Galactic bulge observations were interpreted in Gardner et al. (2014) based on their N-body models; they found a coherent minimum along $l = 0°$ in the mean radial velocity difference between the near and far sides, which is absent in other velocity components and all the velocity dispersions. Qin et al. (2015) systematically explored the kinematics (both the radial velocity and the proper motion) of the X-shape in the S10 model. Along $l = 0°$, the near and far sides of the bar/bulge show excess of approaching and receding particles, reflecting the coherent orbital motion inside the bar structure. Qin et al. (2015) found only very weak anisotropy in the stellar velocity within the X-shape, hinting that the underlying orbital family of the X-shape may not be dominated by simple banana orbits. Contrary to Poleski et al. (2013), Qin et al. (2015) found that the proper motion difference between the near/far sides of the X-shape may not be used to constrain the bar pattern speed. They also confirmed that

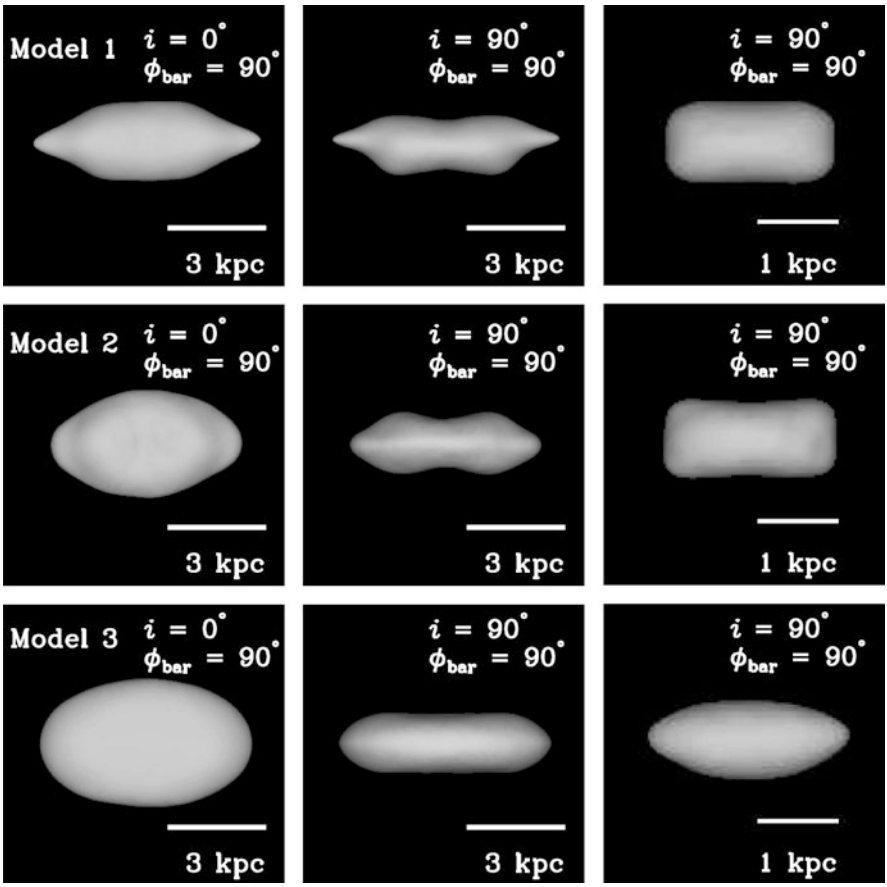

Fig. 10.7 Isodensity surfaces of three *N*-body bars with different buckling strengths, namely, Model 1 (*top row*, strongest buckling), Model 2 (*middle row*, intermediate buckling, the S10 model) and Model 3 (*bottom row*, negligible buckling). The *left* and *middle columns* show the face-on and side-on appearance of the bar at large scale (∼3 kpc). The *right column* shows the side-on shape of the isodensity surfaces at small scale (∼1 kpc)

the Galactic center may be located by fitting the arms of the X-shape, which was originally proposed by Gardner et al. (2014).

It is important to keep in mind that the true 3D shape of the X-shape should not be visualized as simple as a letter "X" with four or eight conspicuous arms sticking out. Figure 10.6 may give you such an impression because human eyes are easily biased to pick out the small-scale density enhancement. The true 3D shape or structure of iso-density surfaces should really be more like a peanut. This is demonstrated in Li and Shen (2015) who estimated the 3-D volume density for three *N*-body simulations with the adaptive kernel smoothing technique (Silverman 1986; Shen and Sellwood 2004); these three bars have undergone different amplitudes/strengths

of buckling instability. Figure 10.7 shows clearly that a buckled bar is composed of three components with increasing sizes: a central boxy core, a peanut bulge and an extended thin bar (Fig. 10.7). The true 3D structure of the X-shape is actually more peanut-shaped (Fig. 10.7), but the peanut-shaped bulge can still qualitatively reproduce the observed bimodal distance distributions that were used to infer for the X-shape. Our visual perception of seeing an "X" is enhanced by the pinched concave shape of the inner peanut structure.

10.4 More Sophisticated Chemo-Dynamical Models of the Galactic Bulge

Despite its simplicity, the self-consistent Milky Way bar/bulge model described in Sect. 10.2 is successful in explaining many aspects of the Galactic bulge, such as the boxy shape, the stellar kinematics, the X-shape, and gives reasonable bar angle, length, and the pattern speed. It may also explain, in principle, the vertical metallicity gradient (Martinez-Valpuesta and Gerhard 2013 and Sect. 10.2.2). However, in order to match the full sophisticated distribution of the stellar populations and chemical composition in the Galactic bulge, more realistic chemo-dynamical simulations must eventually supersede the simple N-body disc simulations (Sect. 10.2) in the future. It is not trivial to model gas properly in simulations, because we need to treat many complicated micro-physical processes of the multi-phase medium with simplified prescriptions. In particular, there are still considerable uncertainties in how to model the star formation and feedback processes.

Most chemo-dynamical models are motivated to explain the vertical metallicity abundance of the Galactic bulge, which was thought to be the main challenge for the secularly evolved bar/bulge model. However, as we discuss in Sect. 10.2.2, the vertical metallicity gradient may be explained by the simple bar/bulge model as well. With additional mass components in the more complicated chemo-dynamical simulations, and many more free parameters, the vertical metallicity gradient may also be reproduced in these simulations.

10.4.1 Two-Component Disc Scenario

Bekki and Tsujimoto (2011) reported that their pure thin disc model failed to reproduce the vertical metallicity gradient in the Galactic bulge, which is opposite to the conclusion reached in Martinez-Valpuesta and Gerhard (2013). This difference is due mainly to the different initial setup in the two studies. Unlike Bekki and Tsujimoto (2011), Martinez-Valpuesta and Gerhard (2013) did not try to link the initial radial metallicity profile to the metallicities of the present-day Galactic disc near the Sun, since the buckling instability in the Milky Way must have occurred long ago when the outer disc was only incompletely assembled.

Nevertheless, in order to explain the observed metallicity gradient Bekki and Tsujimoto (2011) proposed a two-component disc scenario where the bulge is formed from a disc composed of thin and thick discs. In this scenario, the first thin disc was disturbed and heated into a thick disc via a minor merger with a dwarf galaxy at early times. A subsequent thin disc is gradually built up with the inner part developing a bar structure. Since more metal-poor stars at higher latitude originate from the already dynamically hotter thick disc, which was not strongly influenced by vertical mixing of the later bar, they are able to stay in-situ for much longer and keep the metallicity low at high vertical distance. Consequently, a vertical metallicity gradient of the bulge can be produced. A similar model was also suggested in Di Matteo et al. (2014). This scenario may help explain the similarity in stellar populations between the bulge and the thick disc (Meléndez et al. 2008; Alves-Brito et al. 2010; Bensby et al. 2011). However, it is still not entirely clear whether or not the bulge stars are a distinct population with different kinematics and compositions from the thick disc stars (e.g., Lecureur et al. 2007; Fulbright et al. 2007; Minniti and Zoccali 2008).

10.4.2 Clump-Origin Bulges

Clump-origin bulges form through mergers of clumps in a primordial galactic disc. There have been attempts to link the Milky Way bulge with a clump-origin bulge. More discussions of clump-origin bulges may be found in Chap. 12 of this book.

Primordial galaxies are expected to be highly gas-rich in early stage of the disc formation, and massive star-forming clumps may form by gravitational instabilities. The clump can spiral into the center of the galaxy rapidly by dynamical friction, then merge to form a central bulge component (Noguchi 1999; Immeli et al. 2004a,b; Bournaud et al. 2007; Elmegreen et al. 2008; Inoue and Saitoh 2012). These results are consistent with the clumps in the chained galaxies observed at high redshift (Elmegreen et al. 2004).

The reported properties of the clump-origin bulges still differ considerably in various numerical simulations. Elmegreen et al. (2008) found the similarity between clump coalescence and major galaxies mergers in terms of orbital mixing. In their simulations, these giant star forming clumps migrated towards the galaxy center within a few dynamical time scales to form a classical bulge, that is thick, rotates slowly and follows a Sérsic density profile with large index (i.e. close to the $R^{1/4}$ law profile). Inoue and Saitoh (2012) performed high resolution N-body/SPH simulations of clump-origin bulges by assuming a collapsing gas sphere embedded in an NFW halo. They found that their bulge has many properties indicating for a pseudobulge, such as a nearly exponential surface density profile, a barred boxy shape and strong rotation. They also found that this bulge consists of old and metal-rich stars, similar to stars in the Galactic bulge. However, the clump-origin bulges made in these studies all failed to produce the defining characteristic of the Milky Way bulge, i.e., the strong cylindrical rotation pattern (Howard et al. 2009; Shen

et al. 2010). The relevance of clump-origin bulges to the Milky Way needs to be examined in greater depth in the future.

10.4.3 The Milky Way Bulge Formation in the Cosmological Setting

Ideally one would prefer to simulate the full evolution history of Milky Way formation with cosmological initial conditions. Such simulations will simulate the formation of the Galactic bulge in addition to thin and thick discs. The ambitious full chemo-dynamical simulations combine 3-D hydrodynamical simulations with the calculation of chemical enrichment, and obtain the positions, ages, chemical compositions, and kinematics of all star particles. Such detailed predictions can be compared to observations in large surveys. However, cosmological chemo-dynamical simulations are very computationally expensive, and much realism was still fudged in sub-grid physics.

With improved star formation and feedback models, cosmological disc simulations have made progress in making late-type disc galaxies in recent years. These simulations often use strong feedback models to prevent overproduction of stars at early times (see the recent review by Gerhard 2014). Obreja et al. (2013) analyzed and compared the bulges of a sample of L_* spiral galaxies in hydrodynamical simulations in a cosmological context. They found that the bulges show an early starburst-collapse fast phase of mass assembly, followed by a second phase with lower star formation rate, driven by disc instabilities and/or minor mergers. They suggested that one may associate the old population formed during the first rapid phase with a classical bulge, and the young one formed during the slow phase with a pseudobulge. The young population is more oblate, generally smaller, more rotationally supported, with higher metallicity and less α-enhanced than the old one. Guedes et al. (2013) followed the formation and evolution of the pseudobulge in the Eris hydrodynamic cosmological simulation with a very high resolution. Their pseudobulge was built from the inner disc, and composed of mainly old stars that formed in the first step in the inside-out formation of the baryonic disc. So far these cosmological simulations (Guedes et al. 2013; Kobayashi 2014) still do not have a boxy/peanut-shaped bulge as in the Milky Way. Cosmological simulations need a huge dynamic range to model the bulge and halo simultaneously, since the bulge is only $\sim$ 1 kpc in size, and the halo is around $\sim$ 200 kpc. So the spatial resolution required to resolve structures in the bulge may be too high. There is still a long way to go for the current chemo-dynamical simulations to explain the full evolution history of the Milky Way's bulge.

The ultimate goal of chemo-dynamical simulations is not only to reproduce the final results similar to observations, but also to make clear which process is responsible for each particular aspect of observations, which may require a large set of parameter studies. Only until we identify the basic factors contributing to the

more complex features can we claim to understand all the physics involved in the formation and evolution of the Milky Way.

10.5 Other Modeling Techniques

10.5.1 Bar Properties Constrained from Gas Kinematics

The presence of a bar structure in the Milky Way was first hinted by the non-circular gas kinematics (e.g., de Vaucouleurs 1964). One may further use the features in the asymmetric gas flow pattern to infer the properties of the Galactic bar/bulge. Non-circular motions of atomic and molecular gas in the Galaxy are commonly presented in the $l - v$ diagram, which shows the distribution of gas emission line intensity as a function of Galactic longitude and line-of-sight velocity since distances to individual gas clouds are difficult to measure (e.g., Burton and Liszt 1993; Dame et al. 2001). The high density features in the $l - v$ diagram represent the over-dense regions of gas distribution driven mainly by the large-scale non-axisymmetric structures such as the Galactic bar and spiral arms. The features in the $l-v$ diagram, due to their unknown distances, must be interpreted through gas dynamical models, and they can provide important constraints on the properties of the bar and spiral arms.

There have been many hydrodynamic models of the gas flow in barred potentials derived from COBE near-infrared maps or star counts (e.g., Englmaier and Gerhard 1999; Bissantz et al. 2003; Rodriguez-Fernandez and Combes 2008), or in self-consistent barred models (e.g., Fux 1999; Baba et al. 2010). These models have been able to reproduce many of the strong features in the $l-v$ diagram, even though no model was able to provide a good match to all the observed features. Fux (1999) modelled gas dynamics with 3D N-body + SPH simulations. He found that the gas flow driven by a self-consistent bar is asymmetric and non-stationary. Snapshots at some specific times can qualitatively reproduce the observed $l - v$ diagrams of HI and CO . His model could reproduce the connecting arms, which represent the dust lanes as a result of strong bar-driven shocks, 3-kpc arm and 135-km s^{-1} arm (both arms are emanating from the ends of the bar). Based on his modeling results, he found that a bar angle of $25° \pm 4°$, a bar co-rotation radius of 4.0–4.5 kpc, and a bar pattern speed of $\sim$50 km s^{-1}kpc^{-1}, consistent with his stellar modelling results (Fux 1997).

Englmaier and Gerhard (1999) studied gas dynamics in a rotating gravitational potential of the deprojected COBE near-infrared bar and disc. In their models, gas formed a pair of shocks at the leading side of the bar and a nuclear ring, typical of the gas flow pattern in a barred potential. Many observed gas dynamical features could be found in their models, such as the four-armed spiral structure, the 3-kpc arm, the terminal velocity curve (i.e., the envelope line of the $l - v$ diagram), tangent points, although some features are not exactly identical to those in observations.

They predicted a bar pattern speed of $\sim 60\,\mathrm{km\,s^{-1}kpc^{-1}}$ and a bar angle of about 20°–25°, similar to the results from Fux (1999). Bissantz et al. (2003) simulated the gas flow with an updated potential further constrained by COBE maps and clump giant star counts in several bulge fields. They adopted separate pattern speeds for the bar and spiral arms, and suggested that such a configuration would help to make spiral arms pass through the bar co-rotation radius where the spiral arms dissolve in the single pattern speed simulations. The 3-kpc arm and its far-side counterpart in this work cannot be reproduced very well unless they use a massive spiral arm potential. They predicted a bar pattern speed of $\sim 60\,\mathrm{km\,s^{-1}kpc^{-1}}$ and spiral arm pattern speed of $\sim 20\,\mathrm{km\,s^{-1}kpc^{-1}}$, similar to previous results.

The bar pattern speed derived from gas dynamics may have some degeneracy with the bar size; a large bar length coupled with a lower bar pattern speed may work quite well to match gas observations. Li et al. (2015) modelled gas flow pattern for the Milky Way using grid-based hydrodynamical simulations. Their basic bar potential was from an *N*-body model constrained by the density of bulge red clump stars (Portail et al. 2015a; Wegg and Gerhard 2013). They found that a low pattern speed model for the Galactic bar may work, and the best model can give a better fit to the $l - v$ diagram than previous high pattern speed simulations.

10.5.2 Orbit-Based and Particle-Based Modeling

Although numerical simulations such as *N*-body can offer the full evolutionary history from plausible initial conditions, they also have weaknesses. Numerical simulations are inflexible in the sense that a lot of trials are required to reproduce the desired results by adjusting the initial conditions – this becomes very challenging especially for more sophisticated chemo-dynamical simulations which often rely on fudged sub-grid physics and are computationally costly, thus limiting the systematic exploration of parameter space to match the observational results.

Other modelling approaches such as the **Schwarzschild** and **made-to-measure** methods are complementary to *N*-body simulations. Both methods are good at steering models to match the desired final results.

The basic principle of the Schwarzschild orbit-superposition method is given in Schwarzschild (1979). One first computes and finds the typical orbital families in a potential arising from an assumed triaxial density distribution. The time-averaged density along each orbit in a lattice of cells spanning the volume of the model is simply the total cumulative time spent by that orbit in each cell. Then linear/quadratic programming techniques are used to find the non-negative weights of each orbit to fit the assumed mass distribution and the kinematical data to achieve self-consistency. There is no unique solution for the orbital weights, but one may seek to maximize some objective function for a balance of χ^2 minimizations and smoother phase-space distributions (e.g., Richstone and Tremaine 1988; Thomas et al. 2005). The stability of the constructed model is also not guaranteed, and generally needs to

be tested with an N-body code. The weighted orbital structure resulting from the Schwarzschild modeling can offer important clues to the formation history of a system.

Based on the Schwarzschild orbit-superposition method, Zhao (1996) developed the first 3D rotating bar model that fitted the density profile of the COBE light distribution and kinematic data at Baade's window. His model was constructed with 485 orbit building blocks, and little stellar kinematic data were available to explore the uniqueness of this steady-state model. Häfner et al. (2000) extended the classical Schwarzschild technique by combining a distribution function that depends only on classical integrals with orbits that respect non-classical integrals, i.e., Schwarzschild's orbits were used only to represent the difference between the true galaxy distribution function and an approximating classical distribution function. They used the new method to construct a dynamical model of the inner Galaxy with an orbit library that contains about 22,000 regular orbits. For definiteness, they assumed a bar angle of 20° and bar pattern speed of $60\,\mathrm{km\,s^{-1}kpc^{-1}}$. The model reproduced the 3D mass density obtained through deprojection of the COBE surface photometry, and the then-available kinematics within the bar corotation radius (3.6 kpc).

Wang et al. (2012) extended the Schwarzschild implementation of Zhao (1996) and applied it with the extra kinematic constraints from the full BRAVA dataset (Kunder et al. 2012). Using χ^2 minimization, their best-fitting Galactic bar model has a pattern speed of $60\,\mathrm{km\,s^{-1}kpc^{-1}}$, a disc mass of $10^{11}\mathrm{M}_\odot$ and a bar angle of 20° out of 36 models varying these parameters. Compared to Zhao (1996), Wang et al. (2012) can better reproduce the average radial velocity and the surface brightness distribution. However, their model over-predicted the longitudinal proper motions compared to the observed values. N-body tests showed that the model was stable only for a short period of 0.5 Gyr. They suspected that the instability arises because no self-consistency was imposed for the disc outside 3 kpc. Wang et al. (2013) made further tests of their implementation using the N-body bar model in Shen et al. (2010), with the hope to recover the given bar pattern speed and the bar angle in Shen et al. (2010). They concluded that BRAVA radial velocities alone do not constrain well the bar angle and/or the pattern speed using their Schwarzschild implementation, and the observed proper motions may help to reduce the model degeneracy. Their method appeared to over-fit the BRAVA data points, indicating that the implemented smoothing of the phase space distributions may need improvement.

Building a complete and representative orbit library in bars, essential for the Schwarzschild method, is non-trivial. It is necessary to explore systematically which of the many possible orbit families could contribute to a self-consistent model, and to understand how they are affected by properties of the bar potential. For example, Schwarzschild modelling may help elucidate the actual orbital compositions supporting the prominent X-shaped/peanut-shaped structure in the Galactic bulge. There seem to be a large number of irregular/chaotic orbits in bars (e.g., Wang et al. 2012; Patsis and Katsanikas 2014a,b). We need to have a better idea on the fraction

of chaotic orbits, classify them into major families, and identify the location of resonant orbits.

Uniqueness of the solution is also an undesired feature in the Schwarzschild modeling of the Galactic bar. There is considerable freedom to reproduce the existing data by different sets of orbital weights. More systematic studies are needed to explore how many different combinations of orbits still reach the same goodness-of-fit for a given potential, and how much the properties of the final bar can vary but still satisfy the same observational constraints.

Unlike the Schwarzschild method, **made-to-measure (M2M)** method (Syer and Tremaine 1996) slowly adjusts the weights of the particles in an N-body system, instead of the orbital weights as in the Schwarzschild method, as particles proceed in their orbits until the time-averaged density field and other observables converge to a prescribed observational value. The particle weights are adjusted through a weight evolution equation according to the mismatch between the model and target observables. In the Schwarzschild method orbits are first separately integrated in a fixed potential and then superimposed, whereas in the M2M method the two steps are merged – orbits are integrated and the weights of particles are adjusted at the same time, thus eliminating the need for an orbit library. Also M2M can allow us to dynamically adjust the potential while Schwarzschild does not.

The M2M method was first applied to construct a dynamical model for the barred bulge and disc model of the Milky Way in Bissantz et al. (2004). Since then the M2M method has been continuously improved in various implementations, and has gained growing interests in the dynamical modelling of galaxies, especially spheroidals and early-type galaxies (e.g., de Lorenzi et al. 2007, 2008, 2009; Dehnen 2009; Long and Mao 2010, 2012; Morganti and Gerhard 2012; Hunt and Kawata 2013; Hunt et al. 2013). A modified χ^2M2M was implemented to improve the algorithm to model both the density and kinematic data, account for observational errors and seeing effects, and incorporate a maximum-likelihood technique to account for discrete velocities (de Lorenzi et al. 2007, 2008). Long and Mao (2012) applied their design and implementation of the M2M method (Long and Mao 2010) to 24 SAURON galaxies previously analysed by Cappellari et al. (2006), and found generally good agreement between M2M and Schwarzschild methods in determining the dynamical mass-to-light ratio.

Long et al. (2013) constructed a M2M model of the Galactic bar/bulge constrained by the BRAVA kinematics (Kunder et al. 2012). They took the N-body model in Shen et al. (2010) as initial condition and the target luminosity density. They ran a suite of 56 models with different pattern speeds and bar angles in search of the best-fitting one. Their best-fitting model recovered the bar angle and pattern speed of the Shen et al. (2010) N-body model, and reproduced both the mean radial velocity and radial velocity dispersion of the BRAVA data very well. Since they used BRAVA results as kinematic constraints and the Shen et al. (2010) model as the target luminosity density, this work is actually a cross-check between the direct N-body modelling and the M2M method. Hunt and Kawata (2013) and Hunt et al. (2013) modelled disc systems with their own design and implementation of the M2M method (particle-by-particle M2M method, or PRIMAL). They showed that

PRIMAL can recover the radial profiles of the surface density, velocity dispersions, the rotational velocity of the target discs, the apparent bar structure and the bar pattern speed of the bar.

Recently, Portail et al. (2015a) constructed dynamical models of the Galactic boxy/peanut bulge, using the 3D density of red clump giants (Wegg and Gerhard 2013) and BRAVA kinematics as observational constraints. They tried to match the data using their M2M code (de Lorenzi et al. 2007, 2008), starting with N-body models for barred discs in different dark matter haloes. In this work, they estimated the total dynamical mass (including both stellar and dark matter halo) as $1.84 \pm 0.07 \times 10^{10} \mathrm{M}_{\odot}$ inside the rectangular box of $\pm 2.2 \times \pm 1.4 \times \pm 1.2$ kpc. They used BRAVA kinematical data to constrain the models, but the proper motion data (Rattenbury et al. 2007a) are used only as a check of their modelling. Their models tend to be more anisotropic than the data. Given the different significance of the disc component in their initial conditions, their five models sample a wide range of pattern speeds of the final bar structures, ranging from $R \sim 1.08$ to 1.80, where $R = R_{\mathrm{CR}}/R_{bar}$ is the dimensionless parameter characterizing the pattern speed of the bar. They got a scaled value of 25–30 $\mathrm{km\,s^{-1}kpc^{-1}}$, significantly lower than previous estimates with various methods (40–60 $\mathrm{km\,s^{-1}kpc^{-1}}$). If confirmed, this puts the Galactic bar among slow rotators ($R \geq 1.5$).

In summary, both the Schwarzschild and M2M methods are designed to steer models with pre-determined initial conditions towards prescribed observed results. M2M models include aspects of both Schwarzschild methods and regular N-body simulations. When the gravitational potential of the target system is held fixed, the searching process for a distribution of particle weights is closely related to that for a distribution of orbital weights in Schwarzschild's method to fit the same observational constraints. Conversely, when the adjustment of particle weights is switched off and the potential is allowed to evolve, M2M particle codes can reduce to N-body simulations (Gerhard 2010). On the other hand, both types of modelling only construct self-consistent equilibrium models, but they do not tell us how the Galaxy evolved into the current equilibrium configuration from what initial conditions. The most important value of these modelling techniques is that they give us predictive power and suggest further observational tests to confirm or constrain the structural parameters of the bar/bulge.

10.6 Summary and Future Outlook

Understanding the structure and formation of our Milky Way bulge is nontrivial, mostly because of our location in the disc plane and the severe dust extinction in the optical band. Near infrared images from the COBE satellite presented the first clear evidence of a boxy bulge in the Galaxy. Recent large dedicated surveys have allowed a large number of bulge stars to be studied individually in detail. Most bulge stars are very old with a wide range of metal abundances, and they formed earlier than most disc stars on a rapid formation time scale. Observationally, we still need to

better understand the bulge metallicity components identified by Ness et al. (2013a) and their kinematic signatures (Ness et al. 2013b). Future large surveys will also need to settle whether or not the recently identified X-shaped structure is populated mainly by metal-rich stars, instead of metal-poor ones (Nataf et al. 2014).

The Galactic bulge contains crucial information about the formation of evolutionary history of the Milky Way. To unravel these clues theoretical modelling of the bulge is essential. Here we have reviewed recent advances in modelling the Galactic bulge with *N*-body, chemo-dynamical simulations, and other modelling techniques. The main body of the Milky Way bulge appears to be a buckled/thickened bar seen somewhat end-on, as hinted from its asymmetric boxy shape. One can construct a fully evolutionary bar model that matches many properties of the Galactic bulge reasonably well (Sect. 10.2). The dynamical evolution of the bar/bulge was driven mainly by two consecutive disc instabilities. The bar forms naturally from a cold massive precursor disc via the well-known bar instability. Shortly after its formation, the bar suffers from a vigorous buckling instability, and becomes a thickened structure that appears boxy or peanut-shaped when seen edge-on. Such a model self-consistently evolves from plausible simple initial conditions, and is successful in explaining many aspects of the Milky Way bulge, such as the excellent match to the kinematics of the whole bulge, the X-shaped structure that naturally arises in the bar buckling process, reasonable bar angle and other bar parameters consistent with independent structural analysis, and the metallicity map.

This simple model provides a promising starting point, but there are still many open questions to be answered in more sophisticated chemo-dynamical models. For example, what is the exact mass fraction of a possible classical bulge hidden underneath the dominant boxy bulge; how the fossil record of the early inner Galaxy (thick disc, old and younger thin discs) is mapped into the bulge structure, i.e., how to better understand the bulge metallicity components identified by Ness et al. (2013a,b) in the ARGOS survey, and their correlation with the kinematics; how the strongly barred X-shaped structure is populated preferentially by metal-rich stars; is there a solid connection between the bulge and the thick disc (Bekki and Tsujimoto 2011; Di Matteo et al. 2014)?

Ongoing and upcoming large surveys will undoubtedly shed new light on the Milky Way bulge. *Gaia* will provide accurate parallaxes and proper motions of about 20 million stars along all the lines of sight towards the bulge (Robin et al. 2005). Complementary to the *Gaia* mission, ongoing ground based surveys such as APOGEE, VVV, *Gaia*-ESO, GIBS will also provide us huge amount of high-resolution spectroscopic data. With the large influx of data and the improvements in theoretical models, we are poised to make greater progress in putting together all puzzle pieces of the Milky Way bulge.

Acknowledgements We thank Shude Mao, Dimitri Gadotti, Eija Laurikainen, Zhi Li, Richard Long, Martin Smith, and Yu-jing Qin for helpful discussions and comments. The research presented here is partially supported by the 973 Program of China under grant no. 2014CB845700, by the National Natural Science Foundation of China under grant nos.11333003, 11322326, 11403072, and by the Strategic Priority Research Program “The Emergence of Cosmological

Structures" (no. XDB09000000) of the Chinese Academy of Sciences. ZYL is grateful for the support from Shanghai Yangfan Talent Youth Program (No. 14YF1407700). This work made use of the facilities of the Center for High Performance Computing at Shanghai Astronomical Observatory.

References

Alves-Brito A., Meléndez J., Asplund M., Ramírez I., Yong D., 2010, A&A, 513, A35
Athanassoula E., 2005, MNRAS, 358, 1477
Baba J., Saitoh T. R., Wada K., 2010, PASJ, 62, 1413
Babusiaux C. et al., 2010, A&A, 519, A77
Bekki K., Tsujimoto T., 2011, MNRAS, 416, L60
Benjamin R. A. et al., 2005, ApJ, 630, L149
Bensby T. et al., 2011, A&A, 533, A134
Bensby T. et al., 2012, in Astronomical Society of the Pacific Conference Series, Vol. 458, Galactic Archaeology: Near-Field Cosmology and the Formation of the Milky Way, Aoki W., Ishigaki M., Suda T., Tsujimoto T., Arimoto N., eds., p. 203
Binney J., 1978, MNRAS, 183, 501
Binney J., Gerhard O. E., Stark A. A., Bally J., Uchida K. I., 1991, MNRAS, 252, 210
Bissantz N., Debattista V. P., Gerhard O., 2004, ApJ, 601, L155
Bissantz N., Englmaier P., Gerhard O., 2003, MNRAS, 340, 949
Bissantz N., Gerhard O., 2002, MNRAS, 330, 591
Blitz L., Spergel D. N., 1991, ApJ, 379, 631
Bournaud F., Elmegreen B. G., Elmegreen D. M., 2007, ApJ, 670, 237
Bureau M., Freeman K. C., 1999, AJ, 118, 126
Burton W. B., Liszt H. S., 1993, A&A, 274, 765
Cabrera-Lavers A., Hammersley P. L., González-Fernández C., López-Corredoira M., Garzón F., Mahoney T. J., 2007, A&A, 465, 825
Cao L., Mao S., Nataf D., Rattenbury N. J., Gould A., 2013, MNRAS, 434, 595
Cappellari M. et al., 2006, MNRAS, 366, 1126
Clarkson W. et al., 2008, ApJ, 684, 1110
Clarkson W. I. et al., 2011, ApJ, 735, 37
Combes F., Debbasch F., Friedli D., Pfenniger D., 1990, A&A, 233, 82
Dame T. M., Hartmann D., Thaddeus P., 2001, ApJ, 547, 792
de Lorenzi F., Debattista V. P., Gerhard O., Sambhus N., 2007, MNRAS, 376, 71
de Lorenzi F. et al., 2009, MNRAS, 395, 76
de Lorenzi F., Gerhard O., Saglia R. P., Sambhus N., Debattista V. P., Pannella M., Méndez R. H., 2008, MNRAS, 385, 1729
De Propris R. et al., 2011, ApJ, 732, L36
de Vaucouleurs G., 1964, in IAU Symposium, Vol. 20, The Galaxy and the Magellanic Clouds, Kerr F. J., ed., p. 195
Debattista V. P., Shen J., 2007, ApJ, 654, L127
Dehnen W., 2009, MNRAS, 395, 1079
Di Matteo P. et al., 2014, ArXiv e-prints
Elmegreen B. G., Bournaud F., Elmegreen D. M., 2008, ApJ, 688, 67
Elmegreen D. M., Elmegreen B. G., Hirst A. C., 2004, ApJ, 604, L21
Englmaier P., Gerhard O., 1999, MNRAS, 304, 512
Erwin P., Sparke L. S., 2002, AJ, 124, 65
Erwin P., Sparke L. S., 2003, ApJS, 146, 299
Freeman K. et al., 2013, MNRAS, 428, 3660

Freeman K. C., 2008, in IAU Symposium, Vol. 245, IAU Symposium, Bureau M., Athanassoula E., Barbuy B., eds., pp. 3–10
Fulbright J. P., McWilliam A., Rich R. M., 2007, ApJ, 661, 1152
Fux R., 1997, A&A, 327, 983
Fux R., 1999, A&A, 345, 787
Gardner E., Debattista V. P., Robin A. C., Vásquez S., Zoccali M., 2014, MNRAS, 438, 3275
Gerhard O., 2010, Highlights of Astronomy, 15, 198
Gerhard O., 2014, ArXiv:1408.0218
Gerhard O., Martinez-Valpuesta I., 2012, ApJ, 744, L8
Gilmore G. et al., 2012, The Messenger, 147, 25
Gonzalez O. A., Rejkuba M., Minniti D., Zoccali M., Valenti E., Saito R. K., 2011a, A&A, 534, L14
Gonzalez O. A. et al., 2011b, A&A, 530, A54
Gonzalez O. A., Rejkuba M., Zoccali M., Valent E., Minniti D., Tobar R., 2013, A&A, 552, A110
Guedes J., Mayer L., Carollo M., Madau P., 2013, ApJ, 772, 36
Häfner R., Evans N. W., Dehnen W., Binney J., 2000, MNRAS, 314, 433
Hill V. et al., 2011, A&A, 534, A80
Howard C. D. et al., 2009, ApJ, 702, L153
Howard C. D., Rich R. M., Reitzel D. B., Koch A., De Propris R., Zhao H., 2008, ApJ, 688, 1060
Howes L. M. et al., 2014, MNRAS, 445, 4241
Hunt J. A. S., Kawata D., 2013, MNRAS, 430, 1928
Hunt J. A. S., Kawata D., Martel H., 2013, MNRAS, 432, 3062
Immeli A., Samland M., Gerhard O., Westera P., 2004a, A&A, 413, 547
Immeli A., Samland M., Westera P., Gerhard O., 2004b, ApJ, 611, 20
Inoue S., Saitoh T. R., 2012, MNRAS, 422, 1902
Johnson C. I., Rich R. M., Fulbright J. P., Valenti E., McWilliam A., 2011, ApJ, 732, 108
Johnson C. I., Rich R. M., Kobayashi C., Fulbright J. P., 2012, ApJ, 749, 175
Johnson C. I., Rich R. M., Kobayashi C., Kunder A., Pilachowski C. A., Koch A., de Propris R., 2013, ApJ, 765, 157
Kobayashi C., 2014, in IAU Symposium, Vol. 298, IAU Symposium, Feltzing S., Zhao G., Walton N. A., Whitelock P., eds., pp. 167–178
Kormendy J., 1993, in IAU Symposium, Vol. 153, Galactic Bulges, Dejonghe H., Habing H. J., eds., p. 209
Kormendy J., Drory N., Bender R., Cornell M. E., 2010, ApJ, 723, 54
Kormendy J., Kennicutt, Jr. R. C., 2004, ARA&A, 42, 603
Kunder A. et al., 2012, AJ, 143, 57
Launhardt R., Zylka R., Mezger P. G., 2002, A&A, 384, 112
Laurikainen E., Salo H., Athanassoula E., Bosma A., Herrera-Endoqui M., 2014, MNRAS, 444, L80
Lecureur A., Hill V., Zoccali M., Barbuy B., Gómez A., Minniti D., Ortolani S., Renzini A., 2007, A&A, 465, 799
Li Z., Gerhard O., Shen J., et al., 2015, ApJ, in preparation
Li Z.-Y., Shen J., 2012, ApJ, 757, L7
Li Z.-Y., Shen J., 2015, ApJ, in preparation
Li Z.-Y., Shen J., Rich R. M., Kunder A., Mao S., 2014, ApJ, 785, L17
Long R. J., Mao S., 2010, MNRAS, 405, 301
Long R. J., Mao S., 2012, MNRAS, 421, 2580
Long R. J., Mao S., Shen J., Wang Y., 2013, MNRAS, 428, 3478
Martinez-Valpuesta I., Gerhard O., 2011, ApJ, 734, L20
Martinez-Valpuesta I., Gerhard O., 2013, ApJ, 766, L3
Martinez-Valpuesta I., Shlosman I., Heller C., 2006, ApJ, 637, 214
McWilliam A., Rich R. M., 1994, ApJS, 91, 749
McWilliam A., Zoccali M., 2010, ApJ, 724, 1491
Meléndez J. et al., 2008, A&A, 484, L21

Minniti D., Zoccali M., 2008, in IAU Symposium, Vol. 245, IAU Symposium, Bureau M., Athanassoula E., Barbuy B., eds., pp. 323–332
Morganti L., Gerhard O., 2012, MNRAS, 422, 1571
Nataf D. M., Cassisi S., Athanassoula E., 2014, MNRAS, 442, 2075
Nataf D. M., Udalski A., Gould A., Fouqué P., Stanek K. Z., 2010, ApJ, 721, L28
Nataf D. M. et al., 2015, MNRAS, 447, 1535
Ness M., Debattista V. P., Bensby T., Feltzing S., Roškar R., Cole D. R., Johnson J. A., Freeman K., 2014, ApJ, 787, L19
Ness M. et al., 2013a, MNRAS, 430, 836
Ness M. et al., 2013b, MNRAS, 432, 2092
Ness M. et al., 2012, ApJ, 756, 22
Nidever D. L. et al., 2012, ApJ, 755, L25
Nishiyama S. et al., 2005, ApJ, 621, L105
Noguchi M., 1999, ApJ, 514, 77
Obreja A., Domínguez-Tenreiro R., Brook C., Martínez-Serrano F. J., Doménech-Moral M., Serna A., Mollá M., Stinson G., 2013, ApJ, 763, 26
Origlia L., 2014, in IAU Symposium, Vol. 298, IAU Symposium, Feltzing S., Zhao G., Walton N. A., Whitelock P., eds., pp. 28–39
Ortolani S., Renzini A., Gilmozzi R., Marconi G., Barbuy B., Bica E., Rich R. M., 1995, Nature, 377, 701
Patsis P. A., Katsanikas M., 2014a, MNRAS, 445, 3525
Patsis P. A., Katsanikas M., 2014b, MNRAS, 445, 3546
Patsis P. A., Skokos C., Athanassoula E., 2002, MNRAS, 337, 578
Peebles P. J. E., Nusser A., 2010, Nature, 465, 565
Pfenniger D., Friedli D., 1991, A&A, 252, 75
Pfenniger D., Norman C., 1990, ApJ, 363, 391
Pietrukowicz P. et al., 2014, ArXiv:1412.4121
Poleski R. et al., 2013, ApJ, 776, 76
Portail M., Wegg C., Gerhard O., 2015b, MNRAS, 450, 66
Portail M., Wegg C., Gerhard O., Martinez-Valpuesta I., 2015a, MNRAS, 448, 713
Qin Y., Shen J., Li Z.-Y., Mao S., Smith M. C., Rich R. M., Kunder A., Liu C., 2015, ArXiv:1503.06774
Quillen A. C., Minchev I., Sharma S., Qin Y.-J., Di Matteo P., 2014, MNRAS, 437, 1284
Raha N., Sellwood J. A., James R. A., Kahn F. D., 1991, Nature, 352, 411
Rangwala N., Williams T. B., Stanek K. Z., 2009, ApJ, 691, 1387
Rattenbury N. J., Mao S., Debattista V. P., Sumi T., Gerhard O., de Lorenzi F., 2007a, MNRAS, 378, 1165
Rattenbury N. J., Mao S., Sumi T., Smith M. C., 2007b, MNRAS, 378, 1064
Rich R. M., 2013, The Galactic Bulge, Oswalt T. D., Gilmore G., eds., p. 271
Rich R. M., Howard C., Reitzel D. B., Zhao H., de Propris R., 2008, in IAU Symposium, Vol. 245, IAU Symposium, Bureau M., Athanassoula E., Barbuy B., eds., pp. 333–338
Rich R. M., Origlia L., Valenti E., 2012, ApJ, 746, 59
Rich R. M., Reitzel D. B., Howard C. D., Zhao H., 2007, ApJ, 658, L29
Richstone D. O., Tremaine S., 1988, ApJ, 327, 82
Robin A. C., Marshall D. J., Schultheis M., Reylé C., 2012, A&A, 538, A106
Robin A. C., Reylé C., Picaud S., Schultheis M., 2005, A&A, 430, 129
Rodriguez-Fernandez N. J., Combes F., 2008, A&A, 489, 115
Rojas-Arriagada A., Recio-Blanco A., Hill V., 2014, A&A, 569, A103
Saha K., Martinez-Valpuesta I., Gerhard O., 2012, MNRAS, 421, 333
Saito R. K., Zoccali M., McWilliam A., Minniti D., Gonzalez O. A., Hill V., 2011, AJ, 142, 76
Schlaufman K. C., Casey A. R., 2014, ApJ, 797, 13
Schwarzschild M., 1979, ApJ, 232, 236
Sellwood J. A., 2014, Reviews of Modern Physics, 86, 1
Sevenster M., Saha P., Valls-Gabaud D., Fux R., 1999, MNRAS, 307, 584

Shen J., 2014, in IAU Symposium, Vol. 298, IAU Symposium, Feltzing S., Zhao G., Walton N. A., Whitelock P., eds., pp. 201–206
Shen J., Debattista V. P., 2009, ApJ, 690, 758
Shen J., Rich R. M., Kormendy J., Howard C. D., De Propris R., Kunder A., 2010, ApJ, 720, L72
Shen J., Sellwood J. A., 2004, ApJ, 604, 614
Silverman B. W., 1986, Density estimation for statistics and data analysis
Skokos C., Patsis P. A., Athanassoula E., 2002, MNRAS, 333, 847
Soderblom D. R., 2010, ARA&A, 48, 581
Soto M., Rich R. M., Kuijken K., 2007, ApJ, 665, L31
Stanek K. Z., Garnavich P. M., 1998, ApJ, 503, L131
Stanek K. Z., Udalski A., SzymaŃski M., KaŁuŻny J., Kubiak Z. M., Mateo M., KrzemiŃski W., 1997, ApJ, 477, 163
Syer D., Tremaine S., 1996, MNRAS, 282, 223
Thomas J., Saglia R. P., Bender R., Thomas D., Gebhardt K., Magorrian J., Corsini E. M., Wegner G., 2005, MNRAS, 360, 1355
Toomre A., 1966, in Geophysical Fluid Dynamics, notes on the 1966 Summer Study Program at the Woods Hole Oceanographic Institution, ref. no. 66–46, p. 111
Uttenthaler S., Schultheis M., Nataf D. M., Robin A. C., Lebzelter T., Chen B., 2012, A&A, 546, A57
Vásquez S. et al., 2013, A&A, 555, A91
Wang Y., Mao S., Long R. J., Shen J., 2013, MNRAS, 435, 3437
Wang Y., Zhao H., Mao S., Rich R. M., 2012, MNRAS, 427, 1429
Wegg C., Gerhard O., 2013, MNRAS, 435, 1874
Weiland J. L. et al., 1994, ApJ, 425, L81
Wyse R. F. G., 1999, in The Formation of Galactic Bulges, Carollo C. M., Ferguson H. C., Wyse R. F. G., eds., p. 195
Zhao H., 1996, MNRAS, 283, 149
Zoccali M., 2010, in IAU Symposium, Vol. 265, IAU Symposium, Cunha K., Spite M., Barbuy B., eds., pp. 271–278
Zoccali M. et al., 2014, A&A, 562, A66
Zoccali M., Hill V., Lecureur A., Barbuy B., Renzini A., Minniti D., Gómez A., Ortolani S., 2008, A&A, 486, 177
Zoccali M. et al., 2003, A&A, 399, 931

Part IV
Coevolution of Bulges and Black Holes

Chapter 11
Galaxy Bulges and Their Massive Black Holes: A Review

Alister W. Graham

Abstract With references to both key and often forgotten pioneering works, this article starts by presenting a review into how we came to believe in the existence of massive black holes at the centers of galaxies. It then presents the historical development of the near-linear (black hole)–(host spheroid) mass relation, before explaining why this has recently been dramatically revised. Past disagreement over the slope of the (black hole)–(velocity dispersion) relation is also explained, and the discovery of sub-structure within the (black hole)–(velocity dispersion) diagram is discussed. As the search for the fundamental connection between massive black holes and their host galaxies continues, the competing array of additional black hole mass scaling relations for samples of predominantly inactive galaxies are presented.

11.1 Overview

Arguably one of the most exciting aspects of galaxy bulges are the monstrous black holes which reside in their cores, sometimes lurking quietly, other times beaming out their existence to the Universe. Not only are they the dominant species on the mass spectrum of individual objects, but they play host to such a range of extremely unusual phenomenon that they appeal to people of all ages and professions.

For extragalactic astronomers, one curious aspect is the apparent coupling between the mass of the black hole, $M_{\rm bh}$, and the host galaxy bulge or spheroid, $M_{\rm sph}$, within which it resides. The importance of this is because it suggests that the growth of the two is intimately intertwined, and unravelling this connection will provide insight into their co-evolution. While the $M_{\rm bh}$–$M_{\rm sph}$ relation may arise from black hole feedback processes such that the black hole regulates the growth of the surrounding spheroid (a remarkable feat given the factor of a billion difference in physical size), correlations between both the central radial concentration of stars and the central stellar density of the spheroid with $M_{\rm sph}$ might be telling us that it

A.W. Graham (✉)
Center for Astrophysics and Supercomputing, Swinburne University of Technology, Hawthorn, VIC 3122, Australia
e-mail: AGraham@swin.edu.au

E. Laurikainen et al. (eds.), *Galactic Bulges*, Astrophysics and Space Science Library 418, DOI 10.1007/978-3-319-19378-6_11

is instead the spheroid mass which (indirectly) dictates the black hole mass through these relations.

This article starts by providing a background briefing to the development of ideas (since Einstein introduced his theories of relativity) which have led to our current understanding of supermassive black holes in galactic nuclei (Sect. 11.2), and the eventual observational proof which ruled out alternative astrophysical suggestions for the dark mass concentrations identified there (Sect. 11.3). Some effort has been made to reference key papers and give credit to the original developers of ideas and solutions, of whom many have been poorly cited in the literature to date.

Not surprisingly, many reviews have been written about supermassive black holes, and far more than the author was aware when approached to write this review. Enjoyable reports are provided by Kormendy and Richstone (1995) and Longair (1996, 2006) which includes a well-written historical perspective, and an impressively extensive overview of many sub-topics can be found in Ferrarese and Ford (2005) which remain highly relevant today. In it, they too provide an historical account of active galactic nuclei (AGN), detail the many methods used to measure the masses of black holes today, and compare the demographics of black holes in distant quasars with local galaxies. It is however their Sect. 11.9, pertaining to the scaling relations between the masses of black holes and the properties of their host galaxy that is the main focus of this article. For references to other aspects of massive black holes, over the past decade or so the following astrophysical reviews have focussed on: Sagittarius A* (Alexander 2005; Genzel et al. 2010); intermediate mass black holes (Miller and Colbert 2004; van der Marel 2004); massive black hole binaries (Merritt and Milosavljević 2005); AGN activity and feedback (Brandt and Hasinger 2005; Ho 2008; McNamara and Nulsen 2007; Heckman and Best 2014), including hot accretion flows (Yuan and Narayan 2014) and cold accretion flows (Kato et al. 2008; Abramowicz and Fragile 2013); connections with distant AGN (Shankar 2009a); redshifted fluorescent iron lines (Reynolds and Nowak 2003; Miller 2007); gravitational radiation (Berti et al. 2009, see also Amaro-Seoane et al. 2012); black hole spin (Gammie et al. 2004; Reynolds 2013); black hole seeds (Volonteri 2010, see also Koushiappas et al. 2004); and a healthy mix of various topics (e.g. Kormendy and Ho 2013; Genzel 2014) as in Ferrarese and Ford (2005).

As noted by Ferrarese and Ford (2005), in 2004 direct black hole mass measurements were known for 30 galaxies, plus another 8 galaxies for which the dynamical models might be in error. Recently, Savorgnan and Graham (2014), see also Kormendy and Ho (2013), tabulate 89 galaxies with reliably measured black hole masses. Not only has the sample size therefore tripled over the past decade, but new scaling relations have been uncovered and old relations have been revised – and dramatically so as we shall see in the case of the $M_{\rm bh}$–$M_{\rm sph}$ and $M_{\rm bh}$–$L_{\rm sph}$ relations (Sect. 11.4). The $M_{\rm bh}$–σ relation, involving the velocity dispersion of the galactic host, is reviewed in Sect. 11.5 and the controversial issue of its slope addressed. The apparent substructure in the $M_{\rm bh}$–σ diagram, reported in 2008 due to barred galaxies and/or pseudobulges, is additionally discussed.

Having dealt in some detail with the two most commonly cited black hole scaling relations in Sects. 11.4 and 11.5, the assortment of related relations are presented.

While not as popular in the literature, it may be one of these relations which provides the fundamental, or at least an important, link between the black hole mass and its host galaxy (an issue raised by Alexander and Hickox 2012). Therefore, Sect. 11.6 examines the connection between the black hole mass and the host spheroid's Sérsic index, i.e. how radially concentrated the spheroid's stellar distribution is; this dictates the radial gradient of the gravitational potential. Section 11.7 describes the expected association between the black hole mass and the central stellar density (prior to core depletion). Section 11.8 explores the link between the mass of the black hole and the missing stellar mass at the centers of giant spheroids. The connection between the black holes and the dense star clusters found in the nuclei of many galaxies – some of which may harbour intermediate mass black holes – is presented in Sect. 11.9. Section 11.10 discusses the black hole mass relation with the halo (baryons plus dark matter) mass, expected to exist for spheroid dominated galaxies, while Sect. 11.11 remarks on the existence of a correlation with the pitch angle of spiral arms in late-type galaxies. Finally, Sect. 11.12 considers the possibility that a third parameter may account for some of the scatter in the above bivariate distributions, leading to a more fundamental plane or hypersurface in 3-parameter space involving black hole mass and two galaxy/spheroid parameters.

11.2 Historical Development: From Mathematical Speculation to Widespread Suspicion

Karl Schwarzschild (1916; 1999; see also Droste 1917 who independently derived the same solution in 1916) is widely recognised for having developed the 'Schwarzschild metric' for a spherical or point mass within Einstein's (1916) theory of general relativity,[1] but it was Finkelstein (1958, see also Kruskal 1960) who realised the true nature of what has come to be called the "event horizon" bounding these gravitational prisons. Finkelstein eloquently describes this Schwarzschild surface as "a perfect unidirectional membrane: causal influences can cross it but only in one direction". Five years later, while working at the University of Texas, the New Zealand mathematician Roy Kerr (1963) formulated the metric for the more realistic[2] *rotating* black hole. Interestingly, solutions to this space-time include closed time-like curves which, in theory, allow one to travel backwards in time (a concept popularised but also questioned by Thorne 1994). Kurt Gödel (1949) was actually the first to derive such strange solutions to the equations of general relativity, although it is commonly suspected that all closed time-like curves are

[1] It is of interest to note that Einstein was not keen on the idea of singularities, and in Einstein (1939) he wrote that *"The essential result of this investigation is a clear understanding as to why the 'Schwarzschild singularities' do not exist in physical reality"*.

[2] Collapsing stars, and (accretion disc)-fed black holes, are expected to have substantial angular momentum.

just a mathematical artifact, in the same way that the original singularity at the Schwarzschild radius was later explained away by a coordinate transformation (e.g. Eddington 1924; Georges Lemaître 1933), leaving just the singularity (i.e. black hole) at the center. But even if we are to be denied our time machines,[3] black holes still offer the curious and unsuspecting property of evaporating over time – radiating like a black body – before possibly then exploding (Hawking 1974, 1975).

Evolving parallel to the above analytical developments, our acceptance of black holes as more than just a mathematical curiosity had additional connections with stellar evolution and dark stars.[4] As detailed by Yakovlev (1994), the Soviet physicist Yakov Frenkel (1928) was the first to derive equations for the energy density and pressure of super-dense stars comprised of a degenerate Fermi-gas of electrons of arbitrary relativistic extent. He is, however, not widely recognised for having done so. Also using results from Albert Einstein's (1905) theory of special relativity, Soviet physicist Wilhelm Anderson (1929) was the first to derive a maximum mass for the fermion degenerate stellar model of white dwarf stars, above which the Fermi pressure is insufficient to overcome gravity. It is however the British physicist Edmund Stoner (1929) who is somewhat better known for having presented the structure for the mass, radius and density of white dwarf stars composed of non-relativistic electrons. Using his uniformly distributed mass density model, Stoner (1930, see also Stoner 1932a,b) refined his work by formulating how the core becomes relativistic at sufficiently high densities (as had already been done by Frenkel 1928) and he too predicted a maximum stable mass (similar to Anderson 1929) for earth-sized, white dwarf stars. But it is Chandrasekhar (1931a, see also Chandrasekhar 1931b) who is well known for calculating, in a short two-page article using *polytropic density models*, that at masses above $\approx 0.91\,M_{\odot}$, electron-degenerate white dwarf stars are not stable. That is, there is a maximum mass (recognised today as $1.4\,M_{\odot}$) that white dwarf stars can have. If more massive than this limit then they must undergo further gravitational compression. Soon after, Soviet physicist Lev Landau (1932) correctly identified that the next level of resistance to their gravitational collapse would be met in the form of the denser neutron star (see also Oppenheimer and Serber 1938; Oppenheimer and Volkoff 1939). Landau (1932) and Chandrasekhar (1932, 1935)[5] predicted that the ultimate fate of an evolved massive star would be to collapse to a singularity of infinite

[3]Time-travel enthusiasts might appreciate a nod to the hypothetical Einstein and Rosen (1935) bridge (aka "wormhole", a term introduced by John Wheeler in 1957, e.g. Misner and Wheeler 1957, and Klauder and Wheeler 1957) which are warped regions of space-time within general relativity (Morris and Thorne 1988; Morris et al. 1988; Hawking 1988). There is additionally the cosmic string time machine of Gott (1991).

[4]John Michell (1784) was the first to calculate the existence of black holes, which he termed "dark stars", whose gravity was so strong that light would not be able to escape from their surface (see McCormmach 1968 and Schaffer 1979). Interestingly, Herschel (1791) subsequently speculated that 'nebulæ' might be regions of space where gravitationally-retarded particles of light are endeavouring to fly off into space.

[5]Miller (2005) details the early work of Chandrasekhar on this topic.

density.[6] Following further work on this idea (e.g. Baade and Zwicky 1934; Zwicky 1938; Datt 1938), Oppenheimer and Snyder (1939) carefully detailed how overly massive neutron stars are not stable and will collapse into stellar mass black holes. Quite simply, if a star is massive enough and the outward pressure from fusion is over, gravity will win over (e.g. Arnett 1967).

Wheeler (1966) wrote *"In all the physics of the postwar era it is difficult to name any situation more enveloped in paradox than the phenomenon of gravitational collapse"*. Then, in the following year (1967), more than three decades after the initial prediction of neutron stars, pulsars were discovered, finally signalling the existence of neutron stars (Hewish et al. 1968; Pilkington et al. 1968; Hewish 1970). Not surprisingly, this bolstered belief in the existence of stellar mass black holes (e.g. Penrose 1965; Vishveshwara 1970), as did (i) mathematical proof that a singularity will form if an event horizon has formed (Penrose 1969; Hawking and Penrose 1970), (ii) the X-ray pulses from Cygnus X-1 (Oda et al. 1971; Thorne and Price 1975), and likely also (iii) the pioneering searches by Weber (1969, 1970) for gravitational radiation coming from even more massive objects at the center of our Galaxy.

As detailed by Longair (1996, 2006, 2010), Ferrarese and Ford (2005) and Collin (2006), the notion that the centers of galaxies may contain massive black holes, millions to hundreds of millions times the mass of our Sun, stems from the discovery of the great distance to, and thus luminosity of, the quasi-stellar radio source 3C 273. The optical counterpart of this radio source was cleverly discovered by Hazard et al. (1963) using the Parkes radio telescope and lunar eclipsing. Its redshift was subsequently taken with the Palomar Observatory's Hale telescope and correctly interpreted by Schmidt (1963), see also Oke (1963) regarding 3C 273 and Greenstein and Matthews (1963a,b) in the case of 3C 48 (whose redshift had remained uninterpreted over the preceding couple of years).

Baade and Minkowski (1954), Ambartsumian (1958), Woltjer (1959), Burbidge (1959) Burbidge et al. (1963, 1964), Lynds and Sandage (1963) and others had already recognised active galactic nuclei (AGN) to be incredibly energetic phenomena.[7] Radio galaxy 3C 273 and other active galactic nuclei emit vasts amount of energy from a small volume of space (as indicated by quasar variability on short time scales Smith and Hoffleit 1963)[8] and were thus thought to be powered from

[6] In passing, it is noted that quark stars (Ivanenko and Kurdgelaidze 1965) are also expected to have a stable configuration, en route between neutron stars and black holes.

[7] While relatively low-luminosity Seyfert (1943) galaxies – with broad emission lines as previously observed by Fath (1909) and Slipher (1917) – were of course already known in 1963, it was not yet fully appreciated that quasars are their high-energy kin, although similarities were noted by Burbidge et al. (1963) and Burbidge (1964).

[8] Reviews of AGN and their variability are given by Mushotzky et al. (1993), Ulrich et al. (1997), and Peterson (1997).

the gravitational potential energy[9] released as matter falls onto a compact massive object (Salpeter 1964; Zel'dovich 1964; Zel'dovich and Novikov 1964; Ne'eman 1965; Shakura and Sunyaev 1973).[10] Based upon Eddington-limiting arguments at the time, it was immediately realised that the central object has to be massive or else the radiation pressure of the quasar would literally blow the quasar apart. Hoyle et al. (1964) acknowledged the possibility of "invisible mass" perhaps from imploded objects of very large mass.[11]

Just 2 years after the high-redshifts were recorded for the star-like[12] radio sources, Sandage (1965) reported on the high abundance of radio-quiet quasars, referring to them as a "major new constituent of the universe". What he had revealed was that in addition to the radio-loud quasars, the Universe was teeming with many more quasars. Encapsulating the ideas of recent years, Lynden-Bell[13] (1969) and Lynden-Bell and Rees (1971) suggested that a massive black hole resides at the cores of many galaxies (see also Wolfe and Burbidge 1970), and that the infall of orbital matter builds an accretion disc (e.g. Thorne 1974) which heats up due to friction. For a rapidly spinning black hole, this process can liberate a substantial fraction (up to 0.42 for a maximally spinning black hole) of the infalling matter's rest mass energy[14] (Bardeen and Wagoner 1969; Bardeen 1970). Further support for the presence of massive black holes were the linear radio features emanating from the nuclei of galaxies – which were likely emitted from a stable gyroscope such as a spinning black hole – and the superluminal speed of these radio jets (e.g. Cohen et al. 1971; Whitney et al. 1971).

The moniker "black hole" was used by Ann Ewing (1964) just a year after the redshift of 3C 273 was announced. She reportedly heard it at a meeting of the American Association for the Advancement of Science (AAAS), and it was later

[9]As stated by Rees (1998), the black hole's gravitational well "must be deep enough to allow several percent of the rest mass of infalling material to be converted into kinetic energy, and then radiated away from a region compact enough to vary on timescales as short as an hour."

[10]Like many capable theorists, Zel'dovich and Novikov did not restrict themselves to one theory, and in Bisnovatyi-Kogan et al. (1967) they proposed that quasars may be billion solar mass stars burning brightly for tens of thousands of years, see also Hoyle and Fowler (1963), while Novikov (1965) additionally advocated what we now know as 'white holes'.

[11]Hoyle and Burbidge (1966) also speculated that quasars may be nearby objects and that their redshifts do not necessarily reflect the expansion of the universe, see also Hoyle et al. (2000) and Burbidge et al. (2006).

[12]Faint halos had been reported around some of these 'star-like' objects, which we now know is due to the host galaxy surrounding the bright AGN (e.g. Gehren et al. 1984; Hutchings et al. 1984, and references therein).

[13]Historical footnote: The daily commute along the A273 to Herstmonceux in Sussex prompted Donald Lynden-Bell to find a satisfactory explanation for the quasar 3C 273 (priv. comm. 2015).

[14]For comparison, nuclear fusion is known to release less than 1 % of the rest mass energy (0.7 % in the conversion of hydrogen to helium) and thus 'super-stars' are not as efficient sources of energy as rapidly spinning accretion discs around supermassive black holes.

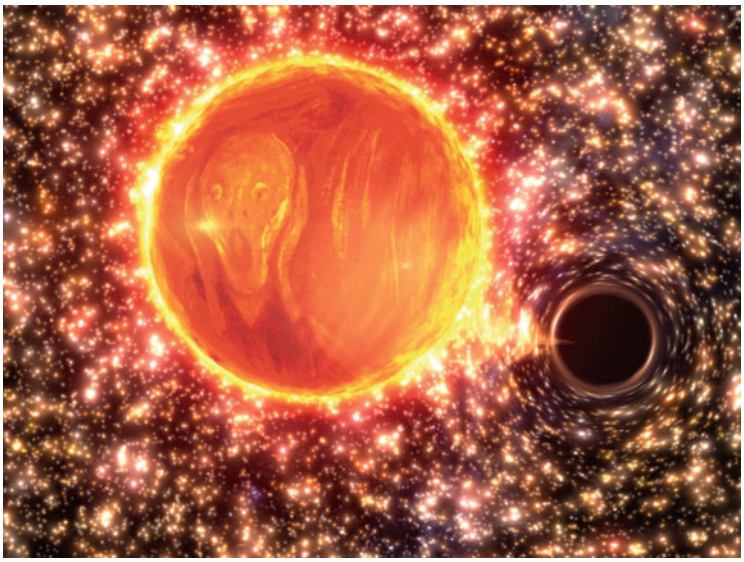

Fig. 11.1 Artist's impression of the horror at a galactic center (Credit: Gabriel Pérez Díaz)

seen used in a scientific paper by John Wheeler (1968).[15] By 1970 the label appears as a familiar term in the literature. It had, at times, previously been used to describe dusty dark patches in our own Galaxy (e.g. Barnard 1897; Campbell 1917). However it became the popular replacement for what the Soviet physicists (e.g. Zel'dovich 1964) called a frozen star,[16] and Western physicists called a collapsed star or a "collapsar" (e.g. Cameron 1971). The term "singularity" had also been, and still is, regularly used by the mathematicians to indicate where any quantity in the field equations becomes infinite.

Despite its strangely endearing name, the phrase "black hole" is often noted to be somewhat unfortunate in that it implies a *hole* in space through which matter may fall through (Fig. 11.1). The idea of an actual singularity – a point of infinite density which arises out of classical physics after division by 0 – is also not popular and considered rather old-school. While a Planck-sized mote may be a better description, what actually exists near the center of a black hole's event horizon is hotly debated. Mathematically-inclined readers who are interested in what a black hole may be like, might enjoy reading about the 'fuzzball' picture from string theory

[15]John Wheeler is first recorded to have used the term "black hole" at his 27 December, 1967, AAAS invited lecture, a few years after Ann Ewing. However, given that he coined the term "worm hole", it seems likely that he also introduced the expression "black hole", although the author does not rule out that it may have been Fritz Zwicky.

[16]For an external observer, time appears to stop inside the Schwarzschild radius, giving rise to the term "frozen star", because the collapse of a star will appear to freeze once the star is within the event horizon.

('t Hooft 1990; Mathur 2005, and associated references), or descriptions of black holes in quantum gravity theories such as spin foam networks (e.g. Penrose 1971a,b; Penrose and Rindler 1986; Rovelli 1998; Domagala and Lewandowski 2004; Perez 2004) or loop quantum gravity (e.g. Ashtekar and Bojowald 2005; Hayward 2006).

11.3 On Firmer Ground

Acceptance of the idea that supermassive black holes reside at the centers of galaxies was not as straight forward as suggested above. During the 1960s and 1970s the AGN community battled it out amongst themselves before (largely) embracing the idea that black holes must be required to power the quasar engines of galaxies. Building on Sandage (1965), Soltan (1982) reasoned that there had to be a lot of mass locked up today in massive black holes because of all the past quasar activity, and Rees (1984) advocated further for the preponderance of massive black holes in the nuclei of galaxies. Then during the 1980s and early 1990s it was primarily the inactive-galaxy community, as opposed to the AGN-community, who remained skeptical until two key papers in 1995 (discussed shortly).

Among the pioneering observational papers for the presence of a massive black hole in individual, nearby, non-AGN galaxies, Sanders and Lowinger (1972) calculated that the Milky Way houses a $0.6 \times 10^6 M_\odot$ black hole and Sargent et al. (1978) concluded that a $5 \times 10^9 M_\odot$ black hole very probably exists in M87 (see also Lynden-Bell 1969 who predicted a $30 \times 10^6 M_\odot$ black hole for the Milky Way.[17] and a 40×10^9 black hole in M87, i.e. an order of magnitude higher). Although these works had revealed that very high masses in small volumes were required at the centers of these galaxies (see also Dressler 1984 and Tonry 1984 in the case of M31 and M31, respectively), it took some years before the observations/measurements improved and alternatives such as a dense cloud of stellar mass black holes or neutron stars could be ruled out. The three following observational works turned the tide of opinion among the remaining naysayers who demanded further proof before accepting the existence of what is indeed an extreme astrophysical object: the supermassive black hole.

(1) Before an object crosses within a black hole's event horizon, any radiation it emits away from the black hole will be gravitationally redshifted, the extent of which depending on how close the object is to the event horizon. Such a tell-tale signature of redshifting was reported on 22 June 1995 by Tanaka et al. (1995) who detected the highly broadened, ionised iron Kα line (6.4 keV) from the galaxy MCG-6-30-15. This highly asymmetric, predominantly redshifted, X-ray emission line had a width corresponding to roughly one-third of the

[17] With the benefit of hindsight, we now know that radio synchrotron emission from Sagittarius A was first seen in the 5 GHz data from Ekers and Lynden-Bell (1971).

speed of light, and was thought to have been emitted at just 3–10 Schwarzschild radii from the black hole. Such relativistic broadening has since been shown to be commonplace (Nandra et al. 1997), thanks to the enhanced sensitivity and spectral resolution of the Japanese ASCA X-ray satellite (Tanaka et al. 1994).

(2) Additional convincing evidence for the reality of massive black holes had came from the very high mass density required to explain the central object in the Seyfert galaxy NGC 4258 (M106). Using the Very Long Baseline Array in New Mexico, Miyoshi et al. (1995) showed that the H_2O maser emission from this galaxy originates from a thin, rotating nuclear gas disc/annulus displaying a clear Keplerian rotation curve and requiring a mass of $3.6 \times 10^7 M_\odot$ within a size of just 0.13 parsec[18] (see also Haschick et al. 1994; Watson and Wallin 1994; Greenhill et al. 1995a,b). In their January 12 paper, Miyoshi et al. (1995) note that the short collisional timescale ($< 10^8$ years) for a swarm of solar mass dark stars with such density ($> 4 \times 10^9 M_\odot$ pc^{-3} inside of the inner 4.1 milliarcseconds) implies that such a hypothetical star cluster could not survive (see also Maoz 1995, 1998); a single supermassive black hole is the only viable candidate. A second example of extreme mass density ($3.2 \pm 0.9 \times 10^8 M_\odot$ pc^{-3}) has since been shown in the Circinus galaxy by Greenhill et al. (2003).

(3) Several years later, high spatial resolution measurements of stellar orbits around the central object in our own Milky Way galaxy also eventually ruled out the possibility that it could be a swarm of neutron stars or stellar mass black holes, with the high density favouring the existence of a massive black hole (Schödel et al. 2002; Ghez et al. 2005, 2008; Gillessen et al. 2009), confirming earlier suspicions (Lacy et al. 1979, 1980; Eckart and Genzel 1996, 1997; Genzel et al. 1996, 1997; Ghez et al. 1998; see also Alexander 2005 and references therein).

As was appropriately emphasized by Merritt and Ferrarese (2001b), within the black hole's sphere-of-influence – whose radius is defined as $r_{\rm infl} = GM_{\rm bh}/\sigma^2_{\rm sph}$ (e.g. Peebles 1972; Frank and Rees 1976) where $\sigma_{\rm sph}$ is roughly the host spheroid's velocity dispersion immediately beyond $r_{\rm infl}$ – one expects to find Keplerian dynamics which are dominated by the black hole. The velocity dispersion of the stars (or the rotational velocity of a relatively lighter disc, as in the case of NGC 4258) inside $r_{\rm infl}$ should thus decline with the inverse square root of the radius, i.e. $\sigma(R) \propto R^{-0.5}$, just as rotational velocities of Keplerian discs or solar systems have $v_{\rm rot} \propto 1/\sqrt{R}$.

The absence of this clear detection for many galaxies has led Merritt (2013) to question their reported black hole measurements, which may be better interpreted as upper limits until we are better able to resolve the sphere-of-influence (see also Valluri et al. 2004). With this cautionary note, we proceed to the topic of black hole scaling relations, which at the very least would still be upper envelopes in the various

[18] Based on a galaxy distance $D = 6.4$ Mpc.

diagrams of black hole mass versus host spheroid properties. It may however then be unusual that all of the clear-cut examples for a definitive black hole reside on this upper envelope (but see Ford et al. 1998; Ho 1999, his section 7; and Batcheldor 2010).

11.4 The M_{bh}–L_{sph} and M_{bh}–M_{sph} Relations

Commenting on the ratio of black hole mass to spheroid mass in M31 and M32, Dressler and Richstone (1988) suspected a relation, and used it to predict billion solar mass black holes in bright elliptical galaxies. While the prediction was not new, in the sense that the authors were aware that past theoretical papers had stated that quasars in big elliptical galaxies could have 10^9 solar mass black holes (e.g. Rees 1984; Begelman et al. 1984, and references therein), the idea of a scaling relation with the *spheroid* does seem to be new.[19] Dressler (1989) further advocated this connection between the black hole and the host spheroid (not the disc), and from a sample of 5 galaxies he noted that there is a "rough scaling of black hole mass with the mass of the spheroidal component".

This differed slightly from Hutchings et al. (1984) who had reported that the "black hole mass is related to that of the galaxy, increasing 60 % faster than that of the galaxy". The study by Hutchings et al. (1984) was of poorly resolved, distant quasars which prevented them from performing a bulge/disc decomposition and as such they did not report on a black hole mass relation with the host spheroid. However, there is an upper limit to the brightness of quasars which has been observed to scale with the brightness of the host galaxy (which are typically spheroid-dominated for the brightest quasars). Using real data, Yee (1992) fit a linear relation to this limit, which he called the M_{QSO}–M_G relationship, and wrote that "it may arise due to a correlation of the mass of the central engine and the galaxy mass", such that "the brightest quasars for a given galaxy mass are the ones shining at or near the Eddington limit (which is set by the mass of the central engine), while others are at lower luminosities".[20] As noted by McLeod (1997, see also McLeod et al. 1999 and result number 4 from Laor et al. 1997), Yee (1992) had effectively discovered the linear, high-mass end of the M_{bh}–M_{sph} distribution.

[19] Jarvis and Dubath (1988) appear to have also picked up on this connection when they wrote in regard to M31 and M32 that: "The likely presence of black holes in two of the closest galaxies with bulge-like components compels us to look at the nuclei of other nearby or large galaxies", which they did for the Sombrero galaxy (NGC 4594).

[20] In passing, and as noted by Alexander and Natarajan (2014), it is possible to exceed the Eddington limit to black hole growth (as noted by Begelman 1979 and Soffel 1982), due to an effective gas drag of the photons. Moreover, non-spherical accretion in the form of a disc can also result in black hole growth superseding the Eddington limit (Nayakshin et al. 2012).

With three more galaxies than Dressler (1989), Kormendy and Richstone (1995, see also Kormendy 1993) wrote a review article in which they plotted this data and reiterated in mathematical form what Dressler had said, and Yee (1992) had shown for massive bulges, i.e. $M_{\rm bh} \propto M_{\rm bulge}$. While they did not fit a relation to the data, they did report a mean $M_{\rm bh}/M_{\rm bulge}$ ratio of 0.22 % (including the Milky Way) and thereby effectively created a more quantitative basis for a linear $M_{\rm bh}$–$M_{\rm bulge}$ relation.

Following the prediction by Haehnelt and Rees (1993) that ≈30 % of nearby galaxies likely house a central massive black hole, Kormendy and Richstone (1995) remarked that at least 20 % of nearby galaxies possess such a black hole – while noting that alternatives such as massive concentrations of dark stars could not yet be ruled out. Magorrian et al. (1998) built on this and suggested that *most* nearby galaxies harbour a massive black hole (see also Sigurdsson and Rees 1997, and the reviews by Ford et al. 1998 and Richstone et al. 1998), supporting the strong suspicion held by many (e.g. Blandford 1986; Rees 1990). Moreover, this followed closely on the heels of the observation that many quiescent galaxies have weak central radio sources (e.g. Keel 1985; Sadler et al. 1989, 1995; Ho et al. 1997), likely signalling low-level accretion onto near-dead quasars.

Rather than the pure 'linear' scaling, a single power-law relation was introduced by Magorrian et al. (1998; see also Franceschini et al. 1998) to describe the distribution of 32 points in the $M_{\rm bh}$–$M_{\rm bulge}$ diagram, such that the log-linear slope was 0.96 ± 0.12 (which is of course still consistent with a slope of 1 and thus a linear relation).[21] In other works, using variously updated masses and samples, Ho (1999) reported a median $M_{\rm bh}/M_{\rm bulge}$ ratio of 0.2 %, and Merritt and Ferrarese (2001c) and Kormendy and Gebhardt (2001) reported a ratio of 0.13 %, although with notable scatter. McLure and Dunlop (2002) noticed that the scatter was considerably reduced once the disc galaxies were excluded, suggestive of poor bulge/disc decompositions used to estimate the bulge masses. Marconi and Hunt (2003) subsequently performed careful bulge/disc decompositions on near-infrared K-band images, less effected by dust and star formation. They also showed that the dynamical/virial mass of the spheroid correlated linearly with the black hole mass, and Häring and Rix (2004) provided improved dynamical masses for the derivation of their near-linear relation. For the next decade, studies of the $M_{\rm bh}$–$L_{\rm bulge}$ and $M_{\rm bh}$–$M_{\rm bulge}$ diagram remained dominated by high-mass galaxies[22] having $M_{\rm bh} >\sim 0.5 \times 10^8 {\rm M}_\odot$ and, despite each paper's incremental improvements, continually recovered a single, near-linear $M_{\rm bh}$–$M_{\rm bulge}$ relation (e.g. Ferrarese and

[21] As suspected by Magorrian et al. (1998), and noted by van der Marel (1999) and Gebhardt et al. (2000), their use of a two-integral distribution function which ignores radial velocity-dispersion anisotropy (see Binney and Mamon 1982) caused them to over-estimate the black hole masses by an average factor of 3–4.5.

[22] Studies were also biased by the inclusion of one or two rare "compact elliptical" galaxies (e.g. M32 in Graham 2007b and Gültekin et al. 2009, their figure 4) that do not represent the population at large.

Ford 2005; Lauer et al. 2007; Graham 2007b, 2008a, his section 6; Gültekin et al. 2009; Sani et al. 2011; Beifiori et al. 2012; Erwin and Gadotti 2012; Vika et al. 2012; van den Bosch et al. 2012; McConnell and Ma 2013; Rusli et al. 2013a). A recent notable exception has been Läsker et al. (2014b) who advocate, with a near-infrared sample of 35 galaxies, that the black hole mass correlates equally well with the total (bulge plus disc) luminosity as it does with the bulge luminosity at 2.2 μm, and that one has $M_{\rm bh} \propto L_{\rm bulge}^{0.75\pm0.10}$ and $M_{\rm bh} \propto L_{\rm galaxy}^{0.92\pm0.14}$. They attribute this to the smaller bulge fluxes obtained from their decomposition of the galaxies' light and the type of linear regression performed. The inclusion of more data will however be welcome, and Savorgnan et al. (2015, in prep.) will double the sample size.

There were, however, a few early deviations from the above (near) convergence of opinion on a linear relation that should be noted. First, while the Abstract of Laor (1998) largely supports the linear relation of Magorrian et al. (1998), the main text reports that $M_{\rm bh} \propto M_{bulge}^{1.5-1.8}$ (although it suggests that this may be partly due to the fact that all their lower mass quasar hosts are disc galaxies for which they may have over-estimated the bulge mass) and Second, it also notes that the low-mass inactive galaxies from Magorrian et al. (1998) better match their steeper $M_{\rm bh}$–$M_{\rm bulge}$ relation than the linear one. Third, Wandel (1999) reported a mean $\log(M_{\rm bh}/M_{\rm bulge})$ ratio of −3.5 for a sample of Seyfert galaxies with black hole masses predominantly less than $10^8\,{\rm M}_\odot$. This is 0.6 dex, i.e. a factor of 4, smaller than reported by Merritt and Ferrarese (2001c) and Kormendy and Gebhardt (2001) who used a sample with ∼80 % of the galaxies having $M_{\rm bh} > 0.8\times10^8\,{\rm M}_\odot$. Wandel (1999) argued and wrote *"It is plausible, therefore, that the Seyfert galaxies in our sample represent a larger population of galaxies with low BBRs [black hole to bulge mass ratios], which is underrepresented in the Magorrian et al. sample"*.[23]

Fourth, while Wandel reported $M_{\rm bh} \propto L_{\rm bulge}^{1.4}$ (which equates to $M_{\rm bh} \propto M_{\rm bulge}^{1.2}$ when using the same $M/L \propto L^{0.18}$ relation as Laor 1998 and Magorrian et al. 1998), the data in Wandel (1999, their figure 1) reveal that a relation with a slope steeper than 1.4 would be likely from a *symmetrical* regression. Fifth, using upper limits for black hole masses, Salucci et al. (2000) reported on hints that the $M_{\rm bh}$–$M_{\rm bulge}$ relation is significantly steeper in spiral galaxies than in [massive] elliptical galaxies. Finally, Laor (2001) reinforced his claim that a steeper, single power-law seems more applicable than a linear relation, finding $M_{\rm bh} \propto M_{\rm bulge}^{1.53\pm0.14}$. Related to this, Ryan et al. (2007) further reveals that the linear $M_{\rm bh}$–$M_{\rm bulge}$ relation over-estimates the masses of black holes in low-mass Seyfert galaxies.

[23] McLure and Dunlop (2001) correctly noted that a better bulge/disc decomposition reduces the observed flux attributed to the bulges by Wandel (1999), however the dust corrections which were not applied can largely cancel this reduction (compare figures 1 and 7 in Graham and Worley 2008).

11.4.1 A Bend in the Road

Before beginning this section, it is necessary to introduce some nomenclature which may be unfamiliar to some readers. The term "Sérsic galaxy" or "Sérsic spheroid" shall be used to denote galaxies or spheroids (elliptical galaxies and the bulges of disc galaxies) whose surface brightness profile is well described by the Sérsic (1963, 1968) model all the way into the center of the galaxy. Two decades ago Caon et al. (1993) demonstrated that the Sérsic model fits the surface brightness profiles of early-type galaxies remarkably well over a large dynamic range. An historical and modern review of Sérsic's model can be found in Graham and Driver (2005). Sérsic galaxies may contain additional nuclear flux components above that of the host Sérsic spheroid. The term "core-Sérsic galaxy" or "core-Sérsic spheroid" refers to a galaxy whose main spheroidal component has a partially-depleted core (i.e. a central stellar deficit of light that is not due to dust) such that the surface brightness profile is well described by the core-Sérsic model (Graham et al. 2003b). The history of galaxy surface brightness models and the impact that the above systematically (with luminosity) varying structures (i.e. non-homology and depleted cores) have on galaxy scaling laws and the unification of bright and faint early-type Sérsic galaxies is discussed at length in Graham (2013).

Re-analysing the dynamical spheroid mass and (updated) black hole mass data for 30 galaxies studied by Häring and Rix (2004), but this time separating the galaxies depending on whether or not they have a partially depleted core, Graham (2012a) found that the two populations follow different relations in the $M_{\rm bh}$–$M_{\rm sph,dyn}$ diagram. While the dozen core-Sérsic spheroids, which are the more massive spheroids, followed the near-linear relation $M_{\rm bh} \propto M_{\rm sph,dyn}^{1.01\pm0.52}$, the Sérsic spheroids followed a much steeper power-law relation, such that $M_{\rm bh} \propto M_{\rm sph,dyn}^{2.30\pm0.47}$. Excluding the barred galaxies, the Sérsic relation was $M_{\rm bh} \propto M_{\rm sph,dyn}^{1.92\pm0.38}$. This near-quadratic relation for the low- and intermediate-mass spheroids had never been reported before and it signalled a bend in the $M_{\rm bh}$–$M_{\rm sph,dyn}$ diagram.

With an increased sample size of 72 galaxies with directly measured black hole masses, Graham and Scott (2013) confirmed this behavior using near-infrared K_s-band magnitudes. Their sample of two dozen core-Sérsic spheroids gave $M_{\rm bh} \propto L_{\rm sph}^{1.10\pm0.20}$, while the four dozen Sérsic spheroids gave the relationship $M_{\rm bh} \propto L_{\rm sph}^{2.73\pm0.55}$, which reduced to $M_{\rm bh} \propto M_{\rm sph,dyn}^{2.34\pm0.47}$ when using $M_{\rm dyn}/L_K \propto L_K^{1/6}$ (e.g., Magoulas et al. 2012; La Barbera et al. 2010). Employing the ARCHANGEL photometry pipeline (Schombert and Smith 2012) applied to Two Micron All-Sky Survey images (Skrutskie et al. 2006), which effectively corrects for missing light at large radii, Scott et al. (2013) converted the K_s-band magnitudes of the spheroids into stellar masses. They found that $M_{\rm bh} \propto M_{\rm sph,*}^{0.97\pm0.14}$ and $M_{\rm bh} \propto M_{\rm sph,*}^{2.22\pm0.58}$ for the Sérsic spheroids and core-Sérsic, respectively.

We therefore now have a situation which is dramatically different to what was believed for the past two decades. It is not simply that we no longer have a single, near-linear $M_{\rm bh}$–$M_{\rm sph}$ relation for all spheroids, but the main growth phase of black holes and bulges, involving gas rich processes, follows a near-quadratic relation,

with gas-poor "dry" mergers subsequently creating the core-Sérsic galaxies which depart from the high-mass end of this near-quadratic relation.[24] That is, the growth of massive black holes has been much more rapid than that of their host spheroids.

Naturally, the simple addition of galaxies and their black holes, through dry merging, will establish the observed near-linear relation for the core-Sérsic galaxies. The average $M_{\rm bh}/M_{\rm sph}$ ratio of these core-Sérsic galaxies then reflects the value obtained at the high-mass end of the near-quadratic Sérsic $M_{\rm bh}$–$M_{\rm sph}$ relation from which they peeled off. In late 2012 Graham and Scott (2013) reported this mass ratio to be 0.49 %, in agreement with that already noted by Laor (2001) for massive spheroids. This ratio is basically the calibration for the Yee (1992) relation between black hole mass and galaxy mass in massive galaxies, modulo the fact that some core-Sérsic galaxies contain large discs. Furthermore, our own galaxy, with an $M_{\rm bh}/M_{\rm sph}$ ratio of 0.05 %, is no longer a low outlying point requiring explanation in the $M_{\rm bh}$–$M_{\rm sph}$ diagram. It has a mass ratio in accord with the near-quadratic scaling relation for Sérsic spheroids.

Adding AGN data from half a dozen recent papers which had observed the AGN black hole masses to reside below the original $M_{\rm bh}$–$M_{\rm sph}$ relation, Graham and Scott (2014) revealed that they depart from the near-linear $M_{\rm bh}$–$M_{\rm sph}$ relation in a systematic manner consistent with the near-quadratic $M_{\rm bh}$–$M_{\rm sph}$ mass scaling relation for Sérsic galaxies. That is, they are not randomly offset. This is shown in Fig. 11.2. This also provides the picture with which we can now interpret the observations by Laor (1998, 2001) and Wandel (1999), who were on the right track over a decade ago.

If one was to separate the galaxies in Fig. 11.2 at $M_{\rm bh} = 2 \times 10^6\,{\rm M}_\odot$, one would (understandably but inappropriately) conclude that the lower mass spheroids do not follow an $M_{\rm bh}$–$M_{\rm sph,*}$ relation (Jiang et al. 2011). This had resulted in these lower mass spheroids being considered distinct by some, and sometimes labelled 'pseudobulges' as opposed to 'classical' bulges (Gadotti and Kauffmann 2009; Kormendy et al. 2011) with the separation said to occur at $n = 2$. This is also where the alleged divide between dwarf elliptical and ordinary elliptical galaxies was said to occur ($M_B = -18$ mag, $M_{\rm gal,*} \approx 2 \times 10^{10}\,{\rm M}_\odot$ $n \approx 2$–2.5, $\sigma \approx 100$–$120\,{\rm km\ s^{-1}}$). However, without the fuller parameter baseline that we now have, or artificially subdividing the data at a Sérsic index of 2, or at $M_B = -18$ mag, or where the curvature in relations using 'effective' radii and surface brightnesses are a maximum (see Graham 2013, for an explanation of this), the continuity between the low- and intermediate-luminosity Sérsic galaxies can be missed, even if the data itself is accurate. This issue is discussed further in Sect. 11.5.2.1.

The distribution of points in Fig. 11.2 reveals that black holes grow faster than the stellar population of their host spheroids, for which abundant evidence is now

[24] Some Sérsic galaxies may follow the near-linear $M_{\rm bh}$–$M_{\rm sph}$ relation, having experienced a major dry merger event in which the nuclear star clusters from the progenitor galaxies have been eroded away but an obvious partially depleted core is not yet formed (see Bekki and Graham 2010). These may well be the galaxies at $-19.5 > M_B > -20$ mag in Côté et al. (2007, their figure 3e).

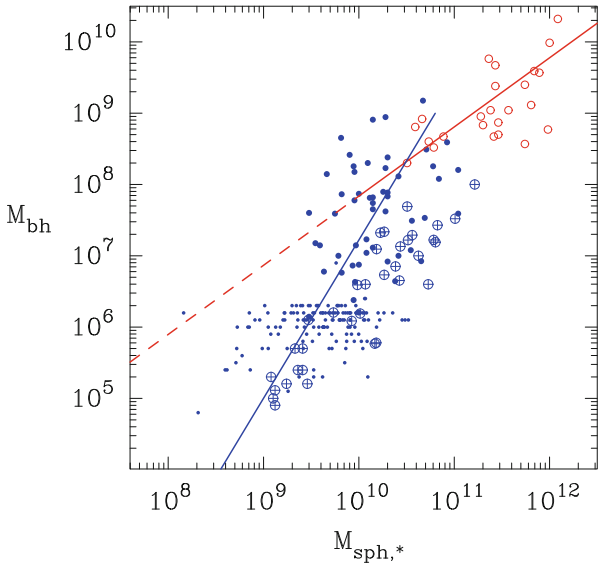

Fig. 11.2 Black hole mass versus host spheroid's stellar mass (in units of solar mass). Core-Sérsic spheroids are shown with open *red circles*, while Sérsic spheroids are shown by the *large blue dots*. A sample of 139 low mass AGN from Jiang et al. (2011) are denoted by the *small dots*, while an additional 35 higher mass AGN (which may have had their host spheroid masses over-estimated by overly-high $(M/L)_{\rm stellar}$ ratios, see Busch et al. 2014) are denoted by the *cross hairs*. The optimal near-linear and near-quadratic scaling relations from Scott et al. (2013) are shown as the *red* (*solid* and *dashed*) and *blue* (*solid*) *line* for the core-Sérsic and Sérsic spheroids, respectively. Of note is that 68 % of the 139 AGN (i.e. $\pm$34 %) are contained within 0.83 dex in the horizontal direction, representing a level of scatter equal to that about the near-linear relation observed at the high-mass end. The non-AGN Sérsic galaxies have more scatter than the non-AGN core-Sérsic galaxies because of the crude way in which their bulge masses were estimated (see Graham and Scott 2014, from which this figure is taken)

appearing (e.g. Diamond-Stanic and Rieke 2012; Seymour et al. 2012; Trakhtenbrot and Netzer 2012; Agarwal et al. 2013; Alonso-Herrero et al. 2013; LaMassa et al. 2013; Lehmer et al. 2013; Drouart et al. 2014). For example, Diamond-Stanic and Rieke 2012 report that the black hole growth rate is proportional to the 1.67 ($= 1/0.6$) power of the star formation rate within the inner kpc (roughly the bulge half-light radii) of their Seyfert galaxies, while the analysis from LaMassa et al. (2013) gives an exponent of 2.78 ($= 1/0.36$) for their sample of $\sim$28,000 obscured active galaxies, quite different from the linear value of 1.

Figure 11.2 also reveals that classical bulges, pseudobulges, clump-bulges (Noguchi 1999), and mixed-bulges containing both a classical bulge and a pseudobulge, all follow the steeper scaling relation, until the onset of relatively dry mergers revealed by the scoured cores seen in the centers of (many of) the most massive spheroids.

With their supernova feedback producing a steeper relation than their AGN feedback prescription, the models of Cirasuolo et al. (2005, their figure 5) and Fontanot et al. (2006, their figure 6) show a bend in the $M_{\rm bh}$–$M_{\rm sph}$ (and $M_{\rm bh}$–M_{σ}) relation at $M_{\rm bh} \approx 10^8 {\rm M}_{\odot}$. At these lower masses, a steeper than linear $M_{\rm bh}$–$M_{\rm sph}$ relation can also be seen in the differing models of Dubois et al. (2012), Khandai et al. (2012, their figure 7); Bonoli et al. (2014, their figure 7) and Neistein and Netzer (2014, their figure 8).

What happens in the $M_{\rm bh}$–$M_{\rm sph}$ diagram at black hole masses less than $10^5\,{\rm M}_{\odot}$ is not yet known. While the absence of a definitive black hole detection in M33 (Kormendy and McClure 1993; Gebhardt et al. 2001; Merritt et al. 2001) had reinforced the idea that black holes are associated with bulges (e.g. Dressler and Richstone 1988; Kormendy and Gebhardt 2001), bulgeless galaxies with massive black holes have since been detected (e.g Reines et al. 2011; Secrest et al. 2012; Schramm et al. 2013; Simmons et al. 2013; Satyapal et al. 2014). Obviously these galaxies do not (yet?) participate in the observed $M_{\rm bh}$–$M_{\rm sph,*}$ scaling relation. As noted in Graham and Scott (2013), there are however tens of galaxies known to contain AGN in bulges whose spheroid magnitudes suggest, based on this near-quadratic $M_{\rm bh}$–$M_{\rm sph,*}$ scaling relation, that they harbour intermediate mass black holes ($10^2 < M_{\rm bh}/{\rm M}_{\odot} < 10^5$). It will be interesting to see (a) if this missing population of intermediate-mass black holes exists and (b) where they reside in the $M_{\rm bh}$–$M_{\rm sph}$ diagram.

11.4.1.1 Implications

Of course the above represents a dramatic revision to the bulge-(black hole) connection , i.e. a completely different relation connecting supermassive black holes with their host bulges, and as such has wide-spread implications. For one, the many-merger scenario proposed by Peng (2007), and explored further by Jahnke and Macciò (2011) and Hirschmann et al. (2010), to produce a linear one-to-one scaling via the central limit theorem can be ruled out. Using a sample of galaxies with a range of initial $M_{\rm bh}/M_{\rm gal,*}$ mass ratios, Peng (2007) noted that after many mergers it would naturally create an $M_{\rm bh}$–$M_{sph,*}$ relation with a slope of 1. Although this concept was independently ruled out by Anglés-Alcázar et al. (2013) who had emphasized that the number of actual major mergers are not frequent enough to have established such a linear relation, the quadratic slope of the $M_{\rm bh}$–$M_{\rm sph}$ relation confirms this ruling.

Some additional implications of the new relation include obvious things like (i) black hole mass predictions in other galaxies, (ii) estimates of the local black hole mass function (e.g. Shankar et al. 2004, 2012; Comastri et al. 2015) and mass density based on local spheroid luminosity functions, and (iii) evolutionary studies of the $M_{\rm bh}/M_{\rm sph}$ mass ratio over different cosmic epochs. In particular, the local $M_{\rm bh}/M_{\rm sph}$ ratio was thought to be 0.14–0.2 % (e.g. Ho 1999; Kormendy 2001; Marconi and Hunt 2003; Häring and Rix 2004). However, Graham (2012a) reported a larger value of 0.36 % for the core-Sérsic galaxies, which was, as noted above,

increased that same year to 0.49 % by Graham and Scott (2013).[25] Nearly a year later this higher ratio for massive spheroids was again noted in the review by Kormendy and Ho (2013) due to its significance.

Additionally impacted areas of research include (iv) galaxy/black hole formation theories, which extends to (v) AGN feedback models, (vi) predictions for space-based gravitational wave detections, (vii) connections with nuclear star cluster scaling relations, (viii) derivations of past quasar accretion efficiency as a function of mass (e.g. Shankar 2009b), (ix) searches for the fundamental, rather than secondary, black hole scaling relation, and (x) calibrations matching inactive galaxy samples with low-mass AGN data to determine the optimal virial factor for measuring black hole masses in AGN. Given that most of these topics could generate a review in their own right, only feedback is briefly commented on here.

A large number of clever theoretical papers have tried to explain the nature of the $M_{\rm bh}$–$M_{\rm sph}$ relation in terms of feedback from the AGN (e.g. Silk and Rees 1998; Haehnelt et al. 1998; Fabian 1999; Kauffmann and Haehnelt 2000; Wilman et al. 2000; Benson et al. 2003; Wyithe and Loeb 2003; Granato et al. 2004; Di Matteo et al. 2005; Springel et al. 2005; Hopkins et al. 2005, 2006; Cattaneo et al. 2006; Sijacki et al. 2007; Somerville et al. 2008; Booth and Schaye 2009, to mention just a fraction). Some papers (but not all those listed here) which have claimed success because they obtained, through gaseous processes, a linear $M_{\rm bh}$–$M_{\rm sph}$ relation over a wide range of mass, now appear in need of tweaking. Encouragingly, while not quite finding a quadratic relation with slope of 2, Hopkins and Quataert (2010) report that the black hole growth rate in their models is proportional to the 1.43 ($= 1/0.7$) power of the star formation rate.

The so-called 'quasar' or 'cold' mode of black hole growth during gas-rich processes, as implemented in semi-analytical models, has typically assumed that black hole growth occurs via accretion which is linearly proportional to the inflowing mass of cold gas (which also produces the host spheroid), modulated by an efficiency which is lower for both unequal mass mergers (Croton et al. 2006) and less massive (more gas-rich) systems with lower virial velocities (e.g., Kauffmann and Haehnelt 2000, their eq. 2; Croton et al. 2006, their eq. 8; Guo et al. 2011, their eq. 36).[26] Graham and Scott (2013) therefore presented a new prescription for the increase in black hole mass, due to gas accretion during wet mergers, such that the black hole would grow quadratically relative to the host spheroid. The short duty (on) cycle of quasars ($\sim 10^7$–10^8 years) may then imply that the bulk of a spheroid's stars are also formed rapidly. Once the gas is largely gone, and significant galaxy/(black hole) growth is attained via major dry merger events, the low-accretion model (e.g. Blandford and Begelman 1999) presumably results in the so-called 'mechanical' or 'radio mode' feedback maintaining the spheroid-(black hole) mass ratio, as is roughly observed for the core-Sérsic galaxies.

[25]This announcement appeared on arxiv.org in mid-November 2012.

[26]Note: Guo et al. (2011) excluded the square on the normalised velocity term in their eq. 36.

11.4.2 The L_{sph}–σ Relation

Around the time that quasars were identified to be at large redshifts, Minkowski (1962) discovered a correlation between velocity dispersion and absolute magnitude for early-type galaxies. He refrained from fitting an equation to it, noting the need to extend the observations to low absolute magnitudes. While Morton and Chevalier (1973) achieved this, finding a continuous distribution of velocity dispersions, it was Faber and Jackson (1976) who were the first to fit an equation to Minkowski's relation. For their sample of 25 galaxies, they reported that $L \propto \sigma^4$, which has since become known as the Faber-Jackson relation. A few years later, exploring the bright end of Minkowski's relation, Schechter (1980) discovered that $L \propto \sigma^5$, a result confirmed by Malumuth and Kirshner (1981; see also von der Linden et al. 2007). Recent studies have suggested that the exponent may be 5.5 in brightest cluster galaxies (Liu et al. 2008) and as high as 6.5 ± 1.3 in core galaxies (Lauer et al. 2007). Shortly after this, Schechter co-authored Davies et al. (1983) in which they revealed that $L \propto \sigma^2$ for low- and intermediate-luminosity early-type galaxies. Many studies have since shown that this result holds from the lowest luminosity dwarf elliptical galaxies up to $M_B \approx -20$ to -21 mag (Held et al. 1992; de Rijcke et al. 2005; Matković and Guzmán 2005; Balcells et al. 2007b; Lauer et al. 2007; Chilingarian et al. 2008; Forbes et al. 2008; Cody et al. 2009; Tortora et al. 2009; Kourkchi et al. 2012). This explained why past samples of intermediate-to-bright early-type galaxies had a slope of around 4, or 3 (Tonry 1981), and confirmed the observation by Binney (1982) and Farouki et al. (1983) that a single power-law was not appropriate to describe the distribution of early-type galaxies in the L–σ diagram. Most recently, Davies has again illustrated this bend, this time in the M_{gal}–σ diagram for early-type galaxies, through co-authorship of Cappellari et al. (2013). Their bent M_{gal}–σ diagram is reproduced in Fig. 11.3.

The bend in Minkowski's relation has been explained by Matković and Guzmán (2005) in terms of Sérsic galaxies (which have low- and intermediate-luminosity) following the $L \propto \sigma^2$ relation of Davies et al. (1983) while core-Sérsic galaxies (which have high-luminosity) follow the $L \propto \sigma^5$ relation of Schechter (1980). This continuity for the low- and intermediate-luminosity Sérsic galaxies, and the break-away of bright galaxies with partially depleted cores, is illustrated further in the L–μ_0 and L–n distributions seen in Graham and Guzmán (2003, their figures 9c and 10; see also Côté et al. 2007, their figure 3e). As noted in footnote 24 of this article, some galaxies may have experienced a major dry merger event but not display a partially depleted core – such as the merger remnants NGC 1316 (Fornax) and NGC 3115 (Schauer et al. 2014; Menezes et al. 2014) – which could explain why some of the high-mass galaxies in Fig. 11.3 do not have depleted cores.[27]

[27]It will be interesting in the future to careful apply the core-Sérsic model to see how all the points are distributed in terms of galaxies with and without partially-depleted cores.

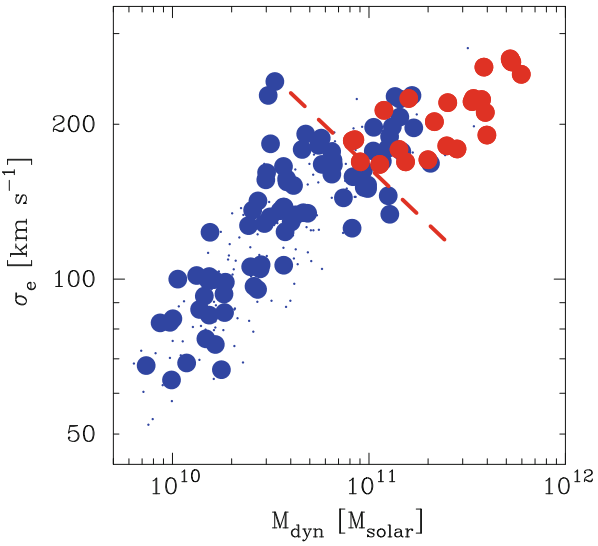

Fig. 11.3 Dynamical galaxy mass (M_{dyn}) – equal to twice the Jeans Anisotropic Multi-Gaussian-Expansion mass within the effective half-light radius R_e – versus the velocity dispersion σ_e within R_e for the ATLAS^{3D} early-type galaxies (Cappellari et al. 2013, see their figure 1). Core galaxies ($\gamma < 0.3$ according to the Nuker model (Grillmair et al. 1994; Lauer et al. 1995) as used by Krajnović et al. 2013) are shown by the large *red circles*, while galaxies having steeper inner profiles ($\gamma > 0.5$) are shown by the *large blue dots*. Galaxies with an unknown inner surface brightness profile slope, or those with $0.3 < \gamma < 0.5$ are shown by the *small dots*

The bend in the M_{gal}–σ diagram, and the M_{bh}–M_{sph} diagram, is likely to have ties with the flattening that is also observed at the bright end of the colour magnitude diagram for early-type galaxies (Tremonti et al. 2004; Jiménez et al. 2011). Dry merging will increase the luminosity while preserving the colour (modulo passive evolution) among the core-Sérsic elliptical galaxies. In contrast, the Sérsic early-type galaxies display a continuous mass-metallicity relation which unites the dwarf and ordinary early-type galaxies (e.g. Caldwell 1983; Caldwell and Bothun 1987).

If the M_{bh}–σ relation (Sect. 11.5) is roughly described by a single power-law, and given that the L–σ (and M_{gal}–σ) relation is notably bent (Fig. 11.3), then the M_{bh}–L relation has to be bent, just as observed and discussed in Fig. 11.2 and Sect. 11.4.1.

11.5 The M_{bh}–σ Relation

While the work on the M_{bh}–L relation from Magorrian received considerable attention, it was the M_{bh}–σ relation (Ferrarese and Merritt 2000; Gebhardt et al. 2000) which really sparked off wide-spread global interest in black hole scaling relations. The reason may likely have been because, after having identified and

removed galaxies with less secure black hole mass estimates, the $M_{\rm bh}$–σ relation was reported by both teams to be consistent with having zero intrinsic scatter (see also Kormendy and Gebhardt 2001).[28] That is, after accounting for the measurement errors, all the scatter was accounted for, suggesting that a new law of physics had been discovered. However, the slope of this potential new law was not agreed upon. Ferrarese and Merritt (2000) had reported $M_{\rm bh} \propto \sigma^{4.8\pm0.5}$, while Gebhardt et al. (2000) reported an exponent of 3.75 ± 0.3. The former slope agreed with the energy-balancing prediction by Silk and Rees (1998, see also Haehnelt et al. 1998) that $M_{\rm bh} \propto \sigma^5$, while the latter slope agreed with the momentum-balancing prediction by Fabian (1999) that $M_{\rm bh} \propto \sigma^4$. This discrepancy was to become a major source of controversy and uncertainty in what has become one of the most famous astronomical relations of recent years. As such, some space is dedicated to this issue here. In the following subsection, the main reason for the different slopes is presented, as this continues to be somewhat misunderstood today.

11.5.1 Slippery Slopes

Ferrarese and Merritt (2000) performed a symmetrical linear regression, using the BCES routine from Akritis and Bershady (1996) which allowed for intrinsic scatter and unique measurement errors on both variables, $M_{\rm bh}$ and σ (which they took to be 13 % for the velocity dispersion of external galaxies). Gebhardt et al. (2000), on the other hand, performed a non-symmetrical ordinary least squares regression by minimising the vertical offsets (i.e. in the $\log M_{\rm bh}$ direction) about their $M_{\rm bh}$–σ relation. This approach effectively assumed that the uncertainty on the velocity dispersion was zero and that the black hole masses all had the same uncertainty.

Merritt and Ferrarese (2001a) addressed the issue of the differing slopes, using four different types of linear regression, two which treated the ($M_{\rm bh}$, σ) data symmetrically and two which did not. They revealed how the slope of the $M_{\rm bh}$–σ relation increased as one assigned an increasing uncertainty to the velocity dispersion and presented a best fit slope of 4.72 ± 0.36 for their expanded sample.

Tremaine et al. (2002) also looked at this issue of different slopes and noted that under certain conditions[29] the minimisation routine from Akritas & Bershady, which was used by Ferrarese and Merritt (2000), can be biased. As noted above, Merritt and Ferrarese (2001a) had additionally used a second symmetrical regression routine, referred to as the "Orthogonal distance regression" which had been

[28] The $M_{\rm bh}$–L relation was reported to have more scatter, but this was in part because of poor bulge/disc decompositions, and the unrecognised bend in the relation.

[29] The slope can be biased if (i) the uncertainty on the x values is large compared to the range of x values, or (ii) the sizes of all the x and y uncertainties are not roughly comparable to each other.

implemented by Press et al. (1992, their Section 15.3) as FITEXY. It was such that the following quantity was minimised during the task of fitting the line $y = a + bx$:

$$\chi^2 = \sum_{i=1}^{N} \frac{[y_i - (a + bx_i)]^2}{\delta {y_i}^2 + b^2 \delta {x_i}^2}, \tag{11.1}$$

where N data pairs of y and x values are available in one's sample, and they have measurement errors δy and δx, respectively. Merritt and Ferrarese (2001a) pointed out that Feigelson and Babu (1992) had already noted that this routine is fine unless the distribution to be fit contains intrinsic scatter, i.e. real departures of the data from the optimal line which are not due to measurement errors. At that time, the $M_{\rm bh}$–σ relation was thought to contain no intrinsic scatter, or was at least consistent with having no intrinsic scatter.

Tremaine et al. (2002) subsequently developed their own modified version of FITEXY. It was such that it minimised the quantity

$$\chi^2 = \sum_{i=1}^{N} \frac{[y_i - (a + bx_i)]^2}{\delta {y_i}^2 + b^2 \delta {x_i}^2 + \epsilon_y^2}, \tag{11.2}$$

where the intrinsic scatter ϵ_y is solved for by repeating the fit until $\chi^2/(N-2)$ equals 1. Although Tremaine et al. (2002) claimed this expression still gave a symmetrical treatment of the data, it did not. By trying to allow for intrinsic scatter, they had inadvertently converted a symmetrical expression into a non-symmetrical expression by minimising the offsets under the assumption that all of the intrinsic scatter lay in the y-direction. They reported a slope of 4.02 ± 0.32 for their $M_{\rm bh}$–σ relation using the smaller uncertainty of 5 % (compare 13 %) for the velocity dispersions of the external galaxies.

Here we look at this a little more carefully, as it continues to cause confusion more than a decade later. If one was to minimise the offsets in the x-direction, about the line $y = a + bx$, or equivalently $x = (y - a)/b$, the expression would be

$$\chi^2 = \sum_{i=1}^{N} \frac{[x_i - \frac{(y_i - a)}{b}]^2}{\delta {y_i}^2/b^2 + \delta {x_i}^2 + \epsilon_x^2},$$

$$\sum_{i=1}^{N} \frac{[-y_i + (a + bx_i)]^2}{\delta {y_i}^2 + b^2 \delta {x_i}^2 + b^2 \epsilon_x^2}, \tag{11.3}$$

where ϵ_x is the intrinsic scatter, but this time implicitly assumed to reside in the x-direction. The difference between Eqs. 11.2 and 11.3 is the final term in the denominator, which has that $\epsilon_y = b\epsilon_x$. Given this (not surprising) dependence on the slope between ϵ_y and ϵ_x, the solution reached by solving for $\chi^2/(N-2) = 1$ in Eqs. 11.2 and 11.3 has a different value of b, i.e. a different slope. To obtain a symmetrical regression therefore requires an average of these two regressions as

discussed in Novak et al. (2006).[30] which are sometimes referred to as the forward and the inverse regression.

Performing a non-symmetrical linear regression analysis and minimising the offsets in just the $\log M_{\rm bh}$ direction is preferred if one wishes to obtain a relation useful for predicting black hole masses in other galaxies, simply because this relation has the smallest offsets in the $\log M_{\rm bh}$ direction (see Feigelson and Babu 1992; Andreon and Hurn 2012). If, on the other hand, one is interested in the underlying/fundamental relation connecting $M_{\rm bh}$ and σ, then one should perform a symmetrical regression. This is discussed by Novak et al. (2006) in terms of the Observer's Question and the Theorist's Question.

Analysing the same data[31] from Tremaine et al. (2002), and assigning a 5 % uncertainty to the velocity dispersion of each galaxy (including the Milky Way), Novak et al. (2006) reported a slope of 4.10 ± 0.30 using Eq. 11.2 and 4.59 ± 0.34 using Eq. 11.3. Had they used an uncertainty of 13 %, they would have reported slopes of 4.39 and 4.59, giving an average value slope of 4.49 that was consistent with Merritt and Ferrarese (2001a) who reported an optimal slope of 4.72 ± 0.36.

To make a point about the ongoing concerns regarding different minimisation routines, and in particular to show that the symmetrical bisector regression routine from Akritas & Bershady was not producing a biased fit in regard to the $(M_{\rm bh}, \sigma)$ data, Graham and Li (2009) used three symmetrical regression routines, one from Akritis and Bershady (1996), the expression from Tremaine et al. (2002) operating in both forward and inverse mode, and an IDL routine from Kelly (2007) based on a Bayesian estimator. All were shown to give very similar results when the same uncertainty on the velocity dispersion was consistently used, a test that was recently confirmed in Park et al. (2012) who additionally used a fourth (maximum likelihood) estimator.

11.5.2 Substructure and Escalating Slopes

In 2007 Graham noticed that all of the barred galaxies in the $M_{\rm bh}$–σ diagram were offset, to either lower black hole masses and/or higher velocity dispersions, relative to the best-fitting line defined by the non-barred galaxies, and that excluding the barred galaxies resulted in a reduced scatter about the $M_{\rm bh}$–σ relation (Graham 2007a). At the same time, Hu (2008) had compiled a larger sample and shown the same apparent substructure within the $M_{\rm bh}$–σ diagram. Hu considered all of his offset galaxies to contain 'pseudobulges', built from the secular evolution of their surrounding disc and containing relatively under-developed black holes. They were also all barred galaxies. Graham (2008a) similarly considered the offset galaxies

[30] An easy way to check if one has performed a symmetrical regression is to swap their x and y data around and re-feed this into their regression routine.

[31] The black hole mass for NGC 821 was updated, but this had almost no impact.

to have undermassive black holes, due to secular evolution over-developing the bulge, or to have elevated velocity dispersions due to the dynamics of the bar. The choice appears answered because Hartmann et al. (2014) have shown that bars are indeed capable of increasing the velocity dispersion in galaxies, and by exactly the average offset observed in the $M_{\rm bh}$–σ diagram (see also Debattista et al. 2013; Monari et al. 2014). Furthermore, Fig. 11.2 shows that pseudobulges and classical bulges (and clump bulges) follow the same broad distribution in the $M_{\rm bh}$–$M_{\rm sph}$ diagram; at low spheroid masses they both reside systematically below the near-linear relation defined by the massive core-Sérsic spheroids. There is not yet evidence that pseudobulges contain smaller black hole masses than classical bulges of the same mass, although more data would be welcome. In particular, removing the contribution of the bar,[32] and the rotational contribution,[33] from the observed central velocity dispersions of the spheroids would be helpful. It may also make more sense to use the quantity $\sqrt{3\sigma_{\rm sph}^2 + v_{\rm sph,rot}^2}$ (Busarello et al. 1992). Although, much of this may be moot in regard to pseudobulges due to the difficult task of actually identifying them, as discussed in the following subsection.

One thing that was clear from Hu (2008) and Graham (2008b) was that the growing sample size had generated an increased scatter about the $M_{\rm bh}$–σ relation,[34] and the intrinsic scatter no longer appeared consistent with zero, a result shown further by Gültekin et al. (2009). The $M_{\rm bh}$–σ diagram was therefore falling from grace, and it also now presented quite a contrast to early claims which had reported that classical bulges and pseudobulges follow the same black hole scaling relations (e.g. Kormendy 2001; Kormendy and Gebhardt 2001). In Kormendy et al. (2011) the offset nature of the pseudobulges was acknowledged, and it was now claimed that black hole masses do not correlate with the properties of pseudobulges. However, the range in absolute magnitude of the pseudobulges was restricted to just 2 mag, making it challenging to identify if there is a relation present. With a fuller data set, Fig. 11.2 reveals that all bulge types appear to follow an $M_{\rm bh}$–$M_{\rm sph}$ relation.

With a sample size of 72 galaxies, McConnell and Ma (2013) used the non-symmetrical, modified FITEXY routine, as coded by Williams et al. (2010) in MPFITEXY. They reported a slope of 5.64 ± 0.32 for their optimal $M_{\rm bh}$–σ relation (their figure 1, which includes the alleged over-massive black hole in NGC 1277: van den Bosch et al. 2012). If they had of additionally used the inverse of this regression, in which the unknown intrinsic scatter is assigned to the log σ direction, they would have obtained a slope of 6.64, and thus an average slope of 6.14. This is steeper than previously reported, and is in part due to their inclusion of the offset barred galaxies at low masses. While McConnell and Ma (2013) do report that their 19 late-type galaxies (with both classical bulges and pseudobulges) have an $M_{\rm bh}$–σ

[32] Graham et al. (2011), their figure 7, offer a first order approximation for this.

[33] See Kang et al. (2013), their figure 9, and Pota et al. (2013) in regard to the velocity dispersion of a globular cluster system.

[34] Potentially, this may in part be due to the inclusion of less accurate black hole mass measurements with under-estimated error bars (see Merritt 2013).

relation with a zero point (i.e. the term 'a' in $y = a + bx$) that is 0.29 dex lower than for their 53 early-type galaxies (8.36 vs 8.07), i.e. offset by a factor of 2, they did not perform a fit to the barred and non-barred galaxies. Given that the early-type galaxies dominate at the high-mass end of the diagram, and the late-type galaxies at the low-mass end, they combine to produce the steeper relation with a slope of $\approx$6.

Graham et al. (2011) highlighted a potential sample selection bias such that the need to resolve (or nearly resolve) the sphere-of-influence of the black holes may be resulting in an artificial floor to the distribution of points in the $M_{\rm bh}$–σ diagram. As such, they additionally used a non-symmetrical regression, but one which minimised the offsets in the horizontal direction, i.e. they performed the 'inverse' regression as this should provide the least biased fit (see Lynden-Bell et al. 1988). Adding eight black hole masses to the compilation of 64 data pairs in Graham et al. (2011) Graham and Scott (2013) reported a slope of 6.08 ± 0.31 using their preferred inverse regression on their sample of 72 galaxies (see Fig. 11.4). For the 51 non-barred galaxies, their optimal slope using the inverse regression was 5.53 ± 0.34. While this is at first glance in agreement with the preferred value of 5.64 ± 0.32 reported by McConnell and Ma (2013), it should be realised that it is a coincidence as different things have been measured: a forward regression for all galaxy types versus an inverse regression for non-barred galaxies.

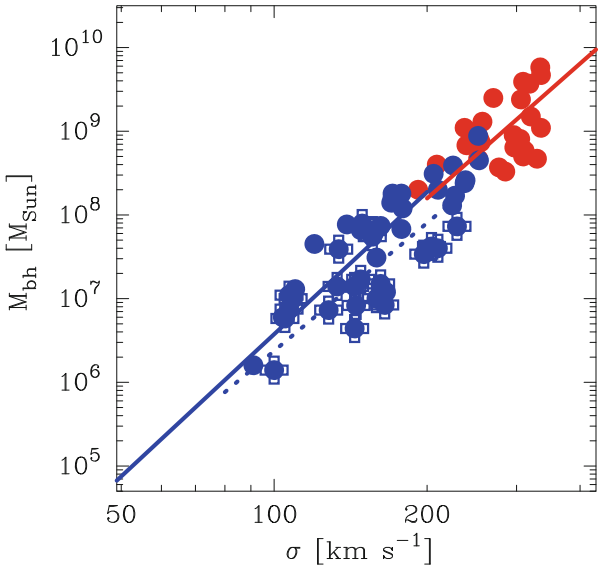

Fig. 11.4 $M_{\rm bh}$–σ diagram taken from Graham and Scott (2013). *Red circles* represent core-Sérsic galaxies; *blue dots* represent Sérsic galaxies. The *crosses* designate barred galaxies, which tend to be offset to higher velocity dispersions. The three lines are linear regressions, in which the barred Sérsic galaxies and the non-barred Sérsic galaxies have been fit separately from the core-Sérsic galaxies (which are not barred)

Using updated and expanded data for 57 non-barred galaxies, taken from the sample of 89 galaxies in Savorgnan and Graham (2014), the forward, inverse and average regression give a slope of 5.10, 6.48 and 5.79. Folding in the offset barred galaxies results in steeper slopes still, as seen with the McConnell and Ma (2013) data. The increase to the slope over the past few years has largely come from increased black hole masses, and new data, at the high mass end. McConnell and Ma (2013) additionally note that the flux-weighted velocity dispersion within one effective radius can be as much as 10–15 % lower in their massive galaxies when excluding data within the black hole's sphere-of-influence. This follows Graham et al. (2011) who noted that the velocity dispersion for M32's spheroid should be reduced from $\sim$75 km s^{-1} to $\sim$55 km s^{-1} (Tonry 1987) for exactly this reason. Increases to black hole masses have also come from efforts to account for dark matter halos, resulting in an average increase of $\sim$20 % (Schulze and Gebhardt 2011; Rusli et al. 2013a), but as high as a factor of 2 in the case of M87 (Gebhardt and Thomas 2009). Incorporating a dark matter halo is akin to relaxing the past assumption/simplification that the stellar mass-to-light ratio is constant with radius.[35]

This new, slightly steeper, $M_{\rm bh}$–σ relation for the non-barred galaxies suggests that if $L_{\rm sph} \propto \sigma^6$ (Lauer et al. 2007) for the core-Sérsic galaxies, then one can expect to recover $M_{\rm bh} \propto L_{\rm sph}$ for the core-Sérsic galaxies. If $L_{\rm sph} \propto \sigma^5$ (e.g. Schechter 1980) then one can expect to find $M_{\rm bh} \propto L_{\rm sph}^{6/5}$, suggestive of a second order effect on the picture of dry mergers maintaining a constant $M_{\rm bh}/L_{\rm sph}$ and $M_{\rm bh}/M_{\rm sph}$ ratio. Resolution to this minor query may simply require consistency with the regression analyses, or perhaps a careful bulge/disc separation of the galaxies involved (e.g. Laurikainen et al. 2005, 2011; Balcells et al. 2007a,b; Gadotti 2008; Läsker et al. 2014a), because core-Sérsic galaxies can contain a fast-rotating disc (e.g. Dullo and Graham 2013; Krajnović et al. 2013).

11.5.2.1 Pseudobulges

Pseudobulges are particularly hard to identify, for the multitude of reasons presented in Graham (2013, 2014). Furthermore, many galaxies contain *both* a disc-like 'pseudobulge' and a classical bulge (e.g. Erwin et al. 2003, 2014; Athanassoula 2005; Gadotti 2009; MacArthur et al. 2009; dos Anjos and da Silva 2013; Seidel et al. 2014). In addition, some may have formed from the (secular) inward migration and (classical) merging of stellar clumps (e.g. Noguchi 1999; Bournaud et al. 2007; Inoue and Saitoh 2012, and references therein). All of this makes the task of labelling galaxies as either containing a pseudobulge or a classical bulge highly

[35]This raises another issue which is yet to be properly addressed in the literature: not only do many spheroids have radial stellar population gradients, but most Sérsic galaxies have nuclear star clusters in addition to massive black holes, and the assumption of a single stellar mass-to-light ratio when modelling the data to derive a black hole mass is therefore not appropriate.

problematic and untenable. In the $M_{\rm bh}$–σ analysis by Graham et al. (2011) and Graham and Scott (2013), they avoided the issue of pseudobulges and separated galaxies based on the presence (or not) of a bar and revealed that the masses of black holes in barred galaxies correlate with the velocity dispersion, despite their heightened dynamics. Given that the majority of Sérsic spheroids (i.e. those without partially depleted cores) also follow the near-quadratic $M_{\rm bh}$–L relation, it appears that the masses of black holes in pseudobulges correlate with at least one property of their host bulge, and unless pseudobulges are restricted to have a narrow range of velocity dispersion, then their black hole masses also correlate with velocity dispersion (or at least define an upper envelope in the $M_{\rm bh}$–σ diagram).

A few of the (often not properly recognised) difficulties with identifying pseudobulges are noted here, in case it is helpful to some readers. From a kinematical perspective, just as with the formation of rotating elliptical galaxies via mergers, mergers can also create bulges which rotate (e.g. Bekki 2010; Keselman and Nusser 2012) and bars can spin-up classical bulges (e.g. Saha et al. 2012), and the smaller the bulges are the easier it is. Rotation is therefore not a definitive signature of a pseudobulge. In spiral galaxies, the observable presence of the disc's inner spiral arms, which cohabit the inner region of the galaxy where the bulge also resides, are of course easier to detect in fainter bulges (which are those that have smaller Sérsic indices) due to the greater bulge/arm contrast. However the detection and presence of these underlying features does not necessitate the presence of a pseudobulge (e.g. Eliche-Moral et al. 2011; dos Anjos and da Silva 2013).

From a selection of hundreds of disc galaxies imaged in the K-band, Graham and Worley (2008) observe no bimodality in the bulge Sérsic indices, questioning the suitability of a divide at a Sérsic index of $n = 2$ which has frequently been used in the recent literature. This divide is roughly halfway between $n = 1$ (which describes the light-profiles of flattened rotating discs) and $n = 4$ (which was in the past thought to describe the majority of elliptical galaxies and large bulges). While pseudobulges are expected to have Sérsic indices $n \approx 1$ – having formed from their surrounding exponential disc (e.g. Bardeen 1975; Hohl 1975; Combes and Sanders 1981; Combes et al. 1990; Pfenniger and Friedli 1991) – the problem is that mergers do not only produce $R^{1/4}$-like light profiles. Mergers can also create bulges with $n < 2$ (e.g. Eliche-Moral et al. 2011; Scannapieco et al. 2011; Querejeta et al. 2015), just as low-luminosity elliptical galaxies (not built from the secular evolution of a disc) are well known to have $n < 2$ and even < 1 (e.g. Davies et al. 1988; Young and Currie 1994).[36]

Prior to the realisation that the Sérsic index changes monotonically with spheroid luminosity and size (e.g. Caon et al. 1993; Andredakis et al. 1995) – referred to as structural nonhomology – the curved but continuous scaling relations involving the

[36]The occurrence of large-scale, rotating stellar discs and kinematical substructure in early-type galaxies on either side of the alleged divide at $M_B = -18$ mag ($n \approx 2$) further reveals the continuity of dwarf and ordinary early-type galaxies (e.g., Emsellem et al. 2007; Krajnović et al. 2008; Scott et al. 2014; Toloba et al. 2014).

'effective' half-light radii and 'effective' surface brightness (which have a maximum curvature around $n = 2$) had suggested that spheroids with $n < 2$ may be a distinct species rather than the low mass extension of spheroids with $n > 2$ (see Graham 2013). However we now know that this was a red-herring, and that all relations involving the 'effective' parameters are curved (e.g. Graham and Guzmán 2003; Gavazzi et al. 2005; Ferrarese et al. 2006a; Côté et al. 2006, 2007). As such, the Kormendy (1977) relation cannot be used to separate dwarf early-type galaxies from ordinary early-type galaxies, nor to separate pseudobulges from classical bulges, because at low-luminosities both types of bulge (classical and pseudo) depart from this relation, which is the tangent to the bright arm of the curved μ_e–R_e distribution.

11.6 The M_{bh}–n Relation

As noted in Graham et al. (2001), it may not be the total amount of mass in a spheroid, but rather how that mass is distributed, when it comes to the connection with the central supermassive black hole. Similarly, the velocity dispersion is but a tracer of the underlying mass distribution, and as such it can not be the fundamental parameter driving the black hole mass scaling relations.

Intriguingly, what Graham et al. (2001) revealed is that the central radial concentration of light, within the inner effective half light radii of spheroids, correlates strongly with the black hole mass. The concentration index which they used, taken from Trujillo et al. (2001), is monotonically related with the Sérsic index n, and thus an M_{bh}–n relation also exists, as shown in Graham et al. (2003a). With an expanded data set, Graham and Driver (2007) revealed that this relation is no longer well described by a single log-linear power-law, and that a log-quadratic relation performs noticeably better (see Fig. 11.5a). Given the log-linear L–n relation observed for both elliptical galaxies (e.g. Young and Currie 1994; Jerjen and Binggeli 1997; Graham and Guzmán 2003; Ferrarese et al. 2006a) and the bulges of disc galaxies (e.g. Andredakis et al. 1995; Graham and Worley 2008, and references therein), and the bent M_{bh}–L_{sph} relation (Sect. 11.4), the M_{bh}–n relation must be bent, such that galaxies which have experienced major, relatively dry, merger events are responsible for the flattening which is seen in Fig. 11.5 at high masses.

The existence of the M_{bh}–L_{sph} relation, coupled with existence of the L_{sph}–n relation, necessitates the existence of the M_{bh}–n relation. Although, as illustrated by Savorgnan et al. (2013), there is a need for care when measuring Sérsic indices, and studies which fail to recover the M_{bh}–n relation for the sample of galaxies with directly measured black hole masses may be dominated by poorly measured Sérsic indices, and in turn erroneous bulge magnitudes which depend on an accurate Sérsic index. Within the literature, measurements for individual galaxies have varied dramatically (e.g. Graham and Driver 2007; Laurikainen et al. 2010; Sani et al. 2011; Vika et al. 2012; Beifiori et al. 2012; Rusli et al. 2013a; Läsker et al. 2014a). Shown in Fig. 11.5b are the average values, after the rejection of extreme outliers, plotted against black hole mass. Savorgnan et al. (2013) divided the sample into

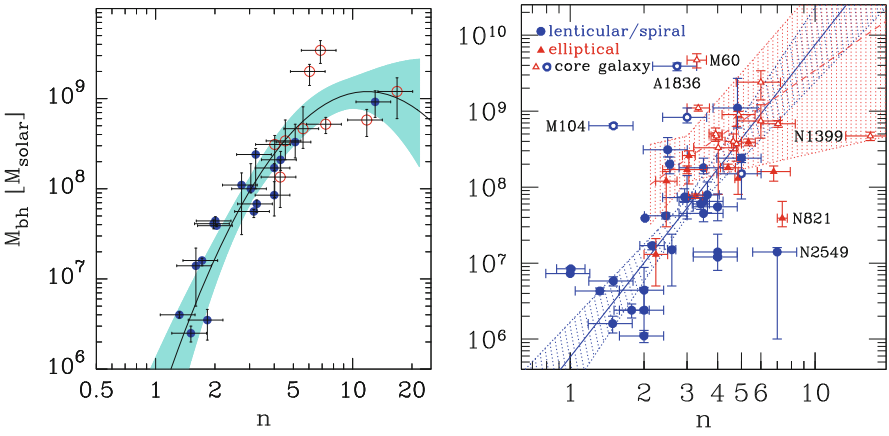

Fig. 11.5 *Left panel*: M_{bh}–n diagram taken from Graham and Driver (2007). The core-Sérsic spheroids are shown here by the *red circles*, while the Sérsic spheroids are shown by the *blue dots*. The lone Sérsic spheroid at the high-mass end is the S0 galaxy NGC 3115, identified to not have a core by Ravindranath et al. (2001). *Right panel*: M_{bh}–n diagram from Savorgnan et al. (2013). Rather than a single log-quadratic relation, two log-linear relations are shown here, one for the Sérsic spheroids and one for the core-Sérsic spheroids

Sérsic and core-Sérsic spheroids, and fit separate linear regressions for each sub-population.

Savorgnan et al. (2015, in prep.) has nearly completed a careful multi-component analysis of all the 72 galaxies used by Graham and Scott (2013) and reconciled the differences between past attempts to measure the Sérsic index. For example, sometimes these discrepancies arise because a lenticular disc galaxy may have been modelled with either a single Sérsic component or more correctly as the sum of a Sérsic-bulge plus an exponential disc by a different author. Other times the presence of an unaccounted for nuclear disc, or a partially depleted core, has biased the luminosity-weighted fits in some studies. The M_{bh}–n relation, more so than the previous relations, is in a state of limbo until this work is completed. Despite the need for care when measuring the Sérsic index, the advantage is that one only requires uncalibrated photometric images.

Readers interested in the development of fitting bulge light profiles since de Vaucouleurs (1959) first noted departures from his $R^{1/4}$ model, may appreciate the references in section 4.1 of Graham (2013). Andredakis et al. (1995) were the first to model the bulges of disc galaxies with Sersic's (1963) light profile model, following its application to elliptical galaxies by Davies et al. (1988) and Caon et al. (1993), and the earlier advocation of its use by Capaccioli (1985, 1987). Some of the difficulty with, and the impact of getting, the Sérsic index correct is illustrated by Gadotti and Sánchez-Janssen (2012) in the case of the Sombrero galaxy.

11.7 The $M_{\rm bh} - \mu_0$ Diagram

It is not unreasonable to expect that the growth of massive black holes may be related to the growth, and subsequent space density, of stars in its immediate vicinity. Gas processes have contributed to the development of both, and the black hole mass may be more connected with the local stellar density than the total stellar mass of the host spheroid. While the de-projected stellar density, ρ_0 is ideally the quantity we would like to have (e.g. Merritt 2006b, his figure 5), and this can be derived under certain assumptions (e.g. Terzić and Graham 2005, their Eq. 4), it is of course the projected surface brightness that is observed.

Binggeli et al. (1984) and Sandage and Binggeli (1984) provide a nice historical account of the detection of dwarf galaxies, and wrote that it was established that "the dwarf elliptical galaxies form a continuum in luminosity with the brighter E systems". Caldwell (1983; his figure 6) and Bothun et al. (1986, their figure 7) revealed this continuum was such that fainter than $M_B \approx -20.5$ mag, there is a log-linear relation between the luminosity and the central surface brightness, μ_0. In addition to this, Binggeli et al. (1984, their figure 11) and Binggeli and Cameron (1991, their figures 9 and 18) found that, when using the inward extrapolation of King models, this L–μ_0 relation extends from $-12 > M_B > -23$ mag. This was further highlighted by Jerjen and Binggeli (1997) and Graham and Guzmán (2003) when using the inward extrapolation of the Sérsic model; extrapolated over partially depleted cores in the case of the brightest spheroids whose cores have been eroded away by coalescing supermassive black holes.

Given this log-linear L–μ_0 relation, and the bent $M_{\rm bh}$–$L_{\rm sph}$ relation (Sect. 11.4), there must be a bent $M_{\rm bh}$–μ_0 relation. It should again be emphasized that this particular value of μ_0 refers to the extrapolated/expected value prior to core depletion. Given the difficulties in routinely obtaining robust Sérsic indices for the spheroids with black hole masses (Sect. 11.6), it is perhaps not surprising that this diagram is yet to be published. Although it may be the fundamental parameter linking black holes with their bulges, to date there is only a prediction by Graham and Driver (2007) for its form. This was derived by coupling the log-quadratic $M_{\rm bh}$–n relation from Graham & Driver with the log-linear n–μ_0 relation from Graham and Guzmán (2003), and is reproduced here in Fig. 11.6.

Given our current understanding, it makes more sense to construct the $M_{\rm bh}$–μ_0 relation using the log-linear $M_{\rm bh}$–L relations for the Sérsic and core-Sérsic spheroids given in Graham and Scott (2013, their table 3) together with the log-linear L–μ_0 relation given in Graham and Guzmán (2003, their figure 9c). Because the latter was derived in the B-band, we use the B-band $M_{\rm bh}$–L relation from Graham & Scott. For the Sérsic galaxies, this gives the relation

$$\log(M_{\rm bh}/{\rm M}_\odot) = 17.24 - 0.63\mu_0, \tag{11.4}$$

and for the core-Sérsic galaxies one has the relation

$$\log(M_{\rm bh}/{\rm M}_\odot) = 13.62 - 0.36\mu_0. \tag{11.5}$$

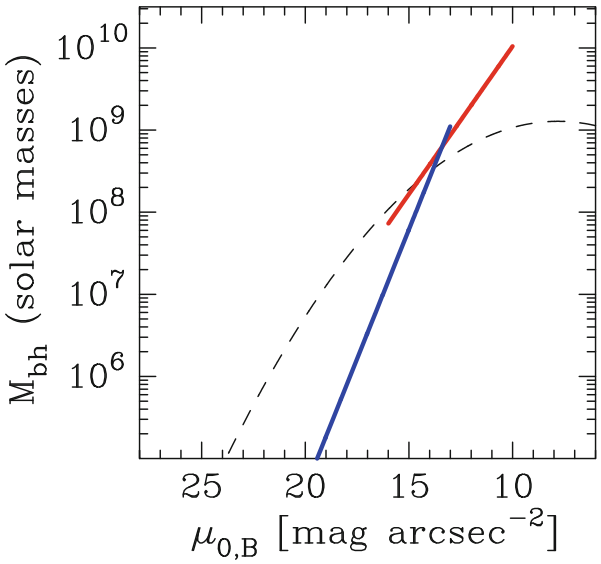

Fig. 11.6 Predictions for the M_{bh}–μ_0 diagram. The *dashed curve* is from Graham and Driver (2007), while the *thin blue* and *thick red lines* show Eqs. 11.4 and 11.5 for the Sérsic and core-Sérsic spheroids, respectively. Clearly the uncertainty on these lines is still quite large, given that the solid lines do not trace the dashed curve, but a bend is nonetheless expected

These predictions are shown in Fig. 11.6. Once the careful Sérsic modelling of galaxies with directly measured black hole masses is completed by Savorgnan et al. (in prep.), it will be possible to populate this diagram and (under certain assumptions) its deprojected cousin.

11.8 Depleted Galaxy Cores and the M_{bh}–M_{def} Relation

As noted previously, the merger of two galaxies without substantial gas, referred to as a dry merger, will result in the supermassive black holes from the progenitor galaxies sinking to the bottom of the newly wed galaxy by transferring much of their orbital angular momentum to the stars near the new galaxy's core (Begelman et al. 1980; Ebisuzaki et al. 1991) (Fig. 11.7). Such collisional construction of galaxies results in an evacuated 'loss cone' showing up as a partially depleted core[37] in the images of nearby galaxies (e.g. King and Minkowski 1966, 1972; Kormendy 1982; Lauer 1983). Typical core sizes, as quantified by the break radius R_b of

[37] See Dullo and Graham (2013, their Section 6.1) for a discussion of alternative concepts for core depletion.

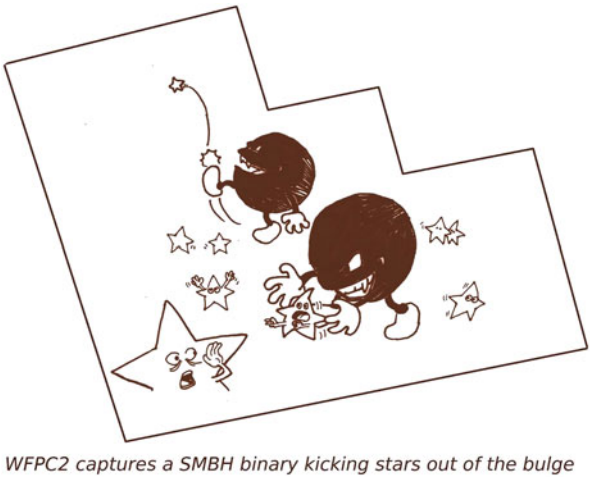

Fig. 11.7 Cartoon showing a pair of supermassive black holes kicking stars away as they dance towards coalescence at the center of a galaxy (Credit: Paolo Bonfini)

the core-Sérsic model, are tens to a few hundred parsec (e.g. Trujillo et al. 2004; Ferrarese et al. 2006a; Côté et al. 2007; Hyde et al. 2008; Richings et al. 2011; Rusli et al. 2013b; Dullo and Graham 2013, 2014; Bonfini 2014), and roughly a factor of 2 smaller than Nuker model break radii (Lauer et al. 1995). Whether or not coalescence of the black holes has already occurred in these galaxies with partially depleted cores is not clear, (although see Khan et al. (2011, 2013), and references therein in regard to the 'final parsec problem').

Using the core-Sérsic model to quantify the central flux deficit, and in turn the stellar mass deficit, Graham (2004) discovered $M_{\rm def} \approx 2M_{\rm bh}$. Previously it was thought that $M_{\rm def}/M_{\rm bh}$ was, on average, an order of magnitude greater (e.g. Milosavljević et al. 2002; Ravindranath et al. 2002), which required a troublingly large number of merger events given that the ejected mass should roughly scale with $N\,M_{\rm bh}$, where N is the cumulative number of (equivalent major) dry merger events (Milosavljević and Merritt 2001; Merritt 2006a). Using the core-Sérsic model, these new lower mass ratios were also found by Ferrarese et al. (2006a) and Hyde et al. (2008). Using the idea from Graham et al. (2003a) that cores can be measured as a deficit of light relative to the inward extrapolation of the outer Sérsic profile, but fitting the Sérsic model rather than core-Sérsic model and identifying the sizes of depleted cores by eye, Kormendy and Bender (2009) reported notably larger mass ratios (typically close to 10 or higher). Hopkins and Hernquist (2010) subsequently resolved this issue in a model-independent manner and revealed that the core-Sérsic model measurements of the central mass deficits were correct. Most recently, Rusli et al. (2013b) found that $\sim$80 % of their 23 galaxies have $1 < M_{\rm def}/M_{\rm bh} < 5$, while Dullo and Graham (2014) reported typical values for their sample of 31 galaxies to be $0.5 < M_{\rm def}/M_{\rm bh} < 4$.

Although the central mass deficit and break radius are obviously not fundamental parameters in establishing the spheroid-(black hole) connection – simply because many galaxies have black holes but not partially depleted cores – there is nonetheless

an $M_{\rm bh}$–R_b relation (Lauer et al. 2007)[38] and an $M_{\rm bh}$–$M_{\rm def}$ relation (e.g., Graham 2004; Rusli et al. 2013b; Dullo and Graham 2014). This relation simply exists over a restricted mass range. Dullo and Graham (2014, their Eq. 18) reported that $M_{\rm def} \propto M_{\rm bh}^{3.70\pm0.76}$ for the population ensemble (not to be confused with growth in individual galaxies). This is of interest for several reasons. One of which is that it may provide insight into the merging scenario, which currently has an unresolved problem. In general, galaxies with the greatest $M_{\rm def}/M_{\rm bh}$ ratio should have experienced the highest number of major dry mergers, and due to the increase in black hole mass but stagnation in velocity dispersion associated with such mergers (e.g. Ostriker and Hausman 1977; Hausman and Ostriker 1978; Ciotti and van Albada 2001), they should be offset to high black hole masses in the $M_{\rm bh}$–σ diagram (see Volonteri and Ciotti 2013). However, they are not (Savorgnan and Graham 2014).

Within low-luminosity early-type galaxies, the nuclear star cluster can be slightly offset ($\sim$100 parsec) from the galaxy's photometric center (Binggeli et al. 2000; Barazza et al. 2003). This is thought to be due to the dense star cluster's harmonic oscillation within the weak gravitational gradient of the galaxy's core. The amplitude of the nuclear cluster's rocking back and forth motion is expected to be greater in spheroids with lower Sérsic index, because they have lower central stellar densities and shallower inner density profiles, and thus less well defined gravitational centers over a greater fraction of their half-light radii (see Terzić and Graham 2005, their figure 2). Similarly, high-luminosity core-Sérsic spheroids have somewhat weakened gravitational centers (Terzić and Graham 2005, their figure 3) due to the partial depletion of stars in their cores. One may then expect to find the supermassive black holes slightly offset from the photometric centers of core-Sérsic galaxies (Miller and Smith 1992; Taga and Iye 1998). However a mechanism capable of creating more extreme ($>$1 kpc) offsets is the recoil from the emission of anisotropic gravitational radiation that a newly merged black hole may receive (e.g. Bonnor and Rotenberg 1961; Peres 1962; Bekenstein 1973). The linear momentum carried away by the gravitational wave is balanced by a kick imparted to the black hole. This recoil process has the ability to evacuate a much greater loss cone, and has been proposed as an explanation for some cores having large $M_{\rm def}/M_{\rm bh}$ ratios (e.g. Boylan-Kolchin et al. 2004; Campanelli et al. 2007; Gualandris and Merritt 2008, 2012), which have been observed in NGC 1399 and NGC 5061. While only small spatial offsets are known for black holes in galaxies with directly measured black hole masses (e.g. Batcheldor et al. 2010; Lena et al. 2014), if this process is operating one might expect to see greater displacements (e.g. Blecha et al. 2013) of black holes in galaxies with larger $M_{\rm def}/M_{\rm bh}$ ratios. However, if the damping timescale of the recoil-induced oscillation is sufficiently short, one may not find this correlation.

[38]Lauer et al. (2007) found that using the radius where the negative, logarithmic slope of the surface brightness profile equals 0.5 (which matches well with the core-Sérsic break radius: Dullo & Graham 2012, their section 5.2) produces a stronger relation than obtained when using the Nuker model break radii.

In passing, it might be remiss if a few words were not said about the gravitational wave signals expected from the final coalescence of massive black holes after they have scoured out the cores of massive spheroids, preferentially removing stars on plunging radial orbits (e.g. Quinlan and Hernquist 1997; Milosavljević and Merritt 2001; Thomas et al. 2014). Binary AGN, and thus massive black holes, are now known in several galaxies (e.g. Komossa et al. 2003; Liu et al. 2014, and references therein). The rapidly changing gravitational field as the black holes spiral (and thus accelerate) around each other, generates a gravitational wave-like ripple which radiates out into space (e.g. Buonanno and Damour 2000; Barack and Cutler 2004; Baker et al. 2006; Blanchet 2006; Sesana 2010; Amaro-Seoane et al. 2012). Travelling at the speed of light, the amplitude of the wave decays linearly (rather than quadratically) with distance and, also unlike light, passes unimpeded through both space and matter. Due to the large orbital size of the binary black hole, space-based interferometers at great separations are required to sample the long wavelength of the waves generated by the black hole binary. Building on the hopes of the Laser Interferometer Space Antenna (LISA: Danzmann and Rüdiger 2003), the European LISA Pathfinder mission[39] (LPF: Anza et al. 2005; McNamara 2013), formerly known as SMART-2, offers the very exciting promise of detecting these waves predicted by Einstein's theory of relativity but not yet observed (Will 2006).

11.9 Intermediate Mass Black Holes and the (Black Hole)–(Nuclear Cluster) Connection

As was noted in Sect. 11.4.1, the bent $M_{\rm bh}$–$M_{\rm sph}$ relation offers hope for detecting the missing population of intermediate mass black holes. This is because the linear $M_{\rm bh}$–$M_{\rm sph}$ relation predicts $10^2 < M_{\rm bh}/{\rm M}_\odot < 10^5$ black hole masses in smaller/fainter spheroids. Although we may not have the spatial resolution at optical/near-infrared wavelengths to resolve the sphere-of-influence of these black holes, and thus directly measure their masses from Keplerian kinematics, there is an independent method which can be used to predict (strengthen/reject) the likely existence of such intermediate mass black holes. It is based on the observation that the black hole mass correlates with the AGN radio and X-ray flux in such a way that they define a 2-dimensional surface in 3-parameter space, which has been dubbed the 'fundamental plane of black hole activity' (Merloni et al. 2003). Therefore, obtaining radio and X-ray data is expected to prove fruitful in the hunt for the elusive intermediate mass black holes. Preferably, this data should be obtained simultaneously because the AGN are known to vary in their flux output over timescales of days.

One of the best candidates for an intermediate mass black hole is the ultraluminous X-ray source HLX-1 in the galaxy ESO 243-49 (Farrell et al. 2009; Webb et al. 2014). Interestingly, this 9000 solar mass black hole candidate does not reside

[39] http://sci.esa.int/lisa-pathfinder/

near the center of its host galaxy but in a compact star cluster (Soria et al. 2010; Wiersema et al. 2010; Farrell et al. 2012) located at a projected distance of ∼3 kpc from the galaxy's nucleus, perhaps shedding insight into the formation location of intermediate mass black holes (see also Mezcua et al. 2013, 2015, in regard to an off-centered intermediate mass black hole candidate in NGC 2276). Despite early hopes for intermediate mass black holes in globular clusters (e.g. Gerssen et al. 2003; Gebhardt et al. 2005; Noyola et al. 2010; Lützgendorf et al. 2013, and references therein), there are not yet any definite candidates (e.g. van den Bosch et al. 2006; Hurley 2007; Anderson and van der Marel 2010; Vesperini and Trenti 2010; Lanzoni et al. 2013; Lanzoni 2015). Observational research programs (e.g. Bellini et al. 2014; Lapenna et al. 2014) continue the hunt as the formation of intermediate mass black holes in dense star clusters seems probable (e.g. Miller and Hamilton 2002; Baumgardt et al. 2004; Gürkan et al. 2004; Portegies Zwart et al. 2004).

Aside from globular clusters, some of the dense star clusters found in the nuclei of many low- and intermediate-luminosity spheroids (e.g. Reaves 1983; Binggeli et al. 1985; Phillips et al. 1996; Carollo et al. 1997) are already known to house massive black holes. Ferrarese et al. (2006b) and Wehner and Harris (2006) originally suggested that these star clusters may be the low-mass extension of the supermassive black holes, in the sense that galaxies housed one type of nucleus or the other. However this idea was soon modified when it was realised that such clusters and massive black hole coexist in substantial numbers of galaxies (e.g. González Delgado et al. 2008; Seth et al. 2008; Graham and Spitler 2009). Ongoing efforts have revealed that nuclear star clusters do not follow the same mass scaling relations as supermassive black holes (Graham 2012b; Leigh et al. 2012; Neumayer and Walcher 2012; Graham and Scott 2013), and the search for intermediate mass black holes continues. Among the most promising targets are the low mass bulges of disc galaxies hosting an AGN (Graham and Scott 2013) and the low mass dwarf galaxies which also display AGN activity (e.g. Reines et al. 2013; Moran et al. 2014); see Fig. 11.8.

Just as there is a relation between spheroid luminosity and the central surface brightness[40] of the spheroid – until the onset of partially depleted cores in massive spheroids – there is also a relationship between spheroid luminosity and the brightness of the nuclear star clusters that they host (Balcells et al. 2003; Graham and Guzmán 2003). In a somewhat similar manner to the establishment of the $M_{\rm bh}$–μ_0 relation presented in Sect. 11.7, one can predict what the $M_{\rm bh}$-$M_{\rm nc}$ relation should be like. Graham (2015) combined the relation $M_{\rm bh} \propto M_{\rm sph}^{2}$ for the Sérsic spheroids (Sect. 11.4.1) with the relation $M_{\rm nc} \propto M_{\rm sph}^{0.6-1.0}$ (references above) to obtain $M_{\rm bh} \propto M_{\rm nc}^{2-3.3}$. A consistent result was obtained by coupling the relation $M_{\rm bh} \propto \sigma^{5.5}$ (Sect. 11.5) with $M_{\rm nc} \propto \sigma^{1.6-2.7}$ (references above) to give $M_{\rm bh} \propto M_{\rm nc}^{2.0-3.4}$. Massive black holes therefore grow rapidly within their host star cluster, until it is evaporated (e.g. Bekki and Graham 2010) or partially devoured (e.g. Hills 1975; Frank and

[40]Technically it is the central surface brightness of the spheroid excluding blips from additional nuclear components such as star clusters.

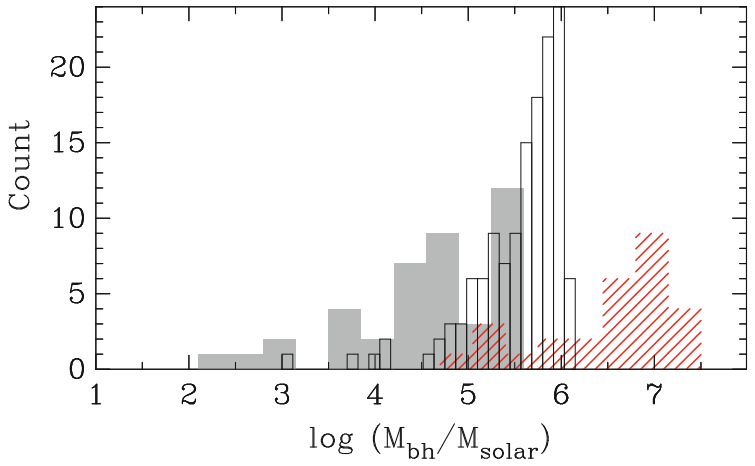

Fig. 11.8 Predicted black hole masses. The solid histogram was obtained using the $M_{\rm bh}$–L_K relation for Sérsic spheroids applied to the K-band bulge magnitudes in Graham and Scott (2013, their table 6). The open histogram was obtained using the $M_{\rm bh}$–$M_{\rm sph}$ relation for Sérsic spheroids (shown in Fig. 11.2) applied to the dwarf galaxy masses in Reines et al. (2013, their table 1). The shaded histogram was obtained in the same way but using the dwarf galaxy stellar masses in Moran et al. (2014, their table 1). The fainter bulges are expected to contain the least massive black holes

Rees 1976; Murphy et al. 1991; Komossa 2013; Donato et al. 2014; Vasiliev 2014). However, disentangling which came first may be an interesting pursuit, and just as there are different types of bulges, there may be different types of nuclear star clusters (e.g. Turner et al. 2012). This $M_{\rm bh}$-$M_{\rm nc}$ relation is somewhat complementary to the $M_{\rm bh}$-$M_{\rm def}$ relation, with each applicable at opposing ends of the black hole mass range currently accessible. Such co-occupancy of black holes and nuclear star clusters is a likely source of stellar tidal disruption events (Komossa et al. 2009; Komossa 2013 and references therein) and gravitational wave emission from the inspiralling of compact stellar remnants (e.g. Hils and Bender 1995; Amaro-Seoane et al. 2007, and references therein), predictions for which are dramatically modified when using the new, near-quadratic $M_{\rm bh}$-$M_{\rm sph}$ relation (Mapelli et al. 2012). Further quantifying the coexistence of massive black holes in dense, compact, nuclear star clusters should help us to predict the occurrence of, and better understand, these exciting phenomena.

11.10 The $M_{\rm bh}$–$M_{\rm halo}$ Relation

Ferrarese (2002) have revealed that there is a relationship between the black hole mass and the galaxy halo mass (baryons plus dark matter), as traced by the circular velocity at large radii (used as a proxy for the halo's virial radius). Due to the relation between this rotational velocity and the galaxy's velocity dispersion (see also Baes

et al. 2003; Pizzella et al. 2005; Ferrarese and Ford 2005, their Eq. 21)[41] one can expect an $M_{\rm bh}$–$M_{\rm halo}$ relation. The extent of this relationship may be applicable only to galaxies with large bulges (or $v_{\rm circ} > \sim 100\,{\rm km\,s^{-1}}$ or $\sigma > \sim 100\,{\rm km\,s^{-1}}$), because of the breakdown in the relationship between circular velocity and velocity dispersion for lower mass systems (e.g. Zasov et al. 2005; Ho 2007; Courteau et al. 2007). Nonetheless, this would make the relationship exist over a larger mass range than the $M_{\rm bh}$–$R_{\rm b}$ and $M_{\rm bh}$–$M_{\rm def}$ relations (Sect. 11.8).

For galaxies built from major dry merger events, in which the black hole mass and the galaxy stellar mass simply add together, the dark matter must also add in this linear fashion. This would then establish a linear $M_{\rm bh}$–$M_{\rm halo}$ relation – just as there is a linear $M_{\rm bh}$–$M_{\rm sph}$ relation preserving the $M_{\rm bh}/M_{\rm sph}$ ratio – at high masses ($M_{\rm bh} >\sim 10^8\,{\rm M}_\odot$). This appears to be consistent with the data in Ferrarese (2002, her figure 5). However, their linear regression to the fuller sample gives $M_{\rm bh} \propto M_{\rm halo}^{1.65-1.82}$, which is in remarkable agreement with the prediction $M_{\rm bh} \propto M_{\rm halo}^{5/3}$ by Haehnelt et al. (1998). Although, with a different sample, Baes et al. (2003) reported $M_{\rm bh} \propto M_{\rm halo}^{1.27}$. Curiously, for elliptical galaxies not built from dry mergers,[42] the prediction by Haehnelt et al. (1998) transforms into $M_{\rm bh} \propto L_{\rm gal}^{20/9} (= L_{\rm gal}^{2.22})$ if $M_{\rm halo}/L_{\rm gal} \propto L_{\rm gal}^{1/3}$ (Jørgensen et al. 1996; Cappellari et al. 2006). This near-quadratic relation has been seen before in Sect. 11.4.

11.10.1 Globular Cluster Systems

Lending support to the $M_{\rm bh}$–$M_{\rm halo}$ relation is the connection between black hole mass and the halo of globular clusters that swarm around galaxies, both in terms of their number (Burkert and Tremaine 2010; Harris and Harris 2011; Rhode 2012; Harris et al. 2014) and their velocity dispersion (Sadoun and Colin 2012; Pota et al. 2013). In Burkert and Tremaine (2010) they used a (self-admittedly limited) sample of 13 galaxies for which the black hole mass and the number of globular clusters was known. They observed an rms scatter of just 0.21 dex about their optimal relation in the $\log(M_{\rm bh})$ mass direction. Not surprisingly this attracted some interest (e.g. Snyder et al. 2011) because it was half of the value observed in the $M_{\rm bh}$–σ diagram. However as more galaxies have been added, the scatter about the relation involving the globular clusters has increased.

[41] It should be noted that the dynamical study by Kronawitter et al. (2000) and Gerhard et al. (2001), which led to the relationship between the circular velocity and the velocity dispersion for elliptical galaxies, was based on a sample of elliptical galaxies that had very similar absolute magnitudes. Consequently, these galaxies will have similar structural and dynamical profiles, and thus their $v_{\rm circ}$–σ relationship may not be applicable to lower- or higher-luminosity elliptical galaxies with different Sérsic indices, i.e. concentration, and dynamical profiles (e.g. Ciotti 1991).

[42] Equal mass, (major) dry mergers preserve the $M_{\rm halo}/L$ ratio and therefore galaxies built from major dry mergers follow the sequence $M_{\rm halo}/L \propto L^0$.

The globular cluster system around individual galaxies are known to display a bimodality in their colour, with the red (metal rich) globular clusters thought to be associated with the galaxy's bulge while the blue (metal-poor) globular clusters are thought to be connected with the halo (Ashman and Zepf 1992; Forbes et al. 1997). Using both the observed velocity dispersion of the globular cluster system, and the velocity dispersion with the rotational component of the system subtracted, Pota et al. (2013) report that while a correlation with black hole mass is evident, it is not yet clear if the black hole mass is better correlated with the red (bulge) or the blue (halo) globular cluster sub-population.

11.11 The $M_{\rm bh}$–(Spiral Arm Pitch Angle) Connection

While the applicability of the $M_{\rm bh}$–$M_{\rm halo}$ relation in lower mass spiral galaxies is unclear, there is a somewhat complementary relation which only operates in spiral galaxies. Seigar et al. (2008; see also Ringermacher and Mead 2009; Treuthardt et al. 2012; Berrier et al. 2013) have presented the relation between black hole mass and spiral arm pitch angle. The spiral arm pitch angle (e.g. Puerari et al. 2014, and references therein) is of course known to vary along the Hubble-Jeans sequence, as does the bulge-to-total flux ratio, or more correctly the luminosity of the bulge (e.g. Yoshizawa and Wakamatsu 1975; Ostriker 1977; Meisels and Ostriker 1984; Trujillo et al. 2002), which may explain the black hole connection with the pitch angle. As with the radial concentration of the bulge light, the pitch angle has the advantage that it can be measured from photometrically uncalibrated images and therefore offers an easy means to predict black hole masses (perhaps even when there is no bulge[43]), from which one can then do clever things like determine the black hole mass function in spiral galaxies (Davis et al. 2014).

Given that this is obviously a secondary relation, although the low level of scatter reported by Davis et al. (2014) is intriguing, less shall be said about this than the relations involving a spheroid's central concentration and density of stars (Sects. 11.6 and 11.7).

11.12 Fundamental Planes: Adding a Third Parameter

As noted in Sect. 11.9, stellar and supermassive black holes roughly define a plane within the 3-dimensional space of black hole mass, radio power and X-ray luminosity (Merloni et al. 2003; Heinz and Sunyaev 2003; Falcke et al. 2004; Körding et al. 2006; Li et al. 2008). While this is both interesting in its own right and highly useful, the relationship between the black hole mass, accretion disc and

[43]The $M_{\rm bh}$–(pitch angle) relation is yet to be established for a sample of bulgeless galaxies.

jet is of a different nature to the other relations presented in this article and as such is not detailed here as it is an AGN phenomenon.

One of the early attempts to introduce a third parameter into the (black hole)–(host galaxy) scaling relations was by Marconi and Hunt (2003). They used the effective half light radius (R_e) of the spheroid, together with the velocity dispersion (σ), to derive a rough virial mass for the spheroid ($M_{virial} \propto \sigma^2 R_e$). They found that the total vertical scatter about their M_{bh}–M_{virial} relation was slightly less than that about their M_{bh}–σ relation (0.25 dex vs 0.30 dex). Using a sample of elliptical galaxies, Feoli and Mele (2005; see also Feoli and Mancini 2009, 2011) reported on a black hole mass relation with the kinetic energy of the host galaxy such that $M_{bh} \propto (M_{gal}\sigma^2)^{\alpha}$, where $0.87 < \alpha < 1.00$ and M_{gal} was derived assuming $R^{1/4}$ light profiles.[44] Given that M_{gal} roughly scales as $\sigma^2 R_e$, their kinetic energy expression roughly scales with $\sigma^4 R_e$. Additional variations of this theme, searching for a fundamental plane using combinations of σ and R_e can be found in de Francesco et al. (2006), who effectively suggested independent exponents for σ and R_e, in Aller and Richstone (2007) in terms of the gravitational binding energy, and in Hopkins et al. (2007) and Soker and Meiron (2011). Given the existence of *the* Fundamental Plane (Djorgovski and Davis 1987) linking the velocity dispersion with the mean effective surface brightness ($\langle\mu\rangle_e$) and effective half light radius, the presence of the M_{bh}–σ relation additionally suggests that there should be an M_{bh}–($\langle\mu\rangle_e$, R_e) plane (Barway and Kembhavi 2007).

With all of these attempts to define different planes, there are two issues that require attention: (i) barred galaxies, and (ii) the accuracy[45] and thus usefulness of R_e.

First, the increased scatter in the M_{bh}–σ diagram due to the inclusion of barred galaxies was reported by Graham (2008a,b) and Hu (2008). Moreover, Graham (2008a) showed that once the barred galaxies were removed, there was no reduction in scatter when going from the M_{bh}–σ diagram to the M_{bh}–(σ, R_e) diagram. If there is a more fundamental relation with some combination of σ and R_e, than compared with σ alone, this should not have been observed. The simulations of Younger et al. (2008, their figure 9) show that (merger built) classical bulges follow a plane, without the need to include (secular-disc-evolution built) pseudobulges. Therefore, if the lower scatter about the hybrid relations is only achieved when including the barred galaxies, it suggests that something else is responsible for the reduction, such as barred galaxies having smaller R_e values than the elliptical galaxies which dominate at the high mass end of one's sample. Younger et al. (2008) suggested that the relatively small dynamic range among the non-barred galaxies with direct black hole mass measurements may have been inadequate to provide a significant detection of this third parameter and thus a plane. It would be interesting to repeat the tests which searched for an optimal plane among the non-barred galaxies, but

[44] It should be noted that the assumption of $R^{1/4}$ light profiles can introduce a systematic bias with galaxy mass, Sérsic index and effective radius (e.g. Trujillo et al. 2001; Brown et al. 2003).

[45] It could be argued that a third issue is the accuracy of the black hole masses (Merritt 2013).

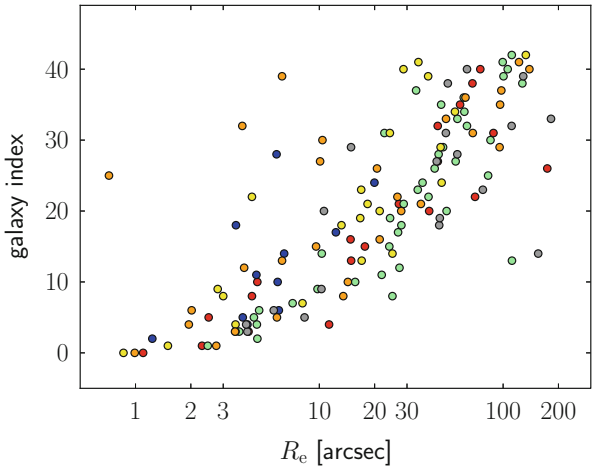

Fig. 11.9 Major-axis effective half-light radii R_e for the spheroidal component of 43 galaxies (having directly measured black hole masses) as determined by different authors (Figure taken from Savorgnan et al. (in prep.)) Legend: *red* = Graham and Driver (2007); *blue* = Laurikainen et al. (2010); *green* = Sani et al. (2011); *yellow* = Vika et al. (2012); *gray* = Beifiori et al. (2012); *orange* = Läsker et al. (2014a)

now using the larger galaxy samples which are available. However this brings us to the second issue.

Given that there have been errors in the measurement of the Sérsic indices n (as revealed by Savorgnan et al. 2013), there are thus errors in the measurements of the published, effective half light radii R_e (see also Bernardi et al. 2014). Harris et al. (2014) show the large range of R_e values (for the same spheroid) reported by different authors for spheroids with directly measured black hole masses. A similar plot is shown in Fig. 11.9 but this time restricting the data to that obtained from Sérsic $R^{1/n}$ model fits by different authors. Consequently, attempts to use R_e for measuring dynamical masses ($\propto \sigma^2 R_e$) or as a third parameter to mop up some of the scatter about the M_{bh}–σ relation should at this time be treated with caution.

11.13 Concluding Remarks

The "attraction" of black holes is vast, as evinced by a huge literature on the subject, of which but a small fraction is noted here. The fundamental physical connection between black-hole and bulge growth still awaits discovery. While it is expected that we may narrow in on the solution as we keep plugging away at more black hole mass measurements, coupled with improving the accuracy of all quantities involved, it is reasonable to expect that something unexpected may be discovered, such is the nature and joy of our collective pursuit.

Given the role that pulsars played in convincing the community that black holes may exist in 1967–1968, it is perhaps fitting that arrays of pulsar beacons are used today (e.g. Sesana et al. 2008; Hobbs et al. 2010; Kramer and Champion 2013) to try and detect the bob and sway of the space antennae as anticipated gravitational waves – from the inspiral of supermassive black holes at the centers of newly merged galaxies – wash by oblivious to our solar system. The future direct detection of such gravitational radiation would provide another strong test of Einstein's theory of general relativity (e.g. Will 2006, 2014), which, starting 100 years ago, led to the modern prediction of dense, dark stars and supermassive black holes.

Acknowledgements This review was made possible by Australian Research Council funding through grant FT110100263. This research has made use of NASA's Astrophysics Data System Bibliographic Services, and the NASA/IPAC Extragalactic Database (NED).

References

Abramowicz, M. A., & Fragile, P. C. 2013, Living Reviews in Relativity, 16, 1
Agarwal, B., Davis, A. J., Khochfar, S., Natarajan, P., & Dunlop, J. S. 2013, MNRAS, 432, 3438
Akritas, M. G., & Bershady, M. A. 1996, ApJ, 470, 706
Alexander, D. M., & Hickox, R. C. 2012, New Astronomy Reviews, 56, 93
Alexander, T. 2005, Physics Reports, 419, 65
Alexander, T., & Natarajan, P. 2014, Science, 345, 1330
Aller, M. C., & Richstone, D. O. 2007, ApJ, 665, 120
Alonso-Herrero, A., Pereira-Santaella, M., Rieke, G. H., et al. 2013, ApJ, 765, 78
Amaro-Seoane, P., Gair, J. R., Freitag, M., et al. 2007, Classical and Quantum Gravity, 24, 113
Amaro-Seoane, P., Aoudia, S., Babak, S., et al. 2012, Classical and Quantum Gravity, 29, 124016
Ambartsumian, V.A. 1958, Solvay Conference on Structure and Evolution of the Universe (R.Stoops, Brussels), p.241
Andreon, S., & Hurn, M. A. 2012, (arXiv:1210.6232)
Anglés-Alcázar, D., Özel, F., & Davé, R. 2013, ApJ, 770, 5
Anza, S., Armano, M., Balaguer, E., et al. 2005, Classical and Quantum Gravity, 22, 125
Anderson, W. 1929, On limiting density of matter and energy, Zeitschrift fur Physik, 56, 851
Anderson, J., & van der Marel, R. P. 2010, ApJ, 710, 1032
Andredakis, Y. C., Peletier, R. F., & Balcells, M. 1995, MNRAS, 275, 874
Arnett, D. 1967, Canadian Journal of Physics, 45, 1621
Ashman, K. M., & Zepf, S. E. 1992, ApJ, 384, 50
Ashtekar, A., & Bojowald, M. 2005, Classical and Quantum Gravity, 22, 3349
Athanassoula, E. 2005, MNRAS, 358, 1477
Baade, W., & Minkowski, R. 1954, ApJ, 119, 206
Baade, W., & Zwicky, F. 1934, Proceedings of the National Academy of Science, 20, 259
Baes, M., Buyle, P., Hau, G. K. T., & Dejonghe, H. 2003, MNRAS, 341, L44
Baker, J. G., Centrella, J., Choi, D.-I., Koppitz, M., & van Meter, J. 2006, Physical Review Letters, 96, 111102
Balcells, M., Graham, A. W., Domínguez-Palmero, L., & Peletier, R. F. 2003, ApJ, 582, L79
Balcells, M., Graham, A. W., & Peletier, R. F. 2007a, ApJ, 665, 1084
Balcells, M., Graham, A. W., & Peletier, R. F. 2007b, ApJ, 665, 1104
Barack, L., & Cutler, C. 2004, Physical Review D, 69, 082005
Barazza, F. D., Binggeli, B., & Jerjen, H. 2003, A&A, 407, 121
Bardeen, J. M. 1970, Nature, 226, 64

Bardeen, J.M. 1975, IAU Symp., 69, 297
Bardeen, J. M., & Wagoner, R. V. 1969, ApJ, 158, L65
Barnard, E. E. 1897, Bulletin of the Yerkes Observatory of the University of Chicago, 5, 446
Barway, S., & Kembhavi, A. 2007, ApJ, 662, L67
Batcheldor, D. 2010, ApJ, 711, L108
Batcheldor, D., Robinson, A., Axon, D. J., Perlman, E. S., & Merritt, D. 2010, ApJl, 717, L6
Baumgardt, H., Makino, J., & Ebisuzaki, T. 2004, ApJ, 613, 1143
Begelman, M.C. 1979, MNRAS 187, 237
Begelman, M. C., Blandford, R. D., & Rees, M. J. 1980, Nature, 287, 307
Begelman, M. C., Blandford, R. D., & Rees, M. J. 1984, Reviews of Modern Physics, 56, 255
Beifiori, A., Courteau, S., Corsini, E. M., & Zhu, Y. 2012, MNRAS, 419, 2497
Bekenstein, J. D. 1973, ApJ, 183, 657
Bekki K., 2010, MNRAS, 401, L58
Bekki, K., & Graham, A. W. 2010, ApJ, 714, L313
Bellini, A., Anderson, J., van der Marel, R. P., et al. 2014, ApJ, in press (arXiv:1410.5820)
Benson, A. J., Bower, R. G., Frenk, C. S., et al. 2003, ApJ, 599, 38
Bernardi, M., Meert, A., Vikram, V., et al. 2014, MNRAS, 443, 874
Berrier, J. C., Davis, B. L., Kennefick, D., et al. 2013, ApJ, 769, 132
Berti, E., Cardoso, V., & Starinets, A. O. 2009, Classical and Quantum Gravity, 26, 163001
Binggeli, B., Barazza, F., & Jerjen, H. 2000, A&A, 359, 447
Binggeli, B., Cameron, L.M. 1991, A&A, 252, 27
Binggeli B., Sandage A., Tammann G.A., 1985, AJ 90, 1681
Binggeli, B., Sandage, A., Tarenghi, M. 1984, AJ, 89, 64
Binney, J. 1982, ARA&A, 20, 399
Binney, J., Mamon, G.A. 1982, MNRAS, 200, 361
Bisnovatyi-Kogan, G. S., Zel'dovich, Y. B., & Novikov, I. D. 1967, Soviet Astronomy, 11, 419
Blanchet, L. 2006, Living Reviews in Relativity, 9, 4 (cited 26-09-2014)
Blandford, R. D. 1986, Quasars, 119, 359
Blandford, R. D., & Begelman, M. C. 1999, MNRAS, 303, L1
Blecha, L., Civano, F., Elvis, M., & Loeb, A. 2013, MNRAS, 428, 1341
Bonfini, P. 2014, PASP, 126, 935
Bonnor, W. B., & Rotenberg, M. A. 1961, Royal Society of London Proceedings Series A, 265, 109
Bonoli, S., Mayer, L., & Callegari, S. 2014, MNRAS, 437, 1576
Booth, C. M., & Schaye, J. 2009, MNRAS, 398, 53
Boylan-Kolchin, M., Ma, C.-P., & Quataert, E. 2004, ApJ, 613, L37
Bothun, G.D., Mould, J.R., Caldwell, N., MacGillivray, H.T. 1986, AJ, 92, 1007
Bournaud, F., Elmegreen, B. G., & Elmegreen, D. M. 2007, ApJ, 670, 237
Brandt, W. N., & Hasinger, G. 2005, ARA&A, 43, 827
Brown, R. J. N., Forbes, D. A., Silva, D., et al. 2003, MNRAS, 341, 747
Buonanno, A., & Damour, T. 2000, Physical Review D, 62, 064015
Burbidge, G. R. 1959, ApJ, 129, 849
Burbidge, G. R. 1964, in Physics of Nonthermal Radio Sources, ed. S.P. Maran and A.G.W.Cameron (Washington, D.C.: Government Printing Office), p.123
Burbidge, G. R., Burbidge, E. M., Sandage, A. 1963, Rev. Mod. Phys. 35, 947
Burbidge, E. M., Burbidge, G. R., & Rubin, V. C. 1964, ApJ, 140, 942
Burbidge, G., Burbidge, E. M., Arp, H. C., & Napier, W. M. 2006, (arXiv:astro-ph/0605140)
Burkert, A., & Tremaine, S. 2010, ApJ, 720, 516
Busarello, G., Longo, G., & Feoli, A. 1992, A&A, 262, 52
Busch, G., Zuther, J., Valencia-S., M., et al. 2014, A&A, 561, A140
Caldwell, N. 1983, AJ, 88, 804
Caldwell, N., & Bothun, G. D. 1987, AJ, 94, 1126
Cameron, A. G. W. 1971, Nature, 229, 178
Campanelli, M., Lousto, C., Zlochower, Y., & Merritt, D. 2007, ApJ, 659, L5

Campbell, W. W. 1917, Journal of the Royal Astronomical Society of Canada, 11, 281
Caon, N., Capaccioli, M., D'Onofrio, M. 1993, MNRAS, 265, 1013
Capaccioli, M. 1985, in New Aspects of Galaxy Photometry, ed. J.-L. Nieto, Springer-Verlag, p.53
Capaccioli, M. 1987, in Structure and Dynamics of Elliptical Galaxies, IAU Symp. 127, Reidel, Dordrecht, p.47
Cappellari, M., Bacon, R., Bureau, M., et al. 2006, MNRAS, 366, 1126
Cappellari, M., McDermid, R. M., Alatalo, K., et al. 2013, MNRAS, 432, 1862
Carollo, C. M., Stiavelli, M., de Zeeuw, P. T., & Mack, J. 1997, AJ, 114, 2366
Cattaneo, A., Dekel, A., Devriendt, J., Guiderdoni, B., & Blaizot, J. 2006, MNRAS, 370, 1651
Chandrasekhar, S. 1931a, ApJ, 74, 81
Chandrasekhar, S. 1931b, MNRAS, 91 456
Chandrasekhar, S. 1932, Zeitschrift für Astrophysik, Vol. 5, p.321
Chandrasekhar, S. 1935, MNRAS, 95, 207
Chilingarian, I. V., Cayatte, V., Durret, F., et al. 2008, A&A, 486, 85
Ciotti, L. 1991, A&A, 249, 99
Ciotti L., van Albada T. S., 2001, ApJ, 552, L13
Cirasuolo, M., Shankar, F., Granato, G. L., De Zotti, G., & Danese, L. 2005, ApJ, 629, 816
Cody, A. M., Carter, D., Bridges, T. J., Mobasher, B., & Poggianti, B. M. 2009, MNRAS, 396, 1647
Cohen, M. H., Cannon, W., Purcell, G. H., et al. 1971, ApJ, 170, 207
Collin, S. 2006, Albert Einstein Century International Conference, AIP Conference Proceedings, 861, 587
Comastri, A., Gilli, R., Marconi, A., Risaliti, G., & Salvati, M. 2015, A&A, 574, LL10
Combes, F., Debbash, F., Friedli, D., and Pfenniger, D. 1990, A&A, 233, 82
Combes, F., Sanders, R.H., 1981, A&A, 96, 164
Côté, P., et al. 2006, ApJ, 165, 57
Côté, P., et al. 2007, ApJ, 671, 1456
Courteau, S., McDonald, M., Widrow, L. M., & Holtzman, J. 2007, ApJ, 655, L21
Croton, D. J., Springel, V., White, S. D. M., et al. 2006, MNRAS, 365, 11
Danzmann, K., & Rüdiger, A. 2003, Classical and Quantum Gravity, 20, 1
Datt, B. 1938, Zeitschrift fur Physik, 108, 314
Davies, J.I., Phillipps, S., Cawson, M.G.M., Disney, M.J., Kibblewhite, E.J. 1988, MNRAS, 232, 239
Davies, R.L., Efstathiou, G., Fall, S.M., Illingworth, G., Schechter, P.L. 1983, ApJ, 266, 41
Davis, B. L., Berrier, J. C., Johns, L., et al. 2014, ApJ, 789, 124
Debattista, V. P., Kazantzidis, S., & van den Bosch, F. C. 2013, ApJ, 765, 23
de Francesco, G., Capetti, A., & Marconi, A. 2006, A&A, 460, 439
de Rijcke, S., Michielsen, D., Dejonghe, H., Zeilinger, W. W., & Hau, G. K. T. 2005, A&A, 438, 491
de Vaucouleurs, G. 1959, in Handbuch der Physik, ed. S. Flugge (Berlin: Springer), 311
Diamond-Stanic, A. M., & Rieke, G. H. 2012, ApJ, 746, 168
Di Matteo, T., Springel, V., & Hernquist, L. 2005, Nature, 433, 604
Djorgovski, S., & Davis, M. 1987, ApJ, 313, 59
Domagala, M., & Lewandowski, J. 2004, Classical and Quantum Gravity, 21, 5233
Donato, D., Cenko, S. B., Covino, S., et al. 2014, ApJ, 781, 59
dos Anjos S., & da Silva, M. B. 2013, Memorie della Societa Astronomica Italiana Supplementi, 25, 33
Dressler, A. 1984, ApJ, 286, 97
Dressler, A. 1989, Active Galactic Nuclei, IAU Symp. 134, 217
Dressler, A., & Richstone, D. O. 1988, ApJ, 324, 701
Droste, J. 1917, Koninklijke Nederlandse Akademie van Wetenschappen Proceedings Series B Physical Sciences, 19, 197
Drouart, G., De Breuck, C., Vernet, J. et al. 2014, A&A, 566, A53
Dubois, Y., Devriendt, J., Slyz, A., & Teyssier, R. 2012, MNRAS, 420, 2662

Dullo, B. T., & Graham, A. W. 2012, ApJ, 755, 163
Dullo, B. T., & Graham, A. W. 2013, ApJ, 768, 36
Dullo, B. T., & Graham, A. W. 2014, MNRAS, 444, 2700
Ebisuzaki, T., Makino, J., & Okumura, S. K. 1991, Nature, 354, 212
Eckart, A., & Genzel, R. 1996, Nature, 383, 415
Eckart, A., & Genzel, R. 1997, MNRAS, 284, 576
Eddington, A. 1924, Nature 113, 192
Einstein, A. 1905, Annalen der Physik, 322, 891
Einstein, A. 1916, Annalen der Physik, 354, 769
Einstein, A. 1939, Annals of Mathematics, 40, 922
Einstein, A., & Rosen, N. 1935, Physical Review, 48, 73
Ekers, R. D., & Lynden-Bell, D. 1971, Astrophysical Letters, 9, 189
Eliche-Moral, M. C., González-García, A. C., Balcells, M., et al. 2011, A&A, 533, 104
Emsellem, E., Cappellari, M., Krajnović, D., et al. 2007, MNRAS, 379, 401
Erwin, P., Beltrán, J. C. V., Graham, A. W., & Beckman, J. E. 2003, ApJ, 597, 929
Erwin, P., & Gadotti, D. A. 2012, Advances in Astronomy, 2012, 946368
Erwin, P., Saglia, R., Thomas, J., et al. 2014, arXiv:1409.7946
Ewing, A.E. 1964, Science News Letter, 85, 39 (January 18)
Faber, S. M., & Jackson, R. E. 1976, ApJ, 204, 668
Fabian, A. C. 1999, MNRAS, 308, L39
Falcke, H., Körding, E., & Markoff, S. 2004, A&A, 414, 895
Farouki, R. T., Shapiro, S. L., & Duncan, M. J. 1983, ApJ, 265, 597
Farrell, S. A., Webb, N. A., Barret, D., Godet, O., & Rodrigues, J. M. 2009, Nature, 460, 73
Farrell, S. A., Servillat, M., Pforr, J., et al. 2012, ApJ, 747, LL13
Fath, E. A. 1909, Lick Observatory Bulletin, 5, 71
Feigelson, E. D., & Babu, G. J. 1992, ApJ, 397, 55
Feoli, A., & Mancini, L. 2009, ApJ, 703, 1502
Feoli, A., & Mancini, L. 2011, International Journal of Modern Physics D, 20, 2305
Feoli, A., & Mele, D. 2005, International Journal of Modern Physics D, 14, 1861
Ferrarese, L. 2002, ApJ, 578, 90
Ferrarese, L., et al. 2006a, ApJS, 164, 334
Ferrarese, L., Côté, P., Dalla Bontà, E., et al. 2006b, ApJ, 644, L21
Ferrarese, L., & Ford, H. 2005, Space Science Reviews, 116, 523
Ferrarese, L., & Merritt, D. 2000, ApJ Lett., 539, L9
Finkelstein, D. 1958, Physical Review, 110, 965
Fontanot, F., Monaco, P., Cristiani, S., & Tozzi, P. 2006, MNRAS, 373, 1173
Forbes, D. A., Brodie, J. P., & Grillmair, C. J. 1997, AJ, 113, 1652
Forbes, D. A., Lasky, P., Graham, A. W., & Spitler, L. 2008, MNRAS, 389, 1924
Ford, H. C., Tsvetanov, Z. I., Ferrarese, L., & Jaffe, W. 1998, The Central Regions of the Galaxy and Galaxies, 184, 377
Franceschini, A., Vercellone, S., & Fabian, A. C. 1998, MNRAS, 297, 817
Frank, J., & Rees, M. J. 1976, MNRAS, 176, 633
Frenkel, J. 1928, Zeitschrift fur Physik (Springer), 50, 234
Gadotti, D. A. 2008, MNRAS, 384, 420
Gadotti, D. A. 2009, MNRAS, 393, 1531
Gadotti, D. A., & Kauffmann, G. 2009, MNRAS, 399, 621
Gadotti, D. A., & Sánchez-Janssen, R. 2012, MNRAS, 423, 877
Gammie, C. F., Shapiro, S. L., & McKinney, J. C. 2004, ApJ, 602, 312
Gavazzi, G., Donati, A., Cucciati, O., et al. 2005, A&A, 430, 411
Gebhardt, K., Bender, R., Bower, G., et al. 2000, ApJ Lett., 539, L13
Gebhardt, K., Lauer, T. R., Kormendy, J., et al. 2001, AJ, 122, 2469
Gebhardt, K., Rich, R. M., & Ho, L. C. 2005, ApJ, 634, 1093
Gebhardt, K., & Thomas, J. 2009, ApJ, 700, 1690
Gehren, T., Fried, J., Wehinger, P. A., & Wyckoff, S. 1984, ApJ, 278, 11

Genzel, R. 2014, Proceedings of the 26th Solvay Conference on Physics: "Astrophysics and Cosmology", R. Blandford and A. Sevrin, eds., World Scientific (arXiv:1410.8717)
Genzel, R., Eckart, A., Ott, T., & Eisenhauer, F. 1997, MNRAS, 291, 219
Genzel, R., Eisenhauer, F., & Gillessen, S. 2010, Reviews of Modern Physics, 82, 3121
Genzel, R., Thatte, N., Krabbe, A., Kroker, H., & Tacconi-Garman, L. E. 1996, ApJ, 472, 153
Gerhard, O., Kronawitter, A., Saglia, R. P., & Bender, R. 2001, AJ, 121, 1936
Gerssen, J., van der Marel, R. P., Gebhardt, K., et al. 2003, AJ, 125, 376
Ghez, A. M., Klein, B. L., Morris, M., & Becklin, E. E. 1998, ApJ, 509, 678
Ghez, A. M., Salim, S., Hornstein, S. D., et al. 2005, ApJ, 620, 744
Ghez, A. M., Salim, S., Weinberg, N. N., et al. 2008, ApJ, 689, 1044
Gillessen, S., Eisenhauer, F., Trippe, S., et al. 2009, ApJ, 692, 1075
Gödel, K. 1949, Reviews of Modern Physics, 21, 447
González Delgado, R.M., Pérez, E., Cid Fernandes, R., & Schmitt, H. 2008, AJ, 135, 747
Gott, J. R., III 1991, Physical Review Letters, 66, 1126
Graham, A. W. 2004, ApJ, 613, L33
—. 2007a, Bulletin of the American Astronomical Society, 39, 759
—. 2007b, MNRAS, 379, 711
—. 2008a, ApJ, 680, 143
—. 2008b, PASA, 25, 167
—. 2012a, ApJ, 746, 113
—. 2012b, MNRAS, 422, 1586
—. 2013, in "Planets, Stars and Stellar Systems", Vol. 6, p.91–140, T.D.Oswalt & W.C Keel (eds.), Springer Publishing (arXiv:1108.0997)
—. 2014, in Structure and Dynamics of Disc Galaxies, Edited by M.S. Seigar and P. Treuthardt. ASP Conference Series, 480, 185
—. 2015, in Star Clusters and Black Holes in Galaxies Across Cosmic Time, IAU Symp. 312, R. Spurzem, F. Liu, S. Li, Y. Meiron (eds), (arXiv:1412.5715)
Graham, A. W., & Driver, S. P. 2005, PASA, 22, 118
Graham, A. W., & Driver, S. P. 2007, ApJ, 655, 77
Graham, A. W., Erwin, P., Caon, N., & Trujillo, I. 2001, ApJ Lett., 563, L11
Graham, A. W., Erwin, P., Caon, N., & Trujillo, I. 2003a, Revista Mexicana de Astronomia y Astrofisica Conference Series, 17, 196
Graham, A. W., Erwin, P., Trujillo, I., & Asensio Ramos, A. 2003b, AJ, 125, 2951
Graham, A. W., & Guzmán, R. 2003, AJ, 125, 2936
Graham, A. W., & Li, I.-H. 2009, ApJ, 698, 812
Graham, A. W., Onken, C. A., Athanassoula, E., & Combes, F. 2011, MNRAS, 412, 2211
Graham, A. W., & Scott, N. 2013, ApJ, 764, 151
Graham, A. W., & Scott, N. 2014, ApJ, in press
Graham, A. W., & Spitler, L. R. 2009, MNRAS, 397, 2148
Graham, A. W., & Worley, C. C. 2008, MNRAS, 388, 1708
Granato, G. L., De Zotti, G., Silva, L., Bressan, A., & Danese, L. 2004, ApJ, 600, 580
Greenhill, L. J., Booth, R. S., Ellingsen, S. P., et al. 2003, ApJ, 590, 162
Greenhill, L. J., Henkel, C., Becker, R., Wilson, T. L., & Wouterloot, J. G. A. 1995a, A&A, 304, 21
Greenhill, L. J., Jiang, D. R., Moran, J. M., et al. 1995b, ApJ, 440, 619
Greenstein, J. L., & Matthews, T. A. 1963a, Nature, 197, 1041
Greenstein, J. L., & Matthews, T. A. 1963b, AJ, 68, 279
Grillmair, C. J., Faber, S. M., Lauer, T. R., et al. 1994, AJ, 108, 102
Gualandris, A., & Merritt, D. 2008, ApJ, 678, 780
Gualandris, A., & Merritt, D. 2012, ApJ, 744, 74
Gültekin, K., Richstone, D. O., Gebhardt, K., et al. 2009, ApJ, 698, 198
Guo, Q., White, S., Boylan-Kolchin, M., et al. 2011, MNRAS, 413, 101
Gürkan, M. A., Freitag, M., & Rasio, F. A. 2004, ApJ, 604, 632
Haehnelt, M. G., Natarajan, P., & Rees, M. J. 1998, MNRAS, 300, 817

Haehnelt, M.G., Rees, M.J. 1993, MNRAS, 263, 168
Häring, N., & Rix, H.-W. 2004, ApJ Lett., 604, L89
Harris, G. L. H., & Harris, W. E. 2011, MNRAS, 410, 2347
Harris, G. L. H., Poole, G. B., & Harris, W. E. 2014, MNRAS, 438, 2117
Hartmann, M., Debattista, V. P., Cole, D. R., et al. 2014, MNRAS, 441, 1243
Haschick, A. D., Baan, W. A., & Peng, E. W. 1994, ApJ, 437, L35
Hausman, M. A., & Ostriker, J. P. 1978, ApJ, 224, 320
Hawking, S. W. 1974, Nature, 248, 30
Hawking, S. W. 1975, Communications in Mathematical Physics, 43, 199
Hawking, S. W. 1988, Physical Review D, 37, 904
Hawking, S. W., & Penrose, R. 1970, Royal Society of London Proceedings Series A, 314, 529
Hayward, S. A. 2006, Physical Review Letters, 96, 031103
Hazard, C., Mackey, M. B., & Shimmins, A. J. 1963, Nature, 197, 1037
Heckman, T. M., & Best, P. N. 2014, ARAA, 52, 589
Heinz, S., & Sunyaev, R. A. 2003, MNRAS, 343, L59
Held, E. V., de Zeeuw, T., Mould, J., & Picard, A. 1992, AJ, 103, 851
Hewish, A. 1970, ARA&A, 8, 265
Hewish, A., Bell, S. J., Pilkington, J. D. H., Scott, P. F., & Collins, R. A. 1968, Nature, 217, 709
Hills, J. G. 1975, Nature, 254, 295
Hils, D., & Bender, P. L. 1995, ApJ, 445, L7
Hirschmann, M., Khochfar, S., Burkert, A., et al. 2010, MNRAS, 407, 1016
Ho, L.C. 1999, in Observational Evidence for Black Holes in the Universe, ed. S.K. Chakrabarti (Dordrecht: Kluwer), ASSL, 234, 157
Ho, L. C. 2007, ApJ, 668, 94
Ho, L. C. 2008, ARA&A, 46, 475
Ho, L. C., Filippenko, A. V., & Sargent, W. L. W. 1997, ApJ, 487, 568
Hobbs, G., Archibald, A., Arzoumanian, Z., et al. 2010, Classical and Quantum Gravity, 27, 084013
Hohl, F. 1975, IAU Symp., 69, 349
Hopkins, P. F., & Hernquist, L. 2010, MNRAS, 407, 447
Herschel, W. 1791, Royal Society of London Philosophical Transactions Series I, 81, 71
Hopkins, P. F., Hernquist, L., Cox, T. J., et al. 2005, ApJ, 630, 705
Hopkins, P. F., Hernquist, L., Cox, T. J., et al. 2006, ApJS, 163, 1
Hopkins, P. F., Hernquist, L., Cox, T. J., Robertson, B., & Krause, E. 2007, ApJ, 669, 67
Hopkins, P. F., & Quataert, E. 2010, MNRAS, 407, 1529
Hoyle, F., & Burbidge, G. R. 1966, ApJ, 144, 534
Hoyle, F., Burbidge, G.R., Narlikar, J.V. 2000, A Different Approach to Cosmology, Cambridge University Press
Hoyle, F., & Fowler, W. A. 1963, Nature, 197, 533
Hoyle, F., Fowler, W. A., Burbidge, G. R., & Burbidge, E. M. 1964, ApJ, 139, 909
Hu, J. 2008, MNRAS, 386, 2242
Hurley, J. R. 2007, MNRAS, 379, 93
Hutchings, J. B., Crampton, D., & Campbell, B. 1984, ApJ, 280, 41
Hyde, J. B., Bernardi, M., Sheth, R. K., & Nichol, R. C. 2008, MNRAS, 391, 1559
Inoue, S., & Saitoh, T. R. 2012, MNRAS, 422, 1902
Ivanenko, D. D., & Kurdgelaidze, D. F. 1965, Astrophysics, 1, 251
Jahnke, K., & Macciò, A. V. 2011, ApJ, 734, 92
Jarvis, B. J., & Dubath, P. 1988, A&A, 201, L33
Jerjen, H., Binggeli, B. 1997, in The Nature of Elliptical Galaxies; The Second Stromlo Symposium, ASP Conf. Ser., 116, 239
Jiang, Y.-F., Greene, J. E., Ho, L. C., Xiao, T., & Barth, A. J. 2011, ApJ, 742, 68
Jiménez, N., Cora, S.A., Bassino L.P., Tecce T.E., & Smith Castelli A.V. 2011, MNRAS, 417, 785
Jørgensen, I., Franx, M., & Kjærgaard, P. 1996, MNRAS, 280, 167
Kang, W.-R., Woo, J.-H., Schulze, A., et al. 2013, ApJ, 767, 26

Kato, S., Fukue, J., & Mineshige, S. 2008, Black-Hole Accretion Discs – Towards a New Paradigm, Kyoto University Press (Kyoto, Japan)
Kauffmann, G., & Haehnelt, M. 2000, MNRAS, 311, 576
Keel, W. C. 1985, in Astrophysics of Active Galaxies and Quasi-Stellar Objects, Mill Valley, CA, University Science Books, p.1–38
Kelly, B. C. 2007, ApJ, 665, 1489
Kerr, R.P. 1963, Phys. Rev. Lett., 11, 237
Keselman, J. A., & Nusser, A. 2012, MNRAS, 424, 1232
Khan, F. M., Just, A., & Merritt, D. 2011, ApJ, 732, 89
Khan, F. M., Holley-Bockelmann, K., Berczik, P., & Just, A. 2013, ApJ, 773, 100
Khandai, N., Feng, Y., DeGraf, C., Di Matteo, T., & Croft, R. A. C. 2012, MNRAS, 423, 2397
King I.R., Minkowski R. 1966, ApJ, 143, 1002
King I.R., Minkowski R. 1972, IAU Symp., 44, 87
Klauder, J., & Wheeler, J. A. 1957, Reviews of Modern Physics, 29, 516
Komossa, S. 2013, IAU Symposium, 290, 53
Komossa, S., Burwitz, V., Hasinger, G., et al. 2003, ApJ, 582, L15
Komossa, S., Zhou, H., Rau, A., et al. 2009, ApJ, 701, 105
Körding, E., Falcke, H., & Corbel, S. 2006, A&A, 456, 439
Kormendy, J. 1977, ApJ, 218, 333
Kormendy, J. 1982, Saas-Fee Advanced Course 12: Morphology and Dynamics of Galaxies, 113
Kormendy, J. 1993, The Nearest Active Galaxies, ed. J. Beckman, L. Colina, & H. Netzer (Madrid: Consejo Superior de Investigaciones Cientficas), 197
Kormendy, J. 2001, Galaxy Discs and Disc Galaxies (ASP Conf. Ser. 230), ed. G. Jose, S. J. Funes, & E. M. Corsini (San Francisco, CA: ASP), 247
Kormendy, J., & Bender, R. 2009, ApJ, 691, L142
Kormendy, J., & Bender, R., Cornell, M.E. 2011, Nature, 469, 374
Kormendy, J., & Gebhardt, K. 2001, 20th Texas Symposium on relativistic astrophysics, 586, 363
Kormendy, J., & Ho, L. C. 2013, ARA&A, 51, 511
Kormendy, J., & McClure, R. D. 1993, AJ, 105, 1793
Kormendy, J., & Richstone, D. 1995, ARA&A, 33, 581
Kourkchi, E., Khosroshahi, H. G., Carter, D., et al. 2012, MNRAS, 420, 2819
Koushiappas, S. M., Bullock, J. S., & Dekel, A. 2004, MNRAS, 354, 292
Krajnović, D., Bacon, R., Cappellari, M., et al. 2008, MNRAS, 390, 93
Krajnović, D., Karick, A. M., Davies, R. L., et al. 2013, MNRAS, 433, 2812
Kramer, M., & Champion, D. J. 2013, Classical and Quantum Gravity, 30, 224009
Kronawitter, A., Saglia, R. P., Gerhard, O., & Bender, R. 2000, A&AS, 144, 53
Kruskal, M. D. 1960, Physical Review, 119, 1743
La Barbera, F., de Carvalho, R. R., de La Rosa, I. G., & Lopes, P. A. A. 2010, MNRAS, 408, 1335
Lacy, J. H., Baas, F., Townes, C.H., & Geballe, T.R. 1979, ApJ Lett., 227, L17
Lacy, J. H., Townes, C. H., Geballe, T. R., & Hollenbach, D. J. 1980, ApJ, 241, 132
LaMassa, S. M., Heckman, T. M., Ptak, A., & Urry, C. M. 2013, ApJ, 765, L33
Landau, L. D. 1932, Phys. Z. Sowjetunion, 1, 285
Lanzoni, B. in Star Clusters and Black Holes in Galaxies Across Cosmic Time, IAU Symp. 312, R.Spurzem, F.Liu, S.Li, Y.Meiron (eds)
Lanzoni, B., Mucciarelli, A., Origlia, L., et al. 2013, ApJ, 769, 107
Laor, A., Fiore, F., Elvis, M., Wilkes, B. J., & McDowell, J. C. 1997, ApJ, 477, 93
Laor, A. 1998, ApJ, 505, L83
Laor, A. 2001, ApJ, 553, 677
Lapenna, E., Origlia, L., Mucciarelli, A., et al. 2014, ApJ, in press (arXiv:1410.5825)
Läsker, R., Ferrarese, L., & van de Ven, G. 2014a, ApJ, 780, 69
Läsker, R., Ferrarese, L., van de Ven, G., & Shankar, F. 2014b, ApJ, 780, 70
Lauer T.R. 1983, in Elliptical Galaxies, Surface Photometry, Santa Cruz: University of California
Lauer, T. R., Ajhar, E. A., Byun, Y.-I., et al. 1995, AJ, 110, 2622
Lauer, T.R., Faber, S. M., Richstone, D., et al. 2007, ApJ, 662, 808

Laurikainen, E., Salo, H., & Buta, R. 2005, MNRAS, 362, 1319
Laurikainen, E., Salo, H., Buta, R., Knapen, J. H., & Comerón, S. 2010, MNRAS, 405, 1089
Laurikainen, E., Salo, H., Buta, R., & Knapen, J. H. 2011, MNRAS, 418, 1452
Lehmer, B. D., Lucy, A. B., Alexander, D. M., et al. 2013, ApJ, 765, 87
Leigh, N., Böker, T., & Knigge, C. 2012, MNRAS, 424, 2130
Lemaître, G. 1933, Annales de la Société Scientifique de Bruxelles, 53, 51
Lena, D., Robinson, A., Marconi, A., et al. 2014, ApJ, 795, 146
Li, Z.-Y., Wu, X.-B., & Wang, R. 2008, ApJ, 688, 826
Liu, F. S., Xia, X. Y., Mao, S., Wu, H., & Deng, Z. G. 2008, MNRAS, 385, 23
Liu, X., Shen, Y., Bian, F., Loeb, A., & Tremaine, S. 2014, ApJ, 789, 140
Longair, M. S. 1996, Our Evolving Universe, Cambridge, New York: Cambridge University Press
Longair, M. S. 2006, The Cosmic Century: A History of Astrophysics and Cosmology, Cambridge University Press, Cambridge, UK
Longair, M. 2010, A Century of Nature (Chapter 9), Laura Garwin, Tim Lincoln, ed., University of Chicago Press
Lützgendorf, N., Kissler-Patig, M., Neumayer, N., et al. 2013, A&A, 555, A26
Lynden-Bell, D. 1969, Nature 223, 690
Lynden-Bell, D., & Rees, M. J. 1971, MNRAS, 152, 461
Lynden-Bell, D., Faber, S. M., Burstein, D., et al. 1988, ApJ, 326, 19
Lynds, C. R., & Sandage, A. R. 1963, ApJ, 137, 1005
MacArthur, L. A., González, J. J., & Courteau, S. 2009, MNRAS, 395, 28
Magorrian, J., Tremaine, S., Richstone, D., et al. 1998, AJ, 115, 2285
Magoulas, C., Springob, C. M., Colless, M., et al. 2012, MNRAS, 427, 245
Malumuth, E.M., & Kirshner. R.P. 1981, ApJ, 251, 508
Maoz, E. 1995, ApJ, 447, L91
Maoz, E. 1998, ApJ, 494, L181
Mapelli, M., Ripamonti, E., Vecchio, A., Graham, A. W., & Gualandris, A. 2012, A&A, 542, A102
Marconi, A., & Hunt, L. K. 2003, ApJ Lett, 589, L21
Mathur, S. D. 2005, Fortschritte der Physik, 53, 793
Matković, A., & Guzmán, R. 2005, MNRAS, 362, 289
McConnell, N. J., & Ma, C.-P. 2013, ApJ, 764, 184
McCormmach, R. 1968, Br. J. Hist. Sci., 4, 126
McLeod, K.K. 1997, in Quasar Hosts, edited by David L. Clements, Ismael Perez-Fournon, Berlin: Springer-Verlag (astro-ph/9701185)
McLeod, K. K., Rieke, G. H., & Storrie-Lombardi, L. J. 1999, ApJ, 511, L67
McLure, R. J., & Dunlop, J. S. 2001, MNRAS, 327, 199
McLure, R. J., & Dunlop, J. S. 2002, MNRAS, 331, 795
McNamara, B. R., & Nulsen, P. E. J. 2007, ARA&A, 45, 117
McNamara, P. W. 2013, International Journal of Modern Physics D, 22, 41001
Meisels, A., & Ostriker, J. P. 1984, AJ, 89, 1451
Menezes, R.B., Steiner, J.E., Ricci, T.V. 2014, ApJ, 796, L13
Merloni, A., Heinz, S., & di Matteo, T. 2003, MNRAS, 345, 1057
Merritt D., 2006a, ApJ, 648, 976
Merritt, D. 2006b, Reports on Progress in Physics, 69, 2513
Merritt D., 2013, Dynamics and Evolution of Galactic Nuclei, Princeton: Princeton University Press
Merritt, D., & Ferrarese, L. 2001a, ApJ, 547, 140
Merritt, D., & Ferrarese, L. 2001b, The Central Kiloparsec of Starbursts and AGN: The La Palma Connection, 249, 335
Merritt, D., & Ferrarese, L. 2001c, MNRAS, 320, L30
Merritt, D., Ferrarese, L., & Joseph, C. L. 2001, Science, 293, 1116
Merritt, D., & Milosavljević, M. 2005, Living Reviews in Relativity, 8, 8 (cited 26-09-2014)
Mezcua, M., Roberts, T. P., Sutton, A. D., & Lobanov, A. P. 2013, MNRAS, 436, 3128
Mezcua, M., Roberts, T. P., Lobanov, A. P., & Sutton, A. D. 2015, MNRAS, 448, 1893

Michell, John (1784). Philosophical Transactions of the Royal Society of London 74: 35
Miller, A.I. 2005, Empire of the Stars, Little Brown/Houghton Mifflin
Miller, M. C., & Hamilton, D. P. 2002, ApJ, 576, 894
Miller, J. M. 2007, ARA&A, 45, 441
Miller, M. C., &
Miller, R. H., & Smith, B. F. 1992, ApJ, 393, 508 Colbert, E. J. M. 2004, International Journal of Modern Physics D, 13, 1
Milosavljević M., & Merritt D. 2001, ApJ, 563, 34
Milosavljević, M., Merritt, D., Rest, A., & van den Bosch, F. C. 2002, MNRAS, 331, L51
Minkowski, R. 1962, IAU Symp, 15 112
Misner, C. W., & Wheeler, J. A. 1957, Annals of Physics, 2, 525
Miyoshi, M., Moran, J., Herrnstein, J., et al. 1995, Nature, 373, 127
Monari, G., Antoja, T., & Helmi, A. 2014, (arXiv:1306.2632)
Moran, E. C., Shahinyan, K., Sugarman, H. R., Velez, D. O., & Eracleous, M. 2014, AJ, 148, 136
Morris, M. S., & Thorne, K. S. 1988, American Journal of Physics, 56, 395
Morris, M. S., Thorne, K. S., & Yurtsever, U. 1988, Physical Review Letters, 61, 1446
Morton, D. C., & Chevalier, R. A. 1973, ApJ, 179, 55
Murphy, B. W., Cohn, H. N., & Durisen, R. H. 1991, ApJ, 370, 60
Mushotzky, R. F., Done, C., & Pounds, K. A. 1993, ARA&A, 31, 717
Nandra, K., George, I. M., Mushotzky, R. F., Turner, T. J., & Yaqoob, T. 1997, ApJ, 477, 602
Nayakshin, S., Power, C., & King, A. R. 2012, ApJ, 753, 15
Ne'eman, Y. 1965, ApJ, 141, 1303
Neistein, E., & Netzer, H. 2014, MNRAS, 437, 3373
Neumayer, N., & Walcher, C. J. 2012, *Advances in Astronomy*, vol. 2012, id. 709038
Noguchi, M. 1999, ApJ, 514, 77
Novak, G.S., Faber, S.M., Dekel, A., 2006, ApJ, 637, 96
Novikov, I. D. 1965, Soviet Astronomy, 8, 857
Noyola, E., Gebhardt, K., Kissler-Patig, M., et al. 2010, ApJ, 719, L60
Oda, M., Gorenstein, P., Gursky, H., et al. 1971, ApJ, 166, L1
Oke, J. B. 1963, Nature, 197, 1040
Oppenheimer, J. R., & Serber, R. 1938, Physical Review, 54, 540
Oppenheimer, J. R., & Snyder, H. 1939, Physical Review, 56, 455
Oppenheimer, J. R., & Volkoff, G. M. 1939, Physical Review, 55, 374
Ostriker, J. P. 1977, Proceedings of the National Academy of Science, 74, 1767
Ostriker, J. P., & Hausman, M. A. 1977, ApJ, 217, L125
Park, D., Kelly, B. C., Woo, J.-H., & Treu, T. 2012, ApJS, 203, 6
Peebles, P. J. E. 1972, ApJ, 178, 371
Peng, C. Y. 2007, ApJ, 671, 1098
Penrose, R. 1965, Physical Review Letters, 14, 57
Penrose, R. 1969, Nuovo Cimento Rivista Serie, 1, 252
1971a, in Quantum Theory and Beyond, ed. T. Bastin, Cambridge University Press, Cambridge
1971b, in Combinatorial Mathematics and its Applications, ed. D. Welsh, Academic Press, New York, pp. 221–244.
Penrose, R., & Rindler, W. 1986, Spinors and space-time. Volume 2: Cambridge University Press, Cambridge
Peres, A. 1962, Physical Review, 128, 2471
Perez, A. 2004, Lectures presented at the II International Conference of Fundamental Interactions, Pedra Azul, Brazil, June 2004, (arXiv:gr-qc/0409061)
Peterson, B. M. 1997, An introduction to active galactic nuclei, Publisher: Cambridge, New York Cambridge University Press
Pfenniger, D., Friedli, D. 1991, A&A, 252, 75
Phillips, A. C., Illingworth, G. D., MacKenty, J. W., & Franx, M. 1996, AJ, 111, 1566
Pilkington, J. D. H., Hewish, A., Bell, S. J., & Cole, T. W. 1968, Nature, 218, 126
Pizzella, A., Corsini, E. M., Dalla Bontà, E., et al. 2005, ApJ, 631, 785

Portegies Zwart, S. F., Baumgardt, H., Hut, P., Makino, J., & McMillan, S. L. W. 2004, Nature, 428, 724
Pota, V., Graham, A. W., Forbes, D. A., et al. 2013, MNRAS, 433, 235
Press, W.H., Teukolsky, S.A., Vetterling, W.T., & Flannery, B.P., 1992, Numerical recipes (2nd ed.; Cambridge: Cambridge Univ. Press)
Puerari, I., Elmegreen, B.G., Block, D.L. 2014, AJ, 148, 133
Querejeta, M., Eliche-Moral, M. C., Tapia, T., et al. 2015, A&A, in press (arXiv:1409.5126)
Quinlan, G. D., & Hernquist, L. 1997, New Astronomy, 2, 533
Ravindranath, S., Ho, L. C., Peng, C. Y., Filippenko, A. V., & Sargent, W. L. W. 2001, Aj, 122, 653
Ravindranath, S., Ho, L. C., & Filippenko, A. V. 2002, ApJ, 566, 801
Reaves G., 1983, ApJS 53, 375
Rees, M. J. 1984, ARA&A, 22, 471
Rees, M. J. 1990, Science, 247, 817
Rees, M. J. 1998, Black Holes and Relativistic Stars, Edited by Robert M. Wald., Chicago: University of Chicago Press, 79
Reines, A. E., Greene, J. E., & Geha, M. 2013, ApJ, 775, 116
Reines, A. E., Sivakoff, G. R., Johnson, K. E., & Brogan, C. L. 2011, Nature, 470, 66
Reynolds, C. S. 2013, Classical and Quantum Gravity, 30, 244004
Reynolds, C. S., & Nowak, M. A. 2003, Physics Reports, 377, 389
Rhode, K. L. 2012, AJ, 144, 154
Richings A. J., Uttley P., Kording E., 2011, MNRAS, 415, 2158
Richstone, D., Ajhar, E. A., Bender, R., et al. 1998, Nature, 395, A14
Ringermacher, H. I., & Mead, L. R. 2009, AJ, 137, 4716
Rovelli, C. 1998, Living Reviews in Relativity, 1, 1 (cited 10-10-2014)
Rusli, S. P., Thomas, J., Saglia, R. P., et al. 2013a, AJ, 146, 45
Rusli, S. P., Erwin, P., Saglia, R. P., et al. 2013b, AJ, 146, 160
Ryan, C. J., De Robertis, M. M., Virani, S., Laor, A., & Dawson, P. C. 2007, ApJ, 654, 799
Sadler, E. M., Slee, O. B., Reynolds, J. E., & Roy, A. L. 1995, MNRAS, 276, 1373
Sadler, E. M., Jenkins, C. R., & Kotanyi, C. G. 1989, MNRAS, 240, 591
Sadoun, R., & Colin, J. 2012, MNRAS, 426, L51
Saha, K., Martinez-Valpuesta, I., & Gerhard, O. 2012, MNRAS, 421, 333
Salpeter, E. E. 1964, ApJ, 140, 796
Salucci, P., Ratnam, C., Monaco, P., & Danese, L. 2000, MNRAS, 317, 488
Sandage, A. 1965, ApJ, 141, 1560
Sandage, A., Binggeli, B. 1984, AJ, 89, 919
Sanders, R. H., & Lowinger, T. 1972, AJ, 77, 292
Sani, E., Marconi, A., Hunt, L. K., & Risaliti, G. 2011, MNRAS, 413, 1479
Sargent, W. L. W., Young, P. J., Lynds, C. R., et al. 1978, ApJ, 221, 731
Satyapal, S., Secrest, N. J., McAlpine, W., et al. 2014, ApJ, 784, 113
Savorgnan, G., & Graham, A.W. 2014, MNRAS in press (arXiv:1410.7405)
Savorgnan, G., Graham, A. W., Marconi, A., et al. 2013, MNRAS, 434, 387
Scannapieco, C., White, S. D. M., Springel, V., & Tissera, P. B. 2011, MNRAS, 417, 154
Schaffer, S. 1979, Journal for the History of Astronomy, 10, 42
Schauer, A. T. P., Remus, R.-S., Burkert, A., & Johansson, P. H. 2014, ApJ, 783, L32
Schechter, P.L. 1980, AJ, 85, 801
Schmidt, M. 1963, Nature, 197, 1040
Schödel, R., Ott, T., Genzel, R., et al. 2002, Nature, 419, 694
Schombert, J., & Smith, A. K. 2012, PASA, 29, 174
Schramm, M., Silverman, J. D., Greene, J. E., et al. 2013, ApJ, 773, 150
Schulze, A., & Gebhardt, K. 2011, ApJ, 729, 21
Schwarzschild, K. 1916 Sitzber. Preuss. Akad. Wiss. Berlin, Math.-Phys. p.189–196
Schwarzschild, K. 1999, (arXiv:physics/9905030)
Scott, N., Davies, R. L., Houghton, R. C. W., et al. 2014, MNRAS, 441, 274
Scott, N., Graham, A. W., & Schombert, J. 2013, ApJ, 768, 76

Scott, N., & Graham, A. W. 2013, Apj, 763, 76
Secrest, N. J., Satyapal, S., Gliozzi, M., et al. 2012, ApJ, 753, 38
Seidel, M.K., Cacho, R., Ruiz-Lara, T., et al. 2014, MNRAS, in press (arXiv:1411.2969)
Seigar, M. S., Kennefick, D., Kennefick, J., & Lacy, C. H. S. 2008, ApJ, 678, L93
Sérsic, J.-L. 1963, Boletin de la Asociacion Argentina de Astronomia, vol.6, p.41
Sérsic, J.-L. Atlas de Galaxias Australes (Córdoba: Argentina Observatorio Astronomico)
Sesana, A. 2010, ApJ, 719, 851
Sesana, A., Vecchio, A., & Colacino, C. N. 2008, MNRAS, 390, 192
Seth, A., Agüeros, M., Lee, D., Basu-Zych, A. 2008, ApJ, 678, 116
Seyfert, C. K. 1943, ApJ, 97, 28
Seymour, N., Altieri, B., De Breuck, C., et al. 2012, ApJ, 755, 146
Shakura, N. I., & Sunyaev, R. A. 1973, A&A, 24, 337
Shankar, F. 2009a, New Astronomy Reviews, 53, 57
Shankar, F., Marulli, F., Mathur, S., Bernardi, M., & Bournaud, F. 2012, A&A, 540, AA23
Shankar, F., Salucci, P., Granato, G. L., De Zotti, G., & Danese, L. 2004, MNRAS, 354, 1020
Shankar, F., Weinberg, D.H. & Miralda-Escude, J. 2009b, ApJ, 690, 20
Sigurdsson, S., & Rees, M. J. 1997, MNRAS, 284, 318
Sijacki, D., Springel, V., Di Matteo, T., & Hernquist, L. 2007, MNRAS, 380, 877
Silk, J., & Rees, M. J. 1998, A&A, 331, L1
Simmons, B. D., Lintott, C., Schawinski, K., et al. 2013, MNRAS, 429, 2199
Skrutskie, M. F., Cutri, R. M., Stiening, R., et al. 2006, AJ, 131, 1163
Slipher, V. M. 1917, Lowell Observatory Bulletin, 3, 59
Smith, H. J., & Hoffleit, D. 1963, Nature, 198, 650
Snyder, G. F., Hopkins, P. F., & Hernquist, L. 2011, ApJ, 728, LL24
Soffel, M.H. 1982, A&A 116, 111
Soker, N., & Meiron, Y. 2011, MNRAS, 411, 1803
Soltan, A. 1982, MNRAS, 200, 115
Somerville, R. S., Hopkins, P. F., Cox, T. J., Robertson, B. E., & Hernquist, L. 2008, MNRAS, 391, 481
Soria, R., Hau, G. K. T., Graham, A. W., et al. 2010, MNRAS, 405, 870
Springel, V., Di Matteo, T., & Hernquist, L. 2005, MNRAS, 361, 776
Stoner, E. 1929, The London, Edinburgh, and Dublin Philosophical Magazine and Journal of Science, Volume 7, p.63
Stoner, E. 1930, The London, Edinburgh, and Dublin Philosophical Magazine and Journal of Science: Series 7, Volume 9, Issue 60, p.944
Stoner, E. C. 1932a, MNRAS, 92, 651
Stoner, E. C. 1932b, MNRAS, 92, 662
Taga, M., & Iye, M. 1998, MNRAS, 299, 111
Tanaka, Y., Inoue, H., & Holt, S. S. 1994, PASJ, 46, L37
Tanaka, Y., Nandra, K., Fabian, A. C., et al. 1995, Nature, 375, 659
Terzić, B., & Graham, A. W. 2005, MNRAS, 362, 197
't Hooft, G. 1990, Nuclear Physics B, 335, 138
Thomas, J., Saglia, R. P., Bender, R., Erwin, P., & Fabricius, M. 2014, ApJ, 782, 39
Thorne, K. S. 1974, ApJ, 191, 507
Thorne, K. S. 1994, Black holes and time warps: Einstein's outrageous legacy, Commonwealth Fund Book Program, New York, NY: W.W. Norton and London: Picador
Thorne, K. S., & Price, R. H. 1975, ApJ, 195, L101
Toloba, E., Guhathakurta, P., Boselli, A., et al. 2014, ApJ, submitted (arXiv:1410.1552)
Tonry, J. 1981, ApJ, 251, L1
Tonry, J. L. 1984, ApJ, 283, L27
Tonry, J. L. 1987, ApJ, 322, 632
Tortora, C., Napolitano, N. R., Romanowsky, A. J., Capaccioli, M., & Covone, G. 2009, MNRAS, 396, 1132
Trakhtenbrot, B., & Netzer, H. 2012, MNRAS, 427, 3081

Tremaine, S., Gebhardt, K., Bender, R., et al. 2002, ApJ, 574, 740
Tremonti, C. A., Heckman, T. M., Kauffmann, G., et al. 2004, ApJ, 613, 898
Treuthardt, P., Seigar, M. S., Sierra, A. D., et al. 2012, MNRAS, 423, 3118
Trujillo, I., Asensio Ramos, A., Rubiño-Martín, J. A., et al. 2002, MNRAS, 333, 510
Trujillo, I., Erwin, P., Asensio Ramos, A., & Graham, A. W. 2004, AJ, 127, 1917
Trujillo, I., Graham, A. W., & Caon, N. 2001, MNRAS, 326, 869
Turner, M. L., Côté, P., Ferrarese, L., et al. 2012, ApJS, 203, 5
Ulrich, M.-H., Maraschi, L., & Urry, C. M. 1997, ARA&A, 35, 445
Valluri, M., Merritt, D., & Emsellem, E. 2004, ApJ, 602, 66
van den Bosch, R., de Zeeuw, T., Gebhardt, K., Noyola, E., & van de Ven, G. 2006, ApJ, 641, 852
van den Bosch, R. C. E., Gebhardt, K., Gültekin, K., et al. 2012, Nature, 491, 729
van der Marel, R. P. 1999, in IAU Symp. 186, Galaxy Interactions at Low and High Redshift, ed. D. B. Sanders & J. Barnes (Dordrecht: Kluwer), p. 333
van der Marel, R. P. 2004, Coevolution of Black Holes and Galaxies, 37
Vasiliev, E. 2014, in Classical and Quantum Gravity, special issue Galactic centers (arXiv:1411.1760)
Vesperini, E., & Trenti, M. 2010, ApJ, 720, L179
Vika, M., Driver, S. P., Cameron, E., Kelvin, L., & Robotham, A. 2012, MNRAS, 419, 2264
Vishveshwara, C.V. 1970, Nature, 227, 936
Volonteri, M. 2010, A&ARv, 18, 279
Volonteri, M., & Ciotti, L. 2013, ApJ, 768, 29
von der Linden, A., Best, P.N., Kauffmann, G., & White, S.D.M. 2007, MNRAS, 379, 867
Wandel, A. 1999,ApJ, 519, L39
Watson, W. D., & Wallin, B. K. 1994, ApJ, 432, L35
Webb, N. A., Godet, O., Wiersema, K., et al. 2014, ApJ, 780, LL9
Weber, J. 1969, Physical Review Letters, 22, 1320
Weber, J. 1970, Physical Review Letters, 25, 180
Wehner, E. H., & Harris, W. E. 2006, ApJ, 644, L17
Williams, M. J., Bureau, M., & Cappellari, M. 2010, MNRAS, 409, 1330
Wheeler, J. A. 1966, ARA&A, 4, 393
Wheeler, J.A., 1968, Amer. Scientist, 56, 1
Whitney, A. R., Shapiro, I. I., Rogers, A. E. E., et al. 1971, Science, 173, 225
Wiersema, K., Farrell, S. A., Webb, N. A., et al. 2010, ApJ, 721, L102
Will, C. M. 2006, Living Reviews in Relativity, 9, 3 (cited 14-10-2014)
Will, C. M. 2014, Living Reviews in Relativity, 17, 4
Wilman R. J., Fabian A. C., Nulsen P. E. J., 2000, MNRAS, 319, 583
Wolfe, A. M., & Burbidge, G. R. 1970, ApJ, 161, 419
Woltjer, L. 1959, ApJ, 130, 38
Wyithe, J. S. B., & Loeb, A. 2003, ApJ, 595, 614
Yakovlev, D. G. 1994, Physics Uspekhi, 37, 609
Yee, H. K. C. 1992, in Relationships Between Active Galactic Nuclei and Starburst Galaxies, ed. A. V. Filippenko, ASP Conference Series (ASP: San Francisco), 31, 417
Yoshizawa, M., & Wakamatsu, K. 1975, A&A, 44, 363
Young, C.K., Currie, M.J. 1994, MNRAS, 268, L11
Yuan, F., & Narayan, R. 2014, ARA&A, 52, 529
Younger, J. D., Hopkins, P. F., Cox, T. J., & Hernquist, L. 2008, ApJ, 686, 815
Zasov, A. V., Petrochenko, L. N., & Cherepashchuk, A. M. 2005, Astronomy Reports, 49, 362
Zel'dovich, Y. B. 1964, Doklady Akad. Nauk, U.S.S.R., 155, 67 (1964, Soviet Physics Doklady, 9, 195)
Zel'dovich & Novikov 1964, Doklady Akad. Nauk, U.S.S.R., 158, 811 (1965, Soviet Physics Doklady, 9, 834)
Zwicky, F. 1938, ApJ, 88, 522

Part V
Theory

Chapter 12
Bulge Formation via Mergers in Cosmological Simulations

Alyson Brooks and Charlotte Christensen

Abstract The latest generation of cosmological simulations are on the verge of being able to resolve the structure of bulges for the first time. Hence, we review the current state of bulge formation in cosmological simulations, and discuss open questions that can be addressed in the near future by simulators, with a particular focus on merger-driven bulge growth. Galaxy mergers have long been assumed to produce classical bulges in disc galaxies. Under this bulge-formation model, though, the high rates of mergers in Cold Dark Matter (CDM) galaxy formation theory predict many more classical bulges than are observed. Furthermore, simulations of galaxy formation continue to generally produce too massive of bulges. Feedback offers a promising avenue for reducing merger-driven bulge growth by maintaining high gas fractions in galaxies and ejecting low-angular momentum gas driven to the centers of galaxies. After reviewing the results of relevant research that has been published to date, we use cosmological simulations to explore the ability of feedback to reduce or even prevent bulge growth during mergers. In dwarf galaxies, mergers actually reduce the central concentration of galaxies as the induced burst of star formation drives out low-angular momentum material. This result shows the potential for feedback to reduce central mass growth. However, we also demonstrate that it is very difficult for current stellar feedback models to reproduce the small bulges observed in more massive disc galaxies like the Milky Way. We argue that feedback models need to be improved, or an additional source of feedback such as AGN is necessary to generate the required outflows.

A. Brooks (✉)
Rutgers University, 136 Frelinghuysen Road, Piscataway, NJ 08854, USA
e-mail: abrooks@physics.rutgers.edu

C. Christensen
Grinnell College, 1116 Eighth Avenue, Grinnell, IA 50112, USA
e-mail: christenc@grinnell.edu

E. Laurikainen et al. (eds.), *Galactic Bulges*, Astrophysics and Space Science Library 418, DOI 10.1007/978-3-319-19378-6_12

12.1 Introduction

Galaxy simulators have made significant progress in recent years in being able to simulate realistic disc galaxies that match a range of observed properties (e.g., Brook et al. 2012b; Aumer et al. 2013). This success has included progress toward resolving the central regions of galaxies and forming more realistic bulges (Christensen et al. 2014a). However, galaxy simulations are, if anything, *too* successful at forming bulges. Even in state-of-the-art simulations, galaxy bulges remain on the massive end of the observed range and the implication is that they also form too easily.

Galaxy simulators spent their formative years trying to understand and overcome the sources of overcooling (e.g., Steinmetz and Navarro 1999; Navarro and Steinmetz 2000; Abadi et al. 2003; Governato et al. 2004; Scannapieco et al. 2009), which leads to an overly dense concentration of mass in the central regions of simulated galaxies compared to observations. Cosmological simulations achieved a major step forward within the past 5 years when they were able to create bulgeless dwarf disc galaxies for the first time (Governato et al. 2010; Teyssier et al. 2013). However, the same star formation and feedback scheme that leads to bulgeless dwarf discs still tends to lead to overly massive stellar bulges in halos of $\sim 10^{11}$ $M_{\odot}$ and higher (e.g. Christensen et al. 2014a). A simple interpretation of this trend suggests that more feedback may be required at higher galaxy masses. Unfortunately, while the most recent simulations have shown that more feedback can indeed lead to smaller bulges in Milky Way-mass galaxies (Aumer et al. 2013; Mollitor et al. 2014), the additional feedback creates new challenges compared to observations (Roškar et al. 2014; Aumer et al. 2014).

Fully cosmological simulations are the best tool for capturing the detailed merger history of galaxies, and thus the best tool to study the impact of mergers on bulge growth. However, analyzing the growth of bulges in cosmological simulations is difficult simply because, until recently, the structure of the bulges was unresolved in these simulations. The highest resolution simulations of Milky Way-mass galaxies (e.g. Hopkins et al. 2014) are only now beginning to have resolved bulges, but over the next few years this sample will greatly expand.

Given that advances in computing will soon allow for higher resolution studies of stellar bulges formed in a cosmological context, we outline in this review the current challenges that will need to be addressed. In particular, we focus on the role of mergers in forming the bulges of galaxies that are disc-dominated at $z = 0$.

We begin in Sect. 12.2 by summarizing the observations that inform our investigations, and in Sect. 12.3 discuss the current formation ideas that explain bulge properties. In Sect. 12.4 we highlight the current theoretical challenges that emerge when favored bulge formation mechanisms are imposed in a Cold Dark Matter galaxy formation context. In Sect. 12.5, we review the state of cosmological bulge formation, including the limited number of studies on the origin of bulges that have so far been carried out with cosmological simulations. We discuss the challenges that remain to forming realistic bulges. In Sect. 12.6 we use simulations

to emphasize bulge trends with galaxy mass, and to point out where simulated trends break down in comparison to observations. We conclude in Sect. 12.7 with a discussion of possible solutions to forming realistic bulges in mergers.

12.2 Observational Properties of Bulges

Bulges are frequently divided into two main types: classical bulges and pseudobulges. Classical bulges generally are more spherically symmetric, are supported by velocity dispersion, have isotropic velocity distributions, and have older stellar populations, while pseudobulges are distinguished by their more disc-like features (Kormendy 1993; Andredakis and Sanders 1994).

Classical bulges resemble elliptical galaxies in a number of ways. As Renzini (1999) stated: "It appears legitimate to look at bulges as ellipticals that happen to have a prominent disc around them." Kormendy and Kennicutt (2004) noted that this statement seems to apply only to classical bulges. One of the most obvious ways that classical bulges resemble elliptical galaxies is that the surface brightness profiles of classical bulges can be fit with a Sérsic profile where n is generally equal to or larger than 2:

$$I(r) = I_0\, exp[(-\frac{r}{r_0})^{(1/n)}], \tag{12.1}$$

where I_0 is the central intensity and r_0 is the scaling radius. The stellar populations in both classical bulges and ellipticals tend to be older (Moorthy and Holtzman 2006), with the stars being typically α-enhanced, indicating that the formation happened rapidly (on a timescale short enough that SN Ia did not yet contribute iron, Weiss et al. 1995; Matteucci 2006; Ganda et al. 2007; Peletier et al. 2007). Finally, there is an argument that many of the scaling relations that elliptical galaxies are observed to follow seem to also be followed by classical bulges (Fisher and Drory 2008; Kormendy and Bender 2012), including the Faber-Jackson relation (a luminosity – velocity dispersion relation, Faber and Jackson 1976), the Kormendy relation (a size – luminosity relation, Kormendy 1977), and the fundamental plane, which relates size, velocity, and luminosity. It should be noted, however, that classical bulges do not appear to follow all elliptical galaxy scaling relations: Gadotti (2009) and Laurikainen et al. (2010) found that the bulge mass-size relation for classical bulges was offset from that for elliptical galaxies.

The bulges of many disc galaxies, however, are not spherically symmetric, are rotationally dominated, and have shallower surface brightness profiles ($n \lesssim 2$). These are known as pseudobulges. Pseudobulges can be further divided into *discy pseudobulges*, which generally have on-going star formation (Fisher 2006) and nuclear bars, spirals or rings (e.g. Fisher 2006), and *boxy/peanut (B/P)* bulges, which are made up of older stellar populations. These B/P bulges have characteristically boxy or peanut isophotal shapes when viewed edge-on (Athanassoula 2005) and

barlens isophotal shapes when viewed face-on (Laurikainen et al. 2011), and they are generally associated with bars. Boxy bulges show cylindrical rotation (i.e., their rotational velocity is constant with height above the midplane), unlike classical bulges.

A review of the observational properties of pseudobulges can be found in Kormendy and Kennicutt (2004). To summarize, though:

- Classical bulges have rounder and more spherically symmetric morphology while pseudobulges may have either discy or boxy morphology.
- The stellar kinematics of classical bulges are generally more dominated by dispersion while in pseudobulges they are more dominated by rotation.
- Most classical bulges have Sérsic indices $n \geq 2$ while most pseudobulges have $n < 2$.
- Classical bulges tend to follow the Faber-Jackson relation and lie along the fundamental plane. Pseudobulges are frequently low-σ outliers from the Faber-Jackson relation. They may also have fainter effective surface brightness at their effective radii than would be expected from the fundamental plane.
- Galaxies with a bulge-to-total (B/T) ratio ≥ 0.5 almost always contain a classical bulge.
- Pseudobulges may contain embedded bars, nuclear rings or, in the case of discy pseudobulges, spiral structure.
- Discy pseudobulges may also contain young stars, gas, and dust, even when the galaxy is not undergoing a merger.

Note that there can be significant overlap in the properties of classical bulges and pseudobulges so the classification between the two should be done by looking at multiple indicators when possible.

12.2.1 Population Studies of Classical and Pseudobulges

It has become increasingly clear that pseudobulges are ubiquitous throughout the Universe. Fisher and Drory (2011) determined that within a 11 Mpc sphere, 80 % of galaxies with a stellar mass of $10^9 M_\odot$ or greater are either bulgeless or contain a pseudobulge (which they defined as any bulge with a low Sérsic index, i.e., including all types of pseudobulges). Similar conclusions were reached by Kormendy et al. (2010) within a 8 Mpc sphere. Current best estimates for the frequency of specifically B/P-shaped pseudobulges are between 20 % (Yoshino and Yamauchi 2015) and 40 % (Lütticke et al. 2000) of spiral galaxies. Classical bulges are more common in more massive galaxies. For instance, they are found in the majority of galaxies with stellar mass greater than $10^{10.5} M_\odot$ and earlier type galaxies show more classical bulges than late-type galaxies (Andredakis et al. 1995; Kormendy and Kennicutt 2004). Similarly, Fisher and Drory (2008) found that bluer galaxies were more likely to host discy pseudobulges, while red galaxies were more likely to host classical bulges. In contrast to discy pseudobulges, B/P bulges are

slightly more common in earlier-type spiral galaxies that have bars (Laurikainen et al. 2014; Yoshino and Yamauchi 2015).

Despite classical bulges being most common in more massive galaxies, even giant ($V_{circ} \geq 200$ km/s) Sc-Scd galaxies frequently lack a classical bulge (Kormendy et al. 2010). Perhaps most notable of this group is the Milky Way itself. Photometric (Blitz and Spergel 1991; Dwek et al. 1995) and kinematic (Howard et al. 2009; Shen et al. 2010) evidence show that the Milky Way's bulge has the boxy shape characteristic of bars seen edge-on (Combes et al. 1990; Raha et al. 1991; Athanassoula 2005). While it is possible that an additional classical bulge component could be hidden by the rest of the bulge, kinematic and metallicity data limit any classical bulge contribution to <10 % the disc mass (Shen et al. 2010; Di Matteo et al. 2014).

Not only are classical bulges more common in higher mass galaxies, they are also less common in low-density environments than in high-density ones (Kormendy et al. 2010). Furthermore, the B/T ratios in low-density environments also tend to be smaller (Kautsch et al. 2009). Theorists must, therefore, explain not only the abundance of massive pure disc galaxies but also their environmental dependency.

12.3 Theoretical Models for the Formation of Bulges

A common view is that classical bulges are formed primarily in mergers of galaxies, while pseudobulges are formed by processes internal to the galaxy.[1] Below, we review the commonly accepted paradigms for the formation of classical and pseudobulges in turn.

12.3.1 Classical Bulges

The similarities between elliptical galaxies and bulges suggest a common formation origin. Mergers have been considered likely triggers for elliptical galaxy formation for even longer than they have been considered the source of bulges (Toomre 1977). Mergers offer several compatible avenues for bulge growth: the violent relaxation of the primary galaxy stellar component, the accretion and violent relaxation of the secondary galaxy stellar component, and the formation of stars from gas undergoing merger-driven angular momentum loss. Given the observed similarities between

[1] One possible internal process for bulge formation we will not discuss here is the build-up of bulges from clumpy discs. In this model, large clumps in massive discs at high z may migrate to the center to form bulges (Genzel et al. 2008; Bournaud et al. 2014; Dekel and Krumholz 2013; Perez et al. 2013). We leave a complete discussion of this formation process to chapter 6.2 (Bournaud 2015). However, it should be noted that the outcomes of gas-rich clumps sinking to the centers of galaxies are not unlike those of gas-rich mergers (Kormendy and Ho 2013).

elliptical galaxies and classical bulges, it is not surprising that the merger hypothesis for elliptical galaxies has been extended to the bulges of spiral galaxies.

12.3.1.1 Merger Formed Ellipticals?

Do elliptical galaxies form in mergers? Simulations of disc galaxy mergers show that the disruption and violent relaxation (Lynden-Bell 1967) of the stellar component results in the formation of a spheroid with the density distribution similar to a de Vaucouleurs ($r^{1/4}$) profile (Barnes 1988; Hernquist 1992). Hopkins et al. (2008) used dissipational mergers of disc galaxies to show that the stars that existed prior to the merger were redistributed into a spheroidal component that could be fit by a Sérsic profile with $n > 2.5$, in agreement with the observed surface brightness profiles of ellipticals (Kormendy et al. 2009). Additionally, many elliptical galaxies are observed to have excess light at their centers compared to what would be extrapolated from a Sérsic fit, in what is termed a "cuspy" profile (Kormendy et al. 2009; Krajnović et al. 2013). Such cuspy profiles are thought to be the signature of a central starburst resulting from a dissipational merger (Mihos and Hernquist 1994; Kormendy 1999). This observation is consistent with the trend for cuspy ellipticals to be less massive (Kormendy et al. 2009) and faster rotators (Krajnović et al. 2013) than ellipticals without excess light. On the other hand, dissipational mergers may not be necessary to produce these observations: simulations of direct collisionless collapse have also been shown to result in a density profile that follows roughly $r^{1/4}$, as well as decreasing line-of-sight velocity dispersions and increasing velocity anisotropy (Hozumi et al. 2000; Trenti et al. 2005), which are all trends observed in ellipticals.

Certainly the old stellar populations in ellipticals require that they form at a time when mergers were more frequent than today. Despite this, there has been some question as to whether mergers alone are enough to reproduce the Fundamental Plane, Faber–Jackson, and Kormendy relations observed for elliptical galaxies. Two merger regimes have been explored: those with gas and those that are purely collisionless. It has been known for a while that there are problems reproducing phase space and elliptical galaxy scaling relations with collisionless mergers alone (Ostriker 1980; Carlberg 1986). For instance, the apparent size growth of ellipticals cannot be explained by gas-poor mergers in the latter half of the age of the Universe (Cimatti et al. 2006; Renzini 2006; Bundy et al. 2007; Scarlata et al. 2007; Nipoti et al. 2009). However, this leaves open the idea that ellipticals were formed in gas-rich mergers early in the age of the Universe. Mergers with significant dissipation do a better job of building the scaling relations of ellipticals than gas-poor mergers (Mihos and Hernquist 1994; Naab et al. 2007; Jesseit et al. 2009) but Ciotti et al. (2007) concluded that some form of initial monolithic collapse was necessary in addition to mergers to match the scaling relations. More recently, however, both semi-analytic models (Porter et al. 2014) and cosmological simulations (Oser et al. 2012) have found that a combination of wet and dry mergers and major and minor

mergers produced galaxies that followed the observed slope and time evolution of the size-mass relation and, in the former case, the Faber–Jackson relation.

Overall, it seems some initial gas-rich collapse and subsequent quenching is required to reproduce the detailed structural properties of ellipticals. However, it is clear that mergers can redistribute existing stars via violent relaxation into a light profile consistent with observations. Hence, both dissipational collapse and mergers are likely involved in the formation of elliptical galaxies. Are these also the processes that form classical bulges?

12.3.1.2 Merger Formed Classical Bulges?

When gas is neglected, major mergers of disc galaxies tend to result in an elliptical galaxy rather than a disc galaxy, as discussed above. In the absence of dissipation, one might imagine that the general distribution of stellar orbits in the remnant correspond roughly to their initial radii prior to the merger. This does not lead to a compact distribution consistent with bulge growth. On the other hand, minor mergers in the mass ratio range 4:1–10:1 can result in discs with bulges (Bournaud et al. 2005). In that case, though, the bulge growth is dominated by gas flows to the central region of the primary galaxy. As we will discuss below, Hopkins et al. (2009b) demonstrated that bulge growth is significantly suppressed as gas fraction increases. Hopkins et al. (2009a) then showed that incorporating this model into the merger histories of halos in ΛCDM can reproduce the trends in spheroid morphology with galaxy mass. A major implication of this successful model is that bulge growth is driven by dissipative processes rather than redistribution of stars. Indeed, Toomre and Toomre (1972) stated: "Would not the violent mechanical agitation of a close tidal encounter – let alone an actual merger – already tend to bring *deep* into a galaxy a fairly *sudden* supply of fresh fuel in the form of interstellar material, either from its own outlying disc or by accretion from its partner?" If channeling of gas in mergers plays a prominent role in bulge formation, then most bulges would appear to be formed in situ to the galaxy. In fact, this is in agreement with current cosmological simulations of disc galaxies (discussed further in Sect. 12.5, Guedes et al. 2013; Okamoto 2013; Christensen et al. 2014a; Pillepich et al. 2015).

Dissipational simulations of mergers result in the build up of a central gas mass (e.g., Negroponte and White 1983). Hernquist (1989) and Barnes and Hernquist (1991) established the theoretical underpinnings for this funneling of gas to the centers of galaxies during mergers. They showed that gas loses angular momentum during mergers through interactions with induced bars, tidal torques and dynamical friction with the disc stars (see also Noguchi 1988; Combes et al. 1990; Barnes and Hernquist 1996). While initially the transfer of gas to the centers of galaxies was primarily seen as a way to fuel Active Galactic Nuclei (AGN), Katz (1992) suggested that bulges form from gas that underwent substantial merger-induced dissipation and from the stars accreted during the merger. This picture of rapid star formation from suddenly condensed gas is consistent with observations of the

blue colors (e.g. Larson and Tinsley 1978), increased star formation rates (Ellison et al. 2008; Jogee et al. 2009), and high central gas densities (Young et al. 1984; Sanders and Mirabel 1985; Sanders et al. 1987) of merging and tidally deformed galaxies. It is also consistent with the apparent funneling of lower metallicity gas seen in merging pairs (Ellison et al. 2013). Finally, the creation of classical bulges through mergers is consistent with the fact that both classical bulges and elliptical galaxies follow the same black hole-mass vs. bulge velocity dispersion relation while pseudobulges do not (Kormendy et al. 2011; Kormendy and Ho 2013). In this model, both classical bulges and supermassive black holes grow through mergers in a process regulated by AGN feedback.

In summary, if classical bulges are formed like elliptical galaxies, it is more likely that the similarities arise due to dissipation in mergers rather than violent relaxation of existing stars. Certainly redistribution of the stars can occur, but may lead to predominantly populating the inner stellar halo (Zolotov et al. 2009; Purcell et al. 2010) rather than a more central, bulge-like concentration.

12.3.2 Pseudobulges

The non-spheroidal-like properties of pseudobulges have led astronomers to question their formation through mergers. As summarized in Kormendy (1993), initially the evidence for non-merger driven growth came from the discy kinematics of many bulges. Additionally, mergers tend to drive Sérsic indices up (van Albada 1982; Aguerri et al. 2001; Kormendy and Fisher 2008), likely placing them above the normal range for both types of pseudobulges. More recently, discy pseudobulges have also been shown to deviate from the photometric projections of the fundamental plane (Kormendy and Kennicutt 2004; Fisher and Drory 2008), implying a separate formation path than either elliptical galaxies or classical bulges.

It is believed that discy bulges grow secularly through the inward transport of material. Bars redistribute gas through galaxies by transferring angular momentum to the outer disc. Near the co-rotation radius gas is collected into rings while gas on smaller orbits is funneled toward the very center (Kormendy and Kennicutt 2004, and references therein). Furthermore, bars cause gas to shock (see Athanassoula 1992, for a detailed analysis; the concept was first proposed by Prendergast, unpublished c1962), resulting in additional inflow. Similarly, other non-axisymmetries like spiral arms can also spur inflow by causing gas to shock. This fresh supply of gas then enables the formation of a discy psuedobulge. Observational evidence for gas being funneled to the centers of galaxies comes from the dips in the stellar velocity dispersion at the centers of galaxies (Emsellem et al. 2001; Marquez et al. 2003; Falcón-Barroso et al. 2006; Peletier et al. 2007). These regions of low dispersion are likely small central stellar discs formed from the inflow of cold gas. The observed correlation between bulge and disc scale length adds further support for bulge growth through secular evolution (Courteau et al. 1996; Aguerri et al. 2005; Carollo et al. 2007).

Similar evidence has been used to argue that B/P bulges form through secular processes. For instance, there is close correspondence between the existence of B/P shaped bulges and rings or bars (Kuijken and Merrifield 1995; Bureau and Freeman 1999), and mergers of discs are unlikely to redistribute stars into the boxy orbits (Bureau 1998) characteristic of B/P bulges. Bars can heat themselves vertically through buckling and resonant star scattering, as has been well established through theoretical modeling (e.g. Combes and Sanders 1981; Combes et al. 1990; Pfenniger and Norman 1990; Raha et al. 1991). This is likely the scenario that leads to B/P bulges, so that B/P bulges tend to form in place rather than through transport of fresh material from the outer disc, as is the case for discy pseudobulges.

Kormendy and Kennicutt (2004) outline three reasons why secular evolution is more likely to create pseudobulges than mergers. First and foremost is the fact that the most obvious pseudobulges are in barred or oval galaxies, i.e., they are associated with galaxies that have a clear non-axisymmetry that should funnel gas to the center. Second, they argue that most pseudobulge galaxies show no sign of tidal interactions in progress. Indeed, time scales may argue against pseudobulges being created in major mergers at high z, since many of them are associated with recent star formation and have blue colors. Finally, Kormendy and Kennicutt (2004) note that mergers should also heat the thin disc. Certainly if pseudobulges are created in major mergers at high z, they may be correlated with thick disc formation instead (Brook et al. 2004). However, more recent minor mergers may also lead to the same driving of gas to the central region, without destroying or heating the thin disc as much as previously believed (Hopkins et al. 2009b; Moster et al. 2010, 2012). Despite these arguments for gas inflow creating pseudobulges, other studies (e.g., Laurikainen et al. 2014) have found that much of the mass in pseudobulges resides in a boxy/peanut/barlens bulge (as opposed to discy pseudobulges), suggesting local heating rather than inflow may dominate the majority of pseudobulge creation.

12.4 Theoretical Challenges

The sheer ubiquity of mergers within a ΛCDM cosmology allows bulge formation to occur easily in mergers. As dark matter halo growth in this cosmology happens through the hierarchical build-up of structure (White and Rees 1978), galaxy mergers, especially at high z, are predicted to be common. Major mergers (mass ratio $\lesssim$1:4) below $z = 1$ are thought to have occurred in only about half of the galaxies (Maller et al. 2006). However, the increasing merger rate with redshift (Fakhouri and Ma 2008; Genel et al. 2009; Fakhouri et al. 2010) leads to even higher rates at earlier times. Minor mergers are more common, and we discuss below whether they may be able to induce bulge growth through tidal torques. These theoretical merger rates have been shown to be in agreement with the observed number density of close pairs (Lotz et al. 2011) and kinematically disturbed galaxies (Puech et al. 2012).

12.4.1 Populations Studies Through Semi-analytic Models

Semi-analytic models (SAMs) consist of a set of analytic models applied to a population of halos generated from cosmological simulations that follow only the dark matter. The dark matter simulation provides the properties of the dark matter halos as a function of time, including their merger history. The analytic models, in turn, describe the evolution of the baryonic component of the galaxies. SAMs have used the frequency of mergers to assess their ability to create bulges through the redistribution of stars (e.g., Kauffmann et al. 1993; Cole et al. 1994; Somerville and Primack 1999). Note, though, that SAMs do not distinguish between morphological types of bulges. They simply lump all bulges together under the label "spheroid." In SAMs, mergers above a given mass ratio result in the galaxy's transformation into a spheroid. Subsequent accretion of gas allows for the formation of a new disc around the spheroid and the galaxy morphology is defined by the spheroid to disc mass ratio. Explicitly linking bulge formation to major mergers enables SAMs to generally reproduce the observed relationship between morphological type and color (Baugh et al. 1996), the color-magnitude relation (Somerville and Primack 1999) and the observed morphological mix of galaxies (Cole et al. 2000), as well as their approximate environmental dependence. Importantly, a merger-driven scenario for spheroids allowed SAMs to reproduce the number density of spheroids at $z = 0$ for galaxies roughly more luminous than $L^{\star}$ (Somerville and Davé 2015). However, for galaxies fainter than $L^{\star}$, the ubiquity of mergers leads to an overproduction of bulges in low mass galaxies.

12.4.1.1 Synergy with Idealized Simulations

The analytical prescriptions used to model the baryonic component in SAMs are often shaped by the results of idealized simulations. Idealized simulations first construct a galaxy according to the simulator's desires, and then follow its evolution. In idealized binary merger simulations, two such galaxies are built and then allowed to merge under the influence of gravity. Idealized simulations differ from cosmological simulations in that they are computationally much less expensive, since they neglect the cosmological context. They generally do not include subsequent gas accretion onto the galaxies, or torques from large-scale structure. This allows idealized simulations to reach relatively high resolutions while exploring a large range of parameter space more quickly than cosmological models. This ability to explore parameter space makes them ideal for deriving analytical prescriptions that can be fed into SAMs.

The overproduction of spheroids in fainter galaxies in SAMs can be alleviated when the gas fractions of merging galaxies are considered. As shown in the binary merger simulations of Hopkins et al. (2009a), angular momentum loss from gas primarily occurs through internal torques generated by the merger. In these situations, the disspational gas bar will lead the dissipationless stellar bar in phase.

The resulting gravitational torque causes angular momentum to be transferred from the gas to the stars (Barnes and Hernquist 1991). In gas rich mergers, the relatively low mass of the stellar bar will result in less angular momentum loss and lower bulge masses. This scenario has been further backed-up by simulations of gas-rich disc mergers (Springel et al. 2005; Governato et al. 2009) and observations that find a significant fraction of $z \sim 1$ galaxies which had sufficient gas fractions to rebuild their disc (Hammer et al. 2009). This dependency on gas fraction results in less efficient bulge formation in lower mass galaxies (Hopkins et al. 2010) and high z galaxies (Stewart et al. 2009). In cosmological simulations, the trend with gas fraction ultimately makes the final bulge-to-disc ratio highly dependent on the ability of stellar feedback to limit star formation prior to and during the merger (Robertson et al. 2006).

While including the role of gas in the resulting bulge-to-disc ratios brings the number of spheroids in low mass galaxies into agreement with observations (Hopkins et al. 2009a; Porter et al. 2014), it may also lead to an under-prediction of the number of spheroids at the massive end. A number of SAMs have found that additional spheroid creation mechanisms, such as those resulting from disc instability, may be required to create spheroids in galaxies brighter than $L^{\star}$(Parry et al. 2009; De Lucia et al. 2011; Porter et al. 2014; Brennan et al. 2015; Somerville and Davé 2015).

12.4.2 The Problem of Pseudobulges

While the SAMs may be able to explain the frequency of spheroids in $L^{\star}$ galaxies and fainter, recall that they do not distinguish between classical and pseudobulges. The frequency of pseudobulges (and apparent lack of classical bulges) in galaxies as massive as the Milky Way raises a potential challenge for ΛCDM (e.g. Weinzirl et al. 2009; Kormendy et al. 2010; Peebles and Nusser 2010). Hierarchical growth is such that interactions and mergers are common at every redshift for massive galaxies. For example, Stewart et al. (2008) found that the majority (70 %) of Milky Way-mass halos have experienced at least one merger with an object 10 % the mass of the Milk Way or greater. If mergers lead to the formation of classical bulges rather than pseudobulges, then it is very mysterious that classical bulges are not more common. Indeed, it is puzzling that classical bulges are not the *dominant* form of bulge found in the Local Universe.

To reconcile the observed frequency of pseudobulges with the hierarchical nature of ΛCDM, one or more of the following possibilities must be true: (1) the merger rates must have been over estimated due to errors in converting halo merger rates to stellar galaxy mergers, (2) pseudobulges must be able to camouflage already-existing classical bulges, (3) pseudobulges can also be formed in mergers, or (4) classical bulge formation during mergers must be less efficient than currently thought, possibly because of feedback or because mergers are happening between galaxies with higher gas fractions.

As far as the first possible solution is concerned, while there is some uncertainty in the merger rates of galaxy discs, *halo* merger rates are very well established and significantly reducing galaxy merger rates would likely require assuming a different matter power spectrum on small scales than generally adopted in ΛCDM models.

In regards to the second possible solution, the existence of bulges containing both pseudo and classical bulge characteristics, i.e. composite bulges, can be presumed from the overlap in populations (Gadotti 2009). A number of individual galaxies with composite bulges have been identified (Nowak et al. 2010; Méndez-Abreu et al. 2014; Erwin et al. 2014). Many of theses galaxies were previously thought to contain only a classical or pseudobulge, so it is clear that either type of bulge can dominate and mask the presence of the other. Unfortunately, since 1-D surface-brightness profiles cannot clearly distinguish between pure pseudobulges and composite bulges (Fisher and Drory 2010; Erwin et al. 2014), and because it is difficult to obtain stellar kinematic information for a wide sample of galaxies, it is currently not possible to make firm estimates of the fraction of pseudobulge-identified galaxies that also contain classical bulges. Méndez-Abreu et al. (2014) found composite bulges in 70 % of their sample of barred galaxies; these composite systems generally had large photometrically-defined classical bulges with an inner pseudobulge-like structure. Erwin et al. (2014) in turn estimated that at least 10 % of S0–Sb barred galaxies were composite-bulge systems and indeed had difficulty entirely ruling out the presence of classical bulges in any of the pseudobulge-identified systems they looked at. We can therefore conclude that the observed frequency of classical bulges may have been underestimated. However, galaxies in which classical bulges are obscured by pseudobulges do not appear common enough to account for all of the discrepancy between observation and theory. Furthermore, the small classical bulges that are masked by pseudobulges in observations tend to contain a much lower stellar fraction than the classical bulges produced by mergers in simulations, as we discuss in the next section. We must, therefore, turn to the third and fourth possible solutions: pseudobulge formation during mergers and less efficient classical bulge formation during mergers. We examine the latter in detail in the following sections but for now, we concentrate on the possibility that some pseudobulge growth could be merger-induced.

The presumed formation of pseudobulges through non-axisymmetries raises some potential issues with distinguishing secular from merger-driven bulge growth. Minor mergers and interactions with satellites can in some cases induce bar formation and result in pseudobulges (e.g., Eliche-Moral et al. 2006; Guedes et al. 2013). Should bulges formed in this manner be considered the result of secular evolution? Alternatively, what do the bulges look like that are created when gas funnels to the center of a merger remnant and forms stars? Would they look like the dissipative collapse that can form spheroidals with large n (discussed in Section 12.3.1), or would the fact that the gas is funneled internally from the galaxy result in a bulge that had the tell-tale signs of discy pseudobulges?

Idealized binary merger simulations should be able to address these questions. Unfortunately, one must be very careful to understand resolution effects. The merger simulations of Keselman and Nusser (2012) adopted 70 pc force resolution for

newly formed stars. They examined the resulting bulge both through a decomposition of the projected density profiles, and kinematically. In all cases, the central component had $n < 1$, and in almost all cases this component is also rotationally supported (at least for a few Gyr after the merger). Hence, for the first time, these authors have demonstrated that mergers of galaxies appear to produce pseudobulges rather than classical bulges.

A similar result was hinted at in the study of "extra light" observed in the central surface brightness profiles of some ellipticals. This extra light is thought to be the signature of a central starburst produced by gas that is funneled to the center during mergers (Kormendy 1999; Hopkins et al. 2008), much like the process expected to create bulges in disc galaxies during mergers. The extra light components could be fit with $n \sim 1$, but with a caveat: the extra light component (and presumably the bulges in Hopkins et al. 2009a) were comparable in size to the force resolution of the simulations. Resolution effects would act to artificially flatten the central profile, and reduce the n of the central light component.

In principle, any computational study of the n value of the resulting bulge formed in mergers needs to undergo a rigorous convergence test. These two simulations, therefore, present promising results that need to be replicated in simulations that can resolve the bulge structure. Once the bulge can be resolved, it will be possible to check whether mergers can produce, in addition to the lower n and the rotational kinematics already hinted at, the other characteristics typical of discy pseudobulges: recent or on-going star formation, dense gas, and morphological substructures such as bars, rings, and spiral arms. It is especially important to examine these other characteristics since so much of the evidence for pseudobulge growth being secularly driven is based on morphological substructures, for instance the strong correlation between pseudobulges and the presence of bars and ovals. Additionally, the ubiquity of star formation within pseudobulges implies that pseudobulge growth is not dominated by episodic events, such as mergers.

In summary, the idea that mergers always lead to classical bulge formation in disc-dominated galaxies is problematic within a hierarchical model like CDM. Historically, the ubiquity of mergers led to an overproduction of bulges in $L^\star$ galaxies and fainter. The formation of bulges was shown to be suppressed in gas-rich mergers, and the adoption of a model that accounted for gas fraction in bulge formation can reproduce the observed trend in morphology with mass up to $L^\star$ (Hopkins et al. 2009a). However, if the remaining bulges that do form in mergers are classical, then tension still remains with CDM theory given that the Local Volume is dominated by pseudobulges (Kormendy et al. 2010; Fisher and Drory 2011). One possible solution to alleviate the tension is if some pseudobulges are induced by minor mergers that trigger bar formation. Indeed, preliminary work using idealized merger simulations suggests that pseudobulges may be the outcome of gas inflow that leads to centralized star formation in gas-rich disc galaxy mergers (Keselman and Nusser 2012). However, a counter-argument to this is that fewer galaxies show rings, ovals, or bars than are likely to have recently experienced minor mergers, suggesting that minor mergers cannot always form pseudobulges, if they ever do.

If discy pseudobulges are not formed during mergers, then it is left to other secular processes and disc instabilities to form them. Given the dearth of classical bulges and evidence that many pseudobulges are B/P bulges that likely formed in situ due to heating from a bar (Laurikainen et al. 2014), it is likely that secular evolution is the primary creator of discy pseudobulges. However, this still requires that the formation of bulges (of all types) must be suppressed in mergers in order to match their low numbers in the local Universe. We explore this possibility below.

12.5 Forming Bulges in Cosmological Simulations

Cosmological simulations are the ideal place to test the physics of bulge formation, owing to the fact that the complex processes of mergers, stellar feedback, and gas inflow and outflow can be self-consistently modeled. Until recently, however, it has been very difficult to specifically study bulge formation because bulges are generally on the same size scale as the force resolution convergence. Convergence in the density profile is only achieved when enough particles are enclosed that the time scale for collisional relaxation of the particles is longer than the age of the Universe (Power et al. 2003). In practice, this means that densities usually converge at 4–6 times the force softening length (Navarro et al. 2010). The highest resolution simulations yet of Milky Way-mass galaxies have achieved a force resolution of $\sim$70 pc (Hopkins et al. 2014), but most simulations published to date have had force resolutions on the order of $\sim$150 pc or more, making the regions interior to $\sim$700 pc officially unresolved. As most bulges have effective radii between 100 and 1000 pc (Fisher and Drory 2010), these resolutions are insufficient to study the structure of the majority of bulges. However, additional simulations with sub-100 pc force resolutions will be achieved within the next few years, and thus the ability to resolve bulges and analyze their growth is becoming a realistic possibility.

Historically, simulations have tended to produce galaxies that are too compact, with a large central mass concentration and large stellar spheroid (e.g., Steinmetz and Navarro 1999; Navarro and Steinmetz 2000; Abadi et al. 2003; Governato et al. 2004; Scannapieco et al. 2009). The resulting overly-massive and concentrated bulges are the direct result of the "overcooling" problem in simulations. In this section we discuss the origin of overcooling, and describe the recent successes in feedback modeling that appear to overcome the overcooling problem. In theory, a fully successful model must also match the observed stellar mass–halo mass relation and its evolution in order to ensure that gas is not being over-consumed in star formation. Over-consumption leads to lower gas fractions, and drives the building of larger bulges than observed. Unfortunately, no simulation that has demonstrated its ability to match this relation back to high z has yet been used to study bulge formation. We instead highlight a few of the best results to date, and point out the open questions that future high resolution cosmological simulations can address.

12.5.1 The Problem of Overcooling

In the overcooling problem, baryons at early times cool rapidly to the center of halos, resulting in galaxies with dense concentrations of gas and stars. In a hierarchical formation model like CDM, these galaxies undergo multiple subsequent mergers. During these mergers, orbital angular momentum is transferred to the dark matter of the accreting halo through dynamical friction. By the time the dense baryons arrive at the center of the accreting halo, little angular momentum remains in them and the resulting galaxies show the classic signs of the angular momentum catastrophe (Navarro and White 1994; Katz et al. 1994; Maller and Dekel 2002; D'Onghia et al. 2006).

Including appropriate stellar feedback has been the most effective method for reducing overcooling in simulations (Governato et al. 2007; Scannapieco et al. 2008; Piontek and Steinmetz 2011). Feedback defends against early cooling of gas in simulated halos by creating a hot gas reservoir that only allows gas to cool onto galaxies at later times. Ideally the feedback hinders cooling prior to the period of rapid mergers, which prevents angular momentum loss in tidal effects and leads to more realistic mass distributions in galaxies (Robertson et al. 2004; Okamoto et al. 2005; Scannapieco et al. 2008; Zavala et al. 2008; Kereš et al. 2009; Piontek and Steinmetz 2011). Stellar and supernova feedback in the disc seems to be the most important source of heating (e.g., Governato et al. 2010; Agertz et al. 2013; Aumer et al. 2013; Ceverino et al. 2014; Hopkins et al. 2014), though pre-heating at reionization also prevents gas from cooling in the lowest mass halos (Quinn et al. 1996; Thoul and Weinberg 1996; Gnedin 2000; Okamoto et al. 2008). As we will discuss later, stellar feedback has other positive effects, such as maintaining the gas fractions of discs and expelling low-angular momentum baryons.

12.5.2 Feedback Implementations and Their Effects on Central Concentration

Stellar feedback offers a promising avenue for reducing the mass and concentration of bulges. However, simulators must grapple with the fact that both star formation and feedback take place on scales much too small to be resolved in cosmological simulations. For example, simulations must adopt a prescription that mimics star formation on kiloparsec scales, rather than the sub-parsec scales where star formation actually takes place (the scheme is then termed "sub-grid"). Thankfully, star formation on galaxy scales does appear to follow a global trend, the Kennicutt-Schmidt relation (Kennicutt 1998; Martin and Kennicutt 2001). However, even if modelers can determine the star formation rate based on the Kennicutt-Schmidt relation, this does not guarantee that the feedback scheme used for subsequent supernova feedback will satisfy observed constraints such as the Tully-Fisher relation or the mass-metallicity relation.

Early simulations found that supernova energy was quickly radiated away in the surrounding dense medium without impacting the galaxy (particularly at high z when the gas is more dense, e.g., Katz 1992; Steinmetz and Navarro 1999). Simulators have thus been forced to develop sub-grid recipes for feedback to model how the energy is transferred to the interstellar media. One way to avoid the immediate radiating away of supernova energy is to turn off cooling in gas particles within the "blastwave" of the supernova remnant for a period of time (McKee and Ostriker 1977; Thacker and Couchman 2000; Stinson et al. 2006). While this cooling delay is designed to mimic the sub-resolution adiabatic expansion of the supernova, it is often considered undesirably artificial. Others avoid disabling cooling by adopting a "multiphase" gas particle model that prevents hot gas particles from being artificially influenced by their cold gas nearest neighbors (Hultman and Pharasyn 1999; Marri and White 2003; Harfst et al. 2006). However, the disconnect between cold and hot gas in this approach can also be considered unphysical and problematic.

More recent works have instead embraced additional sources of energy from young stars (Hopkins et al. 2011; Agertz et al. 2013; Aumer et al. 2013; Kannan et al. 2013; Trujillo-Gomez et al. 2014; Sales et al. 2014; Stinson et al. 2012; Wise et al. 2012) and in these schemes of constant energy injection, cooling need not be turned off for feedback to have a strong effect. Essentially, supernova energy can more easily escape in these schemes because in the $\sim$4 Myr prior to any type II supernova, the massive stars have already contributed to the destruction of their natal birth clouds (Agertz et al. 2013). There are multiple early energy sources which may contribute, e.g., photoionization of the clouds via UV radiation, momentum injection from stellar winds, and radiation pressure on surrounding dust grains (e.g., Murray, et al. 2005; Sharma and Nath 2012; Murray, et al. 2011; Zhang and Thompson 2012; Lopez et al. 2014), but many of them are still poorly constrained. In particular, the strength of the radiation pressure is highly debated. While it is possible that IR trapping causes a single photon to bounce a number of times, increasing its effectiveness, it has also been suggested that a full model of radiative coupling will produce chimneys by which the photons escape, making them ineffective (Krumholz and Thompson 2012, 2013). Despite the debate over the details, the overall trend is to input more energy into the ISM, which has allowed cosmological simulations to successfully reproduce a number of observed galaxy scaling relations in recent years (e.g., Brook et al. 2012b; Aumer et al. 2013).[2]

Along with the increased energy deposition into the ISM, increasing computational power has allowed a change to the distribution of star formation in simulations. Cosmological simulations are now resolving gravitational forces on

[2]Agertz et al. (2011) is notable for producing a galaxy with a relatively low bulge-to-total ratio using low star formation efficiencies, rather than high levels of feedback (B/T = 0.21 for a 1.25×10^{12} $M_\odot$ halo with their preferred feedback model). However, this galaxy produced too many stars overall. As discussed in Agertz et al. (2013), stellar feedback is necessary for producing galaxies with *both* appropriately low stellar masses and small bulges.

scales <100 pc. These high resolutions allow high density peaks in the gas to be resolved. When these peaks are not resolved, star formation takes place in diffuse, warm gas across the entire disc and the supernova energy is quickly radiated away (Ceverino and Klypin 2009; Saitoh et al. 2008). On the other hand, if high density peaks are resolved and the star formation is limited to these peaks (and gas is allowed to cool below 1000 K), the supernova energy is concentrated into smaller physical regions. The overall result is that feedback creates over-pressurized regions and becomes more effective, as well as highly localized. Localized feedback naturally drives gas outflows (galactic "winds," Governato et al. 2010; Guedes et al. 2011; Christensen et al. 2014b; Hopkins et al. 2014; Agertz and Kravtsov 2015) without the need to implement a separate numerical prescription for outflows (Davé et al. 2011; Marinacci et al. 2013; Vogelsberger et al. 2013). Galactic winds appear to be ubiquitous (e.g., Martin 2005; Veilleux et al. 2005; Weiner et al. 2009), so the natural driving of outflows in high resolution simulations can be considered a major success.

These high resolutions with galactic winds led to the simulation of realistic central mass distributions in low-mass dwarf galaxies for the first time: bulgeless dwarf galaxies (Governato et al. 2010, 2012; Teyssier et al. 2013; Di Cintio et al. 2013). Bulgeless discs (no classical or pseudobulge) are more common in low mass dwarf galaxies (Dutton 2009; Kormendy and Freeman 2014). In these galaxies, high resolution and localized feedback lead to gas outflows that preferentially remove low-angular momentum gas (Brook et al. 2011, 2012a). If retained, this low-angular momentum gas could have formed a large stellar bulge. Instead, the loss of it results in a stellar disc with a purely exponential surface brightness profile and higher specific angular momentum than predicted otherwise, consistent with observations (D'Onghia and Burkert 2004; Dutton and van den Bosch 2009; Governato et al. 2010).

Ideally, the same star formation and feedback prescription that produces realistic bulgeless dwarf discs would form realistic bulges as halo mass increases. One might imagine a scenario in which the deeper potential wells in high-mass galaxies prevent the complete loss of low-angular momentum material (Dutton and van den Bosch 2012) so that these galaxies still form bulges. In this scenario, outflows are still required to remove some low-angular momentum material at high z in order to match observed bulge sizes even in Milky Way-mass galaxies (Binney et al. 2001; Bullock et al. 2001; van den Bosch 2001; van den Bosch et al. 2001, 2002). If less low-angular momentum material is lost as galaxy mass increases, this trend could reproduce bulge prominence as a function of galaxy mass.

In practice, it is difficult to reach the same high resolution currently achieved in dwarf galaxy simulations in more massive galaxies. Being more rare, massive disc galaxies like the Milky Way require a larger simulation volume. A larger volume is also necessary to ensure that the large scale tidal torques that deliver angular momentum to the galaxy are included (White 1984; Barnes and Efstathiou 1987). To reach sub-100pc resolutions requires significantly more particles, making this currently computationally challenging, although feasible for the first time (e.g.,

Hopkins et al. 2014). No works have yet examined the bulge properties of massive disc galaxies formed at these high resolutions, though.

12.5.3 Bulge Formation Studies with Cosmological Simulations

The highest resolution studies to yet examine bulges in massive discs in fully cosmological simulations have ∼150 pc resolution (Guedes et al. 2011; Christensen et al. 2014a). Most works have examined central mass distributions by restricting themselves to a study of circular velocities (v_c) and the bulge-to-total (B/T) ratios of their galaxies (e.g., Scannapieco et al. 2010; Stinson et al. 2012; Aumer et al. 2013). The former is useful because large bulges lead to a declining rotation curve rather than the flat curves observed in galaxies. The latter offers many opportunities to compare with observations. A comparison of B/T ratios must be done carefully, though. A number of works have noted that the bulge fractions determined through kinematic decomposition are systematically larger than those determined through photometric decomposition (Governato et al. 2009; Scannapieco et al. 2010; Marinacci et al. 2013; Aumer et al. 2014; Christensen et al. 2014a), although the extent of the discrepancy varies widely with simulation and decomposition methodology. For instance, in the papers cited above, kinematic decomposition produces bulge masses anywhere from 1.25 to 12 times greater than the photometrically determined masses. The need for photometric decompositions (on simulated observations in the appropriate bands and using standard observational decompositions methods) when comparing with observed bulge properties is clear. However, even in the most extreme cases, using photometric rather than kinematic decomposition does not eliminate the problem of too massive or concentrated of bulges.

A few modelers have investigated the structure and growth of their bulges in detail. Guedes et al. (2013) and Okamoto (2013) both found that their bulges were best fit by a Sérsic index <2 (1.4 in the former case, 1.4 and 1.2 in the latter case, as measured through *i*-band photometric decomposition), leading these authors to classify them as pseudobulges (again, we note that resolution may artificially lower *n*, as these simulations would not necessarily yield converged results on scales smaller than ∼750 pc). Despite being classified as pseudobulges, their formation is inconsistent with slow growth via secular evolution processes. Instead, these bulges form fast at high redshift, and mostly in situ from gas funneled to the center of the main galaxy rather than from accreted material. Guedes et al. (2013) noted that mergers contributed a similar fraction of accreted stars to both the bulge and the high *z* disc, rather than preferentially to the bulge and, according to Pillepich et al. (2015), only a quarter of the final bulge stellar mass was formed ex situ. In two of the three galaxies examined in Guedes et al. (2013) and Okamoto (2013), the presence of a bar was tied to bulge formation. However, Guedes et al. (2013) found that the bar formation was itself induced by tidal interactions with accreting galaxies. Hence,

mergers were indirectly responsible for the growth of a bulge with a low Sérsic index in their simulation.

Unfortunately, it is unclear how much merger history plays into the fast pseudobulge formation that was found in these simulations. Most of the galaxies studied so far were chosen to have quiescent merger histories, with their last major mergers occurring at $z \gtrsim 1$. Are the early formation times of these simulated bulges due to a biased selection with all major mergers occurring at high z? Would the bulges continue to grow, or become more classical, with lower z mergers?

One other important consideration is that both Guedes et al. (2013) and Okamoto (2013) suffer from too much star formation at high z compared to abundance matching results (see also Stinson et al. 2012; Agertz et al. 2013). Forming too many stars at high z suggests an overconsumption of gas – and hence lower gas fractions than are realistic. If the simulated galaxies are gas-poor galaxies at high z, then their merger-driven bulge growth would be too efficient (Hopkins et al. 2009a,b). Higher, more realistic gas fractions could possibly be achieved by increased amounts of feedback. Indeed, both Guedes et al. (2013) and Okamoto (2013) conclude that more feedback at high z (possibly in the form of AGN feedback) is likely necessary to form the large, bulgeless disc galaxies that are found in the Local Volume (Kormendy et al. 2010; Shen et al. 2010; Fisher and Drory 2011; Laurikainen et al. 2014).

Recently, Aumer et al. (2014) analyzed the evolution of both the disc and bulge in simulations with greater amounts of feedback. Unlike Guedes et al. (2013) and Okamoto (2013), these simulations included additional feedback from young stars. These simulations did indeed produce more realistic star formation histories for their stellar mass (Aumer et al. 2013) and had low i-band B/T values (typically less than 0.15). However, the stellar distributions reveal discrepancy with observations. Specifically, the simulated Milky Way-mass galaxies show both too little central growth combined with too much outer disc growth compared to results in van Dokkum et al. (2013). It would be tempting to conclude that these unrealistic stellar distributions were the result of ejected bulge gas being recycled to the outer disc. However, Übler et al. (2014) studied these same simulations and showed that most recycled gas returned with similar angular momentum to when it was ejected. Aumer et al. (2014) conclude that their feedback appears to be too strong at $z < 1$, while providing more accurate star formation at higher z. Young stellar feedback has also been shown to produce discs that are too thick compared to observations (Roškar et al. 2014). Taken together, these results suggest that more feedback is necessary at high z to match star formation rates, but that current models of feedback from young stars (prior to supernovae) create new problems. Could the addition of AGN feedback at high z reduce the need for such strong stellar feedback? Or do we simply have yet to understand how stellar feedback operates at high z?

Overall, spiral galaxies with appropriate (if slightly on the massive end of the observable range) bulge-to-total ratios have now been produced and analyzed in a handful of simulations (Guedes et al. 2013; Okamoto 2013; Aumer et al. 2014).

However, as of yet there has been little investigation into how realistic the other bulge properties are. While Christensen et al. (2014a) showed simulations that fit observed bulge scaling relations, those bulges were overly massive compared to the discs, having *H*-band B/T values of 0.43 and 0.53. Similar analysis of the scale lengths, surface brightnesses, and colors of simulated bulges is needed in future simulations, in addition to the more common bulge-to-total ratios.

Moreover, most identification of simulated bulges as being classical bulges or pseudobulges has been based entirely on the Sérsic index. While lower Sérsic indices are well correlated with the discy-properties that indicate a pseudobulge in observed galaxies, it is not clear that simulated galaxies yet produce as clean of a divide. Until it has been shown that pseudo and classical bulges in simulations have the same sets of identifying features as observed galaxies, more holistic classification of bulges in simulations is necessary. Most importantly, simulated bulges should have the defining feature of pseudobulges: being disc-like in terms of a flattened morphology and rotation-dominated stellar kinematics. They should also reproduce the observed sub-types of pseudobulges: discy versus B/P. For instance, simulated bulges should frequently include morphological features such as bars, rings and spiral arms, recent or on-going star formation, and an abundance of dense gas as these are typical observed characteristics of discy pseudobulges.

Reproducing both types of pseudobulges in cosmological simulations is highly dependent on whether the simulations can resolve the instabilities that create bars and other asymmetries. B/P bulges are tied to the presence of bars and it is not clear whether cosmological simulations capture bar formation and destruction. More specifically, long bars can and do form when simulations resolve the perturbation scales sufficiently, but the simulations may not capture the smaller scale disturbances that form shorter bars. Once a bar does form, it is not clear if the simulations will then capture the processes that should lead to its destruction. However, as cosmological simulations achieve ever higher resolution, they are approaching the resolution scales that isolated disc galaxy studies have used to study similar processes. Hence, the ability to answer the question of whether simulations capture these processes is soon to be within reach.

12.6 Limiting Merger-Driven Bulge Formation with Stellar Feedback

Results from both idealized merger simulations and fully cosmological simulations lead us to conclude that the primary mechanism of bulge growth in mergers is tidal torquing of gas within the galaxy, which drives gas into the central regions to undergo a burst of star formation. Recent results from the study of bulgeless dwarfs, however, suggests another step in the story. Bulgeless dwarfs arise in cosmological

simulations regardless of their merger history.[3] While mergers in dwarfs drive gas to the center, subsequent bursts of star formation drive galactic winds that remove that gas from the galaxy. Essentially, mergers in dwarfs can lead to the removal of bulge material, rather than the creation. To what extent could this scenario hold in more massive galaxies with deeper potential wells? At what scale do winds fail to prevent bulge formation?

Some insight into these questions comes from Brook et al. (2012a), which examined the history of a disc galaxy of $2 \times 10^{11}\,\mathrm{M}_{\odot}$ in virial mass. Although this galaxy did eventually form a bulge, the formation was considerably delayed compared to the more massive disc galaxies discussed in the previous section. In fact, the galaxy was still bulgeless at $z = 1$. Bulge formation at higher redshifts was suppressed because it was easier for this galaxy to lose its low-angular momentum gas when the potential well of the galaxy was shallower, i.e. earlier in the galaxy's history (Brook et al. 2012a).

Of course, merger rates were also higher early in the history of the Universe. Is it possible that the shallower potential wells of galaxies at high redshifts (and therefore the greater ability of winds to escape) offset the effects of the increased merger rates? Typically, the existence of massive, bulgeless disc galaxies at $z = 0$ in the Local Volume has been viewed as a challenge to CDM. If mergers instead drive a burst of star formation that expels low-angular momentum gas, could the merger rate predicted in CDM instead be viewed as the solution to the existence of massive, bulgeless discs? In this section we explore this possibility in more detail.

12.6.1 Trends with Galaxy Mass

The mass loading factor (the mass of gas outflowing from the galaxy divided by the mass of stars formed) depends strongly on galaxy mass. Models typically assume an exponential scaling with circular velocity of either -1 for "momentum driven winds" or -2 for "energy driven winds." These scalings imply that dwarf galaxies have mass loading factors a couple of orders of magnitude larger than those of Milky Way mass galaxies. As such, ten to a hundred times more gas is expelled from the central regions of lower mass galaxies than is formed into stars. In other words, as galaxy mass increases, we expect a smaller fraction of the material driven to the centers of galaxies through mergers to be expelled. This should lead to increasingly dominant bulges with increasing galaxy mass.

[3] Due to the required high resolution to form bulgeless dwarf galaxies, a large, statistical sample is difficult to produce. Some observed dwarfs do have bulges, but bulgeless discs dominate the population (Dutton 2009). The current small numbers of simulated dwarfs has limited our ability to produce dwarfs with bulges to understand their origin.

Table 12.1 Characteristics of the examined galaxies and their mergers. Galaxy 5 experienced two qualifying mergers and is, therefore, listed twice. Galaxy 10 is from a separate set of simulations with the more efficient superbubble feedback recipe. The "Primary Halo Mass" listed in column 3 is the mass of the primary at the start of the listed merger.

Halo	Mass at $z = 0$ [$10^9\,M_\odot$]	Primary halo mass [$10^9\,M_\odot$]	Merger redshift	Amount of time for merger [Gyr]	Merger ratio
1	23	7.1	1.3	2.1	1.2
2	38	28	1.1	1.1	3.5
3	38	2.1	1.1	2.6	1.5
4	43	22	1.9	1.1	7.7
5	180	19	1.2	2.1	2.1
"	"	110	1.1	0.9	9.4
6	340	160	1.3	1.1	2.2
7	770	360	1.6	1.3	1.1
8	880	59	1.7	2.5	1.1
9	910	330	1.5	1.2	1.2
10	800	140	2.6	1.0	2.0

Here, we examine the extent to which mergers are able to drive bulge growth as a function of galaxy mass in a current set of high resolution cosmological simulations. We compare a suite of ten simulated galaxies (Table 12.1), all selected from "zoom-in" galaxy simulations produced with the Smoothed Particle Hydrodynamic code, GASOLINE (Wadsley et al. 2004). These galaxies cover a mass range of 10^{10}–$10^{12}\,M_\odot$ at redshift zero. They were selected on the basis of having experienced a 10:1 or greater mass ratio merger since $z = 3$.

The version of GASOLINE used to produce nine of these simulations is described in detail in Christensen et al. (2012). In brief, though, the simulations have gas particle masses between 3.3 and $27.0 \times 10^3\,M_\odot$ and softening lengths between 87 and 174 pc. Star formation occurs probabilistically according to the free fall time and the local molecular hydrogen abundance. Supernova feedback is implemented using a blastwave scheme (Stinson et al. 2006) with the total amount of energy deposited in the ISM being 10^{51} ergs per supernova. This version of the code has been successful at reproducing many observed properties of galaxies, including the shapes of bulges (Christensen et al. 2014a), the cores of dwarf galaxies (Governato et al. 2012), the stellar mass to halo mass relation at $z = 0$ (Munshi et al. 2013), gas fractions at $z = 0$ (Munshi et al. 2013), and the mass distribution of satellite and field dwarf galaxies (Zolotov et al. 2012; Brooks and Zolotov 2014).

The tenth galaxy is produced by a version of GASOLINE with a newer model of supernova feedback, as described in Keller et al. (2014). This feedback model replicates the effect of superbubbles on the surrounding gas. Superbubbles are generated by clustered star formation when the individual winds of supernovae merge. They are also much more efficient at generating gas motion than individual supernovae. For instance, Keller et al. (2014) found that in a Milky Way-mass galaxy, they drove ten times more mass in outflows than the blastwave feedback model.

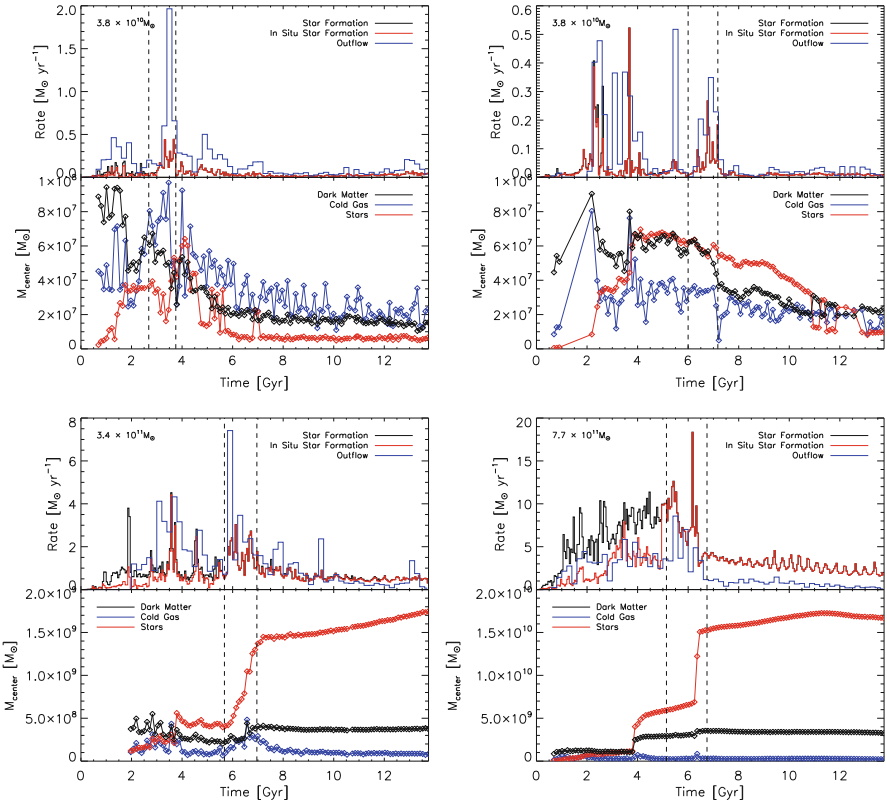

Fig. 12.1 Star formation and outflow history and the evolution of the central mass concentration for four example galaxies. In the *top panels*, the *black curve* is the total star formation history whereas the *red marks* the in situ star formation history for the main progenitor. The *blue curve* shows the history of gas outflow from the disc (gas particles are defined as outflowing if they reach a radius greater than $0.2R_{vir}$). The *dashed vertical lines* mark the beginning and end of major mergers. The *bottom panels* show the evolution of the central mass concentration, i.e. mass within $0.006R_{vir}$ at redshift zero. *Black lines* indicate dark matter mass, *blue* the gas mass, and *red* the stellar mass. For the lower mass galaxies, the merger results in a burst of star formation and, because of their high mass loading factors, an even greater mass of gas outflowing. The result of this expulsion is a decrease in the central total mass following the merger. In contrast, higher mass galaxies expel less mass per stellar mass formed during the merger and their central concentration dramatically increases across the merger

Figure 12.1 illustrates the effect of mergers on the star formation and outflow histories of galaxies (top panels), as well as their central mass concentrations (bottom panels) for four representative galaxies with the blastwave feedback model. Outflows were measured by using particle tracing to detect gas leaving the disc – outflowing material was defined to be gas particles that reached a radius greater than $0.2R_{vir}$ after having been part of the disc. Mergers are marked by vertical dashed lines indicating both the onset (time step where discs first show morphological

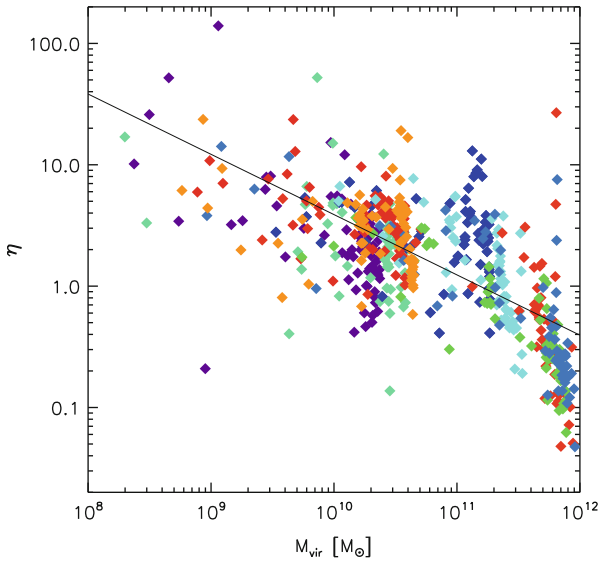

Fig. 12.2 Mass loading factor, η (total gas mass ejected divided by the stellar mass formed), in 0.5 Gyr time bins as a function of the virial mass at that time. The colors mark different galaxies. A power law fit to all the data points results in an exponent of -0.5, indicating that lower mass galaxies are much more efficient at driving outflows

distortion) and end (time of final coalescence) of the mergers. During the mergers in all galaxies both star formation and outflow rates peak. However, the ratio of star formation rate to outflow rate changes with galaxy mass; in the lowest mass galaxy shown the outflow rate is four times that of the star formation rate whereas in the highest mass galaxy the outflow rate is half as much. The mass loading factor (gas outflow rate divided by the star formation rate), η, is shown as a function of halo mass in Fig. 12.2 for the nine galaxies simulated with blastwave feedback. The galaxies in our sample show a -0.5 mass loading factor scaling with halo mass, which is close to that theoretically determined for the energy driven wind model.

Figure 12.1 also shows the history of the central mass of the galaxies. The mass of stars, gas and dark matter mass within 0.006 times the redshift zero R_{vir} are shown as a function of time. This central mass can be seen as a proxy for the bulge mass. In the two lower mass galaxies, the total central mass actually drops following the merger. Based on the outflow rates, it is expected that the gas mass in the central region would decline. We note, however, that the total mass in the central region declines as well. The massive outflow originates as a hot bubble of gas that rapidly expands, and flattens the potential well (Pontzen and Governato 2012; Teyssier et al. 2013). This fluctuation in the potential well also increases the radii of the orbits of the dark matter, causing the total mass to decline, not just the gas mass. The two more massive galaxies, however, instead undergo a dramatic increase in central material (mostly stellar mass) following the merger. In these galaxies, the low mass

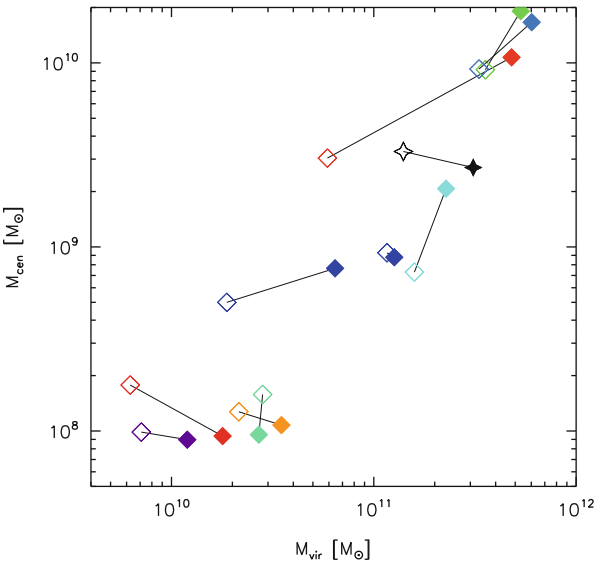

Fig. 12.3 The mass within the central region ($0.006R_{vir}$ at redshift zero) before and after a merger versus the virial mass of the galaxy at each of those times. The *open symbols* show the state of the primary galaxy prior to the merger and *filled symbols* show galaxy post merger. One galaxy (halo 5, seen here as the *blue squares* at approximately $M_{vir} = 10^{11}\,M_\odot$) underwent two qualifying mergers and is shown twice. The *black stars* represent halo 10, a galaxy from a separate cosmological simulation with the more efficient superbubble feedback model. Galaxies with halo masses close to $10^{10}\,M_\odot$ actually have reduced central mass following the merger whereas, except in the case of halo 10, the central mass increases for galaxies with halo masses greater than $\sim 10^{11}\,M_\odot$

loading factors results in less material being blown out of the galaxy, leading to a central stellar bulge.

Figure 12.3 shows the change in central mass following a merger against the initial and final virial mass of the halo. The mass trend is clear: in less massive galaxies, mergers result in lower central mass[4] while in high mass galaxies the central mass increases. This figure also implies a transition mass with $M_{vir} \approx 10^{11}\,M_\odot$. Near this mass, two of the galaxies experienced central growth, whereas the other galaxy had the same central mass before and after the merger. It should be noted, though, that the $10^{11}\,M_\odot$ galaxy that showed almost no central mass growth also had the largest merger ratio (9.4:1).

The exception to these trends is halo 10, shown in black, whose central mass actually decreases following the merger, despite its large mass. This galaxy was

[4]Note that in one case, the total halo mass is slightly lower after the merger as well. This has been seen in other works (Munshi et al. 2013; Sawala et al. 2013), too. When the virial radius is defined at a fixed overdensity, the radius will shrink as the galaxy loses mass in the merger. This results in a lower measured halo mass.

simulated using the more efficient superbubble feedback model. *It is remarkable for being a Milky Way-mass galaxy with one of the smallest bulges yet produced (∼5 % of the stellar mass)* and demonstrates the potential of stellar feedback to control bulge growth during mergers.

12.6.2 Discussion

In the simulations presented here, there is a transition at $M_{vir} \approx 10^{11}\,\mathrm{M}_{\odot}$, above which mergers lead to an increase in central mass using a standard supernova feedback model. While the mass where this transition occurs may vary with the star formation and feedback model, we discuss the broad implications of the model here. The two simulated galaxies at $M_{vir} \approx 10^{11}\,\mathrm{M}_{\odot}$ were also examined in more detail in Christensen et al. (2014b) and Christensen et al. (2014a), where it was shown that the concentration of the bulges matches observed structural relations, but that there is too much early star formation compared to abundance matching results (e.g., Moster et al. 2012). The bulges overall are too massive (by a factor of ∼4 or more assuming a mass-to-light ratio of 1 in the *H*-band). We also include an additional Milky Way-mass galaxy simulated with the more efficient superbubble feedback model. This galaxy not only has a reduced central concentration following a major merger, it also has a very low B/T of 0.05. This galaxy demonstrates the potential for stellar feedback to limit bulge growth, but it will require much more extensive analysis before firm conclusions can be drawn.

There are two potential solutions to reducing the bulge mass in simulated galaxies with $M_{vir} \gtrsim 10^{11}\,\mathrm{M}_{\odot}$. First, if high z star formation were decreased in simulations, then gas fractions would be larger in high z discs, causing mergers to be less efficient at building bulges. Observations show that galaxies at $z > 2$ have higher gas fractions than in similar mass galaxies at $z = 0$ (Tacconi et al. 2010). The gas-rich galaxies observed at high z are progenitors of more massive galaxies than we study here. Nonetheless, at $z = 0$ gas fractions increase as galaxy mass decreases (e.g., Geha et al. 2006; Dutton et al. 2011). Assuming this trend also holds at high z, the progenitors of Milky Way-mass galaxies would be more gas-rich than today, making high z mergers relatively less efficient at bulge formation. Given that simulations are already known to produce excessive high-redshift star formation rates, it is likely that they have tended to be too gas-poor at high z, leading to larger bulges than are realistic. Those simulations that match the high z evolution of the stellar mass-to-halo mass relation (e.g., Brook et al. 2012b; Aumer et al. 2013; Hopkins et al. 2014) may do better at making smaller bulges. Indeed, Aumer et al. (2013) showed that their bulges were smaller, but Aumer et al. (2014) showed that the growth of these central regions was still inconsistent with observations, suggesting that matching the stellar mass-to-halo mass relation is not by itself a sufficient criterion to ensure realistic bulge growth. Other simulations have yet to examine bulge growth.

As discussed in Section 12.5.3, inclusion of feedback from young stars (before they produce supernova) has been shown to bring high redshift simulated star formation rates in line with abundance matching results (Stinson et al. 2012; Aumer et al. 2013). However, the inclusion of this feedback at the levels currently required to reproduce observed properties leads to too thick and extended of stellar discs (Roškar et al. 2014; Aumer et al. 2014). The simulations we have examined in this section lack AGN feedback, as have most of the simulations that examine central mass growth. AGN feedback could be a natural contender to provide extra feedback. Additional motivation for AGN feedback can be found in Dutton et al. (2011), who showed that dark matter halos that host late-type Milky Way-mass galaxies seem to require some halo expansion (assuming a non-evolving Chabrier IMF) in order to match the zero point of the Tully-Fisher relation. Halo expansion at these masses is not reproduced in current simulations that include only stellar feedback (Di Cintio et al. 2013), but AGN feedback could create additional fluctuations in the gravitational potential wells of these massive galaxies that would expand the dark matter orbits (Martizzi et al. 2013).

AGN feedback could be beneficial in two ways; it could regulate star formation across the entire galaxy, potentially bringing simulated star formation rates into agreement with observations, and it could lead to more blowout of low-angular momentum gas that can further shrink the sizes of bulges in massive disc galaxies. For instance, it has been pointed out that there is an intriguing match between the global star formation history of the Universe and the accretion history of black holes (Terlevich 1998; Silverman et al. 2008), indicating that AGN feedback may indeed be tied to star formation regulation in galaxies. Unfortunately, the modeling of AGN feedback is highly uncertain, in particular how it couples with the surrounding gas. AGN feedback models can be broadly classified between those dominated by energy injection (e.g. Springel et al. 2005) and those dominated by momentum injection (e.g. DeBuhr et al. 2010). In the latter case, the velocity of winds has a profound effect on the range over which AGN limit star formation. Low velocity winds (as is typical when the momentum is generated by radiation pressure) affect only the centers of galaxies (DeBuhr et al. 2010) while high velocity winds (like those arising from accretion discs) can affect star formation over a much larger extent (DeBuhr et al. 2012) and, potentially, the growth of bulges in Milky Way-mass galaxies (Choi, private communication).

One strong appeal of AGN feedback is that it might remove gas from the galaxy at early times that could later be re-accreted and contribute to star formation at low z, potentially resulting in more realistic star formation histories. While many simulations form too many stars at high z, an additional consequence is that they underproduce stars at $z < 1$ (Somerville and Davé 2015). Moreover, unlike supernova feedback, AGN feedback can be somewhat independent from the mass of stars formed, which gives it a greater amount of latitude to affect scaling relationships. Given that feedback from young stars combined with supernovae has yet to fully satisfy observational constraints (e.g., simultaneously match stellar-to-halo-mass relations, disc thickness, and bulge/disc size growth), AGN feedback is looking more and more appealing as a potential regulator of star formation.

Perhaps the most attractive aspect of AGN feedback, though, is that it provides a mechanism that may preferentially remove gas from the centers of galaxies. Despite the recent successes of cosmological simulations in making extended discs, the B/T ratios always seems to reside on the high end of what is observed (e.g., Christensen et al. 2014a). As described at the beginning of this section, mergers in dwarf galaxies lead to a burst of star formation that drives outflows of low-angular momentum gas. Are AGN the missing mechanism to reduce bulge mass in higher mass galaxies by removal of low-angular momentum gas? In an ideal scenario, mergers at high redshift might drive gas to galaxy centers, leading to fueling of a black hole and the resultant feedback would reduce bulge growth by expelling excess gas from the center of the galaxy. As an additional bonus, AGN feedback may be able to drive gas at higher velocities than supernova feedback, allowing AGN to be more efficient at removing gas despite deeper potential wells in more massive galaxies.

However, AGN feedback cannot be a panacea. While potentially critical to limiting classical bulge growth, AGN feedback does not explain the presence of massive galaxies that completely lack a classical bulge. Based on the M_{BH}-sigma relation, galaxies with small classical bulges also have small black holes, which would be less effective at removing low-angular momentum gas through feedback. At the far extreme, galaxies with only a pseudobulge do not lie on the M_{BH}-sigma relation (Kormendy and Ho 2013) and tend to have small bulges, if at all. AGN feedback, therefore, has the potential to scale down the mass of classical bulges but to explain the existence of massive, pure-disc galaxies, stellar feedback is likely critical.

12.7 Summary and Future Prospects

Simulators face a number of hurdles in studying the formation of bulges in a cosmological context. Simulations must include large scale structure to capture tidal torques and properly model the angular momentum build-up of galaxies, but to resolve bulges they must also have very high force resolutions. Covering this range of scales is exceptionally computationally expensive. Convergence of the inner few 100 pc will still remain a challenge for the foreseeable future, however, state-of-the-art simulations with sub-100 pc force resolution are now allowing studies of these inner regions that were previously impossible. Until recently, such resolution could only be adopted in idealized merger simulations. Hence, simulators are now in a position to study bulge formation in a fully cosmological setting for the first time.

Much progress has been made: Guedes et al. (2013); Okamoto (2013) and Aumer et al. (2013) were able to form bulges with low bulge-to-total ratios while Christensen et al. (2014a) produced bulges that matched observed scaling relations. However, the B/T ratios of most cosmological simulations still tend to cluster on the high side of what is observed in discs at comparable stellar masses and the bulges are frequently overly-concentrated. Moreover, no simulation has yet showed realistic bulge formation in conjunction with a realistic star formation history. It is

usually assumed that more feedback, particularly at high redshift, can lower bulge masses and reduce their concentration. First, suppressing star formation overall at high redshift will lead to higher gas fractions, which lowers the efficiency of bulge formation in mergers (Hopkins et al. 2009a). Second, feedback can prevent early star formation while increasing later star formation rates through the reaccretion of previously-ejected gas, in better agreement with derived stellar-to-halo mass relations. Third, feedback can eject low-angular momentum gas entirely, reducing the overall size of bulges and bringing them into line with observations (e.g., van den Bosch 2001).

However, the form of the feedback that solves this problem remains elusive. Supernova feedback alone leads to too much early star formation (Stinson et al. 2012) and increasing it without limit results in blown-apart galaxies (Agertz et al. 2013). Including feedback from young stars (UV ionization, radiation pressure, and momentum injection in winds) enables the reproduction of observed stellar-to-halo mass trends (Agertz et al. 2013; Hopkins et al. 2014; Aumer et al. 2013), however these galaxies have too thick of discs (Roškar et al. 2014) and their disc growth is weighted too much to the outer discs (Aumer et al. 2014). As discussed in this chapter, a new model for superbubble feedback shows great promise in its ability to reduce bulge growth but the resulting galaxies require much more extensive evaluation before it is shown to be viable. We are left to wonder if the adopted sub-grid feedback models are the problem, or whether stellar feedback alone simply cannot satisfy all observational constraints. If the latter case, AGN feedback may be invoked to contribute as well.

In addition to the problem of massive bulges, simulations must also contend with the apparent over-production of classical bulges in CDM. Can feedback reduce the formation of classical bulges in significant enough numbers to reproduce observational trends? It has been shown that classical bulges are in the minority in the Local Volume (Weinzirl et al. 2009; Kormendy et al. 2010) and some disc galaxies as massive as the Milky Way appear to be either bulgeless or dominated by pseudobulges. Yet simulations have clearly shown that mergers can create classical spheroids, either through a redistribution of stars in gas-poor mergers, or by inducing gas flows to the center of galaxies that subsequently form stars. Given the ubiquity of mergers in CDM, the lack of classical bulges in galaxies is a serious problem for CDM galaxy formation theory (Peebles and Nusser 2010). If we wish to affirm the CDM model, we are left with two choices: either some mergers must form pseudobulges instead of classical bulges, or mergers must tend to *oppose* bulge formation so that some other mechanism, such as disc instabilities, forms the majority of bulges instead.

Both of these scenarios may be at play to some degree. Minor mergers have been seen to induce bars that create bulges with small n in cosmological simulations (Guedes et al. 2013; Okamoto 2013). Idealized major mergers have also been shown to lead to small n bulges (Keselman and Nusser 2012). These results suggest that a picture in which all mergers lead to classical bulge formation is not complete.

Yet even if some mergers led to pseudobulge formation, current theoretical models would still predict more massive bulges than are observed. This disagreement suggests that some mechanism is suppressing bulge formation. The formation of bulgeless disc galaxies, wherein mergers can fuel the *loss* of bulge material, offers an intriguing case study that may be extended to more massive galaxies. For instance, it is likely that feedback was more effective at high z, when the potential wells of galaxies are shallower (Brook et al. 2012a). Furthermore, some simulations suggest that mass loading factors could have been greater at high redshift (Muratov et al. 2015). Could the progenitors of modern-day $L^\star$ galaxies have had high enough mass loading factors to prevent bulge formation during high redshift mergers? Either AGN feedback or new models of stellar feedback may be able to fuel sufficiently strong galactic winds to remove enough low-angular momentum material.

Within this picture, we can imagine two phases of bulge evolution for a galaxy like our own Milky Way with a relatively quiescent merger history (Hammer et al. 2007). At high z during the era of major mergers, the gas fraction of the galaxy is high. This reduces the size of the bulge that can be formed in mergers, and merger-induced outflows are also more efficient because the potential well is shallower. The combination of these two facts could suppress classical bulge formation at high z. At lower z, secular processes or bars induced by minor mergers could create bulges that look like pseudobulges (Shen et al. 2010).

M31 represents the opposite extreme with its large classical bulge (Kormendy et al. 2010). If high gas fractions and outflows are acting to reduce bulge formation at early times, this suggests a late major merger when gas fractions were lower induced the formation of its classical bulge. Such a lower z massive merger is in agreement with trends observed in M31's stellar halo (Deason et al. 2013; Gilbert et al. 2014).

The contrast between a given massive spiral galaxy that contains a classical bulge, such as M31, and one that does not, such as the Milky Way or M101, may be explained by stochasticity in merger histories. However, the observed correlation between classical bulges and high-density environments requires a more general explanation. For instance, as discussed in greater detail in Kormendy's summary chapter, in dense environments galaxies are more likely to undergo mergers and gas that could otherwise be accreted to regrow a large disc remains suspended as hot, X-ray emitting gas. In low density environments, the galaxies experience fewer mergers, what mergers they do experience are more gas rich, and they are able to continually accrete additional gas from the cosmic web. In this scenario, stellar and AGN feedback could limit bulge-growth through mergers in general and especially at low masses while differences in the environment could account for the three orders of magnitude overlap in mass of disc and elliptical galaxies.

Unfortunately, the computational expense of simulating a broad sample of galaxies at resolutions high enough to resolve the bulge has made it extremely difficult to computationally study the connection between morphology and environment. Cosmological simulations that focus on individual galaxies are just beginning to

be able to resolve bulges, but there are far too few galaxies for population studies. In these simulations, the initial conditions are instead chosen to produce galaxies of the desired morphology. Generally, a quiescent merger history is picked to increase the probability of a galaxy with a low B/T forming. Additionally, embedding high resolution simulations in a dense environment increases the number of high resolution particles required, and drives up the computing costs.

Cosmological simulations of a volume of space (as opposed to a specific galaxy) can achieve larger numbers of galaxies but at the cost of resolution. For instance, Snyder et al. (2015) was able to roughly reproduce the relationship between galaxy morphology and overdensity but with a gravitational softening length of 710 pc, which is larger than most bulges and certainly insufficient for distinguishing pseudobulges from classical bulges. Tantalizingly, Sales et al. (2012) identified the alignment between the angular momentum of the accreting baryons and the galaxy disc as being a key factor in the morphology of galaxies. In galaxies where there was misalignment between the accreting gas and the disc, the net rotation of the galaxy was reduced and it was more likely to be a spheroid. In contrast, if the angular momentum of the accreting gas and existing disc had similar alignment, the galaxy was more likely to be a disc. Once again, though, the resolution was comparatively low (softening lengths of 500 pc) and these simulations are known to produce too many stars (Crain et al. 2009) and, seemingly, too many spheroids.

SAMs offer yet another avenue to examine the connection between galaxy morphology and environment and many of them have been able to reproduce the approximate environmental dependency (e.g. Baugh et al. 1996; Somerville and Primack 1999; Cole et al. 2000). However, recall that SAMs generally do not distinguish between classical and pseudobulges, limiting the reach of these results. Additionally, SAMs have typically been based off of idealized binary merger simulations, which tend to have much lower amounts of stellar feedback than cosmological simulations have found necessary. As SAMs become more nuanced in their modeling of bulges and as the results from larger samples of high-resolution cosmological simulations are analyzed and implemented into them, they will become all the more important for connecting galaxy morphology to environment.

Is it possible for bulge formation to be compatible with merger rates? Can we identify a redshift range over which the fraction of galaxies with classical bulges can be reproduced while simultaneously matching the small fraction of mass in pseudobulges? This remains to be seen. However, it is clear that mergers cannot simply form bulges as historically believed if CDM is the correct model. Despite the fact that a proper treatment of gas fractions can reproduce the number density of observed spheroids for $L^\star$ galaxies and smaller, these bulges always tend to reside on the massive side compared to observations and include too large a fraction of classical bulges. We must explore other options, and feedback-driven outflows generated during mergers are a natural choice for reducing the bulge formation.

References

Abadi M. G., Navarro J. F., Steinmetz M., Eke V. R., 2003, ApJ, 591, 499
Agertz O., Kravtsov A. V., 2015, ApJ, 804, 18
Agertz O., Kravtsov A. V., Leitner S. N., Gnedin N. Y., 2013, ApJ, 770, 25
Agertz O., Teyssier R., Moore B., 2011, MNRAS, 410, 1391
Aguerri J. A. L., Balcells M., Peletier R. F., 2001, A&A, 367, 428
Aguerri J. A. L., Elias-Rosa N., Corsini E. M., Muñoz Tuñón C., 2005, A&A, 434, 109
Andredakis Y. C., Peletier R. F., Balcells M., 1995, MNRAS, 275
Andredakis Y. C., Sanders R. H., 1994, MNRAS, 267, 283
Athanassoula E., 1992, MNRAS, 259, 345
Athanassoula E., 2005, MNRAS, 358, 1477
Aumer M., White S. D. M., Naab T., 2014, MNRAS, 441, 3679
Aumer M., White S. D. M., Naab T., Scannapieco C., 2013, MNRAS, 434, 3142
Barnes J. E., 1988, ApJ, 331, 699
Barnes J. E., Efstathiou G., 1987, ApJ, 319, 575
Barnes J. E., Hernquist L. E., 1991, ApJ, 370, L65
Barnes J. E., Hernquist L. E., 1996, ApJ, 471, 115
Baugh C. M., Cole S., Frenk C. S., 1996, MNRAS, 283, 1361
Binney J., Gerhard O., Silk J., 2001, MNRAS, 321, 471
Blitz L., Spergel D. N., 1991, ApJ, 379, 631
Bournaud F., Jog C. J., Combes F., 2005, A&A, 437, 69
Bournaud F. et al., 2014, ApJ, 780, 57
Bournaud F., 2015, Galactic Bulges, Springer
Brennan R. et al., 2015, MNRAS, 451, 2933
Brook C. B. et al., 2011, MNRAS, 415, 1051
Brook C. B., Kawata D., Gibson B. K., Freeman K. C., 2004, ApJ, 612, 894
Brook C. B., Stinson G. S., Gibson B. K., Roškar R., Wadsley J., Quinn T. R., 2012a, MNRAS, 419, 771
Brook C. B., Stinson G. S., Gibson B. K., Wadsley J., Quinn T. R., 2012b, MNRAS, 424, 1275
Brooks A. M., Zolotov A., 2014, ApJ, 786, 87
Bullock J. S., Dekel A., Kolatt T. S., Kravtsov A. V., Klypin A. A., Porciani C., Primack J. R., 2001, ApJ, 555, 240
Bundy K., Treu T., Ellis R. S., 2007, ApJ, 665, L5
Bureau M., 1998, PhD thesis, Australian National University
Bureau M., Freeman K. C., 1999, AJ, 118, 126
Carlberg R. G., 1986, ApJ, 310, 593
Carollo C. M., Scarlata C., Stiavelli M., Wyse R. F. G., Mayer L., 2007, ApJ, 658, 960
Ceverino D., Klypin A. A., 2009, ApJ, 695, 292
Ceverino D., Klypin A. A., Klimek E. S., Trujillo-Gomez S., Churchill C. W., Primack J. R., Dekel A., 2014, MNRAS, 442, 1545
Christensen C., Brooks A. M., Fisher D. B., Governato F., McCleary J., Quinn T. R., Shen S., Wadsley J., 2014a, Monthly Notices of the Royal Astronomical Society: Letters, 440, L51
Christensen C., Governato F., Quinn T. R., Brooks A. M., Shen S., McCleary J., Fisher D. B., Wadsley J., 2014b, MNRAS, 440, 2843
Christensen C., Quinn T. R., Governato F., Stilp A., Shen S., Wadsley J., 2012, MNRAS, 425, 3058
Cimatti A., Daddi E., Renzini A., 2006, A&A, 453, L29
Ciotti L., Lanzoni B., Volonteri M., 2007, ApJ, 658, 65
Cole S., Aragon-Salamanca A., Frenk C. S., Navarro J. F., Zepf S. E., 1994, MNRAS, 271
Cole S., Lacey C. G., Baugh C. M., Frenk C. S., 2000, MNRAS, 319, 168
Combes F., Debbasch F., Friedli D., Pfenniger D., 1990, A&A, 233, 82
Combes F., Dupraz C., Gerin M., 1990, International Conference on Dynamics and Interactions of Galaxies

Combes F., Sanders R. H., 1981, A&A, 96, 164
Courteau S., de Jong R. S., Broeils A. H., 1996, ApJ, 457
Crain R. A. et al., 2009, MNRAS, 399, 1773
Davé R., Oppenheimer B. D., Finlator K., 2011, MNRAS, 415, 11
De Lucia G., Fontanot F., Wilman D., Monaco P., 2011, MNRAS, 414, 1439
Deason A. J., Belokurov V., Evans N. W., Johnston K. V., 2013, ApJ, 763, 113
DeBuhr J., Quataert E., Ma C.-P., 2012, MNRAS, 420, 2221
DeBuhr J., Quataert E., Ma C.-P., Hopkins P. F., 2010, Monthly Notices of the Royal Astronomical Society: Letters, 406, no
Dekel A., Krumholz M. R., 2013, MNRAS, 432, 455
Di Cintio A., Brook C. B., Macciò A. V., Stinson G. S., Knebe A., Dutton A. A., Wadsley J., 2013, MNRAS, 437, 415
Di Matteo P. et al., 2014, A&A, 567, A122
D'Onghia E., Burkert A., 2004, ApJ, 612, L13
D'Onghia E., Burkert A., Murante G., Khochfar S., 2006, MNRAS, 372, 1525
Dutton A. A., 2009, MNRAS, 396, 121
Dutton A. A. et al., 2011, MNRAS, 26, no
Dutton A. A., van den Bosch F. C., 2009, MNRAS, 396, 141
Dutton A. A., van den Bosch F. C., 2012, MNRAS, 421, 608
Dwek E. et al., 1995, ApJ, 445, 716
Eliche-Moral M. C., Balcells M., Aguerri J. A. L., González-García A. C., 2006, A&A, 457, 91
Ellison S. L., Mendel J. T., Patton D. R., Scudder J. M., 2013, MNRAS, 435, 3627
Ellison S. L., Patton D. R., Simard L., McConnachie A. W., 2008, AJ, 135, 1877
Emsellem E., Greusard D., Combes F., Friedli D., Leon S., Pécontal E., Wozniak H., 2001, A&A, 368, 52
Erwin P. et al., 2014, MNRAS, 446, 4039
Faber S. M., Jackson R. E., 1976, ApJ, 204, 668
Fakhouri O., Ma C.-P., 2008, MNRAS, 386, 577
Fakhouri O., Ma C.-P., Boylan-Kolchin M., 2010, MNRAS, 406, 2267
Falcón-Barroso J. et al., 2006, MNRAS, 369, 529
Fisher D. B., 2006, ApJ, 642, L17
Fisher D. B., Drory N., 2008, AJ, 136, 773
Fisher D. B., Drory N., 2010, ApJ, 716, 942
Fisher D. B., Drory N., 2011, ApJ, 733, L47
Gadotti D. A., 2009, MNRAS, 393, 1531
Ganda K. et al., 2007, MNRAS, 380, 506
Geha M. C., Blanton M. R., Masjedi M., West A. A., 2006, ApJ, 653, 240
Genel S., Genzel R., Bouché N., Naab T., Sternberg A., 2009, ApJ, 701, 2002
Genzel R. et al., 2008, ApJ, 687, 59
Gilbert K. M. et al., 2014, ApJ, 796, 21
Gnedin N. Y., 2000, ApJ, 542, 535
Governato F. et al., 2009, MNRAS, 398, 312
Governato F. et al., 2010, Nature, 463, 203
Governato F. et al., 2004, ApJ, 607, 688
Governato F., Willman B., Mayer L., Brooks A. M., Stinson G. S., Valenzuela O., Wadsley J., Quinn T. R., 2007, MNRAS, 374, 1479
Governato F. et al., 2012, MNRAS, 12, 1
Guedes J., Callegari S., Madau P., Mayer L., 2011, ApJ, 742, 12
Guedes J., Mayer L., Carollo C. M., Madau P., 2013, ApJ, 772, 36
Hammer F., Flores H., Puech M., Yang Y. B., Athanassoula E., Rodrigues M., Delgado R., 2009, A&A, 507, 1313
Hammer F., Puech M., Chemin L., Flores H., Lehnert M. D., 2007, ApJ, 662, 322
Harfst S., Theis C., Hensler G., 2006, A&A, 449, 509
Hernquist L. E., 1989, Nature, 340, 687

Hernquist L. E., 1992, ApJ, 400, 460
Hopkins P. F. et al., 2010, ApJ, 715, 202
Hopkins P. F., Cox T. J., Younger J. D., Hernquist L. E., 2009a, ApJ, 691, 1168
Hopkins P. F., Hernquist L. E., Cox T. J., Dutta S. N., Rothberg B., 2008, ApJ, 679, 156
Hopkins P. F., Kereš D., Onorbe J., Faucher-Giguere C.-A., Quataert E., Murray N., Bullock J. S., 2014, MNRAS, 445, 581
Hopkins P. F., Quataert E., Murray N., 2011, MNRAS, 417, 950
Hopkins P. F. et al., 2009b, MNRAS, 397, 802
Howard C. D. et al., 2009, ApJ, 702
Hozumi S., Burkert A., Fujiwara T., 2000, MNRAS, 311, 377
Hultman J., Pharasyn A., 1999, A&A
Jesseit R., Cappellari M., Naab T., Emsellem E., Burkert A., 2009, MNRAS, 397, 1202
Jogee S. et al., 2009, ApJ, 697, 1971
Kannan R. et al., 2013, MNRAS, 437, 2882
Katz N., 1992, ApJ, 391, 502
Katz N., Quinn T. R., Bertschinger E., Gelb J. M., 1994, MNRAS, 270
Kauffmann G., White S. D. M., Guiderdoni B., 1993, MNRAS, 264
Kautsch S. J., Gallagher J. S., Grebel E. K., 2009, Astronomische Nachrichten, 330, 1056
Keller B. W., Wadsley J., Benincasa S. M., Couchman H. M. P., 2014, MNRAS, 442, 3013
Kennicutt, Robert C. J., 1998, ApJ, 498, 541
Kereš D., Katz N., Davé R., Fardal M. A., Weinberg D. H., 2009, MNRAS, 396, 2332
Keselman J. A., Nusser A., 2012, MNRAS, 424, 1232
Kormendy J., 1977, ApJ, 218, 333
Kormendy J., 1993, Galactic bulges: proceedings of the 153rd Symposium of the International Astronomical Union held in Ghent
Kormendy J., 1999, Galaxy Dynamics, 182
Kormendy J., Bender R., 2012, ApJS, 198, 2
Kormendy J., Bender R., Cornell M. E., 2011, Nature, 469, 374
Kormendy J., Drory N., Bender R., Cornell M. E., 2010, ApJ, 723, 54
Kormendy J., Fisher D. B., 2008, Formation and Evolution of Galaxy Discs ASP Conference Series, 396
Kormendy J., Fisher D. B., Cornell M. E., Bender R., 2009, ApJS, 182, 216
Kormendy J., Freeman K. C., 2014, ArXiv e-prints:1411.2170
Kormendy J., Ho L. C., 2013, ARA&A, 51, 511
Kormendy J., Kennicutt, Robert C. J., 2004, ARA&A, 42, 603
Krajnović D. et al., 2013, MNRAS, 433, 2812
Krumholz M. R., Thompson T. A., 2012, ApJ, 760, 155
Krumholz M. R., Thompson T. A., 2013, MNRAS, 434, 2329
Kuijken K., Merrifield M. R., 1995, ApJ, 443, L13
Larson R. B., Tinsley B. M., 1978, ApJ, 219, 46
Laurikainen E., Salo H., Athanassoula E., Bosma A., Herrera-Endoqui M., 2014, Monthly Notices of the Royal Astronomical Society: Letters, 444, 5
Laurikainen E., Salo H., Buta R., Knapen J. H., 2011, MNRAS, 418, 1452
Laurikainen E., Salo H., Buta R., Knapen J. H., Comerón S., 2010, MNRAS, 405, 1089
Lopez L. A., Krumholz M. R., Bolatto A. D., Prochaska J. X., Ramirez-Ruiz E., Castro D., 2014, ApJ, 795, 121
Lotz J. M., Jonsson P., Cox T. J., Croton D., Primack J. R., Somerville R. S., Stewart K. R., 2011, ApJ, 742, 103
Lütticke R., Dettmar R.-J., Pohlen M., 2000, A&AS, 145, 405
Lynden-Bell D., 1967, MNRAS, 136
Maller A. H., Dekel A., 2002, MNRAS, 335, 487
Maller A. H., Katz N., Kereš D., Dave R., Weinberg D. H., 2006, ApJ, 647, 763
Marinacci F., Pakmor R., Springel V., 2013, MNRAS, 437, 1750

Marquez I., Masegosa J., Durret F., Gonzalez Delgado R. M., Moles M., Maza J., Pérez E., Roth M., 2003, A&A, 409, 459
Marri S., White S. D. M., 2003, MNRAS, 345, 561
Martin C. L., 2005, ApJ, 621, 227
Martin C. L., Kennicutt, Robert C. J., 2001, ApJ, 555, 301
Martizzi D., Teyssier R., Moore B., 2013, MNRAS, 432, 1947
Matteucci F., 2006, ArXiv e-prints:astro.ph.10832
McKee C. F., Ostriker J. P., 1977, ApJ, 218, 148
Méndez-Abreu J., Debattista V. P., Corsini E. M., Aguerri J. A. L., Mendez-Abreu J., Debattista V. P., Corsini E. M., Aguerri J. A. L., 2014, A&A, 572, A25
Mihos J. C., Hernquist L. E., 1994, ApJ, 437, L47
Mollitor P., Nezri E., Teyssier R., 2014, MNRAS, 447, 1353
Moorthy B. K., Holtzman J. A., 2006, MNRAS, 371, 583
Moster B. P., Macciò A. V., Somerville R. S., Johansson P. H., Naab T., 2010, MNRAS, 403, 1009
Moster B. P., Macciò A. V., Somerville R. S., Naab T., Cox T. J., 2012, MNRAS, 423, 2045
Munshi F. et al., 2013, ApJ, 766, 56
Muratov A. L., Keres D., Faucher-Giguere C. -A., Hopkins P. F., Quataert E., Murray N., 2015, eprint arXiv:1501.03155
Murray N., Ménard B., Thompson T. A., 2011, ApJ, 735, 66
Murray N., Quataert E., Thompson T. A., 2005, ApJ, 618, 569
Naab T., Johansson P. H., Ostriker J. P., Efstathiou G., 2007, ApJ, 658, 710
Navarro J. F. et al., 2010, MNRAS, 402, 21
Navarro J. F., Steinmetz M., 2000, ApJ, 538, 477
Navarro J. F., White S. D. M., 1994, MNRAS, 267, 401
Negroponte J., White S. D. M., 1983, MNRAS, 205, 1009
Nipoti C., Treu T., Auger M. W., Bolton A. S., 2009, ApJ, 706, L86
Noguchi M., 1988, A&A, 203, 259
Nowak N., Thomas J., Erwin P., Saglia R. P., Bender R., Davies R. I., 2010, MNRAS, 403, 646
Okamoto T., 2013, MNRAS, 428, 718
Okamoto T., Eke V. R., Frenk C. S., Jenkins A., 2005, MNRAS, 363, 1299
Okamoto T., Gao L., Theuns T., 2008, MNRAS, 390, 920
Oser L., Naab T., Ostriker J. P., Johansson P. H., 2012, ApJ, 744, 63
Ostriker J. P., 1980, Comments on Astrophysics, 8
Parry O. H., Eke V. R., Frenk C. S., 2009, MNRAS, 396, 1972
Peebles P. J. E., Nusser A., 2010, Nature, 465, 565
Peletier R. F. et al., 2007, MNRAS, 379, 445
Perez J., Valenzuela O., Tissera P. B., Michel-Dansac L., 2013, MNRAS, 436, 259
Pfenniger D., Norman C. A., 1990, ApJ, 363, 391
Pillepich A., Madau P., Mayer L., 2015, ApJ, 799, 184
Piontek F., Steinmetz M., 2011, MNRAS, 410, 2625
Pontzen A., Governato F., 2012, MNRAS, 421, 3464
Porter L. A., Somerville R. S., Primack J. R., Johansson P. H., 2014, MNRAS, 444, 942
Power C., Navarro J. F., Jenkins A., Frenk C. S., White S. D. M., Springel V., Stadel J. G., Quinn T. R., 2003, MNRAS, 338, 14
Puech M., Hammer F., Hopkins P. F., Athanassoula E., Flores H., Rodrigues M., Wang J. L., Yang Y. B., 2012, ApJ, 753, 128
Purcell C. W., Bullock J. S., Kazantzidis S., 2010, MNRAS, 404, 1711
Quinn T. R., Katz N., Efstathiou G., 1996, MNRAS, 278, L49
Raha N., Sellwood J. A., James R. A., Kahn F. D., 1991, Nature, 352, 411
Renzini A., 1999, The formation of galactic bulges / edited by C.M. Carollo
Renzini A., 2006, ARA&A, 44, 141
Robertson B. E., Bullock J. S., Cox T. J., Di Matteo T., Hernquist L. E., Springel V., Yoshida N., 2006, ApJ, 645, 986
Robertson B. E., Yoshida N., Springel V., Hernquist L. E., 2004, ApJ, 606, 32

Roškar R., Teyssier R., Agertz O., Wetzstein M., Moore B., 2014, MNRAS, 444, 2837
Saitoh T. R., Daisaka H., Kokubo E., Makino J., Okamoto T., Tomisaka K., Wada K., Yoshida N., 2008, PASJ, 60, 667
Sales L. V., Marinacci F., Springel V., Petkova M., 2014, MNRAS, 439, 2990
Sales L. V., Navarro J. F., Theuns T., Schaye J., White S. D. M., Frenk C. S., Crain R. A., Dalla Vecchia C., 2012, MNRAS, 423, 1544
Sanders D. B., Mirabel I. F., 1985, ApJ, 298, L31
Sanders D. B., Scoville N. Z., Soifer B. T., Young J. S., Danielson G. E., 1987, ApJ, 312, L5
Sawala T., Frenk C. S., Crain R. A., Jenkins A., Schaye J., Theuns T., Zavala J., 2013, MNRAS, 431, 1366
Scannapieco C., Gadotti D. A., Jonsson P., White S. D. M., 2010, Monthly Notices of the Royal Astronomical Society: Letters, 407, L41
Scannapieco C., Tissera P. B., White S. D. M., Springel V., 2008, MNRAS, 389, 1137
Scannapieco C., White S. D. M., Springel V., Tissera P. B., 2009, MNRAS, 396, 696
Scarlata C. et al., 2007, ApJS, 172, 494
Sharma M., Nath B. B., 2012, ApJ, 750, 55
Shen J., Rich R. M., Kormendy J., Howard C. D., De Propris R., Kunder A., 2010, ApJ, 720, L72
Silverman J. D. et al., 2008, ApJ, 679, 118
Snyder G. F. et al., 2015, ArXiv e-prints:1502.07747
Somerville R. S., Davé R., 2015, ARA&A, 53
Somerville R. S., Primack J. R., 1999, MNRAS, 310, 1087
Springel V., Di Matteo T., Hernquist L. E., 2005, MNRAS, 361, 776
Steinmetz M., Navarro J. F., 1999, ApJ, 513, 555
Stewart K. R., Bullock J. S., Wechsler R. H., Maller A. H., 2009, ApJ, 702, 307
Stewart K. R., Bullock J. S., Wechsler R. H., Maller A. H., Zentner A. R., 2008, ApJ, 683, 597
Stinson G. S., Brook C. B., Macciò A. V., Wadsley J., Quinn T. R., Couchman H. M. P., 2012, MNRAS, 428, 129
Stinson G. S., Seth A., Katz N., Wadsley J., Governato F., Quinn T. R., 2006, MNRAS, 373, 1074
Tacconi L. J. et al., 2010, Nature, 463, 781
Terlevich R. J., 1998, MNRAS, 293, L49
Teyssier R., Pontzen A., Dubois Y., Read J. I., 2013, MNRAS, 429, 3068
Thacker R. J., Couchman H. M. P., 2000, ApJ, 545, 728
Thoul A. A., Weinberg D. H., 1996, ApJ, 465, 608
Toomre A., 1977, Evolution of Galaxies and Stellar Populations
Toomre A., Toomre J., 1972, ApJ, 178, 623
Trenti M., Bertin G., van Albada T. S., 2005, A&A, 433, 57
Trujillo-Gomez S., Klypin A. A., Colin P., Ceverino D., Arraki K. S., Primack J. R., 2014, MNRAS, 446, 1140
Übler H., Naab T., Oser L., Aumer M., Sales L. V., White S. D. M., 2014, MNRAS, 443, 2092
van Albada T. S., 1982, MNRAS, 201, 939
van den Bosch F. C., 2001, MNRAS, 327, 1334
van den Bosch F. C., Abel T., Croft R. a. C., Hernquist L. E., White S. D. M., 2002, ApJ, 576, 21
van den Bosch F. C., Burkert A., Swaters R. A., 2001, MNRAS, 326, 1205
van Dokkum P. G. et al., 2013, ApJ, 771, L35
Veilleux S., Cecil G., Bland-Hawthorn J., 2005, ARA&A, 43, 769
Vogelsberger M., Genel S., Sijacki D., Torrey P., Springel V., Hernquist L. E., 2013, MNRAS, 436, 3031
Wadsley J., Stadel J. G., Quinn T. R., 2004, New Astronomy, 9, 137
Weiner B. J. et al., 2009, ApJ, 692, 187
Weinzirl T., Jogee S., Khochfar S., Burkert A., Kormendy J., 2009, ApJ, 696, 411
Weiss A., Peletier R. F., Matteucci F., 1995, A&A, 296, 73
White S. D. M., 1984, ApJ, 286, 38
White S. D. M., Rees M. J., 1978, MNRAS, 183, 341
Wise J. H., Abel T., Turk M. J., Norman M. L., Smith B. D., 2012, MNRAS, 427, 311

Yoshino A., Yamauchi C., 2015, MNRAS, 446, 3749
Young J. S., Kenney J. D., Lord S. D., Schloerb F. P., 1984, ApJ, 287, L65
Zavala J., Okamoto T., Frenk C. S., 2008, MNRAS, 387, 364
Zhang D., Thompson T. A., 2012, MNRAS, 424, 1170
Zolotov A. et al., 2012, ApJ, 761, 71
Zolotov A., Willman B., Brooks A. M., Governato F., Brook C. B., Hogg D. W., Quinn T. R., Stinson G. S., 2009, ApJ, 702, 1058

Chapter 13
Bulge Growth Through Disc Instabilities in High-Redshift Galaxies

Frédéric Bournaud

Abstract The role of disc instabilities, such as bars and spiral arms, and the associated resonances, in growing bulges in the inner regions of disc galaxies have long been studied in the low-redshift nearby Universe. There it has long been probed observationally, in particular through peanut-shaped bulges (Chap. 14). This secular growth of bulges in modern disc galaxies is driven by weak, non-axisymmetric instabilities: it mostly produces pseudobulges at slow rates and with long star-formation timescales. Disc instabilities at high redshift ($z > 1$) in moderate-mass to massive galaxies (10^{10} to a few 10^{11} $M_\odot$ of stars) are very different from those found in modern spiral galaxies. High-redshift discs are globally unstable and fragment into giant clumps containing 10^{8-9} $M_\odot$ of gas and stars each, which results in highly irregular galaxy morphologies. The clumps and other features associated to the violent instability drive disc evolution and bulge growth through various mechanisms on short timescales. The giant clumps can migrate inward and coalesce into the bulge in a few 10^8 years. The instability in the very turbulent media drives intense gas inflows toward the bulge and nuclear region. Thick discs and supermassive black holes can grow concurrently as a result of the violent instability. This chapter reviews the properties of high-redshift disc instabilities, the evolution of giant clumps and other features associated to the instability, and the resulting growth of bulges and associated sub-galactic components.

13.1 Introduction

High-redshift star-forming galaxies mostly form stars steadily over long timescales, merger-driven starbursts being only a minority of galaxies. At redshifts $z > 1$, moderate-mass and massive star-forming galaxies (10^{10} to a few 10^{11} $M_\odot$ of stars) have rapid gas consumption timescales and stellar mass doubling timescales, of the

F. Bournaud (✉)
Laboratoire AIM Paris-Saclay, CEA/IRFU/SAp, CNRS/INSU, Université Paris Diderot, 91191 Gif-sur-Yvette Cedex, France
e-mail: frederic.bournaud@cea.fr

E. Laurikainen et al. (eds.), *Galactic Bulges*, Astrophysics and Space Science Library 418, DOI 10.1007/978-3-319-19378-6_13

order of a Gyr at $z = 2$, depending mostly on redshift and weakly depending on mass, with rare deviations to the mean timescale (Schreiber et al. 2014).

These star-forming galaxies have very irregular morphologies in the optical, especially compared to nearby spirals discs of similar mass, as unveiled by deep surveys over the last two decades. They also have very high gas fractions, about 50 % of their baryonic mass, as probed recently with interferometric studies. The high gas fractions and mass densities cause strong gravitational instabilities in the galactic discs, which results in disc fragmentation, and causes very irregular, clumpy morphologies. These irregular morphologies are often dominated by a few giant clumps of 10^{8-9} $M_\odot$ of baryons, rotating along with the host galaxy.

This violent instability can drive the formation and growth of bulges, either by inward migration and central coalescence of the giant clumps and/or by gravitational torquing of gas and instability-driven inflows. This Chapter reviews the properties of the violent instabilities, and the pieces of evidence that the clumpy morphologies are caused by such violent disc instability rather than mergers or other processes. It then reviews the evolution of the giant clumps, their response to intense star formation and associated feedback processes, and the properties of bulges formed through this process. It eventually reviews recent results on other sub-galactic structures (such as thick discs and central black holes), which may grow concomitantly to bulges through high-redshift disc instabilities, and compares the role of this high-redshift violent instability to the contribution of low-redshift secular evolution through weak instabilities such bars and spiral arms.

13.2 Clumpy Galaxies and the Violent Disc Instability at High Redshift

This section reviews the properties of star-forming galaxies at high redshift, the observed signatures of the underlying disc instabilities, and the main related theories. Throughout, we consider galaxies at redshift $z \approx 1-3$, with stellar masses of 10^{10} to a few 10^{11} $M_\odot$, and that are "normally" star forming on the so-called Main Sequence (Daddi et al. 2007; Elbaz et al. 2011; Schreiber et al. 2014), i.e. with specific star formation rates of the order of a Gyr^{-1} at redshift $z = 2$, as opposed to rare starbursts with faster star formation.

13.2.1 Clumpy Galaxies at Redshift 1–3: Global Morphology

The characterization of the structure of star-forming galaxies at high redshift has steadily developed over the last two decades, driven mainly by deep surveys from the Hubble Space Telescope (HST) in the optical wavelengths (e.g. Cowie et al. 1996), and later-on in the near-infrared, but also accompanied by modern techniques

to identify and select star-forming galaxies in these deep surveys (e.g. Daddi et al. 2004). The highly irregular structure of high-redshift galaxies was first pointed out in the Hubble Deep Field (Abraham et al. 1996; van den Bergh et al. 1996; Cowie et al. 1996). Star-forming galaxies appeared to have highly irregular morphologies, dominated by a few bright patches, with the striking example of the so-called "chain galaxies" where the patches are almost linearly aligned. While reminiscent of nearby dwarf irregulars, these morphologies where found in galaxies 10–100 times more massive – a mass regime at which nearby galaxies are almost exclusively regular disc-dominated galaxies, most often barred spirals (Eskridge et al. 2000; Block et al. 2002), or spheroid-dominated early type galaxies. The lack of regular barred spirals, suspected in such deep optical imaging surveys (van den Bergh et al. 1996; Abraham et al. 1999), actually required deep-enough near-infrared surveys to be confirmed: otherwise the irregular structure could result from band-shifting effects, namely the fact that optical observations of $z > 1$ objects probe the ultra-violet emission, strongly dominated by young star-forming regions, rather than the underlying mass distribution dominated by older stars. The first near-infrared surveys unveiled counterexamples of high-redshift galaxies with a more regular disc structure in the underlying older stellar populations (Sheth et al. 2003), yet deeper and wider fields eventually confirmed the gradual disappearance of regular (barred) spiral discs at $z > 0.7 - 1.0$ (Sheth et al. 2008; Cameron et al. 2010; Melvin et al. 2014; Simmons et al. 2014).

Even before infrared data could resolve kiloparsec-scale structures at $z = 2$, detailed spatially-resolved stellar population studies were used to reconstruct the stellar mass distribution of star-forming galaxies, in particular in the Hubble Ultra Deep Field (Fig. 13.1). It was then found that the bright patches dominating the optical structure were not just random or transient associations of bright stars, but actually massive clumps with sizes in the 100–1000 pc range, stellar masses of a few 10^8 to, in extreme cases, a few $10^9\,M_\odot$, and typical stellar ages of a few 10^8 year indicating relatively young ages (and in particular younger than those of the host galaxies) but suggesting lifetimes that are longer than their internal dynamical timescale (about 10–20 Myr). As random associations would disrupt on such timescales, these data suggested that these bright regions were bound (Elmegreen et al. 2005, 2007). These structures are generally dubbed "giant clumps", and their host galaxies "clumpy galaxies", although these are just the majority of star-forming galaxies at redshift 1–3 and the clumpiness is not a peculiar property of a rare type of galaxy. The morphology of clumpy galaxies suggested that these were disc galaxies, based in particular on the distribution of axis ratios from face-on to edge-on orientations (Elmegreen et al. 2004; Elmegreen and Elmegreen 2006), although the morphology of chain galaxies could have been consistent also with filamentary alignments of separate small galaxies rather than edge-on clumpy discs (Taniguchi and Shioya 2001).

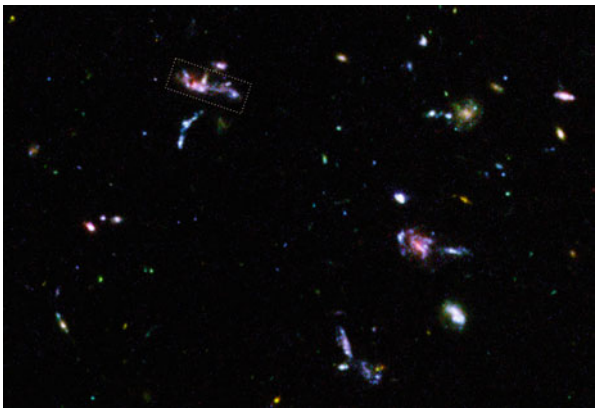

Fig. 13.1 Portion of the Hubble Ultra Deep Field (optical survey) showing more than 10 star-forming galaxies at $z = 1 - 3$ with stellar masses of a few $10^{10}\,M_\odot$ (largest galaxies on the image). The galaxy in the *dashed rectangle* is a typical example of a Main Sequence galaxy about the mass of the Milky Way, located at redshift $z \simeq 1.6$. Its two apparent neighbors lie at very different redshifts. Like many galaxies in this mass and redshift range, it has a very irregular clumpy morphology, with a central reddish bulge and a few clumps of $10^{8-9}\,M_\odot$ each. Only the clump to the right of the center is somewhat redder and contains old stellar populations, and only this particular clump might be a minor merger of an external galaxy. The others formed in-situ by gravitational instability in a gas-rich turbulent disc (Bournaud et al. 2008) and follow a regular rotation pattern around the mass center. The violent instability in the gas-rich medium can also trigger the asymmetry of the galaxy through an $m = 1$ mode, without requiring an external tidal interaction

13.2.2 Kinematics and Nature of Clumpy Galaxies

More robust studies of the nature of clumpy star-forming galaxies were enabled by spatially-resolved spectroscopy of the ionized gas, probing the gas kinematics (velocity field, velocity dispersion) as well as chemical abundances and gradients in the interstellar medium. The pioneering study of Genzel et al. (2006) probed the disc-like nature of one typical star-forming galaxy at redshift two, with a disc-like velocity field, and no signature of an on-going or recent merger, in spite of an irregular and clumpy morphology. In a single particular case, a merger might happen to have a velocity field that resembles that of a disc, with no observable kinematic signature of the merging event, depending on the interaction orbit and on the observer's line-of-sight. However, surveys of tens of star-forming galaxies have now been assembled (Förster Schreiber et al. 2006, 2009; Epinat et al. 2012) and quantitative techniques have been used to interpret the velocity field structure and velocity dispersions of the observed systems (Shapiro et al. 2008). These studies confirmed that only a minority of clumpy galaxies display potential signatures from mergers, and that clumpier galaxies do not harbor more frequent signatures of recent or on-going mergers than smoother galaxies in the same mass range.

The velocity dispersions are high, typically about $50\,\mathrm{km\,s^{-1}}$ with large spatial variations for the Hα gas (e.g., Genzel et al. 2008; Bournaud et al. 2008). Yet, they remain fully consistent with the large scale heights expected for these discs if chain galaxies, which are relatively thick, are the edge-on version of clumpy disc galaxies (Elmegreen and Elmegreen 2006). There are also local irregularities in the velocity field, departing from pure rotation with non circular motions up to 20–$50\,\mathrm{km\,s^{-1}}$, a few times larger than in nearby spirals, but again this is naturally expected from the presence of giant clumps: independently of their origin, massive clumps do stir the surrounding material by gravitational and hydrodynamic interactions, and they also interact with each other. Models of rotating galactic discs with massive clumps do predict such large non-circular motions on kiloparsec scales even when the disc is purely rotating before clump formation (Bournaud et al. 2008).

Parametric classifications of galaxy morphology have long been based on low-redshift data and models are tuned to represent the low-redshift Universe. Such classifications are now started to be tuned also for high-redshift galaxies, and are optimized to avoid confusion between internal clumps and mergers. Such morphological classifications confirm the "clumpy disc" nature of the majority of Main Sequence star forming galaxies (Fig. 13.2) and show close agreement with kinematic classifications (Cibinel et al. 2015).

Signatures of mergers might be more prominent in clumpy galaxies at intermediate redshifts ($z = 0.5-1$), according for instance to Puech (2010). This is a regime in which clumpy galaxies are more rare among star-forming galaxies, most of which have already started to establish a regular barred spiral structure (in the mass range considered here – see Sheth et al. 2008; Kraljic et al. 2012) and have much lower gas fractions and densities (Combes et al. 2013). Merger-induced clump formation may then become more prominent compared to higher redshifts. We also note that these clumps have lower masses so their dynamical impact may be weaker, their response to stellar feedback being likely different, and their role in disc and bulge evolution being potentially different as well. For these reasons the relatively rare clumpy galaxies below $z \simeq 1$ will not be considered hereafter.

13.2.3 Observational Insights on the Nature of Giant Clumps: Gas Content and Stellar Populations

The very nature of clumps and their formation process remain uncertain, in spite of the fact that their host galaxies are generally rotating discs, with a low frequency of mergers. Namely, are these structures formed in-situ, or do they originate from the outside, in the form of small companion galaxies that have been accreted, or clumps of primordial gas that were accreted by the host galaxy before starting to form stars?

The hypothesis of external star-free gas clouds might be ruled-out by the high average density of gas in the clumps (hundreds of atoms or molecules per $\mathrm{cm^3}$, e.g. Elmegreen and Elmegreen 2005) making star formation efficient. This effect would

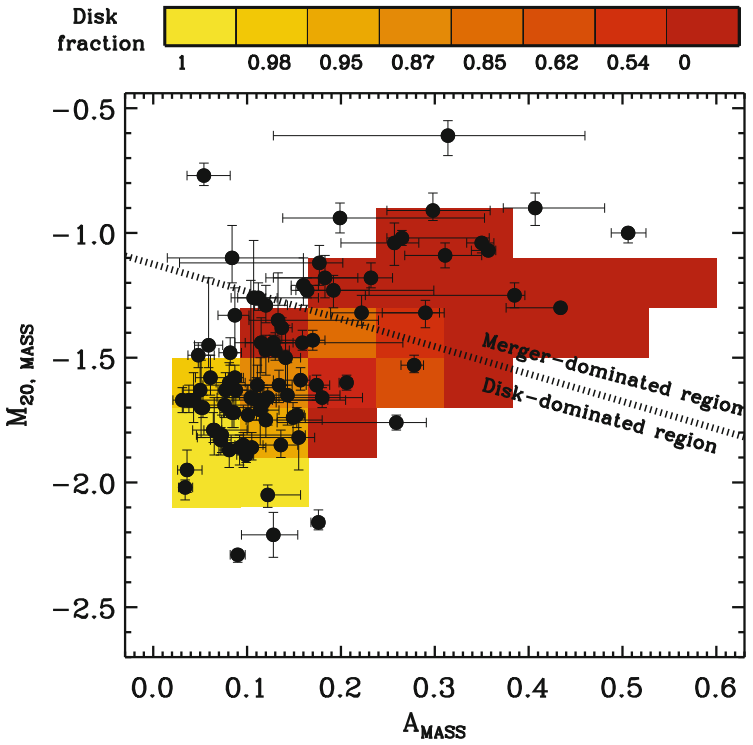

Fig. 13.2 Morphological classification of discs and mergers at $z \simeq 2$ (Cibinel et al. 2015). Combining the Asymmetry A (Conselice et al. 2003) and the M_{20} parameter (Lotz et al. 2004), measured on stellar mass maps, is the most efficient way to distinguish clumpy irregular discs and genuine mergers. The probability of being a disc or a merger according to these parameters is coded using the background colours (note that the scale is logarithmic so discs strongly dominate all colour bins, except the last one). The *black symbols* show a mass-limited sample of star-forming galaxies at $z \sim 2$ in this $A - M_{20}$ plane (Cibinel et al. 2015). About two thirds of these objects are secure discs, and many others have a high probability of being a disc. The disc fraction is even larger when the sample is limited to Main Sequence galaxies, excluding the starbursts. Kinematic classifications by Förster Schreiber et al. (2009) are in close agreement with this morphological classification, when applied to the same galaxies (Figure courtesy of Anna Cibinel)

be increased by the presence of dense substructures, which are likely to arise given the high observed turbulent velocity dispersions (Padoan et al. 1999).

Testing the hypothesis of clumps coming from the outside as small companion galaxies joining a massive galactic disc through dynamical friction requires deep imaging, to be examined through stellar population studies at the scale of individual clumps (Förster Schreiber et al. 2011; Wuyts et al. 2012; Elmegreen et al. 2009). The vast majority of clumps appear younger than expected for small external galaxies at the same redshift. Although the young stellar content of giant clumps may bias the age estimates by outshining the older stellar populations, the comparison with small galaxies at the same redshift shows that the clumps are significantly younger than

small galaxies. Many clumps have estimated stellar ages of only about 100 Myr with no underlying old stellar populations, although such populations would be detectable in small galaxies.

If the clumps really form in-situ in their host galaxy, one should in theory sometimes capture the formation of the clumps during their first internal dynamical timescale (≤ 20 Myr), and hence some clumps should have extremely young ages (about 10 Myr only). However, stellar population studies with broadband imaging with no spectroscopy cannot robustly distinguish such very young ages (Wuyts et al. 2012). Such candidates have recently been identified with deep imaging and spectroscopy (Zanella et al. 2015). Considering the merging of small external galaxies, around a central galaxy of a few 10^{10} $M_\odot$ of stars, a small companion of about 10^9 $M_\odot$ should be found within a projected distance of 10 kpc for about one third of galaxies.[1] If this satellite has not been fully disrupted by the galactic tides, its nucleus should be observed as a giant clump.[2] Such "ex-situ" clumps, with older average stellar ages and an underlying old population, are indeed found in some cases. For instance, a representative clumpy galaxy dissected in Bournaud et al. (2008) contains one clump which is much redder and older than the others, and also exhibits a larger deviation from the underlying disc velocity field, making external origin most likely for this one. Other candidates are found in Förster Schreiber et al. (2011) and appear also in the statistics of Wuyts et al. (2012). Nevertheless, such ex-situ clumps remain relatively rare: most observed clumps are actually different, with younger stellar ages (Elmegreen et al. 2009; Bournaud et al. 2008; Wuyts et al. 2012). The ability to identify such ex-situ clumps is actually reassuring that the non-detection of such old populations in the other clumps is robust, and probes their recent in-situ formation.

Since most of the clumps formed recently inside their host galaxy, and given that they are gravitationally bound (based on the observed stellar masses and velocity dispersions, e.g., Elmegreen et al. 2005; Genzel et al. 2008), their formation likely involves a gravitational (Jeans) instability in a rotating disc, sometimes also called Toomre instability. For such instabilities, leading to the formation of bound objects in a rotating disc to arise, the key requirement is that the Toomre (1964) parameter Q below unity.[3] Based on the observed rotation velocities and velocity dispersions (see previous sections) this typically requires gas density of the order of 100 $M_\odot$ pc^{-2}, an order of magnitude larger than in nearby disc galaxies. This implies interstellar gas masses comparable to the stellar masses, i.e. gas mass fractions of about 50 %

[1] This estimate is simply based on the mass function of galaxies and assuming a random geometrical distribution of satellites within the virial radius.

[2] With a kinematics that could become preferentially consistent with that of the host galaxy disc through gravity torques and dynamical friction within one galactic dynamical time, i.e. about 100 Myr.

[3] Although the Toomre Q parameter is strictly meaningful only in an axisymmetric disc before strong perturbations arise. Note also that in a thick disc the instability limit is about 0.7 rather than $Q < 1$ (Behrendt et al. 2014, and references therein).

of the baryonic mass. Such high gas densities had long been found in the strongest starbursts galaxies (likely merger-induced) at all redshifts (e.g., Tacconi et al. 2008), but not in normal star-forming galaxies. The discovery that Main Sequence galaxies at redshift $z > 1$ are actually very gas-rich with gas fractions of about 50 %, just counting the molecular content (Daddi et al. 2008, 2010; Tacconi et al. 2010, 2013), has shed a new light on this issue. These high gas fractions are estimated from CO line observations, and hence are subject to uncertainties on the conversion of CO luminosity to H_2 mass. Yet, new data probing the CO molecule spectral line energy distribution (Daddi et al. 2015), compared to detailed modelling of the CO excitation and emission in high-redshift galaxies (Bournaud et al. 2015), confirm high luminosity-to-mass conversion ratios and high gas mass fractions. Furthermore, the high gas fractions are also confirmed by independent estimates based on dust properties (Sargent et al. 2014; Magnelli et al. 2014; Genzel et al. 2014).

Hence, the high inferred gas surface densities lead to Toomre Q parameters around unity for velocity dispersions of 30–50 km s^{-1}. The Toomre parameter would be even lower if the velocity dispersions were only a few km s^{-1} as is the case in nearby spirals, in which case the axisymmetric gravitational instability would arise. All numerical experiments modeling discs with masses, sizes and gas fractions, representative for the high-redshift star-forming galaxies discussed above do show clump formation through gravitational instability (see Noguchi 1999; Immeli et al. 2004a; Bournaud et al. 2007, and the more detailed models discussed hereafter). The gravitational stirring of the gas ensures that the turbulent velocity dispersions do not stay below the observed level of $\sim$50 km s^{-1}. Namely, the gas turbulent motions may also be powered by infall and stellar feedback, as we will review in the next sections. But at least the release of gravitational energy through the instability is sufficient to maintain high turbulent dispersions and self-regulate the disc at a Toomre parameter $Q \simeq 1$.

The high velocity dispersions imply that the Jeans mass (or Toomre mass) is high, typically $10^8 - 10^9\,M_\odot$. This sets the high mass of the giant clumps forming through the associated instability. The properties of the instability in these discs was also modeled through analytic models by Dekel et al. (2009b), with results in close agreement with those of numerical models, but using simpler analytic estimates. The giant clumps with a high characteristic masses observed in high-redshift galaxies, can thus be considered as the direct outcome of the disc instability. This is robustly expected from the basic observed properties (mass, size, rotation speed and gas fraction) of these high-redshift galaxies. This probably applies to most of the observed giant clumps, except the few ex-situ clump (minor merger) candidates with older stellar ages (see above). Note that the gravitational instability actually arises in a two-component disc with roughly half of its mass in gas, and half in stars: we refer the reader to Jog (1996) and Elmegreen (2011) for theoretical work on the two-component stability, and Behrendt et al. (2014) for a detailed analysis of the disc stability in numerical simulations. The process is qualitatively unchanged compared to the $Q \simeq 1$ self-regulated instability in a single-component disc described above. Furthermore the gaseous and stellar velocity dispersions are

probably nearly similar in these high-redshift galaxies (e.g., Bournaud et al. 2007) in which case the single-component stability analysis applies.

13.2.4 The Formation of Gas-Rich Clumpy Unstable Galaxies in the Cosmological Context

The irregular and clumpy structure of high-redshift star-forming galaxies is the outcome of their high gas fractions and densities. Theoretically, these high gas fractions are explained by the high rates of external gas infall, which is not compensated by high star formation rate consuming the gas reservoirs, being rather preserved in a long-lasting steady state in the Main Sequence galaxies. Recent cosmological models have highlighted the fact that high-redshift galaxies mostly accrete their baryons in the form of cold diffuse gas, rather than hot gas reservoirs or companion galaxies (Dekel et al. 2009a; Brooks et al. 2009), which further helps the gas to rapidly join the cold star-forming disc. At the opposite, too large contribution of galaxy mergers in the cosmological galaxy growth budget would form massive stellar spheroids (bulge or stellar halo) too early. That would also stabilize the $z \simeq 2$ galaxies against giant clump formation, for having a much lower turbulent speed and characteristic mass for any residual disc instability at $Q \simeq 1$ (Bournaud and Elmegreen 2009). The cold accretion streams do not directly join the star forming disc (see Fig. 13.3). They might be affected by the hot circum-galactic gas (Nelson et al. 2013), and more importantly, the streams need to dissipate

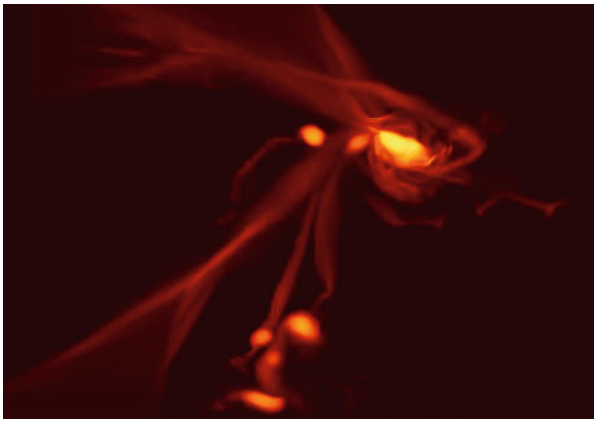

Fig. 13.3 Primordial galaxy fed by three cold streams of gas, in an idealized high-resolution simulation based on typical parameters measured in cosmological simulations (Gabor and Bournaud 2014). The flows join the disc through a turbulent interface with extended circum-galactic reservoirs, before the gas dissipates its energy and feeds the cold star-forming disc, which keeps a high gas fraction, high velocity dispersions self-regulated at a Toomre parameter $Q \simeq 1$, and a clumpy irregular morphology (image size: 100×70 kpc)

the high kinetic energy from the infall, possibly by turbulent dissipation in circumgalactic regions (Elmegreen and Burkert 2010; Gabor and Bournaud 2014) and/or forming extended rotating reservoirs, which would gradually feed the dense star-forming disc (Danovich et al. 2014). Yet, detailed cosmological simulations show that part of the streams can directly feed the central few kiloparsecs of galactic discs in less than one dynamical time (Danovich et al. 2014).

As a result of the high accretion rates, galaxies in cosmological simulations around redshift two have high gas fractions. Actually, modern simulations still have difficulties to preserve sufficient gas reservoirs by avoiding excessive star formation at early epochs (see Dekel and Mandelker 2014, and references therein). Nevertheless, simulations with detailed stellar feedback models do produce some steadily star-forming galaxies with up to ∼30–40 % of gas at $z = 2 - 3$.[4] These simulations (see more details in the next Section) display the expected gravitational instability for such gas-rich discs producing giant clumps and other dense features by gravitational instability (Agertz et al. 2009; Ceverino et al. 2010, 2012). Only a limited fraction of the clumps are "ex-situ" clumps, resulting from the accretion of small nucleated companions or external gas clumps (Mandelker et al. 2014), fully consistent with the observations reviewed above.

13.3 Mechanisms of Bulge Growth Through High-Redshift Disc Instabilities

Knowing the properties of high-redshift star-forming galaxies from the previous Section, in particular the fact that they are subject to a violent clump instability, rather than a weak axisymmetric instability as in nearby barred spirals, we now review the mechanisms through which bulge growth can be triggered and regulated by this instability mode.

13.3.1 Clump Migration and Coalescence

A giant clump in a high-redshift galaxy disc, with a mass of a few $10^{8-9}\,M_\odot$, could behave like a dwarf companion galaxy of a similar mass, except that being dark matter free the mass distribution would be spatially more concentrated. In particular, such a giant clumps undergoes dynamical friction on the underlying gaseous and stellar disc and dark matter halo. Through this process it dissipates its large-scale kinetic energy and angular momentum through increasing the velocity dispersion (i.e., the internal kinetic energy) of the disc and halo. This leads to inward migration

[4] Although these *total* gas fractions seem to remain lower than the observed *molecular* gas fractions, especially if these are the most gas-rich galaxies in simulated samples.

of the giant clump until it reaches the galaxy center – like in a minor galaxy merger. In addition, as the clumps lie in the disc plane, they also undergo gravity torques from other regions of the disc. A clump that forms in a purely rotating disc will break the symmetry of the mass distribution in the disc plane, and induce a kinematic response in the form of a spiral arm or tidal arm, denser than the average disc (Bournaud 2010). This over-dense region will then exchange angular momentum with the clump itself. If most of the mass lies at radii larger than the clump in the galactic disc, as is the case as soon as the disc is sufficiently extended radially, the strongest gravity torques will point from this arm towards the clump. Given that the outer disc has a slower angular velocity than the clump, this arm is trailing with respect to the rotation of the disc, so that the gravity torques exerted on the clump are negative. These gravity torques are thus removing angular momentum from the clump, which accelerates the inward migration already resulting from the dynamical friction process. This torquing process is most efficient in a gas-rich disc as the cold gas component makes the tidal arm response stronger than in a pure stellar disc.

Hence, the clump migration process involves both dynamical friction and gravity torques. Many numerical simulations have been used to study clump migration and estimate the migration timescale, starting with those of Shlosman and Noguchi (1993) and those of Noguchi (1999), the latter being directly motivated by the first observations of chain galaxies by Cowie et al. (1996).

A more detailed treatment of the hydrodynamics and interstellar gas physics was introduced by Immeli et al. (2004a,b). The simulations of Bournaud et al. (2007) were further designed to correspond to the observed properties of star-forming galaxies in the Hubble Ultra Deep field at redshifts $z = 1-2$, with stellar masses of 10^{10}–$10^{11}\,M_\odot$ (see Fig. 13.4). In their simulations the migration timescale of giant clumps to the galaxy center is of the order of 300–500 Myr, depending on the clump initial formation radius, and also of its interaction with the other giant clumps and dense features in the disc. All of the experiments above are idealized models of isolated galaxies, lacking external replenishment of the disc either by cosmological gas infall, accretion of smaller galaxies, or by a few bigger mergers. As a result of star formation the gas fraction gradually decreases, and this can lead to over-estimating the clump migration timescale, as noted for instance by Ceverino et al. (2010). However the clump migration process is so rapid (for clump masses above $10^8\,M_\odot$ at least) that the gas fraction decreases by less than a third of its initial value over this. This is not larger than any other uncertainties, like the fact that it is not possible to evaluate the gas reservoir of atomic gas in these galaxies. Indeed, cosmological simulations with external mass infall have reproduced the clump formation and migration processes, and they found clump migration timescales that are consistent with the above models, or just slightly shorter.[5]

[5]Note that shorter migration timescales in cosmological simulations may also arise if the galaxies are too compact, or have too concentrated dark matter halos enhancing the dynamical friction process. Actually, the cosmological simulations of redshift two galaxies tend to have too low gas fraction because of some largely unexplained early consumption of the gas (e.g., Ceverino et al.

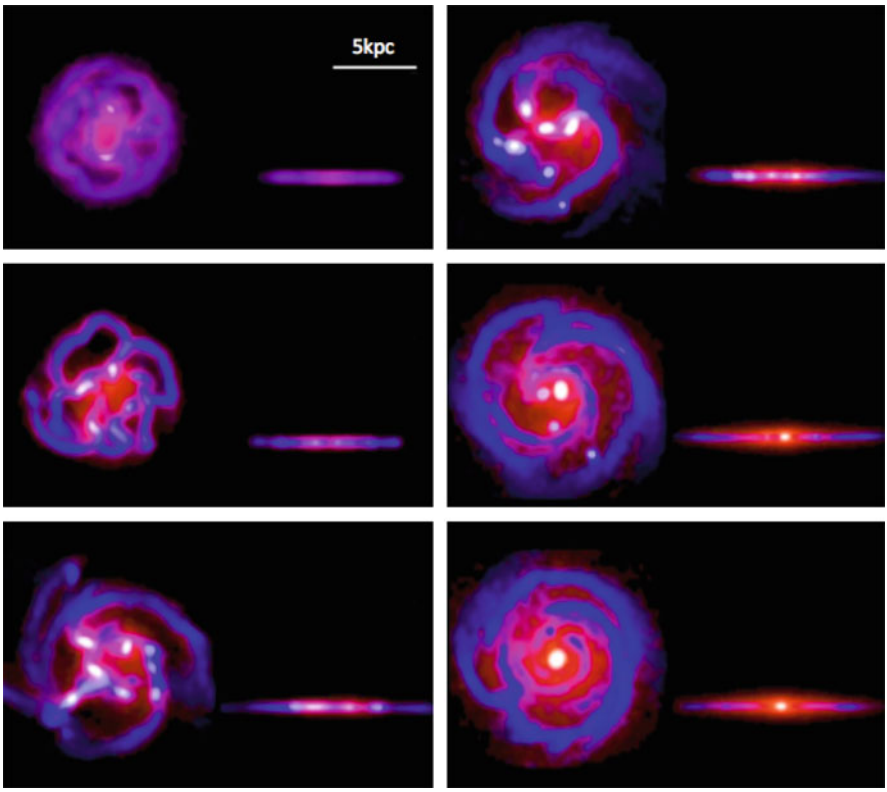

Fig. 13.4 Simulations of a gas-rich (50 % gas fraction) disc galaxy with initial parameters representative for star-forming galaxies at $z \simeq 2$. The unstable gaseous disc forms a ring that quickly fragment into giant clumps. The clumps migrate inward and coalesce into a bulge, while the stellar disc is significantly thickened, and the disc radial profile, initially flat, is re-distributed into an exponential. The bulge formed here is a classical bulge with a Sérsic index of 3.5–4.0. *Blue codes* gas-dominated regions and *red codes* star-dominated ones. Snapshots are separated by 100 Myr. Simulation from Bournaud et al. 2007

13.3.2 Possible Evidence of Clump Migration

An observational signature of inward clump migration, if they survive stellar feedback (see below), could be an age gradient with older clumps found at smaller radii. This is extensively quantified in the simulation sample of Mandelker et al. (2014). In detail clump migration does not imply that young clumps cannot be found at small radii: external gas can feed high gas fraction in the inner disc (Danovich

(2012) and Kereš et al. (2012), with typical gas fractions at best around 30 % at $z = 2$ even counting all the cold gas within a large radius).

et al. 2014) and new clumps can form at small radii in gas-rich discs, except in the central 1–2 kpc, because the innermost regions are stabilized by strong shear and bulge mass (Bournaud et al. 2007; Mandelker et al. 2014). The expected signature is rather an absence of aged clumps in the outermost disc, because clumps formed there might have migrated inward during the last 100–200 Myr. Exceptions could still be found for moderate-mass clumps which can be scattered out to large radii in the interaction with bigger clumps.

Observationally, statistical samples or resolved clumps remain limited, and their ages are hard to estimate. Not only the age of stars in a clump is not a direct tracer of its age (because clumps loose and re-accrete material, see next Section), but also, the stellar age estimators are strongly dependent on many parameters, such as the assumed star formation histories, especially at high redshift (Maraston et al. 2010). Nevertheless, an age gradient is tentatively observed by Förster Schreiber et al. (2011), in quantitative agreement with clump migration and central coalescence within a timescale of at most 500 Myr (see also Guo et al. 2012, 2014).

13.3.3 Stellar Feedback, Outflows, and the Clump Survival Issue

A key issue in the process of inward clump migration (and subsequent coalescence into a central bulge) is their response to stellar feedback. In nearby galaxies molecular clouds are estimated to have short lifetimes of the order of 10–20 Myr, under the effects of supernovae explosions and other feedback processes (Hennebelle and Falgarone 2012; Murray 2011). While giant clumps are typically a thousand times more massive than the biggest gas clouds in the Milky Way, they are also ten times larger in all dimensions, so that their 3-D mass density is not necessarily much higher. As they form stars at high rates, of a few $M_{\odot}\,yr^{-1}$ per clump (Elmegreen et al. 2007; Förster Schreiber et al. 2009; Wuyts et al. 2012), the released energy per unit gas mass is of the same order as that found in nearby star-forming clouds, or is slightly higher. This raises the important question of clump survival against stellar feedback. In particular, having a released feedback energy per unit gas mass of the same order as in nearby molecular clouds, does not mean that the giant clumps will be disrupted in a similar way or on a similar timescale: their gas also lies in a deeper gravitational potential well.

A first attempt to address this issue is in Elmegreen et al. (2008) who concluded that if feedback was strong enough to disrupt the giant clumps within their migration timescale, it would also severely thicken the gas disc and heat the stellar disc well above the observed levels, without also disrupting any pre-existing rotation-dominated stellar disc. This was however based only on energetic supernovae feedback, while other stellar feedback mechanisms might be more likely to disrupt clumps without also completely disrupting the host galaxies. In particular, radiation pressure from young massive stars on the surrounding gas and dust may inject

enough angular momentum into the clumps to disrupt the clumps (Murray et al. 2011).

It has long remained difficult to address this issue in numerical simulations, mostly because stellar feedback can only be modeled through uncertain sub-grid models, even if modern hydrodynamic simulations of galaxies can reach sub-parsec spatial resolutions with mass resolution elements of the order of $100\,M_\odot$ (Renaud et al. 2013). In fact, even the star formation rate which determines the powering rate of feedback relies on sub-grid models. Even if the star formation rate of entire galaxies or giant clumps is realistic compared to observations, changing the sub-grid model may significantly alter the spatial distribution of star formation, especially in resolution-limited simulations. A reassuring point is that idealized simulations of galactic physics can now model gaseous structures up to densities of $10^6\,cm^{-3}$ or more without being at their spatial resolution limit yet: the typical Jeans lengths at such high densities remain larger than a few of resolution elements (without even requiring to add a temperature or pressure floor, Renaud et al. 2013). The fact that stars form with a quasi-universal efficiency in such dense gas (Krumholz and McKee 2005; Gao and Solomon 2004; García-Burillo et al. 2012) implies that at least the first step of star formation in the dense gas is explicitly resolved in these simulations. The subsequent sub-grid modeling of star formation at fixed efficiency in high-density gas is consistent with the observations, down to scales much smaller than that of giant clumps. This is now achieved in idealized simulations, but unfortunately remains out of reach of cosmological simulations so far.

The modeling of supernovae feedback is highly uncertain, in particular because it is often done through thermal dumps of the released energy heating the surrounding gas, while real supernovae remnants include a large fraction of their energy in non-thermal processes, which dissipate on slower timescales (Teyssier et al. 2013). Furthermore, models including the other kind of feedback processes such as stellar winds, photo-ionization, and most importantly radiation pressure were developed only recently (Hopkins et al. 2013; Renaud et al. 2013, see Fig. 13.5). The modeling of radiative feedback remains sub-grid in galaxy simulations and includes free parameters. An important one is the number of scattering events that a photon can undergo in gas cloud before escaping from the cloud (Murray et al. 2011). Another key parameter is the initial mass loading, namely whether the available energy or momentum is diluted into a large or a small mass (and volume) of gas. This loading parameter remained unresolved in numerical simulations until recently, and was sometimes adjusted to generate ad hoc galactic outflows and study their fate (e.g., Oppenheimer and Davé 2006; Genel et al. 2012). The highest resolution simulations of galaxies now become capable of resolving the typical distance over which photons from young stars redistribute their momentum into the ISM and start to estimate this loading factor from physical principles. However, explicit radiative transfer calculations robustly resolving these typical scale lengths are out of reach from galaxy-scale models and become feasible only in cloud-scale or clump-scale simulations.

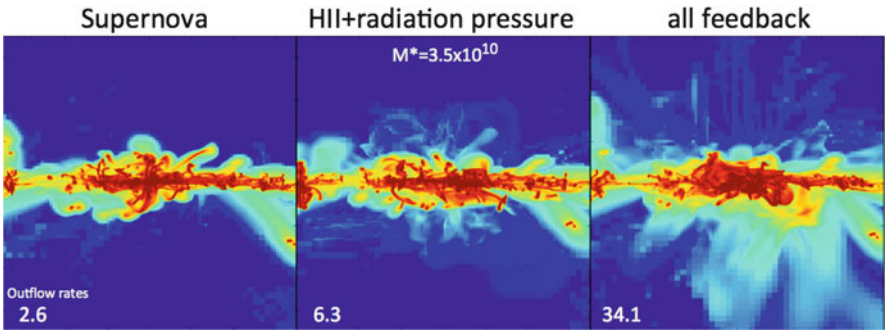

Fig. 13.5 Edge-on views of three simulations of the same gas-rich clumpy galaxy that has been evolved with different stellar feedback models during the last 80 Myr (from left to right: supernovae only, photo-ionization and radiation pressure only, and all mechanisms together, respectively). The gas density is shown and the outflow rates are indicated in the panels in $M_{\odot}\ yr^{-1}$ (measured 2 kpc above/below the disc mid-plane). Outflows are launched by the giant clumps, and the models show the strongly non-linear coupling of feedback mechanisms: the total outflow rate in the simulations with all feedback processes together is well above the sum of the outflow rate in the independent cases. Similar non-linear coupling was noted by Hopkins et al. (2013). These simulations use the feedback models proposed by Renaud et al. (2013) and are similar to those presented in Bournaud et al. (2014), with 3 pc spatial resolution

Some models of gas-rich galaxies with intense feedback have found that the giant clumps could be short lived, even with clump masses of the order of $10^9\,M_{\odot}$. This is the case for instance in the cosmological simulations from Genel et al. (2012), or in the idealized models of Hopkins et al. (2012). It is nevertheless remarkable that in these short-lived clumps models the clump lifetimes are very short, not larger than 50 Myr, hence appearing inconsistent with the stellar ages estimated for real clumps, often reaching 100–200 Myr and more (see above and Wuyts et al. 2012). In these models, the clump disruption is obtained in one or two generation of star formation and evolution, rather than through gradual, steady outflows on the longer term. Models with strong feedback and no long-lived clumps actually tend to lack giant clumps, strongly reducing the mass and/or number of clumps formed. This happens at such a level that the models are inconsistent in forming the majority of observed clumps by in-situ instability, as highlighted recently in the simulations of Tamburello et al. (2014). However, in such models where in-situ clump formation is suppressed, a different (ex-situ) origin of clumps is not explained. In particular their stellar population ages can hardly be reconciled with minor mergers – minor mergers can actually be identified as a source of sub-population of clumps that contain older stellar populations (Bournaud et al. 2008; Elmegreen et al. 2009), but these are only a small fraction of giant clumps. The suppression of in-situ giant clump formation obtained in the models of Tamburello et al. (2014) could in fact result of the low surface density of the discs in their initial conditions, which were

inspired by cosmological simulations (which in turn may consume the disc gas too early). They were not based on the observed gas surface densities estimated from detailed analysis of the dust properties (Sargent et al. 2014; Genzel et al. 2014), or carbon monoxide spectral line distribution studies (Daddi et al. 2015). Hence, a common drawback of all theoretical models, without long-lived clumps, is that either clump formation is suppressed or the clump formation/disruption cycle is very short (<50 Myr). In any case, this appears inconsistent with the observations that commonly probe clump stellar ages of 100–200 Myr or even more than that. On the other hand, for long-lived clumps in models, in a typical star-forming galaxy of stellar mass 10^{10-11} $M_{\odot}$, the migration timescale from the clump birth site to the galaxy central kpc should be 300–500 Myr, which appears to be slightly longer than the observed average stellar ages in giant clumps. This led Wuyts et al. (2012) to argue that clump disruption might be faster than clump inward migration. Yet, the clump stellar population ages provide only a lower limit to the real ages of clumps (see next paragraphs in this Section).

Actually, simulations with a thorough accounting of stellar feedback processes, including not just supernovae, but also radiation pressure and other feedback mechanisms, do not necessarily predict short-lived clumps. In contrast with Genel et al. (2012) and Hopkins et al. (2012), models in Perret et al. (2014), Bournaud et al. (2014) or Ceverino et al. (2014) include non-thermal and radiative feedback schemes and do find long-lived giant clumps – at the same time they do correctly predict short lifetimes for gas clouds below 10^7 $M_{\odot}$ like in low-redshift galaxies. A different approach to feedback modeling by Perez et al. (2013) also find long-lived clumps for any acceptable amount of stellar feedback. That is the case even when strong outflows are launched by the giant clumps and their host galaxies, with outflow rates consistent with the observations obtained by Newman et al. (2012) and Genzel et al. (2011).

Important constraints on the lifetime of giant clumps and their ability to migrate inward toward bulges result from the fact that giant clumps are not quasi-closed-box entities, but rather steadily exchange mass with the surrounding interstellar medium in the host galaxy, either via outflows or inflows of both gas and stars. Hence the ages of stars that lie inside a given clump at a given instant are not equal to the age of this clump. Clumps have a wave-like behavior, although the pattern speed of the $m = 0$ instability is almost equal to the disc rotation speed. Clumps may loose gas through stellar feedback, but more generally they loose material through gravitational tides. At the clump half-mass radius, the gravitational force from the entire clump is only a few times larger than that from the entire galaxy. In other words, clump densities are only marginally higher than the limiting tidal density (Elmegreen and Elmegreen 2005) and clumps gradually loose aged stars by dynamical evaporation toward the galactic potential well (Bournaud et al. 2007).

The clumps have a large cross section (of the order of 0.1–1.0 kpc^2). They wander in a disc that contains substantial amount of gas, even outside the giant clumps themselves.[6] Given this large cross-section of clumps, their low relative velocity of 10–50 $\mathrm{km\,s^{-1}}$ (with respect to surrounding gas), and a density of $\sim$10 $\mathrm{cm^{-3}}$, accretion rates of 1–10 $\mathrm{M_\odot\,yr^{-1}}$ onto each giant clump are expected via pure ballistic capture. The gravitational potential well associated to the giant clumps may actually enhance the accretion. The first detailed estimates of this process were provided by Dekel and Krumholz (2013). Detailed hydrodynamic simulations using the AMR code (Teyssier 2002), which has a very high resolution of 3–6 pc, and include detailed feedback models combining supernovae, photo-ionization and radiation pressure, were presented in Bournaud et al. (2014, see also Perret et al. 2014). These simulations confirmed that, independently on the details of stellar feedback and its "strength", clumps accrete fresh gas at a rate of a few solar masses per year. This gas accretion onto the clumps roughly compensates for both the gas consumption through star formation, and the losses of gas and stars, by gaseous outflows and by dynamical evaporation of aged stars. This means that the clump actually evolves in a steady state, which can be described by a so-called "bathtub model" more commonly used for entire galaxies (Bouché et al. 2010): the gas infall rate is equal to the sum of the star formation rate and gas outflow rate, keeping the total mass constant, thus letting the system to evolve in a steady state. The idea behind the steady state regulation is that any increase in the gas infall rate will be compensated for by the star formation rate, which has a non-linear response, and vice-versa for any decrease in the gas infall rate. The clump mass is then almost stabilized, with some fluctuations around its initial mass.

An important prediction of the long-lived clump scenarios is that the average age of stars contained by a given giant clumps is younger than the actual clump age, measured since its formation by gravitational collapse of the gas-rich disc. The clumps experience a moderate starburst during their first 10–20 Myr, before feedback regulates star formation in a steady state regime (Zanella et al. 2015). Then, they continue to form stars steadily at a higher rate than a closed-box system, due to (re-)accretion of gas from the larger-scale galactic reservoirs. This keeps the average stellar age younger than the clump age. Furthermore, aged stars leave the clump gradually due to the effects of dynamical heating and evaporation, traveling toward the galactic tidal field. As a result, the stellar age becomes even younger than the clump age. Typically stellar ages of 100–200 Myr are predicted, for real clump ages of 300–500 Myr. In long-lived clump models, the stellar age of giant clumps

[6]The presence of large amounts of gas between the giant clumps cannot be mapped spatially in CO surveys yet, but is predicted in the idealized and cosmological simulations of gas-rich unstable discs cited above, and confirmed by two observational arguments: (1) the emission from young stars in the ultraviolet contains a widespread component behind the giant clumps, tracing relatively dense gas (Elmegreen and Elmegreen 2005) and (2) the CO spectral line energy distribution has two components, a high-excitation one attributable to dense clumps, and a low-excitation one corresponding to lower-density, large-scale background gas reservoirs (Daddi et al. 2015; Bournaud et al. 2015).

tends to saturate at 200–250 Myr even for clumps that live more than 500 Myr (Bournaud et al. 2014).

If clumps were disrupted by stellar feedback-driven outflows, the same processes of mass loss and accretion onto the clumps, which are driven by gravitational dynamics, would still be present. Hence the stellar ages would still set a firm minor limit to the ages of the clumps. Hence the observed stellar ages of giant clumps, typically of at least 100–200 Myr (Wuyts et al. 2012; Guo et al. 2012), show evidence that clumps are not disrupted in a few tens of Myr as predicted by some feedback models – actually, all the short-lived clump models reviewed above predict lifetimes smaller than 50 Myr. The observed stellar ages appear consistent with only those models including clump survival and migration toward the galactic center. The ultimate limiting factor to the clump lifetime seems to be their coalescence with other clumps or with the galactic bulge, explaining why Gyr-old giant clumps are not observed either.

A typical star-forming galaxy at redshift $z = 1 - 3$ can thus be expected to experience the migration and central coalescence of giant clumps of $10^{8-9}\,M_\odot$ of gas and stars.[7] Given the observed (and simulated) number of clumps per galaxy, combined with their theoretical lifetimes and observed stellar ages, the central coalescence of a giant clump should typically occur at a rate of $10\,\mathrm{Gyr}^{-1}$ for a galaxy of stellar mass $10^{10-11}\,M_\odot$, i.e. one giant clump every 10^8 years. If the unstable steady state lasts 2 Gyr, this means that the baryonic mass reaching the bulge can be of order of $10^{10}\,M_\odot$ – or even higher without strong stellar feedback. This is because in such case the giant clumps have masses that increase via accretion of the surrounding gas without any outflow regulation.

While the mass reaching the bulge can be very high, we will see later that it does not necessarily mean that too massive bulges are formed. In fact, a large fraction of the mass is still gaseous and can be expelled outward and/or form a central rotating disc rather than a bulge. In the next Sections we first examine the structural properties of the bulges formed by the central coalescence of giant clumps, and then review the issue of bulge mass fraction.

13.3.4 Instability-Driven Inflows

Another mechanism associated to giant clumps and disc instability, but different from giant clump migration and coalescence, can also grow the central mass concentration, and potentially also the bulge mass, in high-redshift disc galaxies. Giant clumps and other dense features, formed by gravitational instability, exert gravity torques on the rest of the disc's gas, which transfers angular momentum. Clumps are located close to their own corotation radius (or slightly inside their

[7]Note that the clumps remain gas-rich as they re-accrete gas and lose aged stars, which compensates for the gas depletion through star formation and gaseous outflows.

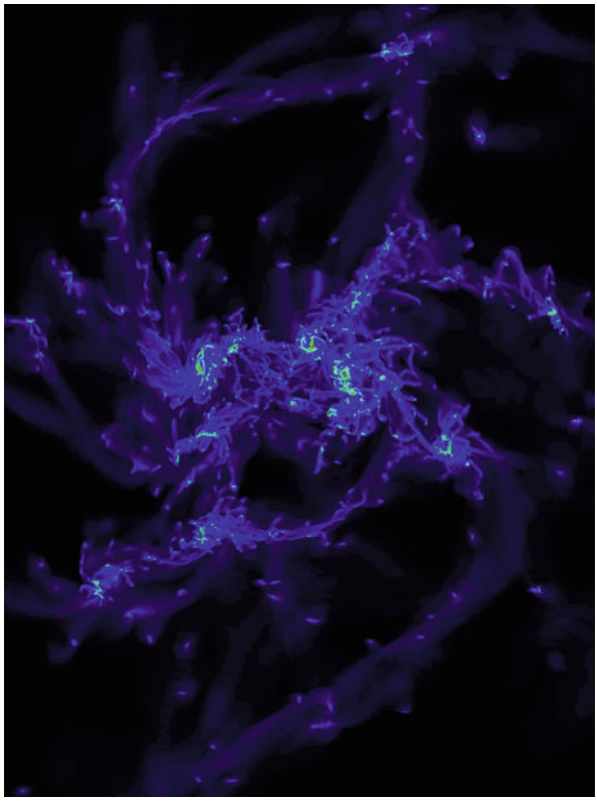

Fig. 13.6 Face-on view of the gas in a high-redshift galaxy simulation (image size: 8×12 kpc). The galactic rotation is counter-clockwise. Note the spiral armlets which are often on the leading side of giant clumps inside the clump radius, and on the trailing side in the outer disc. Gravitational torques from the clumps onto this inter-clump gas drive a continuous inflow of gas toward the galaxy center. Visualization produced with the SDvision software (Thooris and Pomarède 2011)

corotation if dynamical friction has slowed down their rotation speed compared to the rest of the disc material). Material located at smaller radii in the disc thus rotates faster than the clumps, in terms of angular velocity. It then responds mostly as a leading tidal arm, found on the leading side of the clump, compared to the galactic rotation. The presence of multiple clumps and other features can make the tidal pattern hard to identify. A striking example of this phenomenon in simulations is shown in Fig. 13.6.

The material on the leading side of a giant clump undergoes negative gravity torques and loses angular momentum. The material in the outer disc gains angular momentum in exchange. The process is similar for any instability that breaks the disc symmetry (e.g., Combes and Gerin 1985; Bournaud et al. 2005). However, the gravity torques in the case of clump instabilities at high redshifts are typically 10–20 times larger than in case of secular instabilities (namely, spiral arms and bars) at low-redshifts: it can transfer outward even 100 % of the initial angular momentum in just one rotation period (Bournaud et al. 2011), compared to 5–10 % per rotation period for strong bars in low redshift spirals (Bournaud et al. 2005). The corresponding mass inflow rate for a typical high-redshift star-forming galaxy is then of the order of $10\,M_\odot\,yr^{-1}$ or more.

The gravity torques between clumps and non-axisymmetric features are the main mechanism through which gravitational energy is pumped into the interstellar gas. As reviewed in the previous Section, these unstable discs evolve in a self-regulated regime when $Q \simeq 1$, with high velocity dispersions, i.e. $\sigma \sim 50\,\mathrm{km\,s^{-1}}$. Turbulent energy in the interstellar medium typically dissipates in a local crossing-time so that more energy needs to be pumped into the turbulent cascade in steady-state systems (e.g., Mac Low 1999; Bournaud et al. 2011). The specific energy loss rate is then $\sigma^2/(2\tau)$ where τ is about 10 Myr, the energy being dissipated mainly through small-scale compression and shocks that heat the gas, which subsequently radiates the energy away. The radiative losses are balanced by the global inflow of gas down the galactic gravitational potential at a mass inflow rate $\dot{M}$, releasing an energy rate $\dot{M}V_c^2/2$ for a galactic circular velocity V_c. Typical outflow rates estimated for high-redshift star-forming galaxies are of the order of $\sim 10\,\mathrm{M_\odot\,yr^{-1}}$. This compensates the turbulent dissipation in a steady state, which is estimated to be $\sigma^2/\tau \equiv \dot{M}V_c^2$ (Elmegreen and Burkert 2010; Bournaud et al. 2011; Genel et al. 2012).

Studies of the instability-driven inflow (see for instance Krumholz and Burkert 2010; Elmegreen and Burkert 2010; Bournaud et al. 2011) highlight the fact that the inflowing gas is not fully consumed by star formation. Actually, a large fraction of the initial inflow, several solar masses per year, typically flow onto the central kpc region or "bulge region". The gaseous inflow will not necessarily feed a classical bulge as the material is dissipative, but it feeds the central star formation, at a rate of a few solar masses per year. This is consistent with observations showing that this "bulge region" (about the central kpc) has younger stellar populations and more sustained star formation in the most unstable/clumpy galaxies, than in smoother discs of similar mass and redshift (Elmegreen et al. 2009, 2013). The instability-driven inflow thus increases the central concentration of gas *and* young stars, while the central stellar mass can be scattered into a pressure-supported spheroidal bulge during subsequent relaxation events (which can include: coalescence of other giant clumps, major interactions or minor mergers). Few simulations have studied the outcome of the central mass concentration grown by this inflow, compared to direct bulge growth by central coalescence of clumps, mostly because the two processes would be hard to distinguish. Yet, it seems clear that the stellar mass gathered into the central kiloparsec by the clump migration and instability-driven inflow, ends-up in a bulge-like structure rather than just into the innermost regions of a radially-concentrated rotating disc: it comes in excess of the disc exponential mass profile, and has high velocity dispersions and weak residual rotation (Elmegreen et al. 2008; Inoue and Saitoh 2011; Bournaud et al. 2011).

The absence of violent relaxation in the process of instability-driven gaseous inflow should produce only a so-called pseudobulge, namely a low Sérsic index structure with substantial residual rotation. Yet, subsequent relaxation through clump coalescence and/or mergers can make this mass contribute also to a so-called classical bulge, i.e. a highly concentrated structure with virtually no angular momentum left. This global picture has not been studied in detail for disc-dominated galaxies with the Milky Way mass, or up to $10^{11}\,\mathrm{M_\odot}$, but it has been studied for more massive galaxies. As explained in Sect. 13.5, these massive galaxies become

compact spheroid-dominated via the violent disc instability processes. The global instability driven inflow plays a major role in turning the initial discs into compact concentrated objects, whereas relaxation induced by giant clumps and some mergers turn them into "classical" spheroids (see also Zolotov et al. 2014).

13.3.5 Properties of Bulges from High-Redshift Disc Instability

The properties of bulges resulting from the violent instability of high-redshift disc galaxies remain uncertain, as they largely depend on the lifetime and evolution of clumps against stellar feedback. If the clumps are short-lived, disrupted by feedback faster than their inward migration timescale, there is still a diffuse inflow of inter-clump gas driven by the instability (see above, Hopkins et al. 2012, and Bournaud et al. 2011). This will grow a low-concentration pseudobulge if no other relaxation process will affect the central region. On the other hand, the models with long-lived clumps, whose properties are also more consistent with the observed ages of the clumps and their outflow rates, find that the instability can make classical bulges. After repeated clump coalescence (Elmegreen et al. 2008), and due to short star-formation timescales (Immeli et al. 2004b) these bulges have a low rotational support and high Sérsic indices. Bournaud et al. (2007) have shown that for models scaled to the observed properties of galaxies in the Hubble Ultra Deep Field, the disc material is redistributed into an exponential profile during clump migration and classical bulge growth.

Nevertheless, these first models included only supernova-like feedback schemes and lacked a more complete accounting of stellar feedback processes. The full series of stellar feedback processes regulates the mass and gas richness of clumps even if they remain long-lived. Inoue and Saitoh (2012) proposed that the resulting bulge could rather be a pseudobulge, even if its stellar population is old and metal-rich. Nevertheless it seems still possible to grow highly concentrated classical spheroids, with detailed stellar feedback models, at least at high galactic masses (Ceverino et al. 2014; Zolotov et al. 2014). The amount of relaxation was shown to be sufficient to form classical bulges with high Sérsic indices at the centers of exponential discs (Ceverino et al. 2014). Yet, strong subsequent evolution can occur, and even such basic parameters like the bulge-to-disc mass ratio (B/D) can largely evolve between the high-redshift unstable phases and the present-day galaxies (Martig et al. 2012). Bekki and Cioni (2007) highlighted some possible signatures of possible giant clumps and their contribution to present-day bulges.

Thus, a consensus on the resulting bulge properties (mass and type) is far from being reached. The recent efforts have mostly focused on understanding the nature of the giant clumps and their own evolution with respect to star formation and feedback. Note also that the central coalescence of clumps, while it may induce enough relaxation to produce classical bulges, can significantly reduce the central density peak of the dark matter halo (Elmegreen et al. 2008; Inoue and Saitoh 2011).

This could be a way to erode the central cusp produced by hierarchical growth in dark matter halos.

13.3.6 Associated Thick Disc Growth

Another interesting mechanism associated to the instability of high-redshift discs is that pre-existing stars, and stars that formed outside the giant clumps or have left the giant clumps, are rapidly scattered vertically by the local gravitational potential wells associated to the clumps themselves. The scale-height of the stellar disc rapidly increases, thus forming a very thick stellar system ($\geq 1-2$ kpc). Even if the thin disc mass doubles between redshift two and redshift zero, and the old thick disc tends to shrink back by gravitational response (see Villalobos et al. 2010), a thick disc will remain, having a typical scale height of 500–1000 pc. This instability-induced thick disc is decoupled from the younger thin stellar disc formed at lower redshifts: this thick disc will appear as a distinct component in the vertical profile, rather than being just a low-density tail in that profile (Bournaud et al. 2009).

An interesting property of the thick discs formed through this instability mechanism is that its growth is concomitant to bulge growth, possibly accounting for chemical similarities between the two (Chiappini et al. 2009; Chiappini 2009). Another noticeable property of the thick disc is its fairly constant radial thickness throughout the surface brightness profile. While this fails to account for the outer flaring observed for thick discs, which is probably better explained by minor mergers and distant tidal interactions (Villalobos and Helmi 2008; Di Matteo et al. 2011), it does successfully account for the presence of a thick disc in the innermost regions, around central discs and bulges, as observed by Dalcanton and Bernstein (2002). This latter property could not be explained by minor mergers and tidal interactions, which stir and thicken preferentially the low-density outer regions of the stellar disc (Villalobos and Helmi 2008; Bournaud et al. 2009; Martig et al. 2012; Di Matteo et al. 2011). At the same time, clump instability cannot account for all observed thick disc properties and a contribution of other processes such as minor interactions and mergers are likely required, too (Inoue and Saitoh 2014).

Therefore, while interactions and mergers appear needed to explain the outer structure of thick discs, clumpy disc instabilities at high redshift are required to explain their inner one. An interesting property of thick discs is that the fraction of the stellar mass that they gather is larger in later-type galaxies with small bulge fractions (Yoachim and Dalcanton 2006). This relation might be explained by clump-driven bulge growth and disc thickening, if the early-formed stellar mass is distributed between the bulge and the thick disc, with preference for the bulge at high total mass and preference for the thick disc at lower total mass. The relation between bulge properties and thick disc properties, potentially resulting from the role of high-redshift disc instabilities in bulge growth, was further outlined by Comerón et al. (2014) who argue for concurrent growth of the thick disc and central bulgy mass concentrations in the past history of today's spiral galaxies.

13.3.7 *Is Bulge Formation Too Efficient? Stellar Feedback and Bulge Growth Regulation*

A key question related to bulge formation or growth by disc instabilities is whether this mechanism would over-predict bulge formation. The standard ΛCDM galaxy formation models already tend to over-produce bulges and spheroids at the expense of high angular momentum discs, even when violent disc instabilities and giant clumps are neglected, especially in the galaxy mass range of $10^{10} - 10^{11}\,M_{\odot}$. At best, some models with baryonic physics may result in an acceptable distribution of stars among bulges and discs (Agertz et al. 2011; Guedes et al. 2011), but generally they over-produce the stellar mass (Guo et al. 2011). On the other hand, models with more realistic stellar masses remain too dominated by bulges and low angular momentum components (Scannapieco et al. 2011; Guo et al. 2011). These results are often in tension with observations, or can at best be marginally reconciled. However, they are generally consistent with semi-analytic models that do *not* include disc instabilities, or include only low-redshift secular instabilities (bars) that grow bulges much more slowly (e.g., Somerville et al. 2008), as well as cosmological hydrodynamic simulations that do *not* resolve giant clumps and violent disc instabilities[8] or even employ thermal models that suppress strong disc instabilities (Somerville and Davé 2014). Note also that cosmological simulations tend to overproduce stars at early epochs ($z > 3$) and preserve too low gas fractions down to redshifts $z = 1 - 3$ (Dekel and Mandelker (2014) and references therein), which can further damp the disc instability process in these simulations.

The new mechanism of bulge formation by disc instability thus comes on top of a cosmological model which, depending on the assumed (and still uncertain) baryonic physics, already produces enough stellar mass in bulges and low angular momentum components – if not already too much! This could be an indirect argument against clump survival and coalescence into bulges, although the observed clump ages are consistent with long lifetimes and migration to bulges. Note however that the instability driven inflow (see above) is independent of clump survival so that its contribution to the growth of central compact components should not be suppressed in the case of short-lived clumps. The question of whether the proposed high-redshift disc instability mechanisms overproduce bulges is thus naturally raised. The typical numbers for a galaxy of stellar mass $\sim 5 \times 10^{10}\,M_{\odot}$ are, say, five clumps of $5 \times 10^{8}\,M_{\odot}$ in mass, migrating to the bulge in 400 Myr, with unstable steady state maintained for 2 Gyr. This means that 25 % of the total stellar mass coalesces into the bulge through this process, leading to an excessive bulge-to-disc mass ratio of 1:3. Furthermore, the diffuse instability-driven inflow may double this estimate, which was based on the migration and coalescence of giant clumps only. The resulting bulge fraction could thus be above the acceptable levels for such moderate

[8] Resolving the giant clumps requires a resolution that is typically too costly to maintain down to redshift zero (Ceverino et al. 2010).

mass galaxies. Even if the thin disc doubles its mass without further growth of the bulge between $z = 1 - 2$ and $z = 0$, the resulting B/D=1/6 at $z = 0$, would still be in tension with observations. This is the case especially if no other processes, such as minor mergers or some major interactions, which are unavoidable at some level, would also grow the central bulge. These simple estimates highlight the potential problems in the issue.

Early models of clump formation and migration clearly over-produced bulge masses, with final B/D mass ratios about 1:1 after the violent instability period (e.g., Noguchi 1999; Bournaud et al. 2007). A strong limitation of these models was the lack of stellar feedback other than weak supernovae feedback. While the global star formation rate of the galaxies were somehow regulated to realistic values in the galaxies of the Main Sequence, the clumps did not produce gaseous outflows at realistic rates. As a consequence, the clumps in these models accrete surrounding material without being regulated by outflows, so their masses can only increase with time. While the initial clump mass in these models is in agreement with observations (with typical masses of a few $10^8\,M_\odot$ for the main few clumps, and rarely more extreme cases), their masses eventually become excessive beyond the first 10^8 years or so, with clumps masses frequently above $10^9\,M_\odot$. Consequently, the resulting bulge masses after clump coalescence are too high as well.

The realization that clumps actually have their mass content regulated by feedback, with outflows compensating for the sustained gas accretion, helps to solve the problem in two ways. First, the clump masses are regulated to a value fluctuating around their initial mass throughout their migration in the disc, which reduces the mass available for bulge coalescence by a factor of a few. Second, the fact that clumps gradually lose their aged stars and re-accrete gas means that they remain gas-rich, and even gas-dominated, throughout their lifetime (Bournaud et al. (2014) – without these processes they would accumulate large amounts of stars and become star-dominated before reaching the bulge region). More than half of the material reaching the bulge region is thus gaseous, and will form a rotating disc component. Star formation can turn this rotating gaseous component into a rotating stellar component, but stellar and/or AGN feedback can also reduce the amounts of stars formed by ejecting gas from this central component. Detailed simulations quantifying the bulge growth for long-lived clumps having their mass regulated by supernovae, photo-ionization, and radiation pressure feedbacks, show that the growth of bulges by clump migration and instability-driven inflows remains at fully acceptable levels. This is the case at least after 0.5–1.0 Gyr of clump evolution, for galaxies having baryonic masses of $10^{10-11}\,M_\odot$ (see Bournaud et al. (2014) for quantitative results).

Whether a long-lasting disc instability period will eventually over-produce bulges, or whether feedback processes can prevent too much gas to accumulate in the central kpc and turn into stars, remains an open question. Stronger regulation than just clump outflows seems to be needed if the clumps are actually long-lived and can migrate. A first solution to this problem was proposed by Perret et al. (2014). As clumps remain gas-rich along their evolution, their central coalescence conveys large amounts of gas inwards (typically a few $10^8\,M_\odot$ of gas over $\sim$0.1 kpc^2), which provokes a local starburst in the central kpc. The resulting feedback expulses large amounts of gas – from the coalescing clumps, as well as gas brought inward by the global instability-driven inflows. Gas expulsion rates from the central kpc peaking at a few tens of solar masses per year are reported by Perret et al. In addition, this process will affect any pre-existing stellar bulge. The gas mass indeed represents roughly half of the mass in the central kpc (dark matter providing only a minor contribution at such scales) and this major component rapidly fluctuates by clump inflows and feedback-driven gas expulsions. The orbits of stars in the bulge are affected by the rapid fluctuations of the gravitational potential. This process was already pointed out by Bois et al. (2010), in the context of stellar scattering by young star clusters, and gas clouds in mergers, but involving much higher masses at high redshift.

This process of bulge self-regulation by the inflow of giant clumps is illustrated in a simulation by Bournaud et al. (2014) in Fig. 13.6: in this simulation, a galaxy of stellar mass $5.3 \times 10^{10}\,M_\odot$ contains 43 % of gas during the analyzed period. A giant clump of $3.6 \times 10^8\,M_\odot$ of gas and $2.3 \times 10^8\,M_\odot$ of stars coalesces with the central bulge, the stellar mass of which is initially $3.3 \times 10^9\,M_\odot$. The clump brings gas and young stars to the central kpc (from the clump stellar content and from central star formation in the clump gas). The local starburst consumes about 60 % of the clump gas within 25 Myr, with a star formation rate in the central kpc peaking[9] at 13 Myr in Fig. 13.6. Note that this is a high surface density of star formation rate in the central kpc. However, it does not drive the entire host galaxy outside of the typical scatter in the Main Sequence (Schreiber et al. 2014), i.e. the entire host galaxy does not turn into a starburst. The gas mass in the central kpc then decreases by a larger amount than just by gas consumption due to star formation, under the effect of stellar feedback-driven outflows. The response to the sudden mass increase (clump accretion) and decrease (gas outflows) affects the stellar content of the bulge: in particular, some aged stars leave the bulge region migrating toward an extended stellar halo while moving in high-eccentricity orbits. An example is shown in Fig. 13.7: the bulge gains mass of $2 \times 10^8\,M_\odot$ in the clump coalescence process, but rapidly looses $2.3 \times 10^8\,M_\odot$ of aged stars, thus slightly reducing the total bulge mass after this clump coalescence event. Detailed statistical studies remain to be performed, but the simulations studied in Perret et al. (2014) show that the bulge mass can be regulated to reasonable amounts that do not exceed 10–15 % of the

[9] After applying Gaussian time smoothing of FWHM 2 Myr to erase fluctuations related to the numerical sampling of star formation.

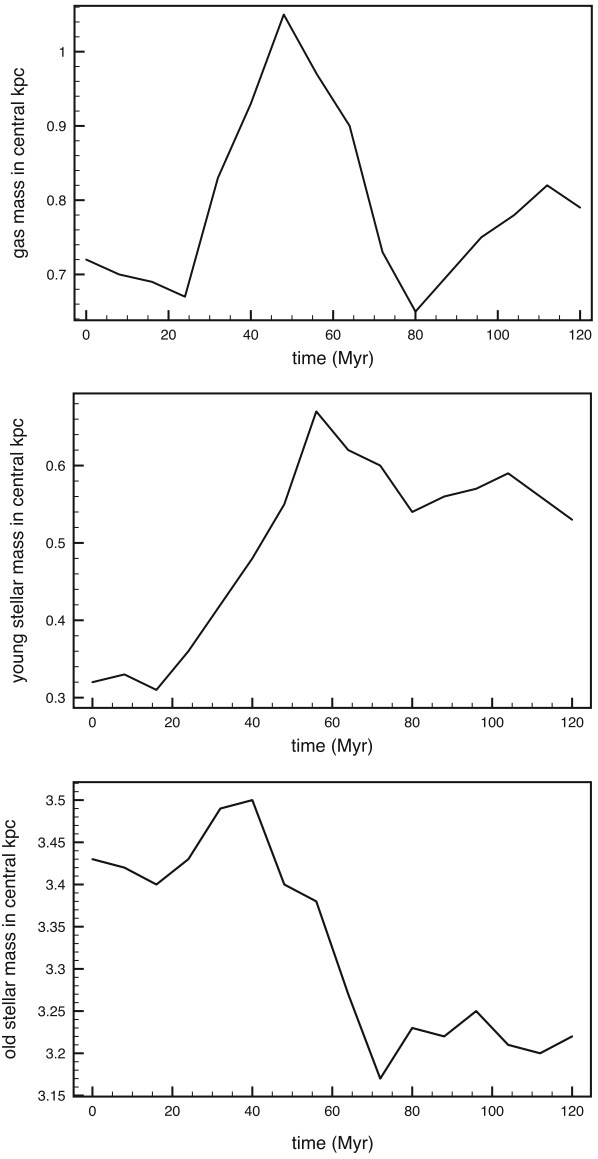

Fig. 13.7 Bulge evolution during the central coalescence of a giant clump (simulations from Bournaud et al. 2014). The panels display mass of gas in the central kpc (radius 500 pc, *top*), the mass of stars younger than 100 Myr plus the current time (i.e. younger than 100 Myr at $t = 0$ and younger than 150 Myr at $t = 50$ Myr, *middle*), and the mass of stars older than 200 Myr plus the current age (*bottom*, still in the central kpc). A massive clump coalesces with the bulge at $t \simeq 60$ Myr. The gas mass increases when the clump comes in, and decreases due to feedback-driven outflows. The mass of young stars in the bulge increases, but that of old star decreases, and the bulge mass is regulated to an almost constant value (even slightly decreasing in this example, although its Sérsic index increases – see text for details). This bulge regulation mechanism was proposed by Perret and collaborators (Perret et al. 2014, and Perret, PhD thesis, 2013)

stellar mass for Milky Way-mass galaxies, owing to the three regulation processes listed above – 1: regulation of the clump mass by steady outflows and dynamical loss of aged stars, 2: regulation of the gas richness of the clumps by re-accretion of gas from the disc, and 3: regulation of the central bulge mass by central starbursts and relaxation during clump coalescence. A detailed accounting in cosmological context however remains required to study the bulge mass budget over the long-lasting clumpy unstable state from $z > 3$ to $z \simeq 1$.

An alternative solution was recently proposed by Combes (2014) who demonstrated than in MOND dynamics, realistic clumpy disc are still predicted by simulations of $z = 2$ galaxies, but the efficiency of bulge formation is lowered as the clump migration timescale increases. Gravitational torquing and inflows should still be present, but without central relaxation through clump coalescence, they may form only a pseudobulge.

13.4 The Associated Growth of Supermassive Black Holes

The violent instability of high-redshift galaxies brings large amounts of gas toward their central regions. This is achieved through the migration of gas-rich clumps, and more generally by a global inflow of gas driven by gravity torques between the dense features arising from the instability, and compensating for the turbulent losses. Simulations of this process (Bournaud et al. 2011) have shown that an inflow of about 1 solar mass per year persists down to the central few parsecs, as the gas is not entirely depleted into star formation. It is then sufficient to have one percent of the mass brought to the central pc accreted by the central supermassive black hole (SMBH) to grow this SMBH in realistic proportions compared to the usual scaling relations for bulges and SMBHs. Various small-scale mechanisms in the central parsec can indeed lead 1 % of the available inflowing gas mass to be accreted by the SMBH (Combes 2001). The process was studied in detail in Gabor and Bournaud (2013) who has shown that bright Eddington-limited episodes of Active Galactic Nuclei (AGN) accretion can be triggered by the disc instability, and could contribute to the bulk of the supermassive black hole mass growth at $z = 1 - 3$ for galaxies of stellar mass $10^{10-11}\,\mathrm{M}_\odot$. The process is illustrated in Fig. 13.8. In the broader cosmological context, the role of cold gas accretion onto gas-rich galaxies and internal instabilities was probed by Dubois et al. (2012, 2013).

Observationally, there is a general lack of correlation between the occurrence of AGN and morphological signatures of major mergers (e.g., Kocevski et al. 2012) except in the most luminous QSOs found preferentially in major mergers. In fact, moderately bright AGN that drive the bulk of SMBH growth are mostly located in normally star-forming, Main Sequence galaxies (Mullaney et al. 2012), which are generally clumpy unstable discs at $z = 1-3$. Searches for a direct link between disc instabilities and AGN are hampered by the high gas column densities, typically a few times $10^9\,\mathrm{M}_\odot\,\mathrm{kpc}^{-2}$ in the central regions of these galaxies, sufficient to reach Compton thickness or at least severely attenuate the X-ray signatures of potential

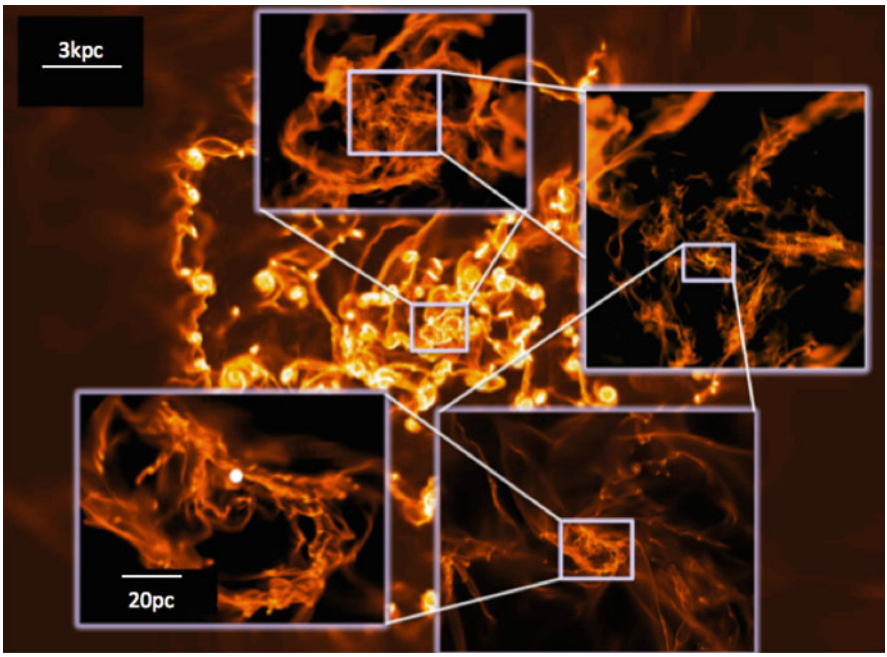

Fig. 13.8 AMR simulations of a high-redshift gas-rich disc galaxy with a central SMBH, using gradual zooms in the AMR refinement toward the central black hole, with a spatial resolution reaching 0.02 pc in the innermost regions. The *white circle* in the last zoom represents the SMBH position and its Bondi radius. The disc instability drives steady gas inflows toward the SMBH. AGN feedback triggers hot winds that escape through low-density holes and leave the accreting channels almost unaffected. The large-scale star-formation activity also remains unaffected in spite of the efficient AGN-driven outflows (Figure courtesy of Jared Gabor)

AGN. Using optical line emission to probe AGN, Bournaud et al. (2012) have shown that at intermediate redshift ($z \approx 0.7$) there are probably more AGN in clumpy unstable discs, than in regular smooth discs of the same mass and size (both clumpy unstable discs and modern spiral types co-exist at such intermediate redshifts). At high redshift $z \geq 1$, Trump et al. (2014) find an AGN frequency as high in clumpy discs as in compact early-type galaxies, which are known to be frequent AGN hosts (compared to star-forming spirals at low redshift), which may indirectly confirm the efficient feeding of AGN in clumpy discs. Yet a direct comparison of AGN feeding in clumpy unstable discs and in more "stable" discs is impossible at $z > 1$, because stable spiral discs are virtually inexistent at $z > 1$.

High-redshift disc instability can contribute to SMBHs in two other ways. First, the clumpy accretion onto black holes can help increase their mass more rapidly at early epochs, which subsequently increases the limiting Eddington rate and makes possible for the SMBH to grow its mass more rapidly. This potential solution to the problem of very massive and bright AGN at very high redshifts ($z \sim 6$, Di Matteo et al. 2012) was studied in DeGraf et al. (2014). Second, the clumps

could be the formation site of SMBH seeds, if they form intermediate mass black holes through runaway stellar collisions, which their estimated star formation rate densities make possible. These seeds could be gathered centrally along with clump migration into an SMBH (Elmegreen et al. 2008), which was potentially supported by some observed spectral signatures (Shapiro et al. 2009).

Studies of the response to feedback show that the feeding of AGN by disc instability does not quench star formation, and not even the fuelling of the AGN itself. AGN from clumpy discs produce high-velocity outflows that are collimated by the density and pressure gradients in the disc, and escape perpendicularly from the disc plane from the nuclear region (Gabor and Bournaud 2014). This is in agreement with recent observations of high-velocity winds emerging preferentially from the nuclear regions (Förster Schreiber et al. 2014). Outflows from star formation are more widespread above the entire disc and its star-forming clumps (observations: Newman et al. 2012, simulations: Bournaud et al. 2014; Hopkins et al. 2013). Hence the AGN feedback does not affect the inflowing, which is the fuel for future AGN feeding, and the extended gas discs including its star-forming regions. This holds even once long-range radiative effects are taken into account (Roos et al. 2014). The AGN luminosity and accretion rate strongly fluctuate over Myr-long timescales, which results from the high heterogeneous, turbulent nature of the inflowing gas, rather than from the regulation by feedback (Gabor and Bournaud 2014; DeGraf et al. 2014).

13.5 Disc Instabilities and Early-Type Galaxy Formation

The instability-driven inflow scales like the circular velocity squared (Sect. 13.3.4) and is thus much more intense in high-mass galaxies. Clump migration is also faster, following the dynamical friction timescale in massive galaxies with high-density discs and halos. This raises the question of whether the violent instability of high-redshift galaxies can form early-type galaxies (ETGs) at high masses, i.e. entirely spheroid-dominated systems rather than just bulges in the center of disc-dominated systems.

Theoretically, these strong inflows can lead to disc contraction in a timescale not larger than 1 Gyr, and the instability-driven bulge growth rate could lead to a bulge-dominated system, through which the disc is stabilized and star formation is quenched (Dekel and Burkert 2014), with the help of stellar spheroids stabilizing gas discs to quench star formation (Martig et al. 2009). Recent cosmological simulations have probed these possible mechanisms, where the strong inflow first forms wet compact star-forming systems, which are subsequently quenched and turned into red compact ETGs (Ceverino et al. 2014; Zolotov et al. 2014). The high Sérsic indices and dispersion-dominated kinematics are consistent with these being the progenitors of modern ETGs. The transitions from the compact star-forming system to a quenched one could correspond to observations of the so-called “blue nuggets” and “red nuggets” at high redshift (Barro et al. 2014).

Observations of giant clumps or clump remnants in the innermost regions of young ETGs in the Hubble Ultra Deep Field (Elmegreen et al. 2005) support this scenario. Bournaud et al. (2011) have also shown that mergers of gas-rich unstable discs lead to compact spheroid formation when the instability in the cold interstellar phase is taken into account during the merger. Nevertheless, it remains unknown whether these processes can explain the detailed phase space structure of modern ETGs, including the observed families of fast and slow rotators (Emsellem et al. 2007) which could also be relatively well explained in the cosmological context without invoking a major role of disc instabilities (Naab et al. 2014).

13.6 Comparison to Secular Disc Instabilities at Lower Redshift

The violent instability where the entire disc is self-regulated at $Q \simeq 1$ persists until about redshift 1, for the galaxy masses that we have studied here (Elmegreen et al. 2007; Genel et al. 2012; Dekel et al. 2009b; Ceverino et al. 2014). This violent phase, with irregular clumpy discs, growing spheroids, and relatively frequent mergers, has a morphology poorly correlated to the final bulge/disc ratio of today's descendent galaxies (Martig et al. 2012). After $z \sim 1$, galaxies enter their secular phase where a stable thin disc grows and slowly evolves, with a bulge/disc ratio close to the final value. This regime differs by having globally $Q > 1$, with $Q \leq 1$ only locally, for instance for gas compressed in spiral arms and in which small molecular clouds form by various local instabilities (Renaud et al. 2013). The evolution from the early violently unstable phase to the secular stable spiral discs is shown for two typical cases of zoom-in simulations in cosmological context in Fig. 13.9.

The mild instability of modern spirals differ from the global instability of their high-redshift progenitors in various ways. Present-day discs globally develop only non-axisymmetric ($m \geq 1$) modes such as spiral arms and bars, and gravitational collapse at $Q \leq 1$ can occur only locally in small over-densities of gas. The associated inflows are much slower, with only a few percent of the angular momentum transferred outwards per rotation period even in strongly barred galaxies (Combes and Gerin 1985; Bournaud et al. 2005). Mass inflows and vertical resonances can secularly grow central spheroids. Yet, simulations in cosmological context in Kraljic et al. (2012) suggest that the contribution of these low-redshift secular instabilities in the bulge mass budget is also more modest than for high-redshift instabilities, although the secular phase last longer and sometimes grows massive peanut-shaped bulges. The absence of violent relaxation, unlike the central coalescence of giant clumps, is such that the process mostly results in pseudobulges rather than classical bulges with high Sérsic indices Chap. 14.

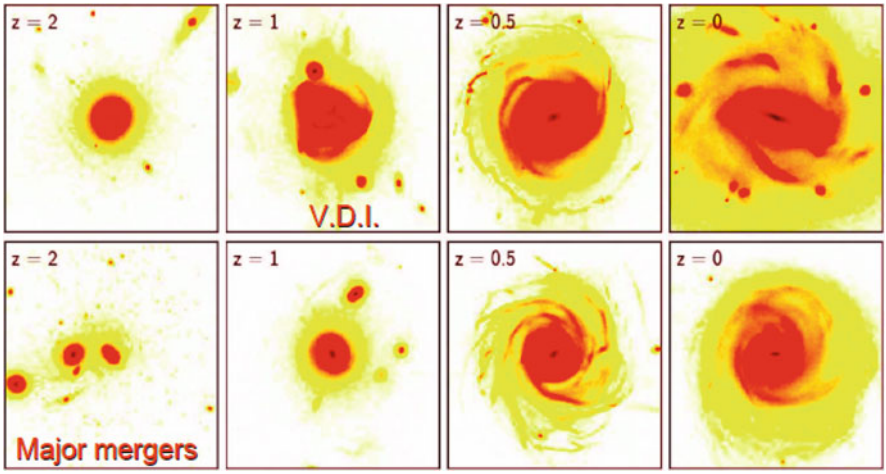

Fig. 13.9 Simulations in cosmological context, zoomed on individual galaxies (From Martig et al. 2012), displaying the stellar mass surface density (panel size: 20×20 kpc). These simulations show the transition from a "violent phase" at $z > 1$ with violent disc instabilities (V.D.I., *top*) and giant clumps and, more rarely, merger-driven starbursts, to a "secular phase" with bars and spiral arms at $z < 1$. Interestingly, this transition shows a "downsizing" behaviour with stellar mass, i.e. it occurs later-on for lower-mass galaxies, which could explain that clumpy disc instabilities persist longer for lower-mass galaxies (Elmegreen et al. 2007; Bournaud et al. 2012) and regular barred spiral morphologies arise earlier-on for high-mass galaxies (Sheth et al. 2008; Kraljic et al. 2012)

The inflow toward AGN and SMBH is also much more modest, but another difference here is the common presence of Inner Lindblad Resonances (ILRs) in low-redshift spiral galaxies – high-redshift discs generally have no ILR associated to the clump instability. As a consequence, the inflow stops and the gas is stored at the ILR radius until a nuclear instability occurs and brings the gas reservoir inwards. The process can be repeated with cyclic AGN feeding, but a large fraction of the inflowing gas can also be depleted through star formation in the meanwhile (Emsellem et al. 2015). Indeed, observations point out that the correlation between galactic bars and AGN is complicated by a number of factors (see e.g. Coelho and Gadotti 2011, and references therein). However, it can be argued that the correlation between nuclear bars and AGN is more straightforward (Combes 2001).

13.7 Summary

High-redshift star-forming galaxies at $z \simeq 1-3$ have irregular optical morphologies dominated by a few bright giant clumps, also faintly detectable in the near-infrared. There is broad evidence that these giant clumps (of a few $10^{8-9}\,M_\odot$ of gas and stars and 500–1000 pc diameter for the biggest ones) form mostly by in-situ gravitational instability in gas-rich, turbulent galactic discs. This is largely supported

by photometry, kinematics, and stellar population studies. Recently, a first example of direct gravitational collapse of a giant clump has been directly probed (in the form of a very massive star-forming blob with almost no underlying aged stellar counterpart, Zanella et al. 2015). Only a small fraction of clumps exhibit older stellar populations and may form ex-situ, in the form of small satellites of gaseous clumps that merge with the disc from the outside.

The modern understanding of galaxy formation in the standard cosmological framework explains the high gas fractions and resulting disc instability as the outcome of steady accretion of cosmological gas reservoirs (and some companion galaxies) at high mass rates. The high cosmic infall rates keep the gas fraction high, the Toomre stability parameter low, and the disc in a globally unstable state. The disc increases its gas velocity dispersion (or turbulent speed) to self-regulated its dynamics in a steady state about $Q \simeq 1$.

Hence the high-redshift progenitors of Milky Way-like spirals differ from modern disc galaxies, which have only weak non-axisymmetric instabilities (bars and spiral arms) and in which gas undergoes gravitational collapse only in limited regions, in the form of transient low-mass molecular clouds.

The giant clumps and the underlying instability can build a galactic bulge in several ways. The first one is the instability-driven inflow, which pumps gravitational energy into the interstellar turbulence cascade to compensate for the radiative losses. This inflow builds a central mass concentration in the form of a pseudobulge – unless another process increases the relaxation and turns this central concentration into a classical bulge.

Detailed numerical models of star formation and feedback in a multi-phase ISM, and observations of stellar population ages, mostly support that the giant clumps can survive against feedback from young massive stars for a few hundreds of Myr, unlike nearby molecular clouds. In this case, the giant clumps undergo dynamical friction from the host galaxy and its dark matter halo and migrate inward in a few 10^8 year, coalesce with the central bulge, or form a bulge if no bulge is present yet. In this case the induced relaxation is generally found to turn the central spheroid into a classical bulge with a high Sérsic index.

The detailed properties of bulges built by disc instabilities remain uncertain, and highly dependent on the physics of stellar feedback. Some studies find that it could be possible to form only a pseudobulge, but others find that in the most massive galaxies the whole system may turn into a classical spheroid through the violent disc instability, consistent with properties of early-type galaxies.

An interesting property of clump migration and central coalescence is that the induced relaxation can affect the stellar orbits of a pre-existing bulge, and cause dynamical evaporation from the central bulge toward a very extended, low-density faint stellar halo. In this case the process gets self-regulated and the bulge mass fraction does not grow above 10–15 % of the stellar mass for a Milky Way-mass high-redshift galaxy.

The violent instability of high-redshift disc galaxies presents other interesting properties that can form other sub-galactic components concurrently with bulges. The instability-driven inflow can typically provide one solar mass per year toward the central parsec, which may be sufficient to dominate the feeding of central supermassive black holes in moderate mass galaxies, and this is potentially supported by observations of active galactic nuclei in Main Sequence galaxies. Along with bulges and central black holes, the violent instability of high redshift galaxies can also grow the old thick stellar discs, which are ubiquitous around present-day spiral galaxies.

Acknowledgements I am grateful to Anna Cibinel, Jared Gabor, Marie Martig, Valentin Perret and Florent Renaud for providing some of the figures and material used in this review, and to Avishai Dekel and Bruce Elmegreen for triggering many new studies on the instability of high-redshift galaxies and the associated growth of bulges. The simulations shown in Fig. 13.7 were carried out on the GENCI computing resources and TGCC/Curie, under allocation GENCI-2015-04-2192.

References

Abraham, R. G., van den Bergh, S., Glazebrook, K., et al. 1996, ApJS, 107, 1
Abraham, R. G., Merrifield, M. R., Ellis, R. S., Tanvir, N. R., & Brinchmann, J. 1999, MNRAS, 308, 569
Agertz, O., Teyssier, R., & Moore, B. 2009, MNRAS, 397, L64
Agertz, O., Teyssier, R., & Moore, B. 2011, MNRAS, 410, 1391
Barro, G., Faber, S. M., Pérez-González, P. G., et al. 2014, ApJ, 791, 52
Behrendt, M., Burkert, A., & Schartmann, M. 2014, arXiv:1408.5902
Bekki, K., & Cioni, M.-R. L. 2007, MNRAS, 377, L20
Block, D. L., Bournaud, F., Combes, F., Puerari, I., & Buta, R. 2002, A&A, 394, L35
Bois, M., Bournaud, F., Emsellem, E., et al. 2010, MNRAS, 406, 2405
Bouché, N., Dekel, A., Genzel, R., et al. 2010, ApJ, 718, 1001
Bournaud, F., Combes, F., & Semelin, B. 2005, MNRAS, 364, L18
Bournaud, F., Elmegreen, B. G., & Elmegreen, D. M. 2007, ApJ, 670, 237
Bournaud, F., Daddi, E., Elmegreen, B. G., et al. 2008, A&A, 486, 741
Bournaud, F., & Elmegreen, B. G. 2009, ApJ, 694, L158
Bournaud, F., Elmegreen, B. G., & Martig, M. 2009, ApJ, 707, L1
Bournaud, F. 2010, Galaxy Wars: Stellar Populations and Star Formation in Interacting Galaxies, 423, 177
Bournaud, F., Chapon, D., Teyssier, R., et al. 2011, ApJ, 730, 4
Bournaud, F., Dekel, A., Teyssier, R., et al. 2011, ApJ, 741, L33
Bournaud, F., Juneau, S., Le Floc'h, E., et al. 2012, ApJ, 757, 81
Bournaud, F., Perret, V., Renaud, F., et al. 2014, ApJ, 780, 57
Bournaud, F., Daddi, E., Weiß, A., et al. 2015, A&A, 575, AA56
Brooks, A. M., Governato, F., Quinn, T., Brook, C. B., & Wadsley, J. 2009, ApJ, 694, 396
Cameron, E., Carollo, C. M., Oesch, P., et al. 2010, MNRAS, 409, 346
Comerón, S., Elmegreen, B. G., Salo, H., et al. 2014, A&A, 571, AA58
Ceverino, D., Dekel, A., & Bournaud, F. 2010, MNRAS, 404, 2151
Ceverino, D., Dekel, A., Mandelker, N., et al. 2012, MNRAS, 420, 3490
Ceverino, D., Klypin, A., Klimek, E. S., et al. 2014, MNRAS, 442, 1545
Ceverino, D., Dekel, A., Tweed, D., & Primack, J. 2014, arXiv:1409.2622
Chiappini, C., Górny, S. K., Stasińska, G., & Barbuy, B. 2009, A&A, 494, 591

Chiappini, C. 2009, IAU Symposium, 254, 191
Cibinel, A., Le Floc'h, E., Perret, V., et al. 2015
Coelho, P., & Gadotti, D. A. 2011, ApJ, 743, L13
Combes, F., & Gerin, M. 1985, A&A, 150, 327
Combes, F. 2001, Advanced Lectures on the Starburst-AGN, 223 (arXiv:0010570)
Combes, F., García-Burillo, S., Braine, J., et al. 2013, A&A, 550, AA41
Combes, F. 2014, A&A, 571, AA82
Conselice, C. J., Bershady, M. A., Dickinson, M., & Papovich, C. 2003, AJ, 126, 1183
Cowie, L. L., Songaila, A., Hu, E. M., & Cohen, J. G. 1996, AJ, 112, 839
Daddi, E., Cimatti, A., Renzini, A., et al. 2004, ApJ, 617, 746
Daddi, E., Dickinson, M., Morrison, G., et al. 2007, ApJ, 670, 156
Daddi, E., Dannerbauer, H., Elbaz, D., et al. 2008, ApJ, 673, L21
Daddi, E., Bournaud, F., Walter, F., et al. 2010, ApJ, 713, 686
Daddi, E., Dannerbauer, H., Liu, D., et al. 2014, ApJ in press (arXiv:1409.8158)
Dalcanton, J. J., & Bernstein, R. A. 2002, AJ, 124, 1328
Danovich, M., Dekel, A., Hahn, O., Ceverino, D., & Primack, J. 2014, arXiv:1407.7129
DeGraf, C., Dekel, A., Gabor, J., & Bournaud, F. 2014, arXiv:1412.3819
Dekel, A., Birnboim, Y., Engel, G., et al. 2009a, Nature, 457, 451
Dekel, A., Sari, R., & Ceverino, D. 2009b, ApJ, 703, 785
Dekel, A., & Krumholz, M. R. 2013, MNRAS, 432, 455
Dekel, A., & Burkert, A. 2014, MNRAS, 438, 1870
Dekel, A., & Mandelker, N. 2014, MNRAS, 444, 2071
Di Matteo, P., Lehnert, M. D., Qu, Y., & van Driel, W. 2011, A&A, 525, LL3
Di Matteo, T., Khandai, N., DeGraf, C., et al. 2012, ApJ, 745, LL29
Dubois, Y., Pichon, C., Haehnelt, M., et al. 2012, MNRAS, 423, 3616
Dubois, Y., Volonteri, M., & Silk, J. 2013, arXiv:1304.4583
Elbaz, D., Dickinson, M., Hwang, H. S., et al. 2011, A&A, 533, A119
Elmegreen, D. M., Elmegreen, B. G., & Hirst, A. C. 2004, ApJ, 604, L21
Elmegreen, B. G., & Elmegreen, D. M. 2005, ApJ, 627, 632
Elmegreen, B. G., Elmegreen, D. M., Vollbach, D. R., Foster, E. R., & Ferguson, T. E. 2005, ApJ, 634, 101
Elmegreen, D. M., Elmegreen, B. G., & Ferguson, T. E. 2005, ApJ, 623, L71
Elmegreen, B. G., & Elmegreen, D. M. 2006, ApJ, 650, 644
Elmegreen, D. M., Elmegreen, B. G., Ravindranath, S., & Coe, D. A. 2007, ApJ, 658, 763
Elmegreen, D. M., Elmegreen, B. G., Ravindranath, S., & Coe, D. A. 2007, ApJ, 658, 763
Elmegreen, B. G., Bournaud, F., & Elmegreen, D. M. 2008, ApJ, 684, 829
Elmegreen, B. G., Bournaud, F., & Elmegreen, D. M. 2008, ApJ, 688, 67
Elmegreen, B. G., Elmegreen, D. M., Fernandez, M. X., & Lemonias, J. J. 2009, ApJ, 692, 12
Elmegreen, B. G., & Burkert, A. 2010, ApJ, 712, 294
Elmegreen, B. G. 2011, ApJ, 737, 10
Elmegreen, B. G., Elmegreen, D. M., Sánchez Almeida, J., et al. 2013, ApJ, 774, 86
Emsellem, E., Cappellari, M., Krajnović, D., et al. 2007, MNRAS, 379, 401
Emsellem, E., Renaud, F., Bournaud, F., et al. 2015, MNRAS, 446, 2468
Epinat, B., Tasca, L., Amram, P., et al. 2012, A&A, 539, A92
Eskridge, P. B., Frogel, J. A., Pogge, R. W., et al. 2000, AJ, 119, 536
Förster Schreiber, N. M., Genzel, R., Lehnert, M. D., et al. 2006, ApJ, 645, 1062
Förster Schreiber, N. M., Genzel, R., Bouché, N., et al. 2009, ApJ, 706, 1364
Förster Schreiber, N. M., Shapley, A. E., Genzel, R., et al. 2011, ApJ, 739, 45
Förster Schreiber, N. M., Genzel, R., Newman, S. F., et al. 2014, ApJ, 787, 38
Gabor, J. M., & Bournaud, F. 2013, MNRAS, 434, 606
Gabor, J. M., & Bournaud, F. 2014, MNRAS, 437, L56
Gabor, J. M., & Bournaud, F. 2014, MNRAS, 441, 1615
Gao, Y., & Solomon, P. M. 2004, ApJ, 606, 271
García-Burillo, S., Usero, A., Alonso-Herrero, A., et al. 2012, A&A, 539, A8

Genel, S., Naab, T., Genzel, R., et al. 2012, ApJ, 745, 11
Genel, S., Dekel, A., & Cacciato, M. 2012, MNRAS, 425, 788
Genzel, R., Tacconi, L. J., Eisenhauer, F., et al. 2006, Nature, 442, 786
Genzel, R., Burkert, A., Bouché, N., et al. 2008, ApJ, 687, 59
Genzel, R., Newman, S., Jones, T., et al. 2011, ApJ, 733, 101
Genzel, R., Tacconi, L. J., Lutz, D., et al. 2015, ApJ, 800, 20
Guedes, J., Callegari, S., Madau, P., & Mayer, L. 2011, ApJ, 742, 76
Guo, Q., White, S., Boylan-Kolchin, M., et al. 2011, MNRAS, 413, 101
Guo, Y., Giavalisco, M., Ferguson, H. C., Cassata, P., & Koekemoer, A. M. 2012, ApJ, 757, 120
Guo, Y., Ferguson, H. C., Bell, E. F., et al. 2014, arXiv:1410.7398
Hennebelle, P., & Falgarone, E. 2012, Ann. Rev. of Astron. and Astrophys., 20, 55
Hopkins, P. F., Kereš, D., Murray, N., Quataert, E., & Hernquist, L. 2012, MNRAS, 427, 968
Hopkins, P. F., Kereš, D., & Murray, N. 2013, MNRAS, 432, 2639
Immeli, A., Samland, M., Westera, P., & Gerhard, O. 2004a, ApJ, 611, 20
Immeli, A., Samland, M., Gerhard, O., & Westera, P. 2004b, A&A, 413, 547
Inoue, S., & Saitoh, T. R. 2011, MNRAS, 418, 2527
Inoue, S., & Saitoh, T. R. 2011, MNRAS, 418, 2527
Inoue, S., & Saitoh, T. R. 2012, MNRAS, 422, 1902
Inoue, S., & Saitoh, T. R. 2014, MNRAS, 441, 243
Jog, C. J. 1996, MNRAS, 278, 209
Kereš, D., Vogelsberger, M., Sijacki, D., Springel, V., & Hernquist, L. 2012, MNRAS, 425, 2027
Kocevski, D. D., Faber, S. M., Mozena, M., et al. 2012, ApJ, 744, 148
Kraljic, K., Bournaud, F., & Martig, M. 2012, ApJ, 757, 60
Krumholz, M. R., & McKee, C. F. 2005, ApJ, 630, 250
Krumholz, M., & Burkert, A. 2010, ApJ, 724, 895
Lotz, J. M., Primack, J., & Madau, P. 2004, AJ, 128, 163
Mac Low, M.-M. 1999, ApJ, 524, 169
Magnelli, B., Lutz, D., Saintonge, A., et al. 2014, A&A, 561, A86
Mandelker, N., Dekel, A., Ceverino, D., et al. 2014, MNRAS, 443, 3675
Maraston, C., Pforr, J., Renzini, A., et al. 2010, MNRAS, 407, 830
Martig, M., Bournaud, F., Teyssier, R., & Dekel, A. 2009, ApJ, 707, 250
Martig, M., Bournaud, F., Croton, D. J., Dekel, A., & Teyssier, R. 2012, ApJ, 756, 26
Melvin, T., Masters, K., Lintott, C., et al. 2014, MNRAS, 438, 2882
Mullaney, J. R., Daddi, E., Béthermin, M., et al. 2012, ApJ, 753, L30
Murray, N., Ménard, B., & Thompson, T. A. 2011, ApJ, 735, 66
Murray, N. 2011, ApJ, 729, 133
Naab, T., Oser, L., Emsellem, E., et al. 2014, MNRAS, 444, 3357
Nelson, D., Vogelsberger, M., Genel, S., et al. 2013, MNRAS, 429, 3353
Newman, S. F., Genzel, R., Förster-Schreiber, N. M., et al. 2012, ApJ, 761, 43
Noguchi, M. 1999, ApJ, 514, 77
Oppenheimer, B. D., & Davé, R. 2006, MNRAS, 373, 1265
Padoan, P., Bally, J., Billawala, Y., Juvela, M., & Nordlund, Å. 1999, ApJ, 525, 318
Perez, J., Valenzuela, O., Tissera, P. B., & Michel-Dansac, L. 2013, MNRAS, 436, 259
Perret, V., Renaud, F., Epinat, B., et al. 2014, A&A, 562, A1
Puech, M. 2010, MNRAS, 406, 535
Renaud, F., Bournaud, F., Emsellem, E., et al. 2013, MNRAS, 436, 1836
Roos, O., Juneau, S., Bournaud, F., & Gabor, J. M. 2014, arXiv:1405.7971
Sargent, M. T., Daddi, E., Béthermin, M., et al. 2014, ApJ, 793, 19
Scannapieco, C., White, S. D. M., Springel, V., & Tissera, P. B. 2011, MNRAS, 417, 154
Schreiber, C., Pannella, M., Elbaz, D., et al. 2015, A&A, 575, AA74
Shapiro, K. L., Genzel, R., Förster Schreiber, N. M., et al. 2008, ApJ, 682, 231
Shapiro, K. L., Genzel, R., Quataert, E., et al. 2009, ApJ, 701, 955
Sheth, K., Regan, M. W., Scoville, N. Z., & Strubbe, L. E. 2003, ApJ, 592, L13
Sheth, K., Elmegreen, D. M., Elmegreen, B. G., et al. 2008, ApJ, 675, 1141

Shlosman, I., & Noguchi, M. 1993, ApJ, 414, 474
Simmons, B. D., Melvin, T., Lintott, C., et al. 2014, MNRAS, 445, 3466
Somerville, R. S., Hopkins, P. F., Cox, T. J., Robertson, B. E., & Hernquist, L. 2008, MNRAS, 391, 481
Somerville, R. S., & Davé, R. 2014, arXiv:1412.2712
Tacconi, L. J., Genzel, R., Smail, I., et al. 2008, ApJ, 680, 246
Tacconi, L. J., Genzel, R., Neri, R., et al. 2010, Nature, 463, 781
Tacconi, L. J., Neri, R., Genzel, R., et al. 2013, ApJ, 768, 74
Tamburello, V., Mayer, L., Shen, S., & Wadsley, J. 2014, arXiv:1412.3319
Taniguchi, Y., & Shioya, Y. 2001, ApJ, 547, 146
Teyssier, R. 2002, A&A, 385, 337
Teyssier, R., Pontzen, A., Dubois, Y., & Read, J. I. 2013, MNRAS, 429, 3068
Thooris, B., & Pomarède, D. 2011, IAU Symposium, 277, 263
Toomre, A. 1964, ApJ, 139, 1217
Trump, J. R., Barro, G., Juneau, S., et al. 2014, ApJ, 793, 101
van den Bergh, S., Abraham, R. G., Ellis, R. S., et al. 1996, AJ, 112, 359
Villalobos, Á., & Helmi, A. 2008, MNRAS, 391, 1806
Villalobos, Á., Kazantzidis, S., & Helmi, A. 2010, ApJ, 718, 314
Wuyts, S., Förster Schreiber, N. M., Genzel, R., et al. 2012, ApJ, 753, 114
Yoachim, P., & Dalcanton, J. J. 2006, AJ, 131, 226
Zanella, A., Daddi, E., Le Floc'h, E., et al. 2015, Nature in press.
Zolotov, A., Dekel, A., Mandelker, N., et al. 2014, arXiv:1412.4783

Chapter 14
Boxy/Peanut/X Bulges, Barlenses and the Thick Part of Galactic Bars: What Are They and How Did They Form?

E. Athanassoula

Abstract Bars have a complex three-dimensional shape. In particular their inner part is vertically much thicker than the parts further out. Viewed edge-on, the thick part of the bar is what is commonly known as a boxy-, peanut-, or X- bulge and viewed face-on it is referred to as a barlens. These components are due to disc and bar instabilities and are composed of disc material. I review here their formation, evolution and dynamics, using simulations, orbital structure theory and comparisons to observations.

14.1 Introduction

Boxy/peanut/X (for short B/P/X, or B/P) bulges protrude out of the central region of galactic discs viewed edge-on. Their name comes from their shape, which is reminiscent of a box, a peanut or an 'X' structure. Good examples are NGC 1381 and ESO 151-G004. There have been many observational studies of such objects over the years, while their formation and evolution have also been extensively studied with the help of simulations, both to understand their origin and as a link to secular evolution. Orbital studies have provided candidate families for the backbone of this structure.

Barlens components (bl for short) were introduced into the picture only quite recently (Laurikainen et al. 2011). They are defined as "lens-like structures embedded in the bars" (Laurikainen et al. 2013). They are thus found in the central part of barred galaxies "but are generally distinct from nuclear lenses by their much larger sizes" (Laurikainen et al. 2011). They are also distinct from standard lenses (Kormendy 1979) because they are shorter than bars (Laurikainen et al. 2013) and because along the bar major axis they blend smoothly in the bar radial density profile, without having any steep drop (Laurikainen et al. 2014; Athanassoula et al.

E. Athanassoula (✉)
Aix Marseille Université, CNRS, LAM (Laboratoire d'Astrophysique de Marseille), UMR 7326, 13388 Marseille 13, France
e-mail: lia@lam.fr

E. Laurikainen et al. (eds.), *Galactic Bulges*, Astrophysics and Space Science Library 418, DOI 10.1007/978-3-319-19378-6_14

2014). NGC 4314 and NGC 4608 are good examples of galaxies with a barlens component. Images of further example galaxies can be found in the NIRS0S (Near Infrared S0 survey) atlas (Laurikainen et al. 2011), the Hubble atlas (Sandage 1961), the S^4G (Spitzer Stellar Structure Survey of Galaxies) sample (Sheth et al. 2010), as well as in Figure 2 of Buta et al. (2006) and Figures 8 and 12 of Gadotti (2008).

Here I will discuss how these components form and evolve and what their properties and dynamics are, basing this discussion on simulations, orbital structure results and on comparison with observations. I will discuss neither the Milky Way bulge, nor bulges in a cosmological setting, and will not give a full account of observations, since all three subjects will be covered elsewhere in this book. I first review orbital structure results (Sect. 14.2), focusing on the families that can be building blocks of B/P/X/bl structures. I then turn to simulation results (Sect. 14.3). In particular, in Sect. 14.3.3 I discuss the ensuing shape of bars and the B/P extent. Comparison with observations is the subject of Sect. 14.4: morphology and photometry of Sect. 14.4.1; kinematics of Sect. 14.4.2. I discuss theoretical aspects of the barlens component in Sect. 14.5. Recent reviews on this or related subjects have been given by Kormendy and Kennicutt (2004), Athanassoula (2008, 2013a) and Kormendy (2008, 2013).

14.2 Orbital Structure

In order to understand the structure, kinematics or dynamics of a given galaxy, or of any of its substructures, it is necessary first to understand the orbits that constitute it. Particularly important for this are the periodic orbits – i.e. orbits that close in a given reference frame after a number of rotations – which constitute the backbone of the structure. These come in two types. *Stable periodic orbits* trap around them regular orbits, while *unstable periodic orbits* are linked to chaos. The latter, however, can also, in certain cases, contribute to the outline of structures.

14.2.1 Periodic Orbits in Two Dimensions

The orbital structure of bars in two dimensions (2D) is relatively simple. The main backbone here is the x_1 family, constituted of orbits which, in a frame of reference co-rotating with the bar, close after two radial oscillations and one revolution around the center, i.e. are in 2:1 resonance (Contopoulos and Papayannopoulos 1980; Athanassoula et al. 1983). They are elongated along the bar and their axial ratio varies with distance from the center, but also from one model to another. At their apocenters they often have cusps or loops (see Athanassoula 1992a for a study of their morphology). There are other families of orbits, such as the x_2 – which is also 2:1 but is elongated perpendicular to the bar – the 3:1, or the 4:1, but they are less

important for the global bar structure, although they are related to several specific aspects such as the shape of the bar, or the structure of the inner kpc.

In 2D studies, by construction, we can study orbital stability only in the plane and the trapped orbits are also planar. A fair fraction of the x_1 orbits are stable, but the amount of chaos depends strongly on the properties of the bar, such as its mass, axial ratio etc. (e.g. Athanassoula et al. 1983; Manos and Athanassoula 2011).

14.2.2 Periodic Orbits in Three Dimensions

In three dimensions (3D) the orbital structure becomes much more complex, even for planar orbits (e.g. Pfenniger 1984; Skokos et al. 2002a,b; Harsoula and Kalapotharakos 2009; Patsis and Katsanikas 2014a,b). Indeed – while in two dimensions periodic orbits can be stable or unstable depending on their response to in-plane perturbations – in 3D all orbits, including the planar periodic ones, can be subject to vertical perturbations, which in turn can introduce instability in the system. The latter is particularly important for our subject matter. At the energy value where a family turns from stable to unstable a new stable family is generated by bifurcation, and this may play an important role in the dynamics of the system. Thus, in barred galaxies there are a number of vertical families named by Skokos et al. as x_1v_1, x_1v_2, x_1v_3 etc.[1] These bifurcate from the x_1 family at the main vertical resonances, such as the 2:1, 3:1, 4:1 etc. There are generally two per resonance, one which crosses the symmetry plane perpendicular to the bar major axis at $z = 0$ and the other with $\dot{z} = 0$. Hence, x_1v_1 and x_1v_2 correspond to the 2:1 vertical resonance, x_1v_3 and x_1v_4 to the 3:1 etc. Trapping around these families determines the vertical thickness and structure of the bar. These vertical families, together with the x_1 family from which they bifurcate, form what is often referred to as the x_1 tree (Skokos et al. 2002a). Thus the backbone of a 3D bar is not the x_1 family but the x_1 tree. Examples of members of the main four vertical families are given in Fig. 14.1. These plots are taken from the work of Skokos et al. (2002a) where the bar is along the y axis, so that the end-on view[2] is the projection on the (x, z) plane and the side-on view[3] is the projection on the (y, z) plane. Since the bar potential is symmetric with respect to the equatorial plane, for each periodic orbit there is also its corresponding symmetric one (not shown here). Thus the side-on view of an x_1v_1 orbit has the shape of either a smile ($\smile$) or a frown ($\frown$).

[1] For certain potentials there is also the z3.1s family whose morphology resembles that of the x_1v_4 family, but it is not related to the x_1 tree . Another potentially useful family is the x1mul2 (Patsis and Katsanikas 2014a).

[2] In the end-on view the galaxy is observed edge-on with the line of sight along the bar major axis.

[3] In the side-on view the galaxy is observed edge-on with the line of sight perpendicular to the bar major axis.

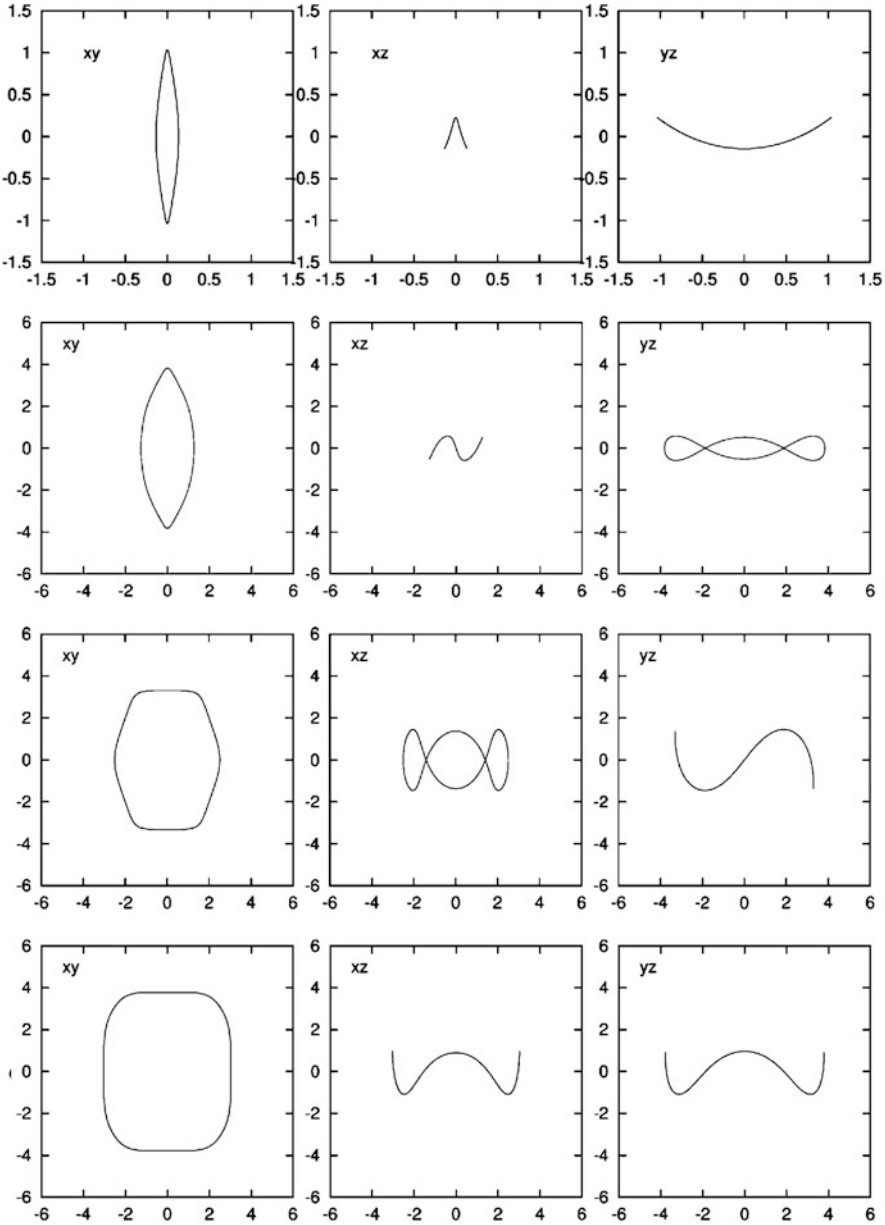

Fig. 14.1 Four examples of periodic orbits from vertical families. From top to bottom we have members of the x_1v_1, x_1v_3, x_1v_4 and x_1v_5 families. There are three views for each orbit: face-on (*left*), end-on (*middle*) and side-on (*right*). Note that the linear scales used in the plots of the various orbits are not the same (This plot is a composite made of parts of figures 8, 9, 10 and 14 of Skokos, Patsis & Athanassoula, *Orbital dynamics of three-dimensional bars – I. The backbone of three-dimensional bars. A fiducial case*, 2002, MNRAS, 333, 847. By permission of Oxford University Press)

The orbits of each family can be useful for building a vertically thick structure only within certain energy ranges and fill only specify regions of the 3D space. As a result, these orbits do not thicken vertically the whole bar; instead they only thicken its inner parts. Thus, if the vertical families are populated, the bar should have two parts: an inner one that is vertically thick and an outer one which is vertically thin.

A further point to note is that the members of the various families have different extents along the bar major axis relative to the bar length, and their vertical extent and face-on shapes differ considerably from one family to another. The x_1v_1 family, which bifurcates at the lowest energy, has the smallest extent along the bar major axis and the largest extent perpendicular to the equatorial plane. Its face-on shape is rather elongated. Higher order families, compared to lower order ones, bifurcate at higher energies, have a larger extent along the bar major axis close to the equatorial plane and a smaller one perpendicular to this plane. Their face-on outline is much less elongated. Measuring the ratio of the bar length (as determined from the orbits that constitute it) to the length of the thick part (also from its orbits), Patsis et al. (2002, hereafter PSA02) find that this number for the x_1v_1 is roughly in the range [2., 4.], while for the x_1v_4 family it is around 1.1 to 1.3. A note of caution is necessary though: the only realistic bar potential used so far in 3D orbital calculations is the Ferrers' bar potential (Ferrers 1877). It is thus not possible to check to what extent these numbers are model dependent. Moreover, the density corresponding to the Ferrers potential does not have an appropriate side-on shape, i.e. it is neither boxy- nor peanut- shaped. Performing more orbital structure calculations using a yet more realistic potential would be highly desirable at this stage.

14.2.3 The Role of Chaotic Orbits

Stable periodic orbits and regular orbits trapped around them are not the only way of building the galactic structures we are discussing here. Unstable periodic orbits are linked to chaos and could, in some cases, provide an alternative. Indeed, sticky chaotic orbits may also contribute to such structures either if they stick to regular tori around the stable families or to unstable asymptotic curves of the unstable periodic orbits (Contopoulos and Harsoula 2008).

Patsis and Katsanikas (2014a,b) examined the evolution of the phase space in a 3D bar and underlined the role that chaotic phenomena may play in building the B/P/X structures. This is a promising alternative and merits further work to establish its role in galaxies. High quality N-body simulations, provided they are realistic, are a perfect test bed for such types of studies, because they offer not only the possibility of viewing the structures from any desired viewing angles, but also allow studies at the level of individual orbits. They can thus give information on the amount of chaotic orbits and also on their specific contributions to the B/P/X structures. First steps in this direction have already been made (Athanassoula 2005c; Harsoula and Kalapotharakos 2009; Manos and Machado 2014) and more specific applications are underway.

14.3 Simulations

14.3.1 General Description

Although inklings of a boxy/peanut structure can be already seen in the edge-on views of the simulations of Hohl and Zang (1979) and Miller and Smith (1979), the first to show it convincingly were those of Combes and Sanders (1981). They were followed by Combes et al. (1990), who found a B/P morphology in all their bar-forming simulations viewed side-on. This forms somewhat after the bar, with a delay of the order of a Gyr (see Sect. 14.3.2). Using axisymmetric definitions for the resonances, the authors found that the horizontal and vertical inner Lindblad resonances (ILRs) coincide by the end of the simulations. This, however, is presumably model dependent (see e.g. Quillen et al. 2014, for a different behavior). Both Combes et al. (1990) and Pfenniger and Friedli (1991) found that the backbone of the peanut should be a vertically 2:1 family.

Pfenniger and Friedli (1991) and Raha et al. (1991), running similar simulations, found that the formation of the B/P structure is preceded by an asymmetric phase during which the equatorial plane is not a symmetry plane anymore. In the latter of these two papers this was ascribed to the fire-hose instability (Toomre 1966), and in the former to orbital instabilities and the ensuing families (Sect. 14.2). Both Combes et al. (1990) and Raha et al. (1991) note that the B/P formation is associated with a drop of the bar strength, which in many cases can be strong and sharp. The latter work conjectured that "bars may be even destroyed by this instability". However, Debattista et al. (2004, 2006) ran a larger set of simulations and found no clear case of bar destruction. From my own, yet larger set of simulations, I also found the same result (unpublished). Strictly speaking, this does not prove that a bar destruction can not occur, it just shows that it is rather unlikely, unless this occurs in a part of the parameter space which has not yet been explored. Note also that after its sharp decrease, the bar strength starts increasing again, or at least stays relatively constant (see Sect. 14.3.2).

Athanassoula and Misiriotis (2002, hereafter AM02) and Athanassoula (2005a) 'observed' the bars and B/P bulges in their simulations and obtained specific results on their shape, extent and kinematics. The quantitative estimates they obtained showed clearly that the B/P bulges are shorter than bars. AM02 and Athanassoula (2003, 2005a) showed that stronger bars produce on average stronger B/P bulges, i.e. bulges which extended further out from the galactic plane, thus confirming the observational result of Lütticke et al. (2000b). They also found that the thick part of relatively weak bars generally has a boxy shape, that of stronger ones a peanut shape, and the very strong ones an X shape.

Mihos et al. (1995) simulated a minor merger of a disc galaxy with its satellite. This induces a strong bar which forms a clear X shape. Strictly speaking, this is not really an example of a B/P formation from a merger, since all the companion does is to drive a bar, which, once formed, buckles and thickens vertically. This driven bar

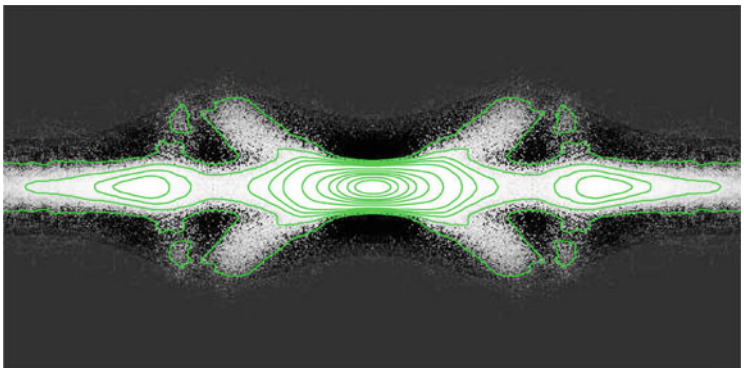

Fig. 14.2 Unsharp masked image of a simulation with a strong bar viewed side-on. The lighter shades in the grey scale plot correspond to higher values and the darkest areas correspond to negative values. The isodensities were chosen so as to show best the relevant features (From figure 6 of Athanassoula, *On the nature of bulges in general and of box/peanut bulges in particular: input from N-body simulations*, 2005, MNRAS, 358, 1477. By permission of Oxford University Press)

is very strong and according to the results discussed above, one would expect an X shaped bulge to form, as indeed occurred in the simulation.

Athanassoula (2005a) unsharp masked[4] a number of images from N-body simulations with the disc viewed edge-on and found a number of interesting morphological features. An example is given in Fig. 14.2, which clearly shows an X-shape, whose four arms do not meet at the center but in pairs at a distance from it. In other examples though (not shown here) these four arms meet together in the center. Schematically, these two types of X shapes can be shown as $>-<$ and $><$, respectively. They were later found also in observations and were dubbed off-centered and centered Xs, respectively (Bureau et al. 2006). There are also two clear maxima, one on either side of the center of the simulated galaxy. In the example of Fig. 14.2 they are due to an inner ring, but they could also have been due to a superposition of appropriate orbit families (PSA02).

Martinez-Valpuesta et al. (2006) witnessed in their simulation a second buckling event occurring between 5 and 8 Gyr, i.e. when the bar is in its secular evolution phase. At the beginning of this time range, the bar length is already of the order of 12 ± 1 kpc, and continues growing after the end of the second buckling, reaching roughly 16 kpc at 12 Gyr. During the first buckling, the asymmetry is strongest in the region closer to the center and during the second one roughly in the middle of the bar region. Such events can also be seen, or inferred, in other simulations (e.g. O'Neill and Dubinski 2003; Athanassoula 2005b; Athanassoula et al. 2013) and even a triple buckling has been reported (Debattista et al. 2006).

[4]Unsharp masking, also called median filtering, consists in replacing the value of each pixel by the difference between it and the median of all pixel values within a circular aperture centered on the pixel. This highlights sharp features.

Including gas in simulations may or may not suppress buckling.[5] Berentzen et al. (1998, 2007) and Villa-Vargas et al. (2010) use an isothermal gas and note that the vertical buckling is much less pronounced than in a similar but collisionless simulation, to the point of being difficult to detect by simple visual inspection. They find that with increasing gas fraction, both the buckling and the B/P strength decrease. When radiative cooling is included, buckling is prohibited (Debattista et al. 2006; Wozniak and Michel-Dansac 2009). This is in agreement with the bar and peanut strength evolutions of the simulations in Athanassoula et al. (2013, further analyzed in Iannuzzi and Athanassoula 2015, hereafter IA15).

14.3.2 Evolution of Bar Related Quantities

In Fig. 14.3 I show the time evolution of bar-related quantities for three different collisionless simulations. The upper panel corresponds to what is referred to in AM02 as a MD model, i.e. a model where the disc dominates in the inner region (a maximum disc model). The two lower panels correspond to what is referred to in AM02 as an MH model. Here the halo and the disc contributions are comparable in the inner parts and the halo plays a more prominent role in the angular momentum redistribution within the galaxy.

In the MD model, the bar starts growing very rapidly, roughly 0.8 Gyr from the beginning of the simulation. Its growth phase lasts also less than a Gyr, after which the strength of the $m = 2$ component reaches a maximum, due to some extent to a strong, but short-lived two-armed spiral (Athanassoula 2012). Between $t = 3.6$ and 4.2 Gyr the bar strength decreases very strongly and rapidly, after which it starts increasing again due to secular evolution. The buckling strength is measured from the asymmetry with respect to the equatorial plane and shows a strong and narrow peak at the buckling time ($t = 3.65$ Gyr). The strength of the B/P increases abruptly in the time interval during which the bar strength drops. Note that the time of maximum asymmetry is within this time range.

The corresponding plots for the first MH run (bottom left panel) show the same qualitative behavior as model MD, but with clear quantitative differences. Namely, the bar starts growing considerably later ($t = 3$ Gyr), grows more during the secular evolution phase and reaches a higher strength by the end of the run. These differences can be easily understood because the halo delays bar formation initially, but at later times helps the bar to grow by absorbing angular momentum emitted from the bar region (Athanassoula 2002, 2003).

The third set of plots (bottom right panel) is also for a MH run but shows an interesting difference from the previous simulation, namely there is a second buckling event, occurring roughly between 7 and 9 Gyr. The second asymmetry

[5] Peanut formation without buckling has also been found in simulations with no gas (Quillen et al. 2014).

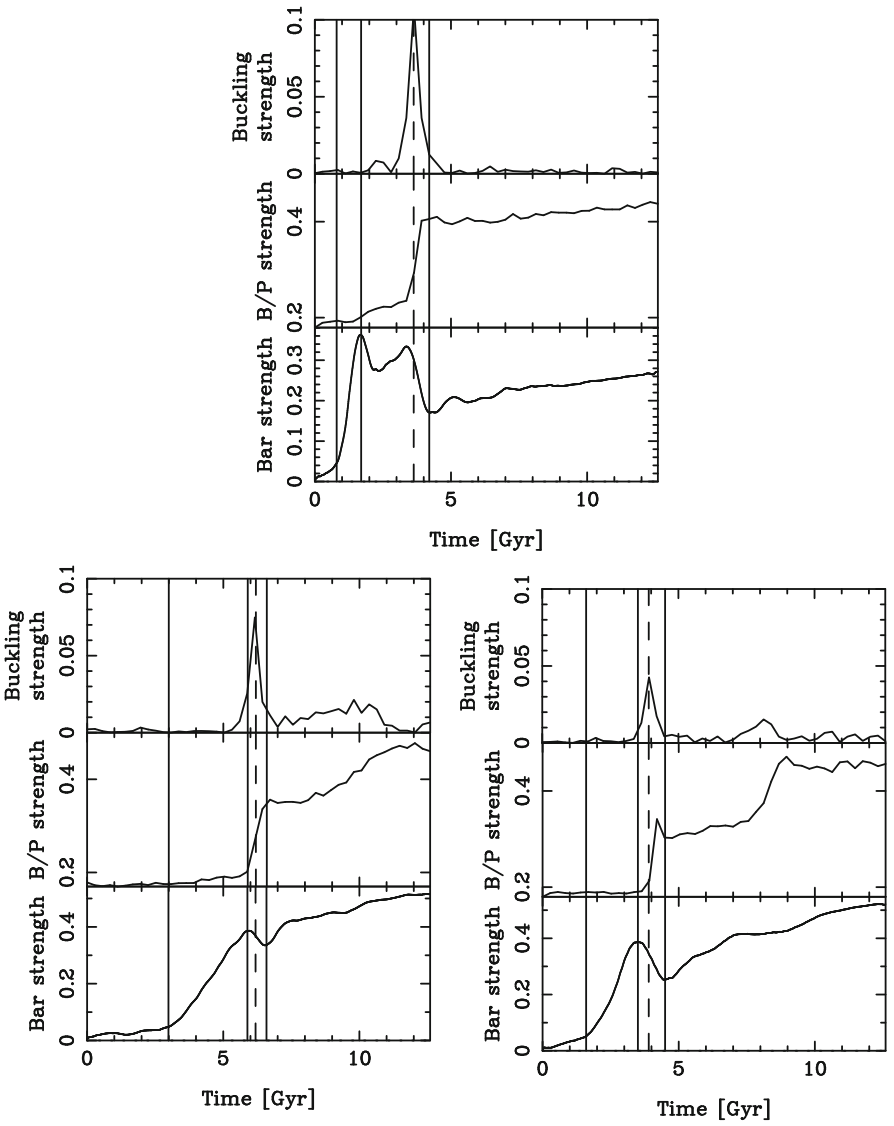

Fig. 14.3 Evolution of bar related quantities for three simulations (see text). Each panel has three sub-panels, showing the evolution of the asymmetry (*top*), of the B/P strength (*middle*) and of the bar strength as given by the m = 2 Fourier component of the density (*bottom*). In all panels, the *first vertical solid line* corresponds to the time the bar starts growing and the second to the end of the growth phase (when the amplitude of the bar strength has reached a local maximum). The *third (dashed) vertical line* shows the maximum of the buckling strength (maximum asymmetry) and the *last (solid) line* the minimum of the bar strength before the start of the secular evolution phase

peak is less high and also broader than the first one, i.e. the second buckling lasts considerably longer but is less strong. The time range during which the peanut strength increases is also somewhat longer, and the increase in B/P strength considerable. During that time the bar strength stops increasing and stays roughly constant.

The buckling episode can also be accompanied by an abrupt change of σ_z/σ_r, where σ_z and σ_r are the z and radial components of the velocity dispersion, respectively (e.g. Debattista et al. 2006; Martinez-Valpuesta et al. 2006; Athanassoula 2008). Saha et al. (2013), however, present a case where a sharp drop occurs well before the buckling and propose an alternative indicator, namely the tilt of the velocity ellipsoid in the meridional plane.

14.3.3 The 3D Shape of Bars

Athanassoula (2005a) presented evidence on the 3D shape of bars coming from various sources, including orbital structure calculations, simulations and various observations of real galaxies. All converges to the same conclusion: Bars have a complex 3D shape with a vertically thick inner part and a thin outer part. Therefore, a B/P/X shaped component is a part of a bar, and, more specifically, its thick part. To visualize this best, it is informative to take a snapshot from an N-body simulation of a bar-forming disc with no classical bulge at a time when both the bar and the B/P feature have formed. Then select only the particles which in the (x, y) view are located roughly within the outer isodensities of the bar and visualize them from many viewing angles. Figure 14.4 shows an example of such a result from a simulation which was chosen so as to have a strong bar with a somewhat X-like edge-on view. The top panel shows the face-on view and the bottom one gives the edge-on one, with two intermediate viewing angles in between (second and third panels). For a better visualization see the complete animation showing the slow rotation around the bar major axis in http://195.221.212.246:4780/dynam/movie/BPreview/BPreview.avi

In the face-on view the bar is seen to have a length of roughly 8 kpc, while in the near-side-on views the thick part is seen to have an extent of roughly 4 kpc, i.e. is clearly less extended than the bar. The ratio of the two extents argues that the main contributor to the B/P/X feature could be the x_1v_1 family. The face-on shape of the thick part of the bar can be described as a squashed oval, because the parts of the isodensities near the bar minor axis form nearly straight lines parallel to the bar major axis. In the second view (second panel from the top), the outermost parts have a clearly rectangular-like outline, which becomes X-shaped in the fully side-on view (bottom panel).

Both in the face-on and in the side-on views the outer part of the bar is quite thin. Near its ends, the bar outline becomes more extended in the face-on view, with a ansae-like shape.

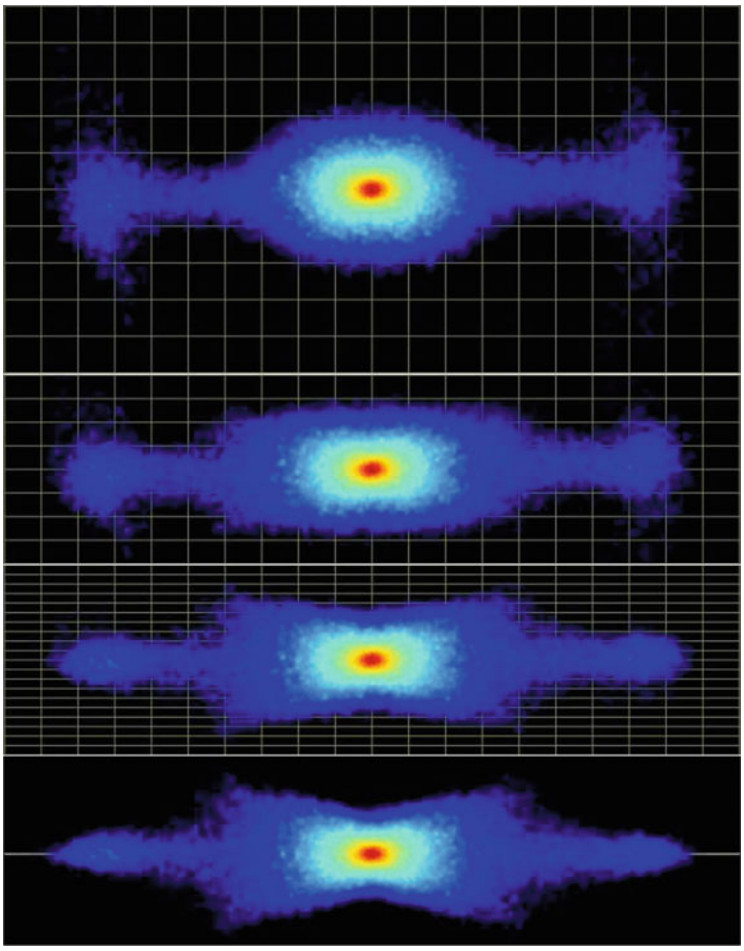

Fig. 14.4 Four views of a strong bar (see text). A Cartesian grid with 1×1 kpc cell size and located on the $z = 0$ (equatorial) plane is also shown in all panels, to give a better understanding of perspective and size

Figure 14.5 gives similar information, but for a weaker bar. In the face-on view the bar has a length of roughly 4 kpc, while in the near-side-on views (not shown here) the thick part is seen to have an extent of roughly 1.5 kpc, i.e. the latter is clearly less extended than the bar along its major axis. The ratio of the two extents now argues strongly that the main contributor to the B/P feature is the $x_1 v_1$ family. The face-on shape of the thick part of the bar is rectangular-like in the inner parts, but not in its outermost parts where it is more oval-like. In the lower panel, the outermost B/P parts have a clearly rectangular outline, so that this feature could be called boxy.

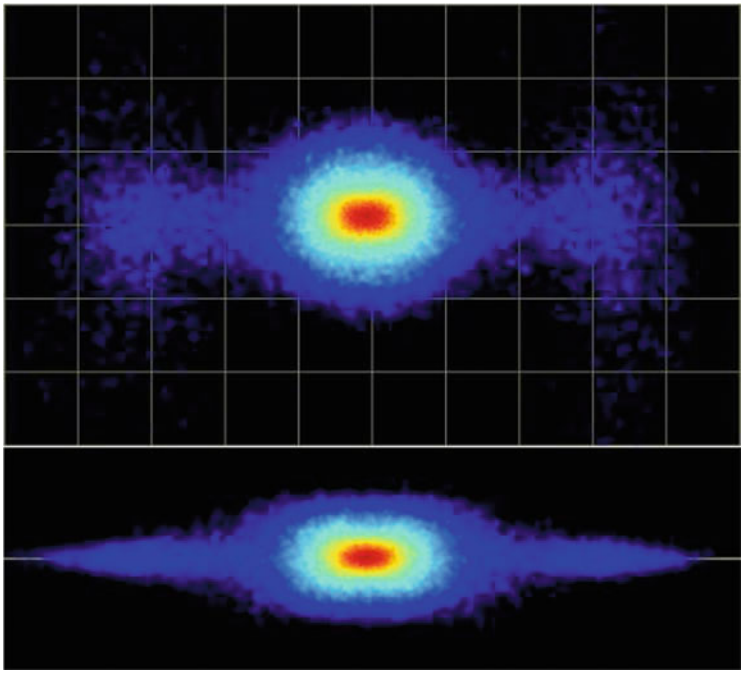

Fig. 14.5 Same as in Fig. 14.4, but for a weaker bar. Only the face-on (*upper panel*) and side-on (*lower panel*) views are shown

In the face-on view the outer part of the bar is relatively less thin than in the previous example, and near its ends, it has extensions similar to the previous example, i.e. shaped as ansae.

14.4 Comparisons with Observations

14.4.1 Morphology and Photometry

As already discussed in the previous section, a face-on view is not favorable to viewing the thick part of the bar, while edge-on views are not favorable for the thin part of it. The best compromise comes from intermediate, but close to edge-on cases. This was first noted by Bettoni and Galletta (1994) for NGC 4442 which has an inclination angle $i = 72°$, Quillen et al. (1997) for NGC 7582 with $i = 65°$ and Athanassoula and Beaton (2006) for M31 with $i = 77°$. In this last paper Athanassoula and Beaton viewed N-body simulations from different viewing angles to compare with the near infrared (NIR) observations of Beaton et al. (2007). The B/P is easily recognized, while the outer thin part of the bar contributes two 'elongations' which appear offset from major axis of the B/P isodensities. For

the inclination of M31, this offset is best seen when the angle between the bar and the galaxy major axes is between 20° and 50°, but this range could well be somewhat model dependent. Erwin and Debattista (2013) extended this study to smaller inclinations and showed that the B/P feature can be detected even at inclinations as low as 40°, although the range of bar position angles for which the 'elongations' (by them called 'spurs') are clearly visible is considerably diminished. Using a sample of 78 nearby early type barred galaxies with inclinations less than 65° they showed that the extent of the thick part of the bar is between 0.4 and 3.8 kpc and the relative extent compared to that of the total bar is 0.38 ± 0.08.

It is possible to obtain information on both the bar and the boxy/peanut in edge-on galaxies by using photometric profiles from strips parallel to the major axis (i.e. the projected equatorial plane). The signature of the bar on the profile along the major axis is a ledge followed by a sharp drop of the intensity. The distance of the drop from the center of the galaxy gives the length of the bar projected on the plane of the sky. Similarly, profiles from strips parallel to and offset from the major axis give the projected length of the B/P feature. This technique has been widely used (e.g. Wakamatsu and Hamabe 1984; Dettmar and Barteldrees 1990; D'Onofrio et al. 1999).

Lütticke et al. (2000a) analyzed a sample of about 1350 edge-on disc galaxies and found that about 45 % of all bulges are B/P shaped. In a sequel paper (Lütticke et al. 2000b) they analyzed photometry of 60 edge-on galaxies in the NIR to minimize the effect of dust and concentrate on the old stellar population. They found a correlation between prominent B/P bulges and strong bar signatures, which they interpret as a dependence of the boxiness on the bar strength, as was later confirmed by simulations (Sect. 14.3.1). They also give the ratio of the bar extent to that of the B/P. Unfortunately, they measured the bar length up to the end of the density drop, which systematically overestimates the bar length and makes comparisons with other works difficult.

Bureau et al. (2006) analyzed the structure and morphology of 30 edge-on galaxies using *K*n-band images. With the help of unsharp masking they showed that galaxies with a B/P structure have more complex morphology than those without it, revealing centered or off-centered X shapes and secondary maxima. These are an "essentially near-perfect match" to the unsharp masks of images of N-body simulations given by Athanassoula (2005a) (Sect. 14.3). ESO 151-G004 (Fig. 14.6) is a good example of an off-centered X shape and NGC 1381 of a centered one (see Fig. 1 of Bureau et al. 2006). A large fraction of the galaxies have also two secondary maxima, one on each side of the center, similar to and at similar locations as the unsharp masked simulated galaxies (Athanassoula 2005a). More unsharp masked galaxies, agreeing equally well with simulations, can be found in Aronica et al. (2003) and Patsis and Xilouris (2006).

Bureau et al. also compared two types of surface brightness radial profiles, one from the major axis surface brightness (lower curve in the bottom panel of Fig. 14.6) and the other by summing the data vertically until the noise level of the image was reached (upper, brighter curve in the same panel and figure). The difference between the two argues that the vertical scale length varies with radius. Axisymmetric disc

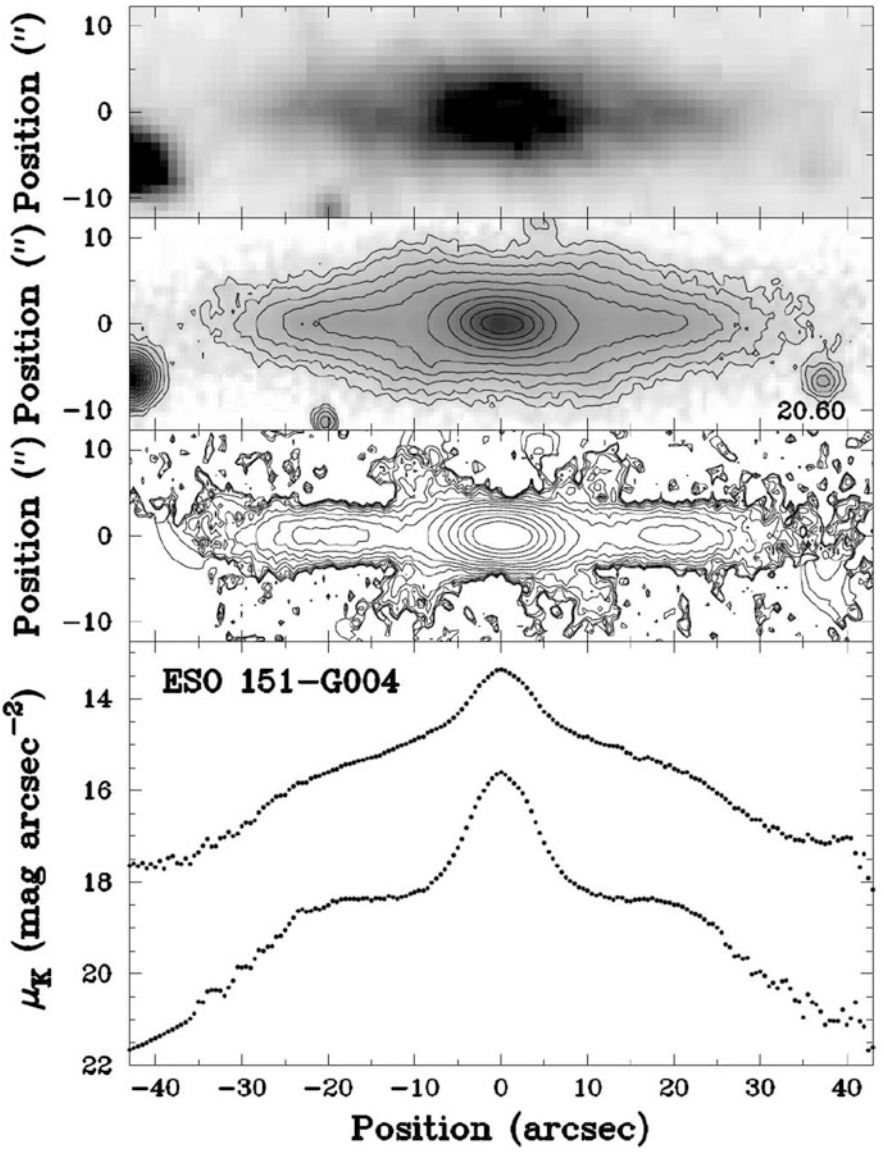

Fig. 14.6 Images and surface brightness profiles of ESO 151-G004. From top to bottom we have a SDSS image of the galaxy, a *K*n-band image, a median-filtered *K*n-band image, and major-axis (*fainter*) and vertically summed (*brighter*) surface brightness profiles, all spatially registered (Panel from figure 1 of Bureau et al., *K-band observations of boxy bulges – I. Morphology and surface brightness profiles*, 2006, MNRAS, 370, 753. By permission of Oxford University Presa)

galaxies generally have only two major components[6]: the disc and the classical bulge. Yet galaxies with a B/P structure have three or four characteristic regions. From the innermost to the outermost, the first region has a very steep profile and is generally associated with the bulge(s). Then follows a shallow or even flat region which is associated with the bar and in some cases links outwards to the disc component. In other cases, in between this shallow component and the disc there is a steep drop, associated with the corresponding features seen at the end of face-on bars both in observed and in simulated galaxies. All these features show up better on the cuts along the major axis than on vertically summed ones, as expected.

14.4.2 Kinematics

Position velocity diagrams (hereafter PVDs) obtained from emission line, long slit spectra of galaxies with B/P bulges (Kuijken and Merrifield 1995; Merrifield and Kuijken 1999; Bureau and Freeman 1999) show a number of interesting features, of which the most important has the form of a tilted X with one near-vertical branch and the other at an angle, and a clear gap between the two. There is also material in the so-called forbidden quadrants. These features were already linked to bars by Kuijken and Merrifield (1995).

Bureau and Athanassoula (1999) made model PVDs from the planar periodic orbits in a barred galaxy model. Although this approach is too crude to reproduce, even approximately, observed PVDs it can give valuable insight. There are clear signatures of the x_1 and the x_2 families. The latter is near-vertical in the PVD space, while the former is at an angle to it. Furthermore there is signal in the forbidden quadrants, resulting from the elongated shape of the orbits. To actually model emission line PVDs, Athanassoula and Bureau (1999) used the gas flow simulations of Athanassoula (1992b) viewing them edge-on. They found that the shocks along the leading edges of the bar and the resulting inflow lead to the characteristic gap seen in observed PVDs. This gap thus reliably indicates the presence of a bar and the existence of an ILR. It also sets strong constraints on the orientation of the bar with respect to the line of sight.

Chung and Bureau (2004) made long-slit absorption line kinematic observations along the major axis of the 30 galaxies of the Bureau and Freeman (1999) sample. They used Gauss-Hermite series up to fourth order and obtained the integrated light, the mean stellar velocity V, the velocity dispersion σ and the third and fourth order moments h_3 and h_4. Bureau and Athanassoula (2005) used the same techniques and, in as much as possible, also the same software to 'observe' N-body simulations from an edge-on perspective. They found similar signatures in these profiles, namely (i) a rotation curve with characteristic double hump, (ii) an h_3 that correlates with

[6]Since here I concentrate on the structure of the inner parts, I do not discuss outer breaks and the discs beyond them.

V over most of the bar extent and (iii) a velocity dispersion with a central peak which in the center-most region may be flat or have a relatively shallow minimum. At intermediate radii σ has a plateau, which may end on either side by a shallow maximum before a steep drop (see also AM02).

The work described so far has only considered 1D velocity information on a slit along the major axis. Obtaining information beyond this for NGC 4565, Kormendy and Illingworth (1982) made a very interesting finding, namely that, within the bulge, the rotational velocity changes very little with height, which was dubbed 'cylindrical rotation'. This was confirmed for other galaxies by many other studies (e.g. Bettoni and Galletta 1994; Fisher et al. 1994; Falcon-Barroso et al. 2004; Williams et al. 2011, and references therein). From the simulation side, a very spectacular cylindrical rotation was found by AM02 for a strongly barred galaxy viewed side-on. Nevertheless, although there may be some rough relation between bar strength and cylindrical rotation, it is far from being a clear correlation, as was found from the observational side by Williams et al. (2011) and from the simulations by IA15.

IA15 extended previous work, by including the second dimension and by using Voronoi binning and the software of Cappellari (Cappellari and Copin 2003). They also used simulations including gas, star formation, feedback and cooling, partly from Athanassoula et al. (2013). They recover the results of Bureau and Athanassoula (2005) and also find peanut related signatures (elongated wings of large h_3 values and X-shaped regions of deep h_4 minima) roughly in an area covering the peanut.

When viewed end-on, bars can be mistaken for classical bulges (e.g. AM02). This holds also for small departures of the bar major axis from the line of sight, not exceeding 10° (Athanassoula 2005a). IA15 investigated the case where both a classical bulge and an end-on viewed bar are present and note that the existence of the bar can be seen in the kinematics, although its signatures are considerably weaker than in the absence of the classical bulge, erroneously hinting to a much weaker bar than actually present.

Similar work, but for face-on views showed that the kinematic signature of a face-on peanut is two minima, one on either side of the center (Debattista et al. 2004; Mendez-Abreu et al. 2008). These results were recovered also by IA15, who also examined the kinematic signatures of the second bucklings. These are much deeper than the corresponding ones of the first buckling and could therefore be easier to observe. Furthermore, the second buckling lasts longer than the first one, which means there would be a higher probability to observe it.

Note that a few large integral-field spectroscopic surveys of nearby galaxies are already available, and many more are starting. Such data, particularly from large telescopes, can provide important new information to further our understanding of bars.

14.5 Barlenses

As mentioned in the Introduction, barlenses (Fig. 14.7) were introduced as separate components only very recently, so very little theoretical work on these structures has so far been made. Athanassoula et al. (2013) ran a number of high resolution simulations including gas and its physics (star formation, feedback and cooling) and found very realistic morphologies (see their figures 4 and 5 for face-on views). In particular, the inner parts of the bars showed structures whose morphology is very reminiscent of barlenses (see also Figs. 14.4 and 14.5 here). To substantiate this visual impression and to understand the origin of these structures, Athanassoula et al. (2014, hereafter ALSB) created fits images from the snapshots of these runs and analyzed them using the same procedures and software as those used for the analysis of real galaxy images (e.g. Laurikainen et al. 2010).

The comparison to observations started by a visual morphological assessment, which allowed ALSB to make comparisons of observed and simulated galaxy images. The simulated radial projected density profiles along the bar major and minor axes are very similar to those found from observations. Ellipse fits and decompositions of the simulated galaxy images allowed further comparisons. The results are in very good agreement with those found from observed galaxies and showed that the structures found in the simulations can indeed be called barlenses.

An understanding of the nature of the barlens components was now possible from an analysis of the simulations. By viewing snapshots from many different angles, ALSB showed that *barlenses are the vertically thick part of the bar viewed face-on, i.e. a barlens and a boxy/peanut/X bulge are the same component, but simply viewed from a different viewing angle*.

ALSB, furthermore, came up with a rule of thumb to estimate the extent of the thick part of the bar along the bar major axis, simply from the shape of the isophotes. Based on this, it is possible to estimate galactic potentials more accurately (Fragkoudi et al. 2015), leading to improvements both in orbital and gas flow calculations. ALSB also found from the simulation data correlations between the bar strength and barlens related quantities. These were confirmed by observations in Laurikainen et al. (2014).

A further interesting point is that the barlens component can be, in some cases, mistaken for a classical bulge (ALSB). Thus the fraction of disc galaxies with no classical bulge is presumably larger than what is actually acknowledged. Furthermore, in decompositions where the barlens is taken into account as a separate component, the mass of the classical bulge relative to the total (B/T) is considerably smaller than that found when a single component is used to model the bar. Laurikainen et al. (2014) find for their sample that $< B/T >= 0.1$ when a bl component is included in the decomposition, compared to $< B/T >= 0.35$ obtained from similar decompositions when the barlens component is omitted.

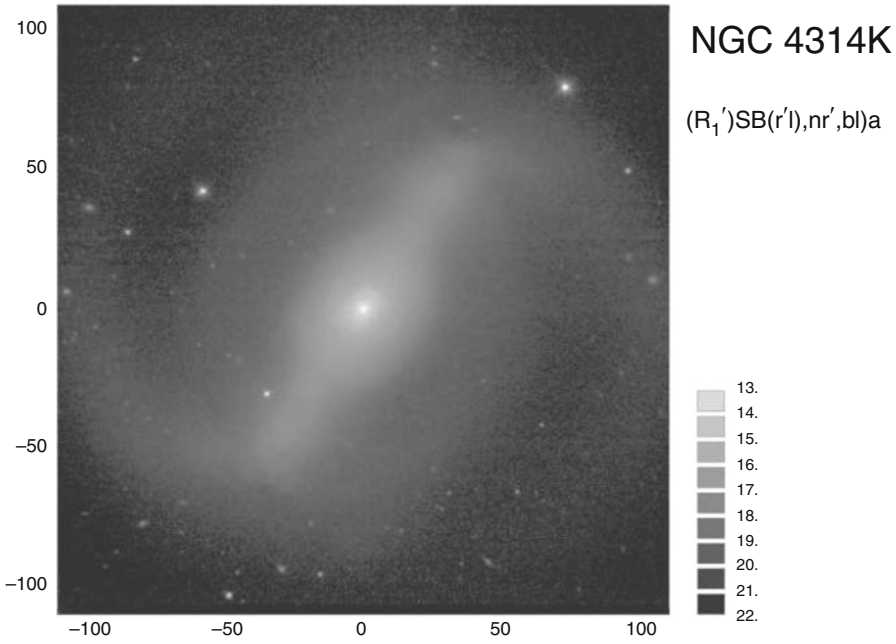

Fig. 14.7 NIRS0S image of NGC 4314. The two components of the bar are clearly discernible. The inner component is shorter and fatter and the outer one longer and more elongated (Reproduced from Laurikainen et al. 2011, *Near-infrared atlas of S0-Sa galaxies (NIRS0S)*, 2011, MNRAS, 418, 1452. By permission of Oxford University Press)

14.6 Nomenclature

This situation in which the same object, namely the thick part of the bar, is known by several different names (B/P/X bulges, barlenses) depending on the viewing angle is not very satisfactory. It comes from the fact that observations preceded theory and the thick part of the bar was observed from different angles well before N-body simulations and orbital structure studies established the 3D shape of bars.

The situation is further complicated by the fact that the thick part is rightfully called a bulge by the two most widely used definitions of a bulge. According to the first definition, a bulge has a smooth light distribution that swells out of the central part of a disc viewed edge-on. B/P/Xs clearly fulfill this definition. The second definition of bulges is based on radial photometric profiles. Here the bulge is identified as the additional light in the central part of the disc, above the exponential profile fitting the remaining (non-central) part. Barlenses clearly fulfill this definition (ALSB, Laurikainen et al. 2014).

Thus B/P/X/bl objects (i.e. the inner thick part of the bar) deserve to be called ‘bulges’ with both current definitions. This is unsatisfactory and calls for a change of the definition of a ‘bulge’ so as to include kinematics. Bulges should be defined

as objects that protrude out of the galactic disc in edge-on galaxies, AND contribute to the additional light in the inner parts of the radial photometric profile, above the disc exponential profile, AND are clearly more pressure than rotationally supported (as measured e.g. by their $<V>/\sigma$ value). Under this definition, only what is now known as classical bulges (Kormendy and Kennicutt 2004; Athanassoula 2005a) would qualify as bulges. B/P/X/bl objects could then rightfully be called the thick part of the bar, while discy pseudo-bulges (Kormendy and Kennicutt 2004; Athanassoula 2005a; Erwin 2008) could then be called inner discs. This suggestion deserves some consideration, since the nomenclature problem in this subject is becoming quite acute.

14.7 Summary

Shortly after their formation, bars become vertically unstable. At that point they may, or may not buckle out of the equatorial plane of the galaxy. Following this possible asymmetric stage, or directly after the onset of the instability, the inner parts of the bar thicken considerably and take the shape of a box. At the same time the bar weakens. Subsequently in most cases the bar amplitude starts growing again, although many cases have been found where it stays roughly constant. The thickness of its inner part also increases with time and its shape can evolve to peanut- or X-like.

By singling out the particles that constitute the bar in the face-on view and then viewing the volume they occupy, it becomes clear that the bar has a very complex and interesting three dimensional shape. It has a vertically thick inner part and a thin outer part. Seen face-on the inner part is elongated along the bar; seen edge-on it has a box, or peanut, or 'X' shape. This global bar geometry has clear signatures when seen from different viewing angles.

Orbital structure theory has provided the families of 3D orbits that can constitute the backbone of this component. The extent of these orbits along the bar major axis is always smaller than that of the bar, but it varies from one family to another as do their vertical height and shape. Thus the x_1v_1 family provides the building blocks that are shortest along the bar major axis, vertically thickest and face-on most elongated, while higher order families have orbits which are relatively more extended along the bar major axis, vertically thinner and less elongated.

Simulations, orbital structure results and observations have been extensively inter-compared and an excellent agreement has been found. It is clear that all three are describing the same objects.

The vertically thick part of the bar is known by different names. Viewed edge-on it is usually referred to as boxy, peanut, or X-shaped bulge. Viewed face-on it is known as the barlens component.

Acknowledgements I thank Albert Bosma for many stimulating discussions and the editors for inviting me to write this review. Figures 14.4 and 14.5 were made using glnemo2 (http://projets.lam.fr/-projects/glnemo2). I acknowledge financial support from the People Programme (Marie Curie Actions) of the European Union's Seventh Framework Programme FP7/2007-2013/ under REA grant agreement number PITN-GA-2011-289313 to the DAGAL network. I also acknowledge financial support from the CNES (Center National d'Etudes Spatiales – France) and from the "Programme National de Cosmologie et Galaxies" (PNCG) of CNRS/INSU, France, and HPC resources from GENCI- TGCC/CINES (Grants x2013047098 and x2014047098) and from the Mesocentre of Aix-Marseille Université (program DIFOMER).

References

Aronica, G., Athanassoula, E., Bureau, M., Bosma, A., Dettmar, R.-J., Vergani, D., Pohlen, M., 2003, Ap&SS, 284, 753
Athanassoula E., 1992a, MNRAS, 259, 328
Athanassoula E., 1992b, MNRAS, 259, 345
Athanassoula E., 2002, ApJL, 569, L83
Athanassoula E., 2003, MNRAS, 341, 1179
Athanassoula E., 2005a, MNRAS, 358, 1477
Athanassoula E., 2005b, in *Planetary Nebulae as Astronomical Tools*, Szczerba R., Stasinska G., Gorny S. K., eds., AIP Conference Proceedings, 804, 333
Athanassoula E., 2005c, Ann. New York Acad. Sciences, 1045, 168
Athanassoula E., 2008, in *Formation and Evolution of Galaxy Bulges*, IAU Symp. 245, eds. M. Bureau, E. Athanassoula & B. Barbuy, Cambridge, UK: Cambridge University Press, 93
Athanassoula E., 2013a, in *Secular Evolution of Galaxies*, eds. J. Falcón-Barroso & J.H. Knapen, Cambridge, UK: Cambridge University Press, 305
Athanassoula E., 2012, MNRAS, 426, L46
Athanassoula, E., Beaton, R. 2006, MNRAS, 370, 1499
Athanassoula, E., Bienaymé, O., Martinet, L. & Pfenniger, D. 1983, A&A, 127, 349
Athanassoula, E., Bureau, M. 1999, ApJ, 522, 699
Athanassoula, E., Laurikainen, Salo & Bosma, 2014, arXiv:1405.6726 (ALSB)
Athanassoula, E., Machado, R. E. G., & Rodionov, S. A. 2013, MNRAS, 429, 1949
Athanassoula, E., Misiriotis, A., 2002, MNRAS, 330, 35 (AM02)
Beaton, R., Majewski, S.R., Guhathakurta, P., Skrutskie, M.F., Cutri, R.M., Good, J., Patterson, R.J., Athanassoula, E., Bureau, M., 2007, ApJ, 658, L91
Berentzen I., Heller C. H., Shlosman I., Fricke K. J., 1998, MNRAS, 300, 49
Berentzen I., Shlosman I., Martinez-Valpuesta I., Heller C. H., 2007, ApJ, 666, 189
Bettoni, D., Galletta, G., 1994, A&A, 281, 1
Bureau M., Aronica G., Athanassoula E., Dettmar R.-J., Bosma A., Freeman K. C., 2006, MNRAS, 370, 753
Bureau, M., Athanassoula, E. 1999, ApJ, 522, 686
Bureau M., Athanassoula E., 2005, ApJ, 626, 159
Bureau, M., Freeman, K. C. 1999, AJ, 118, 126
Buta, R., Laurikainen, E., Salo, H., Block, D., Knapen, J.H., 2006, AJ, 132, 1859
Cappelari, M., Copin, Y., 2003, MNRAS, 342, 345
Chung, A., Bureau, M. 2004, AJ, 127, 3192
Combes F., Debbasch F., Friedli D., Pfenniger D., 1990, A&A, 233, 82
Combes F., Sanders R. H., 1981, A&A, 96, 164
Contopoulos G., Harsoula, M. 2008, Intern. J. of Bifurcation and Chaos, 18, 2929
Contopoulos G., Papayannopoulos, T. 1980, A&A, 92, 33
Debattista V. P., Carollo C. M., Mayer L., Moore B., 2004, ApJ, 604, L93

Debattista V. P., Mayer L., Carollo C. M., Moore B., Wadsley J., Quinn T., 2006, ApJ, 645, 209
Dettmar, R.J., Barteldrees, A., 1990, in *ESO/CTIO Workshop on Bulges of Galaxies*, Proceedings (A92-18101 05-90)
D'Onofrio M., Capaccioli M., Merluzzi P., Zaggia S., Boulesteix J., 1999, A&AS, 134, 437
Erwin, P., 2008, in *Formation and Evolution of Galaxy Bulges*, IAU Symp. 245, eds. M. Bureau, E. Athanassoula & B. Barbuy, Cambridge University Press, 113
Erwin, P., Debattista, V.P., 2013, MNRAS, 431, 3060
Falcon-Barroso, J. et al. 2004, MNRAS, 350, 35
Ferrers N. M. 1877, Q.J. Pure Appl. Math., 14, 1
Fisher, D., Illingworth, G., Franx, M., 1994, AJ, 107, 160
Fragkoudi, F., Athanassoula, E., Bosma, A., Iannuzzi, F., MNRAS, 2015, 450, 229
Gadotti D. A., 2008, MNRAS, 384, 420
Harsoula M., Kalapotharakos C., 2009, MNRAS, 394, 1605
Hohl, F., Zang, T.A. 1979, AJ, 84, 585
Iannuzzi, F., Athanassoula, E., 2015, MNRAS, 450, 2514 (IA15)
Kormendy, J., 1979, ApJ, 227, 714
Kormendy, J., 2008, in *Formation and Evolution of Galaxy Bulges*, IAU Symp. 245, eds. M. Bureau, E. Athanassoula & B. Barbuy, Cambridge Univ. Press, 107
Kormendy, J., 2013, in *Secular Evolution of Galaxies*, eds. Jesús Falcón-Barroso & Johan H. Knapen, Cambridge, UK: Cambridge University Press, 2013, 1
Kormendy, J., Illingworth, G., 1982, ApJ, 256, 460
Kormendy J., Kennicutt R. C., Jr., 2004, ARA&A, 42, 603
Kuijken, K., Merrifield, M. R. 1995, ApJ, 443, L13
Laurikainen E., Salo H., Buta R., Knapen J. H., Comeron, S, 2010, MNRAS, 405, 1089
Laurikainen E., Salo H., Buta R., Knapen J. H., 2011, MNRAS, 418, 1452
Laurikainen, E., Salo, H., Athanassoula, E., Bosma, A., Buta, R., Janz, J. 2013, MNRAS, 430, 3489
Laurikainen, E., Salo, H., Athanassoula, E., Bosma, A., Herrera Endoqui, M. 2014, MNRAS, 444, L80
Lütticke R., Dettmar R.-J., Pohlen M., 2000a, A&AS, 145, 405
Lütticke R., Dettmar R.-J., Pohlen M., 2000b, A&A, 362, 435
Manos, T., Athanassoula, E., 2011, MNRAS, 415, 629
Manos, T., Machado, R. 2014, MNRAS, 438, 2201
Martinez-Valpuesta I., Shlosman I., Heller C., 2006, ApJ, 637, 214
Mendez-Abreu, J., Corsini, E.M., Debattista, V.P., De Rijcke, S., Aguerri, J.A.L., Pizzella, A., 2008, ApJ, 679, L73
Merrifield, M. R., Kuijken, K. 1999, A&A, 345, L47
Miller, R.H., Smith, 1979, ApJ, 227, 785
Mihos, J.C., Walker, I.R., Hernquist, L., Mendes de Oliveira, C., Bolte, M., 1995, ApJ, 447, L87
O'Neill J. K., Dubinski J., 2003, MNRAS, 346, 251
Patsis P. A., Katsanikas, M. 2014a, MNRAS, 445, 3525
Patsis P. A., Katsanikas, M. 2014b, MNRAS, 445, 3546
Patsis P. A., Skokos, Ch., Athanassoula E., 2002, MNRAS, 337, 578 (PSA02)
Patsis P. A., Xilouris, M., 2006, MNRAS, 366, 1121
Pfenniger, D. 1984, A&A, 134, 373
Pfenniger D., Friedli D., 1991, A&A, 252, 75
Quillen, A.C., Kuchinski, L.E., Frogel, J.A., DePoy, D.L., 1997, ApJ, 481, 179
Quillen, A.C., Minchev, I., Sharma, S., Qin, Y.-J., Di Matteo, P., 2014, MNRAS, 437, 1284,
Raha N., Sellwood J. A., James R. A., Kahn F. D., 1991, Nature, 352, 411
Sandage, A., *The Hubble Atlas of Galaxies*, Carnegie Institution of Washington, 1961
Saha, K., Pfenniger, D., Taam, R.E., 2013, ApJ, 764, 123
Sheth, K. et al. 2010, PASP, 122, 1397
Skokos, Ch., Patsis, P.A., Athanassoula, E. 2002a, MNRAS, 333, 847
Skokos, Ch., Patsis, P.A., Athanassoula, E. 2002b, MNRAS, 333, 861

Toomre A. Geophys. Fluid Dyn., No. 66–46, 111
Villa-Vargas J., Shlosman I., Heller C., 2010, ApJ, 719, 1470
Wakamatsu, K.I., Hamabe, M., 1984, ApJS, 56, 283
Williams, M.J., Zamojski, M.A., Bureau, M., Kuntschner, H., Merrifield, M.R., de Zeeuw, P.T., Kuijken, K., 2013, MNRAS, 414, 2163
Wozniak H., Michel-Dansac L., 2009, A&A, 494, 11

Chapter 15
Explaining the Formation of Bulges with MOND

Françoise Combes

Abstract In the cold dark matter (CDM) paradigm, bulges easily form through galaxy mergers, either major or minor, or through clumpy discs in the early universe, where clumps are driven to the center by dynamical friction. Also pseudobulges, with a more discy morphology and kinematics, can form more slowly through secular evolution of a bar, where resonant stars are elevated out of the plane, in a peanut/box shape. As a result, in CDM cosmological simulations, it is very difficult to find a bulgeless galaxy, while they are observed very frequently in the local universe. A different picture emerges in alternative models of the missing mass problem. In MOND (MOdified Newtonian Dynamics), galaxy mergers are much less frequent, since the absence of dark matter halos reduces the dynamical friction between two galaxies. Also, while clumpy galaxies lead to rapid classical bulge formation in CDM, the inefficient dynamical friction with MOND in the early-universe galaxies prevents the clumps to coalesce together in the center to form spheroids. This leads to less frequent and less massive classical bulges. Bars in MOND are more frequent and stronger, and have a more constant pattern speed, which modifies significantly the pseudobulge morphology. The fraction of pseudobulges is expected to be dominant in MOND.

15.1 Introduction

Although the standard CDM model for dark matter is the best frame to represent the universe at large scales, and account for galaxy formation, it experiences difficulties at galaxy scale (e.g. Moore et al. 1999; Silk and Mamon 2012). Cosmological simulations in the standard model predict an over concentration of dark matter in galaxies, and cuspy density profiles, instead of the density cores derived from rotation curves, especially in low-mass galaxies (e.g. de Blok et al. 2008; Swaters et al. 2009). Also simulations have difficulties to form large galaxy discs, since the angular momentum of baryons is lost against massive dark halos (e.g. Navarro and

F. Combes (✉)
Observatoire de Paris, LERMA, CNRS, 61 Av. de l'Observatoire, 75014 Paris, France
e-mail: francoise.combes@obspm.fr

E. Laurikainen et al. (eds.), *Galactic Bulges*, Astrophysics and Space Science Library 418, DOI 10.1007/978-3-319-19378-6_15

Steinmetz 2000), and the missing satellites problem remains unsolved (Diemand et al. 2008). In addition, observed low-mass satellites of the Milky Way have a much larger baryonic fraction than expected from halo abundance matching (e.g. Boylan-Kolchin et al. 2011, 2012).

A large numerical effort has been spent to solve these problems by the detailed physics of the baryonic component, in particular star formation and AGN feedback (e.g. Vogelsberger et al. 2014; Schaye et al. 2015). Another track is to explore alternatives to dark matter models, and in particular modified gravity scenarios, able to account for the missing mass in galaxies.

Already 30 years ago, Milgrom (1983) had the idea of the MOdified Newtonian Dynamics (MOND), based on the fundamental observation that the missing mass problem occurs only in the weak field regime, at low acceleration, when it is lower than the characteristic value of $a_0 = 210^{-10}\,\mathrm{ms}^{-2}$. The observed flat rotation curves in the outer parts of galaxies suggests that in this regime the actual acceleration varies in 1/r. Galaxies are also following the baryonic Tully-Fisher relation (McGaugh et al. 2000), where the baryonic mass of a system is proportional to the 4$^{\mathrm{th}}$ power of the maximum rotational velocity (see Fig. 15.1). Milgrom then proposes that at acceleration below $a_0 = 2\ 10^{-10}\,\mathrm{ms}^{-2}$, the gravitational attraction will tend to the formulation $a = (a_0\ a_N)^{1/2}$, where a_N is the Newtonian value. This effectively produces an acceleration in 1/r, implying a flat rotation curve in the limiting regime, and leading automatically to the Tully-Fisher relation. The transition between the Newtonian and MOND regime is controlled by an interpolation function $\mu(x)$, of $x=a/a_0$, of which the standard form is $\mu(x) = x/(1+x^2)^{1/2}$. It essentially tends to x in the MOND regime, when x is smaller

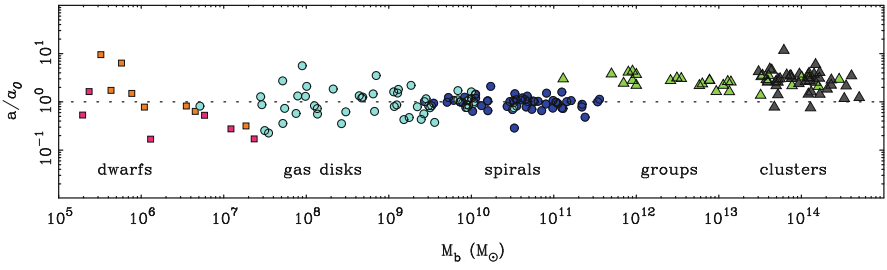

Fig. 15.1 The observed parameter $V_f^4/(GM_b)$, where V_f is the rotational velocity taken in the flat portion of the rotation curve, and M_b is the baryonic mass, can be also written as the acceleration of the system: $a = V_f^2/R$, and $R = GM/V_f^2$. The very small deviation of a from the constant a_0 is remarkable, given the large range of ten decades in baryonic mass M_b. This observation is somewhat puzzling for the standard dark matter model, but is the basis of the modified gravity (MOND) model (From Famaey and McGaugh 2012)

than 1, and to unity in the Newtonian regime. This phenomenology has a large success explaining rotation curves and kinematics of galaxies, from dwarf irregulars dominated by dark matter (and therefore in the MOND regime), to the giant spirals and ellipticals, dominated by baryons (e.g. Sanders and McGaugh 2002). Although the model is still empirical, it is possible to build relativistically covariant theories, able to reproduce gravitational lensing and other phenomena, while tending asymptotically to the above formulation in the non-relativistic limit (Bekenstein 2004).

The galaxy dynamics is quite different in the MOND hypothesis with respect to the standard dark matter model. Some phenomena have already been explored (see e.g. the review by Famaey and McGaugh 2012), but many are still to be discovered, in particular related to galaxy formation, and high redshift evolution. The stability of galaxy discs is fundamentally different, provided that they have low surface brightness (LSB), and are close to the MOND regime (Milgrom and Sanders 2007). Since the MOND discs are completely self-gravitating, they could be much more unstable, however the acceleration is varying asymptotically as the square root of the mass (and not linearly with the mass), so the final effects are not intuitive. Bars are forming quickly in MOND discs, and their pattern speed is not declining through dynamical friction against a dark matter halo, so resonances are long-lived, and may have more impact (Tiret and Combes 2007). Galaxy interactions with no extended dark halos suffer much less dynamical friction, and mergers are rare (Tiret and Combes 2008b). This changes very significantly the hierarchical scenario of galaxy formation, and in particular bulge formation. Therefore, although bulges are now generally in the Newtonian regime today, their formation is certainly very different in the MOND frame with respect to the standard model. Bulges are increasingly important along the Hubble sequence towards the early-types, which correspond to the more massive end. For giant galaxies, the low acceleration regime is encountered only in the outer parts, and the central parts remain Newtonian. Only dwarf galaxies and LSB objects without bulges are still in the MOND regime in their center. This means that bulges today are not likely to be affected by a modified dynamics.

In the following, we will consider in turn the main dynamical mechanisms to form bulges in the ΛCDM paradigm:

- Mergers, major or a series of minor mergers
- Secular evolution, bars and the formation of pseudobulges
- Clumpy galaxies at high redshift and dynamical friction

Are all these processes also at work in MOND, and with which efficiency? It is well known that the standard ΛCDM model has difficulties to account for the large number of observed bulge-less galaxies (Kormendy et al. 2010). Is this problem solved by MOND?

15.2 Galaxy Mergers

In the standard hierarchical scenario, galaxy mergers play a large role in mass assembly, and one of the results of the repeated coalescence of galaxies is to randomly average out the angular momentum of the system, and to form spheroids (e.g. Toomre 1977; Barnes and Hernquist 1991; Naab and Burkert 2003; Bournaud et al. 2005, 2007a). In these last works, it was shown how repeated minor mergers progressively accumulate stars in a central spheroid and grow the bulge, to transform the galaxy in a more early-type spiral. Eventually, N minor mergers of mass ratio N:1 result in an elliptical remnant quite similar to those formed in a 1:1 merger. As shown by Barnes (1988), mergers are very efficient in forming long tidal tails while the main baryonic components merge quickly, because of the existence of extended and massive dark halos, which take the orbital angular momentum away. It can then be expected that the frequency of mergers will depend crucially on the model assumed for the missing mass.

15.2.1 Major Mergers in MOND

One of the main questions is to know whether the MOND dynamics is able to produce long tails in major mergers of galaxies, like in the prototypical Antennae system (Fig. 15.2). These tails have also helped to constrain the dark matter halos

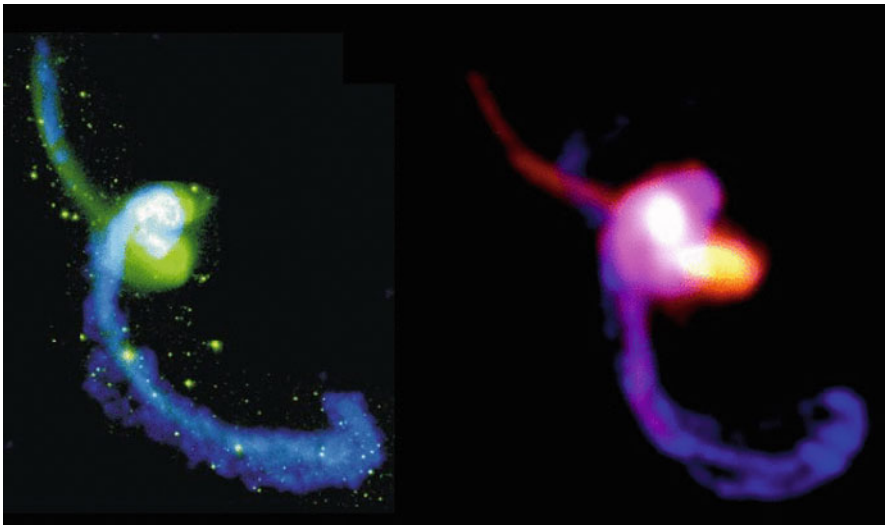

Fig. 15.2 Simulation of tidal interactions in a major merger in MOND (*right*, with gas in *blue* and stars in *red*) compared to the Antennae galaxies (Hibbard et al. 2001, HI gas in *blue*, and stars in *green*). The two long tidal tails are reproduced (Tiret and Combes 2008b)

potential (Dubinski et al. 1996). With MOND, the result is not easy to predict, and numerical simulations are necessary, since the External Field Effect (EFE) perturbs the MONDian dynamics in the outer parts of galaxies. This new effect particular to MOND comes from the fact that it violates the Strong Equivalence Principle of General Relativity. In the Newtonian frame, the internal gravitational forces of a system are independent of their external environment: if the object is embedded in a large system, exerting a force which can be considered constant all over the object, then the internal dynamics is unchanged. Of course, if the force is varying across the object, its differential gives rise to tidal forces, which impact the object. But in the MOND dynamics, even a constant force may create an acceleration above the critical a_0, and get the object out of the MOND regime (Milgrom 1983, 1998).

Several cases can be distinguished to model the EFE, according to the respective values of the external acceleration a_e with respect to the internal acceleration a of the object under consideration, and the critical acceleration a_0. If $a_e < a < a_0$, then the standard MOND effects are retrieved, and if $a < a_0 < a_e$, then the EFE is strong enough to make the system purely Newtonian. But in the intermediate regime, where $a < a_e < a_0$ then the system is Newtonian with a re-normalized gravitational constant G. It can be estimated for instance in a one-dimensional system, that the effective gravitational constant is then $G_{eff} = G\,[\mu_e(1 + L_e)]^{-1}$, where $\mu_e = \mu(a_e/a_0)$, and L_e is the logarithmic gradient of μ (Famaey and McGaugh 2012). In the outer parts of a given system, the internal acceleration is always vanishing, and there will always be a small $a_e < a_0$, therefore this represents the general case: the gravitational force falls again as $1/r^2$, and the potential as $1/r$ and not logarithmically, as could be extrapolated. This allows to define the escape velocity of the system, as in the Newtonian case. Computations of the EFE in the Milky Way, due to the nearby Andromeda galaxy, have given results compatible with the observations (Wu et al. 2007).

Simulations with a 3D adaptive-mesh code able to solve the MOND equations, and including gas and stars, have shown that two long tidal tails can develop in a major merger similar to the Antennae (cf. Fig. 15.2). In absence of dark matter particles as receivers of the orbital angular momentum of the two galaxies, baryons are playing this role, and tidal tails can be very long. In addition, tidal dwarf galaxies can be naturally formed at the tip of the tidal tails in MOND, while it requires radially extended dark matter halos in the standard model (Bournaud et al. 2003). The big difference between the two models is the efficiency of the dynamical friction. While mergers can take only one orbit, or less than 1 Gyr in the standard model, it will take several Gyrs with MOND, and mergers will occur only with selected impact parameters, and initial relative angular momenta. At a distance of $\sim$100 kpc, two galaxies in circular orbits will not merge in a Hubble time with MOND (Fig. 15.3). On the contrary, in the standard model, galaxies have

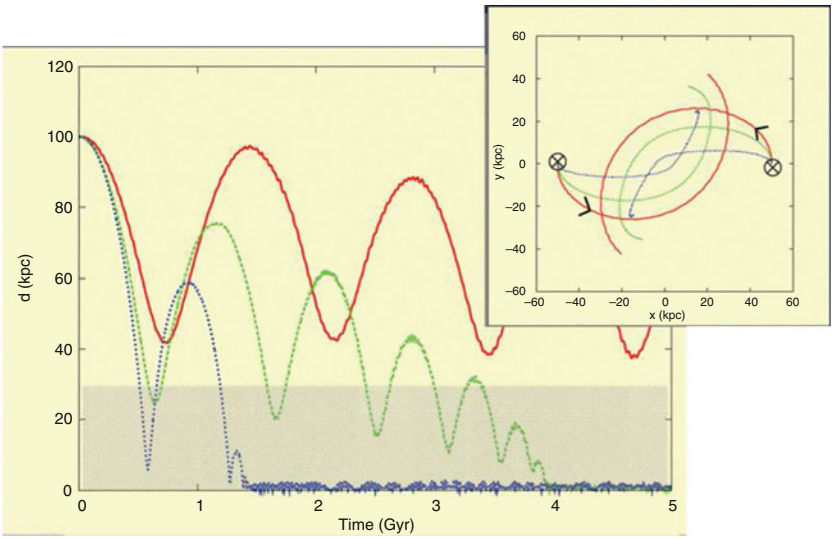

Fig. 15.3 Radial decay during the tidal interactions between two equal-mass spiral galaxies, in the MOND model (Tiret and Combes 2008b). At *left* is shown the relative distance in kpc versus time in Gyr, while the insert at *right* shows the corresponding trajectories (Image by O. Tiret)

already plunged well inside their dark matter halos, of radius ∼200 kpc. Then local dynamical friction is already effective, while in the MOND case, the relative decay relies only on the friction at distance, which is much weaker.

15.2.2 Dynamical Friction

As described above, the gravitational forces between galaxies at large distance are likely to vary as $1/r^2$ as in the Newtonian regime, but with a boosted constant, so the long-distance approach of galaxies could be thought similar. However the phenomena associated to dynamical friction are completely different. Answers to this problem have been controversial at the start, since Ciotti and Binney (2004) computed the relaxation time in the MOND regime with strong approximations: very small fluctuations, impulse approximation for deflection or orbits, linear summation of effects, etc. They compare this two body relaxation time with that in the Newtonian regime, considering the dark matter halo as a rigid background, not participating in the fluctuations. Then they extrapolate their finding of a shorter relaxation time in MOND to the dynamical friction time, obtained for test particles for the local formula of Chandrasekhar (1943), and conclude that globular clusters

should spiral inwards to the center in dwarf galaxies in a few dynamical time-scales, as well as galaxies in groups and in clusters. Nipoti et al. (2008) tried to confirm these findings in simulations, by applying the same hypotheses of a tiny perturbation: the massive bodies subject to the friction, either globular clusters or a rigid bar, have to contain less than 5 % of the baryonic mass, so that particles absorbing the energy and angular momentum are not globally perturbed. In realistic systems though, Nipoti et al. (2007) found that the merging timescales for spherical systems are significantly longer in MOND than in Newtonian gravity with dark matter, and Tiret and Combes (2007) found that bars keep their pattern speed constant in MOND, while they are strongly slowed down in the Newtonian equivalent system with a dark matter halo. In summary, dynamical friction is very slow in MOND, since galaxies are not embedded in extended and massive spheroids of dark matter particles, able to accept the orbital angular momentum. A short merging time-scale for equal-mass interacting galaxies, as short as the CDM, is possible only for nearly radial orbits. Although the impact of very small fluctuations could be larger in MOND than in Newtonian dynamics, the effect saturates quickly when the perturbation is no longer infinitesimal, and on the contrary the equivalent Newtonian system with dark matter has shorter response time-scales, and a massive body (either a companion, or a galactic bar) is slowed down very efficiently. The case of bars, their pattern speeds, and their impact on bulge formation will be explained in detailed in the next Sect. 15.3.

Could the smaller merger frequency predicted by MOND be tested in observations? Unfortunately, the actual merger frequency is not directly accessible. Observers tend to quote galaxy pair frequency, or starbursts due to mergers (e.g. Bell et al. 2006; Lopez-Sanjuan et al. 2013; Stott et al. 2013). However, there is a degeneracy here, since galaxy can appear in pairs during either a short or long time-scale, and starbursts can occur at each closer passage. In the standard DM models, an assumption is done on the duration of galaxy interactions, and the number of starbursts: according to the initial relative velocity and the geometry of the encounter, the merger is expected to occur in one or two passages. An intense starburst is associated to the final phase, and the number of starbursts is thought to count the number of mergers (e.g. Di Matteo et al. 2007). In the MOND model, many passages in binary galaxies will be required before the final merging, and a starburst may be triggered at each pericenter. The number of starbursts as a function of redshift could then be similar, and cannot discriminate the two models. The degeneracy cannot be raised between a limited number of long-lived mergers, or a high frequency of short-lived mergers.

15.3 Bars

To probe realistically the stability of discs with the MOND dynamics, numerical simulations have been run, solving the N-body problem on a grid, through the equations of Bekenstein and Milgrom (1984). Brada and Milgrom (1999) showed

that discs were always more instable in MOND. For the equivalent Newtonian system with a spherical dark halo, the more unstable galaxies are those with massive discs, which are more self-gravitating, while low-mass discs are stabilized by their halo. In MOND, the instability is about the same for massive discs, which are still in the Newtonian regime. However, low-mass discs remain unstable, and their growth rate tend to a constant, instead of vanishing.

15.3.1 Disc Stability in MOND

From detailed comparison of two identical initial discs simulated with Newtonian dynamics+dark matter and MOND, Tiret and Combes (2007) have shown that bars develop quicker with modified gravity (see Fig. 15.4). To have identical starts, the baryonic disc is first computed in equilibrium with its velocity distribution in MOND, and then, the amount of dark matter required to obtain the same derived rotation curve, is added for the Newtonian dynamics run. The evolution of the bar strength in Fig. 15.4 reveals that both bars experience a drop in their strength, and this is due to the vertical resonance, building a peanut-shape feature, evolving in a pseudobulge (e.g. Combes and Sanders 1981; Combes et al. 1990; Bureau and Freeman 1999). The peanut occurs later in MOND. The bar remains strong during a longer time-scale, but then weakens, while the Newtonian bar can strengthen again, by exchanging angular momentum with the dark halo (e.g. Athanassoula 2002).

This different way of growing results also in a different final morphology of the stellar discs: in MOND the disc is more extended, since the bar has grown by

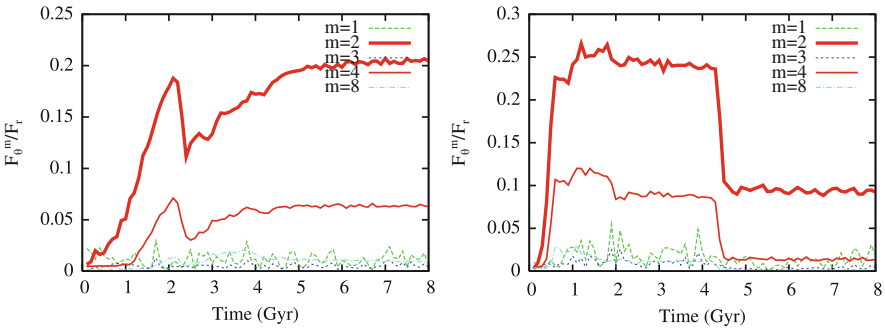

Fig. 15.4 Strength of the bar formed in an Sa-type galaxy purely stellar simulation, measured by its Fourier harmonics m = 2,3,4 and 8 (ratio of tangential to radial force), for the CDM-Newton model (*left*) and MOND (*right*). The bar settles earlier in MOND, and stays longer, but after dropping at 4.5 Gyr, it does not develop again as in the CDM (cf. Tiret and Combes 2007). The drop at 2.5 Gyr in the DM model as in the MOND model at 4.5 Gyr is due to the formation of a peanut bulge, through the vertical resonance (e.g. Combes et al. 1990)

angular momentum exchange with the outer disc particles. Figure 15.4 represents an early-type spiral Sa. When all types are considered, the bar occurs much later in Newtonian models, because later types are more dominated by the dark matter halo, and are less self-gravitating. In MOND it is the contrary, the bar is first stronger in late-types, and then the disc is heated too much and the bar weakens. When the statistics are computed over the whole Hubble sequence, it appears that bars are stronger and more frequent in MOND, when only stellar components are taken into account. The higher MOND bar frequency is more in agreement with observations, where 2/3 of spiral galaxies are barred (e.g. Laurikainen et al. 2004, 2009).

15.3.2 Pattern Speed Evolution

The bar pattern speed evolutions are also different in the two models. As shown in Fig. 15.5 left, Ω_{bar} is almost constant in MOND, while it drops by a factor 3 in 7 Gyr time in the equivalent Newtonian system. This is clearly due to the exchange of angular momentum from the bar to the dark matter halo, through dynamical friction. Indeed, the test run when the Newtonian system is computed with a rigid halo, which cannot deform and produce dynamical friction, has an almost constant Ω_{bar} too.

This drop in Ω_{bar} for the Newtonian+dark matter model has several consequences. First the Lindblad resonances in the plane and the vertical resonance move in radius, as shown in Fig. 15.5 right. The pattern speed at the end of the simulation is shown as a thick dash line, and the inner/vertical resonance moves from 2 to

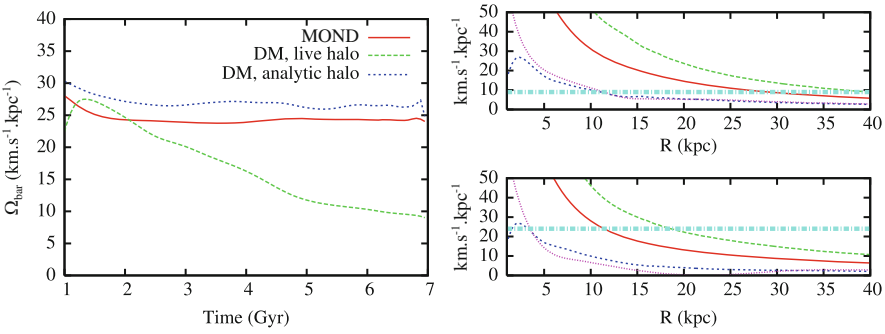

Fig. 15.5 *Left* Bar pattern speeds versus time: in MOND, the pattern speed remains constant, as in the Newtonian galaxy with a rigid dark matter halo. When the dark halo particles are taken into account self-consistently, the bar slows down, losing its angular momentum through dynamical friction. *Right* Frequency curves (from bottom to top, $\Omega - \kappa/2$, $\Omega - \nu_z/2$, Ω and $\Omega + \kappa/2$) for the CDM case (*top*) and MOND (*bottom*). The *thick horizontal line* is the pattern speed of the bar in each case (cf. Tiret and Combes 2007)

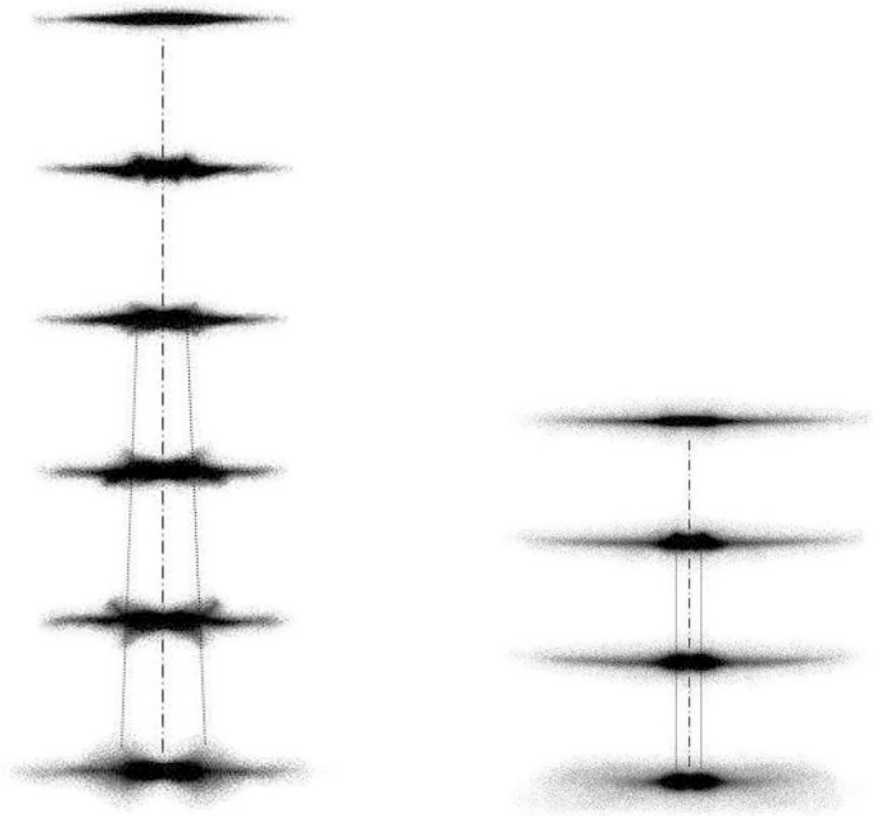

Fig. 15.6 Peanut-shape bulge formation, through vertical resonance with the bar. With CDM (*left*), the bar slows down with time, and the resonance moves to larger radii. Two peanut features are formed along the evolution, and the last one is rather extended in radius, while with MOND (*right*), there is only one peanut formed, centrally concentrated (Tiret and Combes 2007). These runs consider only the stellar component. Peanuts are less developed, when the disc is rich in gas

12 kpc. Since the peanut represents stars vertically up-lifted at resonance, this means that the radius of the peanut is moving radially outwards, as shown in Fig. 15.6. In MOND on the contrary, resonances are more long-lived, and can produce more robust effects.

15.3.3 Bulges and Pseudobulges

Until now, the comparison between MOND and the Newtonian equivalent systems has been discussed with purely stellar discs. However, the presence of gas, and its interaction with stars change the picture. Gas as a dissipational component, is

subject to a phase shift in its response to the bar pattern. There is a torque from the bar to the gas, that drives it to the center. This changes the potential there, and therefore the Ω frequencies and the resonances. The final result is a weakening of the bar, which can only develop again through gas accretion (e.g. Bournaud and Combes 2002). Gas dissipation and star formation have been taken into account in MOND simulations by Tiret and Combes (2008a). Statistically, bars occur even more rapidly in gas rich discs, and especially in the Newtonian models, which were too stable in the purely stellar discs. This makes the two models more similar, as far as the frequency of bars is concerned. Since the baryonic mass is more concentrated with gas in any model, the vertical resonance and the peanut occur at smaller radii, therefore the pseudobulges are smaller and more boxy in appearance.

Finally, the gas is driven by gravity torques inwards inside corotation, and outwards outside. It accumulates in rings at the inner (outer) Lindblad resonances respectively, in star forming rings that reproduce the blue rings observed in barred galaxies (e.g. Buta and Combes 1996). In MOND, this phenomenon is even more remarkable, since first bars are still stronger and more frequent than in the Newtonian dynamics, but also the exchange of angular momentum between the stellar and the gas components is favored, while in the Newtonian case, there is competition with the dark halo for this exchange.

Summarizing the previous learnings, bars are more frequent in MOND, and consequently the formation of pseudobulges is favored. The fraction of classical bulges formed in major or minor mergers is likely to be much less, so that the picture of bulge formation is significantly different in the two regimes. These conclusions are applicable mainly to the local galaxies, at very low redshifts. First bars are less frequent in the past (Sheth et al. 2008), and pseudobulges are thought to be the dominant bulge formation at lower redshift (e.g. Kormendy and Kennicutt 2004). Second, it is not well known how the MOND model can be extended at high redshift. It has been remarked that the critical acceleration a_0 is of the same order as $c\ H_0$, with H_0 the Hubble constant today, and therefore the critical acceleration could increase with z as H(z). Similarly $a_0 \sim c\ (\Lambda/3)^{1/2}$ (with Λ being the dark energy parameter), and any kind of variation with time of a_0 is possible.

In the standard model, there is another mechanism to form bulges, which is more dominant at high redshift, that we will consider now.

15.4 Clumpy Discs

When the universe was about half of its age ($z \sim 0.7$) and earlier, the morphology of spiral galaxies were significantly different from what we know today, in the Hubble sequence. Galaxies were much more clumpy, with clumps of gas and stars of kpc

size (e.g. Elmegreen 2007). These very irregular morphologies are thought to result from the very high gas fraction of these early galaxies. Noguchi (1999) simulated the formation of galaxies from highly gaseous systems, and found that they form giant clumps, which by dynamical friction can spiral inwards to the center rather quickly to form a bulge. Bournaud et al. (2007b) developed further the dynamical mechanisms, and showed that rather quickly, clumpy discs form an exponential disc, a bulge, and also a thick disc due to the stars formed in the turbulently thick gaseous disc. The disruption of the clumps by the feedback of star formation (supernovae, winds) is not yet well known, and can be adjusted to maintain the clumpy discs at the observed frequency (Elmegreen et al. 2008). The large increase of the gas fraction of spiral galaxies with redshift has been confirmed by direct observations of the molecular gas (e.g. Tacconi et al. 2010).

The very high efficiency of bulge formation through dynamical friction in clumpy discs might be a problem for the standard dark matter model, since bulge-less galaxies are quite frequent today (e.g. Weinzirl et al. 2009). Since dynamical friction occurs mainly against dark matter halos, it is expected that it will be much less important in the MOND dynamics, and the rapid bulge formation could be avoided. This was indeed demonstrated in a recent paper, comparing formation of bulges in gas-rich clumpy galaxies, in the two gravity models, Newtonian with dark matter and MOND (Combes 2014).

This work first computes the dynamical time-scale in an idealized situation, where the galaxy discs are purely stellar, to isolate the main dynamical phenomenon, from the more complex gas hydrodynamics, star formation or feedback. When several clumps are launched randomly in the disc, the dynamical friction efficiency is difficult to predict, since the wakes of the different massive bodies interfere (Weinberg 1989). With typical clump mass fraction (25–30 %), in the Newtonian model, the dynamical time-scale for clumps to spiral into the center of a galaxy with baryonic mass 6 10^{10} $M_\odot$ is 0.3 Gyr, and 1 Gyr for a galaxy with baryonic mass 6 10^9 $M_\odot$. In the MOND regime, the clumps do not fall into the center before 3 Gyr. When the gas and star formation/feedback are taken into account, the simulated galaxy discs are rapidly unstable to clump formation, due to the gas fraction of 50 %. In the Newtonian gravity with dark matter, previous results are retrieved, i.e. an increasing clump mass fraction in the first 200 Myr, and the coalescence of clumps towards the center, with a spheroidal bulge formation, in less than 1 Gyr (Noguchi 1999; Immeli et al. 2004; Bournaud et al. 2007b). With MOND gravity, clumps form quickly too (cf. Fig. 15.7), but they maintain in the disc for the whole simulation of 3 Gyr, until the gas has been consumed in stars. The clump mass fraction does not decrease much, being just eroded through stellar feedback and shear forces (Fig. 15.8). Bulges are clearly not formed in the early clumpy phase of galaxy formation, as in the Newtonian equivalent systems.

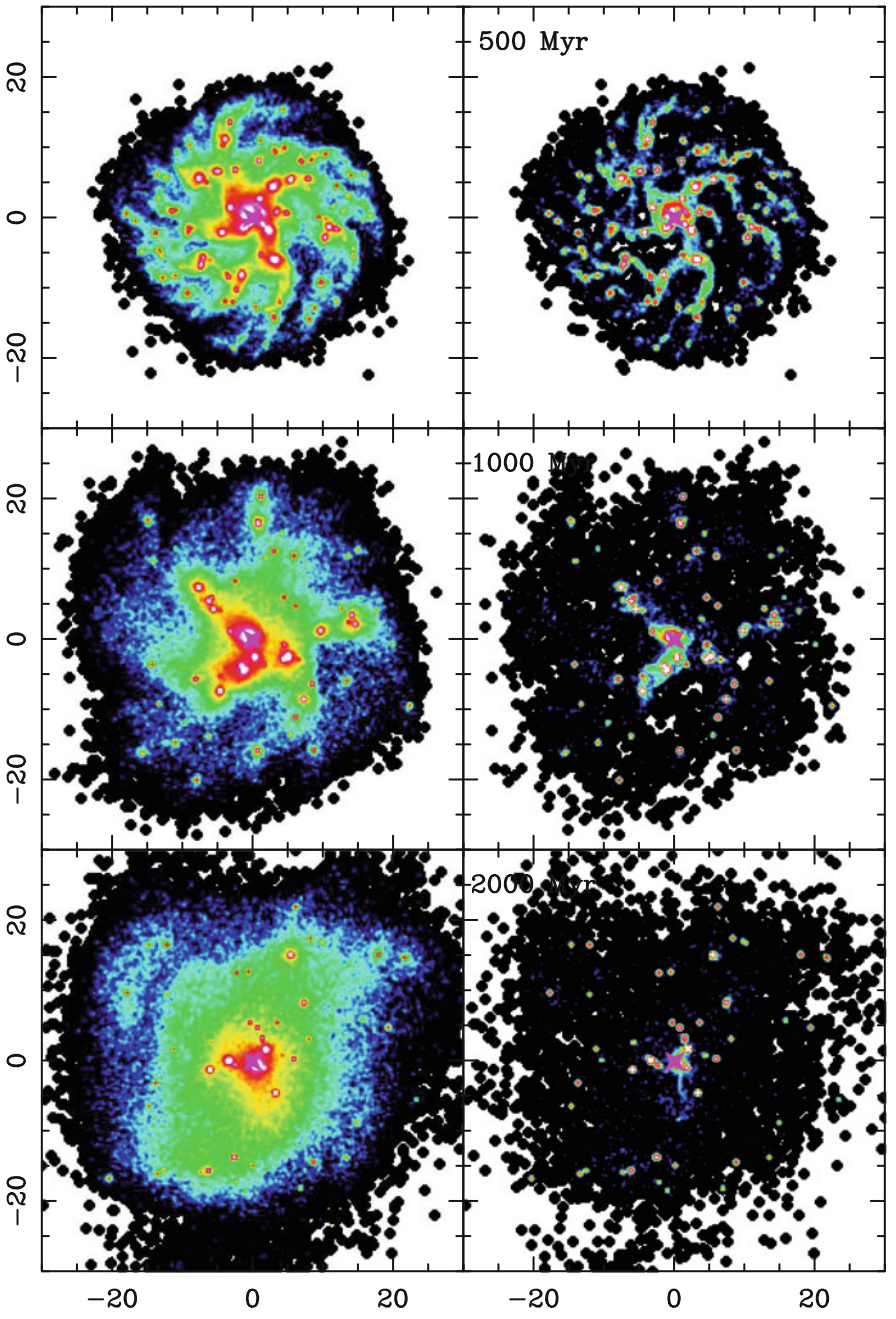

Fig. 15.7 All baryons (*left*) and gas (*right*) surface densities of the dwarf clumpy galaxy, simulated with MOND gravity, at epochs 0.5, 1 and 2 Gyr. Each panel is 60 kpc in size. The color scale is logarithmic and the same for all plots (From Combes 2014)

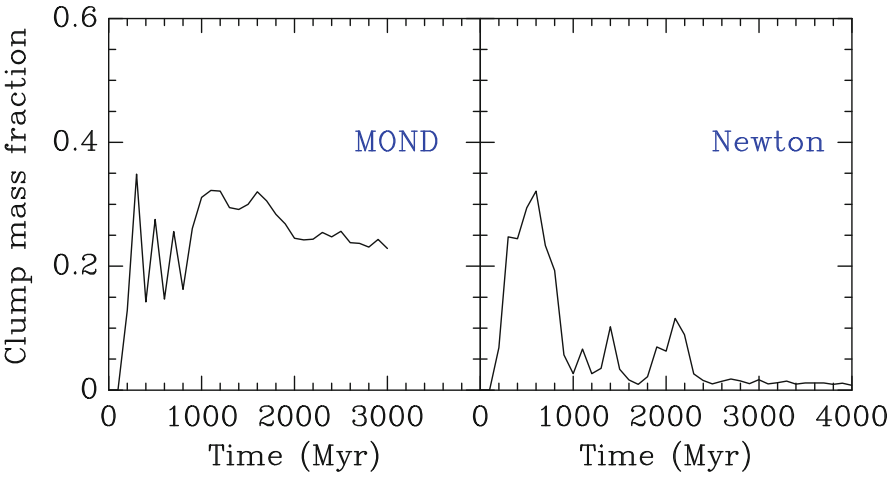

Fig. 15.8 Evolution of the clump mass fraction for the giant galaxy, in the MOND gravity (*left*) and in the Newtonian gravity (*right*)

15.5 Conclusions

In the standard model, classical bulges are thought to be formed essentially in galaxy mergers, which are very frequent in the hierarchical scenario of galaxy formation. In addition, a small classical bulge is also formed in the first Gyr of the galaxy lives, during the clumpy phase, where their disc is gas dominated. Later on, pseudobulges formed out of bar resonances adding their contribution to the classical bulges.

In the frame of MOND, bulges are hardly formed in early times, in the clumpy phase of galaxy formation, since the dynamical friction without dark matter halos is not efficient enough to drive clumps towards the center, before they are destroyed or reduced by stellar feedback and shear forces. Classical bulges can form later, through hierarchical merging, with a frequency which is smaller than what occurs in the analogous Newtonian systems with dark matter. They however form with comparable frequency through secular evolution, by vertical resonances with bars. It is therefore expected that the contribution of pseudobulges with respect to classical bulges is higher in MOND. Globally, bulges are expected less frequent and less massive, which might be more compatible with observations of local galaxies (Weinzirl et al. 2009; Kormendy et al. 2010). These tendencies have to be confirmed with more simulations. A complete cosmological context is however not yet possible, given the uncertainties of the modified gravity models in the early universe.

References

Athanassoula, E. 2002 ApJ 569, L83
Barnes, J. E. 1988, ApJ 331, 699
Barnes, J. E., and Hernquist, L. E. 1991, ApJ 370, L65
Bekenstein, J., and Milgrom, M. 1984, ApJ 286, 7
Bekenstein, J. 2004 PhRvD 70h3509
Bell, E.F., Phleps, S., Somerville, R.S. et al. 2006, ApJ 652, 270
Bournaud, F., and Combes, F. 2002, A&A 392, 83
Bournaud, F., Duc, P.-A., and Masset, F. 2003, A&A 411, 469
Bournaud, F., Jog, C.J., and Combes, F. 2005, A&A 437, 69
Bournaud, F., Jog, C.J., and Combes, F. 2007, A&A 476, 1179
Bournaud, F., Elmegreen, B.G., and Elmegreen, D.M. 2007, ApJ 670, 237
Boylan-Kolchin, M., Bullock, J. S., and Kaplinghat, M. 2011, MNRAS 415, L40
Boylan-Kolchin, M., Bullock, J. S., and Kaplinghat, M. 2012, MNRAS 422, 1203
Brada, R., and Milgrom, M. 1999, ApJ 519, 590
Bureau, M., and Freeman, K. C 1999, AJ 118, 126
Buta, R., and Combes, F. 1996, F^{als} of Cosmic Physics, Volume 17, pp. 95–281
Chandrasekhar, S., 1943 ApJ 97, 255
Ciotti, L., and Binney, J. 2004, MNRAS 351, 285
Combes, F., and Sanders, R. H. 1981, A&A 96, 164
Combes, F., Debbasch, F., Friedli, D., and Pfenniger, D. 1990, A&A 233, 82
Combes, F. 2014, A&A, 571, A82
de Blok, W. J. G., Walter, F., Brinks, E. et al. 2008, AJ 136, 2648
Diemand, J., Kuhlen, M., Madau, P. et al. 2008, Nature 454, 735
Di Matteo, P., Combes, F., Melchior, A-L, and Semelin, B. 2007, A&A 468, 61
Dubinski, J., Mihos, J. C., and Hernquist, L. 1996, ApJ 462, 576
Elmegreen, D.M. 2007, in IAU S235, ed. F. Combes & J. Palous, CUP, p. 376
Elmegreen, B.G., Bournaud, F., and Elmegreen, D.M. 2008, ApJ 688, 67
Famaey, B., McGaugh, S. S. 2012, Living Reviews in Relativity, vol. 15, no. 10
Hibbard, J.E., van der Hulst, J.M., Barnes, J.E., and Rich, R.M. 2001, AJ 122, 2969
Immeli, A., Samland, M., Gerhard, O., and Westera, P. 2004, A&A 413, 547
Kormendy, J., and Kennicutt, R. C. 2004, ARAA 42, 603
Kormendy, J., Drory, N., Bender, R., and Cornell, M. E. 2010, ApJ 723, 54
Laurikainen, E., Salo, H., Buta, R., and Vasylyev, S. 2004, MNRAS 355, 1251
Laurikainen, E., Salo, H., Buta, R., and Knapen, J. H. 2009, ApJ 692, L34
Lopez-Sanjuan, C., Le Fèvre, O., Tasca, L.A.M. et al.: 2013, A&A 553, A78
McGaugh, S.S., Schombert, J.M., Bothun, G.D., and de Blok W.J.G. 2000, ApJ 533, 99
Milgrom, M. 1983, ApJ 270, 365
Milgrom, M. 1998, ApJ 496, L89
Milgrom, M., and Sanders, R.H. 2007 ApJ 658, 17
Moore, B., Ghigna, S., Governato, F. et al. 1999, ApJ 524, L19
Naab, T., and Burkert, A. 2003, ApJ 597, 893
Navarro, J.F., and Steinmetz, M. 2000, ApJ 528, 607
Nipoti, C., Londrillo, P., and Ciotti, L., 2007, MNRAS 381, 104
Nipoti, C., Ciotti, L., Binney, J., and Londrillo, P. 2008, MNRAS 386, 2194
Noguchi, M. 1999, ApJ 514, 77
Sanders, R.H., and McGaugh, S. 2002, ARAA 40, 263
Schaye, J., Crain, R. A., Bower, R. G. et al. 2015, MNRAS 446, 521
Sheth, K., Elmegreen, D. M., Elmegreen, B. G. et al. 2008, ApJ 675, 1141
Silk, J., and Mamon, G.A. 2012, Research in Astronomy and Astrophysics, Volume 12, Issue 8, pp. 917–946
Stott, J. P., Sobral, D., Smail, I. et al. 2013, MNRAS 430, 1158

Swaters, R.A., Sancisi, R., van Albada, T.S., and van der Hulst, J.M. 2009 A&A 493, 871
Tacconi, L., Genzel, R., Neri, R. et al. 2010, Nature 463, 781
Tiret, O., and Combes, F. 2007, A&A 464, 517
Tiret, O., and Combes, F. 2008a, A&A 483, 719
Tiret, O., and Combes, F. 2008b ASPC 396, 259
Toomre, A. 1977, in Evolution of Galaxies and Stellar Populations, Proceedings of a Conference at Yale University, p. 401
Vogelsberger, M., Genel, S., Springel, V. et al. 2014, Nature 509, 177
Weinberg, M.D. 1989, MNRAS 239, 549
Weinzirl, T., Jogee, S., Khochfar, S. et al. 2009, ApJ 696, 411
Wu, X., Zhao, H-S., Famaey, B. et al. 2007, ApJ 665, L101

Part VI
Recent Progress and Remaining Unresolved Problems

Chapter 16
Elliptical Galaxies and Bulges of Disc Galaxies: Summary of Progress and Outstanding Issues

John Kormendy

Abstract Bulge components of disc galaxies are the high-density centers interior to their outer discs. Once thought to be equivalent to elliptical galaxies, their observed properties and formation histories turn out to be richer and more varied than those of ellipticals. This book reviews progress in many areas of bulge studies. Two advances deserve emphasis: (1) Observations divide bulges into "classical bulges" that look indistinguishable from ellipticals and "pseudobulges" that are discier and (except in S0s) more actively star-forming than are ellipticals. Classical bulges and ellipticals are thought to form by major galaxy mergers. Discy pseudobulges are a product of the slow ("secular") evolution of galaxy discs. Nonaxisymmetries such as bars and oval distortions transport some disc gas toward the center, where it starbursts and builds a dense central component that is discier in structure than are classical bulges. Secular evolution explains many regular structures (e.g., rings) seen in galaxy discs. It is a new area of galaxy evolution work that complements hierarchical clustering. (2) Studies of high-redshift galaxies reveal that their discs are so gas-rich that they are violently unstable to the formation of mass clumps that sink to the center and merge. This is an alternative channel for the formation of classical bulges.

This chapter summarizes big-picture successes and unsolved problems in the formation of bulges and ellipticals and their coevolution (or not) with supermassive black holes. I present an observer's perspective on simulations of cold dark matter galaxy formation including baryonic physics. Our picture of the quenching of star formation is becoming general and secure at redshifts $z < 1$. I conclude with a list of major uncertainties and problems. The biggest challenge is to produce realistic bulges + ellipticals and realistic discs that overlap over a factor of >1000 in mass but that differ from each other as we observe over that whole range. A related difficulty is how hierarchical clustering makes so many giant, bulgeless galaxies in field but not cluster environments. I present arguments that we rely too much on star-formation feedback and AGN feedback to solve these challenges.

J. Kormendy (✉)
Department of Astronomy, University of Texas at Austin, 2515 Speedway, Mail Stop C1400, Austin, TX 78712-1205, USA
e-mail: kormendy@astro.as.utexas.edu

E. Laurikainen et al. (eds.), *Galactic Bulges*, Astrophysics and Space Science Library 418, DOI 10.1007/978-3-319-19378-6_16

16.1 Introduction

This final chapter summarizes areas of major progress in understanding galaxy bulges and tries to distill the important unresolved issues that need further work.

I do not revisit the subjects covered by all chapters – Madore (2015: historical review), Méndez-Abreu (2015: intrinsic shapes), Falcón-Barroso (2015: kinematic observations), Sánchez-Blázquez (2015: stellar populations), Laurikainen and Salo (2015: observations of boxy bulges), Athanassoula (2015: modeling of boxy bulges), Gonzalez and Gadotti (2015: observations of the Milky Way boxy bulge), Shen and Li (2015: modeling of the Milky Way boxy bulge), Cole and Debattista (2015: nuclear star clusters), and Combes (2015: bulge formation within MOND). I comment briefly on Zaritsky's (2015) chapter on scaling relations.

I concentrate in this summary chapter on three main areas of progress and on two main areas where there are unresolved difficulties:

Two additions to our picture of bulge formation are (1) formation by massive clump instabilities in high-z discs; Bournaud (2015) develops this story, but it deserves emphasis here, too, and (2) our picture of secular evolution of galaxy discs that produces two distinct kinds of dense central components in galaxies, discy pseudobulges (reviewed here by Fisher and Drory 2015) and boxy pseudobulges (discussed in four chapters listed above). Both deserve emphasis here, too.

The main areas with unresolved issues come in two varieties:

Probably the most important chapter in this book is Brooks and Christensen (2015) on the modeling of galaxy – and thus also bulge – formation. These models that add baryonic physics to giant N-body simulations of the hierarchical clustering of cold dark matter (CDM) in a ΛCDM universe define the state of the art in the most general version of galaxy formation theory. Much has been accomplished, and progress is rapid. Brooks and Christensen (2015) is an excellent review of the state of the art as seen by its practitioners. In this chapter, I would like to add the viewpoint of an observer of galaxy archaeology. I suggest a slightly different emphasis on the successes and shortcomings of present models. My main purpose is to promote a dialog between theorists and observers that may help to refine the observational constraints that are most telling and the modeling exercises that may be most profitable. Baryonic galaxy formation is an extraordinarily rich and difficult problem. Many groups struggle honorably and carefully with different aspects of it. In this subject, besides a strong push on remaining limitations such as resolution, the main need seems to me to be a broader use of observational constraints and a consequent refinement of the physics that may succeed in explaining them.

A second issue involves Graham's (2015) chapter on supermassive black holes. It is inconsistent with all other work that I am aware of on this subject, including McConnell and Ma (2013) and Kormendy and Ho (2013). Section 16.6 summarizes this subject using results from Kormendy and Ho (2013, hereafter KH13).

Section 16.7 reviews the quenching of star formation in galaxies. Many different lines of research are converging on a consistent picture of how quenching happens.

Finally, I conclude with a personal view of the most important, big-picture issues that are still unsolved by our developing picture of galaxy evolution.

16.2 Secular Evolution and the Formation of Pseudobulges

Progress on bulge formation is dominated by two conceptual advances. This section revisits secular evolution in disc galaxies. This is a major addition that complements our picture of galaxy evolution by hierarchical clustering. I begin here because *all further discussion depends on the resulting realization that the dense central components in galaxies come in two varieties with different formation processes, classical and pseudo bulges.* Section 16.3 discusses the second conceptual advance, the discovery of a new channel for the formation of classical bulges. This is the formation at high z of unstable clumps in gas-rich discs; they sink to the center along with lots of disc gas and starburst and relax violently. In this way, bulge formation proceeds largely as it does during major mergers. This leads to a discussion of the merger formation of both bulges and ellipticals in Sect. 16.4.

Our pictures of the merger formation of classical bulges and ellipticals and the secular growth of pseudobulges out of discs both got their start in the late 1970s. The importance of major mergers (Toomre and Toomre 1972; Toomre 1977) in a hierarchically clustering universe (White and Rees 1978) got a major boost from the realization that CDM halos make galaxy collision cross sections much bigger than they look. This subject "took off" and rapidly came to control our formation paradigm. Secular evolution is a more difficult subject – slow processes are hard to study – and it did not get a similar boost from the CDM revolution. However, the earliest papers on the subject come from the same time period: e.g., Kormendy (1979a) emphasized the importance of slow interactions between nonaxisymmetric galaxy components; Kormendy (1979b) first pointed out the existence of surprisingly discy bulges; Combes and Sanders (1981) showed that boxy pseudobulges are edge-on bars. Kormendy (1981, 1982) reviewed and extended the results on discy bulges. This subject did not penetrate the galaxy formation folklore; rather, it remained a series of active but unconnected "cottage industries" for the next two decades. Nevertheless, by the 1990s, the concept – if not yet the name – of discy pseudobulges was well established (see Kormendy 1993 for a review), and the idea that boxy bulges are edge-on bars was well accepted (see Athanassoula 2005 for a more recent and thorough discussion). I hope it is fair to say that the comprehensive review by Kormendy and Kennicutt (2004) has helped to convert this subject into a recognized paradigm – it certainly is so in this book – although it is still not as widely understood or taken into account as is hierarchical clustering.

Kormendy and Kennicutt (2004) remains up-to-date and comprehensive on the basic results and on observations of prototypical pseudobulges. However, new reviews extend and complement it. Kormendy and Fisher (2005, 2008) and

Kormendy (2008, 2012) provide the most important physical argument that was missing in Kormendy and Kennicutt (2004): Essentially all self-gravitating systems evolve toward more negative total energies (more strongly bound configurations) by processes that transport kinetic energy or angular momentum outward. In this sense, the secular growth of pseudobulges in galaxy discs is analogous to the growth of stars in protostellar discs, the growth of black holes in black hole accretion discs, the sinking of Jupiters via the production of colder Neptunes in protoplanetary discs, core collapse in globular clusters, and the evolution of stars into red (super)giants with central proto white dwarfs, neutron stars, or stellar-mass black holes. All of these evolution processes are related. So secular disc evolution and the growth of pseudobulges is fundamental, provided that some process redistributes angular momentum in the disc. My Canary Islands Winter School lectures (Kormendy 2012) are an up-to-date observational review that includes environmental secular evolution. Sellwood (2014) provides an excellent theoretical review.

Boxy pseudobulges are discussed in four chapters of this book; I concentrate on discy pseudobulges. Fisher and Drory (2015) review the distinction between classical and pseudo bulges from a purely phenomenological point of view. That is, they intercompare observational diagnostics to distinguish between the two bulge types with no reference to physical interpretation. This is useful, because it gives relatively unbiased failure probabilities for each diagnostic. They are not wholly independent, of course, because they are intercompared. But they are independent enough in execution so that we get a sufficient estimate of the failure probability when they are combined by multiplying the individual failure probabilities.

Kormendy and Kennicutt (2004), Kormendy (2012), and KH13 strongly advocate the use of as many bulge classification criteria as possible. The reason is that any one criterion has a non-zero probability of failure. Confusion in the literature (e.g., Graham 2011) results from the fact that some authors use a single classification criterion (e.g., Sérsic index) and so get results that conflict with those derived using multiple criteria. But we have long known that most classical bulges have $n \geq 2$, that most pseudobulges have $n < 2$, and that there are exceptions to both criteria. No-one should be surprised that Sérsic index sometimes fails to correctly classify a bulge. This is the point that Fisher and Drory (2015) make quantitative.

Fisher and Drory (2015) show that the failure probability of each classification criterion that they test is typically 10–20 %. A few criteria are completely robust (if $B/T \gtrsim 0.5$, then the bulge is classical) and a few are less reliable (star formation rate cannot be used for S0s). But, by and large, it is reasonable to conclude that the use of M criteria, each with failure probability ϵ_m, results in a classification with a failure probability of order the product of the individual failure probabilities, $\Pi_1^M \epsilon_m$. This becomes very small very quickly as M grows even to 2 and especially to $M > 2$. For example, essentially all bulge-pseudobulge classifications in KH13 were made using at least two and sometimes as many as five criteria.

Fisher and Drory (2015) also contribute new criteria that become practical as new technology such as integral-field spectroscopy gets applied to large samples of galaxies. These are incorporated into an enlarged list of classification criteria below.

A shortcoming of Fisher and Drory's approach is that it is applied without regard to all galaxy Hubble types. But we know that both many S0s and many Sbcs contain pseudobulges, but the latter all tend to be star-forming whereas the former generally are not. This is one reason for their conclusion (e.g.) that high star formation rate near the galaxy center robustly implies a pseudobulge, but no star formation near the center fails to prove that the bulge is classical. Classification criteria that involve gas content and star formation rate cannot be applied to S0 galaxies. Application to Sas is also fragile. Fortunately, most criteria do work for early-type galaxies.

16.2.1 Enlarged List of Bulge-Pseudobulge Classification Criteria

Kormendy and Kennicutt (2004), Kormendy (2012), and Fisher and Drory (2015) together provide the following improved list of (pseudo)bulge[1] classification criteria. I note again: The failure rate for individual criteria ranges from 0 % to roughly 25 %. Therefore the use of more criteria quickly gives much more reliable results.

(1) If the galaxy center is dominated by young stars and gas but there is no sign of a merger in progress, then the bulge is mostly pseudo. Ubiquitous star formation must be secular. Fisher and Drory (2015) make this quantitative: if the specific star formation rate sSFR $\geq 10^{-11}$ yr^{-1}, then the bulge is likely to be pseudo; whereas if sSFR $< 10^{-11}$ yr^{-1}, then the bulge is likely to be classical. Also, if the bulge is very blue, $B - V < 0.5$, then it is pseudo. Criteria (1) cannot be used for S0s.

(2) Discy pseudobulges (a) generally have apparent flattening similar to that of the outer disc or (b) contain spiral structure all the way to the galaxy center. Classical bulges are much rounder than their discs unless they are seen almost face-on, and they cannot have spiral structure. Criterion 2(a) can be used for S0s; 2(b) can not.

(3) Pseudobulges are more rotation-dominated than are classical bulges in the $V_{\rm max}/\sigma - \epsilon$ diagram; $V_{\rm max}$ is maximum rotation velocity, σ is near-central velocity dispersion, and ϵ is ellipticity. Integral-field spectroscopy often shows that the central surface brightness excess over the inward extrapolation of the disc profile is a flat central component that rotates rapidly and has small σ.

(4) Many pseudobulges are low-σ outliers in the Faber-Jackson (1976) correlation between (pseudo)bulge luminosity and velocity dispersion. Integral-field spectra often show that σ decreases from the disc into a pseudobulge. Fisher and Drory make this quantitative: Pseudobulges have rather flat logarithmic

[1]Editorial comment: "(Pseudo)bulge" means classical and pseudo bulge, without prejudice. In this chapter, "Pseudobulge" includes both boxy and discy central components grown out of galaxy discs. When the distinction is particularly important, the text explicitly says (e.g.) "discy pseudobulges".

derivatives of the dispersion profile $d\log\sigma/d\log r \geq -0.1$ and $V^2/\sigma^2 \geq 0.35$. In contrast, if $d\log\sigma/d\log r < -0.1$ or if central $\sigma_0 > 130\,\mathrm{km\,s^{-1}}$, then the bulge is classical.

(5) Small bulge-to-total luminosity ratios do not guarantee that a bulge is pseudo, but almost all pseudobulges have $PB/T \lesssim 0.35$. If $B/T \gtrsim 0.5$, the bulge is classical.

(6) Most pseudobulges have Sérsic index $n < 2$; most classical bulges have $n \geq 2$.

(7) Classical bulges fit the fundamental plane correlations for elliptical galaxies. Some pseudobulges do, too, and then the correlations are not useful for classification. More extreme pseudobulges are fluffier than classical bulges; they have larger effective radii r_e and fainter effective surface brightnesses μ_e. These pseudobulges can be identified using fundamental plane correlations.

(8) In face-on galaxies, the presence of a nuclear bar shows that a pseudobulge dominates the central light. Bars are disc phenomena. Triaxiality in giant Es involves different physics – slow (not rapid) rotation and box (not x_1 tube) orbits.

(9) In edge-on galaxies, boxy bulges are edge-on bars; seeing one identifies a pseudobulge. The boxy-core-nonrotating side of the "E – E dichotomy" between two kinds of elliptical galaxies (see Sect. 16.4.1.1) cannot be confused with boxy, edge-on bars because boxy ellipticals – even if they occur in disc galaxies (we do not know of an example) – are so luminous that we would measure $B/T > 0.5$. Then point (5) would tell us that this bulge is classical.

(10) Fisher and Drory (2015) conclude that pseudobulges have weak Fe and Mg b lines: equivalent width of [Fe λ5150 Å] < 3.95 Å; equivalent width of [Mg b] < 2.35 Å. In their sample, no classical bulge has such weak lines. Some pseudobulges have stronger lines, so this criterion, like most others, is not 100 % reliable.

(11) If a bulge deviates from the [Mg b] – σ or [Mg b] – [Fe] correlations for elliptical galaxies by Δ[Mg b] < -0.7 – that is, if the [Mg] line strength is lower than the scatter for Es – then the bulge is likely to be pseudo (Fisher and Drory 2015).

It is important to emphasize that classical and pseudo bulges can occur together. Fisher and Drory (2015) review examples of dominant pseudobulges that have small central classical bulges. And some giant classical bulges contain nuclear discs (e.g., NGC 3115: Kormendy et al. 1996b; NGC 4594: Kormendy et al. 1996a).

Criterion (9) for boxy pseudobulges works only for edge-on and near-edge-on galaxies. In face-on galaxies, it is easy to identify the elongated parts of bars, but they also have rounder, denser central parts, and these are not easily distinguished from classical bulges (Athanassoula 2015; Laurikainen and Salo 2015). So the above criteria almost certainly fail to find some pseudobulges in face-on barred galaxies.

16.2.2 Secular Evolution in Disc Galaxies: Applications

Progress in many subjects depends on a full integration of the picture of disc secular evolution into our paradigm of galaxy evolution. Examples include the following:

(1) If the smallest bulges are pseudo and not classical, then the luminosity and mass functions of classical bulges and ellipticals are very bounded: $M_K \lesssim -19$; $M_V \lesssim -16$; $L_V \gtrsim 10^{8.5}\ L_\odot$; stellar mass $M_{\rm bulge} \gtrsim 10^9\ M_\odot$. In simulations (Brooks and Christensen 2015; Sect. 16.4 here), the physics that makes classical bulges and ellipticals does not need to explain objects that are smaller than the above. More accurately: If the same generic physics (e.g., major mergers) is relevant for smaller objects, it does not have to produce remnants that are consistent with low-mass extrapolations of parameter correlations for classical bulges and ellipticals. One possible reason may be that the progenitors of that physics are very gas-rich.

(2) Our understanding that, below the above limits, lower-mass bulges are essentially all pseudo makes it harder to understand how galaxy formation by hierarchical clustering of CDM makes so many giant, classical-bulge-less (i. e., pure-disc) galaxies. This was the theme of the observational papers by Kormendy et al. (2010) and Fisher and Drory (2011). It is addressed in Brooks and Christensen (2015). We return to this issue in Sect. 16.4.

(3) Understanding how supermassive black holes (BHs) affect galaxy evolution requires an understanding that classical and pseudo bulges are different. Classical bulges participate in the correlations between BH mass and bulge luminosity, stellar mass, and velocity dispersion. Pseudobulges essentially do not. This is some of the evidence that BHs coevolve with classical bulges and ellipticals in ways to be determined, whereas BHs exist in but do not influence the evolution of discs or of disc-grown pseudobulges. We return to this subject in Sect. 16.6.

16.3 Giant Clumps in High-z Gas-Rich Discs Make Classical Bulges

The second major advance in our picture of bulge formation involves the observation that many high-z discs are very gas-rich and dominated by $10^8 - 10^9\ M_\odot$, kpc-size star-forming clumps (Elmegreen et al. 2005, 2007, 2009a,b; Bournaud et al. 2007; Genzel et al. 2006, 2008, 2011; Förster Schreiber et al. 2009, 2011a,b; Tacconi et al. 2010). These galaxies evidently accrete cold gas so rapidly that they become violently unstable. Bulgeless discs tend to have small epicyclic frequencies κ. If the surface density Σ rapidly grows large and is dominated by gas with low velocity dispersion σ, then the Toomre (1964) instability parameter $Q = 0.30\sigma\kappa/G\Sigma \lesssim 1$ (G = gravitational constant). The observed clumps are interpreted to be the result.

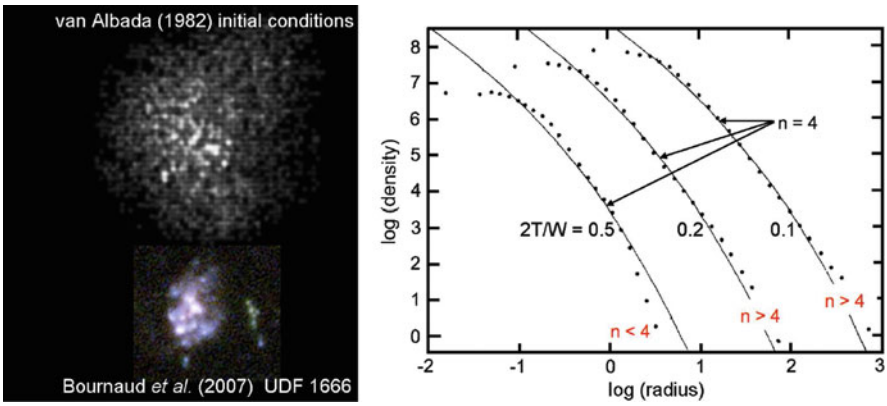

Fig. 16.1 Mergers of clumpy initial conditions make Sérsic et al. (1968) function remnants with indices $n \sim 2$–4. A remarkably early illustration is the n-body simulation of van Albada (1982), whose initial conditions (*grayscale densities*) resemble the clumpy high-z galaxy UDF 1666 studied by Bournaud et al. (2007). Van Albada's initial conditions were parameterized by the ratio of twice the total kinetic energy to the negative of the potential energy. In equilibrium, $2T/W = 1$. For smaller values, gentle collapses ($2T/W = 0.5$) make Sérsic profiles with $n < 4$. Violent collapses ($2T/W \lesssim 0.2$) make $n \gtrsim 4$. Clump sinking in high-z discs is inherently gentle. The hint is that the clumps merge to make classical bulges with $n < 4$ (This figure is from Kormendy 2012)

Theory and simulations suggest that the clumps sink rapidly toward the center by dynamical friction. They also dump large amounts of additional cold gas toward the center via tidal torques. The result is violent relaxation plus a starburst that produces a classical bulge. Many papers discuss this evolution (e.g., Dekel et al. 2009b; Ceverino et al. 2010, 2015; Cacciato et al. 2012; Forbes et al. 2014). Bournaud (2015) reviews this subject in the present book. I include it here for two reasons, it is a major advance, so it deserves emphasis in this concluding chapter, and I want to add two science points:

Figure 16.1 illustrates my first point: *Evolution by clump sinking, inward gas transport, violent relaxation, and starbursts proceeds much as it does in our picture of wet major mergers. That is, in practice (if not in its beginnings), classical bulge formation from clump instabilities is a variant of our standard picture of bulge formation in wet major mergers.* The process starts differently than galaxy mergers – what merges here are not finished galaxies but rather are clumps that formed quickly and temporarily in unstable discs. Nevertheless, what follows – although two- and not three-dimensional – is otherwise closely similar to a wet merger with gas inflow and a starburst. That is, it is a slower, gentler version of Arp 220.

Early models by Elmegreen et al. (2008) confirm that gas-rich galaxy discs violently form clumps like those observed. The clumps quickly sink, merge, and make a high-Sérsic-index, vertically thick bulge. It rotates slowly, and rotation velocities decrease with increasing distance above and below the disc plane. These are properties of classical bulges, and Elmegreen and collaborators conclude that

this process indeed makes classical (not pseudo) bulges. Many of the later papers summarized above and reviewed by Bournaud (2015) reach similar conclusions.

However, Bournaud (2015) goes on to review more recent simulations that – among other improvements – include strong feedback from young stars. The results complicate the above picture. For example, Genel et al. (2012) find that "galactic winds are critical for [clump] evolution. The giant clumps we obtain are short-lived and are disrupted by wind-driven mass loss. They do not virialize or migrate to the galaxy centers as suggested in recent work neglecting strong winds." Other simulations produce pseudobulge-like, small Sérsic indices. Some results are inherently robust, such as the conclusion that gas-rich, violently unstable discs at high z gradually evolve into gas-poor, secularly evolving discs at lower redshifts (Cacciato et al. 2012; cf. Ceverino et al. 2010). However, the conclusions from the models are substantially more uncertain than the inferences from the observations. This is part of a problem that I emphasize in the next section:

Simulations of baryonic galaxy evolution inside CDM halos formed via N-body simulations of cosmological hierarchical clustering are making rapid progress as the baryonic physics gets implemented in better detail. But these simulations still show clearcut signs of missing important physics. In contrast, practitioners of this art who carefully put great effort into improving the physics tend to be overconfident about its results. We are – I will suggest – still in a situation where robust observational conclusions that are theoretically squishy are more trustworthy than conclusions based on state-of-the-art simulations, at least when baryonic physics is involved.

Another caveat is the observation that the clumps in high-z discs are much less obvious in the inferred mass distributions than they are in rest-frame optical or blue light (Wuyts et al. 2012). Frontier observations have opened up a popular new window on the formation of classical bulges, but its importance is not entirely clear.

In the present subject of bulge formation, it seems provisionally plausible that formation via high-z disc instabilites and consequent clump sinking represents a significant new channel in the formation of classical bulges. Meanwhile, a large body of work from the 1980s and 1990s continues to tell us that major galaxy mergers make classical bulges, too. Can we distinguish the results of the two processes? We do not yet know, but my second point is that Fig. 16.1 provides a hint: Although results are still vulnerable to unknown details in (for example) feedback, it seems likely that the classical bulges produced by sinking clumps have Sérsic indices that are systematically smaller than those made by major galaxy mergers. This is one aspect of many that deserves further work. See also point (8) in Sect. 16.8.

16.4 Making Classical Bulges and Ellipticals by Major Mergers

Brooks and Christensen (2015) is perhaps the most important chapter in this book. A parallel ARA&A review of the same subject is by Somerville and Davé (2015). The mainstream of theoretical work on galaxy formation has come to be the simulation in a cosmological context first of purely collisionless CDM but now with gloriously messy baryonic physics included. Progress is impressively rapid, but we are far from finished. This subject is well reviewed from the perspective of its practitioners by Brooks and Christensen. This includes a discussion of uncertainties and shortcomings in the models, again as seen by theorists. As an observer, I have a complementary perspective on which measurements of galaxies provide the most useful constraints on and "targets" for formation models. It gives me the feeling that modelers are at least partly "barking up the wrong tree." This section complements Brooks and Christensen (2015) by reviewing these observations.

Pseudobulge formation was covered in Sect. 16.2. Here, I focus on the formation of classical bulges and ellipticals. My discussion uses the observations that classical bulges are essentially indistinguishable from coreless-discy-rotating ellipticals (see, e.g., Fig. 16.4). The inference is that they formed in closely related ways.

16.4.1 Observer's Perspective on Bulge Formation via Major Mergers

I begin with giant ellipticals and classical bulges: their structure and formation are understood in the most detail. Classical bulges are identified by the criteria listed in Kormendy and Kennicutt (2004), Kormendy (2012), KH13, Fisher and Drory (2015), and Sect. 16.2 here. I know no observational reason to seriously doubt our understanding of bulges with $B/T \gtrsim 0.8$. Then, as B/T drops to $\lesssim 1/2$, the situation gets less clear. Our formation picture may still essentially be correct, but it gets less directly based on observations as B/T or bulge luminosity decreases. Meanwhile, the theoretical problem is that simulations make too many bulges, especially big ones. In this section, I review things that we know and outline things that we do not know. It is critically important to start with a discussion of ellipticals, because our understanding of classical bulges must be within this context.

16.4.1.1 Observed Properties of Ellipticals: Clues to Their Formation

The observed properties of elliptical galaxies are reproduced by simulations of wet and dry mergers in remarkable detail. These are not embedded in large-scale cosmological simulations, but this is not a fundamental fault if the initial conditions are realistic – galaxies with typical $z \sim 0$ gas fractions and encounter velocities that are roughly parabolic. Kormendy et al. (2009, hereafter KFCB) provide an

ARA&A-style review and develop some of the evidence. Hopkins et al. (2009a, 2009b) provide the most detailed models for wet and dry mergers, respectively. These papers are comprehensive; a concise summary of the "E – E dichotomy" in Kormendy (2009) is updated below. The critical observation is that ellipticals come in two varieties and that bulges are similar to one (but not both) of these varieties.

The E – E dichotomy of ellipticals into two kinds is based on these observations:

Giant ellipticals ($M_V \lesssim -21.5 \pm 1$ for $H_0 = 70\,\mathrm{km\,s^{-1}\,Mpc^{-1}}$) generally

(1) have Sérsic function outer profiles with $n > 4$;
(2) have cores; i. e., central missing light with respect to the outer Sérsic profile;
(3) rotate slowly, so rotation is of little importance dynamically; hence
(4) are anisotropic and modestly triaxial;
(5) are less flattened (ellipticity $\epsilon \sim 0.2$) than smaller ellipticals;
(6) have boxy-distorted isophotes;
(7) mostly are made of very old stars that are enhanced in α elements (Fig. 16.2);
(8) often contain strong radio sources (Fig. 16.3), and
(9) contain X-ray-emitting gas, more of it in more luminous galaxies (Fig. 16.3).

Normal ellipticals and dwarf ellipticals like M 32 ($M_V \gtrsim -21.5$) generally

(1) have Sérsic function outer profiles with $n \simeq 2$ to 3;
(2) are coreless – have central extra light with respect to the outer Sérsic profile;
(3) rotate rapidly, so rotation is dynamically important to their structure;
(4) are nearly isotropic and oblate spheroidal, albeit with small axial dispersions;
(5) are flatter than giant ellipticals (ellipticity $\epsilon \sim 0.35$);
(6) have discy-distorted isophotes;
(7) are made of younger stars with little α-element enhancement (Fig. 16.2);
(8) rarely contain strong radio sources (Fig. 16.3), and
(9) generally do not contain X-ray-emitting gas (Fig. 16.3).

These results are established in many papers (e.g., Davies et al. 1983; Bender 1988; Bender et al. 1989; Nieto et al. 1991; Kormendy et al. 1994; Lauer et al. 1995, 2005, 2007a,b; Kormendy and Bender 1996; Tremblay and Merritt 1996; Gebhardt et al. 1996; Faber et al. 1997; Rest et al. 2001; Ravindranath et al. 2001; Thomas et al. 2002a,b, 2005; Emsellem et al. 2007, 2011; Cappellari et al. 2007, 2011, 2013b; KFCB; Kuntschner et al. 2010). A few ellipticals are exceptions to one or more of (1)–(9). The above summary is quoted from Kormendy (2009).

Why is this relevant here? The answer is that classical bulges are closely similar to coreless-discy-rotating ellipticals. No bulge is similar to a core-boxy-nonrotating elliptical as far as I know. This is a clue to formation processes. First, though, we need to understand the difference between the two kinds of ellipticals:

How did the E–E dichotomy arise? The "smoking gun" for an explanation is a new aspect of the dichotomy originally found in Kormendy (1999) and observed in all low-luminosity ellipticals in the Virgo cluster by KFCB. Coreless galaxies do not have featureless power-law profiles. Rather, all coreless galaxies in the KFCB sample show a new structural component, i.e., central extra light above the inward extrapolation of the outer Sérsic profile. Kormendy (1999) suggested that the extra light is produced by starbursts fed by gas dumped inward during dissipative mergers.

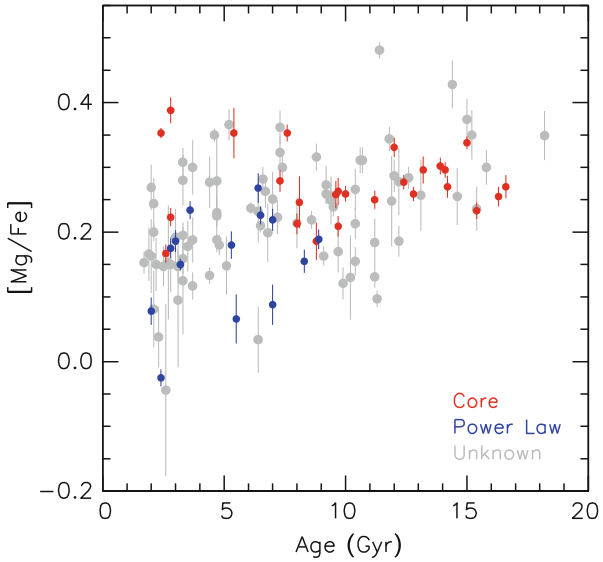

Fig. 16.2 Alpha element overabundance (log solar units) versus relative age of the stellar population. *Red* and *blue* points denote core and "power law" (i. e., coreless) ellipticals (The [Mg/Fe] and age data are from Thomas et al. (2005); this figure is from KFCB)

Starbursts were predicted by merger simulations as soon as these included gas, dissipational gas inflow, and star formation (Mihos and Hernquist 1994). Mihos and Hernquist were concerned that extra components had not been observed. The reason turns out to be that we had not measured ellipticals with enough surface brightness range and spatial resolution. Like Faber et al. (1997, 2007), KFCB suggest that the origin of the E – E dichotomy is that core ellipticals formed in dry mergers whereas coreless ellipticals formed in wet mergers. Simulations of dry and wet mergers reproduce the structural properties of core and extra light ellipticals in beautiful detail (Hopkins et al. 2009a,b). And, although the formations scenarios differ, Khochfar et al. (2011) similarly conclude that the difference between fast and slow rotators is related to cold gas dissipation and star-formations shutdown, respectively.

Cores are thought to be scoured by supermassive black hole binaries that were formed in major mergers. The orbit shrinks as the binary flings stars away. This decreases the surface brightness and excavates a core (Begelman et al. 1980; Ebisuzaki et al. 1991; Makino and Ebisuzaki 1996; Quinlan and Hernquist 1997; Faber et al. 1997; Milosavljević and Merritt 2001; Milosavljević et al. 2002; Merritt 2006). The same process should happen during wet mergers; although gas accelerates the orbital decay (Ivanov et al. 1999; Gould and Rix 2000; Armitage and Natarajan 2002, 2005; Escala et al. 2004, 2005; Dotti et al. 2007; Hayasaki 2009; Cuadra et al. 2009; Escala and Del Valle 2011; see Mayer 2013 for a recent review). However, we observe that the fraction of the luminosity that is in extra light in low-luminosity ellipticals is larger than the fraction of the light that is "missing" in the

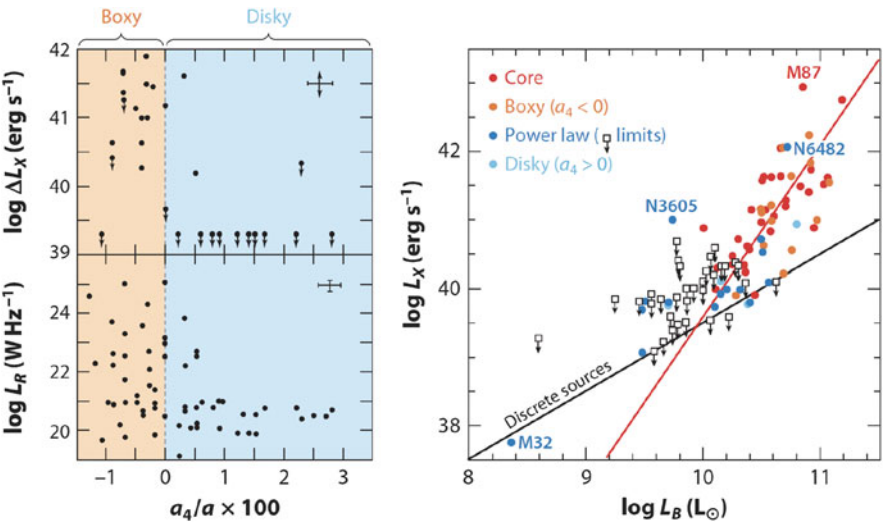

Fig. 16.3 (*Left*) Correlation with isophote shape parameter a_4 of (*top*) X-ray emission from hot gas and (*bottom*) radio emission (from Bender et al. 1989). Boxy ellipticals ($a_4 < 0$) contain hot gas and strong radio sources; discy ellipticals ($a_4 > 0$) generally do not. (*Right*) KFCB update of the X-ray correlation. Detections are color-coded according to the E – E dichotomy. The emission from X-ray binary stars is estimated by the *black line* (O'Sullivan et al. 2001); this was subtracted from the total emission in constructing the *left panels*. The *red line* is a bisector fit to the core-boxy-nonrotating ellipticals. They statistically reach $L_X = 0$ from hot gas at $\log L_B \simeq 9.94$. This corresponds to $M_V \simeq -20.4$, a factor of 2 fainter than the luminosity that divides the two kinds of ellipticals. Thus, if a typical core E was made in a merger of two equal-mass galaxies, then both were marginally big enough to contain X-ray gas and the remnant immediately was massive enough so that hot gas could quench star formation. KFCB suggest that this is why these mergers were dry. For similar results, see Pellegrini (1999, 2005) and Ellis and O'Sullivan (2006). This figure is from KH13

cores of high-luminosity ellipticals. KFCB suggest that core scouring is swamped by the starburst that makes the extra light in coreless-discy-rotating ellipticals.

When did the E–E dichotomy arise? Figure 16.2 shows observation (7) that core ellipticals mostly are made of old stars that are enhanced in α elements. In contrast, coreless ellipticals are made of younger stars with more nearly solar compositions. This means (Thomas et al. 2002a,b, 2005) that the stars in core Es formed in the first few billion years of the universe and over a period of $\lesssim 1$ Gyr, so quickly that Type I supernovae did not have time to dilute with Fe the α-enriched gas recycled by Type II supernovae. This does not mean that core ellipticals were made at the same time as their stars. Mass assembly via dry mergers as required to explain their structure could have happened at any time after star formation stopped. Our problem is to explain how star formation was quenched so quickly and not allowed to recur. In contrast, coreless ellipticals have younger, less-α-enhanced stellar populations. They are consistent with a simple picture in which a series of wet mergers with accompanying starbursts formed their stellar populations and assembled the galaxies

more-or-less simultaneously over the past 9 billion years. Faber et al. (2007) discuss these issues in detail. A big problem with the present state of the art is that we know so little about mergers and merger progenitors at high z.

Why did the E–E dichotomy arise? The key observations are: (8) core-boxy ellipticals often are radio-loud whereas coreless-discy ellipticals are not, and (9) core-boxy ellipticals contain X-ray gas whereas coreless-discy ellipticals do not (Bender et al. 1989). Figure 16.3 (from KH13) illustrates these results. KFCB suggest that the hot gas keeps dry mergers dry and protects giant ellipticals from late star formation. This is the operational solution to the above "maintenance problem". I return to the problem of star-formation quenching in Sect. 16.7.

In the above story, the challenge is to keep the hot gas hot, given that X-ray gas cooling times are short (Fabian 1994). KFCB review evidence that the main heating mechanism may be energy feedback from accreting BHs (the active galactic nuclei [AGNs] of observation 8); these may also have helped to quench star formation. Many details of this picture require work (Cattaneo et al. 2009). Cosmological gas infall is an additional heating mechanism (Dekel and Birnboim 2006). Still, Fig. 16.3 is a crucial connection between X-ray gas, AGN physics, and the E – E dichotomy.

"Bottom line:" In essence, only giant, core ellipticals and their progenitors are massive enough to contain hot gas that helps to engineer the E–E dichotomy.

16.4.1.2 Classical Bulges Resemble Coreless-Discy-Rotating Ellipticals

Are both kinds of ellipticals also found as bulges? So far, observations indicate that the answer is "no". Classical bulges closely resemble only the coreless-discy-rotating ellipticals. There are apparent exceptions in the literature, but all the exceptions that I know about are classification errors brought about (e.g.) by the very large Sérsic indices of some core galaxies (see KFCB Table 1 for examples and KFCB Section 5.2 for discussion). This comment also does not include ellipticals with nuclear discs. All signs are that these involve different physics, so these really are ellipticals, not S0 bulges.

There is physics in this conclusion. The X-ray gas prevents cooling and dissipation during any subsequent mergers or any $z \lesssim 1$ cold accretion. Plausibly, it should also prevent there from being any cold gas left over to make a new disc after a merger is complete. Further checks, both of the observational conclusion and of the theoretical inference, should be made.

16.4.1.3 The Critically Important Target for Galaxy Formation

The most fundamental distinction between galaxy types is the one between bulges + ellipticals and discs. Bulges and discs overlap over a factor of about ∼1500 in luminosity and mass (Fig. 16.4), but over that entire overlap range, they are dramatically different from each other. This includes differences in specific angular momentum (Romanowsky and Fall 2012; Fall and Romanowsky 2013), in orbit structure, in flattening, and in radial density profiles (discs are roughly exponential; coreless-discy-rotating ellipticals have $^{n>}_{\sim}$ 2). At absolute magnitude $M_V \simeq -16.7$ and outer circular-orbit rotation velocity $V_{\rm circ} \sim 85\,{\rm km\,s^{-1}}$, M 32 is a normal small elliptical galaxy (KFCB). At $M_V \simeq -21.6$ and $V_{\rm circ} = 210 \pm 15\,{\rm km\,s^{-1}}$, M 101 is almost 100 times more luminous but is thoroughly different from M 32 or from $M_V \simeq -21.6$ ellipticals (Kormendy et al. 2010).

I believe that the goal of galaxy formation modeling should be to produce realistic discs and realistic ellipticals that overlap over the observed factor of ∼1500 in luminosity but that differ as we observe them to differ over the whole of that range. And over the whole of that range, discs and bulges can be combined with B/T and $D/T \simeq 1 - B/T$ ratios that have the observed distribution (i. e., $B/T \sim 1$ near the upper end of the range, but it can be $\ll 1$ at the bottom of the range). The properties of individual discs and bulges are essentially independent of B/T with structural parameters shown in Fig. 16.4.

Of course, bulges and discs are not different in *every* parameter; e.g., the r_e – μ_e correlations overlap at high luminosities (Fig. 16.4). This makes sense: At the highest masses, it does not require much dissipation to turn a disc into an elliptical, at least in terms of virial parameters. All that is required is to scramble disc orbits into an ellipsoidal remnant. A larger amount of dissipation is required to make the high-density centers, and in *central* parameters and parameter correlations, discs and bulges + ellipticals are very different (Kormendy 1985, 1987).

16.4.1.4 Critical Observational Clue: The Problem of Giant, Pure-Disc Galaxies Depends on Environment, Not on Galaxy Mass

The most difficult challenge in our picture of galaxy formation – I suggest – is to understand how hierarchical clustering produces so many giant, pure-disc galaxies that have no sign of a classical bulge. CDM halos grow by merging; fragments arrive from all directions, and not all fragments are small. There are two parts to this problem: (1) It is difficult to understand how cold, flat discs survive the violence inherent in the mergers that grow DM halos. And (2) it

(continued)

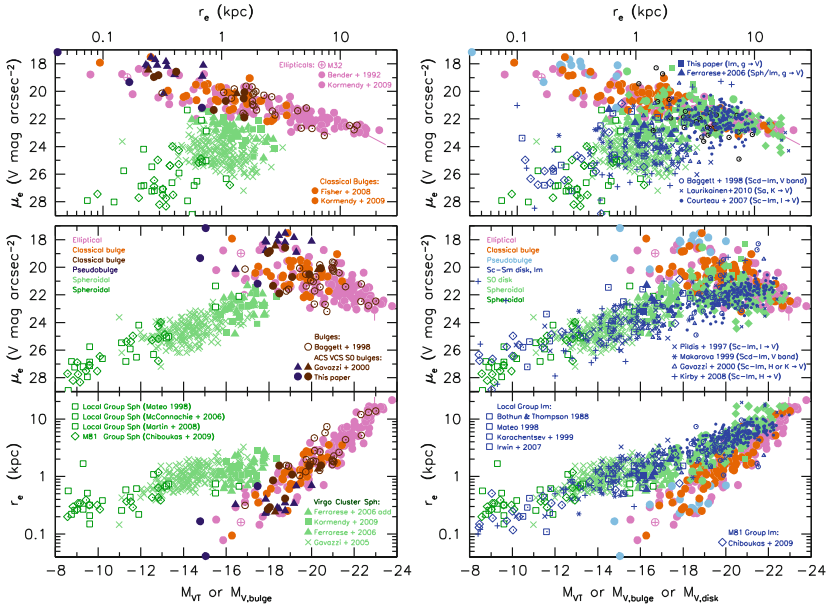

Fig. 16.4 Correlations between effective radius r_e, effective brightness μ_e, and absolute magnitude M_V for classical bulges and ellipticals (*brown* and *pink points*), for spheroidal (Sph) galaxies and S0 discs (*green points*), and for spiral galaxy discs (*blue points*). When bulge-disc decomposition is necessary, the two components are plotted separately. Bulges and discs overlap from $M_V \simeq -15$ to $M_V \simeq -23$, i. e., over a factor of about 1500. The *left panel* shows (1) that Sph galaxies are distinct from bulges + ellipticals and (2) that classical bulges and ellipticals satisfy the same structural parameter correlations. The *right panel* adds S0 and S galaxy discs. It shows that all discs satisfy the same structural parameter correlations over the whole range of luminosities. Note that discs and ellipticals have similar r_e and μ_e at the highest luminosities, but they have very different Sérsic indices ($\sim$1 and 2 to > 10, respectively). As a result, the central surface brightnesses in bulges and ellipticals are more than an order of magnitude higher than the central surface brightnesses of discs (Kormendy 1985, 1987). Bulges + ellipticals and discs also have non-overlapping distributions of intrinsic flattening (e. g., Sandage, Freeman, and Stokes 1970). From Kormendy and Bender (2012)

is difficult to prevent the stars that arrive with the latest accretion victim from adding to a classical bulge that formed in (1) from the scrambled-up disc.

Brooks and Christensen (2015) review how the modeling community tries to solve this problem. In spite of several decades of evidence that mergers make bulges, they do not use mergers to turn discs into bulges. Instead, they use feedback from young stars and active galactic nuclei to "whittle away" the low-angular-momentum part of the distribution of gas angular momenta and argue that this prevents bulge formation. And they use feedback to delay

(continued)

disc formation until the halo is assembled. Feedback is likely to be important in the formation of dwarf galaxies (Governato et al. 2010), and indeed, they essentially never have bulges (e.g., Kormendy and Freeman 2015, Figure 10).

However, it is difficult for me to believe that feedback, either from star formation or from AGNs, is responsible for the difference between bulges and discs. Feedback is fundamentally an internal process that is controlled by the galaxy's potential well depth. It is not clear how *only* tweaking the feedback can make a small elliptical like M 32 (different from small discs) and a giant disc like M 101 (different from similarly giant ellipticals) with no intermediate cases. Bulge-to-total ratios vary widely, but classical bulges are always like ellipticals no matter what the B/T ratio, and discs are always different from ellipticals no matter what the D/T ratio. Observations do not suggest that it is primarily feedback that results in this difference. Rather:

There is a fundamental observational clue that modelers are not using:

Whether evolution makes discs or whether it makes bulges does not depend mainly on galaxy mass. Rather, it is a strong function of environment. Kormendy et al. (2010) show that, in the extreme field (i. e., in environments like the Local Group), most giant galaxies ($V_{\rm circ} \geq 150\,{\rm km\,s^{-1}}$) are pure discs. Only 2 of 19 giant galaxies closer to us than 8 Mpc have B/T as big as 1/3. Only 2 more are ellipticals. A few have smaller classical bulges, but 11 of the 19 galaxies have essentially no classical bulge. In contrast, >2/3 of all stars in the Virgo cluster live in bulges or elliptical galaxies. *There is no problem of understanding giant pure-disc galaxies in the Virgo cluster.* It is a mature, dense environment that contains large amounts of X-ray-emitting, hot gas. Rich clusters are places where most of the baryons live suspended in hot gas (e.g., Kravtsov and Borgani 2012). I argue in Sect. 16.4.1.1 that various heating processes maintain this situation for very long times. In contrast, poor groups are environments in which accretion of cold gas from the cosmic web can dominate, as long as the galaxies involved – i. e., the aforementioned pure discs – are low enough in mass so that they cannot hold onto X-ray gas.

As long as this environmental dependence is not a primary, essential part of the explanation, I believe that attempts to solve the problem of overproduction of bulges in ΛCDM cosmology are "barking up the wrong tree".

Why can't we use feedback to delay star formation until the halo is assembled? As reviewed by Brooks and Christensen (2015), this is commonly suggested. The counterexample is our Galaxy: The oldest stars in the thin disc are $\sim 10^{10}$ yr old, so much of the growth of our Galaxy happened when the thin disc was already in place (Kormendy et al. 2010, p. 73).

16.4.1.5 It Is Not a Problem that Major Mergers Are Rare

The prevailing theoretical paradigm is more and more converging on the view that major mergers are rare – are, in fact, almost irrelevant – and that, instead, minor mergers make both bulges and ellipticals (see Naab 2013 for a review), even some core-boxy-nonrotating ellipticals (Naab et al. 2014). It will be clear from this writeup that, based on observational evidence, I agree that major mergers are rare. But I disagree that they are unimportant in the formation of bulges and ellipticals.

The above papers make important points that are robust. They argue convincingly that major mergers are rare – that only a small fraction of galaxies undergo several of them in their recent history (say, since $z \sim 2$). And many authors argue that most star formation does not occur during mergers; rather, it occurs in a "main sequence" of discs of various masses, with higher star formation rates at higher masses (e.g., Schiminovich et al. 2007; Noeske et al. 2007; Elbaz et al. 2007; Daddi et al. 2007; Finlator and Davé 2008; Karim et al. 2011; Peng et al. 2010; Rodighiero et al. 2011; Wuyts et al. 2011; Salmi et al. 2012; Whitaker et al. 2012; Tacconi et al. 2013; Speagle et al. 2014). These authors conclude that the duty cycle of star formation is large. Therefore most star formation does not occur in rare events. I made the same argument in Sect. 16.2: If almost all galaxies of a particular type are energetically forming stars, then star formation must be secular; it cannot be episodic with short duty cycles. Caveat: the star formation that is associated with mergers is not instantaneous. Puech et al. (2014) argue that merger-induced star formation is significant. Are these results consistent with a picture in which essentially all formation of classical bulges and ellipticals happens via major mergers?

I believe that the answer is yes, although the details need further work. Elliptical galaxies are observed to be rare; the morphology-density relation (Dressler 1980; Cappellari et al. 2011) shows that they are a small fraction of all galaxies except in rich clusters. Classical bulges are rarer than we thought, too; this is a clear conclusion of the work on disc secular evolution. *Therefore the events that make bulges must be rare.* It is also not a problem if most star formation happens in discs. For example, only a small fraction of the galaxy mass is contained in the extra light components that are identified by KFCB and by Hopkins et al. (2009a) as the parts of coreless/discy/rotating ellipticals that formed in the most recent ULIRG-like starburst (Genzel et al. 2001). Most of the mass was already in stars before these late, wet mergers. And in dry mergers, essentially all the mass was already in stars (or in X-ray gas that stays X-ray gas) and essentially no new stars are formed.

How many mergers do we need to explain elliptical galaxies? Toomre (1977) already pointed out that a reasonable increase in merger rate with increasing z would suffice. He based this on ten mergers-in-progress that he discussed in his paper. He assumed that such objects are identifiable for $\sim$ half a billion years. Then, if the number of mergers in progress increased as (lookback time)$^{5/3}$ consistent with a flat distribution of binding energies for galaxy pairs, the result is that the number of remnants is consistent with the number of elliptical and early-type disc galaxies. This estimate was made for the level of completeness of the Second Reference Catalogue of Bright Galaxies (de Vaucouleurs et al. 1976).

Conselice (2014) reviews observational estimates of how merger rates depend on z. As Toomre predicted, the major merger rate is inferred – e.g., from counting close pairs of galaxies – to increase rapidly with z. Observations of high-z galaxies show that close binary fractions increase roughly as $(1 + z)^m$ with $m \sim 2$ to 3 (e.g., Bluck et al. 2009, 2012; Conselice et al. 2009; López-Sanjuan et al. 2013; Tasca et al. 2014). ULIRGs increase in comoving energy density even faster toward higher redshift, at least out to $z = 1$ (Le Floc'h et al. 2005). The necessary connections between these results to establish or disprove whether bulges + ellipticals are made via major mergers have not been established. Important uncertainties include (1) the low-mass end of the mass functions for ellipticals and especially for classical bulges, and (2) the degree to which mass-clump sinking in discs contributes. However, the above results on merger frequencies appear at least qualitatively consistent with the conclusion that bulges and ellipticals are made in major mergers, as the pre-2000 history of observational work established (see Schweizer 1998 for a review).

A shortcoming of many current investigations is that they concentrate on a few parameter distributions for large galaxy samples and not specifically on the histories of bulges and discs. E.g., they look at the statistics of what fraction of galaxies experience mergers. Outcomes are difficult to estimate, because with samples of 10^4 to 10^5 $z \sim 0$ galaxies or 10^2 high-z galaxies, the typical galaxy is only a few pixels in radius. Then it is difficult to identify and classify galaxy components.

16.4.1.6 Uncertainties with Our Picture of Bulge Formation in Major Mergers

Two major uncertainties are a concern (see also Brooks and Christensen 2015). Virtually all observational evidence on mergers-in-progress (e.g., Toomre 1977; Joseph and Wright 1985; Sanders et al. 1988a,b; Hibbard et al. 1994, 2001a, b; Hibbard and Mihos 1995; Hibbard and van Gorkom 1996; see Schweizer 1987, 1990, 1998 for reviews) involves giant galaxies. And the detailed evidence is for $z \sim 0$ galaxies with gas fractions of a few to $\sim$10 %. (1) We do not have comparable evidence for dwarfs. That is, we have not studied a sample of dwarfs that fill out a merger sequence from close pairs to mergers engaged in violent relaxation to train wrecks that are still settling down to mature objects. And (2) we do not have comparably detailed studies of galaxies at high z that have gas fractions $\gtrsim$ 50 %. It is possible that mergers behave differently for such objects.

16.4.1.7 The Problem of Giant, Pure-Disc Galaxies: Conclusion

My most important suggestion in this section is that the modeling community relies too strongly on feedback as the only way to prune excessive bulge formation. On the contrary, I suggest that environmental differences in the amount of dynamical violence in galaxy formation histories are the central factor. I suggest that the solution is not to whittle away the low-angular-momentum tail of the distribution

of angular momenta in forming galaxies. Nearby galaxies dramatically show us the importance of violent relaxation. To me, the issue is: How much does violent relaxation dominate? How much is the evolution controlled by gentle accretion? And how do the answers depend on environment?

16.5 Universal Scaling Relations for All Galaxies?

How we best construct parameter correlations depends on what we want to learn. Projections of the fundamental plane correlations *separate* galaxy classes; e.g., bulges+ellipticals from discs+Sphs (Fig. 16.4). So they teach us about differences in formation processes. In contrast, it is possible to construct parameter correlations that make most or all galaxy types look continuous. *These encode less information about galaxy formation*. E.g., in a projection of the structural parameter correlations that encodes mass-to-light ratio, the difference between ellipticals, spheroidals, and even irregulars largely disappears (Bender et al. 1992). Zaritsky (2015) regards this as progress – as replacing correlations that are flawed with ones that capture some inherent simplicity. That simplicity is real. But it is insensitive to the power that other correlations clearly have to tell us things about galaxy formation.

I therefore disagree, not with Zaritsky's operational results but with his motives. If you look at the fundamental plane face-on, it contains lots of information. If you look at it edge-on, then it looks simple. This may feel like a discovery. But it just means that you are looking at a projection that hides the information content in the parameter plane. Other combinations of parameters make still more types of objects looks continuous and indistinguishable. But this means that we learn still less, not more, about their nature and origin. The simple correlations are not uninteresting, but the ones that teach us the most are the ones that correctly identify differences that turn out to have causes within formation physics.

16.6 Coevolution (Or Not) of Supermassive Black Holes and Host Galaxies

The observed demographics of supermassive black holes (BHs) and their implications for the coevolution (or not) of BHs and host galaxies are discussed in Kormendy and Ho (2013). This is a 143-page ARA&A review that revisits methods used to measure BH masses $M_\bullet$ using spatially resolved stellar and gas dynamics. It also provides a detailed analysis of host galaxy morphologies and properties. Careful treatment of the $M_\bullet$ and galaxy measurements allows Kormendy and Ho to reach a number of new science conclusions. They are summarized in this section.

Graham (2015) reviews the same subject in the present book. Some of his review is historical, especially up to the beginning of his Sect. 11.4.1 but also sporadically

thereafter. I do not comment here on the historical review. However, on the science, I cannot "duck" my responsibility as author of this concluding chapter:

I disagree with most of the scientific conclusions in Graham (2015). Starting in his Sect. 11.4.1, his discussion uses data and repeats conclusions from Graham and Scott (2013, 2015). Problems with the 2013 data are listed in KH13 (p. 555); a point made there that is not repeated further here is that many of Graham's galaxy classifications are incorrect. Here, rather than write a point-by-point rebuttal to Graham (2015), I first concentrate on a summary of the unique strengths of the KH13 analysis and data. However, a few comments are added to further explain the origin of the disagreements with Graham (2015). I then summarize the KH13 results and conclusions about $M_\bullet$ – host-galaxy correlations (Sects. 16.6.1 and 16.6.2).

Before I begin, a comment is in order on how readers react to disagreements in the literature. The most common reaction is that the subject needs more work. Specialists may know enough to decide who is correct. But the clientele community of non-specialists who mainly want to use the results often do not delve into the details deeply enough to decide who is correct. Rather, their reaction is that this subject needs further work until everybody agrees that the disagreement is resolved. Sometimes, this is an appropriate reaction, when the issues are more complicated than our understanding of the physics, or when measurements are still too difficult, or when results under debate have low significance compared to statistical errors or systematic effects. My reading of the community is that reactions to disagreements on BH demographics take this form.

However, I suggest that we already know enough to decide who is correct in the disagreement between KH13 and Graham (2015). Our ARA&A review and the Graham and Scott papers both provide enough detail to judge the data and the analysis. It is particularly important to note how these separate discussions do or do not connect up with a wide body of results in other published work, including other chapters in this book. A strength of the Kormendy and Ho analysis is that it connects up with – i. e., it uses and it has implications for – a wide variety of aspects of galaxy formation.

Strengths of the data and supporting science that are used by KH13 include the following. Some of these points are discussed more fully in the Supplemental Material of KH13.

(1) BH masses based on absorption-line spectroscopy are now derived by including halo dark matter in the stellar dynamical models. This generally leads to an upward revision in $M_\bullet$ by a factor that can be $\gtrsim 2$ for core galaxies. Kormendy and Ho use these masses. For some galaxies (e. g., M 87), Graham uses them; for other galaxies (e. g., NGC 821, NGC 3377, NGC 3608, NGC 4291, and

NGC 5845), he does not, even though such masses are published (Schulze and Gebhardt 2011).

(2) Kormendy and Ho include new $M_\bullet$ determinations for mostly high-mass galaxies from Rusli et al. (2013). Graham and Scott (2013) did not include these galaxies. It is not clear whether they are included in Graham (2015), but observation that the highest $M_\bullet$ values plotted in his Fig. 11.4 are $\sim 6\times10^9\,M_\odot$ and not $> 10^{10}\,M_\odot$ suggests that they are not included, at least in this figure.

(3) BH masses derived from emission-line gas rotation curves are used without correction when the emission lines are narrow. However, when the emission lines are wide – often as wide in $\mathrm{km\,s^{-1}}$ as the rotation curve amplitude – some authors have ignored the line widths in the $M_\bullet$ determinations. KH13 argue that these BH masses are underestimated and do not use them. Graham (2015) uses them.

(4) All disc-galaxy hosts have B/T values based on at least one and sometimes as many as six bulge-disc decompositions. Graham and Scott (2013) use a mean statistical correction to derive some bulge magnitudes from total magnitudes.

(5a) All disc-galaxy hosts have (pseudo)bulge classifications that are based on at least two and as many as five criteria such as those listed here in Sect. 16.2.1. Graham (2015) rejects this approach and instead compares BH–host correlations for barred and unbarred galaxies. However, Kormendy and Ho emphasize that some barred galaxies contain classical bulges, whereas many unbarred galaxies contain pseudobulges. If classical and pseudo bulges correlate differently with their BHs (Fig. 16.7), then a division into barred and unbarred galaxies does not cleanly see this. It should be noted that other derivations of BH–host correlations (e. g., the otherwise very good paper by McConnell and Ma 2013), also do not differentiate between classical and pseudo bulges. They compare early and late galaxy types. But many S0s contain pseudobulges, and a few Sbcs contain classical bulges (e.g., NGC 4258: Kormendy et al. 2010).

(5b) The picture of disc secular evolution and the conclusion that pseudobulges are distinguishable from classical bulges is fully integrated into the analysis. Graham (2011, 2015) does not use this picture and argues that classical and pseudo bulges cannot reliably be distinguished. Kormendy and Kennicutt (2004), Kormendy (2012), Kormendy and Ho (2013), Fisher and Drory (2015) in this book, and Sect. 16.2 in this summary chapter disagree. The subject is growing rapidly, and whole meetings are devoted to it (e.g., 2012 IAU General Assembly Special Session 3, "Galaxy Evolution Through Secular Processes," http://bama.ua.edu/~rbuta/iau-2012-sps3/proceedings.html and Kormendy 2015; XXIII Canary Islands Winter School, "Secular Evolution of Galaxies", Falcón-Barroso and Knapen 2012). Kormendy and Ho make a point of distinguishing classical and pseudo bulges by purely morphological criteria such as those given in Sect. 16.2.1. The fact that we then discover that BHs correlate differently with classical and pseudo bulges is a substantial success of the secular evolution picture.

(6) KH13 find that the $\log M_\bullet - M_{K,\mathrm{bulge}}$, $\log M_\bullet - \log\sigma$ and $\log M_\bullet - \log M_{\mathrm{bulge}}$ correlations for classical bulges and ellipticals have intrinsic scatter of 0.30,

0.29, and 0.28 dex, respectively. This small scatter is a consequence of the care taken in (1)–(5), above, in implementing a uniform, accurate distance scale based as much as possible on standard candles, in correcting galaxy classifications when detailed photometry reveals errors, and in correcting K-band magnitudes for systematic errors. Given this small scatter, it was possible to discover a new result; i. e., that five sample galaxies that are major mergers in progress deviate from the above correlations in having undermassive BHs for their host size (see Figure 14 in KH13). Having noted this result, the five mergers are omitted from our correlation fits shown below. However, mergers in progress are included in Graham (2015) and in McConnell and Ma (2013).

These procedural differences plus others summarized in KH13 and omitted here for the sake of brevity account for most of the differences in the correlation plots shown in Graham (2015) and those in KH13. Generically, they have the following effects (ones in italics also apply to McConnell and Ma 2013). (1) *At the high-$M_\bullet$ end, Graham's BH masses are biased low, because he uses underestimated values from emission-line rotation curves,* because he uses $M_\bullet$ values that are not corrected for effects of halo dark matter, and because he does not consistently use the Rusli et al. (2013) high-$M_\bullet$ galaxies. (2) At the low-$M_\bullet$ end, Graham's BH masses are biased low, because he includes pseudobulges. Differentiating barred and unbarred galaxies is not sufficient to solve this problem. *McConnell and Ma also include pseudobulges, differentiating early- and late-type galaxies helps, although many S0s contain pseudobulges.* (3) Graham regards M 32 as pathological and omits it. KFCB show that it is a normal, tiny elliptical. Including it in KH13 helps to anchor the BH correlations at low BH masses. (4) *The result is that the BH–host correlations have much larger scatter in Graham (2015) and in McConnell and Ma (2013) than they do in KH13 (see Figs. 16.5 and 16.7 below).* Also, Graham sees a kink in the $\log M_\bullet - M_{K,\mathrm{bulge}}$ correlation whereas we do not, and he sees no kink in the $\log M_\bullet - \log\sigma$ correlation whereas we see signs of a kink at high σ where $M_\bullet$ becomes largely independent of σ. McConnell and Ma (2013) and KH13 agree on the kinks (and lack of kinks) in the $M_\bullet$ – host-galaxy correlations.

16.6.1 Correlations Between BH Mass and Host Galaxy Properties from Kormendy and Ho (2013)

This section summarizes the BH – host-galaxy correlations from KH13.

The procedures summarized above lead in KH13 to Table 2 for 44 elliptical galaxies and Table 3 for 20 classical bulges and 21 pseudobulges. Figure 16.5 shows the resulting $\log M_\bullet - M_{K,\mathrm{bulge}}$ and $\log M_\bullet - \log\sigma$ correlations for classical bulges and ellipticals. Mergers in progress are omitted as explained above, and three "monster" BHs that deviate above the correlations are illustrated in faint symbols but are omitted from the fits. Also shown are symmetric, least-squares fits (Tremaine et al. 2002) symmetrized around $L_{K,\mathrm{bulge}} = 10^{11}\,L_{K\odot}$ and $\sigma_e = 200\,\mathrm{km\,s^{-1}}$:

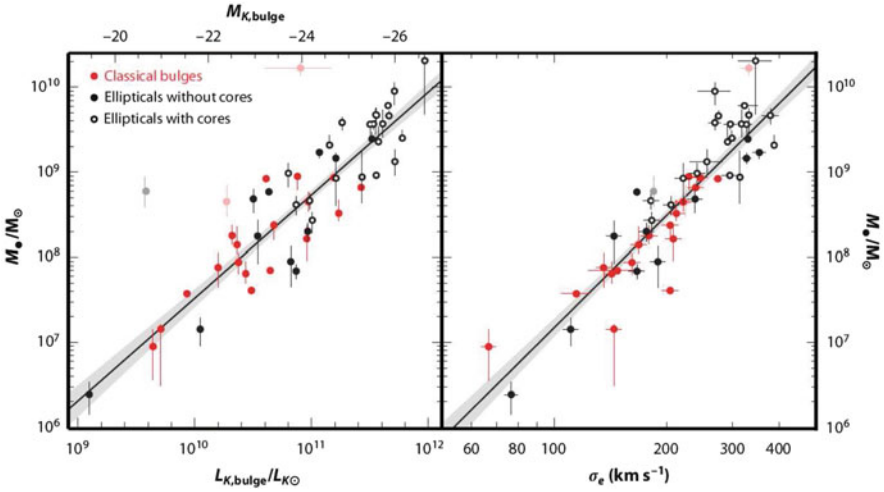

Fig. 16.5 Correlations of BH mass $M_\bullet$ with the K-band absolute magnitude and luminosity of the host bulge (*left panel*) and with its velocity dispersion at radii where σ_e is unaffected by the BH (*right panel*). *Black points* are for ellipticals; a *white center* indicates that this galaxy has a core. *Red points* are for classical bulges. The lines are Eqs. (16.1) and (16.2). Note: the $M_\bullet$–$M_{K,\mathrm{bulge}}$ correlation remains log-linear with no kink at high luminosities. In contrast, the biggest BH masses look essentially independent of σ_e in ellipticals that have cores (From KH13)

$$\log\left(\frac{M_\bullet}{10^9\,M_\odot}\right) = -(0.265 \pm 0.050) - (0.488 \pm 0.033)(M_{K,\mathrm{bulge}} + 24.21); \quad (16.1)$$

$$\log\left(\frac{M_\bullet}{10^9\,M_\odot}\right) = -(0.509 \pm 0.049) + (4.384 \pm 0.287)\log\left(\frac{\sigma}{200\ \mathrm{km\ s^{-1}}}\right). \quad (16.2)$$

Here, we adopt equal errors of $\Delta M_{K,\mathrm{bulge}} = 0.2$ and $\Delta \log M_\bullet = 0.117$, i. e., the mean for all fitted galaxies. Then the intrinsic scatters in Eqs. (16.1) and (16.2) are 0.30 and 0.29 dex, respectively. In physically more transparent terms,

$$\frac{M_\bullet}{10^9\ M_\odot} = \left(0.544^{+0.067}_{-0.059}\right)\left(\frac{L_{K,\mathrm{bulge}}}{10^{11}\ L_{K\odot}}\right)^{1.22\pm0.08}; \quad (16.3)$$

$$\frac{M_\bullet}{10^9\ M_\odot} = \left(0.310^{+0.037}_{-0.033}\right)\left(\frac{\sigma}{200\ \mathrm{km\ s^{-1}}}\right)^{4.38\pm0.29}. \quad (16.4)$$

Both relations have shifted to higher BH masses because of corrections to $M_\bullet$, because mergers in progress are omitted, and because pseudobulges are postponed.

The $\log M_\bullet - L_{K,\mathrm{bulge}}$ correlation in Fig. 16.5 is converted to a correlation with bulge stellar mass M_{bulge} by applying mass-to-light ratios that were engineered by KH13 to be independent of the papers that determine $M_\bullet$, to have zeropoints based on the Williams et al. (2009) dynamical models, but also to take variations in stellar

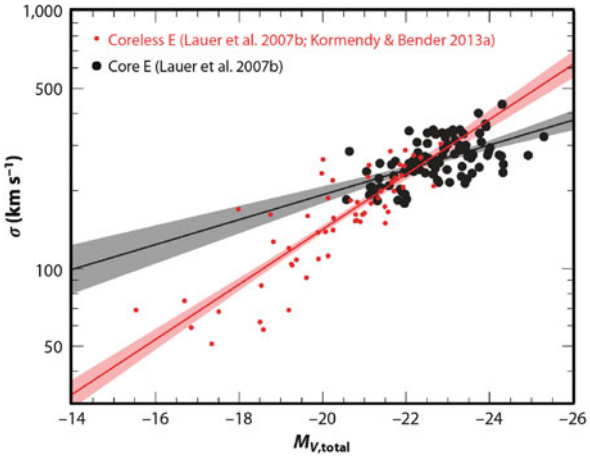

Fig. 16.6 Faber-Jackson (1976) correlations for core ellipticals (*black*) and coreless ellipticals (*red*). Total V-band absolute magnitudes $M_{V,\rm total}$, velocity dispersions σ, and profile types are mostly from Lauer et al. (2007b) or otherwise from KFCB. The lines are symmetric least-squares fits to core Es (*black line*) and coreless Es (*red line*) with 1-σ uncertainties shaded. The coreless galaxies show the familiar relation, $\sigma \propto L_V^{0.27\pm0.02}$. But velocity dispersions in core ellipticals increase only very slowly with luminosity, $\sigma \propto L_V^{0.12\pm0.02}$. As a result, $M_\bullet$ becomes almost independent of σ for the highest-σ galaxies in Fig. 16.5. This figure from KH13 is based on Kormendy and Bender (2013). Lauer et al. (2007a) and Cappellari et al. (2013a,b) show closely similar diagrams

population age into account. The resulting mass correlation is:

$$100\left(\frac{M_\bullet}{M_{\rm bulge}}\right) = \left(0.49^{+0.06}_{-0.05}\right)\left(\frac{M_{\rm bulge}}{10^{11}\,M_\odot}\right)^{0.15\pm0.07}, \qquad (16.5)$$

with an intrinsic scatter of 0.28 dex. The BH mass fraction, $M_\bullet/M_{\rm bulge} = 0.49^{+0.06}_{-0.05}\,\%$ at $M_{\rm bulge} = 10^{11}\,M_\odot$, is approximately a factor of 4 larger than we thought before the $M_\bullet$ values were corrected (Merritt and Ferrarese 2001; Kormendy and Gebhardt 2001; McLure and Dunlop 2002; Marconi and Hunt 2003; Sani et al. 2011).

Note again that $M_\bullet$–$L_{\rm bulge}$ is a single power law with no kink, whereas $M_\bullet$–σ is a power law that "saturates" at high $M_\bullet$ (see also McConnell and Ma 2013). That is, $M_\bullet$ becomes nearly independent of σ in the highest-σ galaxies that also have cores (Fig. 16.5). We understand why: The Faber-Jackson L–σ correlation saturates at high L, because σ does not grow very much once galaxies are massive enough so that all mergers are dry (Fig. 16.6). This is seen in simulations of dry, major mergers (e.g.) by Boylan-Kolchin et al. (2006) and by Hilz et al. (2012). Section 16.4.1.1 reviewed arguments why core ellipticals are remnants of dry mergers.

The pseudobulges that were postponed from Fig. 16.5 are added to the BH–host correlations in Fig. 16.7. Hu (2008) was the first person to show that pseudobulges deviate from the $M_\bullet - \sigma_e$ correlation in having small BH masses. This was confirmed with larger samples and extended to the $M_\bullet - M_{K,\rm bulge}$ and $M_\bullet - M_{\rm bulge}$ correlations

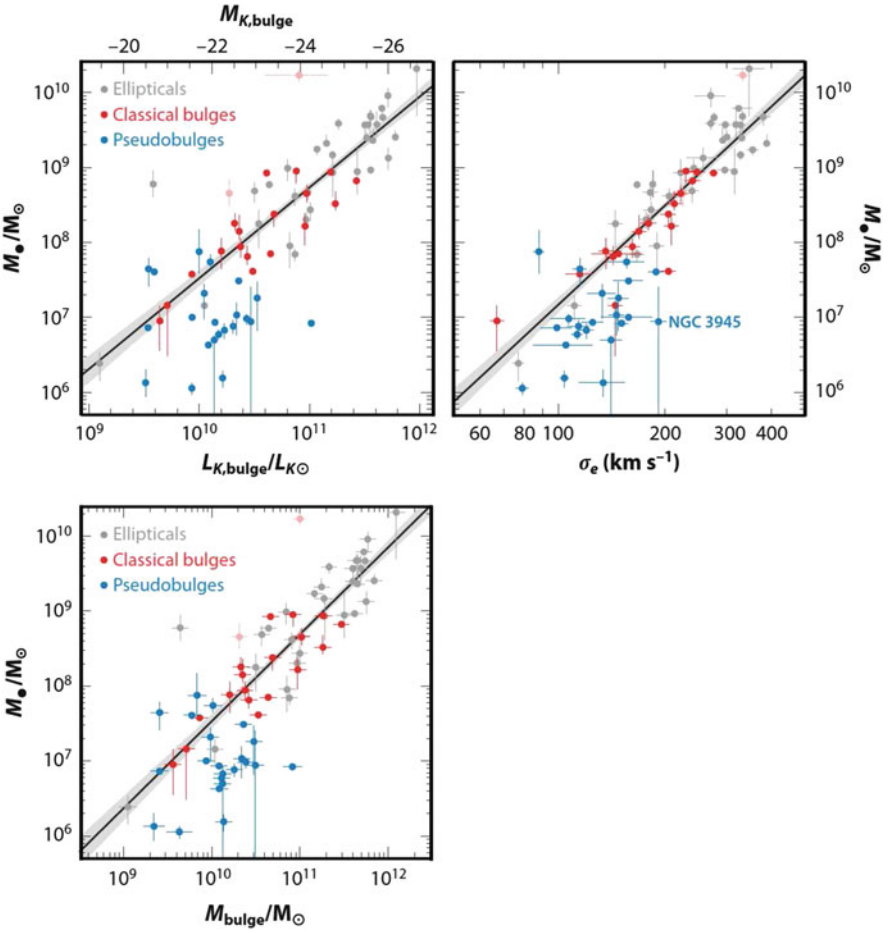

Fig. 16.7 Correlations of BH mass with the *K*-band absolute magnitude and luminosity of the host bulge (*top-left panel*), with its stellar mass (*bottom panel*), and with the mean velocity dispersion of the host bulge at radii that are large enough so that σ_e is unaffected by the BH (*right panel*). *Gray points* are for ellipticals, *red points* are for classical bulges, and *blue points* are for pseudobulges. The lines with shaded 1-σ uncertainties are symmetric least-squares fits to the classical bulges and ellipticals. In all panels, pseudobulge BHs are offset toward smaller $M_\bullet$ from the correlations for classical bulges and ellipticals. Absent any guidance from the *red* and *gray points*, we conclude the pseudobulge BHs do not correlate with their hosts in any way that is strong enough to imply BH-host coevolution (From KH13, who tabulate the data and give sources)

by Greene et al. (2010) and by Kormendy et al. (2011). Figure 16.7 now shows this result for the largest available sample, that of KH13.

Hints of this result are seen in McConnell and Ma (2013); they compare early- and late-type galaxies and note that many late-type galaxies have undermassive BHs. This captures some of the result in Fig. 16.7 but not all of it, because many

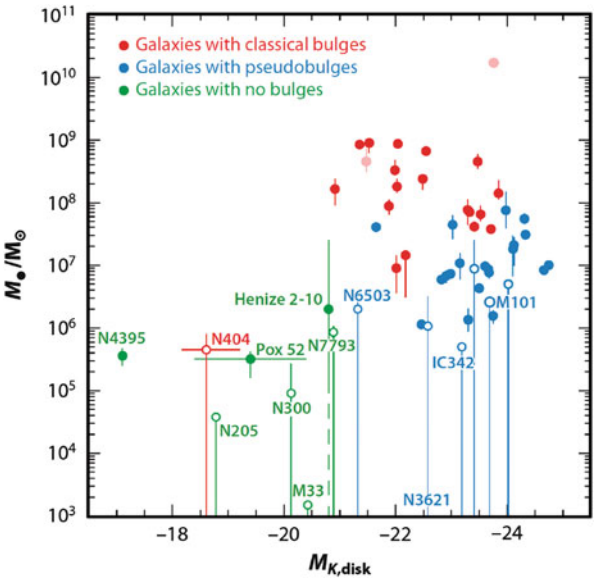

Fig. 16.8 Black hole mass $M_\bullet$ vs K-band absolute magnitude of the disc of the host galaxy. *Filled circles* are for galaxies with BH detections based on spatially resolved stellar or gas dynamics; *open circles* are for galaxies with upper limits on $M_\bullet$. The strongest upper limit is $M_\bullet \lesssim 1500\, M_\odot$ in M 33 (Gebhardt et al. 2001). *Red* and *blue circles* are for galaxies with classical and pseudo bulges, respectively. *Green points* are for galaxies with no classical bulge and (almost) no pseudobulge but only a nuclear star cluster (From KH13, who tabulate the data and give sources)

S0 galaxies contain pseudobulges. Similarly, Graham (2015) compares barred and unbarred galaxies and concludes that many barred galaxies have undermassive BHs. Again, this result is related to Fig. 16.7 – many (but not all) barred galaxies contain pseudobulges, and many (but not all) unbarred galaxies contain classical bulges.

In Fig. 16.7, the highest-$M_\bullet$ pseudobulge BHs largely agree with the correlations for classical bulges and ellipticals; the lowest-$M_\bullet$ BHs deviate, but not by much more than an order of magnitude. Note that the BHs that we find in pseudobulges may be only the high-$M_\bullet$ envelope of a distribution that extends to much lower BH masses. Still, why are pseudobulge BHs even close to the correlations? KH13 argue that this natural: even one major merger converts a pseudobulge to a classical bulge, and then merger averaging manufactures an essentially linear correlation with a zeropoint near the upper end of the mass distribution of progenitors (see Figure 37 in KH13 and Peng 2007; Gaskell 2010, 2011; Hirschmann et al. 2010; Jahnke and Macciò 2011, who developed this idea).

Turning next to discs: Fig. 16.8 confirms the conclusion reached in Kormendy and Gebhardt (2001) and in Kormendy et al. (2011) that BH masses are completely uncorrelated with properties of their host discs.

M 33, with its strong upper limit on $M_\bullet$, briefly gave us the feeling that pure discs might not contain BHs. But it was clear all along that they can have AGNs. Figure 16.8 includes bulgeless galaxies in which we find $10^{6\pm1}$-$M_\odot$ BHs. The prototypical example is NGC 4395, a dwarf Sd galaxy with $M_V = -18.2$, with no classical or pseudo bulge, but with only a nuclear star cluster that has an absolute magnitude of $M_B \simeq -11.0$ and a velocity dispersion of $\sigma \lesssim 30 \pm 5\,\mathrm{km\,s^{-1}}$ (Filippenko and Ho 2003; Ho et al. 2009). And yet, NGC 4395 is the nearest Seyfert 1 galaxy known (Filippenko and Ho 2003). It shows the signatures of BH accretion

– broad optical and UV emission lines (Filippenko et al. 1993), variable X-ray emission (Shih et al. 2003), and a compact, flat-spectrum radio core (Wrobel and Ho 2006). Peterson et al. (2005) get $M_\bullet = (3.6 \pm 1.1) \times 10^5\, M_\odot$ by reverberation mapping. This is the smallest BH mass measured by reverberation mapping. But the BH in NGC 4395 is much more massive than $M_\bullet \lesssim 1500\, M_\odot$ in the brighter pure-disc galaxy M 33 ($M_V = -19.0$).

This is the best example of many that are revealed in the observing programs of Ho, Barth, Greene, and collaborators and reviewed by Ho (2008) and by KH13. Other important galaxies include Pox 52 (Barth et al. 2004; Thornton et al. 2008) and Henize 2–10 (Reines et al. 2011). Broader AGN surveys to find low-mass BHs, many of them in late-type, pure-disc galaxies, include Greene and Ho (2004, 2007), Barth et al. (2008), and Dong et al. (2012). The general conclusion is that classical and even pseudo bulges are not necessary equipment for the formation and nurture of supermassive BHs.

We need one more result before we discuss implications for galaxy evolution:

Very popular for more than a decade has been the suggestion that the fundamental correlation between BHs and their host galaxies is not one with bulge properties but rather is a correlation with halo DM. This was suggested by Ferrarese (2002) and supported by papers such as Baes et al. (2003). The idea is attractive for galaxy formation theory, because then halo mass is the natural parameter to control AGN feedback (e.g., Booth and Schaye 2010). The most robust part of our effort to model galaxy formation is the calculation of DM hiararchical clustering. Conveniently, DM mass is then provided by halo-finder algorithms.

However, we can now be confident that *halo DM does not correlate directly with $M_\bullet$ independent of whether or not the galaxy contains a bulge* (Kormendy and Bender 2011). This result is reviewed in detail and with the largest galaxy sample in KH13. They list eight arguments against Ferrarese's conclusion. Some are based on examining the proxy parameters that she used to make her arguments (σ for $M_\bullet$ and $V_{\rm circ}$ for the DM; e. g. we now know that σ is not a proxy for BH mass for pseudobulge galaxies: Fig. 16.7 here). Some arguments are based on the direct correlation of measured $M_\bullet$ with $V_{\rm circ}$: there is essentially no correlation unless the galaxy has a classical bulge. Perhaps the most telling argument is based on the well determined relationship between the stellar mass M_* and the DM mass $M_{\rm DM}$ of galaxies. Behroozi et al. (2013) show that $M_*/M_{\rm DM}$ reaches a maximum at $M_{\rm DM} \simeq 10^{12}\, M_\odot$ and is smaller at both higher and lower $M_{\rm DM}$ (see also Fig. 16.9 here). Together with the correlation (Eq. 16.5) between $M_\bullet$ and $M_{\rm bulge} \simeq M_*$ (exact for ellipticals and approximate for bulge-dominated galaxies), Behroozi's result implies that the relationship between $M_\bullet$ and $M_{\rm DM}$ is complicated,

$$M_\bullet \propto M_{\rm DM}^{2.7} \quad \text{at} \quad M_{\rm DM} \ll 10^{12}\, M_\odot \ , \tag{16.6}$$

but

$$M_\bullet \propto M_{\rm DM}^{0.34} \quad \text{at} \quad M_{\rm DM} \gg 10^{12}\, M_\odot \ , \tag{16.7}$$

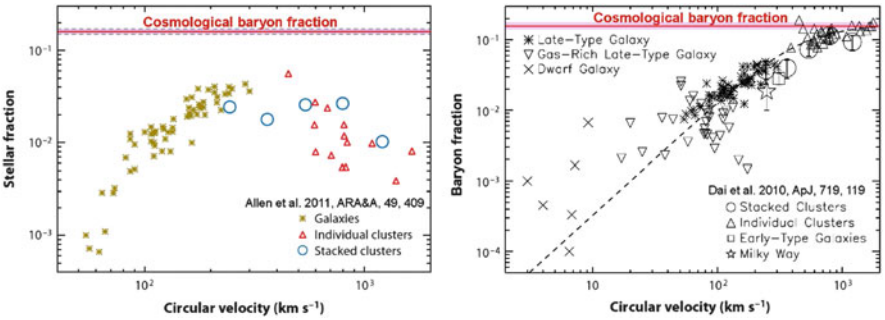

Fig. 16.9 Stellar mass fraction $M_*/(M_{\rm baryon} + M_{\rm DM})$ (*left*) and total baryon mass fraction $M_{\rm baryon}/(M_{\rm baryon} + M_{\rm DM})$ (*right*) versus a circular-orbit rotation velocity $V_{\rm circ} \sim \sqrt{GM_{\rm DM}/r}$ (Dai et al. 2010) that approximately characterizes the total mass distribution. Here M_* is the stellar mass, $M_{\rm DM}$ is the DM halo mass, r is the radius of the halo, and G is the gravitational constant. The cosmological baryon fraction has been adjusted very slightly to 0.16 ± 0.01, i. e., the mean of the WMAP and Planck measurements (Hinshaw et al. 2013 and Planck Collaboration 2014, respectively) (Both figures originally come from Dai et al. 2010)

with a kink in the correlation at $M_{\rm DM} \simeq 10^{12}\,M_\odot$. Meanwhile, the $M_\bullet - M_{\rm bulge}$ correlation is log linear with small scatter from the lowest to the highest bulge masses in Fig. 16.5. This correlation shows no kink at $M_{\rm DM} \sim 10^{12}\,M_\odot$ corresponding to $M_{\rm bulge} \sim 3 \times 10^{10}\,M_\odot$ (see Fig. 16.7). The simplicity of $M_\bullet - M_{\rm bulge}$ versus the complexity of $M_\bullet - M_{\rm DM}$ is another argument in favor of the conclusion that BHs coevolve with bulges and ellipticals but not directly with DM halos.

16.6.2 AGN Feedback and the Coevolution (Or Not) of Supermassive Black Holes and Host Galaxies

Implications for the coevolution (or not) of BHs and host galaxies are reviewed by Kormendy and Ho (2013). They distinguish four modes of AGN feedback:

(1) Galaxies that are not dominated by classical bulges – even ones like NGC 4736 that contain big pseudobulges – can contain BHs, but these grow by low-level AGN activity that involves too little energy to affect the host galaxy. Whether or not AGNs are turned on when we observe them, these galaxies actively form stars and engage in secular evolution by the redistribution of gas. Most AGNs at $z \sim 0$ and probably out to $z \sim 2$ are of this kind. They include giant galaxies such as our Milky Way, with outer circular-orbit rotation velocities $V_{\rm circ} > 220\,{\rm km\,s^{-1}}$. These galaxies are not correctly described by simple prescriptions in which gravitational potential well depth controls AGN feedback.

(2) Most consistent with the prevailing emphasis on AGN feedback are classical bulges and coreless-discy-rotating ellipticals. They satisfy the tight correlations between $M_\bullet$ and bulge properties in Fig. 16.5. It is likely (although the engineering is not fully understood) that AGN feedback helps to establish these $M_\bullet$–host relations during dissipative ("wet") major mergers. This must happen mostly at high z, because gas fractions in major mergers at $z \sim 0$ are small, and indeed, mergers in progress at $z \simeq 0$ do not satisfy the $M_\bullet$ correlations. It is important to note that even small Es with $V_{\rm circ} \lesssim 100\,{\rm km\ s^{-1}}$ (e. g., M 32) satisfy the $M_\bullet$–host correlations, whereas even giant pure discs (e. g., M 101) do not. Coevolution is not about potential well depth. Coevolution (or not) is determined by whether (or not) the galaxy contains a classical bulge or elliptical – i. e., the remnant of at least one major merger.

(3) The highest-mass ellipticals are coreless-boxy-nonrotating galaxies whose most recent mergers were dissipationless ("dry"). These giant ellipticals inherit any feedback magic – including the $M_\bullet$–host relations – from (2). In them, AGN feedback plays a different, essentially negative role. It keeps galaxy formation from "going to completion" by keeping baryons suspended in hot gas. With masses $M > M_{\rm crit}$ in Sect. 16.7, these galaxies hold onto hot, X-ray-emitting gas that is believed to prevent cold-gas dissipation and to quench star formation. However, X-ray gas cooling times are short, and so – given that we observe only weak temperature gradients – something must keep the hot gas hot. One such process is gas infall from the cosmological web (Dekel and Birnboim 2006). Another is "maintenance-mode AGN feedback" (see Fabian 2012 for a review). All proposed heating processes may be important. See Sect. 16.7.

(4) The averaging that is inherent in galaxy mergers may significantly decrease the scatter in the $M_\bullet$–host correlations. That is, during a merger, the progenitors' stellar masses add and so do their BH masses. In the absence of new star formation, the effect is to decrease the correlation scatter. Recall a conclusion in Sect. 16.4 that only a modest amount of star formation happens during mergers. So the central limit theorem ensures that the scatter in BH correlations with their hosts decreases as $M_\bullet$ increases via either wet or dry mergers.

In summary, KH13 provides the largest available database on BH detections via spatially resolved dynamics, putting the many heterogeneous discovery papers on a homogeneous system of (for example) distances and magnitudes, and incorporating many $M_\bullet$ corrections from the recent literature. Homogeneous data are also provided for all BH host galaxies, including all disc-galaxy hosts, many of which had not previously been studied. Bulge-pseudobulge classifications are provided based on multiple classification criteria (cf. Sect. 16.2.1 here), and (pseudo)bulge-disc photometric decompositions are derived for all galaxies that did not previously have photometry. The results (their Tables 2 and 3) are an accurate enough database to allow Kormendy and Ho (2013) to derive a number of new conclusions about BH-host correlations and their implications. Some of these are reviewed above. Others, such as correlations (or not) with nuclear star clusters and globular cluster systems, are omitted here, in part to keep the length of this paper manageable, and in part

because the connection with galaxy bulges is less direct than it is for subjects that we cover.

Many of our conclusions disagree with Graham (2015). Within the subjects that I have reviewed in this paper, I have tried to explain why. Readers are encouraged to compare the accuracy of our data sets (particularly $M_\bullet$ measurements), our results, and the physical picture in which they are embedded. We believe that the observational conclusions reached in KH13 are robust, and the essential implications for galaxy evolution – the big picture of what happens, if not the engineering details – are well established. Section 16.7 is an important example.

16.7 Quenching of Star Formation

Many papers on star formation histories begin by setting up a "straw-man target" that the quenching of star formation is mysterious. In contrast, it strikes me that the literature shows encouraging convergence on a picture at least at $z < 1$ in which well defined processes convert "blue cloud" star-forming galaxies to "red sequence" red and dead galaxies. This section rephrases Sect. 16.6.2 to describe this picture.

The essential observation that has driven progress on this subject is summarized in Fig. 16.9. The left panel shows the Allen et al. (2011) version of the Behroozi et al. (2013) result that led to Eqs. (16.6) and (16.7) in Sect. 16.6.1. I use it because the abscissa is in the same units as in the right panel. It shows that the ratio of stellar mass to total mass reaches a maximum at $V_{\rm circ} \sim 300\,{\rm km\,s^{-1}}$ or, in Behroozi et al. (2013), at $M_{\rm DM} \sim 10^{12}\,M_\odot$. This maximum is ∼1/5 of the cosmological baryon fraction, so most baryons in the universe have not yet made stars. Lower-mass halos have smaller stellar fractions (*left panel*) and smaller baryon fractions (*right panel*) because – we believe – the baryons have increasingly been ejected from DM halos by star-formation and supernova feedback or never accreted after cosmological reionization. But the focus here is on higher DM masses. They, too, have smaller stellar mass fractions than at the "sweet spot" halo mass of $10^{12}\,M_\odot$. But Fig. 16.9 (*right*) shows that these baryons are not "missing" at $M_{\rm DM} \gg 10^{12}\,M_\odot$. On the contrary, the total baryon fraction converges to essentially the cosmological value in the highest-mass halos, which are halos of rich clusters of galaxies. This is the by-now well known result that, as $M_{\rm DM}$ grows above $10^{12}\,M_\odot$ and $V_{\rm circ}$ grows above $300\,{\rm km\ s^{-1}}$, an increasingly large fraction of the baryons are indeed present but have not made stars. Rather, they are suspended in hot, X-ray-emitting gas, until in rich clusters of galaxies, that hot gas outmasses the stellar galaxies in the cluster by 1.0 ± 0.3 dex (Kravtsov and Borgani 2012). This has led to the essential idea of "$M_{\rm crit}$ quenching" of star formation by X-ray-emitting gas, which can happen provided that the DM mass is larger than the critical mass, $M_{\rm DM} \gtrsim M_{\rm crit} \simeq 10^{12}\,M_\odot$, that is required to support the formation and retention of hot gas halos (e. g., Birnboim and Dekel 2003; Kereš et al. 2005; Cattaneo et al. 2006, 2008, 2009; Dekel and Birnboim 2006, 2008; Faber et al. 2007; KFCB; Peng et al. 2010, 2012; KH13; Knobel et al. 2015; and Gabor and Davé 2015).

The transition mass between galaxies that should contain X-ray gas and those that should not is consistently derived by a variety of theoretical arguments and is consistent checked via a variety of observational tests. It should occur at the DM mass at which the hot gas cooling time is comparable to the infall time (Rees and Ostriker 1977). Birnboim and Dekel (2003) and Dekel and Birnboim (2006, 2008) argue from theory and Kereš et al. (2005) find from SPH simulations that gas that is accreted during hierarchical clustering falls gently into shallow potential wells and makes star-forming discs, whereas gas crashes violently onto giant galaxies and is shock-heated to the virial temperature. It is this hot gas that quenches star formation. Calculated hot-gas cooling times are short; this led to the well known "cooling flow problem" (Fabian 1994). But X-ray measurements of temperature profiles now show that they are much shallower than cooling-time calculations predict in the absence of heating (McNamara and Nulsen 2007; Kravtsov and Borgani 2012; Fabian 2012). Debate continues about how the gas is kept hot; Dekel and Birnboim (2006, 2008) suggest that the required heating is caused by continued accretion; AGN feedback is another candidate (e.g., Best et al. 2006; Best 2006, 2007a,b; Fabian 2012; Heckman and Best 2014), and dying stars return gas to the intergalactic medium at just the right kinetic temperature (Ostriker 2006). The engineering details need to be sorted out. It is likely that all processes are important. But from the point of view of this paper, the engineering is secondary. The important point is that the galaxies and clusters tell us that they know how to keep the gas hot.

Many observed properties of galaxies can be understood in the context of $M_{\rm crit}$ quenching. E. g., it allows semianalytic models of galaxy formation to reproduce the color bimodality of galaxies ("red sequence" versus "blue cloud"; Blanton and Moustakas 2009) as a function of redshift (Cattaneo et al. 2006, 2008, 2009).

Faber et al. (2007) and KFCB emphasize the connection of the above results to this paper: *$M_{\rm crit}$ star-formation quenching is believed to explain the difference between the two kinds of ellipticals discussed in Sect. 16.4.1.1*. I noted there that classical bulges and coreless-discy-rotating ellipticals generally do not contain X-ray-emitting gas, whereas core-boxy-nonrotating ellipticals contain more X-ray gas as their luminosities increase more above $L_{\rm crit} = 10^{10.2}\ L_{B\odot}$ (Fig. 16.3). Now, $L_{\rm crit}$ corresponds to $M_V \simeq -20.9$; i. e., 0.6 mag fainter than the divide between coreless-discy-rotating and core-boxy-nonrotating ellipticals. This is a factor of almost 2. If the most recent event that made an elliptical was an equal-mass merger, then *the divide between coreless-discy-rotating and core-boxy-nonrotating ellipticals happens at a luminosity below which neither of the merger progenitor galaxies should have contained X-ray gas and above which one or both progenitor galaxies should have contained X-ray gas. Thus KFCB point out that the E–E dichotomy occurs at the correct luminosity so that coreless-discy-rotating ellipticals formed in wet mergers whereas core-boxy-nonrotating ellipticals formed in dry mergers.*

Specifically, $M_V \simeq -20.7$ for merger progenitors corresponds (using $M/L_V \sim 6$) to a stellar mass of $M_* \simeq 1 \times 10^{11}\ M_\odot$ or, using a baryon-to-total mass ratio of 1/6 (Komatsu et al. 2009), to $M_{\rm DM} \simeq 6 \times 10^{11}\ M_\odot$. And the divide between coreless-discy-rotating Es and core-boxy-nonrotating Es happens at $M_{\rm DM} \simeq 10^{12}\ M_\odot$. So the agreement with the above picture of $M_{\rm crit}$ star-formation quenching is good.

Thus our picture of the formation of classical bulges and elliptical galaxies by wet and (at $M_{\rm DM} > 10^{12}\,M_\odot$) dry major mergers (Sect. 16.4 of this paper) is a tidy addition to our developing paradigm of star-formation quenching. Many details of the structure of classical bulges and ellipticals (e. g., the list in Sect. 16.4.1.1) fit into and support this paradigm. But the paradigm is more general than just an explanation of the E – E dichotomy. I turn to these more general aspects next:

In a seminal paper, Peng et al. (2010) use a few robust observations to derive very general conclusions about how quenching must work. They do this completely operationally, without any need to identify the physical mechanism(s) of quenching. At redshift $z \sim 0$ (Sloan Digital Sky Survey) and out to $z \sim 1$ (zCOSMOS survey: Lilly et al. 2007), the most essential observations used are (1) that the specific star formation rate is almost independent of galaxy mass (there is a "main sequence" of star formation) but with rapidly decaying specific star formation rate as $z \to 0$, and (2) that star-forming galaxies satisfy a Schechter (1976) mass function whose characteristic mass is almost independent of z. From a discussion of how star formation operates to reproduce the above and other observations, they deduce that quenching is driven by galaxy mass and by galaxy environment and that these two modes (not identified physically) are separable and independent. Plus there must be an additional quenching mode that is associated with bulge formation via mergers. Fig. 16.10 connects their picture with the quenching paradigm that we review here.

Peng et al. (2010) emphasize that their analysis is operational: it identifies the conditions in which quenching must operate, but it does not identify quenching mechanisms. However, with this section's background on $M_{\rm crit}$ quenching and with results from KH13 on BH – host-galaxy coevolution (or not), we can identify aspects of our developing physical picture of star-formation quenching with the conclusions of Peng et al. (2010). This is illustrated in Fig. 16.10.

The masses used in Peng et al. (2010) are estimated by integrating star formation rates and by fitting spectral energy distributions; in essence, they are stellar masses. Figure 16.10 suggests that mass quenching tends to happen at masses $\sim 10^{10.5}\,M_\odot$. In Figure 7 of Peng et al. (2010), the fraction of quenched galaxies (independent of environment) reaches 50 % at $\sim 10^{10.6}\,M_\odot$ and 80 % at $\sim 10^{11.25}\,M_\odot$. These correspond to $M_{\rm DM} \sim 10^{11.4}$ to $10^{12}\,M_\odot$. The good agreement with $M_{\rm crit}$ suggests that Peng's "mass quenching" is precisely our "$M_{\rm crit}$ quenching" by hot gas.

Peng et al. (2010) conclude further that some low-mass galaxies are quenched by their environments. That is, these galaxies are quenched because they are satellites of higher-mass objects – ones (either individual galaxies or clusters of galaxies) that *can have* masses $M_{\rm DM} \gtrsim M_{\rm crit}$. *I suggest that Peng's "environmental quenching" is the same physical process as mass quenching, but in Peng's mass quenching, the X-ray gas that does the work belongs to the galaxy that is being quenched, whereas in environmental quenching, the X-ray gas that does the work belongs to somebody else; i. e., to the quenched galaxy's parent giant galaxy or galaxy cluster.* This idea is verified by Peng et al. (2012), Knobel et al. (2015), and Gabor and Davé (2015).

The suggested connection with KH13 then is this: Both mass and environment quenching are aspects of point 3 in Sect. 16.6.2 – they are effects of hot gas that is kept hot by a combination of maintenance-mode AGN feedback and other processes

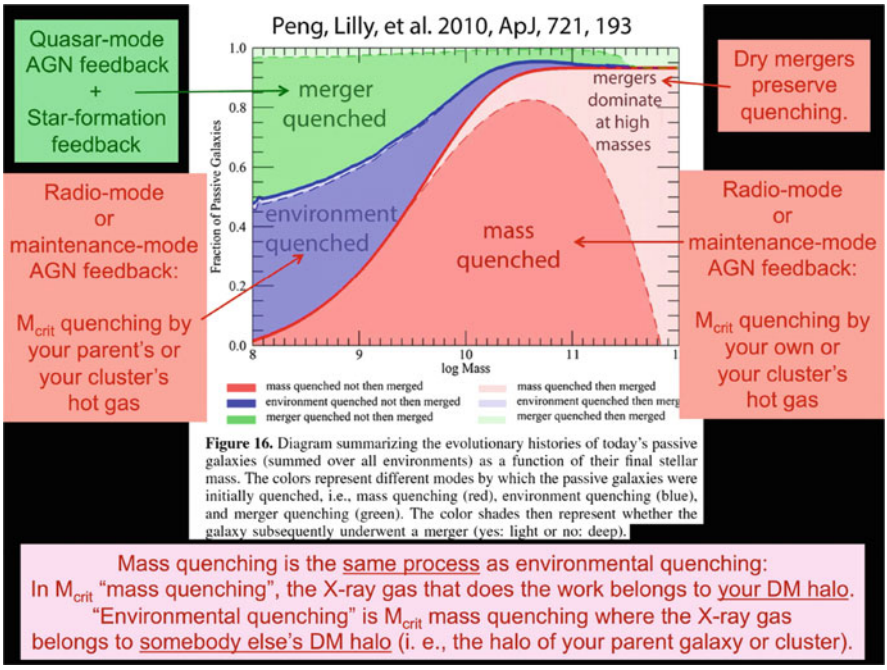

Fig. 16.10 Powerpoint slide connecting the star-formation quenching picture of Peng et al. (2010: central figure and its caption) with the picture that is summarized in this paper (surrounding text)

such as continued infall of gas from the cosmological hierarchy and the injection of the kinetic energy of gas that is shed by dying stars.

But the above quenching processes are not sufficient. It is easy to explain why – to give an example that mass quenching and environment quenching cannot explain. *What quenches field S0 galaxies with masses* $M \ll M_{\rm crit}$*?* Kormendy and Ho (2013) suggest that they are quenched in the context of wet galaxy mergers that include starbursts, with energy feedback from the starburst beginning the job of quenching and AGN feedback (Sect. 16.6.2, point 2) finishing the job. It seems natural to suggest that this is the Peng's "merger quenching". Observations of gas outflows in high-z, star-forming galaxies such as submillimeter galaxies – at least some of which are mergers – are reviewed in KH13. Of course, bulge-formation and $M_{\rm crit}$ quenching can be mutually supportive (e.g., Woo et al. 2015).

Once star formation is quenched at $M > M_{\rm crit}$, then dry mergers preserve both the quenched state and the $M_\bullet$ – host correlations (Sect. 16.6.2, point 4 and modes "mass quenched then merged", "environment quenched then merged", and "merger quenched then merged" in Fig. 16.10).

The biggest remaining question in our $z < 1$ picture is this: *In merger-quenched galaxies that have* $M \ll M_{\rm crit}$*, i. e., in objects in which X-ray gas is not available even after the merger is finished, what preserves the quenched, red and dead state? We do not know, but episodic, low-level AGN feedback may be the answer.*

The biggest overall uncertainty is that quenching may operate differently at $z \gtrsim 2$. Dekel and Birnboim argue (1) that $M_{\rm crit}$ is higher at high z, when gas fractions in galaxies and gas accretion rates onto galaxies are both higher and (2) that cold streams can penetrate hot gas at high z and contribute to the growth of discs at masses that are unattainable at $z \sim 0$ (Dekel et al. 2009a). Another difference involves the observation that most star-forming galaxies define a main sequence of star formation with few outliers, implying that duty cycles are long and hence that star formation is not driven primarily by short-duration events such as mergers (Sect. 16.4.1.5). When strong gas outflows are seen in star-forming galaxies at $z \sim 2$, the inference is that some combination of star formation and AGN feedback is responsible but that these are not primarily driven by major mergers (e.g., Förster Schreiber et al. 2014; Genzel et al. 2014). Because these processes are also associated with bulge growth in disc galaxies (Lang et al. 2014), the most consistent interpretation that also includes the $M_\bullet$ correlation results is that the bulge growth in these objects is by clump cluster sinking (Sect. 16.3 here). Genzel (private communication) suggests that Peng's mass quenching may be this outflow process associated with more-or-less steady-state star formation, AGN feedback, and classical bulge growth. On the "plus side", there is clearly a danger that our tidy picture is basically correct at $z < 1$ but not a description of what happens at $z \gg 1$. On the other hand, we already know that many details of galaxy structure are well explained by the $z \sim 0$ picture. Particularly important is the natural explanation of cores in dry-merger remnants and central extra light in wet-merger remnants (see KFCB). Alternative suggestions for quenching mechanisms at high z have not addressed and solved the problem of also explaining these aspects of $z \sim 0$ galaxy structure. This is not a proof that the suggested high-z processes are wrong.

It seems reasonable to conclude that our $z < 1$ picture of star formation quenching is robust. Mostly, it needs clarification of engineering details. In marked contrast, star formation quenching at $z \gtrsim 2$ is less well understood, although progress is rapid.

16.8 A Partial Summary of Outstanding Problems

I conclude with a summary of the most important outstanding problems. I restrict myself to big-picture issues and do not address the myriad engineering details that are unsolved by our present state of the art. They are, of course, vitally important. But a comprehensive list would require a paper of its own. I therefore refer readers to earlier chapters of this book, which discuss many of these problems in detail.

(1) I emphasized in Sect. 16.4.1.3 that, to me, the most important goal is to produce realistic classical bulges + ellipticals and realistic discs that overlap over a factor of >1000 in mass but that differ from each other in ways that we observe over the whole of this range. They can

combine with any B/T from 0 to 1, but the differences between bulges and discs depend very little on B/T.

(2) Four decades of work on $z \simeq 0$ galaxies showed convincingly that major mergers convert discs into classical bulges and ellipticals with the observed properties, including Sérsic index, fundamental plane parameter correlations, intrinsic shape and velocity distributions, both as functions of mass, the presence of cores or central extra light, and isophote shape. This work also suggested that merger rates were higher in the past, and modern observations confirm this prediction. By the mid-1990s, we had converged on a picture in which classical bulges and ellipticals were made in major mergers. Enthusiasm for mergers was probably overdone, but now, the community is overreacting in the opposite direction. The successes of the 1970s–1990s are being forgotten, and – I believe – we have come to believe too strongly that minor mergers control galaxy evolution. Reality probably lies between these extremes. For today's audience, the important comment is this: The observations that led to our picture of E formation via major mergers have not been invalidated. I suggest that the profitable way forward is to use what we learn from $z \simeq 0$ mergers-in-progress to explore how mergers make bulges and ellipticals at higher z, including (of course) differences caused (for example) by large gas fractions and including new ideas such as violent disc instabilities that make clumps that make bulges. For this still-elusive true picture, it is OK that mergers are rare, because ellipticals are rare, too, and classical bulges are rarer than we thought. And it is OK that most star formation does not happen in mergers, because ellipticals are rare anyway, and because their main bodies are mostly made up of the scrambled-up remnants of already-stellar progenitor discs.

(3) The most important unsolved problem is this: How did hierarchical clustering produce so many giant galaxies (say, those with $V_{\rm circ} \gtrsim 150\,{\rm km\,s^{-1}}$) with no sign of a classical bulge? This problem is a very strong function of environment – in field environments such as the Local Group, most giant galaxies are bulgeless, whereas in the Virgo cluster, most stars live in classical bulges and elliptical galaxies. The clue therefore is that the solution involves differences in accretion (gentle versus violent) and not largely internal physics such as star-formation or AGN feedback.

(4) Calculating galaxy evolution ab inito, starting with ΛCDM density fluctuations, constructing giant N-body simulations of halo hierarchical clustering, and then adding baryonic physics is the industry standard today and the way of the future. It is immensely difficult and immensely rewarding. It is not my specialty, and I have only one point to add to the excellent review by Brooks and Christensen: *Observations hint very strongly that we put too much reliance on feedback to solve our engineering problems in producing realistic*

galaxies. Observations of supermassive BH demographics tell us that AGN feedback does not much affect galaxy structure or star formation until mergers start to make classical bulges. And point (3) emphasizes that environment and not gravitational potential well depth is the key to solving the problem of giant, pure-disc galaxies.

(5) We need to fully integrate our picture of disc secular evolution into our paradigm of galaxy evolution. As observed at $z \simeq 0$, this picture is now quite detailed and successful. Essentially all of the commonly occurring morphological features of galaxies – bars, (nuclear, inner, and outer) rings, nuclear bars, and pseudobulges – are at least qualitatively explained within this picture. Some of these details are beyond the "targets" of present galaxy-formation simulations. But pseudobulges are immediately relevant, because our recognition of them has transformed our opinions about classical bulges. They are much rarer than we thought. In particular, small classical bulges are *very* rare. And although some galaxies have structure that is completely determined by the physics of hierarchical clustering, others – and they dominate in the field – appear to have been structured almost exclusively by secular processes. Incorporating these processes is a challenge, because slow processes are much more difficult to calculate than rapid processes. But secular evolution is an idea whose time has come (Sellwood 2014), and we need to include it in our paradigm.

(6) At the same time, our *quantitative* understanding of secular evolution needs more work. For example, we need a study similar to Dressler's (1980) work on the morphology-density relation: We need to measure the luminosity and mass functions of discs, pseudobulges, and classical bulges+ellipticals, all as functions of environmental density. At present, we have essentially only two "data points" – the extreme field (Kormendy et al. 2010; Fisher and Drory 2011) and the Virgo cluster (see Kormendy et al. 2010). This is already enough to lead to point (3) in this list. We need corresponding studies in more environments that span the density range from the field to the richest clusters. This will not be easy, first because we need high spatial resolution whereas observing more environments drives us to larger distances, and second because of point (7).

(7) Our picture of disc secular evolution predicts that many galaxies should contain both a classical and a pseudo bulge. Work on the subject has concentrated on extremes – on galaxies that are dominated by one kind of bulge or the other. Samples of large numbers of galaxies will inevitably have to face the challenge of separating at least three components (bulge, pseudobulge, and disc) and in many cases more (bar, lens, ...). We also need to be able to find pseudobulges in face-on barred galaxies (see Sect. 16.2.1). But it is easy to overinterpret details in the photometry. The best way to

approach this problem is probably to begin with infrared observations of nearly-edge-on galaxies (e.g., Salo et al. 2015).

(8) Are classical bulges really indistinguishable from ellipticals? The structural parameter scaling relations shown in Fig. 16.4 (based on many authors' work) show that they are closely similar. I use this result throughout the present paper. It is central to Renzini's (1999) paraphrase of the classical morphological definition: "A bulge is nothing more nor less than an elliptical galaxy that happens to live in the middle of a disc." But not everybody agrees. Based on multi-component decompositions, different fundamental plane correlations for classical bulges and ellipticals have been found by Gadotti (2008, 2009, 2012) and by Laurikainen et al. (2010). We need to resolve these differences. At stake is an understanding of whether classical bulges and ellipticals form – as I suggest – by essentially the same major merger process or whether important variations in that process produce recognizably different results. In particular, it is not impossible that we can learn to distinguish ellipticals and perhaps *some* bulges that form via mergers of distinct galaxies from other bulges that form via the mergers of mass clumps that form in unstable discs. Both processes drive additional gas toward the center, but it is possible that bulge formation via disc instabilities is intrinsically more drawn out in time with the result (for example) that "extra light components" such as those studied in Kormendy (1999), KFCB, and Hopkins et al. (2009a) are smoothed away and unrecognizable in the resulting classical bulges but not in discy-coreless-rotating ellipticals.

(9) Returning to elliptical galaxies: KFCB present a detailed observational picture and ARA&A-style review of the two kinds of ellipticals in large part as seen in the Virgo cluster. Hopkins et al. (2009a,b) present modeling analyses of wet and dry mergers, respectively. *We need to know how this very clean picture as seen in the nearest rich cluster translates into other environments.* Much of the work published by Lauer et al. (1995, 2005, 2007a,b), by Faber et al. (1997), by Kormendy and Bender (1996, 2013), and by Bender et al. (1989) applies to broader ranges of environments. It suggests that the picture summarized here in Sect. 16.4.1.1 is basically valid but that the distinction between coreless-discy-rotating and core-boxy-nonrotating galaxies is somewhat "blurred" in a broader range of environments. For example, $M_V = -21.6$ cleanly separates the two kinds in Virgo, with only one partial exception (NGC 4621 at $M_V = -21.54$ has $n = 5.36^{+0.30}_{-0.28}$ characteristic of core galaxies, but it has a small amount of extra light near the center). However, the above papers and others show that the two galaxy types overlap over a range of absolute magnitudes from about $M_V = -20.5$ to about $M_V = -23$. In the overlap range and occasionally outside it, some classification criteria in Sect. 16.4.1.1 conflict with the majority. We should not

be surprised that heterogeneous formation histories can have variable outcomes; on the contrary, it is encouraging to see as much uniformity as we see. Still, a study of how the systematics depend on environment should be profitable.

(10) Still on ellipticals and classical bulges: The SAURON and ATLAS^{3D} teams have carried out an enormous amount of truly excellent work on nearly all aspects of bulge+E structure and evolution. A review is in preparation by Cappellari (2015). *It is natural to ask how the picture of bulges and ellipticals developed by the SAURON and ATLAS^{3D} papers compares with the one outlined in Sect. 16.4 here. The answer is that they agree exceedingly well.* There are differences in emphasis, and the large SAURON + ATLAS^{3D} teams address many subjects that are beyond the scope of studies by our team or by the Nuker team. There is also one difference in analysis that makes me uncomfortable – in their work, they generally do not decompose galaxies into bulge and disc parts. *It is therefore all the more remarkable that careful work without using component decomposition and our work that always is based on component decomposition converge on pictures that are so similar.* E.g., the separate parameter correlations for bulges and discs that are shown here in Fig. 16.4 are visible as pure-bulge and pure-disc boundaries of parameter correlation *regions* shown in Cappellari et al. (2013b). In their diagrams, the parameter space between our bulge and disc correlations is filled in with intermediate-Hubble-type galaxies that have $0 < B/T < 1$. Similarly, Cappellari et al. (2011) and Kormendy and Bender (2012) both revive the "parallel sequence" galaxy classification of van den Bergh (1976), as do Laurikainen et al. (2011). Kormendy and Bender (2012) also add Sph galaxies (as distinct from ellipticals) to the classification.
What may appear as a difference between Sect. 16.4 and the SAURON + ATLAS^{3D} work is our emphasis on many E–E dichotomy classification criteria versus their distinction based only on fast versus slow rotation. However, Lauer (2012) shows that the SAURON + ATLAS^{3D} division into fast and slow rotators is essentially equivalent to the division between coreless and core galaxies. The equivalence is not exact based in the rotation amplitude parameter $\lambda_{r_e/2}$ (within 1/2 of the effective radius r_e) chosen by the SAURON and ATLAS^{3D} teams. But it becomes much more nearly exact if slow and fast rotators are divided at a slightly higher rotation rate, $\lambda_{r_e/2} = 0.25$. In unpublished work, I found an essentially equivalent result for the original SAURON kinematic classification, in which slow rotators have $\lambda_R < 0.1$ and fast rotators have $\lambda_R > 0.1$ as defined in Emsellem et al. (2007). If the division is instead made at $\lambda_R = 0.175$, then core and coreless ellipticals are separated essentially perfectly. (The only exception in KFCB is NGC 4458, which is slowly rotating but coreless. But it is almost exactly round, and rotating galaxies that are

seen face-on will naturally look like slow rotators.) The more nuanced ATLAS^{3D} look at elliptical galaxy dynamics leads to a revised suggestion that fast and slow rotators should be separated at $\lambda_{r_e/2} = (0.265 \pm 0.01) \times \sqrt{\epsilon_{e/2}}$ (Emsellem et al. 2011, Equation 4). A typical $\epsilon = 0.2$ for core-boxy galaxies and $\epsilon = 0.35$ for coreless-discy galaxies (from Tremblay and Merritt 1996) then implies a division at $\lambda_{r_e/2} = 0.16$ and 0.12, respectively. The typical intrinsic ellipticity of 0.4 found by Sandage et al. (1970) for all ellipticals implies $\lambda_{r_e/2} = 0.17$. These values are closer to the rotation parameters 0.25 and 0.175 that divide core and coreless galaxies as found by Lauer (2012) and by my work, respectively.

I suggest that the best way to divide slow rotators from fast rotators is not to pick some arbitrary value of the rotation parameter but rather to ask the galaxies what value of the rotation parameter produces the cleanest distinction into two kinds of galaxies as summarized in Sect. 16.4.1.1. When this is done, the E – E dichotomy as discussed in this paper and the large body of work done by the SAURON and ATLAS^{3D} teams are remarkably consistent.

A partial exception to the above conclusion is some of the *N*-body simulation work, e.g., by Naab et al. (2014). They acknowledge the importance of major mergers in some ways that are consistent with the story advocated in this paper. But their conclusion that "The galaxies most consistent with the class of non-rotating round early-type galaxies grow by gas-poor *minor* mergers alone" (emphasis added) is at best uncomfortable within the picture presented here. The core-boxy-nonrotating galaxies have a large range of mostly homogeneous properties with respect to which the round ones do not stand out as different (e.g., KFCB). In particular, our understanding of cores – especially the tight correlations between core properties and BH masses – depends on our picture that cores are scoured by black hole binaries that are formed in major mergers (see KFCB and Kormendy and Bender 2009 for both the data and a review). At best, *it remains to be demonstrated that minor mergers – which necessarily involve many small galaxies with* (from Fig. 16.7) *undermassive BHs – can produce the very large BH masses and cores that are seen in giant core ellipticals. Dry minor mergers cannot do better than to preserve the* $M_\bullet/M_{\rm host}$ *mass ratio. Also, if many minor mergers are necessary – and these galaxies are so massive that very many minor mergers are necessary to grow them – then there is a danger of producing a central cluster of low-mass BHs that is never observed as a cluster of compact radio sources and that is inherently unstable to the ejection of objects in small-n n-body systems* (see KH13, p. 634).

(11) I conclude with two sociological points: It is worth emphasizing that galaxy evolution work did not start in the 2000s. Many results that were derived in the 1960s–1990s remain valid today. We should not

forget them. We should integrate them into our current picture of galaxy evolution.

(12) And finally: Galaxy evolution work has changed profoundly in the SDSS and HST eras. Before the early 1990s, *our goal was to understand the evolution of galaxy structure.* Now, most emphasis on galaxy structure has disappeared. *Now, our goal is to understand the history of star formation in the universe.* The main reason for this change is the common ground found between SDSS studies of many thousands of galaxies and HST studies of very distant galaxies. Necessarily, both kinds of studies concentrate on galaxies whose images are a few arcsec across. We do not resolve structural details. Mainly, we measure colors and magnitudes. So galaxy evolution has evolved into the study of the red sequence and blue cloud in the color-magnitude relation. Star formation and its quenching are, of course, important. But it would be enormously healthy if we could improve the dialog between SDSS+HST people and those – such as this author – who work on nearby galaxies whose star formation histories and structures can be studied in great detail. Conselice (2014) is an example of a paper that tries to bridge the gap. We would benefit greatly if we could completely connect the two approaches to galaxy evolution.

Acknowledgements Many of my ideas about galaxy evolution were forged in intense and enjoyable collaborations with Ralf Bender, Luis Ho, and the Nuker team. It is a pleasure to thank all these people and many more who I do not have room to list for fruitful conversations over many years. I am especially grateful to Reinhard Genzel for stimulating and insightful discussions and to Ralf Bender, Dimitri Gadotti, and Eija Laurikainen for very helpful comments on this paper. Any errors of interpretation that remain are of course my responsibility. I thank Steve Allen, Xinyu Dai, Ying-Jie Peng, and Simon Lilly for permission to copy figures. My work on this paper was supported by the Curtis T. Vaughan, Jr. Centennial Chair in Astronomy at the University of Texas.

References

Allen, S. W., Evrard, A. E., & Mantz, A. B. 2011, ARA&A. 49, 409
Armitage, P. J., & Natarajan, P. 2002, ApJ, 567, L9
Armitage, P. J., & Natarajan, P. 2005, ApJ, 634, 921
Athanassoula, E., 2005, MNRAS, 358, 1477
Athanassoula, E. 2015, in Galactic Bulges, ed. E. Laurikainen, R. F. Peletier, & D. A. Gadotti (New York: Springer), pp. 393–414 (arXiv:1503.04804)
Baes, M., Buyle, P., Hau, G. K. T., & Dejonghe, H. 2003, MNRAS, 341, L44
Baggett, W. E., Baggett, S. M., & Anderson, K. S. J. 1998, AJ, 116, 1626
Barth, A. J., Greene, J. E., & Ho, L. C. 2008, AJ, 136, 1179
Barth, A. J., Ho, L. C., Rutledge, R. E., & Sargent, W. L. W. 2004, ApJ, 607, 90
Begelman, M. C., Blandford, R. D., & Rees, M. J, 1980, Nature, 287, 307
Behroozi, P. S., Wechsler, R. H., & Conroy, C. 2013, ApJ, 770, 57
Bender, R. 1988, A&A, 193, L7

Bender, R., Burstein, D., & Faber, S. M. 1992, ApJ, 399, 462
Bender, R., Surma, P., Döbereiner, S., Möllenhoff, C., & Madejsky, R. 1989, A&A, 217, 35
Best, P. N. 2006, Paper Presented at the Workshop on The Role of Black Holes in Galaxy Formation and Evolution, Potsdam, Germany, 2006 September 10 – 13 (see Cattaneo et al. 2009)
Best, P. N. 2007a, in ASP Conf. Ser. 379, Cosmic Frontiers, ed. M. Metcalfe & T. Shanks (San Francisco, CA: ASP), 213
Best, P. N. 2007b, New Astron. Rev., 51, 168
Best, P. N., Kaiser, C. R., Heckman, T. M., & Kauffmann, G. 2006, MNRAS, 368, L67
Birnboim, Y., & Dekel, A. 2003, MNRAS, 345, 349
Blanton, M. R., & Moustakas, J. 2009, ARA&A, 47, 159
Bluck, A. F. L., Conselice, C. J., Bouwens, R. J., et al. 2009, MNRAS, 394, 51
Bluck, A. F. L., Conselice, C. J., Buitrago, F., et al. 2012, ApJ, 747, 34
Booth, C. M., & Schaye, J. 2010, MNRAS, 405, L1
Bothun, G. D., & Thompson, I. B. 1988, AJ, 96, 877
Bournaud, F. 2015, in Galactic Bulges, ed. E. Laurikainen, R. F. Peletier, & D. A. Gadotti (New York: Springer), pp. 357–392 (arXiv:1503.07660)
Bournaud, F., Elmegreen, B. G., & Elmegreen, D. M. 2007, ApJ, 670, 237
Boylan-Kolchin, M., Ma, C.-P., & Quataert, E. 2006, MNRAS, 369, 1081
Brooks, A., & Christensen, C. 2015, in Galactic Bulges, ed. E. Laurikainen, R. F. Peletier, & D. A. Gadotti (New York: Springer), pp. 319–356
Cacciato, M., Dekel, A., & Genel, S. 2012, MNRAS, 421, 818
Cappellari, M. 2015, ARA&A, in preparation
Cappellari, M., Emsellem, E., Bacon, R., et al. 2007, MNRAS, 379, 418
Cappellari, M., Emsellem, E., Krajnović, D., et al. 2011, MNRAS, 416, 1680
Cappellari, M., McDermid, R. M., Alatalo, K., et al. 2013b, MNRAS, 432, 1862
Cappellari, M., Scott, N., Alatalo, K., et al. 2013a, MNRAS, 432, 1709
Cattaneo, A., Dekel, A., Devriendt, J., Guiderdoni, B., & Blaizot, J. 2006, MNRAS, 370, 1651
Cattaneo, A., Dekel, A., Faber, S. M., & Guiderdoni, B. 2008, MNRAS, 389, 567
Cattaneo, A., Faber, S. M., Binney, J., et al. 2009, Nature, 460, 213
Chiboucas, K., Karachentsev, I. D., & Tully, R. B. 2009, AJ, 137, 3009
Ceverino, D., Dekel, A., & Bournaud, F. 2010, MNRAS, 404, 2151
Ceverino, D., Dekel, A., Tweed, D., & Primack, J. 2015, MNRAS, 447, 3291
Cole, D. R., & Debattista, V. P. 2015, in Galactic Bulges, ed. E. Laurikainen, R. F. Peletier, & D. A. Gadotti (New York: Springer), pp. 117–134 (arXiv:1504.05879)
Combes, F. 2015, in Galactic Bulges, ed. E. Laurikainen, R. F. Peletier, & D. A. Gadotti (New York: Springer), pp. 415–430 (arXiv:1501.03603)
Combes, F., & Sanders, R. H. 1981, A&A, 96, 164
Conselice, C. J. 2014, ARA&A, 52, 291
Conselice, C. J., Yang, C., & Bluck, A. F. L. 2009, MNRAS, 394, 1956
Courteau, S., Dutton, A. A., van den Bosch, F. C., et al. 2007, ApJ, 671, 203
Cuadra, J., Armitage, P. J., Alexander, R. D., & Begelman, M. C. 2009, MNRAS, 393, 1423
Daddi, E., Dickinson, M., Morrison, G., et al. 2007, ApJ, 670, 156
Dai, X., Bregman, J. N., Kochanek, C. S., & Rasia, E. 2010, ApJ, 719, 119
Davies, R. L., Efstathiou, G., Fall, S. M., Illingworth, G., & Schechter, P. L. 1983, ApJ, 266, 41
Dekel, A., & Birnboim, Y. 2006, MNRAS, 368, 39
Dekel, A., & Birnboim, Y. 2008, MNRAS, 383, 119
Dekel, A., Birnboim, Y., Engel, G., et al. 2009a, Nature, 457, 451
Dekel, A., Sari, R., & Ceverino, D. 2009b, ApJ, 703, 785
de Vaucouleurs, G., de Vaucouleurs, A., & Corwin, J. R. 1976, Second Reference Catalogue of Bright Galaxies (Austin, TX: University of Texas Press)
Dong, X.-B., Ho, L. C., Yuan, W., et al. 2012, ApJ, 755, 167
Dotti, M., Colpi, M., Haardt, F., & Mayer, L. 2007, MNRAS, 379, 956
Dressler, A. 1980, ApJ, 236, 351
Ebisuzaki, T., Makino, J., Okamura, S. K. 1991, Nature, 354, 212

Elbaz, D., Daddi, E., Le Borgne, D., et al. 2007, A&A, 468, 33
Ellis, S. C., & O'Sullivan, E. 2006, MNRAS, 367, 627
Elmegreen, B. G., Bournaud, F., & Elmegreen, D. M. 2008, ApJ, 688, 67
Elmegreen, B. G., & Elmegreen, D. M. 2005, ApJ, 627, 632
Elmegreen, B. G., Elmegreen, D. M, Fernandez, M. X., & Lemonias, J. J. 2009a, ApJ, 692, 12
Elmegreen, D. M., Elmegreen, B. G, Marcus, M. T., et al.2009b, ApJ, 701, 306
Elmegreen, D. M., Elmegreen, B. G, Ravindranath, S., & Coe, D. A. 2007, ApJ, 658, 763
Emsellem, E., Cappellari, M., Krajnović, D., et al. 2007, MNRAS, 379, 401
Emsellem, E., Cappellari, M., Krajnović, D., et al. 2011, MNRAS, 414, 888
Escala, A., & Del Valle, L. 2011, Int. J. Mod. Phys. E, 20, 79
Escala, A., Larson, R. B., Coppi, P. S., & Mardones, D. 2004, ApJ, 607, 765
Escala, A., Larson, R. B., Coppi, P. S., & Mardones, D. 2005, ApJ, 630, 152
Faber, S. M., & Jackson, R. E. 1976, ApJ, 204, 668
Faber, S. M., Tremaine, S., Ajhar, E. A., et al. 1997, AJ, 114, 1771
Faber, S. M., Willmer, C. N. A., Wolf, C., et al. 2007, ApJ, 665, 265
Fabian, A. C. 1994, ARA&A, 32, 277
Fabian, A. C. 2012, ARA&A, 50, 455
Falcón-Barroso, J. 2015, in Galactic Bulges, ed. E. Laurikainen, R. F. Peletier, & D. A. Gadotti (New York: Springer), pp. 169–192 (arXiv:1503.04590)
Falcón-Barroso, J., & Knapen, J. H. 2012, eds., Canary Islands Winter School of Astrophysics, Vol XXIII, Secular Evolution of Galaxies (Cambridge: Cambridge University Press)
Fall, S. M., & Romanowsky, A. J. 2013, ApJ, 769, L26
Ferrarese, L. 2002, ApJ, 578, 90
Ferrarese, L., Côté, P., Jordán, A., et al. 2006, ApJS, 164, 334
Filippenko, A. V., & Ho, L. C. 2003, ApJ, 588, L13
Filippenko, A. V., Ho, L. C., & Sargent W. L. W. 1993, ApJ, 410, L75
Finlator, K., & Davé, R. 2008, MNRAS, 385, 2181
Fisher, D. B., & Drory, N. 2008, AJ, 136, 773
Fisher, D. B., & Drory, N. 2011, ApJ, 733, L47
Fisher, D. B., & Drory, N. 2015, in Galactic Bulges, ed. E. Laurikainen, R. F. Peletier, & D. A. Gadotti (New York: Springer), pp. 51–86
Forbes, J. C., Krumholz, M. R., Burkert, A., & Dekel, A. 2014, MNRAS, 438, 1552
Förster Schreiber, N. M., Genzel, R., Bouché, N., et al. 2009, ApJ, 706, 1364
Förster Schreiber, N. M., Genzel, R., Newman, S. F., et al. 2014, ApJ, 787, 38
Förster Schreiber, N. M., Shapley, A. E., Erb, D. K., et al. 2011a, ApJ, 731, 65
Förster Schreiber, N. M., Shapley, A. E., Genzel, R., et al. 2011b, ApJ, 739, 45
Gabor, J. M., & Davé, R. 2015, MNRAS, 447, 374
Gadotti, D. A. 2008, Mem. Soc. Astron. Ital., 75, 1 (arXiv:1208.2295)
Gadotti, D. A. 2009, MNRAS, 393, 1531
Gadotti, D. A. 2012, in IAU Symposium 295, The Intriguing Life of Massive Galaxies, ed. D. Thomas, A. Pasquali, & I. Ferreras (Cambridge: Cambridge Univ. Press), 232
Gaskell, C. M. 2010, in The First Stars and Galaxies: Challenges for the Next Decade, ed. D. J. Whalen, V. Bromm, & N. Yoshida (Melville, NY: AIP), 261
Gaskell, C. M. 2011, in SF2A-2011: Proceedings of the Annual Meeting of the French Society of Astronomy and Astrophysics, ed. G. Alecian, K. Belkacem, R. Samadi, & D. Valls-Gabaud (Paris: SF2A), 577
Gavazzi, G., Donati, A., Cucciati, O., et al. 2005, A&A, 430, 411
Gavazzi, G., Franzetti, P., Scodeggio, M., Boselli, A., & Pierini, D. 2000, A&A, 361, 863
Gebhardt, K., Lauer, T. R., Kormendy, J., et al. 2001, AJ, 122, 2469
Gebhardt, K., Richstone, D., Ajhar, E. A., et al. 1996, AJ, 112, 105
Genel, S., Naab, T., Genzel, R., et al. 2012, ApJ, 745, 11
Genzel, R., Burkert, A., Bouché, N., et al. 2008, ApJ, 687, 59
Genzel, R., Förster Schreiber, N. M., Rosario, D., et al. 2014, ApJ, 796, 7

Genzel, R., Newman, S., Jones, T., et al. 2011, ApJ, 733, 101
Genzel, R., Tacconi, L. J., Eisenhauer, F., et al. 2006, Nature, 442, 786
Genzel, R., Tacconi, L. J., Rigopoulou, D., Lutz, D., & Tecza, M. 2001, ApJ, 563, 527
Gonzalez, O. A., & Gadotti, D. A. 2015, in Galactic Bulges, ed. E. Laurikainen, R. F. Peletier, & D. A. Gadotti (New York: Springer), pp. 205–238 (arXiv:1503.07252)
Gould, A., & Rix, H.-W. 2000, ApJ, 532, L29
Governato, F., Brook, C., Mayer, L., et al. 2010, Nature, 463, 203
Graham, A. W. 2011, Discussion comment following Kormendy, Bender, & Cornell 2011
Graham, A. W. 2015, in Galactic Bulges, ed. E. Laurikainen, R. F. Peletier, & D. A. Gadotti (New York: Springer), pp. 267–318 (arXiv:1501.02937)
Graham, A. W., & Scott, N. 2013, ApJ, 764, 151
Graham, A. W., & Scott, N. 2015, ApJ, 798, 54
Greene, J. E., & Ho, L. C. 2004, ApJ, 610, 722
Greene, J. E., & Ho, L. C. 2007, ApJ, 670, 92
Greene, J. E., Peng, C. Y., Kim, M., et al. 2010, ApJ, 721, 26
Hayasaki, K. 2009, PASJ, 61, 65
Heckman, T. M., & Best, P. N. 2014, ARA&A, 52, 589
Hibbard, J. E., Guhathakurta, P., van Gorkom, J. H., & Schweizer, F. 1994, AJ, 107, 67
Hibbard, J. E., & Mihos, J. C. 1995, AJ, 110, 140
Hibbard, J. E., van der Hulst, J. M., Barnes, J. E., & Rich, R. M. 2001a, AJ, 122, 2969
Hibbard, J. E., & van Gorkom, J. H. 1996, AJ, 111, 655
Hibbard, J. E., van Gorkom, J. H., Rupen, M. P., & Schiminovich, D. 2001b, in ASP Conference Series, Vol. 240, Gas and Galaxy Evolution, ed. J. E. Hibbard, M. P. Rupen, & J. H. van Gorkom (San Francisco: ASP), 659
Hilz, M., Naab, T., Ostriker, J. P., et al. 2012, MNRAS, 425, 3119
Hinshaw, G., Larson, D., Komatsu, E., et al. 2013, ApJS, 208, 19
Hirschmann, M., Khochfar, S., Burkert, A., et al. 2010, MNRAS, 407, 1016
Ho, L. C. 2008, ARA&A, 46, 475
Ho, L. C., Greene, J. E., Filippenko, A. V., & Sargent, W. L. W. 2009, ApJS, 183, 1
Hopkins, P. F., Cox, T. J., Dutta, S. N., Hernquist, L., Kormendy, J., & Lauer, T. R. 2009a, ApJS, 181, 135
Hopkins, P. F., Lauer, T. R., Cox, T. J., Hernquist, L., & Kormendy, J. 2009b, ApJS, 181, 486
Hu, J. 2008, MNRAS, 386, 2242
Irwin, M. J., Belokurov, V., Evans, N. W., et al. 2007, ApJ, 656, L13
Ivanov, P. B., Papaloizou, J. C. B., & Polnarev, A. G. 1999, MNRAS, 307, 79
Jahnke, K., & Macciò, A. V. 2011, ApJ, 734, 92
Joseph, R. D., & Wright, G. S. 1985, MNRAS, 214, 87
Karachentsev, I., Aparicio, A., & Makarova, L. 1999, A&A, 352, 363
Karim, A., Schinnerer, E., Martínez-Sansigre, A., et al. 2011, ApJ, 730, 61
Kereš, D., Katz, N., Weinberg, D. H., & Davé, R. 2005, MNRAS, 363, 2
Khochfar, S., Emsellem, E., Serra, P., et al. 2011, MNRAS, 417, 845
Kirby, E. M., Jerjen, H., Ryder, S. D., & Driver, S. P. 2008, AJ, 136, 1866
Knobel, C., Lilly, S. J., Woo, J., & Kovač, K. 2015, ApJ, 800, 24
Komatsu, E., Dunkley, J., Nolta, M. R., et al. 2009, ApJS, 180, 330
Kormendy, J. 1979a, in Photometry, Kinematics and Dynamics of Galaxies, ed. D. S. Evans (Austin: Dept. of Astronomy, Univ. of Texas at Austin), 341
Kormendy, J. 1979b, ApJ, 227, 714
Kormendy, J. 1981, in The Structure and Evolution of Normal Galaxies, ed. S. M. Fall & D. Lynden-Bell (Cambridge: Cambridge Univ. Press), 85
Kormendy, J. 1982, in Twelfth Advanced Course of the Swiss Society of Astronomy and Astrophysics, Morphology and Dynamics of Galaxies, ed. L. Martinet & M. Mayor (Sauverny: Geneva Observatory), 113
Kormendy, J. 1985, ApJ, 295, 73

Kormendy, J. 1987, in Nearly Normal Galaxies: From the Planck Time to the Present, ed. S. M. Faber (New York: Springer), 163
Kormendy, J. 1993, in IAU Symposium 153, Galactic Bulges, ed. H. Dejonghe & H. J. Habing (Dordrecht: Kluwer), 209
Kormendy, J. 1999, in Galaxy Dynamics: A Rutgers Symposium, ed. D. Merritt, J. A. Sellwood, & M. Valluri (San Francisco, CA: ASP), 124
Kormendy, J. 2008, in IAU Symposium 245, Formation and Evolution of Galaxy Bulges, ed. M. Bureau, E. Athanassoula, & B. Barbuy (Cambridge: Cambridge University Press), 107
Kormendy, J. 2009, in ASP Conference Series, Vol. 419, Galaxy Evolution: Emerging Insights and Future Challenges, ed. S. Jogee, I. Marinova, L. Hao, & G. A. Blanc (San Francisco: ASP), 87 (arXiv:0812.0806)
Kormendy, J. 2012, in Canary Islands Winter School of Astrophysics, Vol. XXIII, Secular Evolution of Galaxies, ed. J. Falcón-Barroso & J. H. Knapen (Cambridge: Cambridge University Press), 1
Kormendy, J. 2015, Highlights of Astronomy, 16, 316
Kormendy, J., & Bender, R. 1996, ApJ, 464, L119
Kormendy, J., & Bender, R. 2009, ApJ, 691, L142
Kormendy, J., & Bender, R. 2011, Nature, 469, 377
Kormendy, J., & Bender, R. 2012, ApJS, 198, 2
Kormendy, J., & Bender, R. 2013, ApJ, 769, L5
Kormendy, J., Bender, R., Ajhar, E. A., et al. 1996a, ApJ, 473, L91
Kormendy, J., Bender, R., & Cornell, M. E. 2011, Nature, 469, 374
Kormendy, J., Bender, R., Richstone, D., et al. 1996b, ApJ, 459, L57
Kormendy, J., Dressler, A., Byun, Y.-I., et al. 1994, in ESO/OHP Workshop on Dwarf Galaxies, ed. G. Meylan & P. Prugniel (Garching: ESO), 147
Kormendy, J., Drory, N., Bender, R., & Cornell, M. E. 2010, ApJ, 723, 54
Kormendy, J., & Fisher, D. B. 2005, in The Ninth Texas-Mexico Conference on Astrophysics, ed. S. Torres-Peimbert & G. MacAlpine, RevMexA&A, Serie de Conferencias, 23, 101
Kormendy, J., & Fisher, D. B. 2008, in ASP Conference Series, Vol. 396, Formation and Evolution of Galaxy Discs, ed. J. G. Funes & E. M. Corsini (San Francisco: ASP), 297
Kormendy, J., Fisher, D. B., Cornell, M. E., & Bender, R. 2009, ApJS, 182, 216 (KFCB)
Kormendy, J., & Freeman, K. C., 2015, ApJ, submitted (arXiv:1411.2170)
Kormendy, J., & Gebhardt, K. 2001, in 20th Texas Symposium on Relativistic Astrophysics, ed. J. C. Wheeler & H. Martel (Melville, NY: AIP), 363
Kormendy, J., & Ho, L. C. 2013, ARA&A, 51, 511
Kormendy, J., & Kennicutt, R. C. 2004, ARA&A, 42, 603
Kravtsov, A. V., & Borgani, S. 2012, ARA&A, 50, 353
Kuntschner, H., Emsellem, E., Bacon, R., et al. 2010, MNRAS, 408, 97
Lang, P., Wuyts, S., Somerville, R. S., et al. 2014, ApJ, 788, 11
Lauer, T. R. 2012, ApJ, 759, 64
Lauer, T. R., Ajhar, E. A., Byun, Y.-I., et al. 1995, AJ, 110, 2622
Lauer, T. R., Faber, S. M., Gebhardt, K., et al. 2005, AJ, 129, 2138
Lauer, T. R., Faber, S. M., Richstone, D., et al. 2007a, ApJ, 662, 808
Lauer, T. R., Gebhardt, K., Faber, S. M., et al. 2007b, ApJ, 664, 226
Laurikainen, E., & Salo, H. 2015, in Galactic Bulges, ed. E. Laurikainen, R. F. Peletier, & D. A. Gadotti (New York: Springer), pp. 87–116 (arXiv:1505.00590)
Laurikainen, E., Salo, H., Buta, R., & Knapen, J. H. 2011, MNRAS, 418, 1452
Laurikainen, E., Salo, H., Buta, R., Knapen, J. H., & Comerón, S. 2010, MNRAS, 405, 1089
Le Floc'h, E., Papovich, C., Dole, H. et al. 2005, ApJ, 632, 169
Lilly, S. J., Le Fèvre, O., Renzini, A., et al. 2007, ApJS, 172, 70
López-Sanjuan, C., Le Fèvre, O., Ilbert, O., et al. 2013, in ASP Conference Series, Vol. 477, Galaxy Mergers in an Evolving Universe, ed. W.-H. Sun, K. Xu, N. Scoville, & D. Sanders (San Francisco: ASP), 159

Madore, B. F. 2015, in Galactic Bulges, ed. E. Laurikainen, R. F. Peletier, & D. A. Gadotti (New York: Springer), pp. 13–24
Makarova, L. 1999, A&AS, 139, 491
Makino, J., & Ebisuzaki, T. 1996, ApJ, 465, 527
Marconi, A., & Hunt, L. K. 2003, ApJ, 589, L21
Mateo, M. 1998, ARA&A, 36, 435
Mayer, L. 2013, Class. Quantum Grav. 30, 244008
McConnell, N. J., & Ma, C.-P. 2013, ApJ, 764, 184
McLure, R. J., & Dunlop, J. S. 2002, MNRAS, 331, 795
McNamara, B. R., & Nulsen, P. E. J. 2007, ARA&A, 45, 117
Méndez-Abreu, J. 2015, in Galactic Bulges, ed. E. Laurikainen, R. F. Peletier, & D. A. Gadotti (New York: Springer), pp. 25–50 (1502.00265)
Merritt, D. 2006, ApJ, 648, 976
Merritt, D., & Ferrarese, L. 2001, MNRAS, 320, L30
Mihos, J. C., & Hernquist, L. 1994, ApJ, 437, L47
Milosavljević, M., & Merritt, D. 2001, ApJ, 563, 34
Milosavljević, M., Merritt, D., Rest, A., & van den Bosch, F. C. 2002, MNRAS, 331, L51
Naab, T., 2013, in IAU Symposium 295, The Intriguing Life of Massive Galaxies, ed. D. Thomas, A. Pasquali, & I. Ferreras (Cambridge: Cambridge Univ. Press), 340
Naab, T., Oser, L., Emsellem, E., et al. 2014, MNRAS, 444, 3357
Nieto, J.-L., Bender, R., & Surma, P. 1991, A&A, 244, L37
Noeske, K. G., Weiner, B. J., Faber, S. M., et al. 2007, ApJ, 660, L43
Ostriker, J. P. 2006, Paper Presented at the Workshop on The Role of Black Holes in Galaxy Formation and Evolution, Potsdam, Germany, 2006 September 10 – 13 (see Cattaneo et al. 2009)
O'Sullivan, E., Forbes, D. A., & Ponman, T. J. 2001, MNRAS, 328, 461
Pellegrini, S. 1999, A&A, 351, 487
Pellegrini, S. 2005, MNRAS, 364, 169
Peng, C. Y. 2007, ApJ, 671, 1098
Peng, Y.-J., Lilly, S. J., Kovač, K., et al. 2010, ApJ, 721, 193
Peng, Y.-J., Lilly, S. J., Renzini, A., & Carollo, M. 2012, ApJ, 757, 4
Peterson, B. M., Bentz, M. C., Desroches, L.-B., et al. 2005, ApJ, 632, 799; Erratum. 2006, ApJ, 641, 638
Pildis, R. A., Schombert, J. M., & Eder, J. A. 1997, ApJ, 481, 157
Planck Collaboration 2014, A&A, 571, A16
Puech, M., Hammer, F., Rodrigues, M., et al. 2014, MNRAS, 443, L49
Quinlan, G. D., & Hernquist, L. 1997, New Astron., 2, 533
Ravindranath, S., Ho, L. C., Peng, C. Y., Filippenko, A. V., & Sargent, W. L. W. 2001, AJ, 122, 653
Rees, M. J., & Ostriker, J. P. 1977, MNRAS, 179, 541
Reines, A. E., Sivakoff, G. R., Johnson, K. E., & Brogan, C. L. 2011, Nature, 470, 66
Renzini, A. 1999, in The Formation of Galactic Bulges, ed. C. M. Carollo, H. C. Ferguson, & R. F. G. Wyse (Cambridge: Cambridge Univ. Press), 9
Rest, A., van den Bosch, F. C., Jaffe, W., et al. 2001, AJ, 121, 2431
Rodighiero, G., Daddi, E., Baronchelli, I., et al. 2011, ApJ, 739, L40
Romanowsky, A. J., & Fall, S. M. 2012, ApJS, 203, 17
Rusli, S. P., Thomas, J., Saglia, R. P., et al. 2013, AJ, 146, 45
Salmi, F., Daddi, E., Elbaz, D., et al. 2012, ApJ, 754, L14
Salo, H., Laurikainen, E., Laine, J., et al. 2015, ApJS, in press (arXiv:1503.06550)
Sánchez-Blázquez, P. 2015, in Galactic Bulges, ed. E. Laurikainen, R. F. Peletier, & D. A. Gadotti (New York: Springer), pp. 135–168 (1503.08105)
Sandage, A., Freeman, K. C., & Stokes, N. R. 1970, ApJ, 160, 831
Sanders, D. B., Soifer, B. T., Elias, J. H., et al. 1988a, ApJ, 325, 74
Sanders, D. B., Soifer, B. T., Elias, J. H., Neugebauer, G., & Matthews, K. 1988b, ApJ, 328, L35

Sani, E., Marconi, A., Hunt, L. K., & Risaliti, G. 2011, MNRAS, 413, 1479
Schechter, P. 1976, ApJ, 203, 297
Schiminovich, D., Wyder, T. K., Martin, D. C., et al. 2007, ApJS, 173, 315
Schulze, A., & Gebhardt, K. 2011, ApJ, 729, 21
Schweizer, F. 1987, in Nearly Normal Galaxies: From the Planck Time to the Present, ed. S. M. Faber (New York: Springer), 18
Schweizer, F. 1990, in Dynamics and Interactions of Galaxies, ed. R. Wielen (New York: Springer), 60
Schweizer, F. 1998, in 26th Advanced Course of the Swiss Society of Astronomy and Astrophysics, Galaxies: Interactions and Induced Star Formation, ed. D. Friedli, L. Martinet, & D. Pfenniger (New York: Springer), 105
Sellwood, J. A. 2014, Rev. Mod. Phys., 86, 1
Sérsic, J. L. 1968, Atlas de Galaxias Australes (Córdoba: Observatorio Astronómico, Universidad de Córdoba)
Shen, J., & Li, Z.-Y. 2015, in Galactic Bulges, ed. E. Laurikainen, R. F. Peletier, & D. A. Gadotti (New York: Springer), pp. 239–266 (arXiv:1504.05136)
Shih, D. C., Iwasawa, K., & Fabian, A. C. 2003, MNRAS, 341, 973
Somerville, R. S., & Davé, R. 2015, ARA&A, 53, 51
Speagle, J. S., Steinhardt, C. L., Capak, P. L., & Silverman, J. D. 2014, ApJS, 214, 15
Tacconi, L. J., Genzel, R., Neri, R., et al. 2010, Nature, 463, 781
Tacconi, L. J., Neri, R., Genzel, R., et al. 2013, ApJ, 768, 74
Tasca, L. A. M., Le Fèvre, O., López-Sanjuan, C., et al. 2014, A&A, 565, A10
Thomas, D., Maraston, C., & Bender, R. 2002a, Rev. Mod. Astron., 15, 219 (arXiv:astro-ph/0202166)
Thomas, D., Maraston, C., & Bender, R. 2002b, Ap. Space Sci., 281, 371
Thomas, D., Maraston, C., Bender, R., & Mendes de Oliveira, C. 2005, ApJ, 621, 673
Thornton, C. E., Barth, A. J., Ho, L. C., Rutledge, R. E., & Greene, J. E. 2008, ApJ, 686, 892
Toomre, A. 1964, ApJ, 139, 1217
Toomre A. 1977, in The Evolution of Galaxies and Stellar Populations, ed. B. M. Tinsley & R. B. Larson (New Haven: Yale Univ. Obs.), 401
Toomre, A., & Toomre, J. 1972, ApJ, 178, 623
Tremaine, S., Gebhardt, K., Bender, R., et al. 2002, ApJ, 574, 740
Tremblay, B., & Merritt, D. 1996, AJ, 111, 2243
van Albada, T. S. 1982, MNRAS, 201, 939
van den Bergh, S. 1976, ApJ, 206, 883
Whitaker, K. E., van Dokkum, P. G., Brammer, G., & Franx, M. 2012, ApJ, 754, L29
White, S. D. M., & Rees, M. J. 1978, MNRAS, 183, 341
Williams, M. J., Bureau, M., & Cappellari, M. 2009, MNRAS, 400, 1665
Woo, J., Dekel, A., Faber, S. M., & Koo, D. C. 2015, MNRAS, 448, 237
Wrobel, J. M., & Ho, L. C. 2006, ApJ, 646, L95
Wuyts, S., Förster Schreiber, N. M., Genzel, R., et al. 2012, ApJ, 753, 114
Wuyts, S., Förster Schreiber, N. M., van der Wel, A., et al. 2011, ApJ, 742, 96
Zaritsky, D. 2015, in Galactic Bulges, ed. E. Laurikainen, R. F. Peletier, & D. A. Gadotti (New York: Springer), pp. 193–204

Index

E. Laurikainen et al. (eds.), *Galactic Bulges*, Astrophysics and Space Science Library 418, DOI 10.1007/978-3-319-19378-6